CRANFIELD UNIVERSITY

Centre for Materials Science and Engineering
Department of Materials and Medical Sciences

Bonded Repair of Composite Structures

A Finite Element Approach

Submitted in partial fulfilment of the requirements for
the Degree of Doctor of Philosophy
by

A. Randolph A. ODI

Supervisor
Professor C. M. FRIEND

Internal Examiner
Dr M. J. Iremonger
Cranfield University

External Examiner
Mr F. L. Matthews
Imperial College

Submitted
19 December 1997

Examined
09 February 1998

28 May 1998

I hereby declare that the contents of this thesis represents solely my own work and has not been submitted for any other academic or professional award. The thesis is submitted on the conditions contained in the Regulations for the Presentation of Thesis, and the work for it has not been carried out previously.

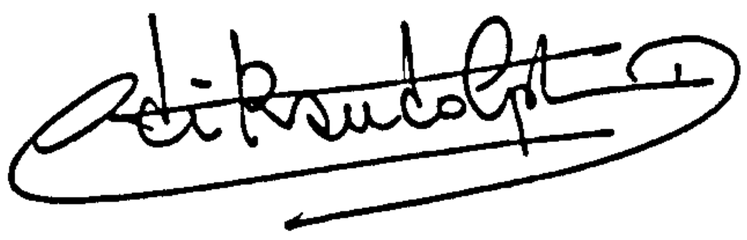

A Randolph A Odi

SUMMARY

This thesis addresses the issues surrounding the application of the finite element method to analyse composite structure repairs with an emphasis on aircraft applications. A comprehensive literature survey has been carried out for this purpose and the results are presented.

A preliminary study and a comparative study of different modelling approaches have been completed. These studies aim to explore and identify the problems in modelling repairs on simple composite panels with special attention given to adhesive modelling.

Three modelling approaches have been considered: Siener's model which is an extension of the traditional plane strain 2D model used for adhesively bonded joints, Bair's model which is a promising new approach and a full 3D model. These studies have shown that these methods are complementary providing a different insight into bonded repairs. They have also highlighted the need for a new modelling approach which will provide an overall view of bonded repairs.

Improved modelling approaches have been developed for externally bonded patch and flush repairs. These models enable the study of adhesive failure as well as composite adherend failures. These approaches have been applied to real repairs and the predicted results compared to experimental data. Four case studies have been conducted: external bonded patch repairs to composite plates, a scarf joint for bonded repairs, a flat panel repaired with a scarfed patch and a repaired curved panel.

These case studies have shown that bonded repairs to composite structures can be analysed successfully using PC-based commercial finite element codes.

Dedication

Seek first his Kingdom and his righteousness,
and all these things will be given to you as well.
Matthew 6:33

A mon père Marc Odi Assamoi:

Ton amour du travail bien fait, ton abnégation et ta conscience professionelle seront toujours une inspiration à donner le meilleur de moi-même. Ton amour discret mais profond, que j'ai mis du temps à comprendre et à apprécier, sera toujours mon compagnon de route tout au long de mon existence. Merci pour tout.

A ma mère Georgette Alla Seni:

Tu as toujours su trouver les mots justes pour me réconforter, surtout dans les moments difficiles. Savoir que tu m'aimes sans conditions sera toujours mon plus grand trésor. Merci d'être ma Maman.

A mes frères et soeurs Yves, Marie-Florence, Georges, Guy, Evelyne, Marie-Reine, Marc-Ange, et Marie-Emmanuelle:

Pour tous les sacrifices consentis. Recevez toute ma gratitude et ma reconnaissance. En vous tous, j'ai trouvé de vrais amis. Que Dieu nous garde toujours unis.

A mes parents, amis et connaissances:

Merci pour tous vos encouragements.

A ma fiancée Edith Laurette:

Ton soutien m'a été précieux tout au long de ce travail. Tu as fait preuve de beaucoup de compréhension à mon égard afin que cette thèse puisse s'achever. En témoignage de l'amour merveilleux que nous partageons et pour tous les sacrifices consentis. Cette thèse est aussi la tienne. Que le Seigneur te bénisse et te guide toujours.

"Préoccupez-vous d'abord du Royaume de Dieu
et de la vie juste qu'il demande, et Dieu
vous accordera aussi tout le reste."
Matthieu 6:33

Acknowledgements

I am particularly indebted to Prof. Cliff Friend for his guidance and supervision. I would like to thank Prof. Alex Brown and Cranfield University for the financial support and also Prof. David Bulman, my original supervisor, who initiated this research programme.

I would like thank also Dr David Bray at the Defence Evaluation and Research Agency (Farnborough) for providing the experimental data used for this project. Many thanks to Mike Prachar for the useful discussions in the latter part of the work.

Many thanks to Dr Jennifer Oakeshott (Imperial College) for the discussions and advice on using NISA and Adam Towse and Andrew Clark (Bristol University) for providing some of the references on adhesive failure criteria. Dr Keith Rogers' help is acknowledged for writing some of the BASIC programmes used in this project.

I am indebted to all the NISA support team at Wilde & Partners, in particular to David Deakin and Tim Morris whose help went far beyond the call of duty.

I would like to express my gratitude to all the people who supported and encouraged me during this period of study. I am thinking in particular of:

Christopher Thorpe for innumerable discussions in the office, much appreciated breaks from this work.

John Economou for many late nights (and early morning) discussions on engineering. They really put the philosophy back into the PhD!

Dr and Mrs Ron Colyer for their encouragement and support.

Dr and Mrs Paul Gibbons, members of the Prayer and Bible Reading Group and the Christian community in Faringdon, Oxon.: for their treasured friendship which made Faringdon feel like home away from home.

Dr Trebi-Ollennu, Dr and Mrs Marek Myszko, Chris Elvidge, Lee Kirkham and Peter Bruce

Antonis Tsourdos, Anna Blumel and the PhD students in the Postgraduate Room.

Mr and Mrs Venance Djouka (Ivory Coast Permanent Representation), Mr and Mrs Jonas Tiero and my friends in the Ivorian community in the UK.

CONTENTS

LIST OF FIGURES

Chapter 1

Literature Survey

Repair and Modelling Issues

1.0 - Introduction

Over the past twenty years, the use of composite materials in aircraft structures has become increasingly widespread as the need for improved aircraft performance and capabilities grew stronger during the last part of the Cold War era. For many of the industry experts, "the future can only be one of increased composite usage" [1]. Although the progress made was spurred by the aeronautical industry, composites today have found applications in several key engineering sectors, ranging from electronics to space applications.

As bigger and more important components are manufactured in composites, the problems concerning their damage and repair become more significant because the associated spare parts costs make the "replace rather than repair" policy for metallic components rather less attractive.

In this chapter, the issues surrounding composites service damage, damage detection and repair have been reviewed. The particular example of the aircraft industry has been taken to illustrate various points. However the issues raised here and in subsequent sections will be more or less valid in other areas where composites have found applications.

Composite materials basic concepts and constituents are discussed in greater details in Appendix A.

1.1 - Service Experience of Composite Structures

Composite structures have been flying throughout the world in different operating conditions for over 25 years now. A considerable amount of information has been gathered about their service history. Like any other engineering structures, they were found to be liable to damage and defects. These could arise during manufacture or during service. Manufacturing defects will not be discussed in this review as it is assumed that before entering service, composite components would have undergone stringent quality assurance controls able to detect and eliminate faulty parts. The focus therefore will be on service damage.

1.1.1 - Damage in Composite Materials

Composite structures are prone to a wide range of damages which adversely affect their residual properties. These damages can be classified into two distinct categories: those due to the operational environment and those due to mechanical effects and hazards.

Table 1 Typical service mechanical damage [2]

Defect	Typical causes
Cuts, scratches	Mishandling
Delaminations	Impact damage
Disbonds	Impact damage Overload
Hole elongation	Overload/bearing failure
Dents (delamination and crushed core)	Impact damage Walk in no-step regions Runway stones
Edge damage	Mishandling of doors and removable parts
Penetration	Battle damage Severe mishandling (e.g. fork lift)

Table 2 Typical service environmental damage [2]

Defect	Typical causes
Abrasion	Rain/grit erosion
Surface oxidation	Lightning strike Overheat Battle damage (e.g. laser designator)
Delamination	Freeze/thaw stressing (due to moisture expansion) Thermal spike (causing steam formation)
Honeycomb panel disbonds	Same as for delaminations
Core corrosion	Moisture penetration into honeycomb
Surface swelling	Use of undesirable solvents, e.g. paint stripper

Typical service damage are listed in Table 1 and Table 2.

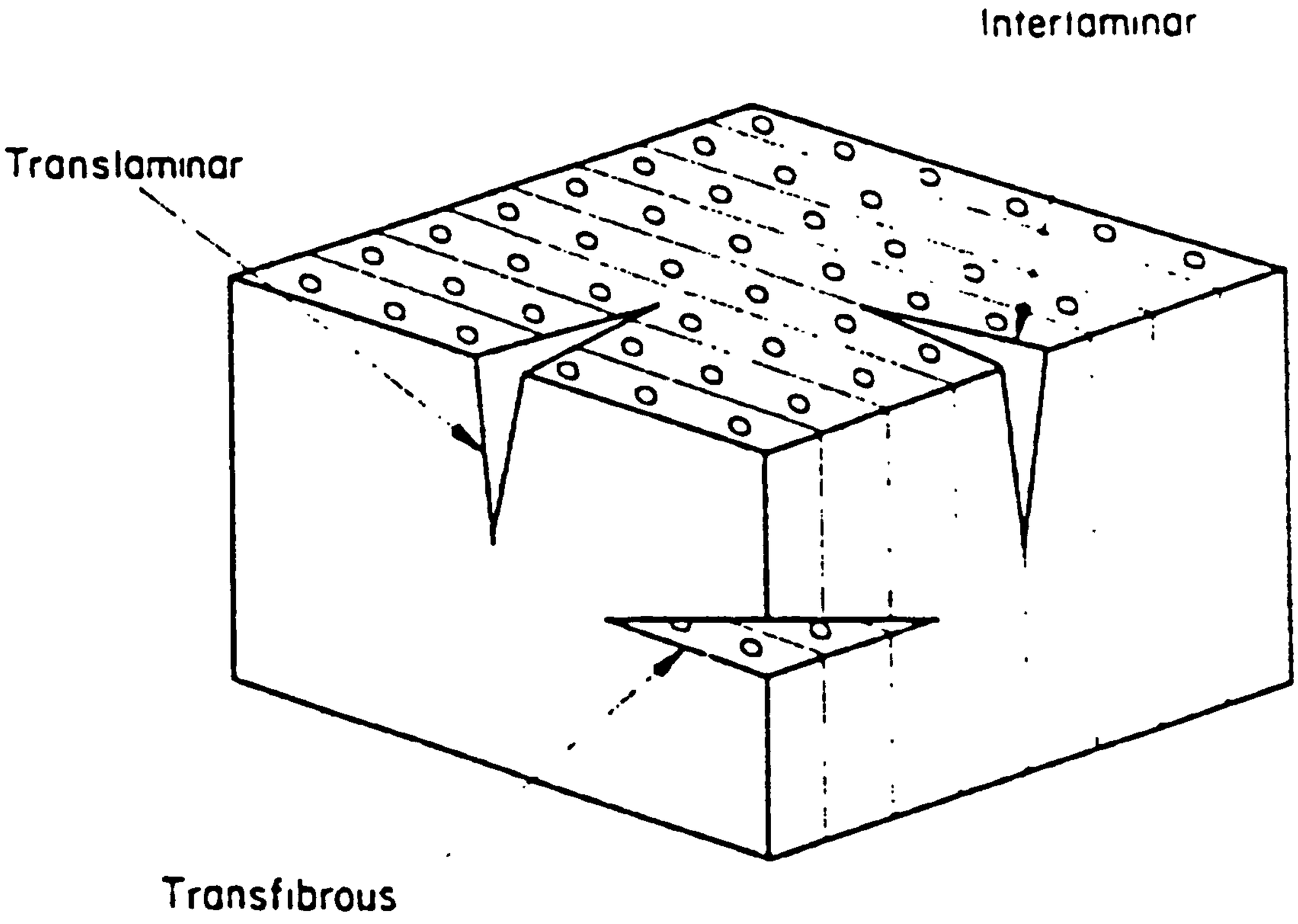

Figure 1 Flaws in a layered fibre reinforced composites [3]

According to Adams and Cawley [3] these defects can be put into three main groups: translaminar, interlaminar and transfibrous cracks as illustrated in Figure 1. Translaminar cracks are not common and transfibrous cracks (i.e. fibre breakage) usually occur after interlaminar failure if the structure is further stressed.

Heslehurst [4] conducted an extensive analysis of the various failure modes and mechanics of all defects commonly found in composite aircraft structures. He concluded that for adequate damage modelling, the principal damage types could be put in three main groups: delaminations, transverse matrix cracks and holes.

Table 3 Generalised defect types [4]

Delaminations	**Matrix cracks**	**Holes**
Bearing surface damage	Bearing surface damage	Bearing surface damage
Blistering	Contamination	Crushing
Contamination	Corner/edge crack	Cuts and scratches
Corner/edge crack	Cracks	Fastener holes
Corner radius delamination	Edge damage	Fibre kinks
Delaminations	Matrix cracking	Fracture
Debond	Matrix crazing	Holes and penetration
Edge damage	Porosity	Rework areas
Fastener holes	Translaminar cracks	Surface damage
Fibre/matrix debond	Voids	
Holes and Penetration		
Pills and fuzz balls		
Surface swelling		

Thus the main defects found in these groups are shown in Table 3.

Interlaminar cracks, often described as delaminations, are by far the most common defects to occur during service. They are single or multiple internal cracks whose planes are parallel to the surface of a component. They are the most serious defects because they are often difficult to detect. Several studies have shown that they have serious detrimental effects on composite residual properties, especially compression strength [2].

Delaminations can have environmental or mechanical causes. They occur most frequently at holes, free edges, regions of section change and bonded joints because high interlaminar stresses can exist there. The existence of interlaminar stresses was first proven by Hayashi in 1967 and then by the work of Pagano and Pipes who expanded Hayashi's original ideas [4]. During service, the most important cause of delamination is impact. Mainly because it is most likely to occur during ground handling operations. Tools can easily be dropped by maintenance personnel. Also stones can be thrown up from the runway, especially if the aircraft operates from semi-prepared strips as in military operations. The laminated nature of composite structures makes it very difficult for such delaminations to be detected because not only do they occur within the laminates but there is often no visible damage on the outer plies apart from very small surface indentations. Such damage is sometimes referred to as Barely Visible Impact Damage (BVID). Because of the concern about delamination effects on composite properties, several studies have been conducted in this growing research field. The most important ones connected to carbon fibre reinforced epoxy structures are included in an excellent review by Baker *et al.* [2]. A good introduction to the field of delaminations and additional information can be found in [5].

Disbonds are also of concern for composite sandwich aircraft structures. They can be caused by impacting or overloading the structure. They can also result from water, grease or oil seeping through the structure. During routine aircraft operations which include going through a series of freezing and thawing cycles, these substances deteriorate the core and destroy the interface bond [6].

Moisture absorption is a particular problem especially with carbon fibre reinforced epoxy structures because it degrades their hot/wet performance. Moisture going through freeze/thaw stressing causes delaminations by expanding. Or when it migrates in the structure, overheating creates a rapid heat build up which causes internal pressure to overcome laminate bonding [7]. The amount of moisture absorbed is a function of matrix and fibre type, time, component geometry, temperature, relative humidity and exposure conditions. AFRP are more susceptible to moisture absorption with about 2.6% by weight over a 10 year period ground based exposure programme by NASA Langley Research Centre. For CFRP, this varied from 0.7 to 2.2%. Equilibrium was reached after 3 years for CFRP structures and 7 years for AFRP [8].

These service damages need to be detected during routine maintenance checks as their presence and/or continued evolution could seriously hamper future aircraft operations with catastrophic consequences. A range of non destructive inspection (NDI) techniques have been developed over the years for composite structures to cope with this particular need.

1.1.2 - Damage Detection in Composite Structures

There are several damage detection techniques available to the maintenance engineer to check for service defects on aircraft structures. Most of them have evolved from methods used for metallic aircraft structures. They range from the low tech visual inspection to sophisticated ultrasonic techniques. They are usually comparative methods, using standards as reference, and therefore they require competence and skill from inspection personnel.

Table 4 NDI Methods

NDI Method	Delaminations	Disbonds	Cracks	Debris	Moisture	Condition of internal component
Radiography • Low kV, high definition			X	X		X
Ultrasonic • Attenuation • Resonance • Holography • Spectroscopy	X X X X	X X X X				X
Optical • Holography • Speckle interferometry • Laser photography	X X X	X X X	X		X	
Acoustic • Emission • Transmission	X X	X X	X X	X		
Thermal • Thermography	X	X		X		
Mechanical • Tapping test • Mechanical impedance	X	X X				X

The main NDI methods are listed in Table 4. Of the methods shown, only ultrasonic and radiographic ones are commonly used with composites. The main techniques only are discussed in this review.

1.1.2.1 - Radiographic NDI

Low voltage, high definition X-rays are used to inspect composite structures. GFRP and BFRP structures are best suited to this conventional X-radiography. CFRP give more problems but can be inspected if glass tracer fibres are incorporated in the material. Detection of delamination is very difficult because they are usually normal to the X-ray beam. Of the new radiography techniques being investigated, penetrant-enhanced X-radiography and neutron radiography have shown much promise. For the former, the presence of a radio-opaque penetrant in defects such as delaminations

significantly improves detection. The main problems are the toxicity of most penetrants and the fact that defect needs to be surface breaking. Neutron radiography could be used to check for transverse cracks. This technique uses the fact that composites absorb a certain amount of neutron depending on the presence of elements such as hydrogen. The main limitation is that it cannot be used for large-scale NDI as neutron sources are then not practical. There is therefore more chances for these developments to remain at laboratory level [3]

1.1.2.2 - Ultrasonic NDI

This is the most widely used technique. The structure is inspected by ultrasonic waves. This is done using a single or two transducers. When one is used, the inspection is said to be carried out in the pulse-echo mode. This means that the transducer is used to detect the reflection of the wave sent. With two transducers, one is employed as transmitter and the other as receiver. This is called the through-transmission mode. Because of severe impedance mismatch between the air and the structure, a liquid or solid medium called a couplant is used as a sort of conduit or guide for the ultrasonic waves. Water is often used as a couplant because it offers the best characteristics. The structure can be immersed in it or if it is too large water jets are used.

A variety of methods are used to display the results, the most common being A, B or C scans. The A scan is usually sent to a visual display unit (VDU) as a description of the echoes time history. The presence of echoes can be indicated by intensity variation if time is plotted on the vertical axis. Then the horizontal axis indicates where the echoes are located. This is a B-scan which allows a cross section to be built. C-scans are constructed around the same principle but use the amplitude of each echo at each point of the component surface being monitored. This gives a plan view of defect locations but no information on their depths.

Several types of measurements are possible with the same equipment described above. This determines the sub-type of ultrasonic NDI. For attenuation-type, the amplitude of the signal received in the time domain is monitored. The transducer is placed normal to the structure. In ultrasonic spectroscopy, echo measurements are made in the frequency domain. This is particularly advantageous for thin structures where it is difficult to resolve successive pulses. Still in development is ultrasonic holography where the measurements are translated into visual information by digital signal enhancement techniques. It is also possible to process the ultrasonic test signal in both frequency and time domains if the structure is being tested for a variety of defects [3, 9].

1.1.2.3 - Other NDI Techniques

Acoustic transmission NDI is sometimes referred to as Acousto-ultrasonic and as such can be classified as an ultrasonic NDI method. It involves using two transducers working together as in through-transmission mode. The pulse sent is transformed into mechanical displacement at the surface. Elastic stress waves are then produced in the structure by the release of energy as most structures tend to exist at their lowest

energy level. When they emerge to the receiver they are greatly deformed if they have encountered significant defects. [10].

Thermography NDI methods reveal the presence of defects through the analysis of temperature distribution in a structure. Infra-red cameras are often used. If the heating is produced by applying cyclic stresses through fatigue or vibration testing then the method is deemed active. If only the reaction to an applied temperature change is monitored then it is a passive method. This method is quick and can even detect moisture ingression but is generally less sensitive than ultrasonic methods. Equipment costs are also very high [3].

There are several other techniques which are discussed in greater details by Teagle [9], Wegman *et al.* [10] and Adams and Cawley [3] who also give several references about comprehensive reviews of NDI techniques by different researchers.

Each NDI method has its limitations and is best suited for given applications. The problem of moisture detection remains, especially for carbon-epoxy composite structures.

Once the structure has been inspected and service defects have been found, the maintenance engineer goes through the process of evaluating them. This will determine whether or not the component needs to be repaired or replaced. Thus NDI is the first step in the repair process because component damage can be assessed properly. After a decision is taken to repair the component, the engineer is faced with the prospect of designing a suitable repair scheme usually following the recommended practice included in the aircraft manufacturer structural repair manual (SRM) if the damage meets a set of criteria outlined in the SRM.

Very often, the damage will fall outside the criteria laid down, either because it is a new type or more often because SRM guidelines can be restrictive. Operators have in several cases found that the area of damage specified as repairable is far too small and the limits set too tight. Repair recommendations have been found to be ineffective in practice in specific cases such as delamination repairs [11]. It is therefore more than likely that the repair engineer will have to design a suitable repair for cases beyond the scope of the SRM that will need to be certified by both the aircraft manufacturer and the aviation authority.

1.2 - Repairing Aircraft Composite Structures

Repairs to aircraft structures outside the scope of manufacturers SRM have been successful. There are several examples which can be found in the literature [12]. Robson however[11] found that in most cases there was almost no systematic studies of the effect of damage size on repair efficiency. Heslehurst [4] also noted that current repair methodology tended to circumvent the damage analysis phase and based most repair designs on past experience or similar structural damage. Damage analysis is a vital step in the repair process if appropriate and economic repair designs are to be made.

Table 5 Typical repair methodology process [4]

1. Locate the damage area
2. Assess the extent of the damage
3. Evaluate the damage area stress state
4. Design the repair scheme
5. Fabricate and prepare the repair scheme
6. Apply the repair scheme
7. Conduct post-repair quality checks
8. Monitor the repair region

Table 5 shows a typical repair methodology process proposed by Heslehurst [4].

1.2.1 - Damage Analysis

Damage analysis must be an integral part of the repair process if optimum and cost-effective results are to be obtained. This analysis will rely essentially on the stress state around the damaged area. Given the complexity of composites, it is often very difficult to use closed form analysis techniques to evaluate accurately the stress distribution in the damaged structure. Numerical analysis will be necessary.

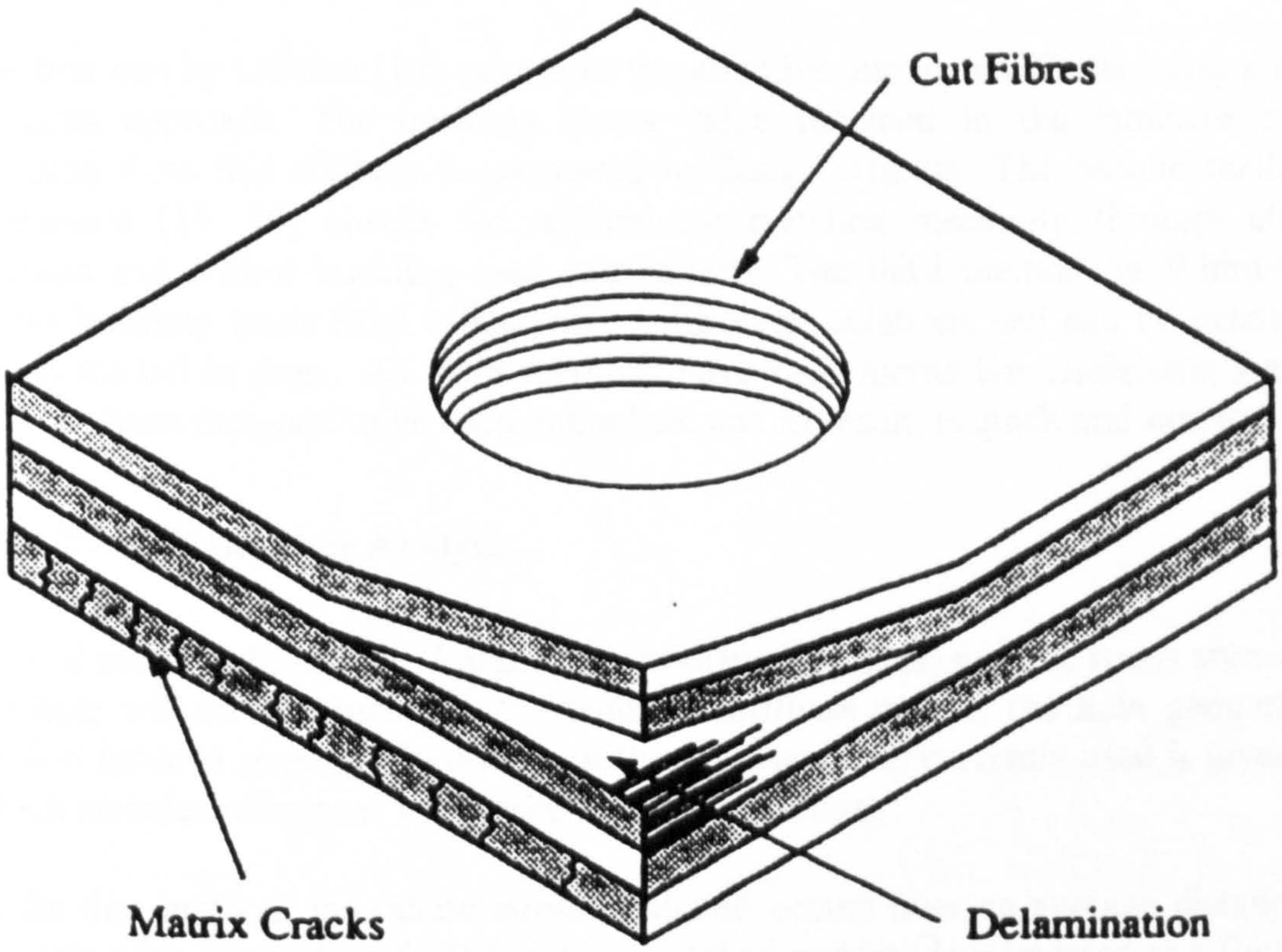

Figure 2 Principal damage types in composite laminates [4]

The three defect categories defined by Heslehurst [4] and shown on Figure 2 are well suited to numerical analysis. In general composite structures experience a local loss in stiffness for transverse matrix cracks whereas holes lead to a reduction in strength due to stress concentration effects. Delaminations may lead to structural instability when the component is loaded in compression or in shear.

The stress state in composite materials is in three dimensions. The existence of six stress components makes any analysis difficult. The interlaminar stresses can be difficult to evaluate or measure experimentally but they are necessary for a full stress analysis. Several methods have been devised to estimate them. In depth treatment of this subject can be found in [13, 14, 15]. On a more practical level, it is possible to use in-plane stress analysis in conjunction with current design variables to provide sufficient damage tolerance for interlaminar stresses, an approach suggested by Heslehurst [4].

1.2.1.1 - Matrix Crack and Delamination Analysis

An assessment of the damage caused by transverse matrix cracks will be concerned mainly with local buckling instability because a severe loss in local stiffness may lead to buckling. If compression loads are present then this may even cause delaminations.

There are three main methods that can be used for delamination analysis. They belong to the point stress analysis group which is the main alternative to analyses based on linear elastic fracture mechanics (LEFM). Point stress analysis tends to be preferred to LEFM because the properties required for the latter are difficult to correlate with basic composite material properties [4].

The first one by O'Brien [16] calculates the effective laminate stiffness using a rule of mixtures approach. The buckling stress value obtained in the laminate primary direction from this stiffness is compared to design stresses. The second method by Heslehurst [13, 14] checks for sublaminate buckling instability through effective stiffness and critical buckling load calculations. The third method by Whitney [17] assess buckling loads from sublaminate stiffness calculations and can be extended to panels loaded in shear. All three methods have their merits but Heslehurst's analysis [13] has been designed to be used in the field and as result, is quick and simple.

1.2.1.2 - In-Plane Hole Analysis

Several methods have been designed for in-plane hole analysis. The stress state around the hole will be influenced by the laminate stiffness matrix, the hole geometry and applied far-field stresses. An outline of the main methods currently used is given in [4] which includes references with more in-depth coverage.

In the first method, the failure stress predicted occurs over an average distance from the hole edge. The ratio of notched to unnotched strength is calculated as a function of this average distance, the hole radius and the normalised in-plane laminate stiffness matrix coefficients. In the point stress failure criterion method, the failure stress is predicted at a fixed distance from the hole boundary. A ratio of notched to unnotched strength is calculated and is a function of the same parameters as in the average stress failure criteria method described above. These two methods are suitable for uniaxial loading conditions and for circular holes.

For biaxial loading, the Gresczcuk and Tan-Tsai methods [4] are appropriate. The latter one being suitable for skewed elliptical holes. The methods devised by Ko and Hart-Smith are also convenient for biaxial stress states but use the principle of superposition [4]. They are both used for circular shaped holes. In addition, the Hart-Smith method has more assumptions but is simpler and thus more suited for field repair situations.

Once the decision has been taken to repair the damaged structure, there is the need to define the goals to be attained by this repair. These goals will usually be set in terms of repair criteria. These criteria will be defined in most cases by the original aircraft manufacturer in their SRMs. They will be similar to those described by Cook *et al* [18].

1.2.2 - Repair Criteria

Ideally the main objective of a repair is to restore the damaged structure to its original functional capacity. This restored capability will be evaluated in terms of strength, functional performance, safety, cosmetic appearance and service life. There will be special situations where repairs will not restore the component to its full capability but will still be necessary. This will be the case for combat emergency or the evacuation flight of an aircraft. In these particular cases, the conditions will dictate which criteria will be met by the temporary repair until such time when more appropriate measures will be taken [18]. This review will not be concerned by such cases as they are usually guided by unique policies and technical criteria.

1.2.2.1 - Strength, Stiffness and Stability

Structural repair will be required to restore a structure's full strength and stiffness in most cases. This will be done by selecting appropriate repair materials and designing adequate repairs.

The minimum requirement for primary structures will be the ultimate load limit. This limit is 50% greater than the maximum load expected in service. For secondary structures, the minimum requirement may be less stringent and less than full strength and stiffness may be deemed acceptable. However there is always a penalty in terms of the repaired structure durability and service life. As full strength and stiffness repair are usually no more difficult and time consuming than marginal ones, they should always be the recommended target.

In addition to strength and stiffness, there will be a need to consider stability if the structure is loaded primarily in compression or shear. This will be the case for components such as airframe panels which may buckle between major supports. Other structures such as stabilisers are designed primarily for stiffness, in bending and in torsion, to cope with aerodynamic loading. Repairs for such components will be designed primarily to restore stiffness rather than strength. Thus the predominant criterion will be closely related to the primary function of the structure. Care should be taken to avoid differences in stiffness between the repair and the parent. An overly stiff

repair will cause the interface with the parent structure to be over-stressed and lead to premature failure . If the parent structure is stiffer, then the repair will not take its share of loading and thus will fail to relieve the parent structure. The end result will be failure in the repair surroundings.

1.2.2.2 - Durability

For most current aircraft composite structures, fatigue is not a problem because they are designed for strain levels much below those at which fatigue could be an issue. This is because of the uncertainties still surrounding composite damage propagation and characterisation. However, environmental degradation will be important. Special attention will be given to the hot/wet properties. These should match those of the parent structure.

1.2.2.3 - Aerodynamic Smoothness

Abrupt changes in thickness and contours will affect the aerodynamic features of any aircraft structure. Depending on the component function, this can be detrimental. In the case of control and lifting surfaces, the overall effect will be a reduction in aircraft efficiency through increased drag. For fixed wing aircraft, aerodynamic smoothness will in general be more important. For rotorcraft, for example, this requirement will not be critical except for rotor blades, hubs and horizontal lifting surfaces such as the stabilator.

1.2.2.4 - Weight and Balance

Although the total weight added by a repair will be insignificant compared to the aircraft gross weight, there will be a need to pay attention to the weight being added in relation to the component functionality. For rotor blades, this will be of particular interest as they need to be statically and dynamically balanced.

1.2.2.5 - Economic Criteria

Most of the time it will be more economical to repair a damaged part than to replace it. Any repair scheme should consider the costs that will be involved in effecting it. These include aircraft downtime which should be minimised, repair personnel skills and training which require simplicity in repairs, facilities, tools and equipment as well as repair material costs. Special attention should be paid in particular to special handling, storage and material processing requirements.

Other repair criteria may include stealth characteristics and the repair in relation to other aircraft systems such as fuel systems, lightning protection and mechanical systems.

More in depth treatment of repair criteria parameters can be found in [19] and [20].

1.2.3 - Repair Types

The repair design will also be influenced by engineering factors other than stress analysis. These include the availability of repair facilities (tools, equipment and materials), the type of damage (the degree of structural degradation), compromise between engineering objectives and economic considerations (e.g. aircraft downtime) and the accessibility of the damaged area.

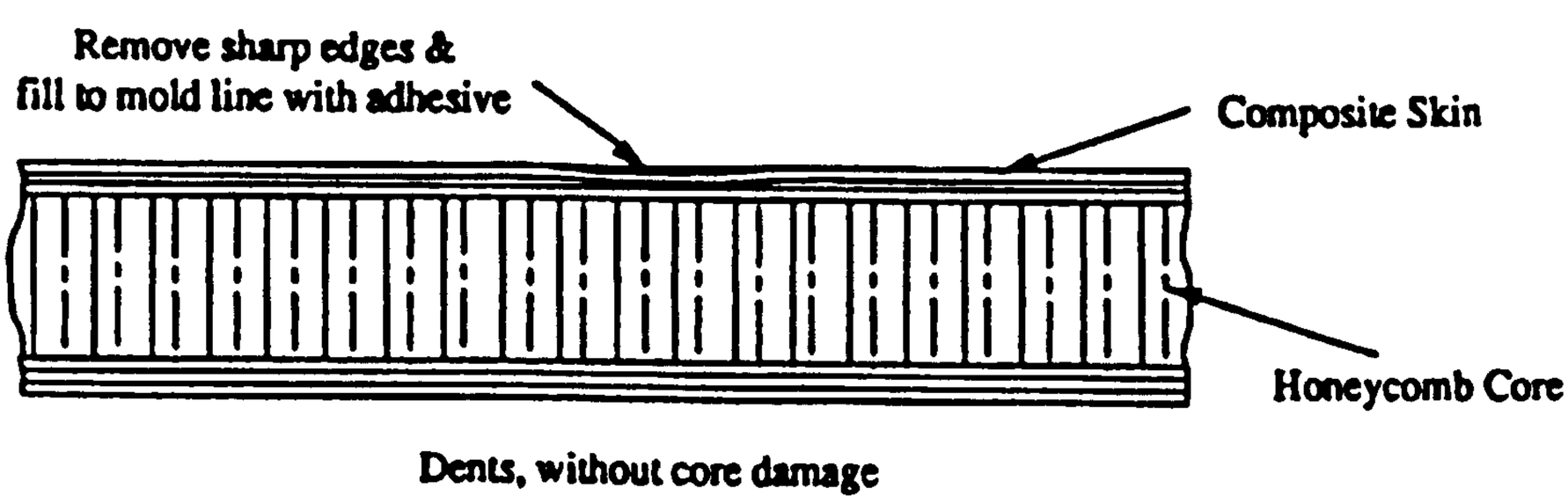

Figure 3 Cosmetic Repair [4]

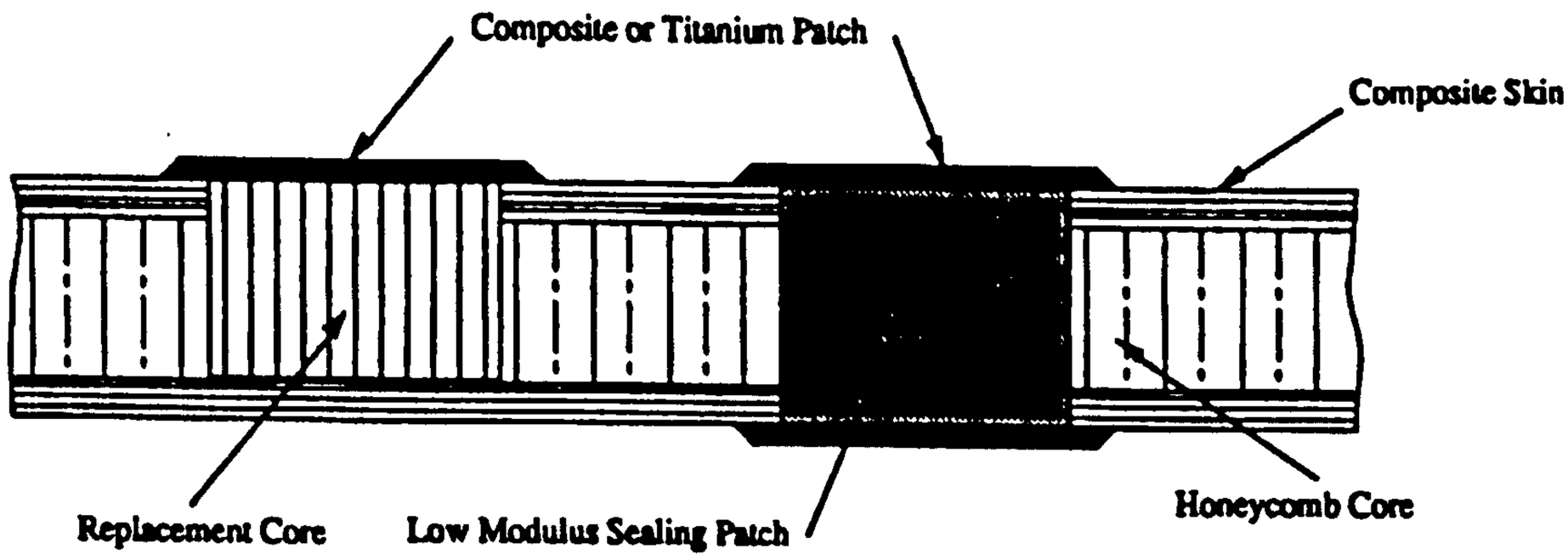

Figure 4 Semi-structural repair [4]

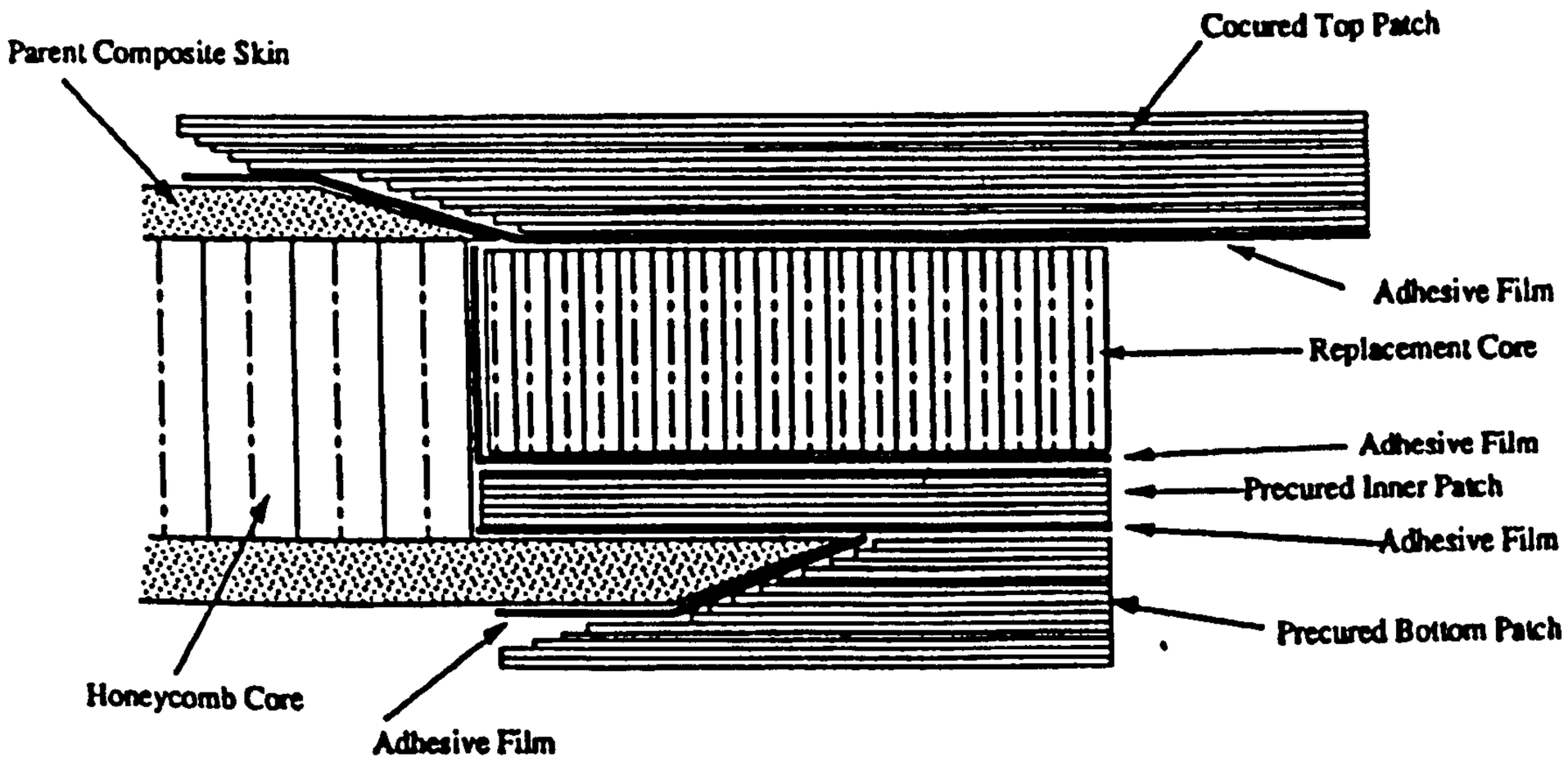

Figure 5 Adhesively bonded structural repair [4]

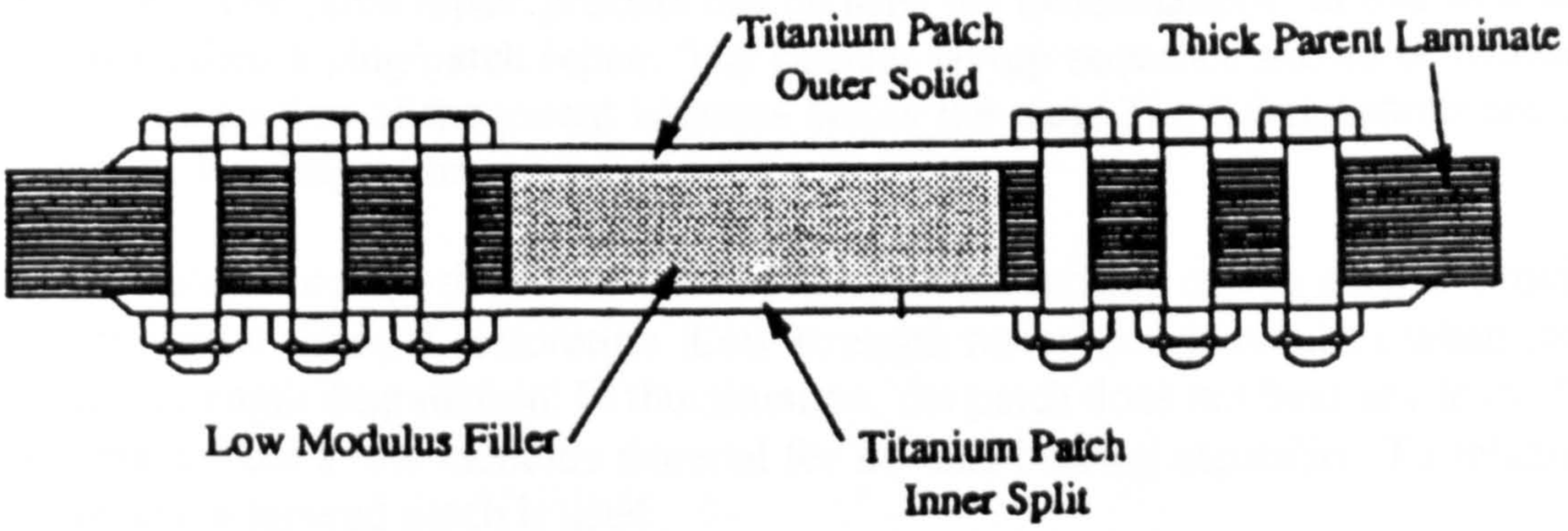

Figure 6 Mechanically fastened structural repair [4]

Whichever design is considered, it will be one of the four basic types of generic repair designs [4]:

- Non-structural or cosmetic repair (Figure 3): required when the damage is minor but environmental protection is necessary to avoid further degradation.
- Semi-structural repair (Figure 4): for damage more important than minor scratches. The damaged area is usually filled with an adhesive foam or a core replacement. The part is then covered by a thin patch called a doubler. Doublers may or may not be load carrying.
- Adhesively bonded structural repair (Figure 5): used for major damage. A patch is adhesively bonded over the damage area and has significant load bearing capabilities. Mainly used on thin composite skins.
- Mechanically fastened structural repair (Figure 6): also used for major damage. In this case, the patch is often bolted to the parent structure. It is used mostly on thick structural components.

1.2.3.1 - Non-Structural Repairs

These are carried out for minor defects. The main aim is to protect against the service environment as further exposure may lead to more serious degradation. For example, moisture can be absorbed through transverse matrix cracks. The use of a filler will prevent further moisture ingression. The filler is usually made from a compatible resin, such an epoxy, with chopped-glass fibre or glass sphere reinforcement. The surface is then re-finished. This type of repair is easy to carry out.

1.2.3.2 - Semi-Structural Repairs

In this type of repair, some load carrying capability is available from the doubler. The potting compound used is similar to that for cosmetic repair. The damaged region is filled with this compound. An alternative is to use glass-epoxy prepregs. The inconvenience there may be a weight penalty which may not be acceptable for control surfaces.

Semi-structural repair using a doubler can be used for transverse matrix cracks when damage analysis indicates the likelihood of local instability. The damage is filled with a low viscosity resin and the doubler is used to restore local stiffness. The damaged area

is not removed because load carrying fibres are still present. However there is a need to dry it out. The same repair process can be used for delaminations. In this case it is sometimes called a plug/patch repair. The doubler lay-up sequence should be identical to that of the portion of the parent laminate below the plug. The delaminations are cut out down to the deepest one.

To repair holes in composite structures, this plug/patch scheme can be used to provide low to moderate strength restoration. Low strength restoration is required when there is minimal strength degradation. In this situation, the patch does not bear any load. The plug is made from a low modulus material for no-load bearing capability. To minimise peel stresses, a tapered patch is used.

1.2.3.3 - Adhesively Bonded Structural Repairs

These are employed to repair major damage by replacing or supplementing the lost load path in the damaged material. Adhesively bonded structural repairs (ABSR) are carried out by bonding a patch to the parent laminate. This provides the most effective load transfer mechanism [21].

ABSR share similar features with adhesively bonded joints. Thus they can be classified into three main configurations: single lap, step-lap and scarf repair joints which can all be doubled to give three further categories (double-lap, double stepped and double scarf). ABSR can also be divided into external patch repair (single and double-lap repair joints mainly) and flush patch repair (step and scarf joints).

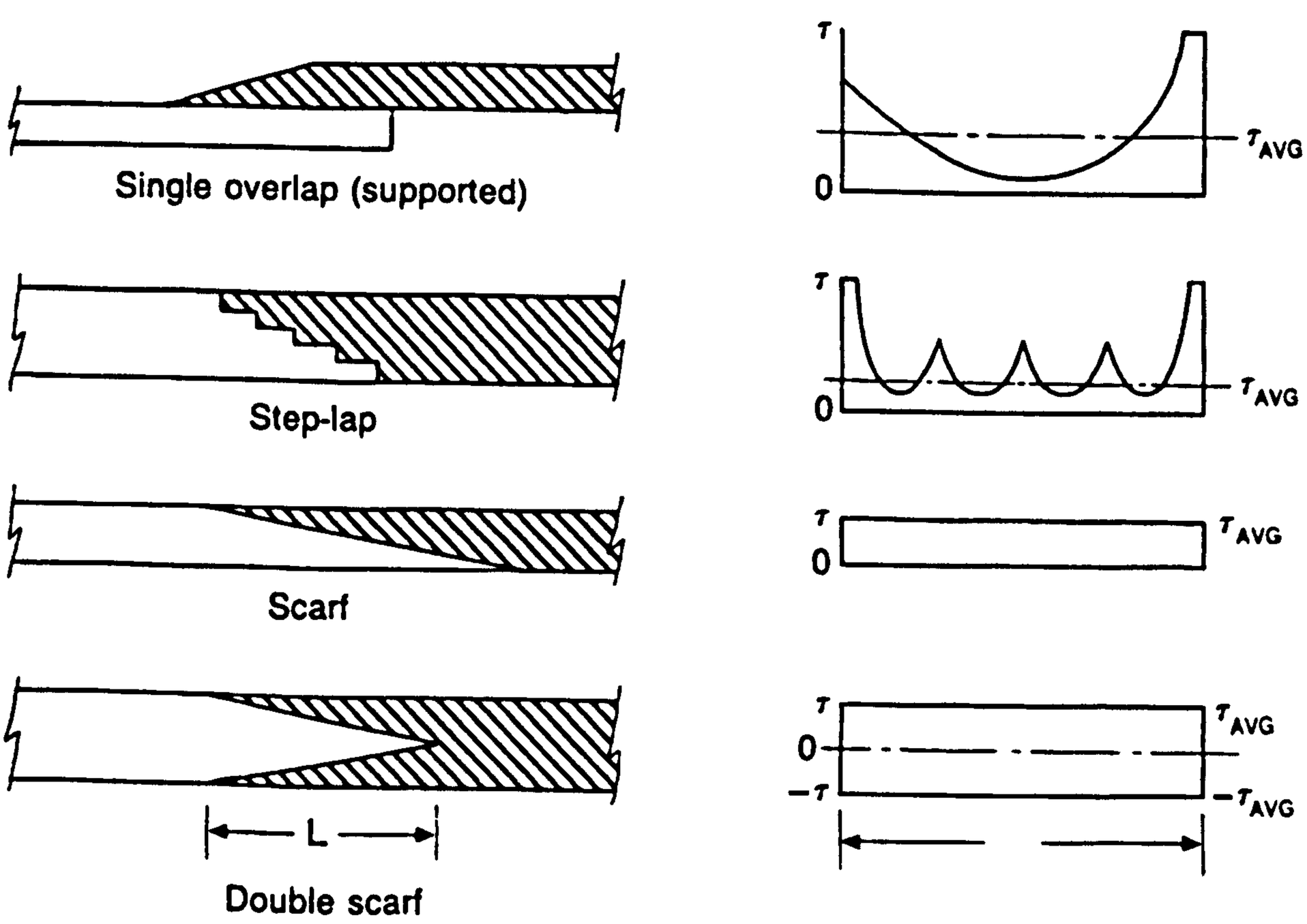

Figure 7 Main adhesive bonded joint types [21]

The various joints are illustrated in Figure 7 along with their theoretical resulting shear stress distribution in the adhesive.

External patch repairs are relatively easy to apply under field conditions because they are less critical in nature. Strength recovery between 70 and 100% can be achieved. In practice, this figure is around 60 to 80% [22]. They are used on thin structures and in situations where there is limited back side access or substructure interference. The load is taken over and around the damaged area. To minimise peel and shear stresses at the ends of the patch, tapering is used. One of the main problems encountered with this type of repair is the existence of an eccentric load path. This results in severe bending in the patch and peel stresses in the adhesive. Under compressive loading, this may produce buckling instability. To alleviate this problem, a sub-structure such as a honeycomb core can provide sufficient support to react against the bending.

Flush repairs are more time consuming because of the effort involved in preparing the surfaces. Scarf joints are the most difficult to realise because of their dimensional tolerances but they provide the highest joint efficiency of all repair types. Step-joints are an alternative which are easier to make. Scarf joints offer a uniform shear stress distribution in the adhesive and a low peel stress due to the lack of load eccentricity. Given the complexity of manufacturing appropriate scarf joints, they will usually be done under depot conditions. The patch lamination is designed to match that of the parent laminate with extra plies being added. A study by Myhre and Beck [23] found that premature failure occurred in the longest 0° outer ply due to peel stresses unless the ends of the ply were serrated. The exact additional number of plies to be added was determined empirically. Recently, Robson *et al* [24] have attempted to determine the number of additional plies required and in which direction they should be by using classical laminated plate theory.

Table 6 Guideline for use of extra plies on repair patches [24]

Base Lay-up	Loading	To restore stiffness		To restore strength	
		Extra Ply Orientation	Proportions*	Extra Ply Orientation	Proportions*
Quasi-iso.	longitudinal	0°	1 per 16 plies	0°	1 per 16 plies
Cross-Ply	longitudinal	0°	1 per 16 plies	0°	1 per 6 to 8 plies
Angle-Ply	longitudinal	±45°	1 pair per 16 plies	±45°	1 pair per 8 plies
	shear	±45°	1 pair per 16 plies	±45°	1 pair per 16 plies

*Extra plies are indicated for each group, or part group of plies, of the number shown in the original laminate

Guidelines for the use of extra plies are summarised in Table 6. Despite the limitations of the approach, the guidelines are very useful because they are the first one resulting from logical rather than empirical considerations.

ABSR patches can be co-cured, i.e. bonded then cured on the damaged laminate, or pre-cured, i.e. cured then bonded to the damaged area. The first method allows any contours to be matched by the patch and as such is well suited for highly curved or double-curved components. The inconvenience is moisture related problems that can

arise from a poorly dried component. This is avoided by using pre-cured patches but these are less flexible.

The design of bonded joints has been investigated by several researchers. More details about joint stress analysis and design can be found in [25] which contains several references to earlier works by Hart-Smith and other researchers.

1.2.3.4 - Mechanically Fastened Structural Repairs

This is an alternative concept to bonded repairs for restoring load bearing capabilities to seriously damaged composite structures. They are usually used for thick laminates where the shear stress requirement is excessive for adhesives. Bolted repairs are well suited to battle damage repairs because they can be applied by relatively unskilled personnel. External and flush patches can be used.

An external bolted patch repair is similar to a bolted single or double lap joint. The patch must be thick enough for the use of flush head fasteners but there is a limit to the thickness that can be used based on aerodynamic considerations. The pattern of fasteners will affect the repair efficiency. Bolted repair analysis is complex however. There are several methods quoted by Heslehurst [4].

For a flush patch, the damage is completely removed. There is a need to use doublers as well. The bolts are applied through the patch to the doublers and also through the undamaged area to the doublers. Limited back side access may be an obstacle for doubler installation.

The main materials used for patches are aluminium and titanium. The former has the advantage of being lighter but is well known to react electrolytically when in contact with the carbon contained in CFRP. A remedy is to use a scrim cloth or a sealant to isolate the aluminium patch from the carbon fibres. Titanium will not corrode in the presence of graphite but is far less machinable and formable than aluminium. Special titanium alloys have been developed for repair purposes with increased machinability and formability.

Mechanically fastened structural repairs (MFSR) can be time consuming because of the drilling operations required which can also cause significant additional damage to the parent structure if not performed properly.

1.2.3.5 - Adhesive Bonded or Mechanically Fastened Structural Repair?

As both methods can be used for repairing major damage, it is useful to compare them.

One of the main advantages of MFSR is that they require little or no surface preparation. For ABSR, surface preparation will have a strong influence on the quality of the bond. Therefore it must be performed with care. The environment is also important. Moisture is a particular problem for ABSR and there is a need to dry out the component completely before effecting the repair.

MFSR is well suited for field operation as the tools used are simple and can easily be carried. For ABSR, pressure and some form of heating may be required. Thus vacuum bags and heater lamps or blankets are often amongst the repair tools.

One of the main disadvantages of MSFR is the weight penalty compared to ABSR. It is also difficult to use them for certain components because of the need to reproduce the original contour. Doubly curved structural components are out of reach for this type of repair. ABSR can always reproduce the contours and they usually take higher strain levels.

The use of MFSR requires a certain amount of bearing strength from the parent laminate. The best lay-ups in terms of bearing strength are quasi-isotropic. This is not always the case for many components which may use a lay-up optimally suited for a particular loading configuration. Thus most composites lay-ups have low bearing strength. MFSR may not be designed with adequate bearing strength for most composite lay-ups. This is not a problem with ABSR.

The answer as to which one of MFSR and ABSR is best lies with the original design for the damaged component. There are no generally agreed conditions in the literature. Some authors such as Hart-Smith [26], Heslehurst [4], and Robson [11] favour the use of MFSR for field repairs, thick monolithic structures and highly loaded structures, whereas ABSR should be used for structures under light to moderate loads and thin structures. Hart-Smith [26] goes further in favouring MSFR over ABSR at all times if sufficient thought on repairability is given at the design stage. This would require the provision of mostly-quasi-isotropic lay-ups for sufficient bearing strength. To do so would not make the best use of composites as their fundamental versatility will be discarded to provide a material that mimics isotropic ones.

The opposite argument in favour of ABSR is put by Myhre and Beck [23] who note that fibre reinforced composite are essentially bonded in nature. Thus the use of bonding to repair damaged structures is a natural step. The weight penalty associated with bolts and rivets has led manufacturers in recent years to move away from bolted and riveted construction in favour of bonded ones. Thus as more structures are designed with a bonded construction, ABSR becomes the natural choice. The same view is shared by Baker [21]. The move towards virtually all-composite aircraft may see sandwich structures used increasingly, especially for the fuselage of large transport aircraft. MFSR are notoriously known to be incompatible with sandwich structures [22].

Given the trend being developed by aircraft manufacturers, ABSR will gain more prominence even for field repair as improvements are being made to provide suitable equipment [27]. Also, the advent of thermoplastic composites opens the way for even quicker novel bonding methods such as microwave joining [28] which may be more adapted to the field environment.

1.2.4 - Experience From Composite Repair Programmes

Several research programmes sponsored by the US defence establishment in the 1970s have established beyond any doubt that structures made from composites are repairable. These programme results were used as the basis for well-established advanced composite repair manuals [18, 29]. In addition several papers on composite repair can be found in the literature detailing the on-going work into this increasingly important area. All of them cannot be mentioned in this review, however attention can be drawn to a few landmark published works which illustrate the experience gained from various research studies in this area.

A review of the early US DOD/NASA sponsored programmes can be found in [30]. These started with the use of metal patch (notably titanium) to repair composite aircraft structures. Most of these repair techniques relied on an external patch. New ground was broken by Myhre and Beck [23] in the development of a successful scarf repair concept using adhesive bonding technology. This concept proved also to be able to cope with larger damaged areas than before. The use of serration was shown to be successful in dealing with peel stress problems. This modified scarf joint repair design was used in an another programme looking at the extension of the use of existing military aircraft repair techniques for commercial transport aircraft. The results of this programme have been published by Knauss and Stone [31] and Stone [32]. These together with other earlier works covering various aspects of composite repair technology including repair to thermoplastic and high temperature composites can be found in an excellent book edited by Brown [33].

Another significant publication is from the Advisory Group for Aerospace Research and Development (AGARD) conference series [34]. This was convened around the same period when Brown [33] edited his monograph.

Most researchers mainly reported in this conference their own experience in repairing composite structures. Thus several papers are rather general [35, 36, 37, 38, 39]. Others reported the problems linked with the repair of specific aircraft components such as stiffened panels [40, 41]. Due to earlier repair studies, the consensus seems to establish MFSR as best suited to the field environment whereas ABSR are preferred at depot level. As in Brown [33], most researchers have been successful in repairing composite structures.

AGARD organised another conference [42] on composite repair as a follow-up to the one held eight years before in 1986 [34]. In contrast to the previous proceedings, ABSR seemed to be established as the preferred repair method even for field repair. This was mainly due to the development of more adapted tools for field operation such as the vacuum-mould bag [43] which is even suitable for large area damage repair.

There was also an increased emphasis on improving scarfed repairs [44, 45, 46, 47]. Thus the 'hard patch' concept was developed by Deutsche Aerospace to repair a Canadian Forces CF-18 aircraft vertical stabiliser leading edge where the damage sustained was not covered by the SRM [45]. This method was developed first by Bauer and Maier and tested in-situ for a fighter aircraft integrally stiffened fuselage skin [44]. It was based on the preparation of a scarf in the parent structure and then a tool was generated in which the hard patch was cured under autoclave conditions.

Excellent results were obtained. However the procedure was lengthy and needs to be further improved.

Another point developed was the repair of honeycomb structures. This was done by improving earlier generic concepts [48] or using the new 'hard patch' concept [45].

Efforts were also made to deal with moisture associated problems with composites by developing and improving adhesives for curing temperatures below the boiling point of water. Successful work has been done in this area by Cochran *et al.* [49].

Useful developments of thermoplastic composite repair technology were also reported by [50] together with those for high temperature composites using modified scarf repair techniques [51].

Outside these conferences, several other papers were published on the repair of composites. Some give a good general introduction to this field [52, 53, 7].

1.2.4.1 - The Experimental Approach

The overwhelming impression in reading most published works on the subject of composite repair is the very strong experimental approach used by most researchers. This gave a very practical orientation to their work. This can be seen very strongly with the earlier papers [23, 30-32]. Even for the latest publications, the emphasis on experimental work is still very strong.

This fact can be explained in great part by the circumstances the pioneers found themselves in. They were introducing new materials and new processes into a very safety conscious environment. Thus they needed hard evidence to justify their products beyond the highly perceptible weight gain advantage. The results they gained from these experimental programmes vindicated their point as to the repairability of these new structural materials [23].

However composites by their very nature are complex. Any experimental programme requires taking into account several parameters. This either led to system specific results or very costly and long programmes. For example investigating moisture related problems may take several months to condition test specimens alone. Given the costs of raw materials for these test specimens, limitations inevitably came into play as to how many parameters or characteristics could be investigated at any one time. Thus the need to get the most out of a limited number of specimens, a goal which some such as Christian *et al.* [30], managed to achieve. This is in turn might raise questions on the validity of such results.

An exclusively experimental approach requires that the same experiments be conducted for every new type of material. With the versatility of composites, the combinations are endless. Also this approach encouraged conservatism in repair design in the early years as manufacturers usually went for what they knew best. Hence this tendency in current design methodology to create repair designs based on past experience or similar structural damage [4].

As the industry no longer possesses the kind of resources once devoted to research by defence budgets, the need for an analytical approach is being recognised more and more [4]. In their proposed composite repair methodology, Hall *et al.* [54] advocated strongly the development of analytical techniques to design and evaluate repair techniques. This in turn would help focus any required validation testing. This process will be helped by the improvement in computing capabilities.

1.2.4.2 - The Need for Analytical Methods

Although not much is said about analytical methods in most published works, certainly for earlier works, it would be inaccurate to state that this aspect was completely discarded even for programmes with a very strong experimental emphasis.

Most of the analysis carried out for repair programmes have been based on closed-form semi-empirical solutions. In the specific case of ABSR, the calculations for the repair joint design were based on the work by Hart-Smith on adhesive bonded joints [55, 56, 57, 58]. Several computer codes have been developed, based on these solutions and incorporated in hand-held programmable calculators for repair engineers. They form an intrinsic part of the first guides produced for advanced composite repair [18, 29]. Similar work by the same author has been conducted for MFSR, namely bolted and riveted repairs. The code developed from these solutions was also incorporated in a composite repair expert system developed by Sandow [59].

Closed-form semi-empirical solutions form the first group of analytical methods. They were popular because they could be programmed and thus give the repair engineer easy access to a good design aid. However, they have their limitations which make them suitable only as first stage tool for estimation and sizing of the design. When used exclusively they lead to very conservative designs because of their semi-empirical nature which requires safety factors to added. This analytical method cannot deal with thick, heavily loaded joints and is also restricted to shear stresses in the adhesive. Peel stresses must be minimised by the joint configuration. Hart-Smith has published to that respect a very useful paper on minimising peel stresses in adhesive joints [60]. His recommendations have been widely used for that purpose.

Given the limitations encountered with the first group of analytical methods, the need to look elsewhere for better solutions is very strong. A second group of methods have been suggested by Hall *et al.* [54]. This group is composed of numerical techniques such as finite elements, finite difference or boundary elements solutions.

These numerical techniques have been designed for solving continuum problems in engineering. They work by reducing a complex problem to a series of smaller problems requiring simpler solutions. This action is called domain discretisation. Once these smaller problems are solved, they are put together thus giving an answer to the more complex problem. Most engineering problems can be described mathematically by a set of differential equations which are complemented by a set of initial or boundary value conditions. Numerical methods such as finite difference (FD), finite elements (FE) or

boundary elements (BE) aim to solve these problems by solving these differential equations using some form of domain discretisation.

For the FD method, a grid is used as the domain discretisation form. The derivatives in the differential equations are approximated by using some type of truncated Taylor expansion. They are thus expressed in terms of the values at a number of discrete mesh points. The boundary conditions are then applied to the resulting algebraic equations to solve the problem at hand. The scheme used to discretise the problem domain is usually straightforward. The method is simple enough to use. However, there are serious limitations on using it for curved geometries. The usual FD grid is unable to cope with general boundaries. Also, if the boundary conditions are expressed with equations which contain derivatives, the need arises for the creation of fictitious external points or the formulation of lower order Taylor expansion. The net result is a decrease in accuracy [61]. An introduction to this method can be found in [62] where further information is available. In spite of these short-comings, FD method remains popular within the engineering community because it is economical to run on computers due to its simple matrix generation and manipulation.

The limitations encountered above with the FD technique led to the formulation of the FE method. This method relies on a series of elements to discretise the domain. The problem's variables are approximated in this case over these small parts of the domain constituted by the elements using polynomial interpolation functions. The properties of each element are expressed in terms of a discrete number of nodes and contained in matrices. The assembly of these matrices gives a global matrix which contains the properties of the continuum. The boundary conditions are then applied and the problem solved. The use of elements allows any geometry, in particular curved ones, to be represented. Also, the presence of derivatives in boundary conditions is not an obstacle as these can be expressed in terms of the same interpolation functions used to discretise the problem domain. Thus this method is more flexible than the FD one and also offers additional flexibility through easier mesh grading capabilities. However, the FE technique requires large amount of data to successfully discretise the full problem domain. This can be particularly acute for three dimensional analysis of engineering problems. The method may give inaccurate results for problems involving discontinuous functions, singularities or functions which vary rapidly [61] (e.g. interlaminar direct stresses at a laminated composite structure free edges).

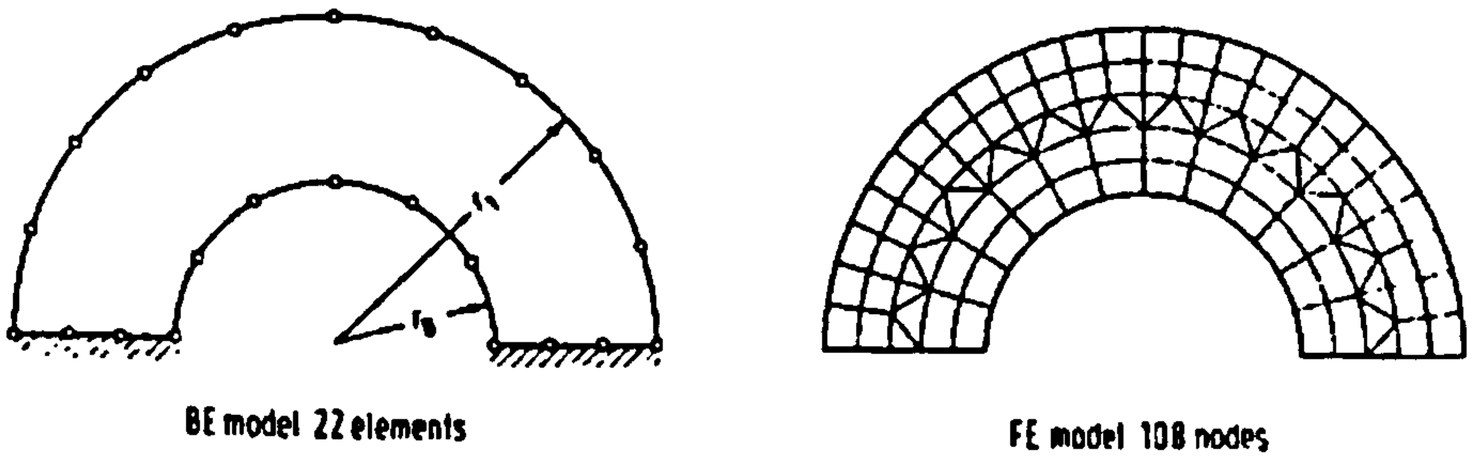

Figure 8 Modelling of an arch by BEM and FEM [61]

The boundary element method (BEM) was developed as a possible solution to the problems encountered with the FE technique. In this method, only the boundary of the

problem domain is discretised using a series of elements. Thus the amount of data required is significantly reduced (see Figure 8). The variables at different boundary points are related by using the original equations formulating the problem to be solved. This results in a number of influence coefficients which are then arranged into matrix form. The application of boundary conditions is done in a way similar to the FE method. The elements used can be of any shape making them adaptable to any general boundary. The inaccuracies found with FE for problems involving discontinuities and singularities no longer exist because the fundamental (original) equations are used. However, the use of the fundamental equations requires special integration techniques if an accurate solution to the problem is to be found because the integrals resulting from relating the variables in this case are far more complex [61]. The BEM was not very successful at first for solving potential flow and stress analysis problems which made it unpopular amongst scientists and engineers. However continued research in the field has solved this earlier stumbling block and has revealed this technique as an excellent alternative to finite elements. Compared to FD and FE, BEM is very much in its infancy and remains to this day very much a research tool.

On the basis of this short account of the main differences between the three numerical methods mentioned above, the FE method emerges as the most promising analytical technique to use for the design and evaluation of repair techniques as advocated by Hall *et al.* [54]. This method has been used in virtually every engineering field and is a proven technology. There are several commercial codes available in addition to others written for research purposes.

The finite element method is described in greater details in Appendix B with an emphasis on its use to model composite structures. The information is drawn from the introductory textbook by Astley [63] and the book by Ochoa and Reddy [64]on the finite element analysis of composite laminates. This is complemented by the definitive work by Zienkiewicz and Taylor [65, 66] on the FEM and the coverage by Smith and Griffiths [67] on its computer implementation. The existing literature on the use of FE for modelling and designing composite repair is reviewed in the next section.

1.3 - Finite Element Modelling of Composite Repair

The review carried out above on the experience gained from composite repair programmes has highlighted the need for a systematic approach to the design of composite repairs. It was further shown that the finite element method was the most promising analytical technique currently available able to fulfil this need. This section reviews how the FE method has been used so far to model, analyse and design composite repairs.

It was noted earlier that a bonded joint and a repair joint share essentially the same features. Therefore, it will be of interest to look first at the use of the finite element method in the design and analysis of composite bonded joints, before moving to a review of previous work on modelling composite repair using the FEM.

1.3.1 - Adhesively Bonded Joints With Composite Adherends

Adhesive bonding technology for composites has evolved from the technology used to bond aircraft metal components which was already mature when first extended to these new materials. As such the starting point in understanding adhesive bonded joints are the pioneering works by Volkersen [68] and Goland and Reissner [69]. These, along with other early methods of analysis for isotropic adherends proposed by Szepe [70], De Bruyne [71] and others have been reviewed extensively by several authors: Kutscha and Hofer [72] covered all work done in this field up to 1969, Vinson and Sierakowski [73] have reviewed the adhesive bonded technology up to 1986 and before that, Matthews *et al.* [74] covered all published work relating to adhesively bonded joints in composite materials in 1982 in an excellent article. A good understanding of the theoretical analysis of bonded joints can be found in [75].

1.3.1.1 - Limitations of Closed-Form Analysis

The main limitations of the earlier works, relying on closed-from analysis, were the fact that the peel and shear stresses were assumed constant across the adhesive thickness, the shear was maximum at the overlap ends and the adherends were assumed to deform only in tension. Renton and Vinson [76,77,78] and Allman [79] improved these models by including bending, shear and normal stresses effects with the adhesive shear stresses falling to zero at the overlap ends. Allman's analysis also allowed the peel stress to vary linearly across the adhesive but with the adhesive shear stress constant through the thickness.

Further developments came with the work of Adam and Peppiatt [80] which concentrated on the effect of transverse stresses in the adhesive joint (i.e. across the width of the joint). The adherends shear deformations were considered but bending effects neglected along with tearing and peeling stresses and the adhesive normal stresses. Their results show that there was a significant variation in stress along the joint width.

The use of closed-forms analyses, which are part of the continuum mechanics approach, is limited to very idealised joints and neglects the non-linear behaviour of the adhesive. Several researchers agree that only numerical methods can take the analysis of bonded joints further [73, 74 and 80].

1.3.1.2 - Limitations of Other Continuum Mechanics Approaches

The next logical step in the use of continuum mechanics was to remedy some of the limitations of the close-form analyses. Central to this was a better modelling of the adhesive behaviour. The addition of more realistic features such as the adhesive non-linear characteristics meant that the resulting equations could no longer be solved by closed-form expressions. Numerical methods had to be used to solve some of the differential equations which resulted from more complete analyses of bonded joints.

Several authors have shown that non-linearity effects are always much more important than those deriving from through-thickness adherend strains [74]. As a result, most non-linear analyses of adhesive bonded joints with composite adherends have centred around the adhesive non-linear behaviour.

The main advocate of the use of continuum mechanics supported by numerical solutions has been Hart-Smith who has published a great deal on the subject over the years [55-58, 81]. Single lap, double lap, scarf and stepped-lap joints have all been studied in great detail. Most of his work has been reviewed by himself in [82] and the main results summarised there.

The key element of Hart-Smith joint design philosophy is that every effort should be made to ensure that the adhesive is not the weak link in the joint. Thus he advocates tapering the adherends or locally thickening the adhesive to alleviate any peel stresses. Another aspect of Hart-Smith analysis is the choice of an elastic- perfectly plastic model to characterise the adhesive non-linear behaviour.

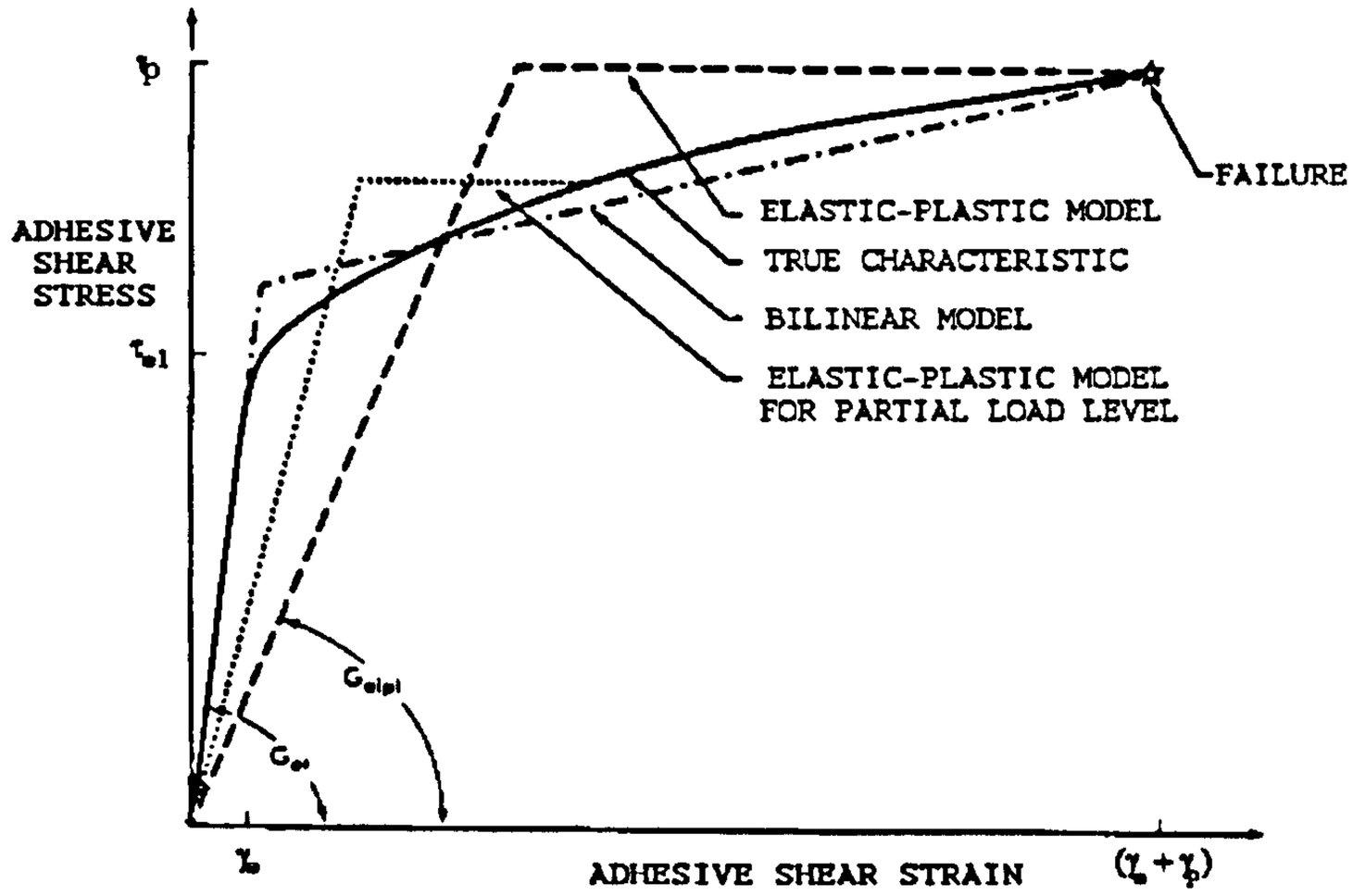

Figure 9 Adhesive shear stress-strain curve and various mathematical models [82]

In the model shown in Figure 9, the adhesive shear strain energy (as represented by the area under the curve) is retained as the main important characteristic. Thus the true characteristic is idealised by adjusting the elastic strain (γ_e) and keeping the maximum plastic strain (γ_p) the same as in the true shear stress-strain curve in such a way that the area under the idealised curve is equal to that under the true characteristic, i.e. the shear strain energy of both curves are equal.

Hart-Smith analysis of double lap joints has been based on earlier classical analyses by Volkersen [68]. He showed that increasing the adhesive maximum plastic strain will increase the joint strength. The exact shape of the stress-strain curve influences the adhesive shear stress along the joint length. So for the purpose of the analysis, the adhesive model chosen was adequate. He also included the effects of having thermally mismatched adherends. This highlighted the adverse effect of increasing adherend thickness and stiffness on the joint strength in this situation.

Hart-Smith used Goland and Reissner work [69] as the starting point of his analysis of single lap joints. Taking into account geometric and material non-linearity, he found that the adhesive behaviour had little influence on the joint strength. This was governed essentially by adherend properties and peel stresses. The joint strength was further influenced by the overlap length. Thermal effects were also included in the analysis and shown to affect the results.

Analysis of scarf joints showed that the adhesive stress is indeed uniform but only when the adherends were identical. If any difference was introduced either through a stiffness variation or a thermal mismatch, then the stress is adversely affected, becoming more non-uniform as the disparities increased. These were shown also to act independently of one another. In analysing, stepped-lap joints, Hart-Smith omitted the joint overall eccentricity and peel stresses. The solution he proposed was iterative and greatly influenced by the choice of initial values. This is due to the fact that in stepped-lap joints, the load is transferred mainly through the first three steps.

Most researchers agree that the main advantage of the continuum mechanics approach is that it offers the possibilities of parametric studies of joint characteristics at low costs. However, the assumptions used limits its use to very idealised joint configurations. As such exact stress distribution throughout the joint is not always available. Also, real joint features such as adhesive spew fillets cannot be modelled at all. These are the considerations which lead to the use of the finite element analysis of composite adhesive bonded joints.

1.3.1.3 - Finite Element Analysis Of Composite Adhesively Bonded Joints

The use of the finite element method (FEM) to study bonded joints with composite adherends has brought a new level of understanding of these structures. The biggest advantage of the method is the ability to determine the stresses within a body of arbitrary geometry. The inclusion of real joint features such as spew fillets has been a stumbling block for continuum mechanics approaches because this method could not cope with complex geometries. The use of the FEM also circumvented many of the continuum mechanics approximations because the contribution from all stresses within the adhesive joint could be included in the analysis. Thus more accurate prediction could be made.

The use of the technique was greatly investigated by Adams and his co-workers [83] after the pioneering work of Wooley and Carver [84] who first applied the FEM to study single lap joints. Their main results have been summarised by Adams and Wake in [83]. Their work has been set to study two main aspects of bonded joints which could not be dealt with continuum mechanics: joints end effects (which includes spew fillets and adherend tapering) and material non-linearity of both adhesive and adherends. Although the main joint types were all studied by Adams and his co-workers, most of their work has been around single-lap joints. Their biggest contribution has been on understanding the role of adhesive spew fillets in the reduction of peak adhesive stresses [80] and the influence of local geometry on joint strength predictions [85,86]. For joint strength predictions, the use of maximum value criteria (e.g. maximum stress or strain) was advocated in non-linear analyses. Although good correlation with experimental results have been obtained, this approach could not be generalised to other joint types. This was strongly criticised by Clark and McGregor [87] who felt that the Adam's approach had not reached the stage of quantitative joint strength predictions.

Another distinctive approach has been the use of fracture mechanics in FE analysis of bonded joints. This approach has been developed extensively by Groth [88] in his investigation of the effects of stress singularities at bonded joints corners. He relied

essentially on stress intensity factors in joint strength prediction. However, this method is not favoured by Adams and Harris [85] given the doubts cast by Kinloch and Shaw [89]. They showed that for adhesive joints, the fracture energy (from which stress intensity factors can be obtained) is not independent of the joint geometry and as such cannot be treated as an adhesive property.

Further improvement to the study of bonded joints has been brought about by Remy *et al.* [90] whose work included the prediction of initial and final joint failure for a single-lap joint. To achieve this, they relied on the formulation of various post-failure behaviour (PFB) models. Although added accuracy was gained through this process, better PFB models are required if all composite failure modes are to be taken into account. Also, the FE formulation of the problem relies on independent non-linear stress-strain curves which may prove costly in terms of required experimental characterisation if this approach is to be used for various materials. Thus, the improved predictions may be outweighed by the analytical complexity.

Finally, John *et al.* [91] have explored the capability of the FEM to predict joint strength variation with time under hot/wet conditions. Joint failure strength was predicted using a new criterion which relied on the scaled shear stress distribution along the joint length for various overlap lengths and their common crossover point which corresponds to the adhesive yield stress in shear. Reasonable agreement with experimental data was obtained. A non-linear analysis might have provided better results. However further work by Charalambides *et al.*[92] has revealed that John's criterion was not very good because the relationship with respect to the common crossover point was not very strong. Nevertheless, the study by John and co-workers is an important step towards the characterisation of the long-term behaviour of bonded joints.

These few references reveal the capabilities of the FE method in the analysis of bonded joints with composite adherends. Numerous studies on the subject have been published, a lot of them concerned with the definition of appropriate failure criteria for improved joint strength predictions. Most of them have been covered in the excellent review by Matthews and co-workers [74]. Later reviews include that by Lee and McCarthy [93] which include a good comparison between continuum mechanics and finite element analysis of bonded joints with composite adherends. Further information can be found there. It must be noted that because of the preoccupation with adhesive failure criteria, most of the bonded joints in those studies were designed to fail in the adhesive first [e.g. 87] with a few notable exceptions such as [94]

When non-linearity is included in the analysis, it can be one of the following: geometric non-linearity (large deflections such as in single lap-joint) or material non-linearity. The latter is further divided between the adhesive and the adherends.

For composite materials, the non-linearity is due mainly to the matrix material. Two distinct approaches can be used to model the non-linear behaviour of composites: one uses independent non-linear stress-strain curves which are obtained from uniaxial experimental tests and the other uses plasticity theory. For the first method, a stress-strain curve is required for each composite strain component and these are interpolated

and integrated in various ways. In the plasticity theory, the material behaviour is characterised by three properties: yield condition, flow and hardening rule.

The yield condition or yield criterion defines the specific stress combinations that will initiate the inelastic response. The hardening rule defines the evolution of the yield surface with stress, strain and other parameters. The flow rule relates the plastic strain increment to the current stress level and stress increment. These are used in conjunction with the linear elastic characteristics of the material.

For the adhesive, plasticity theory can also be used. This constitutes the **elastic-plastic** model, one of the two basic approaches currently used. The yield criterion used is the von Mises one which can be written as:

$$(\sigma_1-\sigma_2)^2+(\sigma_2-\sigma_3)^2+(\sigma_3-\sigma_1)^2=2\sigma_y^2$$

where σ_1, σ_2, and σ_3 are a combination of principal stresses and σ_y is the yield stress. This model has been used in most papers on non-linear analysis of composite bonded joints. A few examples can be found in [95, 96, 97, 98, 99]. The other approach is based on the so-called Rhagava criterion. Rhagava *et al.*[100] have shown that most polymers, including epoxy resins, have different yield stress in tension and compression. The following yield criterion was proposed:

$$(\sigma_1-\sigma_2)^2+(\sigma_2-\sigma_3)^2+(\sigma_3-\sigma_1)^2+2(|\sigma_c|-\sigma_t)[\sigma_1+\sigma_2+\sigma_3]=2|\sigma_c|\sigma_t$$

where σ_c and σ_t are the uniaxial compressive and tensile yield stresses. It is worth noting that when the two yield stresses are equal in absolute value, the von Mises yield criterion is obtained. The Raghava yield criterion has been used by successfully by Adams *et al.* [85] and Remy *et al.* [90] .

Two main conclusions can be drawn from the review above:

1. Closed form analysis are useful in determining basic joint geometry and in conducting parametric studies at low computing costs.
2. Numerical analysis in the form of the finite element method is essential if real joint features are to be represented and joint strength predicted accurately.

1.3.2 - Modelling Of Repair Joints: A Review

Given the growing popularity of the finite element method as a valuable engineering tool, it is surprising that the literature survey conducted for this project uncovered only a few papers directly concerned with the finite element modelling of composite repairs. This may be due to the fact that repair joints and structural joints share several common features. Thus given the amount of work devoted to understanding the latter, modelling specifically repair joints has not been pursued with the same endeavour. One can also notice that for several researchers the two types are considered the same when it comes to the analysis phase. Hence in several papers such as [101,102], the analyses which are carried out on structural joints using a particular modelling approach are often implied as entirely suitable for repair joints.

However, it is being recognised more and more that repairing aircraft structures, and repairing composite structures in particular, is a discipline in its own right, with its specific difficulties quite different from those associated with designing these structures for the first time [103]. Also, the view is emerging that some modelling approaches used for structural bonded joints (e.g. representing the adhesive by equivalent peel and shear springs) may not be suitable for bonded repairs of composite structures [104]

Furthermore, in their repair methodology, Hall *et al.* [54] called specifically for improvement in numerical analysis methods if more efficient repairs are to be designed. This view is also shared by Davis [104]in his report on the development of a standard for composite repairs for the Royal Australian Air Force. This can only be achieved by re-thinking the whole approach to the modelling of bonded repairs.

Published papers on the use of the FEM in the modelling of composite repairs are now reviewed.

1.3.2.1 - Modelling Approaches Evolved From Bonded Joints Studies

The following papers illustrate the main approaches used to model composite repairs which have evolved from bonded joints studies. Their common characteristic is the use of equivalent properties.

The first approach is that proposed by Loss and Kedward in their analysis of peel and shear stresses in adhesively bonded joints [101] in the early 80s. Although they did not model repairs specifically, they anticipated that their approach could be used in the context of repair design. The key feature of their analysis is the representation of the adhesive as a series of spring elements orientated in the longitudinal and the normal directions. The adherends are modelled with beam elements with equivalent membrane, bending and transverse shear properties.

The results presented compare well with classical solutions and other numerical techniques with the added benefit of being low on computing cost. However serious doubts have been expressed about the suitability of such an approach for composites[104]. Simply working out equivalent isotropic properties from composite laminates to input as beam element properties will not be sufficient to deal with failure modes peculiar to composites (e.g. interlaminar failure). Some experimental studies have shown that adhesively bonded composite joint failure can be associated exclusively with failure within the adherends themselves [102].

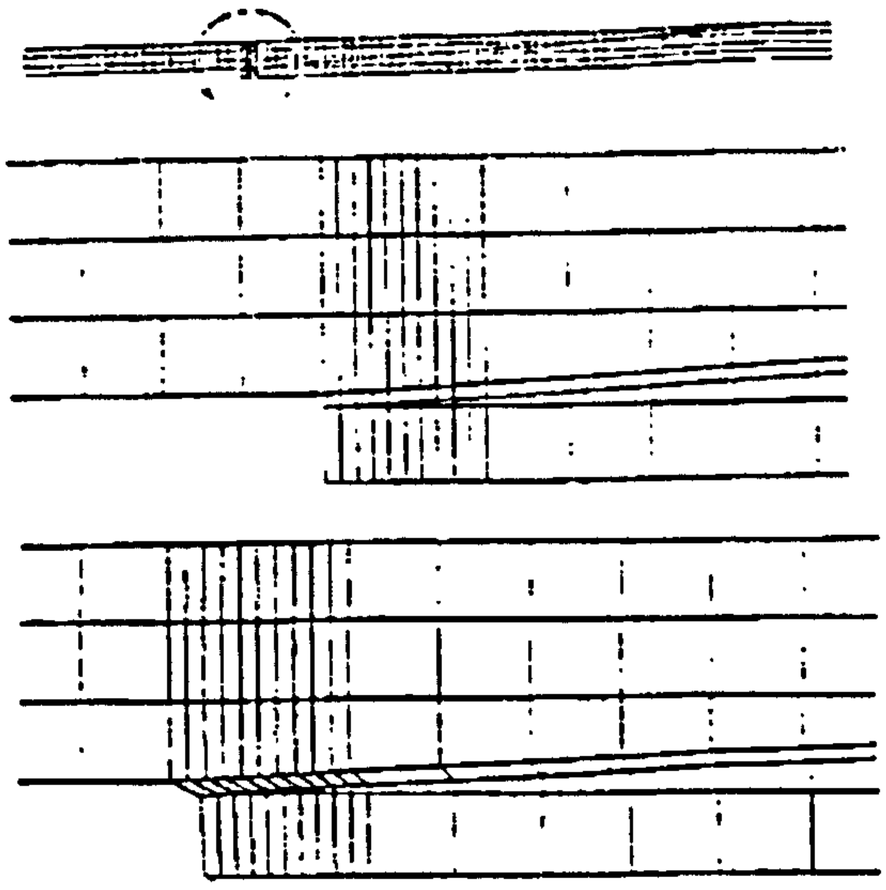

Figure 10 Finite element mesh in a repaired panel [102]

In his modelling of composite patch repairs, Siener [102] followed a method similar to Loss and Kedward [101] by working out equivalent properties for the composite adherends and inputting them into his FE model. The investigation was carried out using a 2D plane strain model (Figure 10), typical of those used in early studies of adhesively bonded joints [e.g. 85]. Siener showed that joint strength could be increased while reducing the overlap length by increasing the repair patch stiffness through a variation of lamination sequence. The repair joint failure prediction was not very successful. This was due to the use of equivalent properties and the omission of the adhesive non-linearity in the analysis. In fact, the experimental data revealed that the repair joints failed in modes which were characteristics of laminated composites. As such, the modelling approach could not reproduce it.

Finally, another modelling approach is proposed by Hunter [105]. It is a variation of Loss and Kedward model [101] in the sense that the adhesive was also discretised using spring elements. The adherends were modelled using plate elements which is an improvement. Thus it was a 3D model. Orthotropic properties were calculated from classical laminate theory and used in the model. The results obtained were good as far as the overall structure response was concerned. However, each spring element needed to be calibrated to obtain equivalent adhesive stiffness using a lengthy procedure. Again the criticism levelled against other approaches using equivalent properties applies to this one as well.

1.3.2.2 - Modelling Approaches Developed For Bonded Repairs

The need for more appropriate modelling approaches for bonded repairs was perceived early by Jones *et al.* [106] who proposed their analysis methods also in the early 1980s. They relied on the formulation of a special finite element to model the adhesive layer.

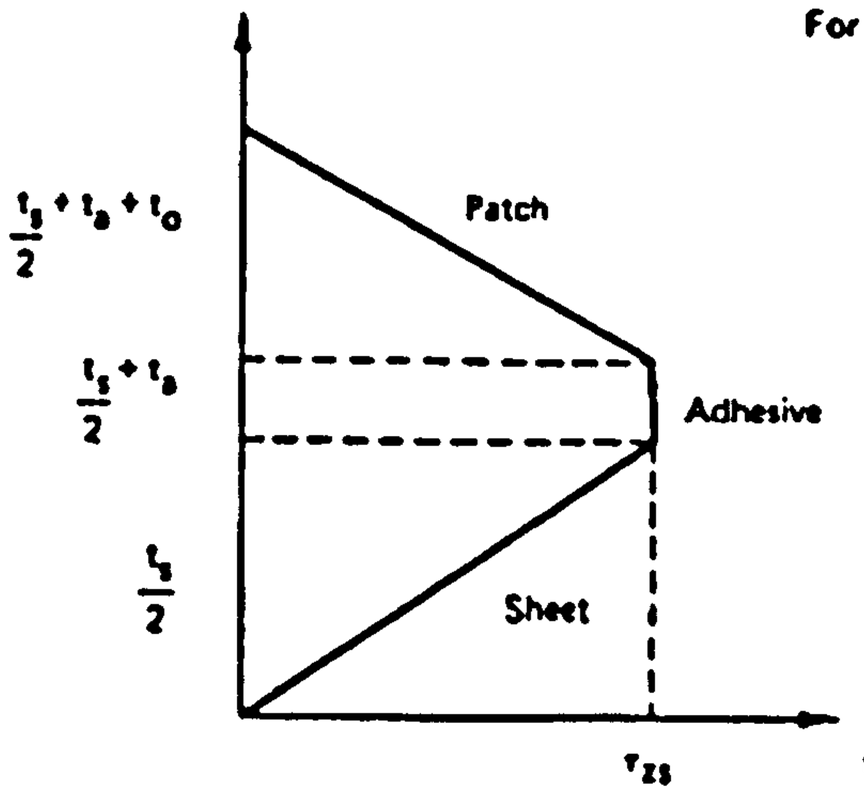

For (a) Doubly reinforced, t_s is the sheet thickness

(b) Singly reinforced, t_s is twice the sheet thickness

Figure 11 Shear stress variation in the repaired structure [106]

Shear stresses were assumed to vary linearly with thickness in the repair patch and the parent laminate. These stresses were zero at free surfaces and planes of symmetry. The adhesive shear stresses were assumed constant through the adhesive layer (Figure 11). A special purpose code was written for the analysis of various external repairs.

Jones *et al.* concluded that either a titanium or quasi-isotropic boron repair patch was equally suited to repair holes whereas a unidirectional laminate with fibres perpendicular to the crack was best to repair cracked laminated panels. The repair efficiency was measured through stress intensity values.

The results and conclusions reached must therefore be put in perspective given the reservation expressed by Kinloch and Shaw [89]. Also material non-linearity was not included for the adhesive. However the modelling approach is of interest because adhesive elements are not normally available in commercial finite element codes.

More recently Soutis and Hu [107] have shown that the traditional 2D plane strain models used for bonded joints were not entirely suitable to represent accurately external bonded repairs to composite panels. A full 3D model using solid elements with equivalent orthotropic properties was used to analyse the repair. Failure was predicted with good success using stress concentration factors. The same approach was used for the study of scarfed repairs [108]. A different failure criterion was used to predict failure. The FE results agreed very well with experimental data, indicating that the optimum scarf angle was around 7° against 4° if a 2D model was used. However, the failure criterion used relied on a characteristic distance which has never been shown to be a material properties. As such, caution needs to be exercised on the implications of the work.

Baker *et al.* [46] have also used a detailed 3D FE model to study scarf repairs to carbon epoxy components (aluminium honeycomb sandwich panels with composite skins). Each ply in the structure was modelled individually as separate elements.
It is not sure from the description given whether 3D solid elements were actually used in the analysis. However this 3D model was used to ensure that coupling between plies was properly accounted for. Linear elastic properties were assumed for the adhesive. Good agreement was obtained between the FE model and experimental results for strains. Stress concentrations due to the repair geometry were successfully predicted at ply drops in the doubler plies at the top of the scarf joint (Figure 12). No attempt was

made to predict failure. However, this paper illustrates the usefulness of the FEM as a design tool for composite repairs.

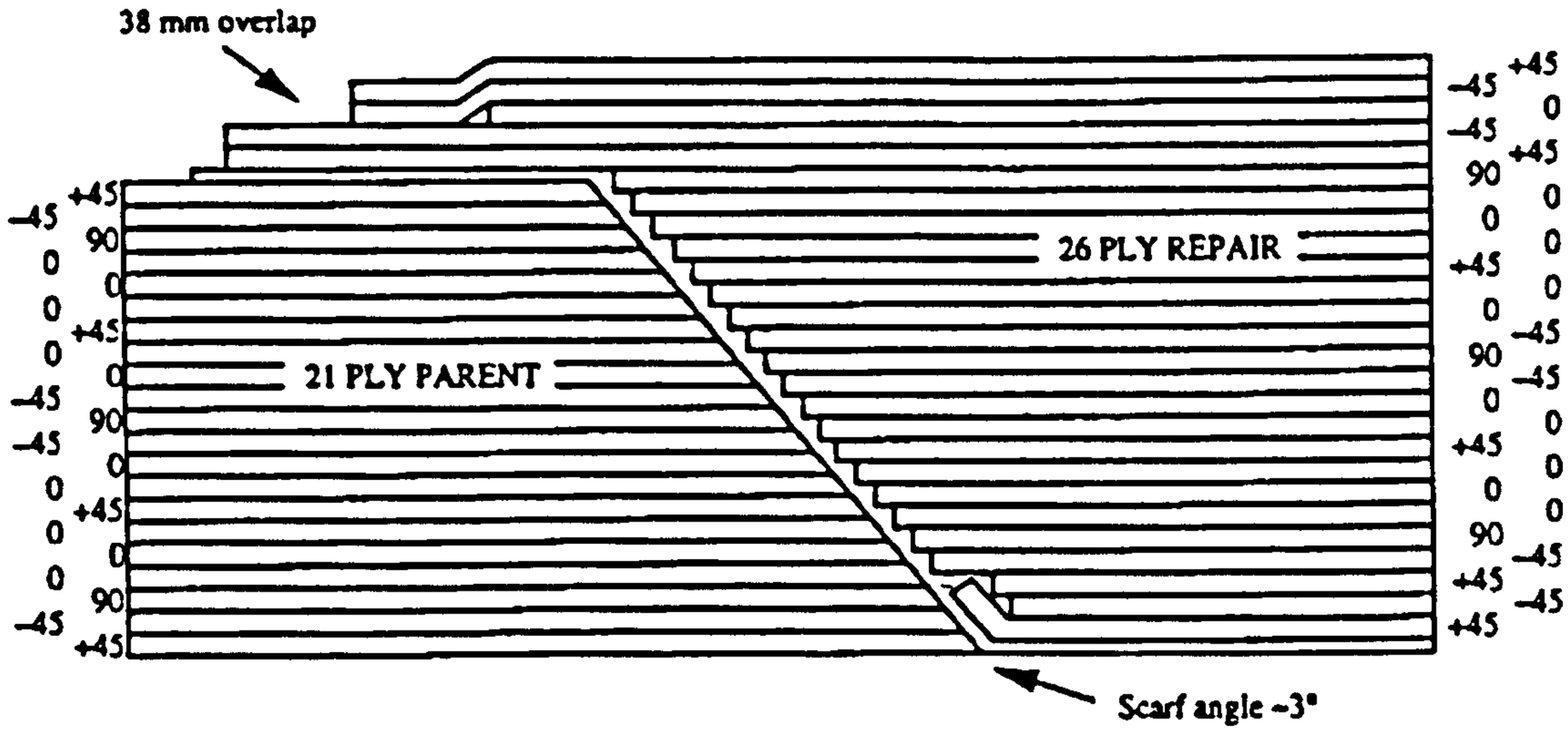

Figure 12 Repaired panel lamination sequence [46]

The study by Bair *et al.* [109] is one of the very few published papers dedicated exclusively to the modelling of composite repairs. The modelling approach is suggested which is quite different from all the others presented so far.

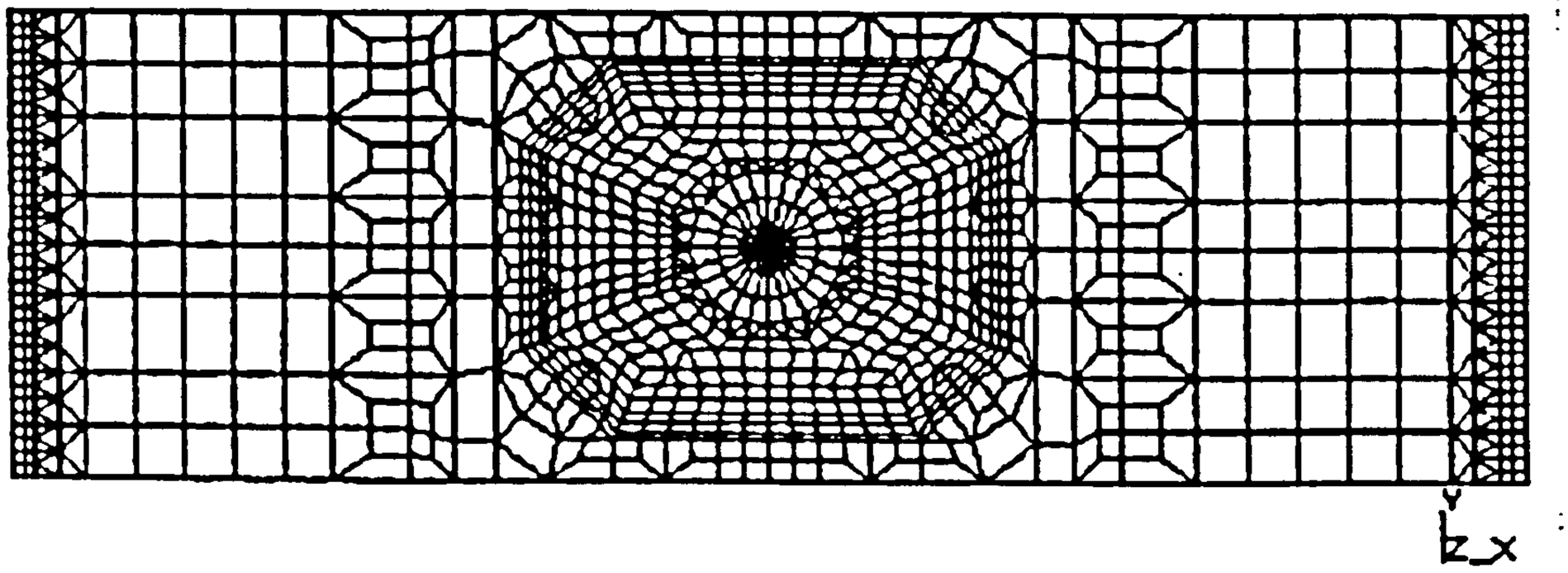

Figure 13 Finite element mesh in a repaired panel [109]

Each layer of adhesive is modelled as a ply at each step. Now with the modelling approach adopted, the correct representation of the number of layers in the repaired panel becomes a problem. This is due to the fact that the total number of plies varies as you move from one edge of the plate to the other.

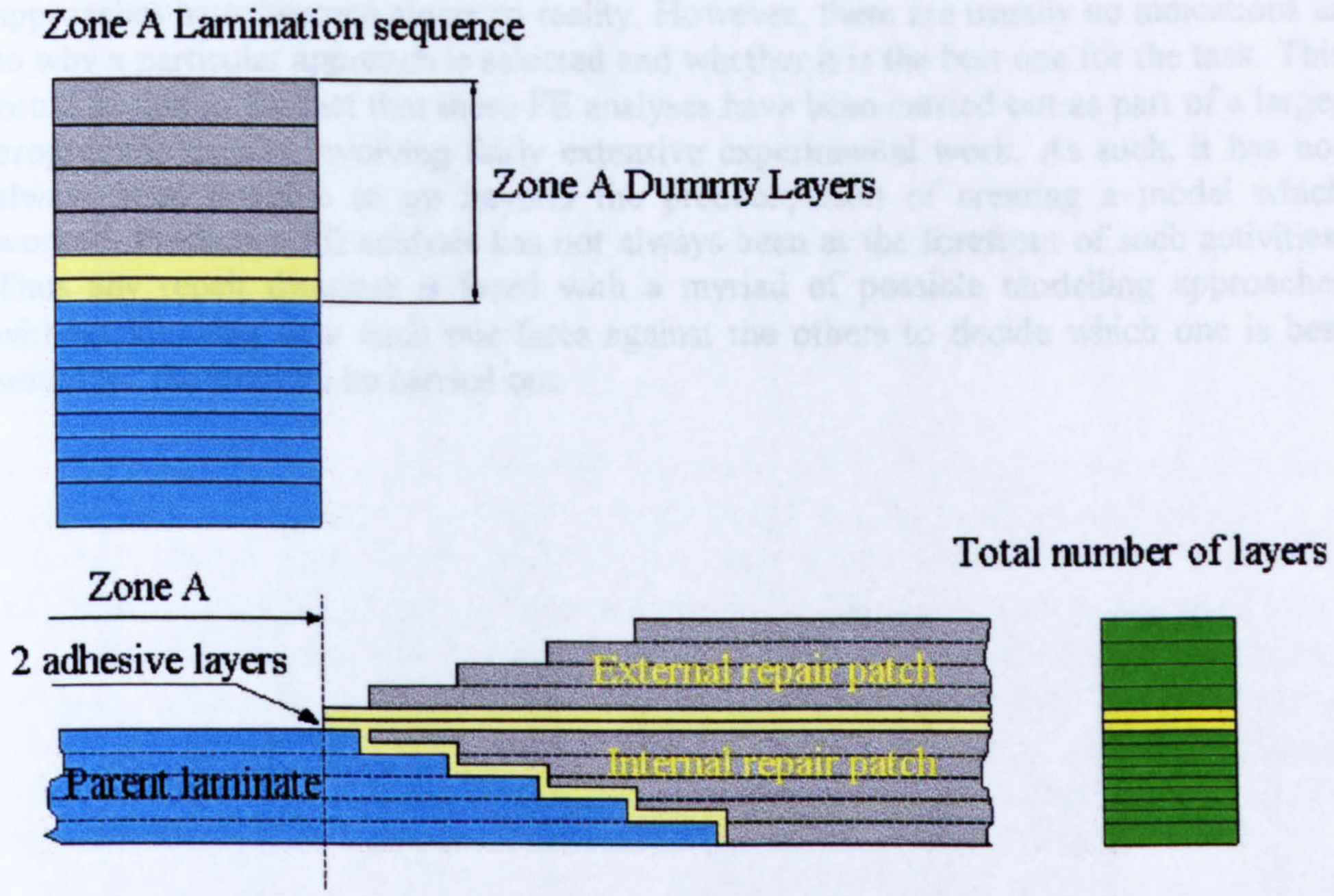

Figure 14 Repaired panel configuration used by Bair et al. *[109]*

To overcome this modelling difficulty, Bair *et al.* resorted to the use of dummy layers with extremely small stiffness. The panel is modelled zone by zone and the appropriate number of dummy layers is added to make up to the maximum number of layers. Thus the number of layers is the same in the whole model. For the panel in Figure 14, the dummy layers are indicated for zone A to illustrate this concept.

The results of the analysis were compared to experimental data. Both sets of data agree very well for strain measurements. No information was given about the stresses in the panel apart from a stress distribution plot in the fibre direction. Also no attempts were made to predict joint strength. No indication was given about the material model used for the adhesive and whether or not a non-linear analysis was carried out. The lack of the above information make the evaluation of this paper rather difficult with respect to other studies. However, useful description of the actual modelling work was given which shed a light on using the FEM for composite repair design and analysis. Bair's model has its merits but there are doubts whether features such as adhesive fillets and local geometry rounding can be represented using this approach. The main conclusion reached from this study is that the FEM can be used successfully on a day to day basis to design and analyse composite repair for large area damage on a personal computer.

1.4 - Conclusions

The modelling approaches used in the papers mentioned above indicate a growing awareness of the specific requirements for analysing bonded repairs. As such, these

approaches have become closer to reality. However, there are usually no indications as to why a particular approach is selected and whether it is the best one for the task. This could be due to the fact that these FE analyses have been carried out as part of a larger programme usually involving fairly extensive experimental work. As such, it has not always been possible to go beyond the preoccupation of creating a model which worked. Predictive FE analysis has not always been at the forefront of such activities. Thus any repair designer is faced with a myriad of possible modelling approaches without knowing how each one fares against the others to decide which one is best suited for the work to be carried out.

Project Aims

Modelling and Analysing Composite Repairs

The literature survey has highlighted the need for the development of analytical techniques for the design of adequate repair schemes. The finite element method was shown to be an appropriate candidate for such a task. Modelling approaches for adhesively bonded joints are well documented in the literature. Although bonded joints and repair joints share similar features, designing repairs and bonded joints are two different tasks. The open literature on modelling approaches specifically for repair joints is not abundant. Furthermore, there is no evidence of any studies undertaken with the specific aim of looking at the fundamental aspects of applying the finite element method to the analysis of bonded repairs to composite structures.

Therefore, this project aimed in the first instance to understand the philosophy behind the modelling approaches that have been used in the past and to compare them in order to gain a better understanding of the current state of affairs.

The second aspect was to evaluate the potential of commercial finite element codes for undertaking the analysis on a PC. The restriction to a PC only was designed to simulate an intermediate repair facility with no access to the types of equipment available at main maintenance depot.

Thirdly, the project aimed to formulate modelling strategies which are an improvement on current approaches for both external and flush repair types and to apply them to real repair schemes in order to test their applicability and predictive capabilities.

Finally, the project aimed to investigate ways of improving existing commercial codes with a special focus on the NISA/DISPLAY family of programmes.

Chapter 2

Comparative Study of Modelling Approaches

2D and 3D Models

2.0 - Introduction

In this chapter, the first aim of the project is tackled by comparing different modelling approaches which have been suggested and used for bonded repairs to composite structures. A better understanding of the philosophy behind each approach was sought. The main objective was to explore the advantages and problems associated with each approach through a linear static analysis of a representative composite repair.

The NISA FE code was selected for this project after a comparison of commercially available FE packages. The selection was centred around the suitability for PC operations and for modelling composite materials. The selection process is detailed in Appendix C which reveals also NISA main capabilities.

2.1 - Modelling Approaches

Three approaches have been selected: the traditional 2D plane strain model adapted for composite structures (Siener [102]), Bair's model [109] and a full 3D model (Soutis and Hu [107]). This selection was based on the principle of suitability for use on a PC, using commercially available FE codes.

Hunter's model [105] and Loss's model [101] were not selected because of the discretisation employed for the adhesive. Although this simplification looks attractive, the current generation of desktop computers have sufficient power to deal with modelling more accurately the adhesive layer without resorting to time consuming discretisation. Jones's model [106] was not included because the current project assumes access to commercially available FE codes on a desktop PC.

2.1.1 - Siener's Model

The main feature of this model is the plane strain assumption. This reduces the analysis to a 2D problem. It has been used before to model bonded joints successfully and thus represents a natural first step into modelling repair joints. From the laminate stacking sequence and material properties, effective properties are calculated using laminate analysis theory. These effective properties (Young's moduli, Poisson's ratios etc.) are then used in the material definition of the finite element model.

2.1.2 - Bair's Model

Bair's model represents a significant departure from the traditional plane strain model. Although in the original paper [109], the authors referred to this approach as being a two-dimensional one, it is in effect a three-dimensional model because it uses 3D composite shell elements which include deformations due to membrane, bending, membrane-bending coupling and transverse shear effects. As explained earlier, a zone-by zone method was used to construct the model with a combination of dummy layers where appropriate (Figure 14). The element used was made up of a number of perfectly bonded layers.

2.1.3 - 3D Model

This model employs 3D solid elements to represent both the adhesive and the composite adherends. Simple isoparametric solid elements are used with equivalent properties. These equivalent properties were obtained from classical lamination analysis. The aim was to obtain a full three dimensional representation of the stress state. Each adherend ply was modelled individually.

2.2 - Modelling Data

2.2.1- Geometry

These three approaches were used to model a scarf repair of a damaged composite plate. Siener's approach could be used to model an exact scarf repair, however, for the Bair approach the scarf joint was approximated by a five step lap joint. For the 3D model both types of repair were modelled. For reference purposes, undamaged and damaged plates were also modelled.

2.2.1.1 - Undamaged Plate

The undamaged plate was a Hercules AS4/3501-6 carbon/epoxy composite with a stacking sequence of $[0_2 / \pm 45 / 90 / \pm 45 / 0_2]_s$. The laminate was 300 mm long, 25 mm wide and 2.5 mm thick, giving a layer thickness of 0.1389 mm for each lamina. Modelling the undamaged plate was straightforward. The three modelling approaches were used. The displacement and stress output from these models were used as references for the repaired plate as the aim in any repair scheme is to restore a damaged component to a fully functional state. 3D composite shell elements (NISA-NKTP 32) were used in Bair's approach, general shell elements (NKTP 20)for Siener's and 3D solid elements (NKTP 4) for the 3D model. Plane strain elements (NKTP 2) could have been used for Siener's model and hybrid solids (NKTP 9) for the adhesive in the 3D model. These hybrid solids are more suitable for thin structures but are more expensive to run in terms of computing power and time.

2.2.1.2 - Damaged Plate

The damaged plate was similar in dimension to the undamaged plate but had a central 10 mm hole. The damaged state corresponds to that where damaged material has been cut out of the plate leaving a circular hole. This represents the plate just before the repair is carried out. Damage propagation was not considered. The damaged plate was

modelled to show the effect of the hole in the structure. The finite element model was constructed using the automeshing facility in NISA/DISPLAY with a stress accuracy option. The resulting mesh was thus fine enough to warrant accurate stress calculations around the hole. This area was more likely to have stress concentrations. The modelling was again straightforward.

2.2.1.3 - Repaired Plate

Using Siener's approach two models were constructed representing the two repair schemes: a scarf repair with a scarf angle of 3° and a stepped repair with five steps. A laminate analysis programme, LAP, was used to generate equivalent orthotropic properties for the laminate material and stacking sequence. This computer software is based on Classical Laminate Theory in which laminates are assumed to be infinite in length and width with plane stress assumed for each layer. This programme was also used to check results from the undamaged plate in tension.

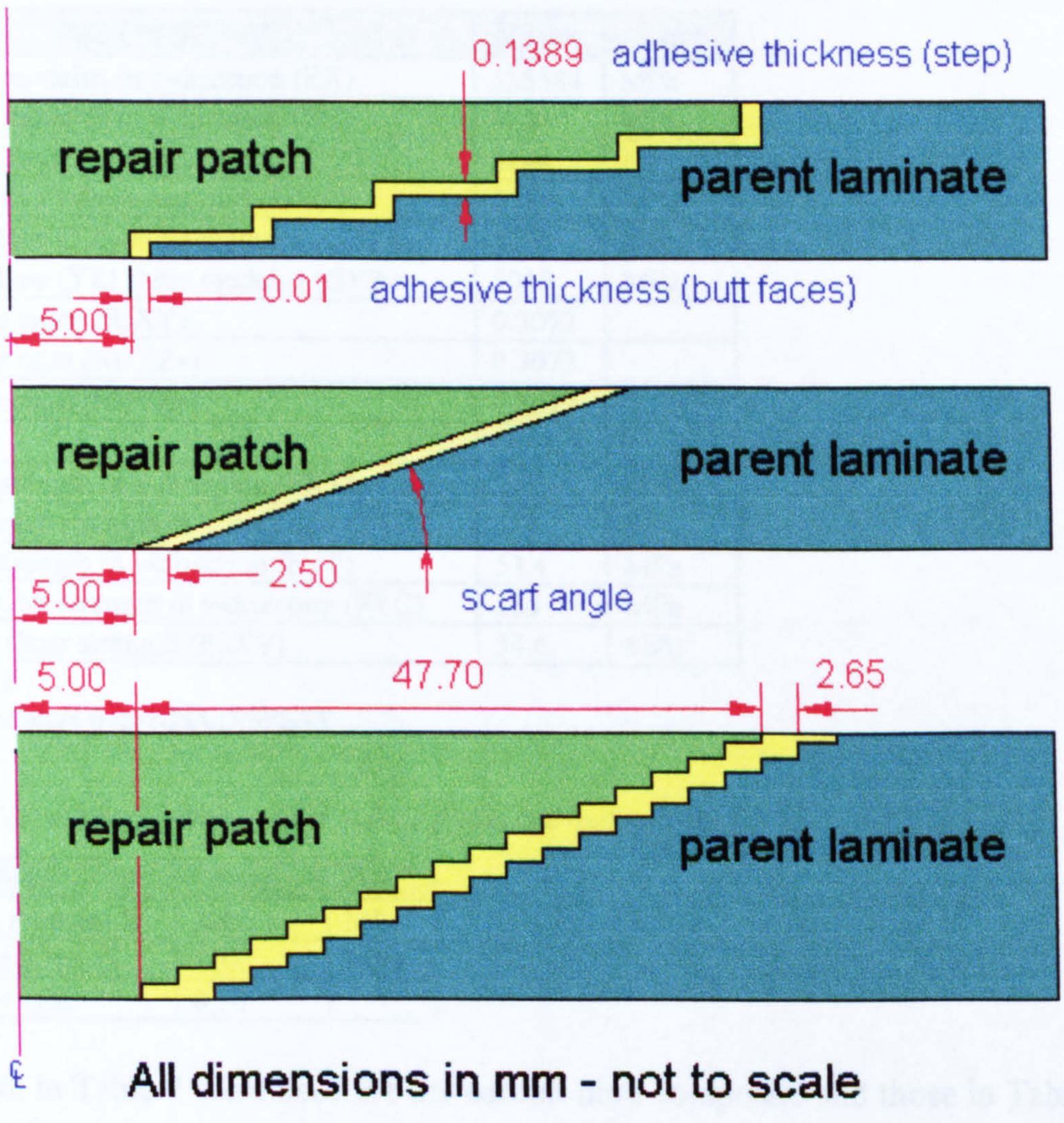

Figure 15 Repair schemes: (a) stepped lap joints (b) scarf joint (c) 18 step scarf joint approximation

For Bair's approach, only a stepped repair could be constructed (Figure 15). The adhesive thickness at each step was 0.1389 mm with a step length of 7.96 mm. The butt faces at each step were 0.01 mm apart as shown on Figure 15. The repair length was only 39.80 mm compared to the scarf repair length of 47.70 mm.

Initially the same stepped repair used in Bair's approach was to be modelled using 3D solid elements with the same adhesive thickness but with a step length of 9.51 mm and butt faces 0.15 mm apart to keep in line with practical repairs. A scarf repair model was also planned. However, for the latter, the model was constructed with a step at each ply as shown in Figure 15(c). From that point of view, the repair modelled using 3D solid elements is closer to actual bonded repairs in its representation of the joint. As a result, the stepped repair used in Bair's was not modelled.

2.2.2 - Materials Data

For all three states, the plate was loaded in tension by 10 kN with the appropriate boundary conditions to simulate a tensile test. Where appropriate, extensive use of symmetry was made..

Table 7 AS4/3501-6 Material Data (Source: NPL, UK)

PROPERTY(°)	Value	Unit
Young's modulus in x-direction (EX)	135584	MPa
Young's modulus in y-direction (EY)	9244	MPa
Young's modulus in z-direction (EZ*)	9244	MPa
In plane (XY) shear modulus (GXY)	5019	MPa
Out-of-plane (XZ) shear modulus (GXZ*)	5019	MPa
Out-of-plane (YZ) shear modulus (GYZ*)	5019	MPa
Poisson's ratio (NUXY)	0.3072	
Poisson's ratio (NUXZ*)	0.3072	
Poisson's ratio (NUYZ*)	0.3072	
Tensile strength in x-direction (FXT)	2178	MPa
Compressive strength in x-direction (FXC)	484	MPa
Tensile strength in y-direction (FYT)	53.4	MPa
Compressive strength in y-direction (FYC)	134	MPa
In-plane shear strength (FSXY)	34.6	MPa

* assumed

(°) nomenclature from NISA/DISPLAY

Table 8 Typical Epoxy Adhesive Material Data (Picket and Holloway [96])

PROPERTY	Value	Unit
Young's modulus E	3000	MPa
Shear modulus, G	1103	MPa
Poisson's ratio	0.36	

The data in Table 7 were used for the carbon fibre composite and those in Table 8 for the adhesive

2.3 - Results And Discussion

The aim of this study was to compare the different modelling approaches. The results obtained are grouped in three main parts: displacement, adhesive tensile stress and adhesive shear stress results. These parameters provide a useful comparison of the data obtained. The main reason for the choice of these quantities as comparison parameters

is the fact that in a repair joint, ultimate characteristics such as strength and efficiency, are strongly influenced by the adhesive stresses (in particular the shear stress). Thus a model's ability to evaluate these stresses is a good indication of its usefulness. Accurate displacement calculation is the first basic requirement any finite element model must meet. A linear static analysis with a relatively low load also allowed an investigation of the structural response predicted by the models.

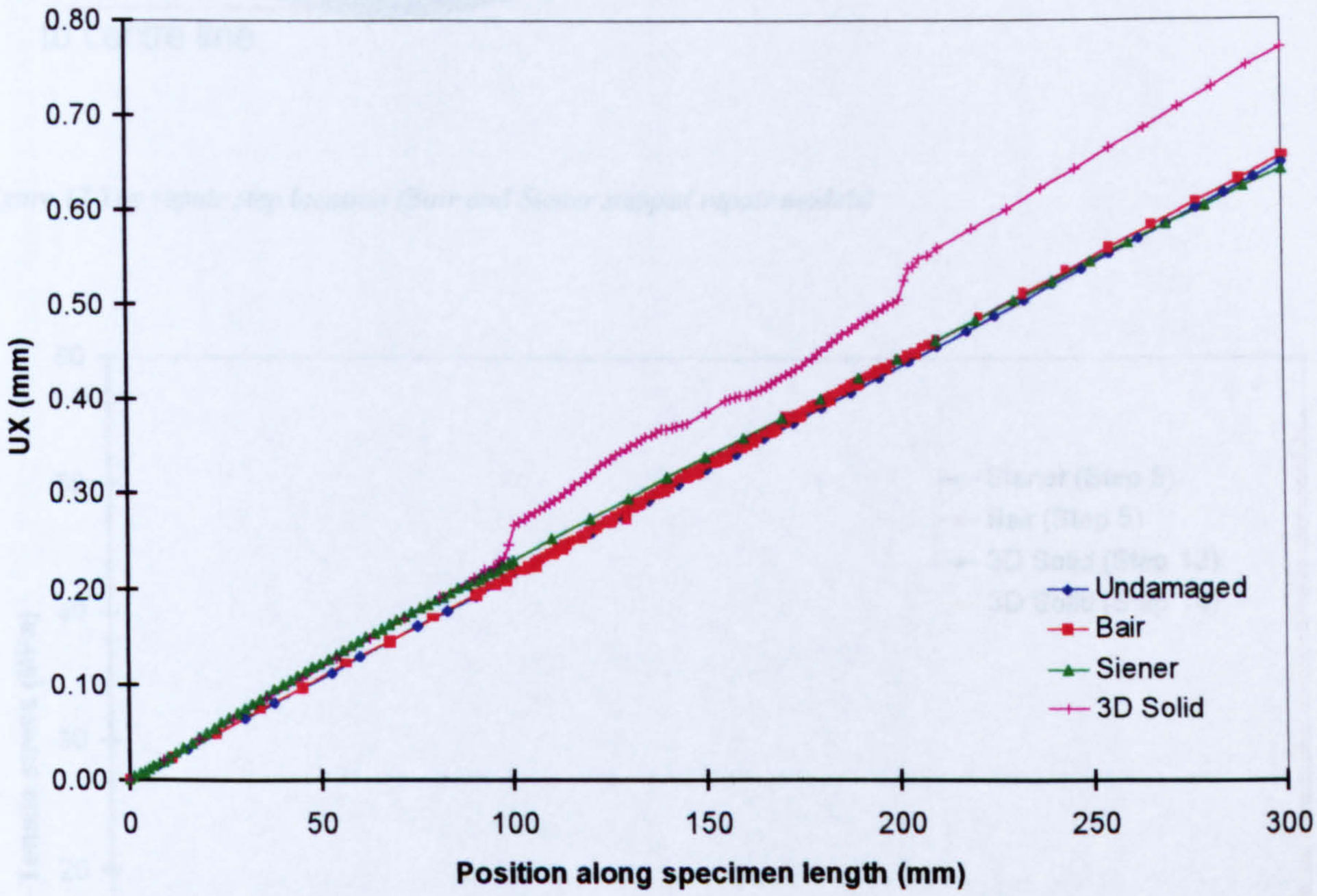

Figure 16 Longitudinal displacement

Figure 16 compares the displacements along the plate centre line, predicted by the models for both undamaged and repaired states. The reference (undamaged) displacement shows good agreement between the models. However the mesh used for the Bair and 3D models was finer. Figure 16 also confirms that the repairs were effective as far as matching the undamaged plate displacement was concerned for the Siener and Bair models. The presence of the repair patch in the 3D model is more apparent. The discontinuities in this displacement curve are located where the patch begins and ends. The curve shows the nodal displacement on the top surface of the plates and the shifts in the curve are due to the presence of adhesive at the edge of the repair patch which is much more compliant that the adherends.

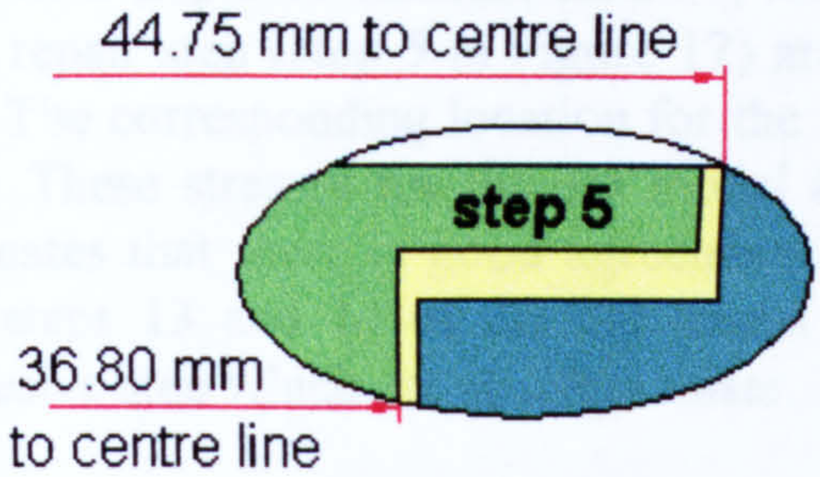

Figure 17 Top repair step location (Bair and Siener stepped repair models)

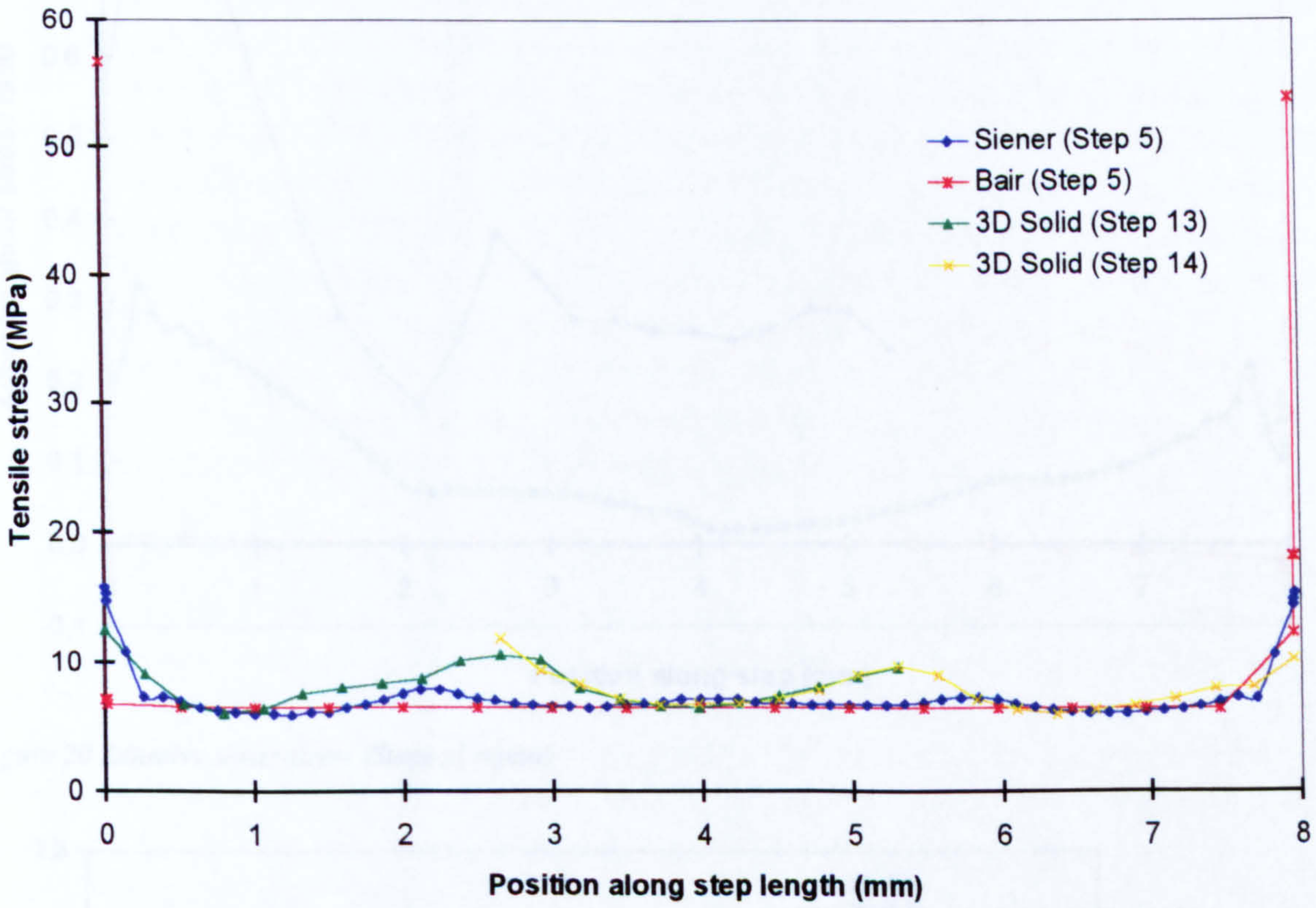

Figure 18 Adhesive tensile stress

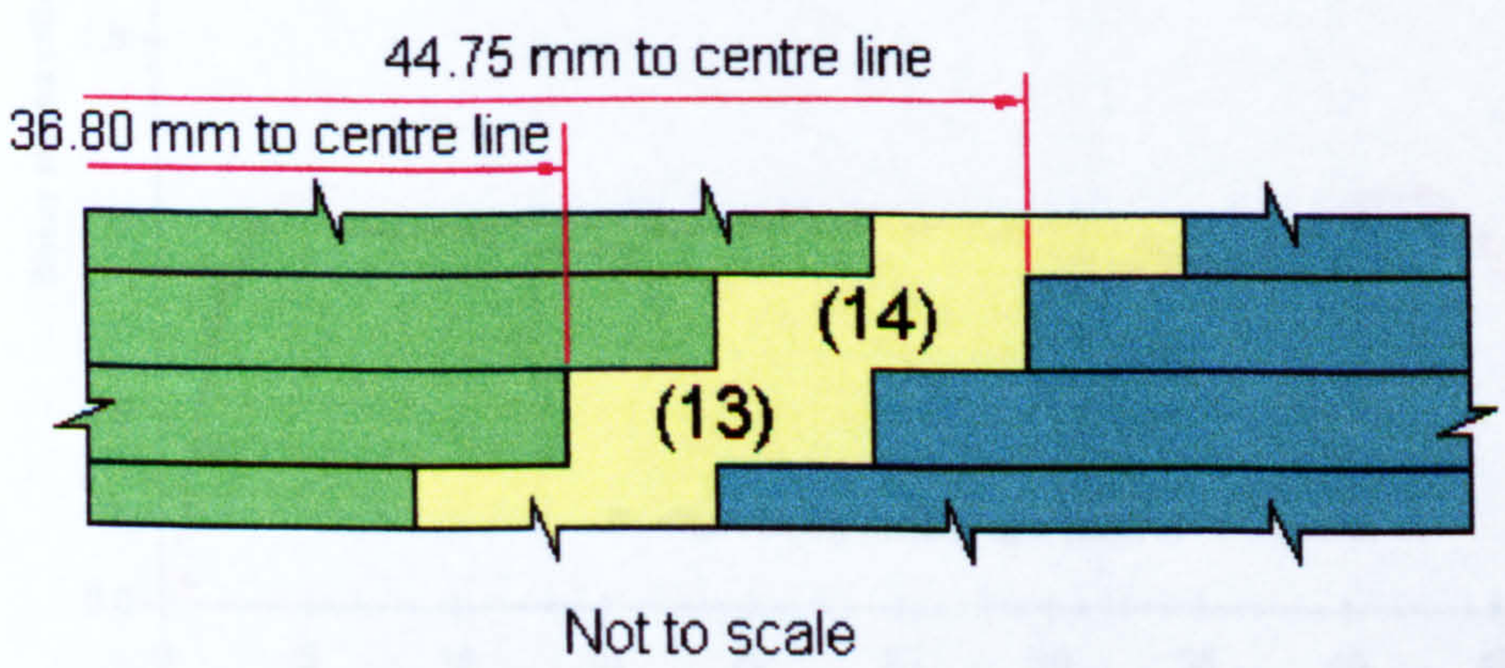

Figure 19 Step 13 and 14 (3D model)

The next step is to consider adhesive tensile stress. The adhesive tensile stresses for the top repair step (step 5 in Figure 17) are plotted for Siener and Bair models in Figure 18. The corresponding location for the 3D model is shown in Figure 19 (steps 13 and 14). These stresses for the 3D model are added to the plot in Figure 18. Figure 18 indicates that there is good agreement between all three models; the peaks observed for steps 13 and 14 of the 3D model were due to the end of the ply above each adhesive step which act as stress raiser.

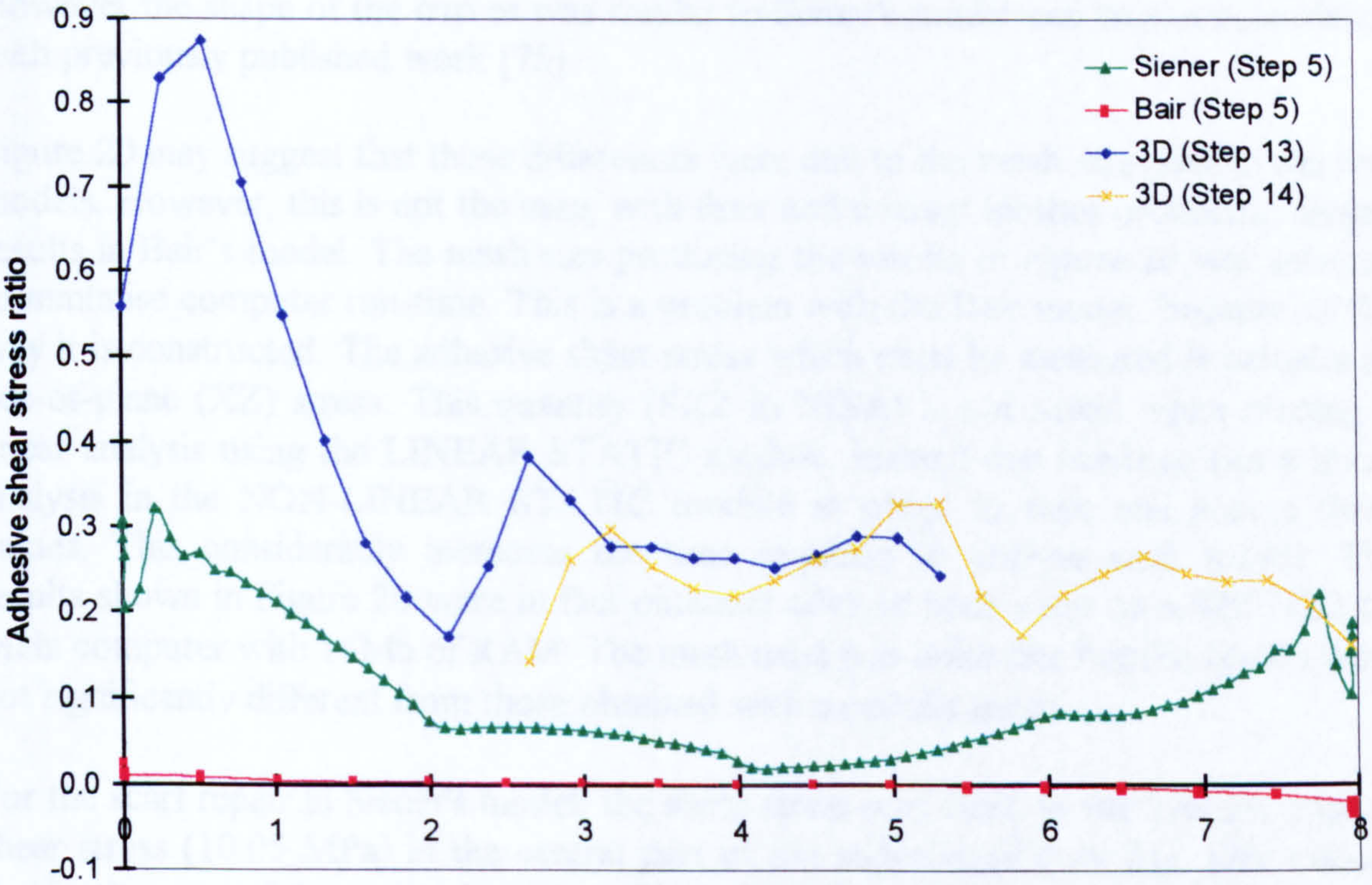

Figure 20 Adhesive shear stress (Stepped repair)

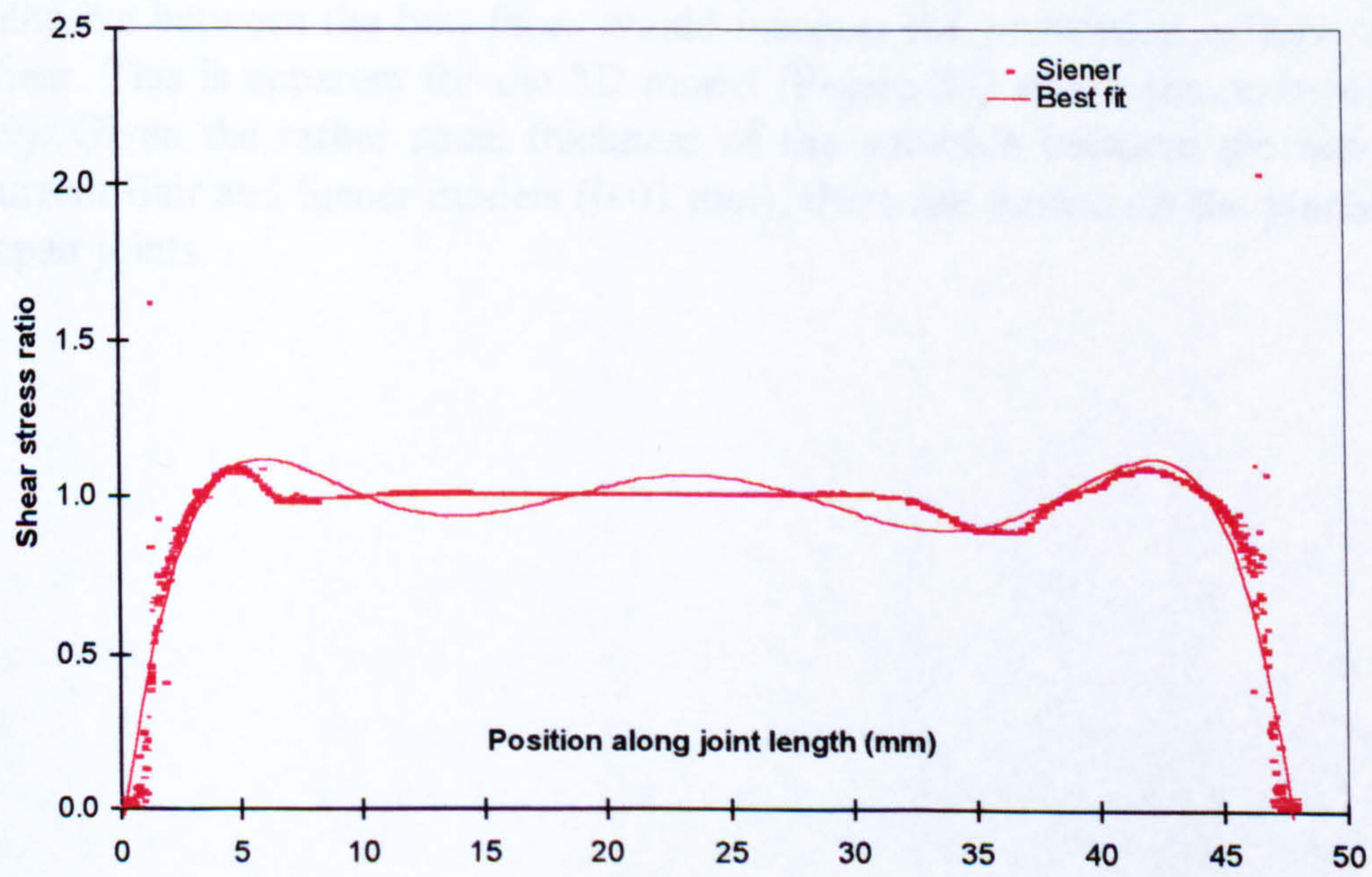

Figure 21 Adhesive shear stress (Scarf repair)

The final comparison parameter, the adhesive shear stress, is shown in Figure 20 and Figure 21 for different repair schemes using the three approaches. This stage of the comparison highlights some interesting results. Figure 20 shows the adhesive shear stress ratio plotted for the same steps as in Figure 18. This ratio expresses the adhesive shear stress as a fraction of the averaged applied shear stress which is 8.37 MPa for the stepped repair used in the Bair and Siener models and 8.38 MPa for the 3D model. The values obtained from Bair's model were very small compared to Siener's and the shape of the curve was completely different from that expected. For the 3D model, the shear stress was higher with larger maximum values because the step length was shorter. However the shape of the curves was similar to Siener's model and was in accordance with previously published work [75].

Figure 20 may suggest that these differences were due to the mesh size used in the two models. However, this is not the case, with finer and coarser meshes producing similar results in Bair's model. The mesh size producing the results in Figure 20 was selected to minimise computer run-time. This is a problem with the Bair model because of the way it is constructed. The adhesive shear stress which must be measured is actually an out-of-plane (XZ) stress. This quantity (SXZ in NISA) is not saved when running a linear analysis using the LINEAR STATIC module. Instead one needs to run a linear analysis in the NON-LINEAR STATIC module in order to save and access these values. This considerably increases the time required to analyse each model. The results shown in Figure 20 were in fact obtained after an hour's run on a 486 DX2 66 MHz computer with 16Mb of RAM. The mesh used was quite fine but the results were not significantly different from those obtained with a coarser mesh.

For the scarf repair in Siener's model, the shear stress was close to the average applied shear stress (10.05 MPa) in the central part of the adhesive (Figure 21). One notices that in the case of the stepped repairs (Figure 20), the maximum value of shear stress ratio was approximately 0.4 i.e. less than half the average applied stress. This is because in that stepped repair a large proportion of the load was transferred by the adhesive between the butt faces rather than by shear. Increasing the thickness of the adhesive between the butt faces would increase the proportion of load transferred by shear. This is apparent for the 3D model (Figure 20) which has no butt faces (Figure 19). Given the rather small thickness of the adhesive between the butt faces in the current Bair and Siener models (0.01 mm), there are doubts on the practicality of such repair joints.

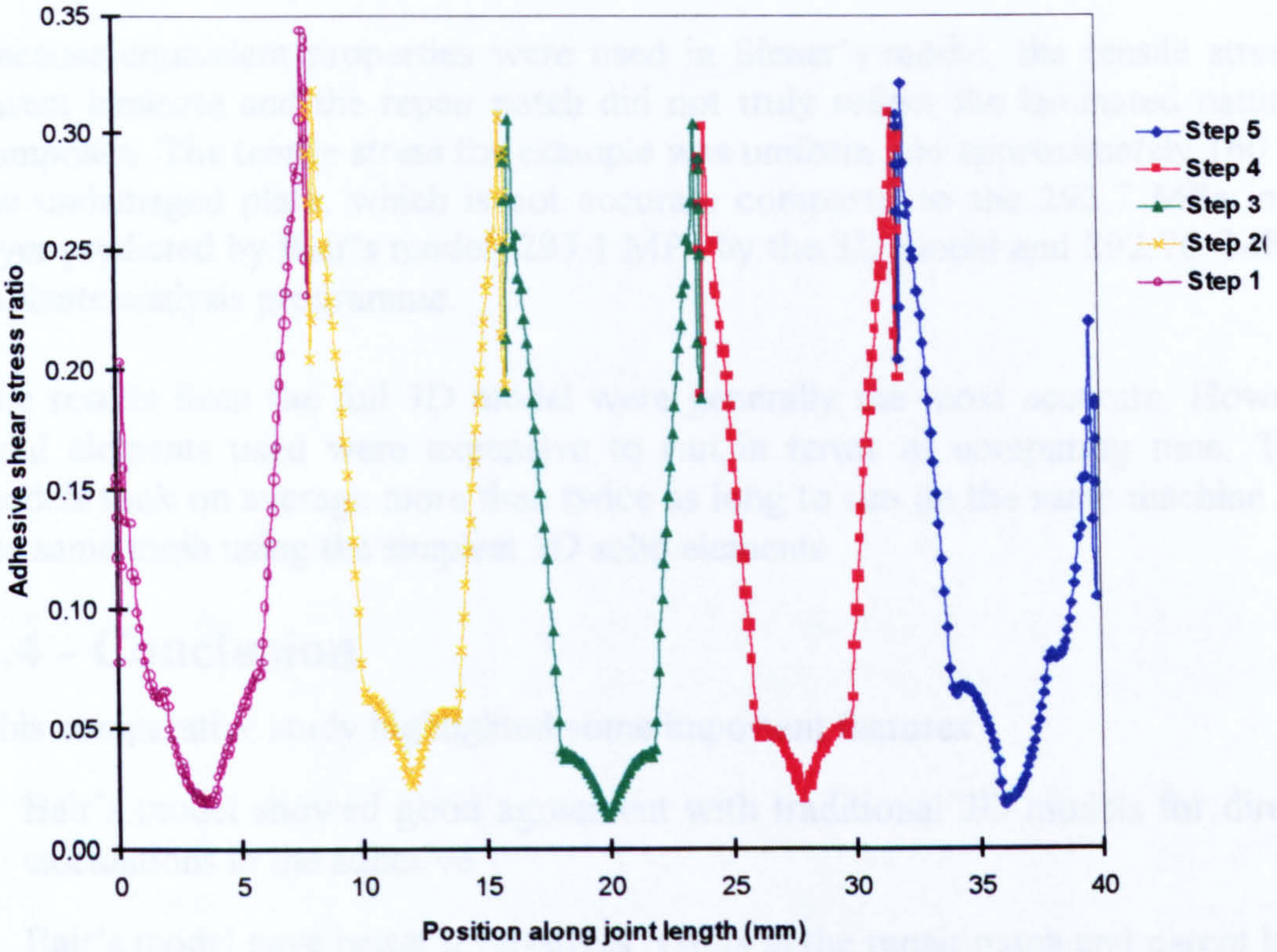

Figure 22 Adhesive shear stress ratio (Stepped repair - Siener)

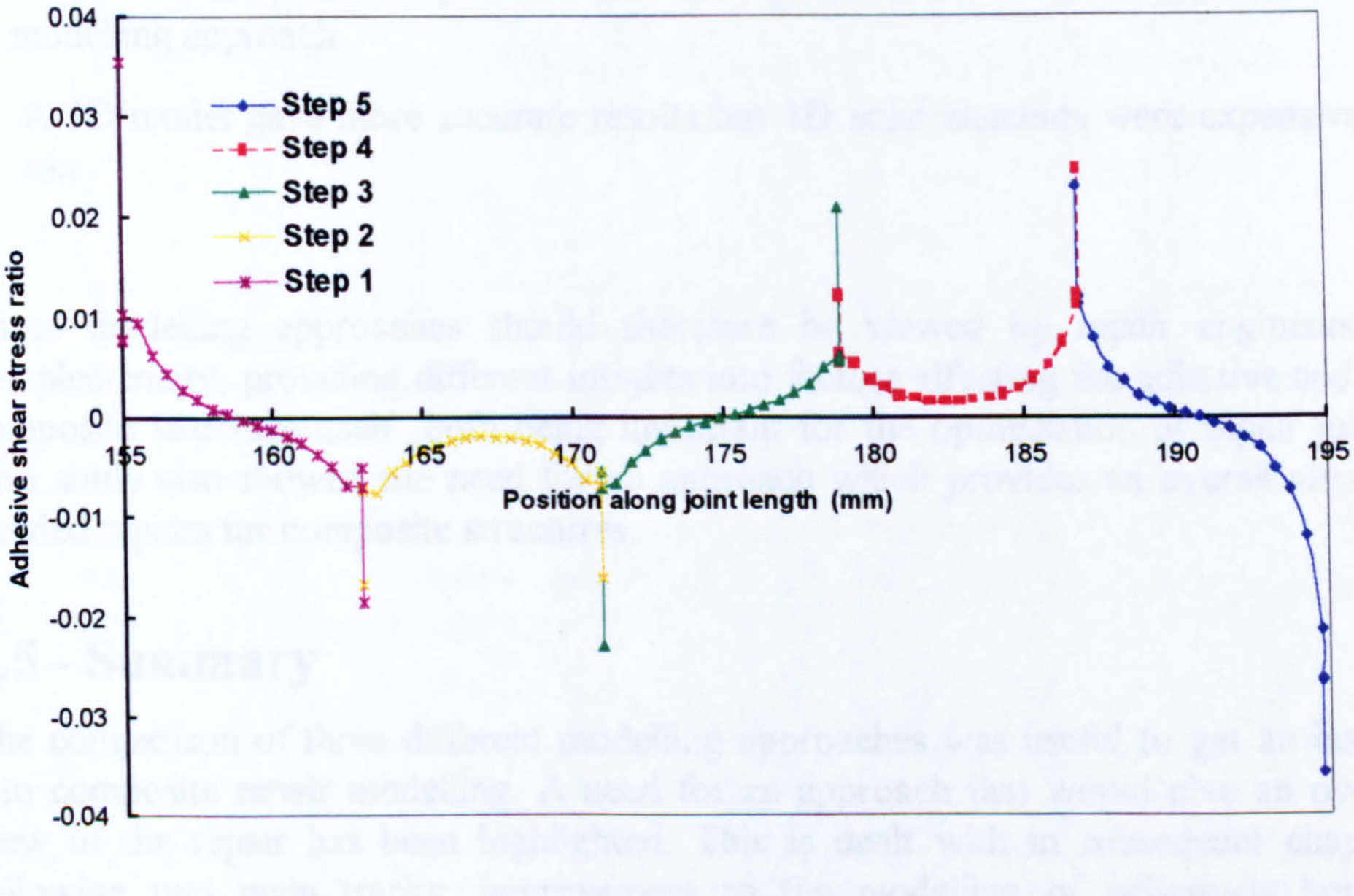

Figure 23 Adhesive shear stress (Stepped repair - Bair)

Figure 22 shows the adhesive shear stress ratio on each step calculated using Siener's model. This stress profile is that expected from previously published work. In contrast, the shear stress distribution in Figure 23 for Bair's model showed a significant departure from both the results from the Siener model and previously published work [21, 57]

Because equivalent properties were used in Siener's model, the tensile stress in the parent laminate and the repair patch did not truly reflect the laminated nature of the composite. The tensile stress for example was uniform and approximately 160 MPa for the undamaged plate, which is not accurate compared to the 292.7 MPa in the top layer predicted by Bair's model, 293.1 MPa by the 3D model and 292.76 MPa by the laminate analysis programme.

The results from the full 3D model were generally the most accurate. However, the solid elements used were expensive to run in terms of computing time. The same models took on average more than twice as long to run on the same machine and with the same mesh using the simplest 3D solid elements.

2.4 - Conclusion

This comparative study highlighted some important features:

- Bair's model showed good agreement with traditional 2D models for direct stress calculations in the adhesive
- Bair's model gave better layer-stress results in the repair patch and parent laminates
- Bair's model produced less reliable results for adhesive shear stresses. These were best obtained using Siener's approach
- Siener's model produced poorer values for layer stresses. This was inherent in this modelling approach
- A 3D model gave more accurate results but 3D solid elements were expensive to run

These modelling approaches should therefore be viewed by repair engineers as complementary, providing different insights into factors affecting the adhesive and the composite structure itself both being important for the optimisation of repair joints. This study also showed the need for an approach which provides an overall view of bonded repairs for composite structures.

2.5 - Summary

The comparison of three different modelling approaches was useful to get an insight into composite repair modelling. A need for an approach that would give an overall view of the repair has been highlighted. This is dealt with in subsequent chapters following two main tracks: improvement to the modelling of adhesively bonded composite repairs and its application to actual repairs for validation purposes.

Chapter 3

Improved Modelling Approaches

Comparative Study

3.0 - Introduction

The improvement of the modelling approach for bonded repairs presented in this thesis follows two directions. The first one seeks to improve the modelling of external repairs and the second one deals with flush scarf repairs.

Two new modelling approaches are proposed which cater for all repairs. The first one uses 3D solid elements to represent accurately the adhesive layer whilst retaining the 3D composite shell element for composite adherend modelling. In the second approach, 3D composite solid elements replace the composite shell elements used in the first approach for the composite adherends.

In this chapter, the new approaches were compared to the more traditional approach of Soutis and Hu [107] who used 3D solid elements with equivalent orthotropic properties. This comparative study was carried out for an external bonded patch repair to a composite plate. This repair type was chosen because both new approaches are suitable for external bonded patch repairs. For flush repairs, only the second approach can be used.

3.1 - Improved Modelling of Bonded Composite Repairs

From the studies in Chapter 2, a need was identified for an approach which would enable the study of both adhesive and composite adherends within a single model. This need spearheaded the development of improved models for bonded repairs. When one considers the analysis of an adhesive bonded composite repair system, there are three key areas where improvements can be effected: modelling components, adhesive material models and failure theories.

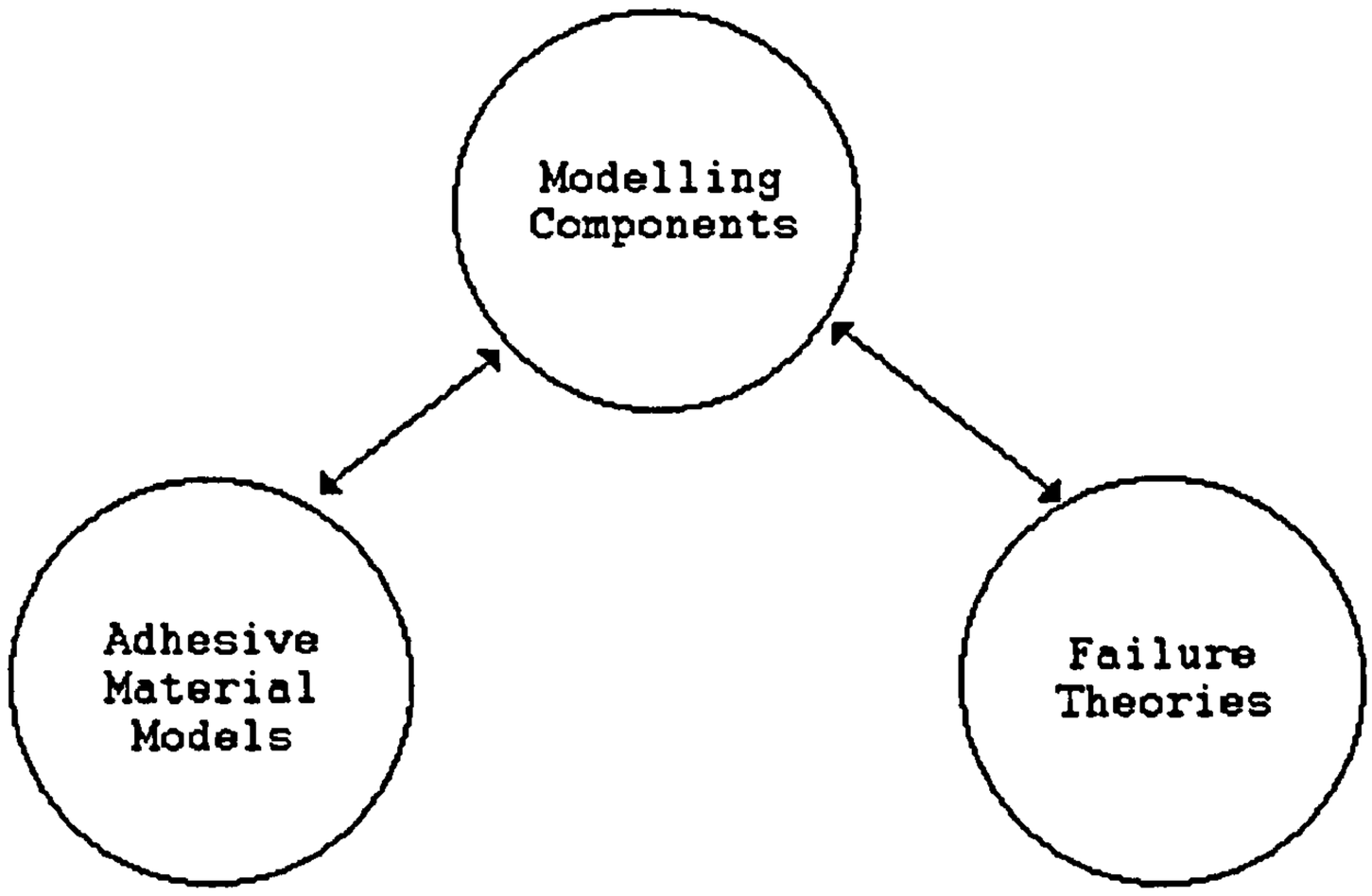

Figure 24 Key areas for improved modelling approaches

These key areas are represented schematically in Figure 24 where the arrows indicate that changes in some of these areas are inter-dependent. For example, a new realistic adhesive material model may require the formulation of a finite element more adapted to the task. This was done by Jones *et al.* [106].

Improvement in the first key area implies a systematic look at the type of elements which are used and what benefit can be gained by switching to other element types. The second area deals with the type of adhesive material model used, especially for non-linear analysis. Improvement can be obtained from using material models which simulate more accurately the behaviour of adhesives (e.g. the use of an appropriate yield criterion such as that proposed by Rhagava and co-workers [100]). Finally improvement can be brought about by better failure theories for composite adherends and for adhesives.

Any investigation to improve these key areas needs to be underpinned by a sound design philosophy. Hart-Smith's design philosophy for adhesive bonded joints states that any such joint should be designed in such a way that the adhesive must never be allowed to become the weak link [82].

In their quest for an appropriate adhesive failure criterion for bonded joints, researchers have tended to produce joints where the adhesive layer was the critical link in order to assess their proposed criterion against experimental results [110, 87]. However, for bonded repairs, the emphasis must be shifted towards a design philosophy which is closer to that advocated by Hart-Smith for bonded joints. No repair scheme must have adhesive layers failing before either the repair patch or the

parent laminate. That design philosophy was identified as a key aspect in seeking to improve the modelling and analysis of bonded repairs to composite structures.

If failure was to occur elsewhere in the repaired structures than in the adhesive layers, it was important for the new models to be able to predict layer stresses and strains, given the laminated nature of the composite adherends. This consideration was implemented by using available elements which could provide layer stresses and strains. That dealt with the first key area where it was concluded that the improved models needed to use either the 3D laminated shell elements or the 3D laminated solid elements to model the composite adherends.

The second key improvement is concerned with the third area. Failure criteria specific to composite materials need to be applied in the prediction of repaired structures failure load and modes. The main criteria considered are the Tsai-Wu interactive and the maximum stress criteria because they are the best ones implemented in NISA. For the adhesive, the failure criterion needs to be a simple but effective way of determining the adhesive failure loads with respect to that of the composite adherends.

The improvements are the only ones which can be envisaged within the context of the FE code selected for the project. Improvement in the third area are concerned with failure prediction of the repairs. Since a better understanding of the new modelling approaches was sought primarily in this chapter, failure prediction issues are addressed in the following chapter.

3.2 - Modelling Data

The work was based on the information published by Soutis and Hu [107] on the design and performance of bonded patch repairs to composite structures. In their study, a 2D analytical model of a double lap joint was used to investigate various joint parameters such as overlap length, patch thickness, patch shape and the influence of the adhesive. From that preliminary study, an optimum joint configuration was obtained and a 3D finite element analysis was then carried out to determine the stress levels in the patch, adhesive layer and the parent laminate. An attempt was also made to predict ultimate repair joint failure load using stress concentration factors.

The modelling data used in this study was adapted since the information provided in Soutis and Hu's paper [107] was not complete. It was therefore decided that different materials would be used but the laminate geometry would be retained. This was possible because the emphasis was on the development of new modelling approaches. The following chapter will look more closely at failure prediction and a comparison with Soutis and Hu's work will then be made.

32.1 - Geometry

3.2.1.1 - Undamaged Plate

The undamaged plate was a symmetric composite laminate. It was 100mm long by 50 mm wide with a thickness of 3 mm. The stacking sequence was $[(\pm 45/0/90)_3]_s$ which indicates a quasi-isotropic lay-up. The undamaged plate was modelled to serve as a reference for the repaired plate.

3.2.1.2 - Damaged Plate

The damaged plate had the same overall dimensions as the undamaged plate. In addition, it had a central hole. The hole diameter was 10 mm. This represented the stage when the damaged material had been identified by suitable NDI and removed. Actual damage progression was not considered.

3.2.1.3 - Repaired Plate

Two external patches with the same quasi-isotropic lay-up as the undamaged plate ($[(\pm 45/0/90)_3]_s$) were bonded to the damaged laminate to provide a loading path

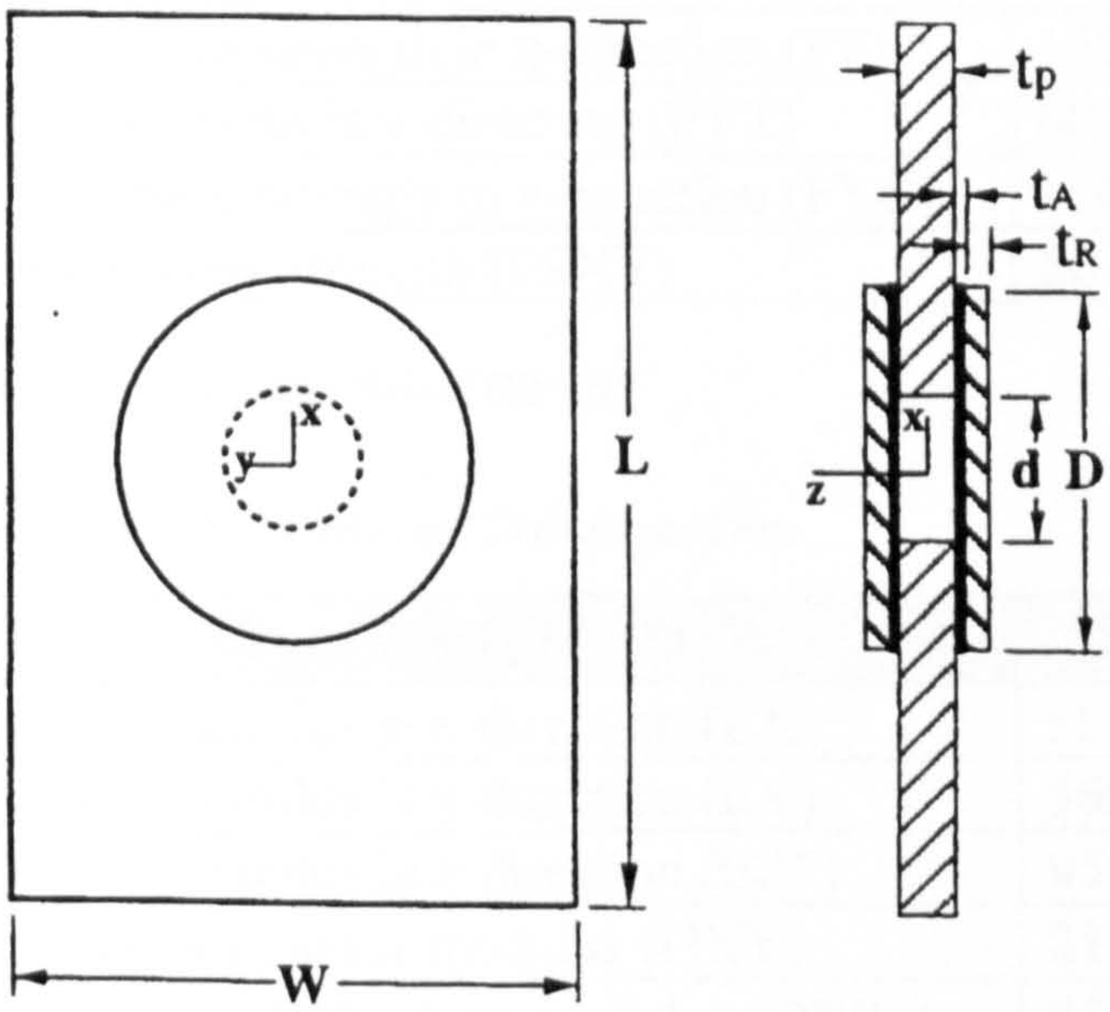

Figure 25 Repaired plate geometry [107]

around the hole. The repaired plate is shown in Figure 25. Each patch was circular with a 35 mm diameter and was 1.5 mm thick. This gave a layer thickness of 0.625 mm. The adhesive layers were 0.1 mm thick.

3.2.2 - Materials

The materials used for the models were not the same as those used by Soutis and Hu [107] because the information at the time of the work was not complete. However, the same matrix resin system was used with similar carbon fibres. A typical epoxy adhesive was selected.

3.2.2.1 - Parent Laminate

The parent laminate was made of XAS carbon fibres embedded in an epoxy resin (Ciba-Geigy 913). The laminate was symmetric and orthotropic with the same stacking sequence as the undamaged plate.

Table 9 XAS/913 UD Material Data (Source: Anaglyph, Imperial College, UK)

PROPERTY(°)	Value	Unit
Young's modulus in x-direction (EX)	144300	MPa

PROPERTY(°)	Value	Unit
Young's modulus in y-direction (EY)	11040	MPa
Young's modulus in z-direction (EZ*)	11040	MPa
In plane (XY) shear modulus (GXY)	5790	MPa
Out-of-plane (XZ) shear modulus (GXZ*)	1158	MPa
Out-of-plane (YZ) shear modulus (GYZ*)	1158	MPa
Poisson's ratio (NUXY)	0.313	
Poisson's ratio (NUXZ*)	0.175	
Poisson's ratio (NUYZ*)	0.175	
Tensile strength in x-direction (FXT)	2185	MPa
Compressive strength in x-direction (FXC)	1500	MPa
Tensile strength in y-direction (FYT)	60	MPa
Compressive strength in y-direction (FYC)	180	MPa
In-plane shear strength (FSXY)	80	MPa

* assumed

(°) nomenclature from NISA/DISPLAY

Table 10 XAS/913 Equivalent Orthotropic Data

PROPERTY(°)	Value	Unit
Young's modulus in x-direction (EX)	56506	MPa
Young's modulus in y-direction (EY)	56506	MPa
Young's modulus in z-direction (EZ*)	9553	MPa
In plane (XY) shear modulus (GXY)	21589	MPa
Out-of-plane (XZ) shear modulus (GXZ*)	4534	MPa
Out-of-plane (YZ) shear modulus (GYZ*)	4534	MPa
Poisson's ratio (NUXY)	0.3087	
Poisson's ratio (NUXZ*)	0.174	
Poisson's ratio (NUYZ*)	0.174	

* assumed

(°) nomenclature from NISA/DISPLAY

The assumed properties in Table 9 were based on approximately the same order as those given by Soutis and Hu. The data given in Table 9 was used for models which required only lamina material properties. The computer program LAP (Laminate Analysis Programme) was used with the appropriate stacking sequence and the above lamina data to generate equivalent orthotropic properties. These are given in Table 10.

3.2.2.2 - Repair Patch

The repair patch was made of the same composite material as the parent laminate with the same stacking sequence.

3.2.2.3 - Adhesive

The adhesive linear elastic properties are given in the table below. These represent typical epoxy adhesive properties.

Table 11 Epoxy Adhesive Material Data (Picket and Holloway [96])

PROPERTY	Value	Units
Young's modulus E	3000	MPa
Shear modulus, G	1103	MPa
Poisson's ratio	0.36	

3.3 - Undamaged and Damaged Plates

The undamaged and damaged plates were analysed for reference purposes. The task was straightforward. The strategy adopted and the analysis results are described in the following sections.

3.3.1 - Modelling Strategy

For the undamaged and damaged plate, the choice was down to the different types of elements available. One could use layered composite shell elements (NKTP-32), composite solid elements (NKTP-7) or 3D solid elements (NKTP-4) with equivalent orthotropic properties.

The composite shell elements (NKTP-32) are the standard elements for modelling composite structures in NISA. They are available as linear, parabolic or cubic types with various number of nodes. They are based on standard shell elements but offer layer stresses and strains as well as interlaminar shear stresses and various composite failure theories.

The 3D solid elements (NKTP-4) are the standard solid elements used to model moderately thin to thick structures. They are available as first or second order elements. They are capable of modelling orthotropic materials. Hence equivalent orthotropic properties must be used with them. No layer stresses or strains are available.

The 3D composite solid elements (NKTP-7) are derived from the 3D solid elements. They offer in addition all layer stresses but do not provide interlaminar stresses.

3.3.1.1 - Undamaged Plate Model

From the comparative study in Chapter 2 and given the simplicity of the undamaged plate, the reference model was constructed using 3D composite solid elements (NKTP-7). Several lamination sequence tables (LAMSEQ tables used in NISA to define the material, thickness and fibre angle of each element) were investigated to identify the effects on the layer stress results. Another model using 3D solid elements (NKTP-4) was done to compare the displacements and various stresses. Various boundary conditions were explored to simulate a compression test on a composite plate using different axes of symmetry. It was concluded that modelling one quarter of the plate with the appropriate symmetrical boundary conditions was sufficient. Strictly speaking, the results were numerically correct but not analytically due to the presence of $\pm 45^{\circ}$ fibres. An undamaged model was also constructed using LAP and the results cross-

checked with those from NISA. The plate was subjected to a compressive pressure loading of 350 MPa.

3.3.1.2 - Damaged Plate Model

Two models were constructed for the damaged plate: one using 3D composite solid elements (NKTP-7) and the other using 3D solid elements (NKTP-4) with orthotropic properties. The mesh density in both cases was exactly the same. For both cases, half the plate was modelled using symmetry about the transverse axis (i.e. perpendicular to the 0° fibre direction). The plate was subjected to a compressive pressure loading of 350 MPa.

Modelling the damaged plate using solid composite elements presented specific problems regarding the definition of the fibres orientation within the laminate in the vicinity of the hole. This was due to the fact that in NISA, the element's first edge (defined by the line connecting the first two nodes) is used to determine the local axes with respect to which the fibre orientation is defined. As the elements were positioned around the hole, the position of their first edge with respect to the global co-ordinates system was not constant. The main result was that a lamination sequence table had to be defined for every single element around the hole.

As this was not practical, a certain degree of approximation had to be applied by defining element lamination tables by angular sector. This made the model very tedious to define. Furthermore, if a finer mesh was required one had to create new tables for the new elements.

3.3.2 - Results and Discussion

A finite element analysis always generates a wealth of data. The most demanding task is to examine and interpret those data. This task can only be performed efficiently when the relevant quantities have been identified. Each problem will have a particular set of relevant data. Longitudinal displacement and stresses are the relevant quantities for the undamaged and damaged models.

3.3.2.1 - Undamaged Plate

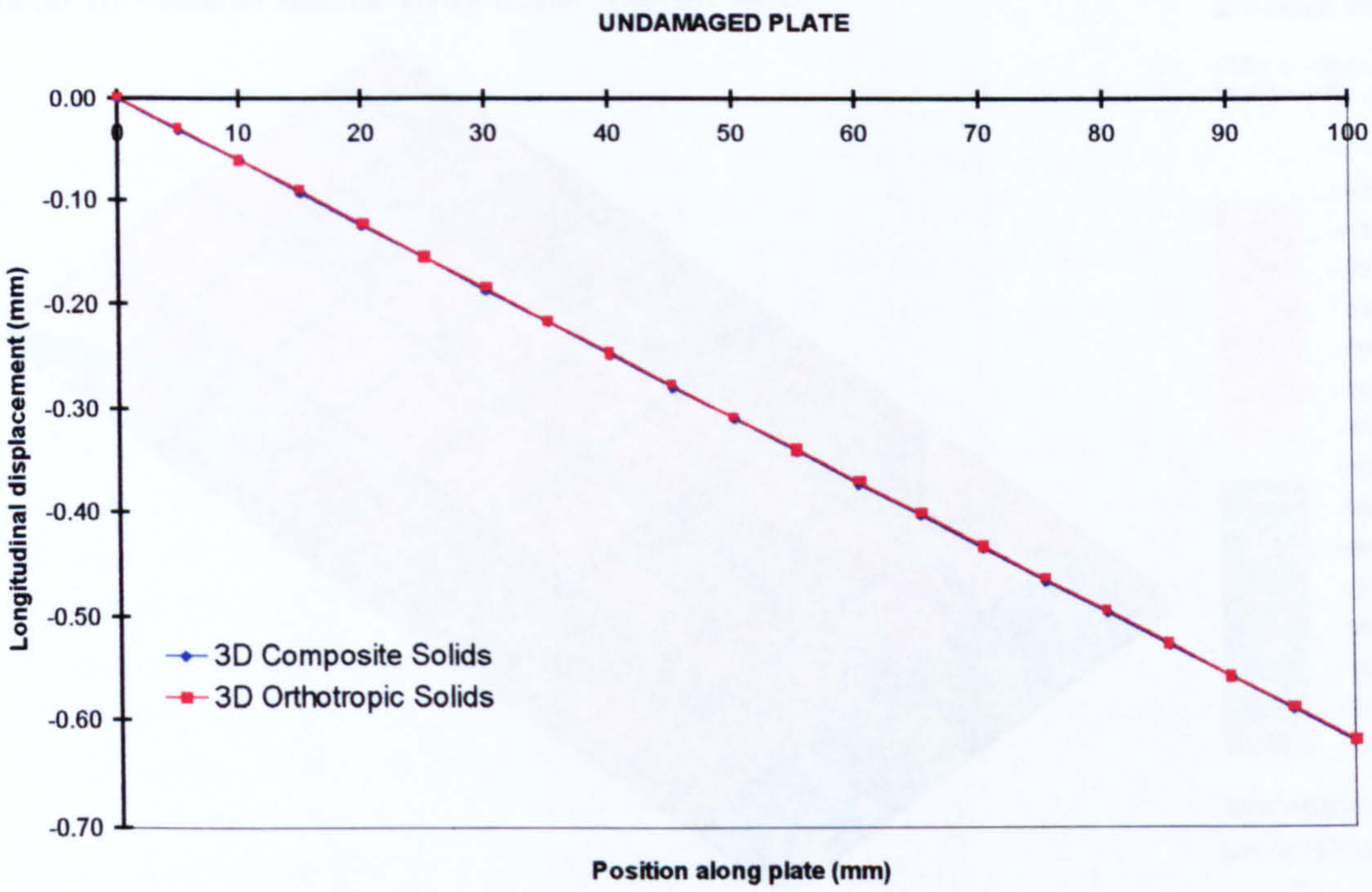

Figure 26 Longitudinal displacement (Undamaged Plate)

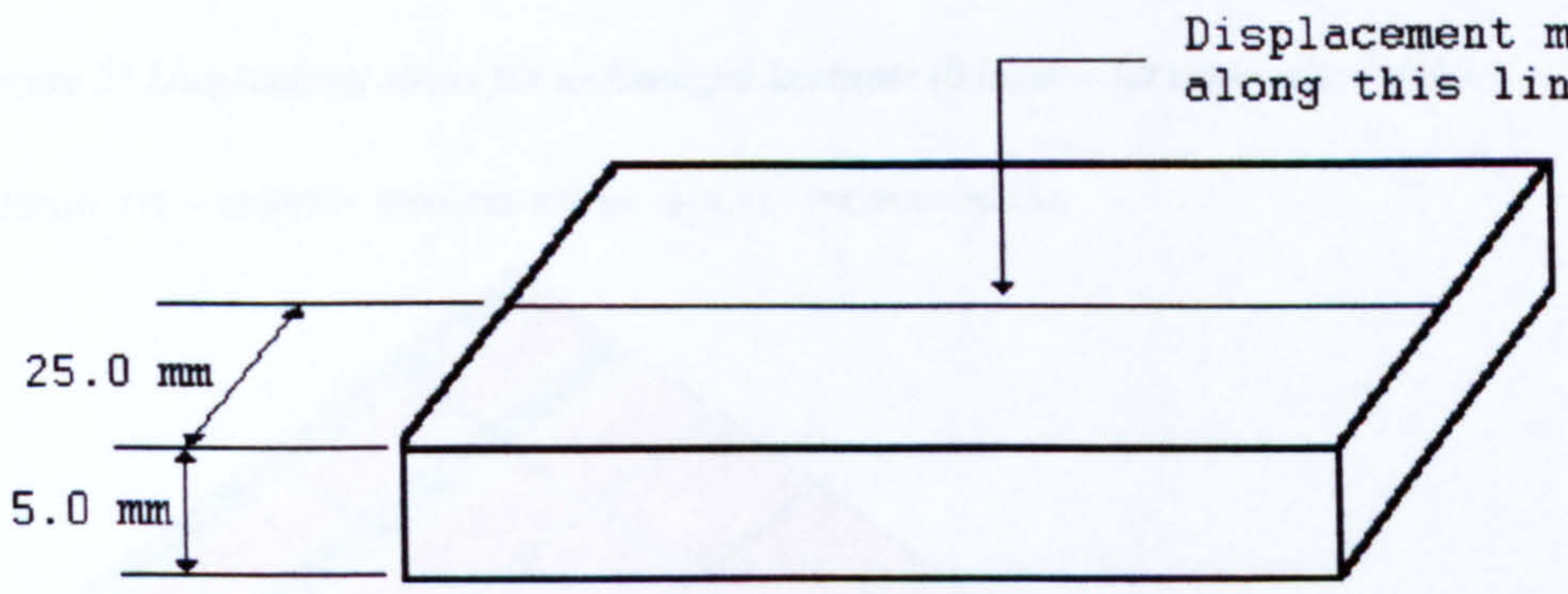

Figure 27 Nodal location for longitudinal displacement curves

Figure 26 shows clearly that using either 3D orthotropic or composite solid elements makes no difference in the predicted longitudinal displacements. The location of the nodes where the displacements are measured is shown in Figure 27.

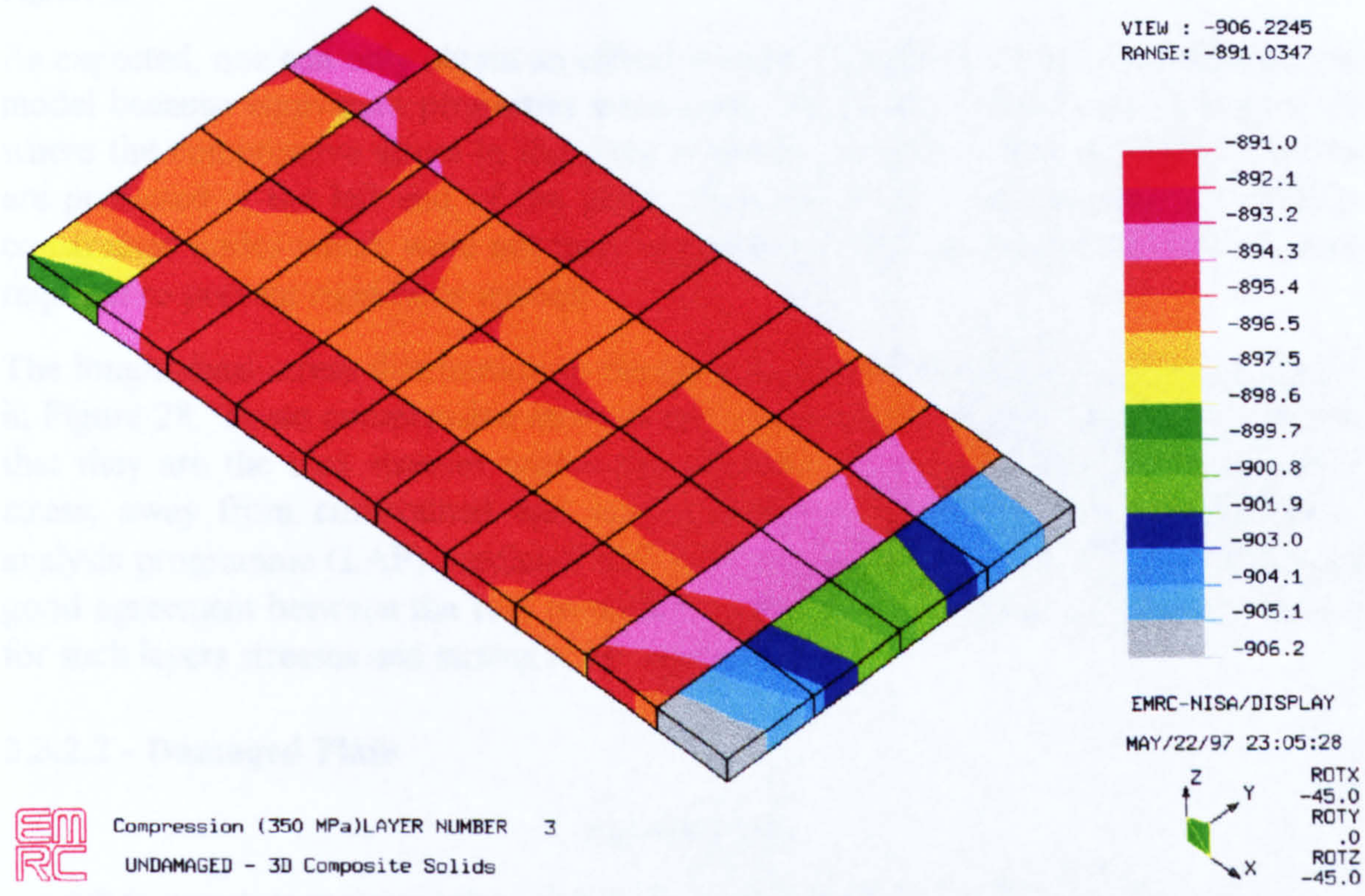

Figure 28 Longitudinal stress for undamaged laminate (0 layer - 3D composite Solids)

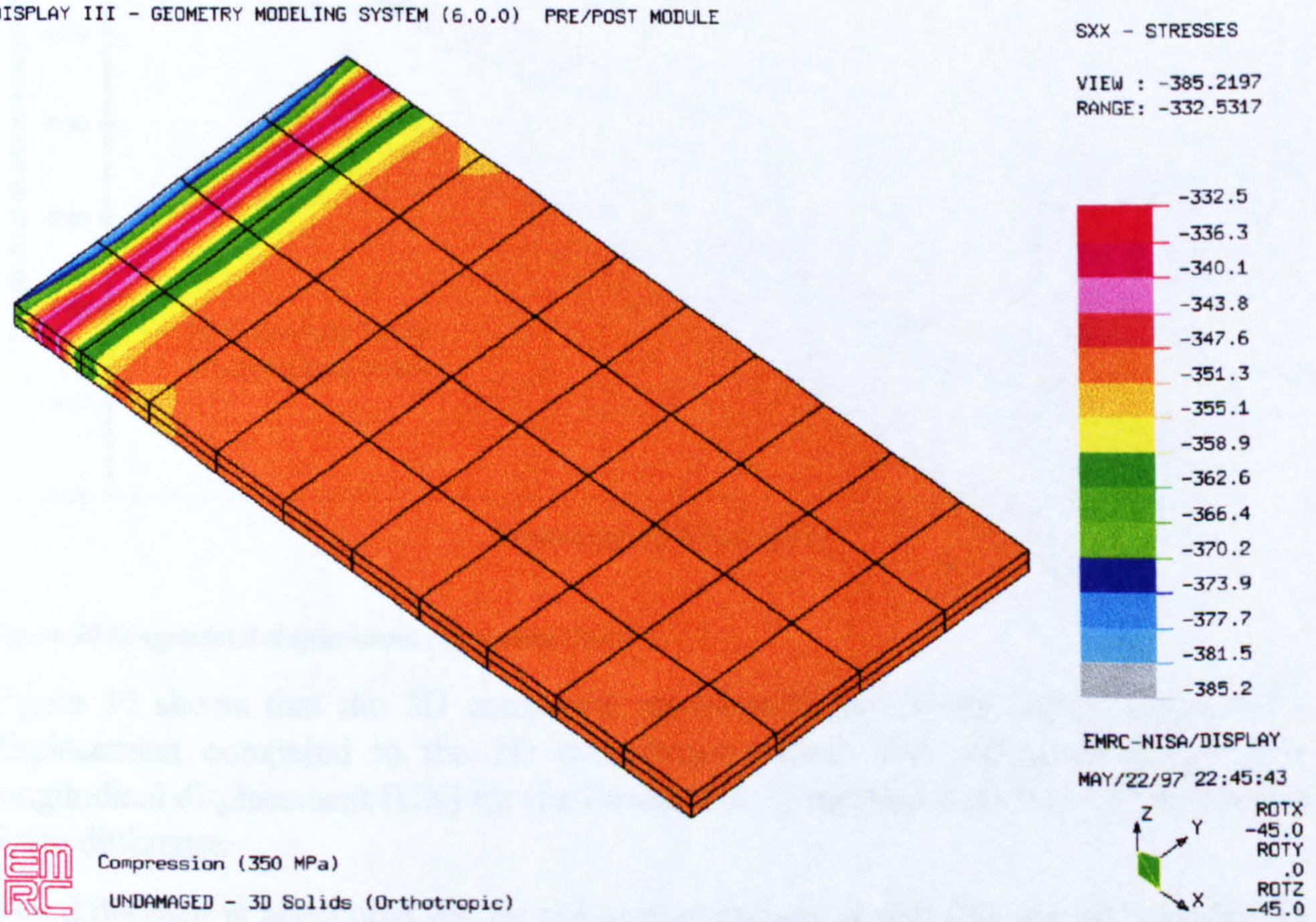

Figure 29 Longitudinal stress contours for undamaged laminate (3D Orthotropic Solids)

The main difference between the two undamaged plate models was their ability to predict layer stresses. The longitudinal stresses in the plate are shown in Figure 28 and Figure 29.

As expected, one can only obtain an effective stress distribution for the 3D orthotropic model because equivalent properties were used. This can be seen easily in Figure 29 where the compressive stress in the plate is about 351 MPa. Slightly higher stresses are predicted at the left end of the plate. This was due to the influence of the fully constrained nodes which were not truly representative of a compression test but were required to prevent rigid body motion.

The longitudinal stress distribution in the third layer (which had fibres at 0°) is shown in Figure 28. These compressive stresses are unaveraged nodal stresses, which means that they are the true stresses within the elements. The mean value of compressive stress, away from constrained and loaded nodes, was 896.5 MPa. The laminate analysis programme (LAP) predicted 893.9 MPa for each 0° layer. Thus there is very good agreement between the two predicted values. The 3D composite model allowed for such layers stresses and strains to be calculated.

3.3.2.2 - Damaged Plate

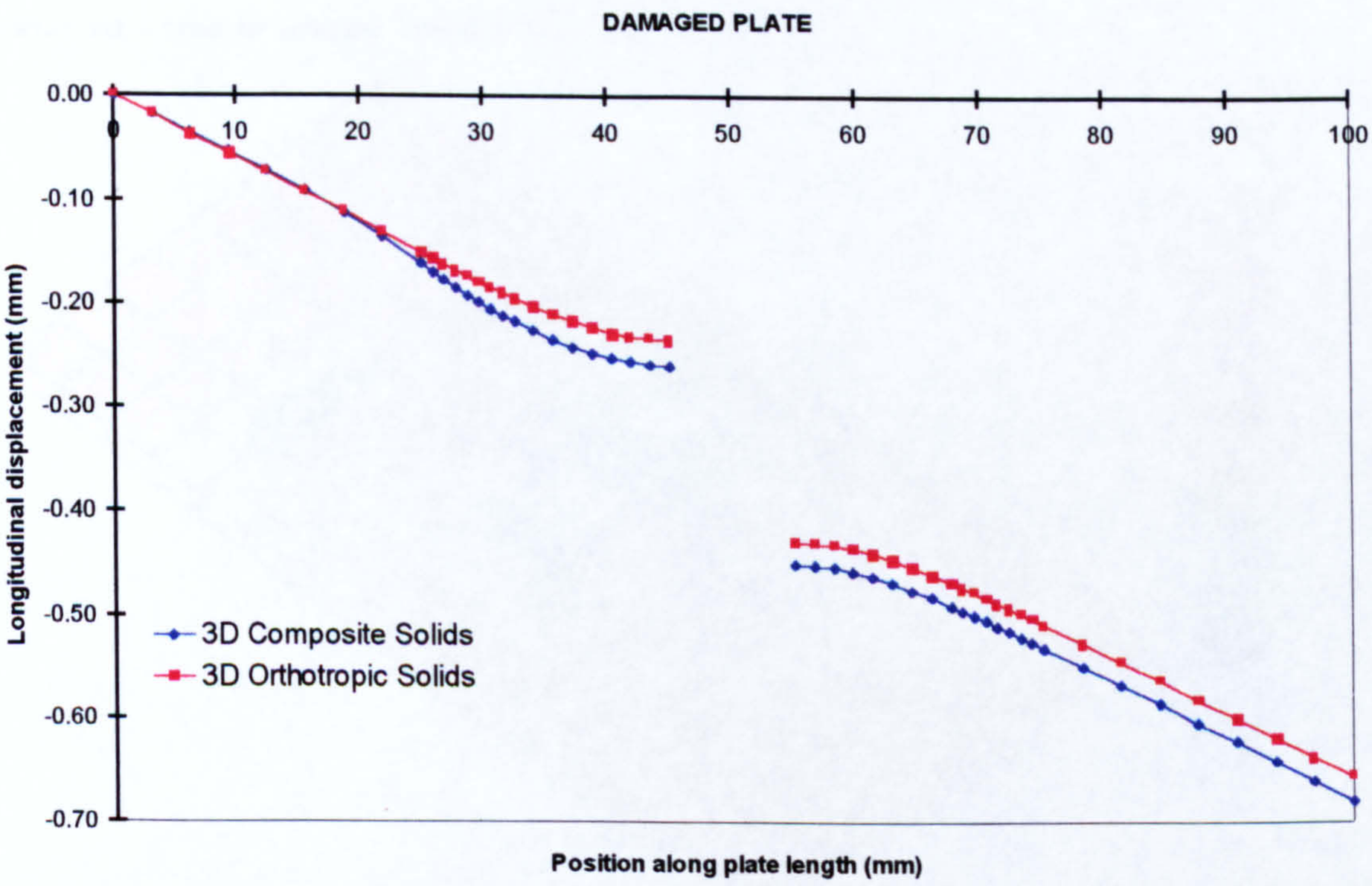

Figure 30 Longitudinal displacement (Damaged Plate)

Figure 30 shows that the 3D composite model predicts slightly higher compressive displacement compared to the 3D orthotropic model. The maximum compressive longitudinal displacement (UX) for the former is 0.71 mm and 0.66 mm for the latter, a 7.6% difference.

The difference is accounted for by the approximation in defining the fibre angles for some elements around the plate hole, as explained on page 51.

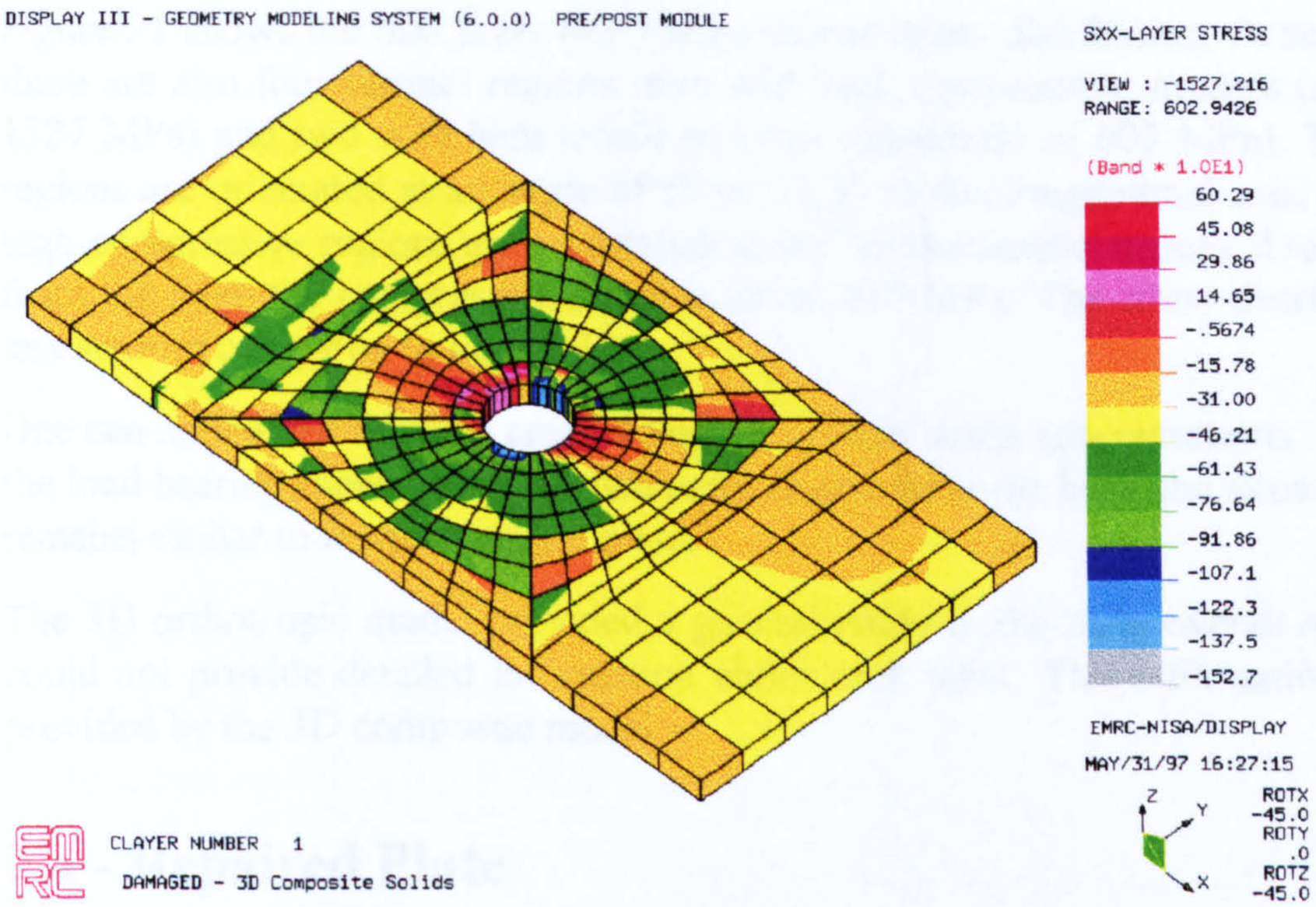

Figure 31 Longitudinal stress for 45° layer (Damaged plate - 3D Composite Model)

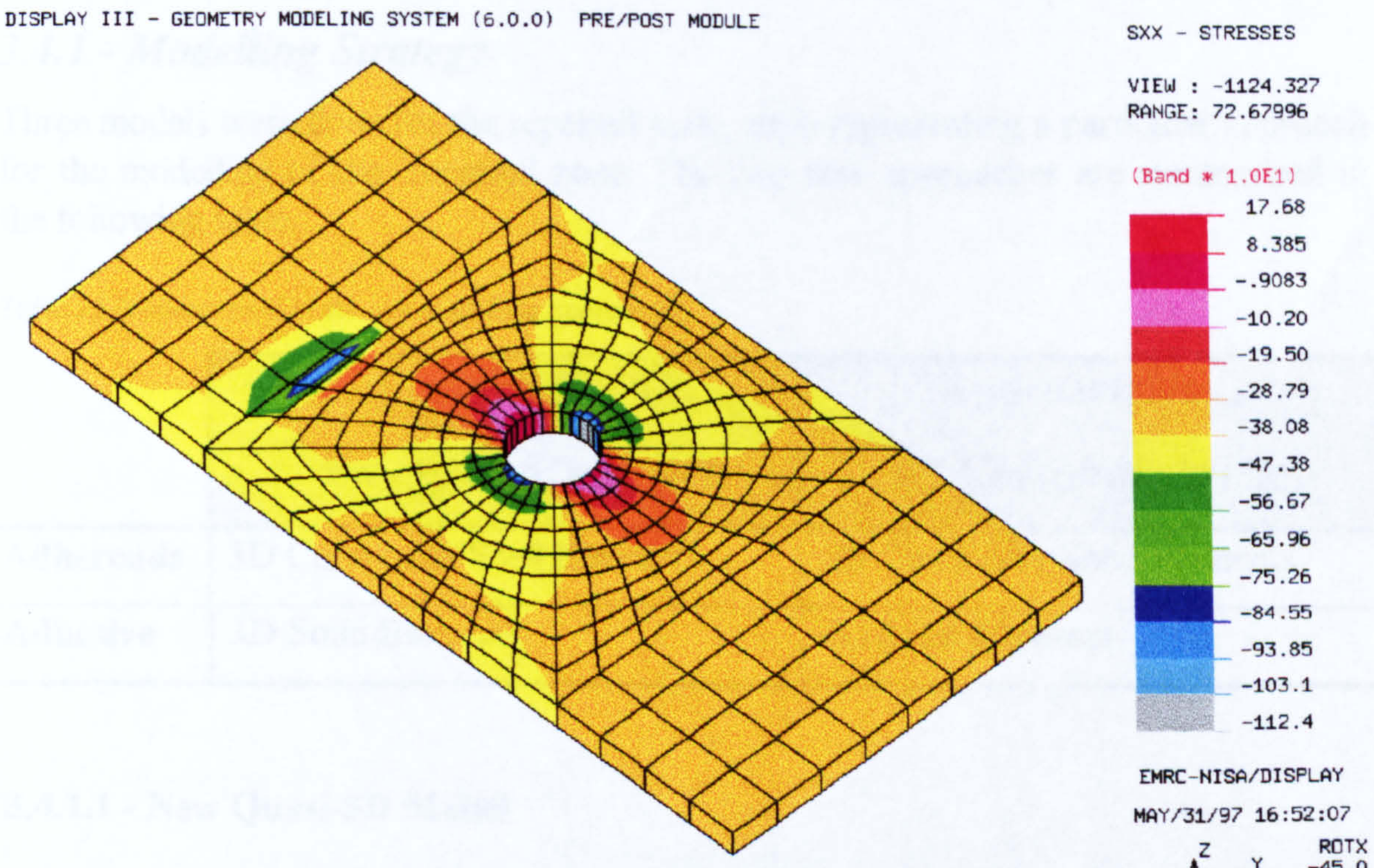

Figure 32 Longitudinal stress (Damaged plate - 3D Orthotropic Model)

The difference in the two models is further highlighted by the longitudinal stress contour plots shown in Figure 31 and Figure 32. For the 3D Orthotropic model (Figure 32), the plot shows two regions of high compressive stresses located around the hole, in the transverse direction. There are two other regions with tensile stresses along the loading axis with a maximum stress of 72.7 MPa. Away from the hole, the stresses are compressive and around 380 MPa.

Figure 31 shows the first layer (45°) longitudinal stress distribution. Around the hole, there are also four distinct regions: two with high compressive stresses (maximum of 1527 MPa) and two with high tensile stresses (maximum of 603 MPa). These tensile regions are orientated at an angle of about 22.5° to the longitudinal axis, whereas the high compressive regions are orientated at 90° to the tensile regions direction. Away from the hole, the compressive stress is about 310 MPa. The stress distribution is far less smooth compared to Figure 32.

One can notice that the hole creates regions of high stress concentrations. This reduces the load bearing capability of the laminate. Away, from the hole, the stress distribution remains similar to the undamaged plate.

The 3D orthotropic model provided a general guide to the plate overall response but could not provide detailed information about each layer. This information was easily provided by the 3D composite model.

3.4 - Repaired Plate

The modelling strategy adopted for the repaired plate and the analysis results are presented in the following sections.

3.4.1 - Modelling Strategy

Three models were done for the repaired plate, each representing a particular approach for the modelling of the repaired zone. The two new approaches are summarised in the following table.

Table 12 Elements used in the new modelling approaches

	Approach No. 1 New Quasi-3D Model	**Approach No. 2 3D Composite Model**
Adherends	3D Composite Shell Elements	3D Composite Solid Elements
Adhesive	3D Solid Elements	3D Solid Elements

3.4.1.1 - New Quasi-3D Model

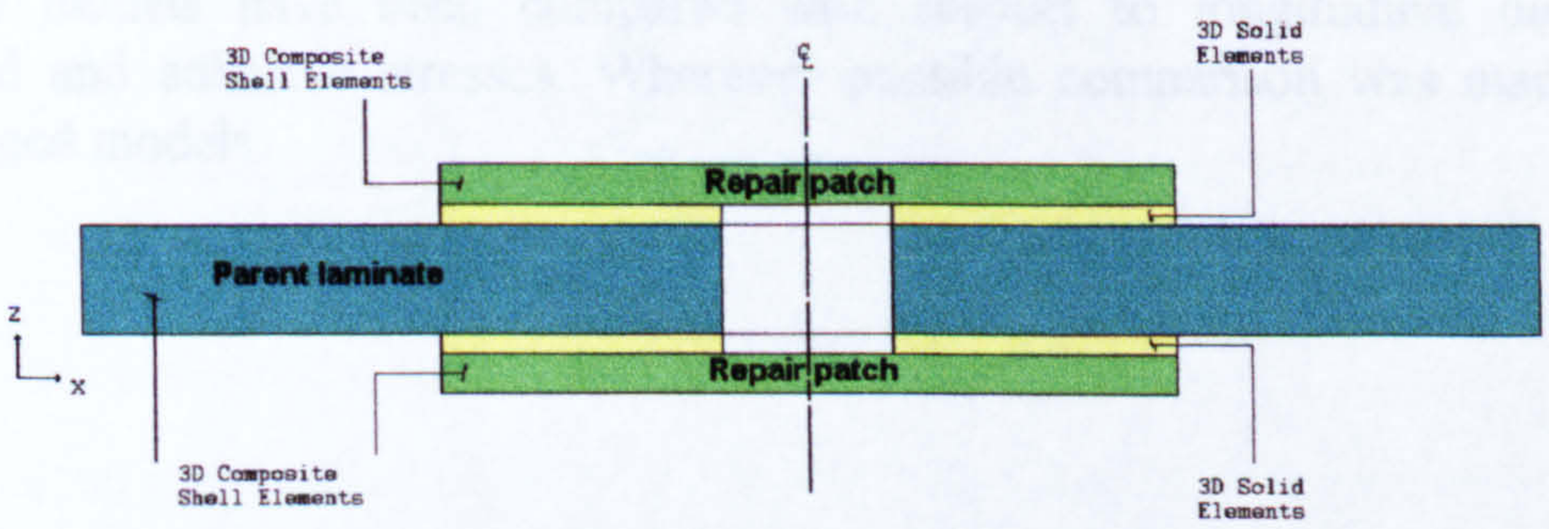

Figure 33 New Quasi-3D Model

This model mixed composite shell elements with 3D solid elements. The composite shell elements were used for the parent laminate and the repair patches. The solid elements were used for the adhesive layers (Figure 33). The laminated nature of the composite adherends was therefore maintained and the solid elements allowed a full 3D stress analysis of the adhesive layers. This model represented the first new approach.

The procedure followed for building this model started with the model geometry definition using geometric entities such as points, lines, surfaces and volumes. The nodes at the interfaces between the adhesive layers and the repair patches and the parent laminates were carefully merged to ensure continuity throughout the model. Second order elements were used and the appropriate lamination sequence pointers defined and assigned. The whole plate was modelled. The following boundary conditions (BC) were applied:

- displacement BC: at x = 0 UX=UZ=RX=RZ=0

  at node (0/0/0) full constraint to prevent rigid body motion
- pressure BC: at x = L pressure load = -350 MPa

3.4.1.2 - 3D Composite Model

In this model, 3D composite solid elements were used for the parent laminate and the repair patches. The adhesive layers were modelled using solid elements. For the parent laminate and the repair patch, approximations in the definition of fibre angles, similar to those used for the damaged plate, around the hole were used. This model represented the second new approach.

3.4.1.3 - 3D Orthotropic Model

3D solid elements were used throughout this model. For the composite adherends, equivalent orthotropic properties were used. The mesh size used was exactly the same as for the 3D composite model. In fact this model was built from the 3D composite model by changing all the elements types to 3D solids and assigning new materials IDs. Thus the model was straight forward to build.

3.4.2 - Results and Discussion

The 3D models have been compared with respect to longitudinal displacement, adherend and adhesive stresses. Wherever possible comparison was made with the undamaged models.

3.4.2.1 - Longitudinal Displacement

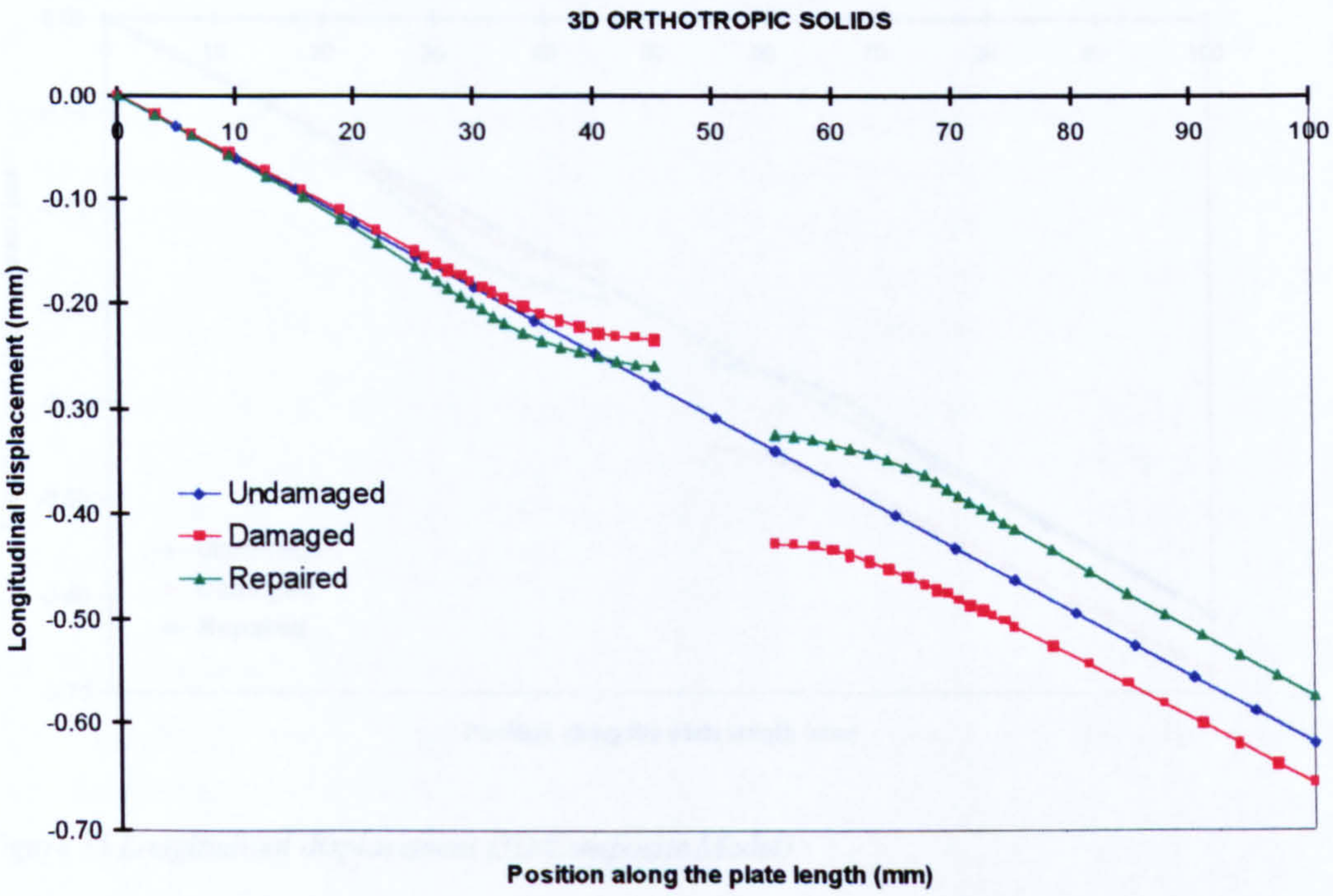

Figure 34 Longitudinal displacement (3D orthotropic Model)

Figure 34 shows the longitudinal displacement from the 3D Orthotropic model for all three states: undamaged, damaged and repaired. The discontinuity of the curves for the damaged and repaired plates indicates the position of the hole (from 45 to 55 mm - which corresponds to the 10 mm diameter).

The red curve indicates that the damaged plate contracts much further than the undamaged plate (blue curve). Considering the left portion of the red curve, it appears to level off as one gets closer to the hole edge. This is consistent with the fact that, as the plate was loaded in compression along its right end side, the absence of material in the hole ensured that no load was transferred directly from the right end of the plate to the left. The load was transferred instead around the hole. Thus, the material in the vicinity of the hole was not displaced as much as it could have been had the hole been filled. On the right side of the hole, the material was displaced further than it would have been. This explains why the left hand portion of the red curve is above the undamaged plate blue curve left hand portion; the reverse being true on the right hand side.

The green curve of the repaired plate is similar in shape to the damaged plate curve. This is because the hole was still present in the parent laminate plate. However, the effect of the repair patches becomes more apparent because they provided load paths above, below and around the hole. One notices also that the left hand portion of the green curve is above the undamaged curve. Thus Figure 34 shows clearly that the patch takes some of the load through the action of the adhesive.

The repaired plate maximum displacement (0.588 mm) was comparable to that of the undamaged plate (0.622 mm). This represents a 5.78% difference. This may indicate that the repaired plate was slightly stiffer than the undamaged one. This could have been clarified by a finer mesh.

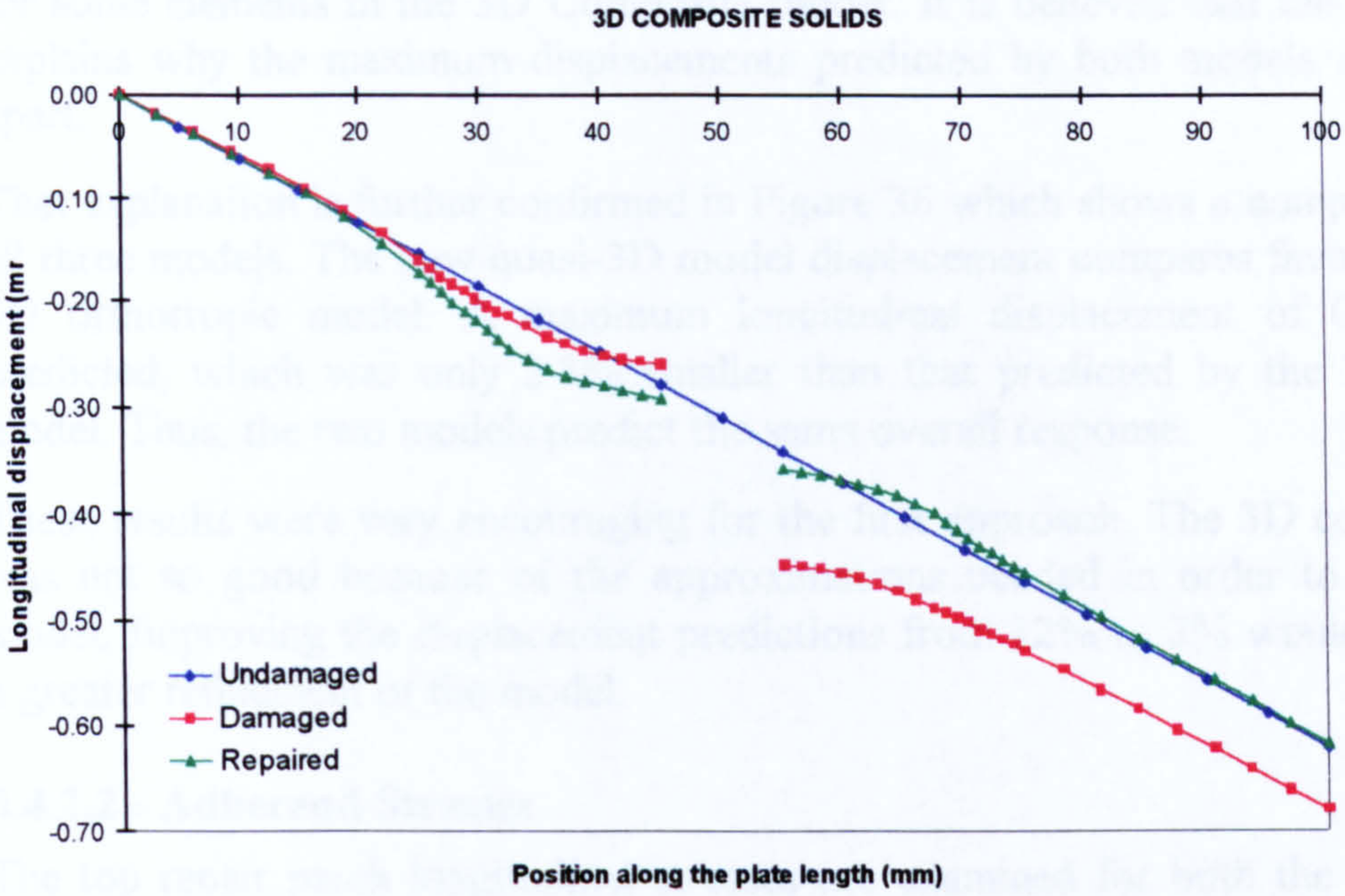

Figure 35 Longitudinal displacement (3D Composite Model)

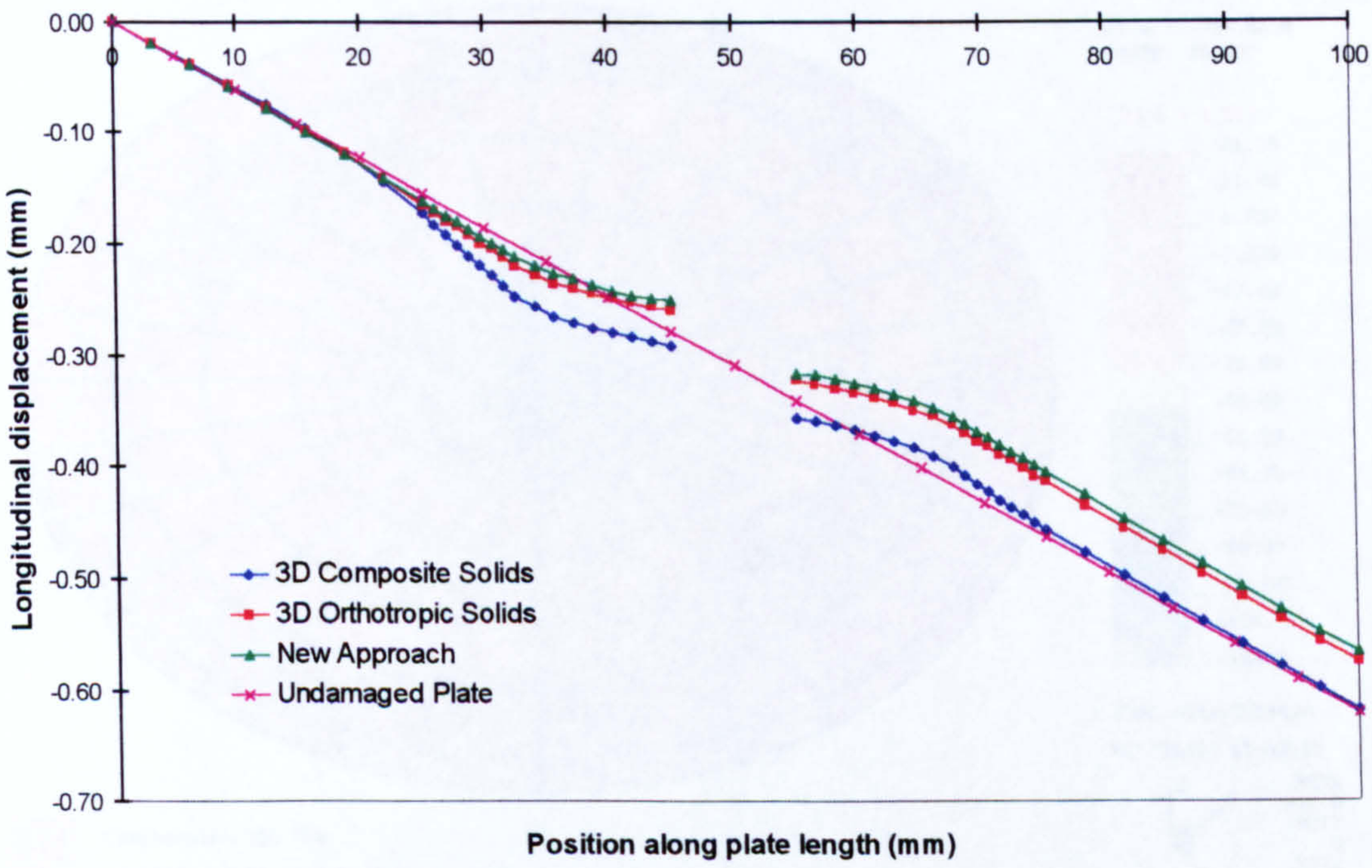

Figure 36 Comparison of longitudinal displacement for the 3D Models

Figure 35 shows the same displacement curves as those in Figure 34 for the 3D Composite model. Again, the discontinuity of the curves for the damaged and repaired plates indicates the position of the hole. One can also notice that the patch was efficient in taking up some of the loads. This is reflected in the displacement curve in the centreline of the plate which is closer to the undamaged plate curve, away from the hole.

The repaired plate maximum displacement was 0.657 mm, i.e. 5.5% higher than that for the undamaged plate. This indicates that the repaired plate was slightly less stiff than the undamaged plate. This finding may contrast with that from the 3D orthotropic model but one has to bear in mind the approximation used in defining the fibre angle

for some elements in the 3D Composite model. It is believed that this approximation explains why the maximum displacements predicted by both models are nearly 12% apart.

That explanation is further confirmed in Figure 36 which shows a comparison between all three models. The new quasi-3D model displacement compares favourably with the 3D orthotropic model. A maximum longitudinal displacement of 0.572 mm was predicted, which was only 2.8% smaller than that predicted by the 3D orthotropic model. Thus, the two models predict the same overall response.

These results were very encouraging for the first approach. The 3D composite model was not so good because of the approximations needed in order to get a working model. Improving the displacement predictions from 12% to 3% would have required a greater refinement of the model.

3.4.2.2 - Adherend Stresses

The top repair patch longitudinal stresses are examined for both the 3D orthotropic model and the new 3D model.

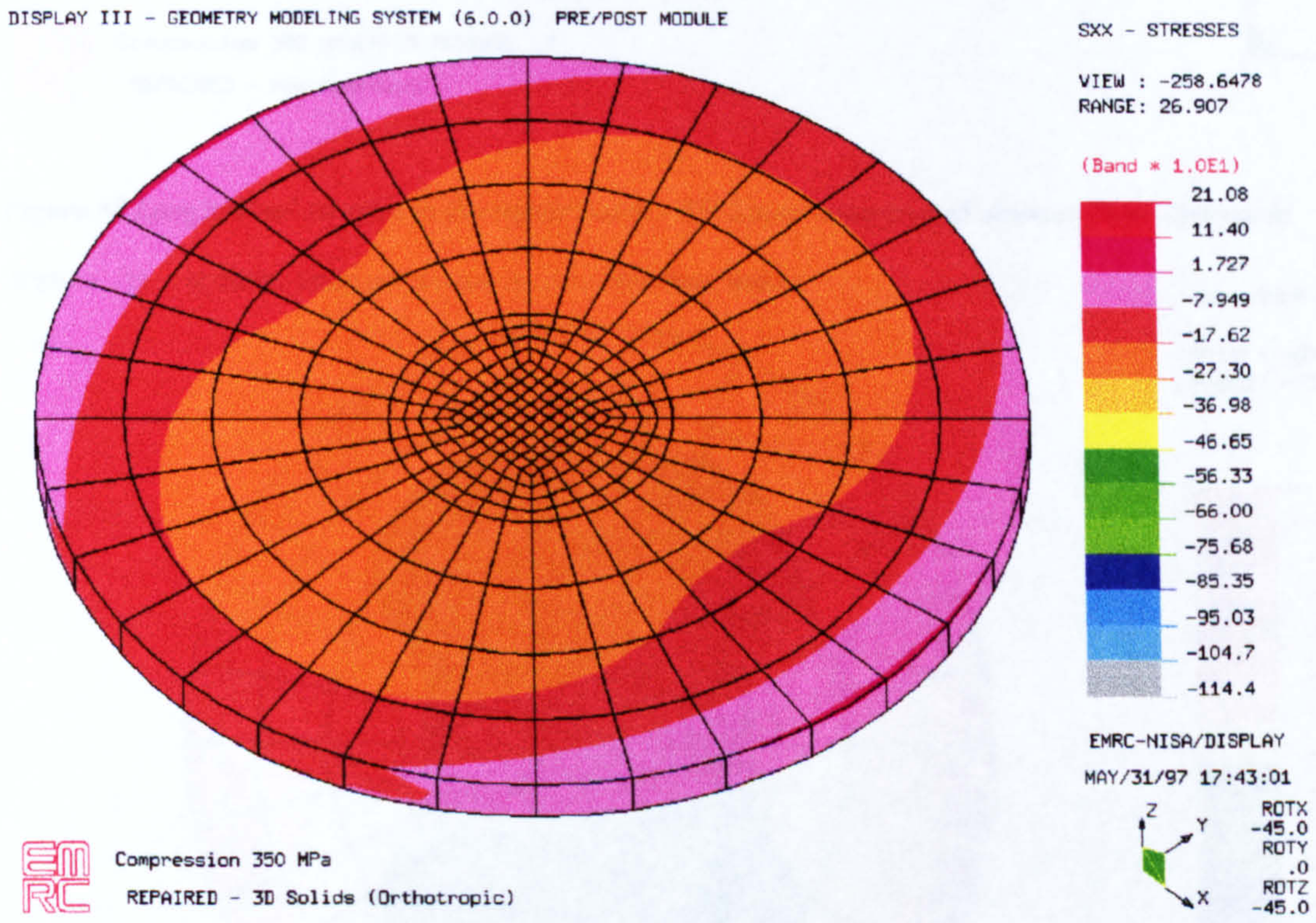

Figure 37 Longitudinal stresses in the repair patch (3D Orthotropic Model)

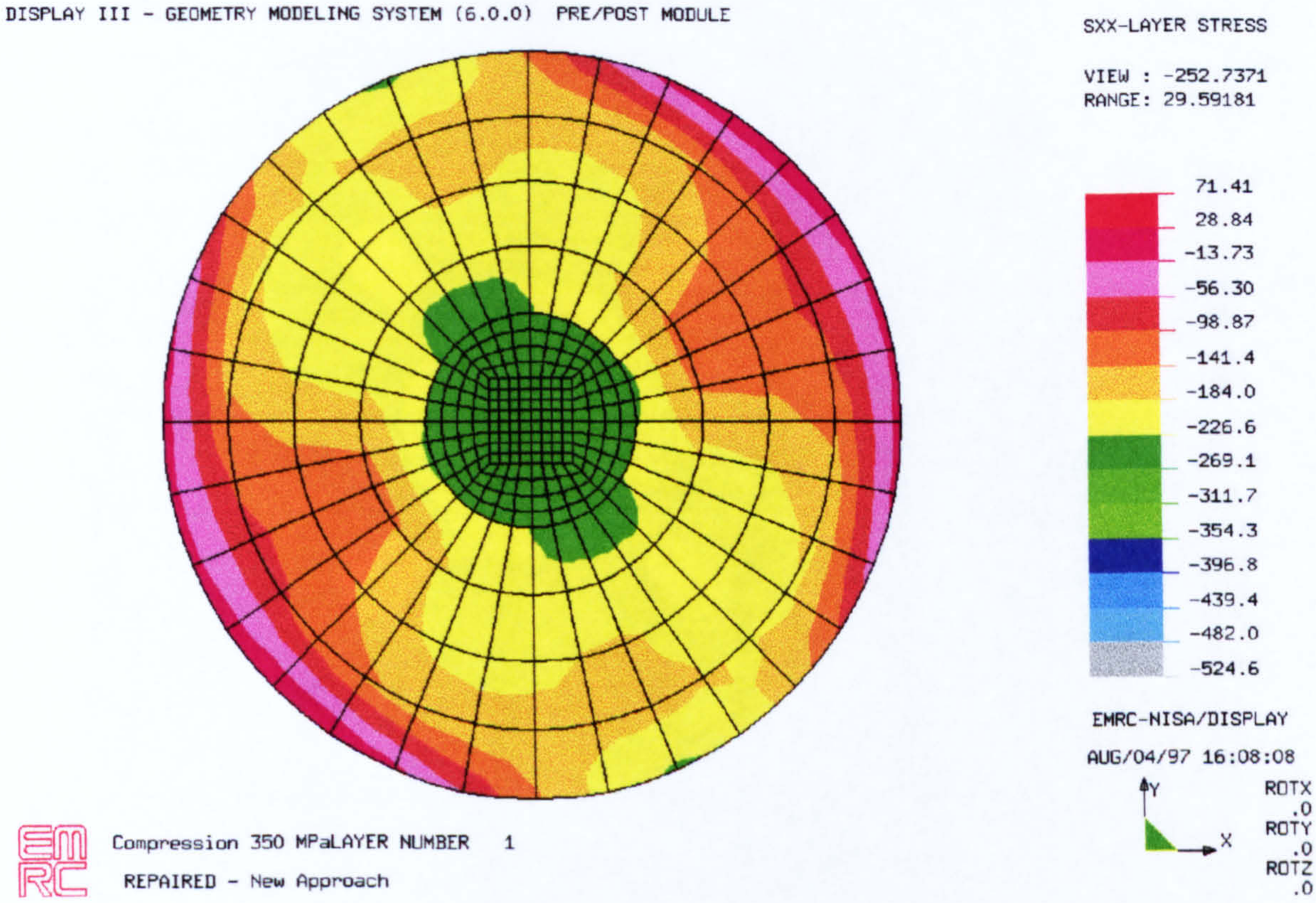

Figure 38 Longitudinal stresses in the repair patch - 45° Layer -unaveraged stresses (New Approach)

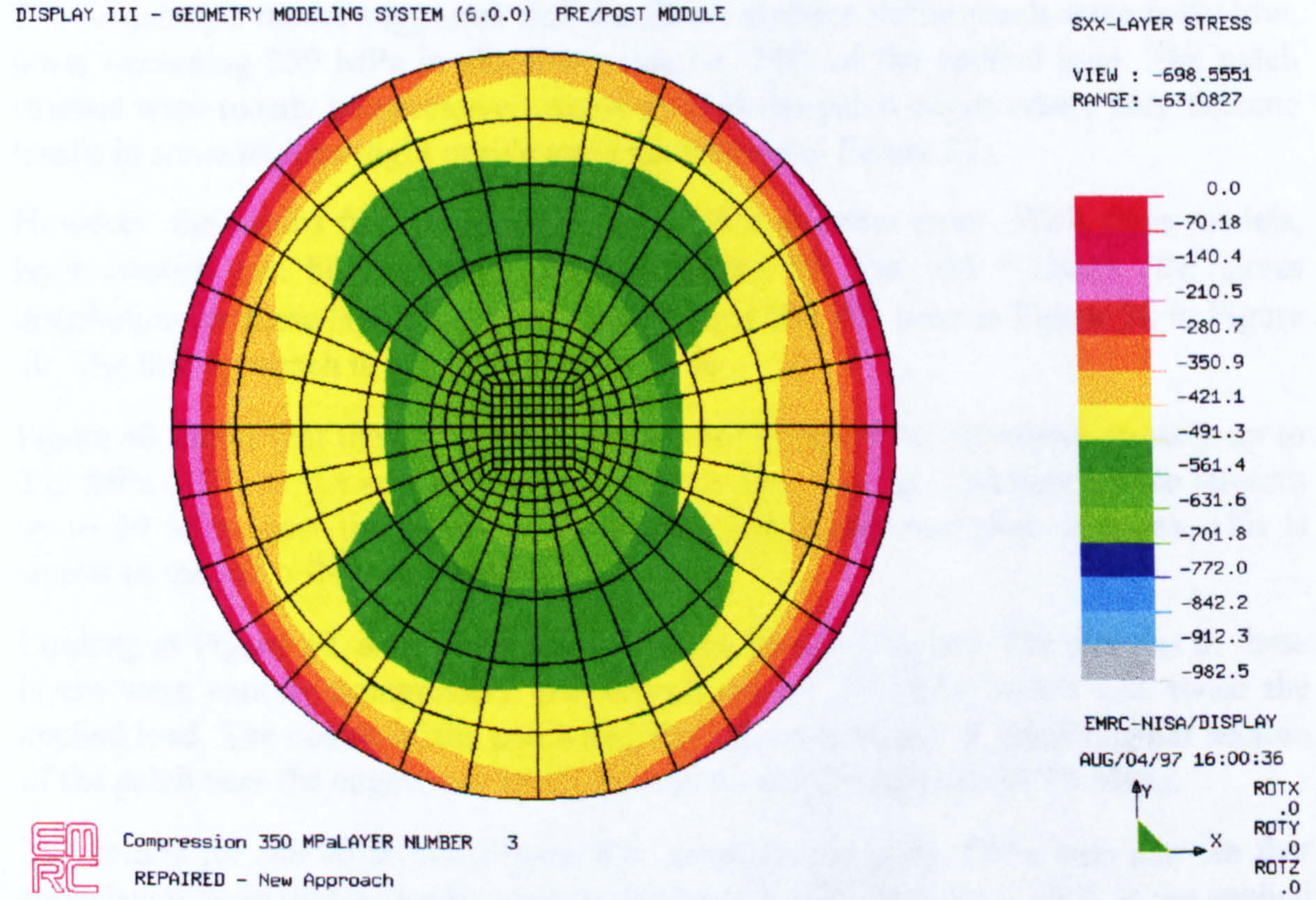

Figure 39 Longitudinal stresses in the repair patch - 0° Layer -unaveraged stresses (New Approach)

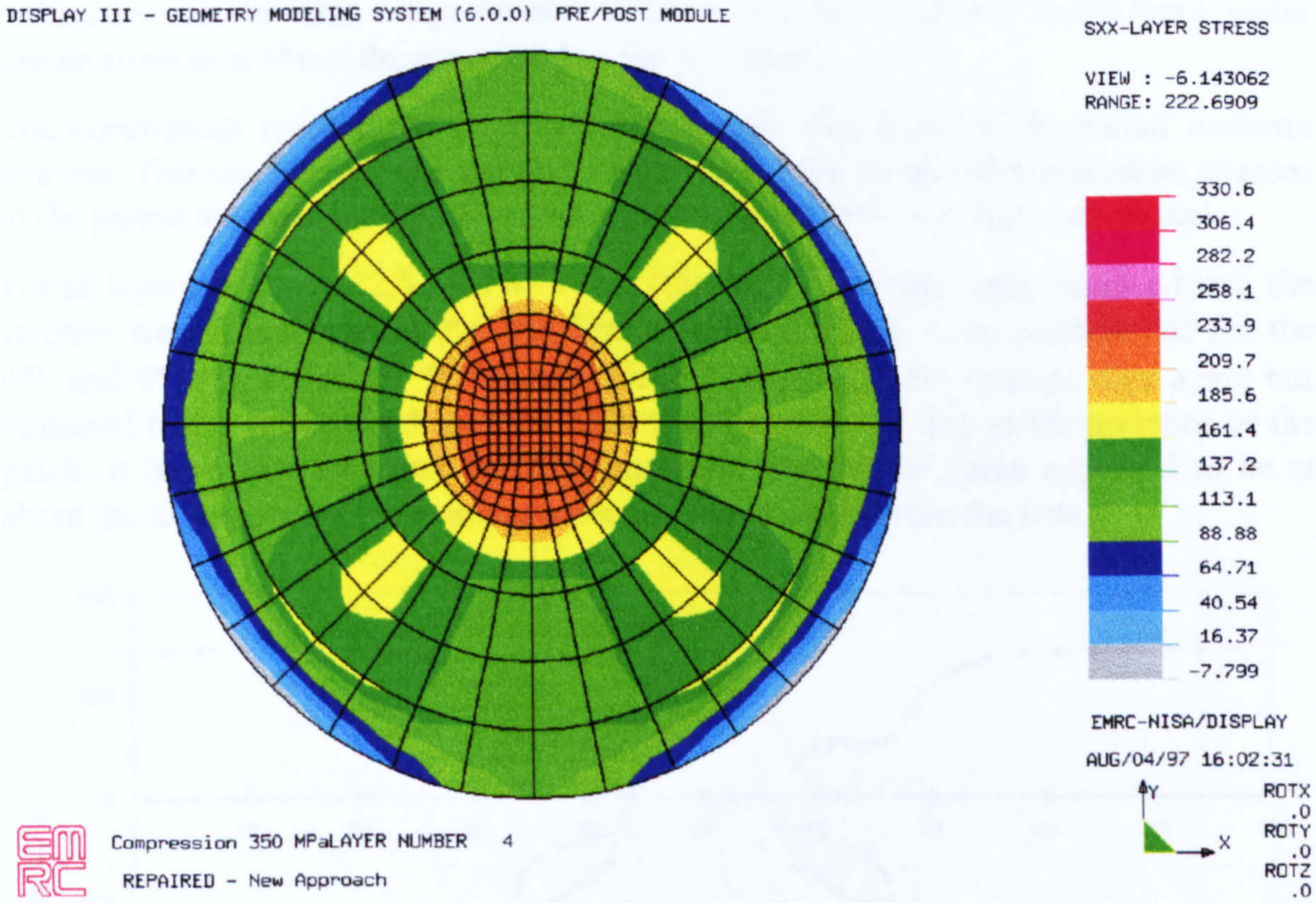

Figure 40 Longitudinal stresses in the repair patch - 90° Layer -unaveraged stresses (New Approach)

The orthotropic model suggested that the direct stresses in the patch were fairly low, never exceeding 259 MPa in absolute value i.e. 74% of the applied load. The patch stresses were mostly compressive, except toward the patch edges where they become tensile in some regions (light purple and pink colours in Figure 37).

However, the results from the new models told a different story. With these models, layer stresses can be examined. This was done for the ±45 ° layers (the stress distribution for these layers are the same), 0° layer and 90° layer in Figure 38 to Figure 40. The first approach is selected as an example.

Figure 38 shows that the 45° layers are subjected to mostly compressive stresses up to 253 MPa (72% of the applied load). There are also regions exhibiting tensile stresses up to 29 MPa, near the edges of the patch (light purple and pink colours). This is similar to the 3D orthotropic model.

Looking at Figure 39, a different story emerges for the 0°layers. The stresses in these layers were entirely compressive and very close to 700 MPa, which was twice the applied load. The centre of the patch had the highest stresses. A great angular section of the patch near the edges was lightly loaded in compression (about 70 MPa).

The results for the 90°layers (Figure 40) complete the story. Here, one can see that these layers were under mostly tensile stresses up to 223 MPa (i.e. 64% of the applied load) apart for some regions near the edges of the patch.

It is apparent that the new models offer more possibilities than the 3D orthotropic model as was anticipated. These patch layer stresses revealed that the 0° layers were under the highest stress level, a feature which could not have been forecast by any

orthotropic model with no prediction of layer stresses. The 90° layers were under tensile stresses at about the same level as the 45° layers.

The conclusions reached for the repair patch were also true for the parent laminate stresses. This can be seen in Figure 41 which shows the predicted longitudinal stresses in the parent laminate for the 3D orthotropic model and the first approach model.

For all layers, between 32.5 and 67.5 mm (the position of the repair patch edges), the stresses were lower than elsewhere. This effect was much more pronounced for the 45° and 0° layers. For the 90° layers, close to the hole, the stresses rose again but remained below the far field stresses. This effect was clearly due to the presence of the patch. It is worth noting that the layer stresses in the repair patch appeared to be at about the same level as those in the parent laminate, away from the hole.

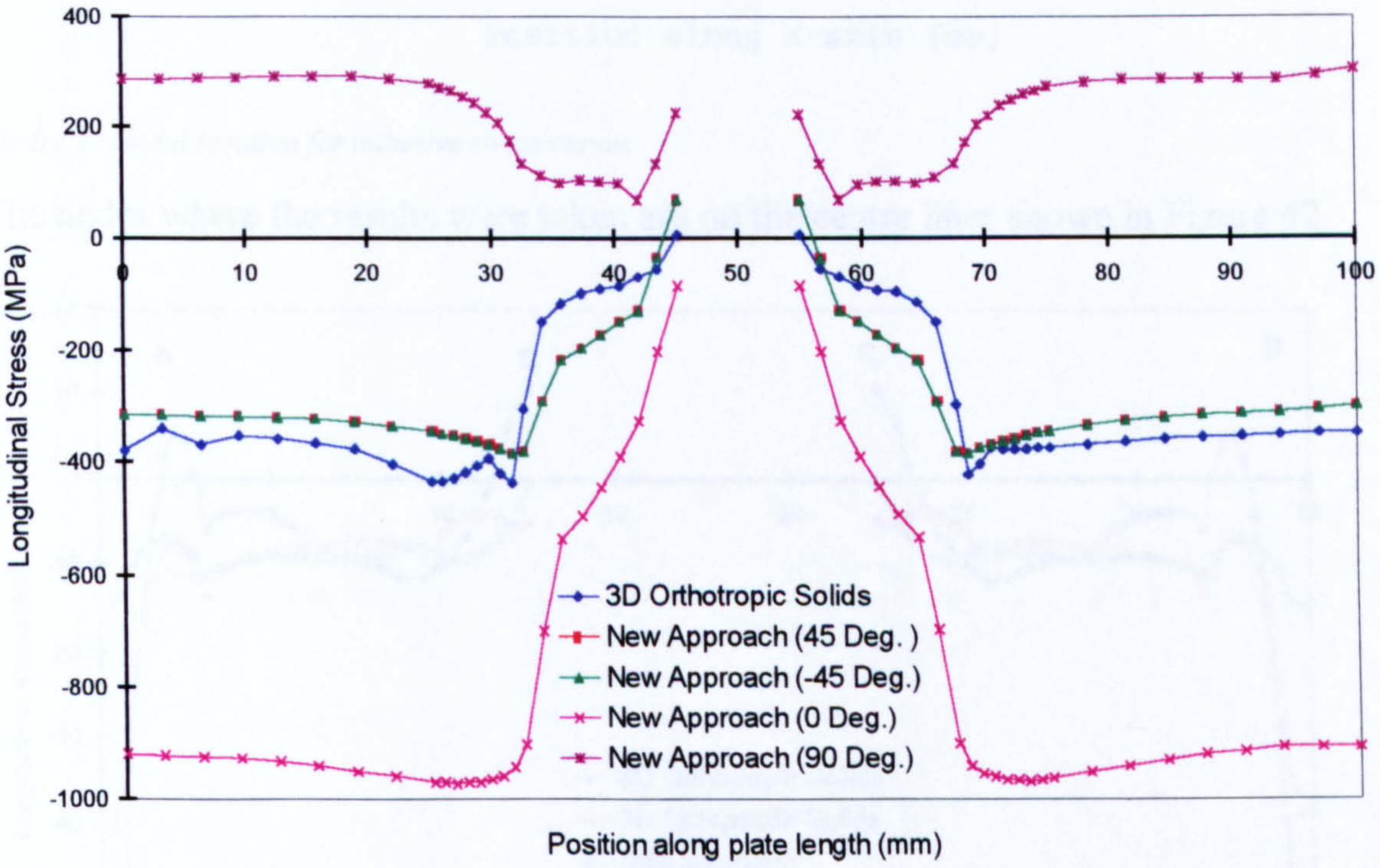

Figure 41 Parent laminate longitudinal stresses

3.4.2.3 - Adhesive Stresses

The adhesive longitudinal stresses were considered along with the more important shear and peel stresses. The next three figures show the first results obtained from adhesive submodels for all three 3D approaches.

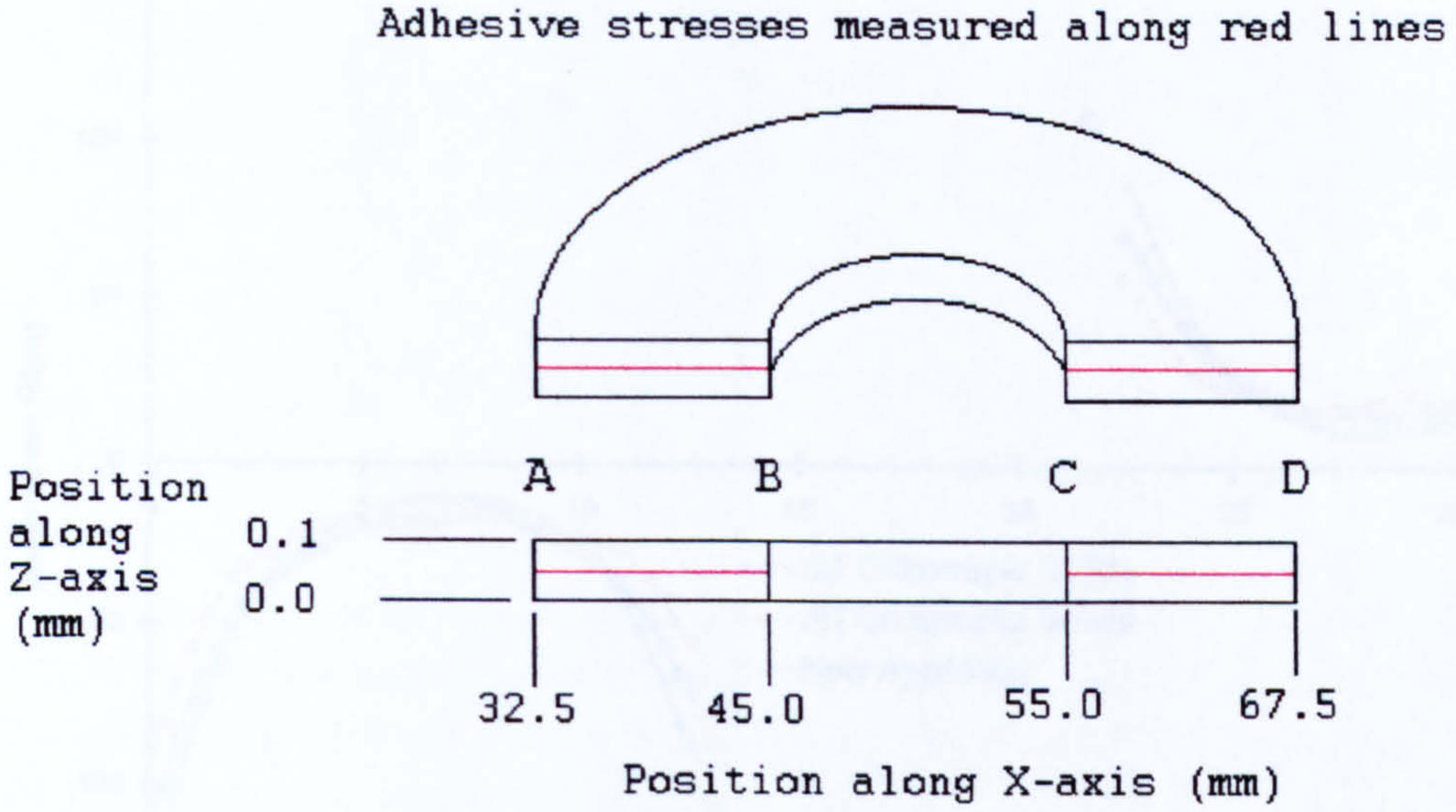

Figure 42 Nodal location for adhesive stress curves

The nodes where the results were taken are on the centre lines shown in Figure 42.

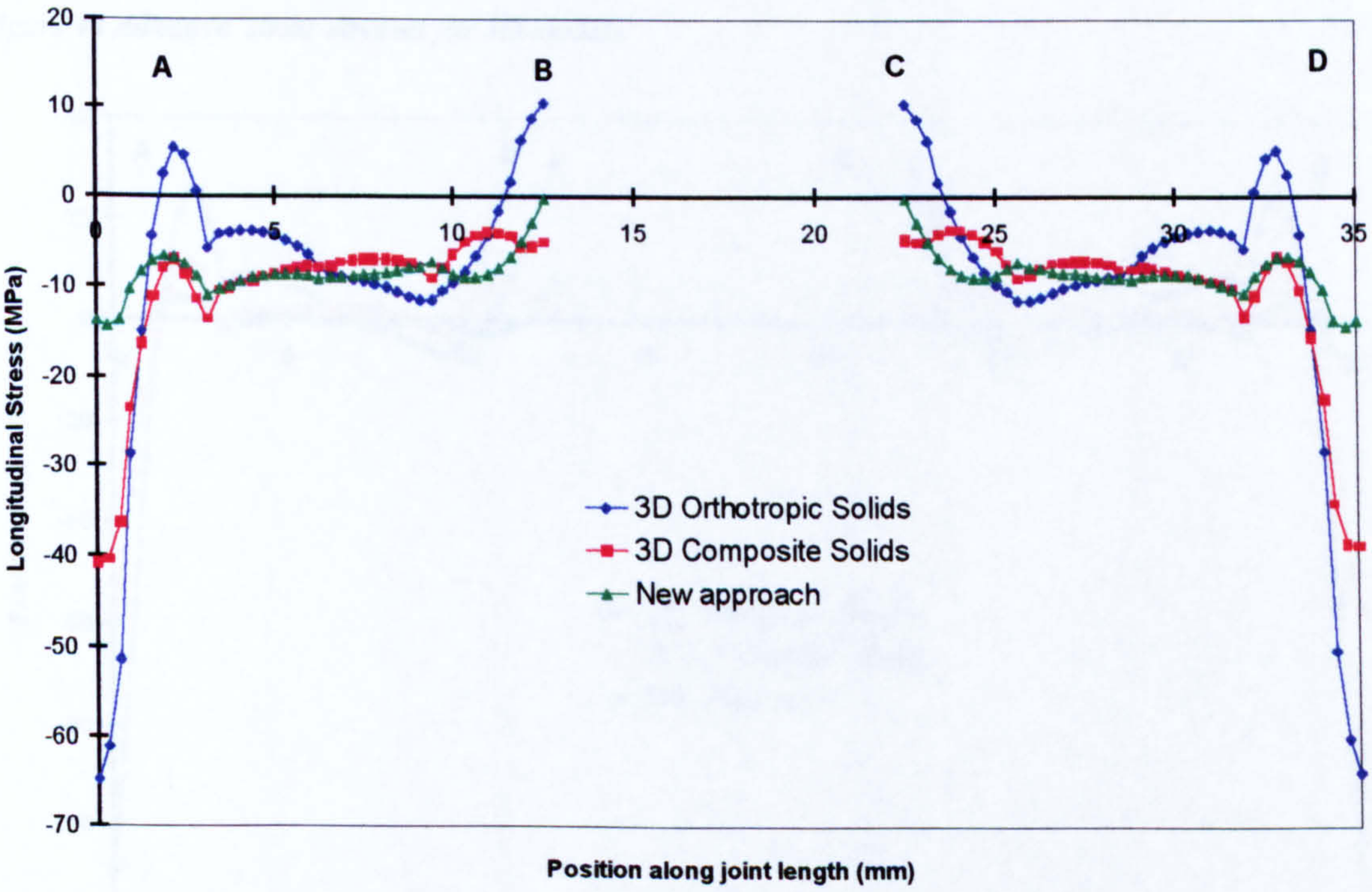

Figure 43 Adhesive longitudinal stresses for 3D models

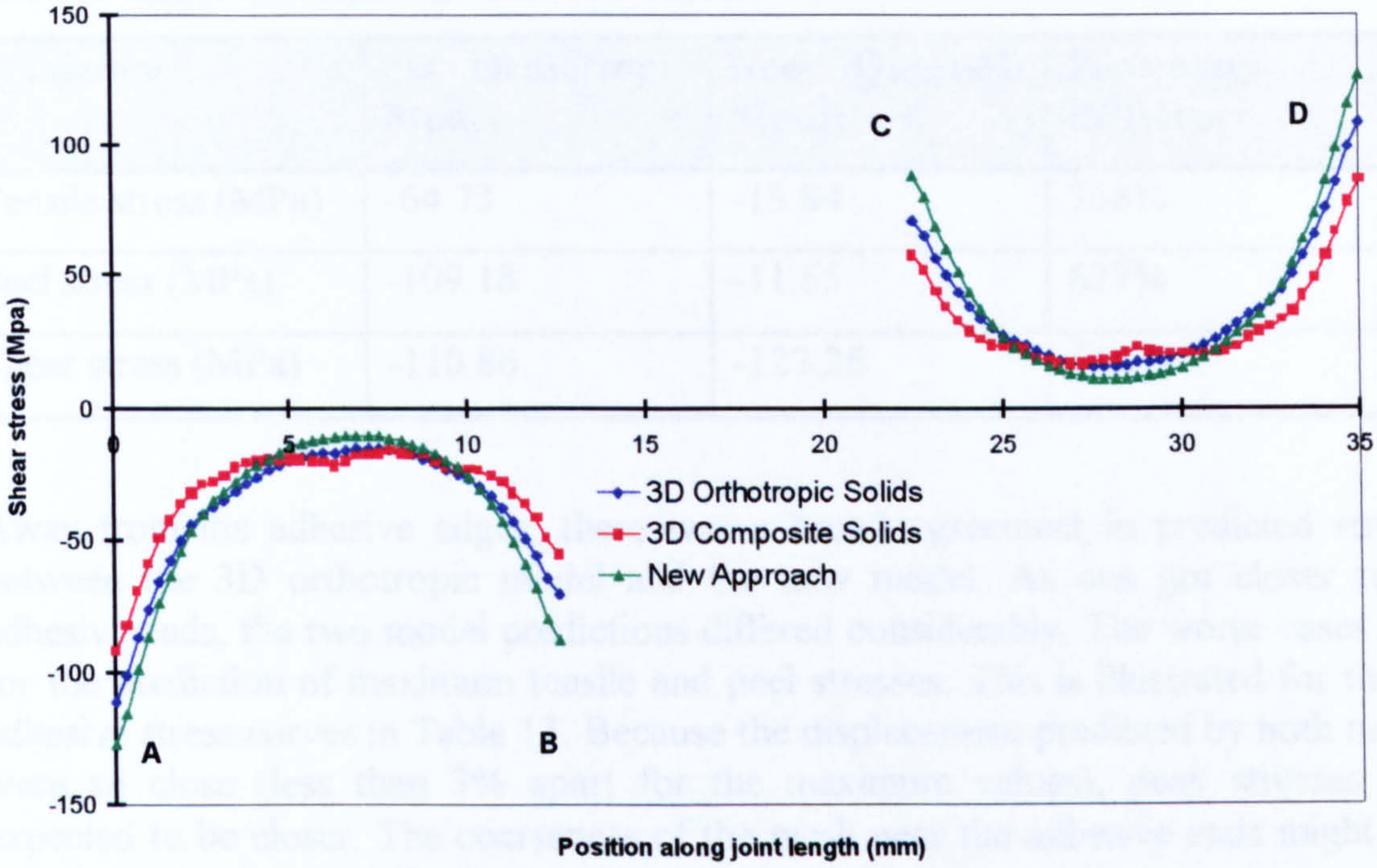

Figure 44 Adhesive shear stresses for 3D models

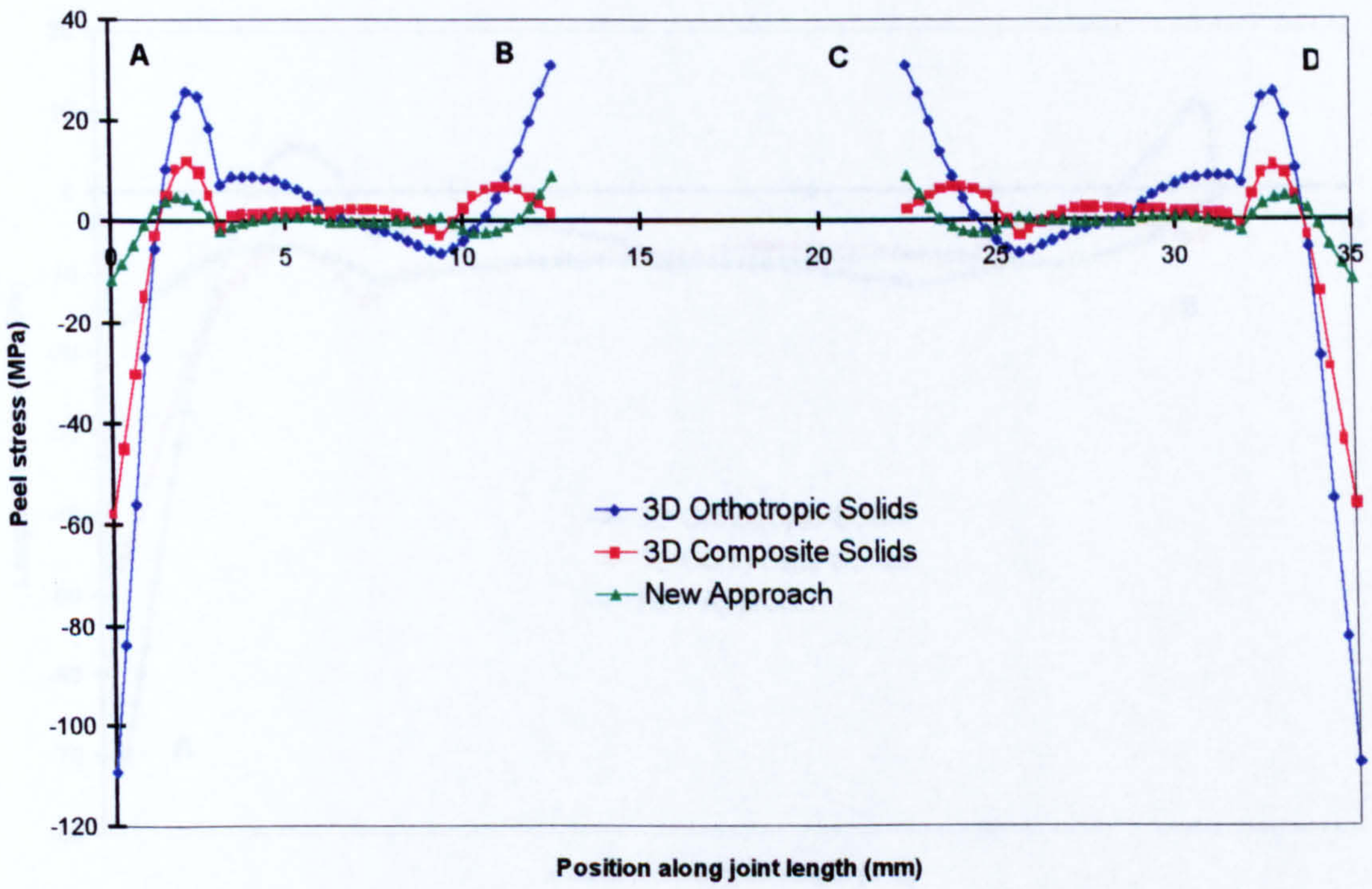

Figure 45 Adhesive peel stresses for 3D Models

All three figures show clearly that there were important differences between the 3D models. First, looking at the longitudinal stresses (Figure 43), one notices that the 3D composite model predicted results which were different from the two other models. This was expected because the displacements were 12% higher than those predicted by the other two models. As stresses were obtained from the integration of the displacements, they were bound to be less in agreement if the models differed already in the predicted displacement.

Table 13 Maximum stresses for LHS adhesive curve left end

Maximum	3D Orthotropic Model	New Quasi-3D Model	Percentage Difference
Tensile stress (MPa)	-64.73	-13.84	368%
Peel stress (MPa)	-109.18	-11.65	837%
Shear stress (MPa)	-110.86	-127.25	14.8%

Away from the adhesive edges, there was a broad agreement in predicted stresses between the 3D orthotropic model and the new model. As one got closer to the adhesive ends, the two model predictions differed considerably. The worse cases were for the prediction of maximum tensile and peel stresses. This is illustrated for the left adhesive stress curves in Table 13. Because the displacement predicted by both models were so close (less than 3% apart for the maximum values), peak stresses were expected to be closer. The coarseness of the mesh near the adhesive ends might have accounted for the big differences.

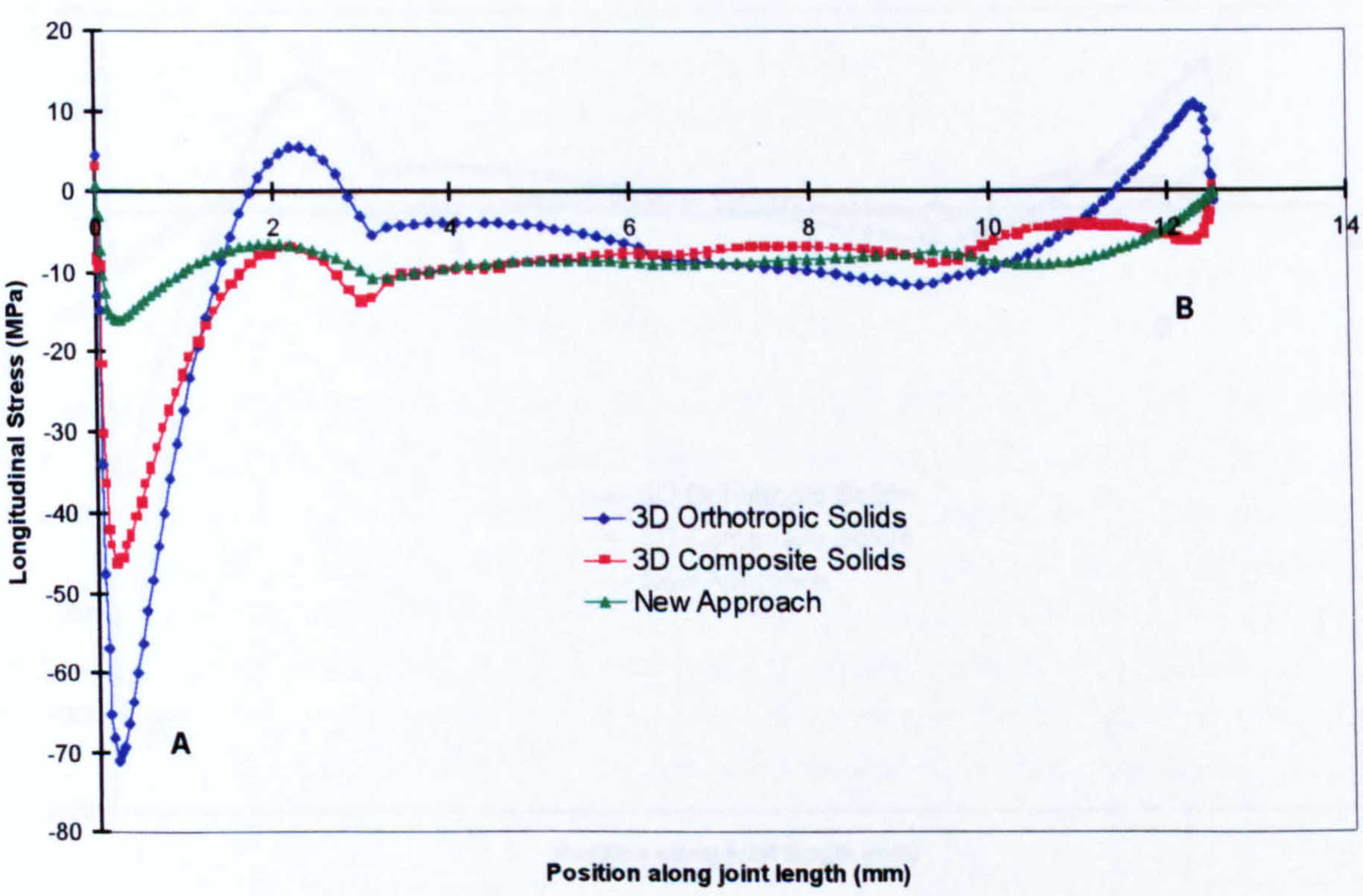

Figure 46 Adhesive longitudinal stresses for refined submodels

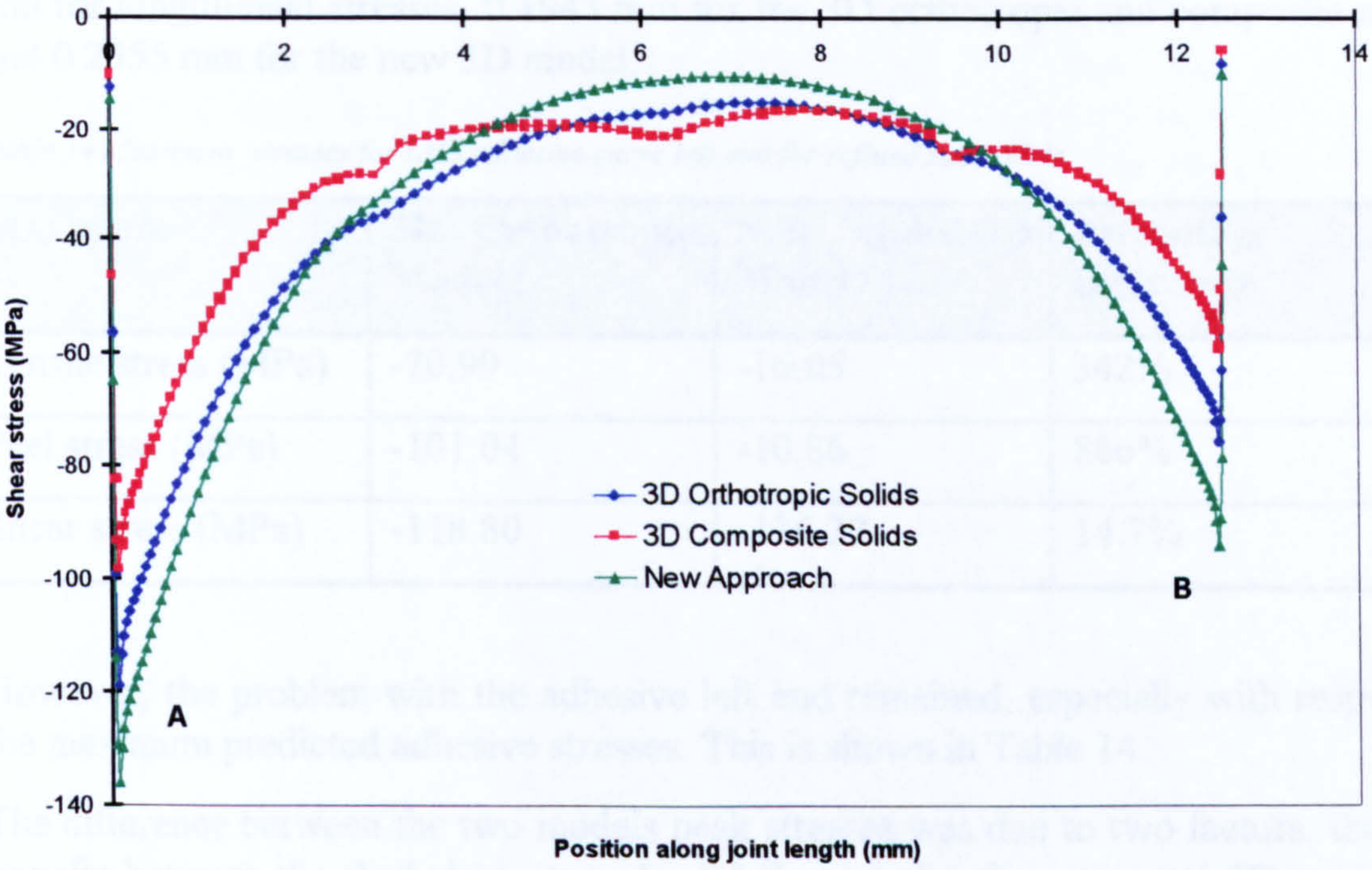

Figure 47 Adhesive shear stresses for refined submodels

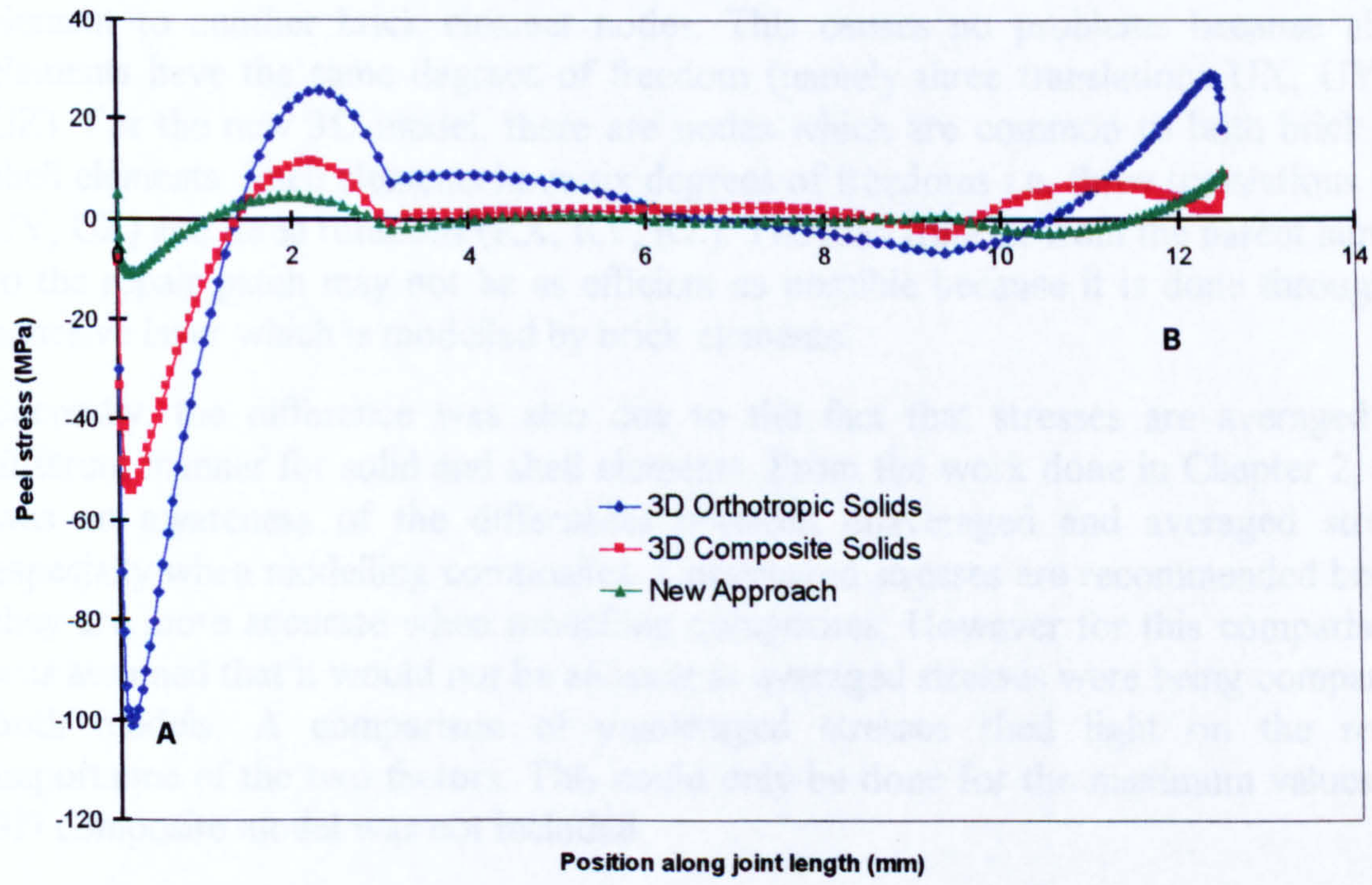

Figure 48 Adhesive peel stresses for refined submodels

To obtain better adhesive stresses, new submodels were constructed with a finer mesh towards the adhesive free edges. The results are shown in Figure 46 to Figure 48 for the LHS adhesive only..

The adhesive shear stresses in Figure 46 fall quite rapidly towards zero near the end of the curves (corresponding to adhesive edges). The shear stresses all peak at a distance of 0.0703 mm from the adhesive end A. For lap joints, adhesive shear stresses usually peak at a distance approximately half the adhesive thickness [111]. So, the stress distribution curves were improved. For the peel stresses, that distance is 0.1255 mm

and for longitudinal stresses, 0.1943 mm for the 3D orthotropic and composite model and 0.2355 mm for the new 3D model.

Table 14 Maximum stresses for LHS adhesive curve left end for refined submodels

Maximum	3D Orthotropic Model	New Quasi-3D Model	Percentage Difference
Tensile stress (MPa)	-70.99	-16.05	342%
Peel stress (MPa)	-101.04	-10.86	886%
Shear stress (MPa)	-118.80	-136.32	14.7%

However, the problem with the adhesive left end remained, especially with respect to the maximum predicted adhesive stresses. This is shown in Table 14.

The difference between the two models peak stresses was due to two factors: the load transfer between the shell elements and solid elements for the new quasi-3D model and the comparison between averaged stresses rather than unaveraged stresses

Firstly for the 3D orthotropic model, the loads are transferred from nodes on one brick element to another brick element nodes. This causes no problems because all the elements have the same degrees of freedom (namely three translations UX, UY and UZ). For the new 3D model, there are nodes which are common to both brick and shell elements. Shell elements have six degrees of freedoms i.e. three translations (UX, UY, UZ) and three rotations (RX, RY, RZ). The load transfer from the parent laminate to the repair patch may not be as efficient as possible because it is done through the adhesive layer which is modelled by brick elements.

Secondly, the difference was also due to the fact that stresses are averaged in a different manner for solid and shell elements. From the work done in Chapter 2, there was an awareness of the differences between unaveraged and averaged stresses, especially when modelling composites. Unaveraged stresses are recommended because they are more accurate when modelling composites. However for this comparison, it was assumed that it would not be an issue as averaged stresses were being compared in both models. A comparison of unaveraged stresses shed light on the relative importance of the two factors. This could only be done for the maximum values. The 3D composite model was not included.

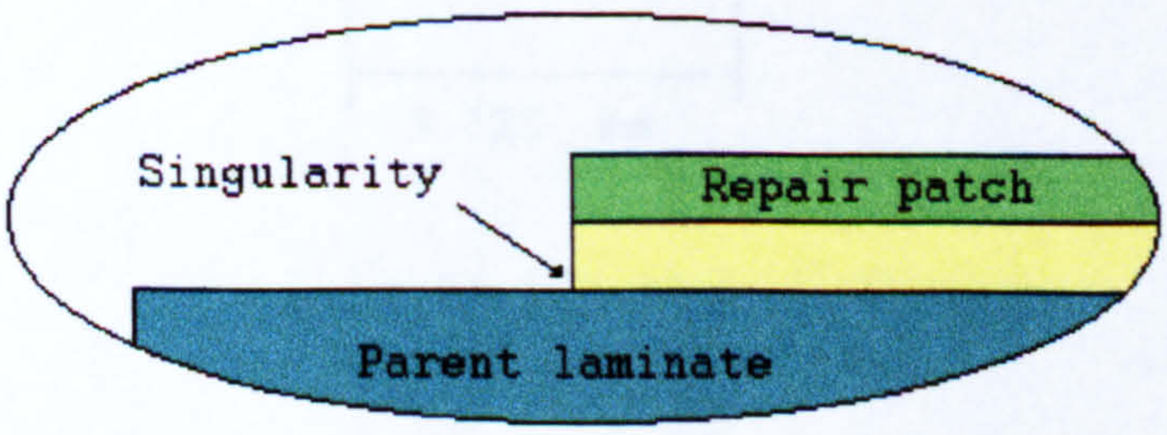

Figure 49 Singularity location for repair joint

One of the main problems in comparing maximum adhesive stresses is the existence of a singularity (Figure 49) where the stress value is mesh dependent. This phenomenon has been well documented by Adams [75] for various bonded joints. In the present study, this was not so much of a difficulty since the same mesh size was used for both models and the difference between peak values was sought.

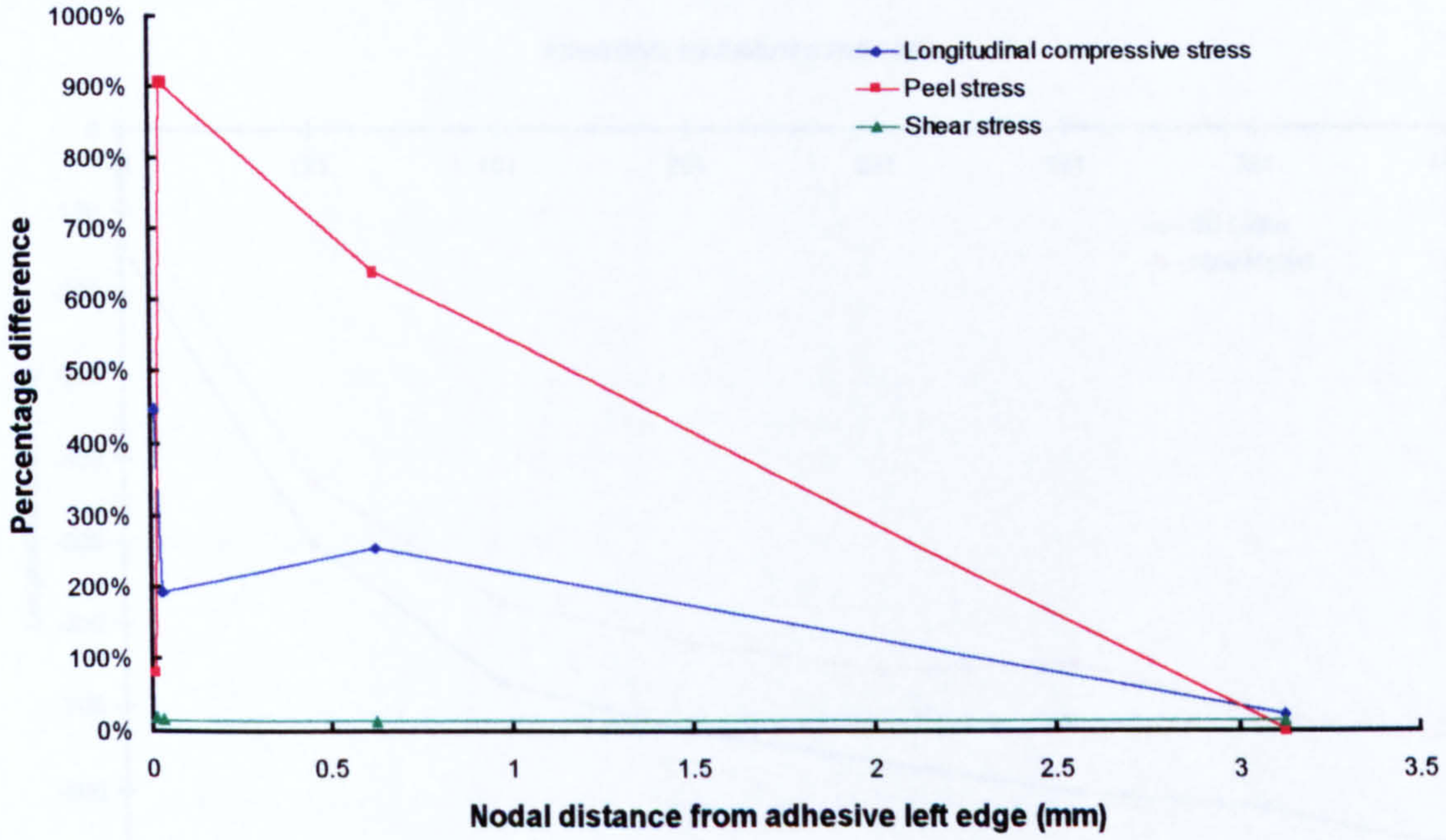

Figure 50 Nodal stress predictions close to adhesive left edge

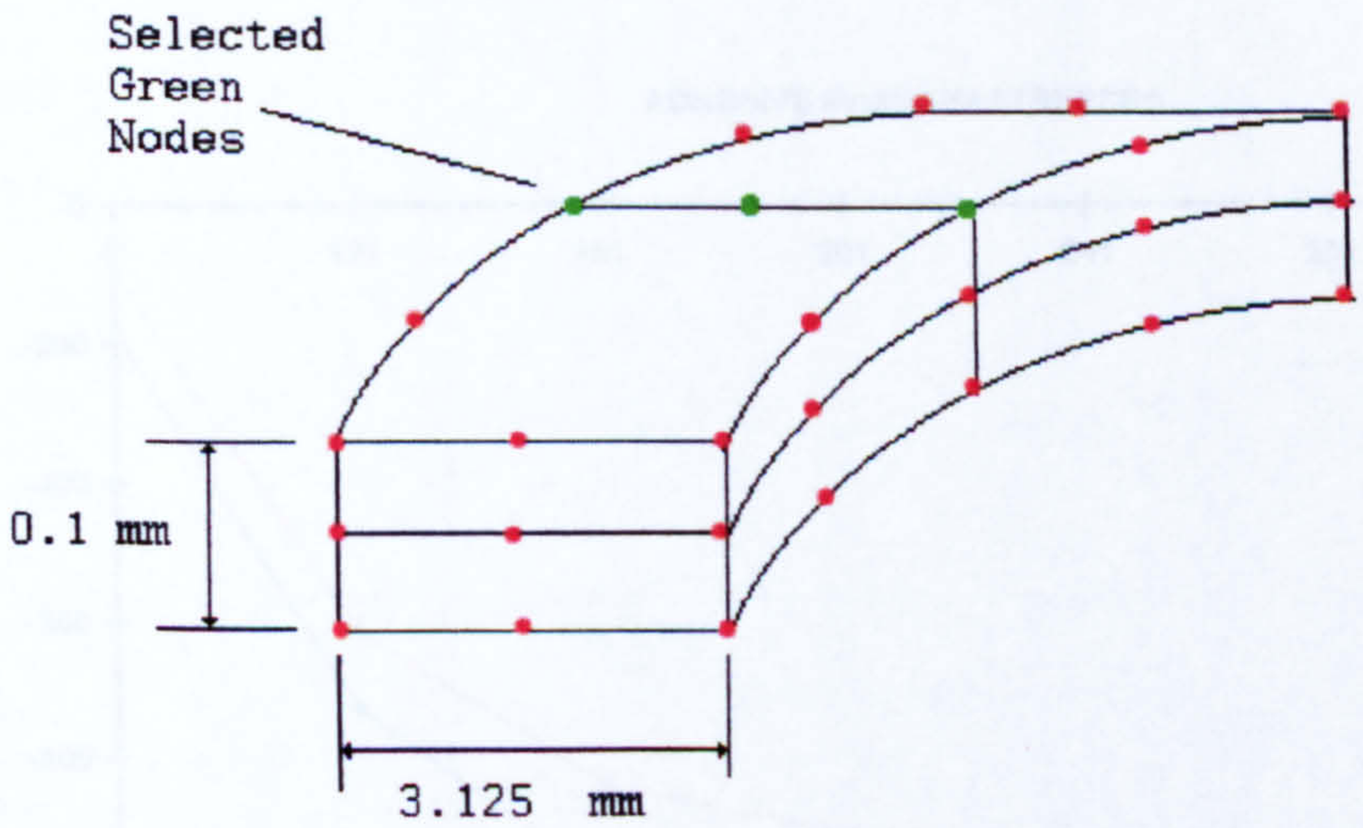

Figure 51 Node location for graphs in Figure 50

The curves in Figure 50 highlight the fact that the singularity affects the numerical results for predicted longitudinal and peel stresses as one gets closer to it. The percentage difference for the shear stress predicted by the two models did not seem to be affected and remained constant. The nodes where the data were recorded are shown as green dots in Figure 51. An improved distribution could be obtained with a finer mesh. These results were obtained from the main models rather than the adhesive submodels thus must be seen as qualitative information only.

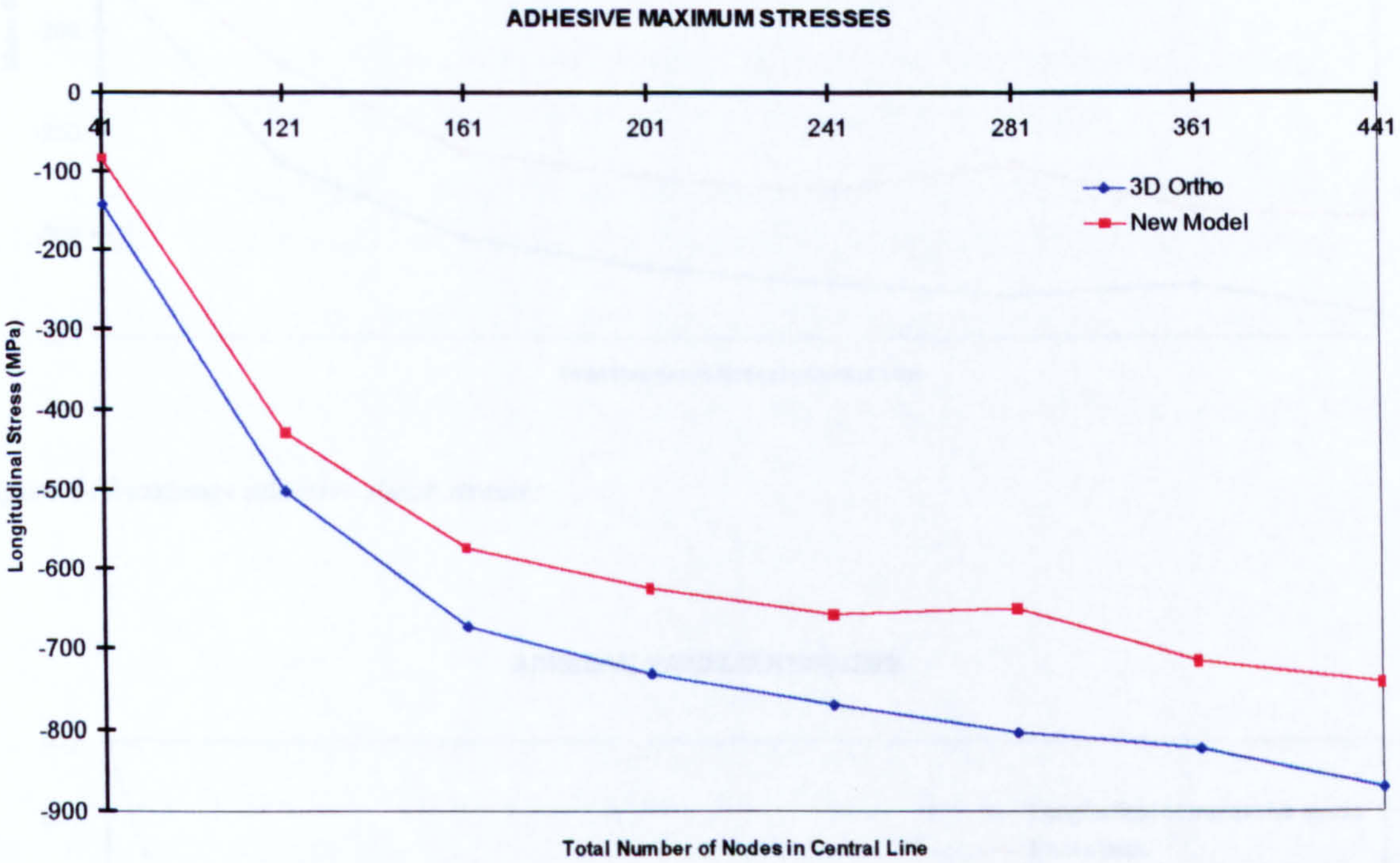

Figure 52 Maximum adhesive longitudinal stresses

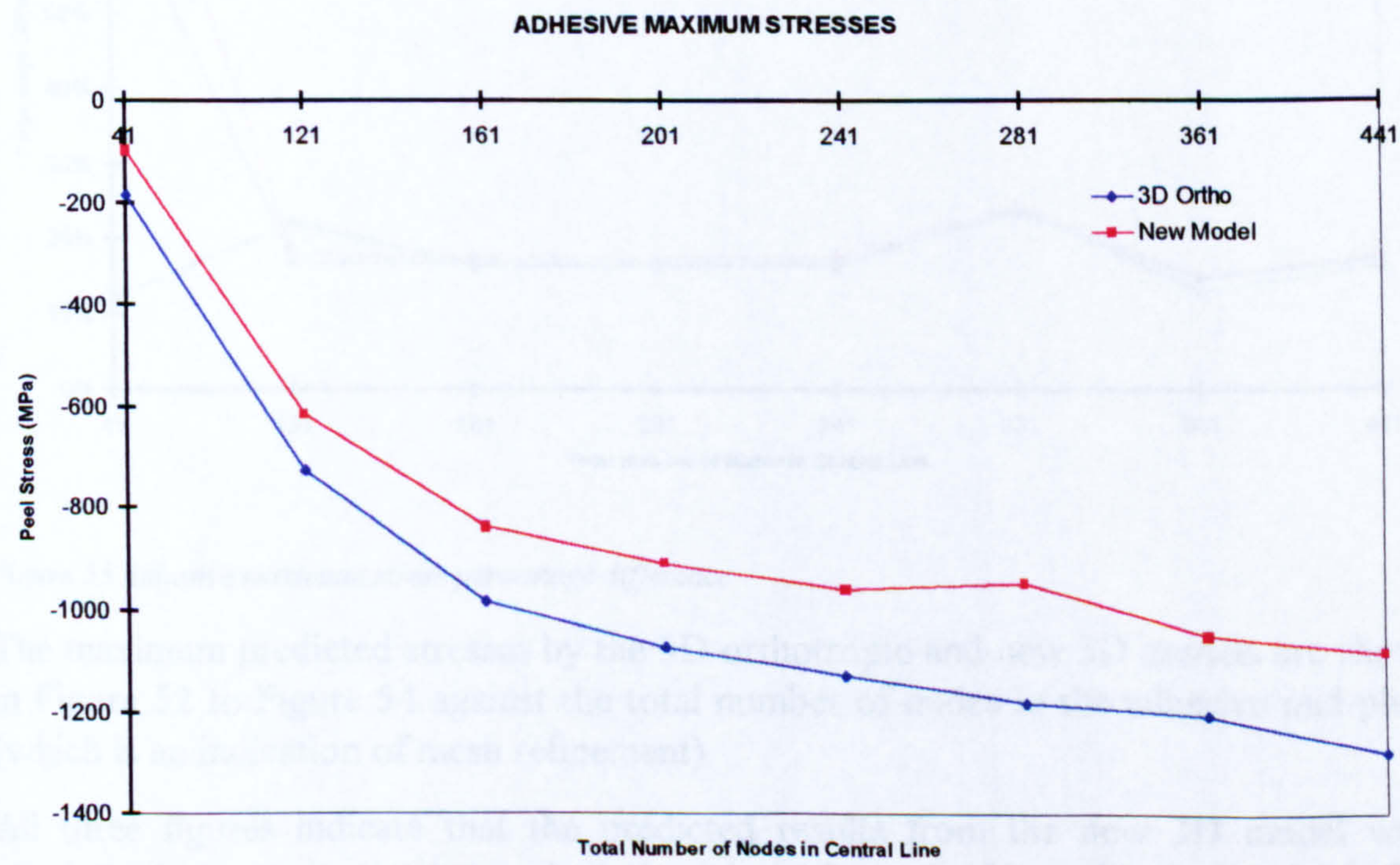

Figure 53 Maximum adhesive peel stresses

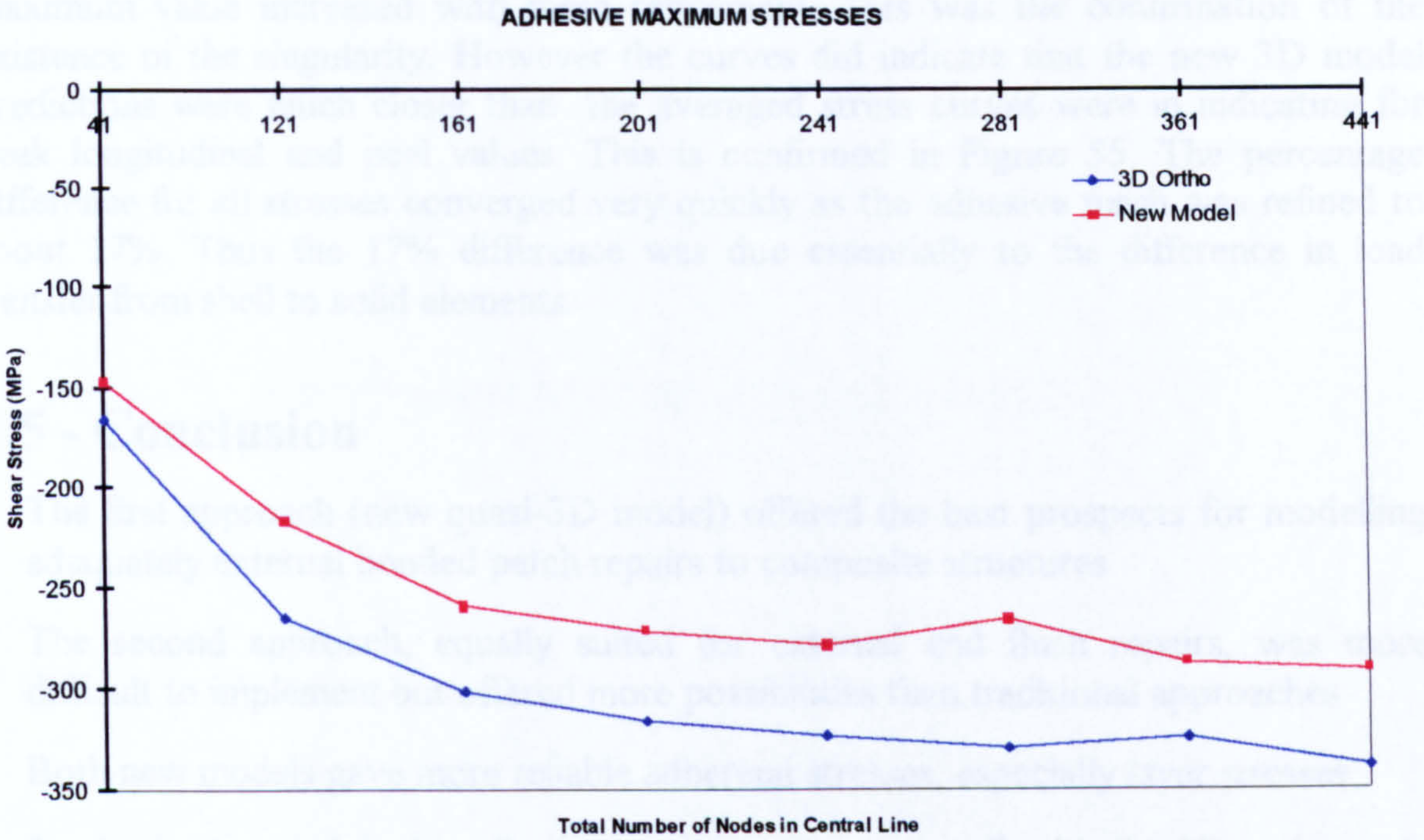

Figure 54 Maximum adhesive shear stresses

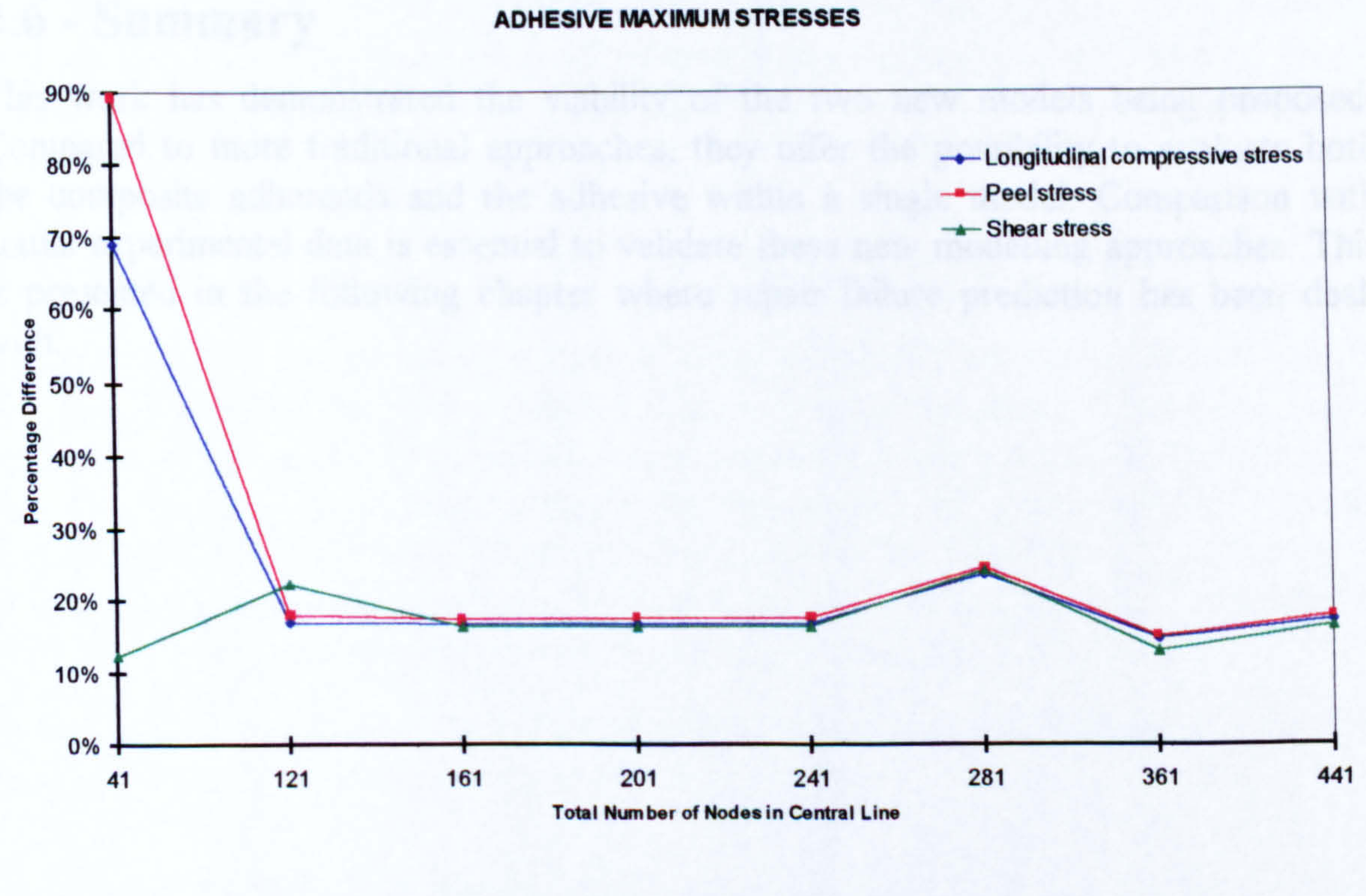

Figure 55 Adhesive maximum stress percentage difference

The maximum predicted stresses by the 3D orthotropic and new 3D models are shown in Figure 52 to Figure 54 against the total number of nodes in the adhesive mid-plane (which is an indication of mesh refinement).

All three figures indicate that the predicted results from the new 3D model were consistently lower in absolute values than those from the 3D orthotropic model. The difference between the models appeared constant for every set of submodels. The

maximum value increased with mesh refinement. This was the confirmation of the existence of the singularity. However the curves did indicate that the new 3D model predictions were much closer than the averaged stress curves were in indicating for peak longitudinal and peel values. This is confirmed in Figure 55. The percentage difference for all stresses converged very quickly as the adhesive mesh was refined to about 17%. Thus the 17% difference was due essentially to the difference in load transfer from shell to solid elements.

3.5 - Conclusion

- The first approach (new quasi-3D model) offered the best prospects for modelling adequately external bonded patch repairs to composite structures
- The second approach, equally suited for external and flush repairs, was more difficult to implement but offered more possibilities than traditional approaches
- Both new models gave more reliable adherend stresses, especially layer stresses
- For both new models the adhesive stresses compared well with the 3D orthotropic model predictions

3.6 - Summary

This work has demonstrated the viability of the two new models being proposed. Compared to more traditional approaches, they offer the possibility to evaluate both the composite adherends and the adhesive within a single model. Comparison with actual experimental data is essential to validate these new modelling approaches. This is presented in the following chapter where repair failure prediction has been dealt with.

Chapter 4

Improved Modelling Approaches

Predicting Failure

4.0 - Introduction

This chapter demonstrates how the first modelling approach introduced in the preceding chapter can be used to predict failure for externally bonded patch repairs to composite structures. Once stresses and strains are calculated, the next step is to apply an appropriate criterion in order to predict failure load and location.

Failure criteria for both composites and adhesive are reviewed first with an emphasis on their relevance to the analysis of bonded repairs. The new quasi-3D model described in Chapter 3 was used for this study which was based on the work by Soutis and Hu [107]. Failure prediction for the repaired panel were compared to both Soutis and Hu's FE predictions using stress concentration factors and the experimental results.

4.1- Failure Criteria for Composites and Adhesives

The ultimate goal for any model is the prediction of failure load, mode and location. To this end, one relies on failure theories. For a bonded composite repair model, it is necessary to investigate both adhesive and composite adherend failure. In both cases numerous studies have been published on the subject of failure criteria. To help understand the current state of affairs, a review has been carried out and the main findings presented in this section. This review is by no means exhaustive but aims to provide a critical understanding of what is currently available.

Failure criteria for composite materials are reviewed first followed by a section on failure criteria for structural adhesives.

4.1.1 - Composite Materials

The prediction of failure in composite materials is a subject which has widely been researched right from the beginning when these materials were being introduced into aircraft structures. Several books [112, 113, 114, 115, 116, 117, 118 and 119] are now available which describe well the main failure theories for composite materials. In addition several surveys of composite failure criteria have been carried out, including an early work by Sandhu [120] and a more recent one by Curtis [121] to name a couple. Additional information can be found in those references.

This short review will be concerned essentially with the main theories, with a special emphasis on those used in numerical analysis. In addition, theories for simple laminates only will be covered.

Despite the growing number of publications in this important area, there is no general consensus on which theory works best. Recently, a special forum on "Failure of Composite Materials" was convened at the 11th International Conference on Composite Materials (14-18 July 1997, Gold Coast, Australia). It emerged from the open discussion, after presentations by the main experts in the field, that there were broadly two schools of thought on the subject: one in favour of the much used interactive criteria (now widely regarded as classical composite failure theories) and a 'new' emerging group in favour of physically based failure criteria. The first group includes composite materials pioneers such as Dr. Stephen Tsai, E.M. Wu and K. W. Shacharov and the second has such advocates as Dr. John Hart-Smith, Dr Alan Baker, Prof. A. Puck and Dr-Ing Ralf Cuntze.

The main classical failure theories for composites materials are presented in the next section followed by a brief survey of the emerging new physically based theories.

4.1.1.1 - Classical Composite Failure Criteria

The main characteristic of laminate strength theories is that they are macroscopic in nature and are expressed in term of single lamina strengths. In addition, they assume that the material is homogeneous and linear elastic to failure. These macromechanical failure theories have evolved from isotropic material failure theories, modifying them to take into account stiffness and strength anisotropy of composites. According to Daniel and Ishai [118], more than forty macromechanical failure theories have been proposed over the years.

Amongst the various theories, four have been widely used and are considered representative of the various approaches:

- Maximum stress theory
- Maximum strain theory
- Deviatoric strain energy theory for anisotropic material (a.k.a. Tsai-Hill)
- Interactive tensor polynomial theory (a.k.a. Tsai-Wu)

The first two are classified as **limit** criteria by Matthews and Rawlings [116] who describe the last two as **interactive** criteria.

Limit Criteria

The Maximum Stress Theory compares each stress component acting on a lamina along the principal material axes to the corresponding strength in that direction. The theory stipulates that failure is deemed to have occurred if at least one stress component exceeds its corresponding strength. This criterion is expressed as follows:

$$\sigma_1 = \begin{cases} F_{1t} \text{ when } \sigma_1 > 0 \\ -F_{1c} \text{ when } \sigma_1 < 0 \end{cases}$$

$$\sigma_2 = \begin{cases} F_{2t} \text{ when } \sigma_2 > 0 \\ -F_{2c} \text{ when } \sigma_2 < 0 \end{cases}$$

$$|\tau_6| = F_6$$

Equation 1

where (σ_1, σ_2, τ_6) is the lamina state of stress resolved along the principal material axes and:

F_{1t}, longitudinal tensile strength

F_{1c}, longitudinal compressive strength

F_{2t}, transverse tensile strength

F_{2c}, transverse compressive strength

F_6, in-plane shear strength

The criterion can easily be expressed for a 3D state of stress by adding sub-criteria for the through-thickness tensile stress (σ_3) and the two remaining out-of-plane shear stresses (τ_4, τ_5).

.

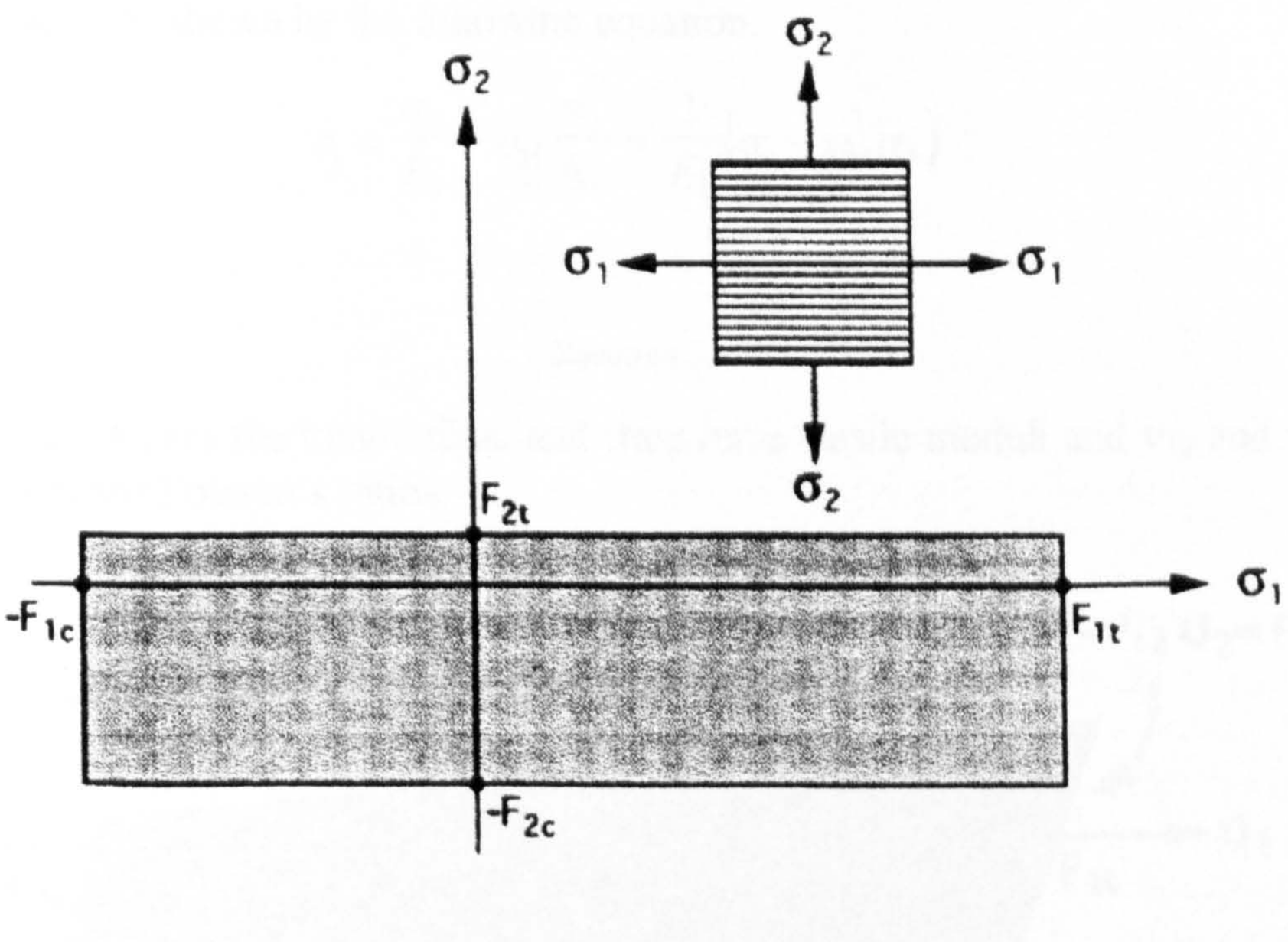

Figure 56 Maximum stress theory failure envelope for a UD lamina [118]

The failure envelope of a lamina under biaxial normal loading using the maximum stress theory is shown in Figure 56

The Maximum Strain Theory is very similar to the maximum stress theory. It states that failure occurs when at least one of the strains along the lamina principal material

directions is greater than the ultimate strain in that direction. The criterion is expressed also as a set of sub-criteria as shown above.

$$\varepsilon_1 = \begin{cases} \varepsilon_{1t}^u \text{ when } \varepsilon_1 > 0 \\ -\varepsilon_{1t}^u \text{ when } \varepsilon_1 < 0 \end{cases}$$

$$\varepsilon_2 = \begin{cases} \varepsilon_{2t}^u \text{ when } \varepsilon_2 > 0 \\ -\varepsilon_{2t}^u \text{ when } \varepsilon_2 < 0 \end{cases}$$

$$\gamma_6 = 2\left|\varepsilon_{12}\right| = \gamma_6^u$$

Equation 2

where (ε_1, ε_2, γ_6) is the lamina state of strain resolved along the principal material axes and:

ε_{1t}^u = Ultimate longitudinal tensile strain

ε_{1c}^u = Ultimate longitudinal compressive strain

ε_{2t}^u = Ultimate transverse tensile strain

ε_{2c}^u = Ultimate transverse compressive strain

γ_6^u = Ultimate in - plane shear strain

Due to Poisson's effect this theory allows for some limited interaction between the different stress components. For example, the longitudinal strain ε_1 is a function of both σ_1 and σ_2 as shown by the following equation:

$$\varepsilon_1 = \frac{\sigma_1}{E_1} - \upsilon_{21}\frac{\sigma_2}{E_2} = \frac{1}{E_1}\left(\sigma_1 - \upsilon_{12}\sigma_2\right)$$

Equation 3

where E_1 and E_2 are the longitudinal and transverse elastic moduli and ν_{12} and ν_{21} the major and minor Poisson's ratios.

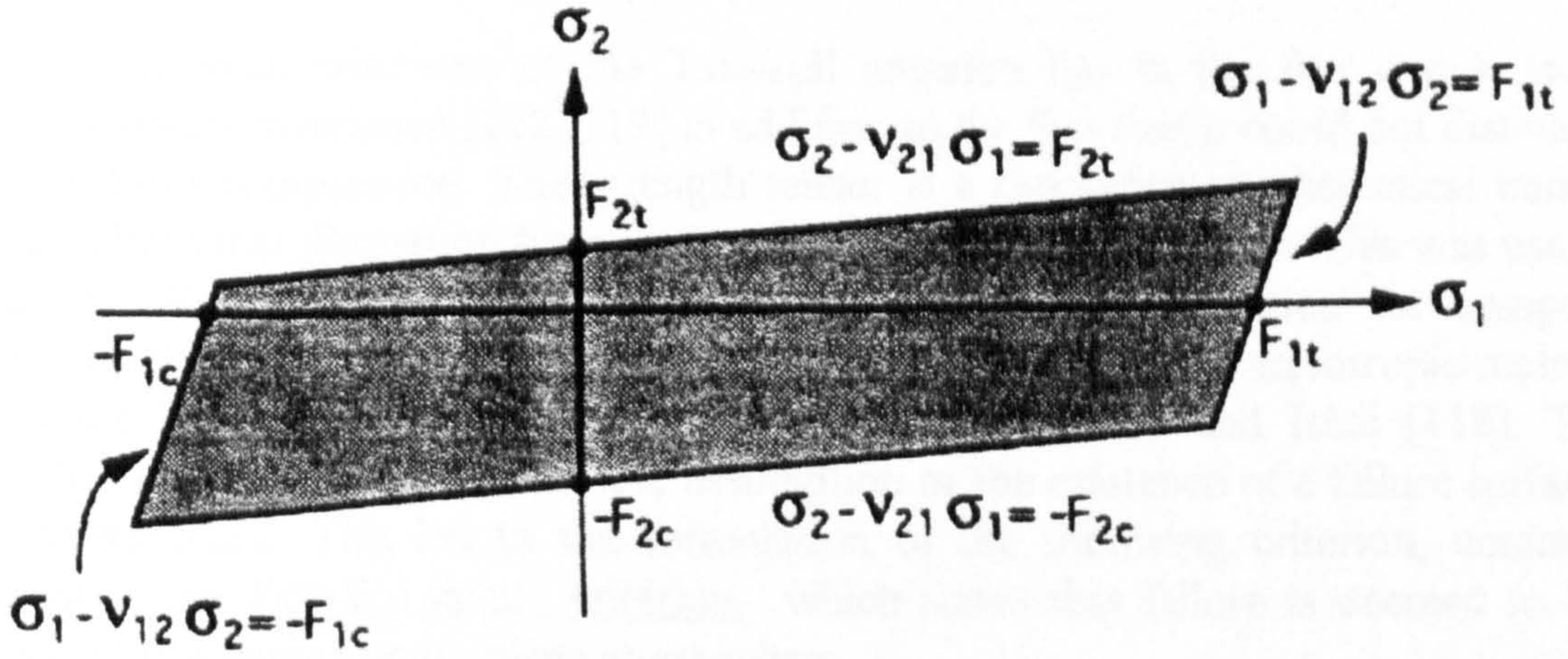

Figure 57 Maximum strain theory failure envelope for a UD lamina [118]

The failure envelope of a lamina under biaxial normal loading using the maximum strain theory is shown in Figure 57 (in the stress space).

The main attraction of the limit criteria is that they are simple to use. However, their agreement with experimental data is good only for fibre angles close to 0° or 90° [116]. This is due to the fact that for lamina with intermediate fibre angles, the two direct stress components can both be significant and thus interact with each other. Also because linearity is assumed in the development of these theories, the two failure criteria will give different answers when the stress-strain response is non-linear (e.g. lamina loaded in shear). In those situations, the maximum strain criterion is more accurate.

Interactive Criteria

These criteria have been devised to account for the interaction between the different stress components.

The Tsai-Hill failure criterion is one of the most widely used criteria because it has proved successful in a wide variety of situations. Its origins go back to von Mises distorsional energy yield criterion for ductile metals which was adapted by Hill to account for anisotropy in ductile metals. The failure criterion is given by:

$$\left(\frac{\sigma_1}{F_1}\right)^2+\left(\frac{\sigma_2}{F_2}\right)^2+\left(\frac{\tau_6}{F_6}\right)^2-\frac{\sigma_1\sigma_2}{F_1^2}\geq 1$$

Equation 4

where F_1 and F_2 are selected from the longitudinal and transverse strengths in accordance with the sign of the corresponding stress (i.e. tensile strength for tensile stress and compressive strength for compressive stress).

This criterion does not explicitly distinguish tensile strengths from compressive ones. However, it does offer a direct correlation between the criterion and the stress state required to cause failure. Furthermore, failure can now be predicted using a single equation rather than three or five subsets for the limit criteria. The relative magnitude of the terms in the failure equation can be used as a guide to determine the dominant failure mode.

One of the main criticisms of the Tsai-Hill criterion lies in the fact that it lacked strength tensor invariance [122, 119] in addition to the fact that it could not distinguish tension from compression. The strength tensor is a theoretical mathematical concept which allows transformation from one co-ordinate system to another. This was used by Tsai and Wu [122] in their proposition for a new failure criterion for composite materials. Their work modified an early general failure theory for anisotropic materials discussed by Goldenblat and Kopnov according to Daniel and Ishai [118]. Their modification was underpinned by the assumption of the existence of a failure surface in the stress space. This led to the formulation of the following criterion, commonly known as the Tsai-Wu failure criterion, which states that failure is deemed to have occurred in a lamina under plane stress when:

$$f_1\sigma_1 + f_2\sigma_2 + f_{11}\sigma_1^2 + f_{22}\sigma_2^2 + f_{66}\tau_6^2 + 2f_{12}\sigma_1\sigma_2 = 1$$

where:

$$f_1 = \frac{1}{F_{1t}} - \frac{1}{F_{1c}} \quad ; \quad f_{11} = \frac{1}{F_{1t}F_{1c}}$$

$$f_2 = \frac{1}{F_{2t}} - \frac{1}{F_{2c}} \quad ; \quad f_{22} = \frac{1}{F_{2t}F_{2c}}$$

$$f_{66} = \frac{1}{F_6^2} \quad ; \quad f_{12} \cong -\tfrac{1}{2}\sqrt{f_{11}f_{22}}$$

Equation 5

The linear terms of the equation cater for the distinction between tension and compression. The coefficient f_{12} is an interaction coefficient which is determined under an equal biaxial tensile test. This test is not easy to perform nor is it very practical. The approximation for f_{12} in Equation 5 above often works well [118]

The Tsai-Wu criterion has the same attractiveness as the Tsai-Hill criterion because it consists of just one equation which can be easily coded. As such, it has been used widely in numerical analysis packages. However, because of the quadratic terms, there is no proportional link between applied load and the failure index when applied for laminates.

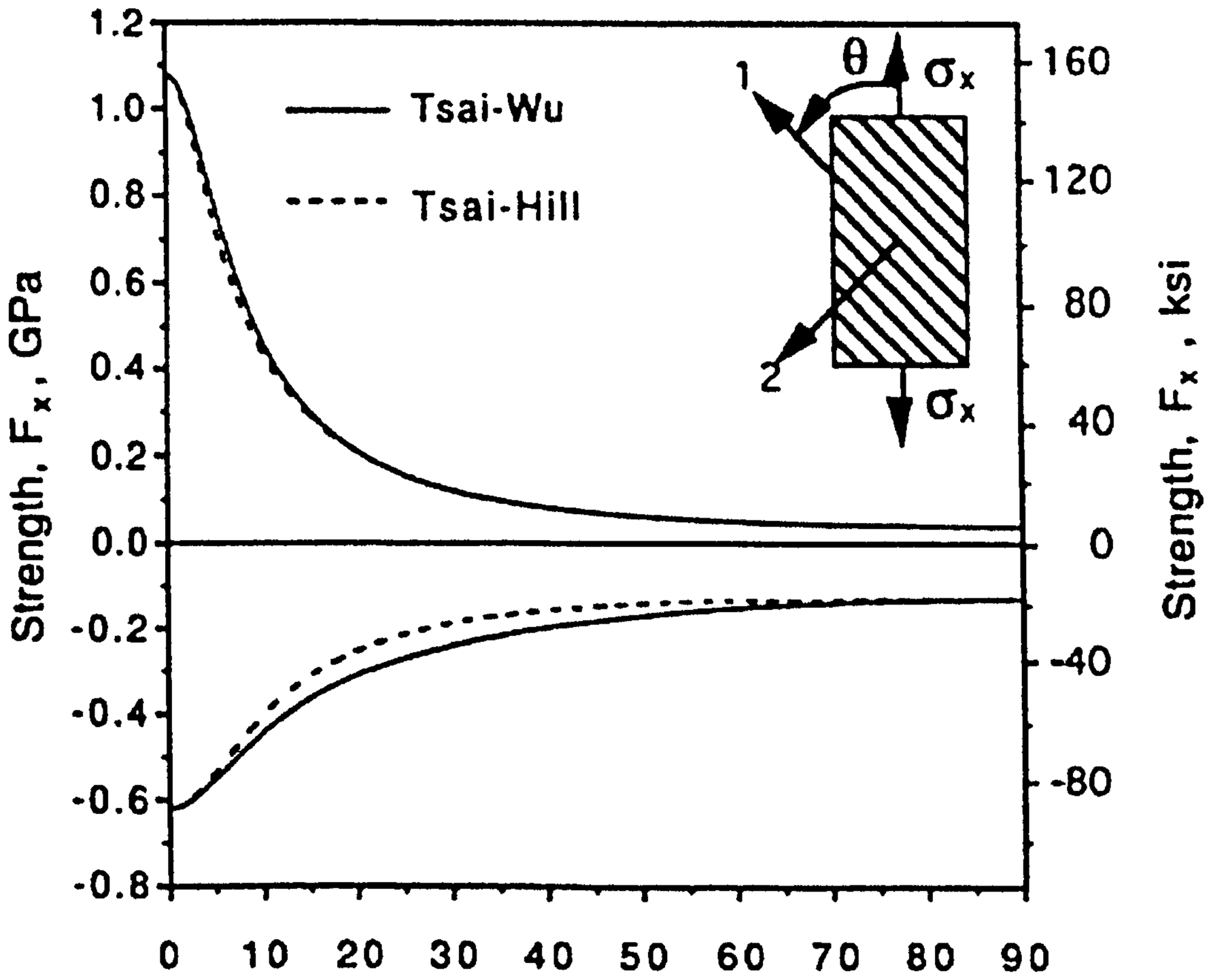

Figure 58 Comparison of Tsai-Wu and Tsai-Hill failure criteria [118]

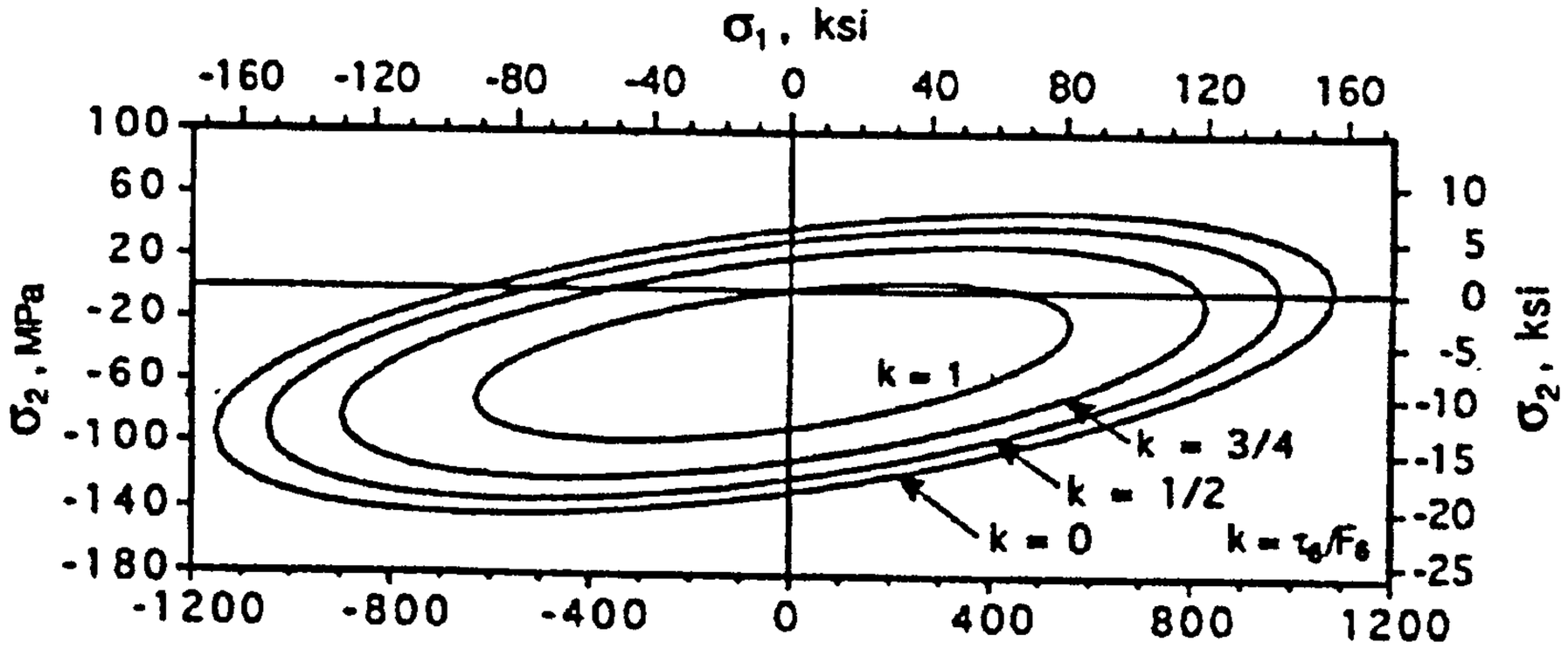

Figure 59 Tsai-Wu failure envelope for a UD lamina [118]

Both criteria are represented in the (σ_1, σ_2, τ_6) stress space by a closed surface. They are compared in Figure 58 through the predicted uniaxial strength of an E-glass/epoxy UD lamina loaded off-axis. The strength is given as a function of the fibre angle,θ. The Tsai-Wu failure envelope for the same lamina under biaxial loading is shown in Figure 59 for various shear stress levels.

The Tsai-Wu criterion as defined above is really an approximation of the general tensor polynomial failure criterion for anisotropic materials advocated by Tsai and Wu [122]. It was shown by Tennyson *et al.* [123] to overestimate failure strength and by Tennyson and Elliott [124] to underestimate it by as much as 30%-40% under biaxial compression loading for example. One way of improving the strength prediction with a tensor polynomial failure criterion, is to use higher order polynomials.

Such an approach was proposed by Tennyson *et al.* [123] using cubic tensor polynomials rather than quadratic ones. This criterion was shown to produce better agreement with experimental data. However, this came at the cost of requiring more strength data than for the Tsai-Wu criterion. In addition, the failure surface predicted by the method was not always closed and thus 'infinite' strength could be predicted, especially in the compression-compression quadrant of the stress space [125]. Jiang and Tennyson [126] refined this criterion further by including requirements that would ensure the closure of the failure surface. This is done in terms of non-intersecting asymptotes and an asymptotic plane. Clearly the full explanation of this method is beyond the scope of this review but it can be noted that these requirements for closure although necessary, further complicate an already complicated criterion, needing additional test data on top of an already long list of tests. Thus, although this criterion improves failure predictions the associated increase in testing and complexity makes it unattractive to use.

4.1.1.2 - Inconsistencies of Interactive Failure Criteria

One of the great drawbacks of the much used interactive criteria, exemplified by the Tsai-Wu criterion, is that they lack any connection between failure predictions and physical phenomena. A fact acknowledged by some of the leading proponents of these theories [127]. This has been the biggest criticism of the interactive theories which, according to Hart-Smith [127] are better suited to characterise *homogeneous* anisotropic solids (e.g. rolled metallic plates or extrusions) than *heterogeneous* fibre-polymer composites.

To illustrate some of the difficulties of the interactive criteria, one can consider the case of the interactive coefficient f_{12} (Equation 5) which is determined by biaxial failure tests. Hashin [128] argued that there was no guarantee that different biaxial tests (e.g. tension-tension, compression-compression, tension-compression) would give the same value for this interactive coefficient or that these values would be similar. Furthermore, he noted that Pipes and Cole [129] found that f_{12} had greatly different values for the different fibre orientations used in the their off-axis tests.

Even assuming that a correct value has been found for the interactive coefficient, there are further inconsistencies between predicted results and what is physically acceptable such as in the case of predicted failure for the following biaxial tensile state of stress described by Hashin [128]:

$$\sigma_1 = \sigma;\ \sigma_2 = \alpha\sigma;\ \tau_6 = 0$$

where α is a real number and σ is to be determined

Equation 6

Substituting the above equation into Equation 5 gives the following expression which can then be solved for σ.

$$a\sigma^2 + b\sigma - 1 = 0$$

Equation 7

where

$$a = f_{11} + \left(f_{22} + 2f_{12}\right)\alpha^2$$

$$b = f_1 + \alpha f_2$$

Equation 8

Hence, from the quadratic Equation 7, the biaxial stress state at failure is (σ, $\alpha\sigma$) where:

$$\sigma = \frac{-b + \sqrt{b^2 + 4a}}{2a}$$

Equation 9

The coefficients a and b are defined as in Equation 8. Now given the definition of the coefficients in the Tsai-Wu criterion (Equation 5), the expression in Equation 9 indicates that the failure stress state for this biaxial test is dependent on both tensile and compressive lamina strengths. This, in turn, implies that failure under biaxial tensile loads depends on the lamina compressive strengths. Such an implication is physically unrealistic. The same absurd conclusion can be drawn for a biaxial compressive test.

These objections to the Tsai-Wu failure criterion point to the conclusion that, whatever the form used to describe it, a physically acceptable failure criterion for composite materials cannot be represented in the stress (or strain) space by a continuous differentiable smooth curve. Furthermore, each section of the failure surface must correspond to one distinct failure mode.

4.1.1.3 - Physically Based Failure Criteria

This category includes all the theories which have been put forward to remedy the perceived shortcomings of the interactive failure criteria, based on the fundamental idea that any acceptable failure theory should reflect somehow experimentally observed phenomena.

Despite a growing number of publications exposing the shortcomings of interactive criteria and the realisation of the need for more physically based criteria, the literature on these criteria is not abundant as far as the proposition for new mechanistically derived theories is concerned. This was due to the fact that, although the anomalies reported above were noticed fairly early on, it took a long time to convince the most influential experts in the composite community [127, 128]. As such, reported studies in this area are fairly recent.

Two main paths have been proposed independently: one by Hart-Smith [130] which is based on the maximum shear stress failure criterion (also known as Tresca criterion) defined in terms of strains and the other based on fracture surfaces (also known as Hashin-Puck Action-Plane Strength criterion [131]). Both are described in the following sections.

Hashin-Puck Action Plane Strength Criterion

Hashin has been one of the first researchers to question the validity of some of the well known interactive failure criteria and to advocate that separate failure modes for fibres and matrices should be included in any failure criterion. He proposed with Rotem in [132] the representation of the failure criterion of a unidirectional fibre composite in a piecewise smooth form, with each smooth section representing a particular failure mode. This was done for fatigue failure prediction of composite laminae under plane stress. This work was extended to a three-dimensional stress state in [128].

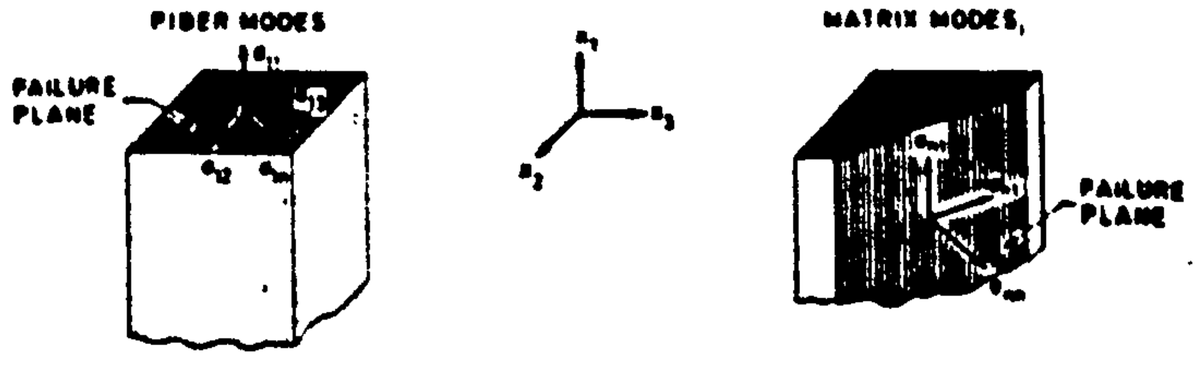

Figure 60 Composite failure modes [128]

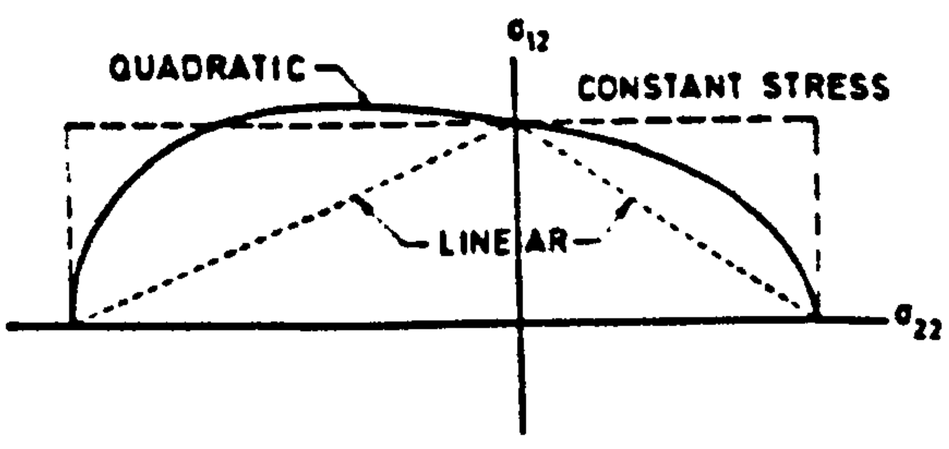

Figure 61 Approximated failure surfaces [128]

Hashin's approach is based on the identification of separate failure modes for fibres and matrix (as illustrated in Figure 60) and the expression of the appropriate failure

criterion for each mode in terms of quadratic stress polynomials giving rise to a piecewise failure surface of the type shown in Figure 61 along with other possible approximations.

Four failure modes (tension & compression for both fibre and matrix) were considered. Hashin's analysis was presented with a great insight into the various stresses affecting each of these modes. Some of the assumptions needed for a consistent and logical set of criteria could not be verified due to lack of experimental data and computational capabilities. This lead to the formulation of simplified criteria for the fibre compressive, the matrix tensile and compressive failure modes. For the case of a lamina under plane stress conditions, these criteria are given by:

Tensile fibre mode	$\left(\frac{\sigma_1}{F_{1t}}\right)^2+\left(\frac{\tau_6}{F_6}\right)^2=1$	$\sigma_1>0$
Compressive fibre mode	$\sigma_1=-F_{1c}$	$\sigma_1<0$
Tensile matrix mode	$\left(\frac{\sigma_2}{F_{2t}}\right)^2+\left(\frac{\tau_6}{F_6}\right)^2=1$	$\sigma_2>0$
Compressive matrix mode	$\left(\frac{\sigma_2}{2F_5}\right)^2+\left[\left(\frac{F_{2c}}{2F_5}\right)^2-1\right]\frac{\sigma_2}{F_{2c}}+\left(\frac{\tau_6}{F_6}\right)^2=1$	$\sigma_2<0$

where F_5 is the transverse shear strength

Equation 10

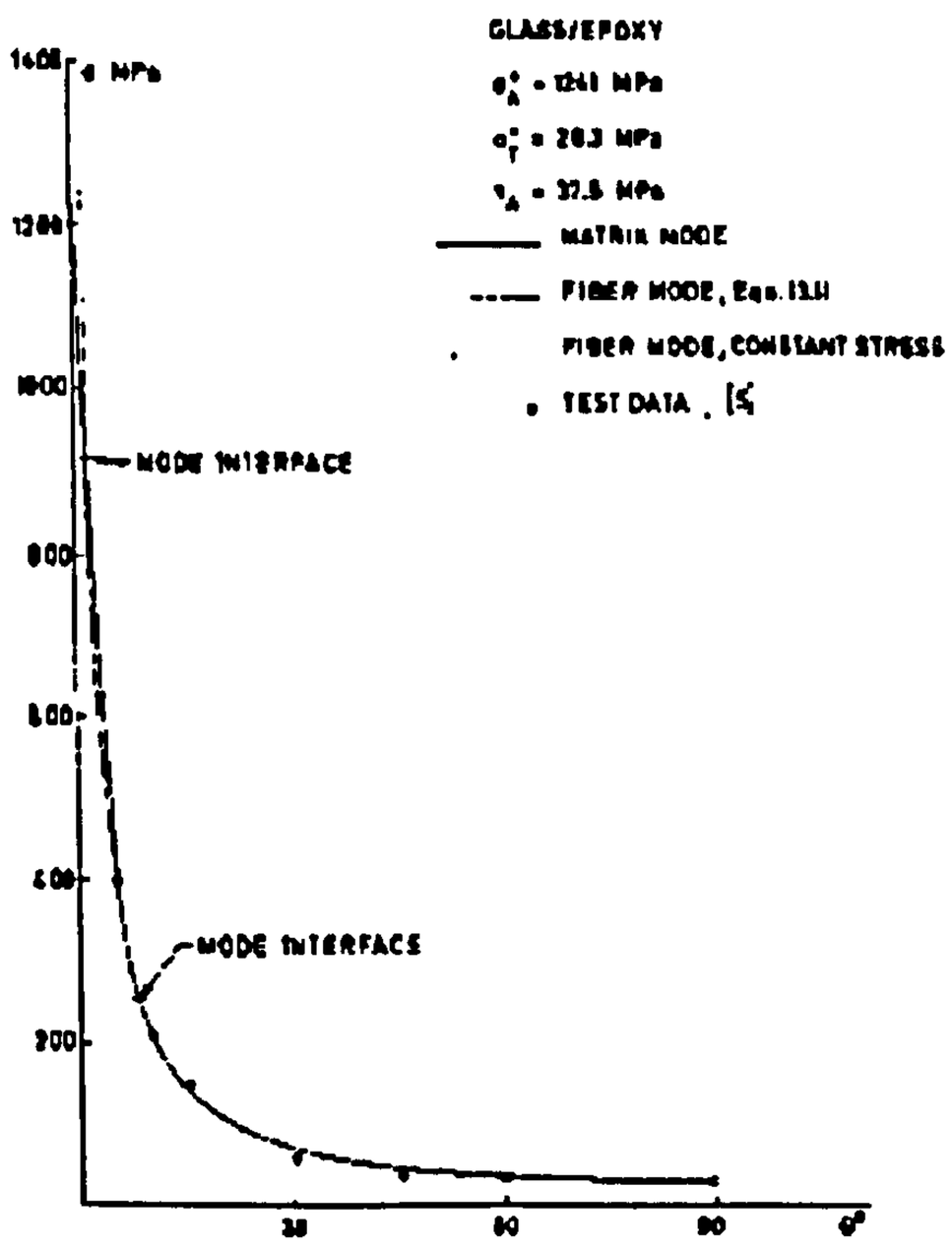

Figure 62 Comparison of with glass-epoxy off-axis test specimens [128]

Comparison with experimental data obtained from off-axis test on boron-epoxy and glass-epoxy specimens showed very good agreement (given some of the

approximations used for the matrix failure modes). The glass-epoxy results are shown in Figure 62.

One of the implications of the quadratic approximations used for the matrix failure modes is that matrix failure always occurs on the maximum transverse shear plane. Such a statement cannot hold for all stress states (e.g. for a stress state where in-plane shear is the dominant component, the failure plane orientation is likely to be governed by the direction of the maximum in-plane shear). Despite these shortcomings, Hashin's work [128] provided the first real step towards more physically acceptable failure criteria for composite materials.

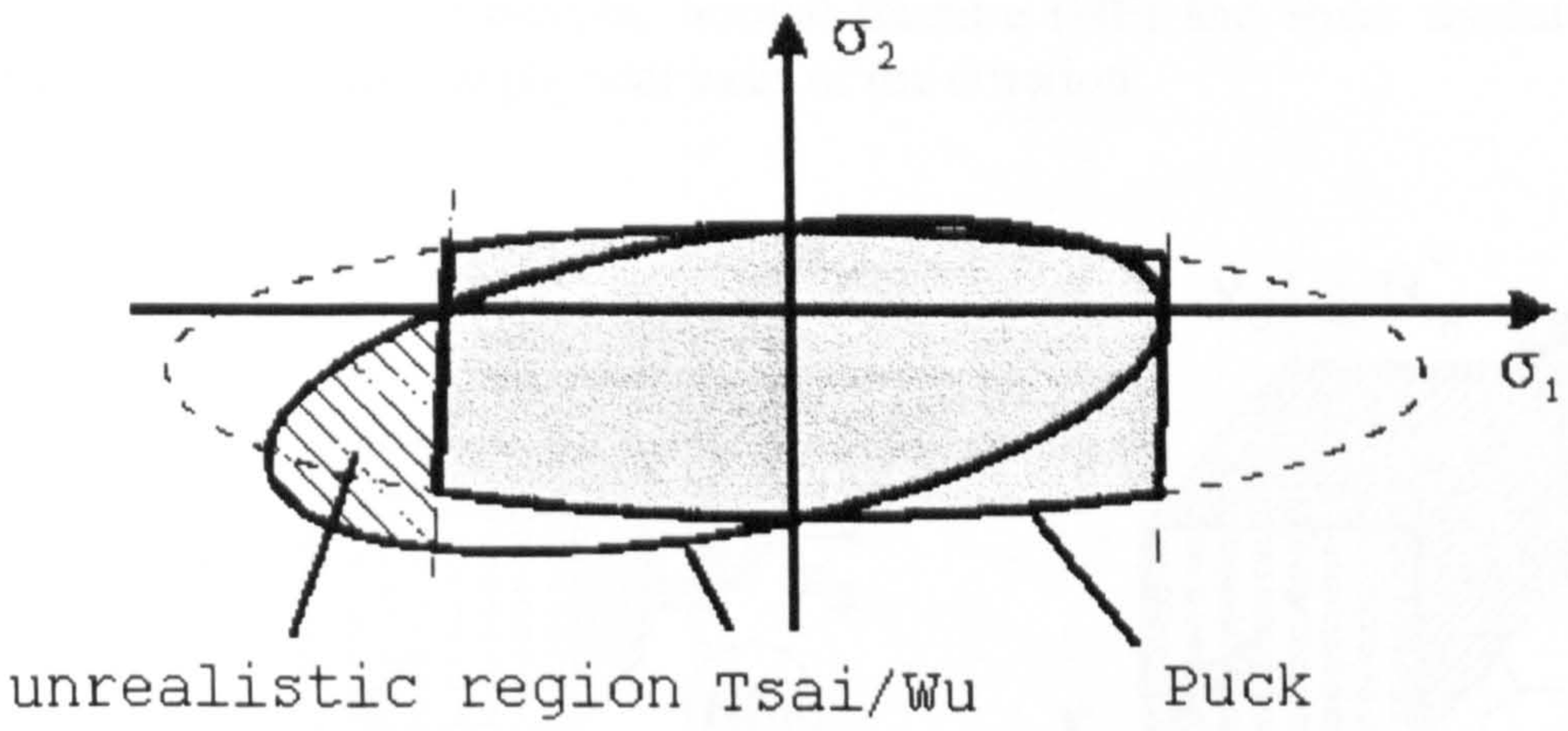

Figure 63 Schematic comparison between the Puck and Tsai-Wu criteria [135]

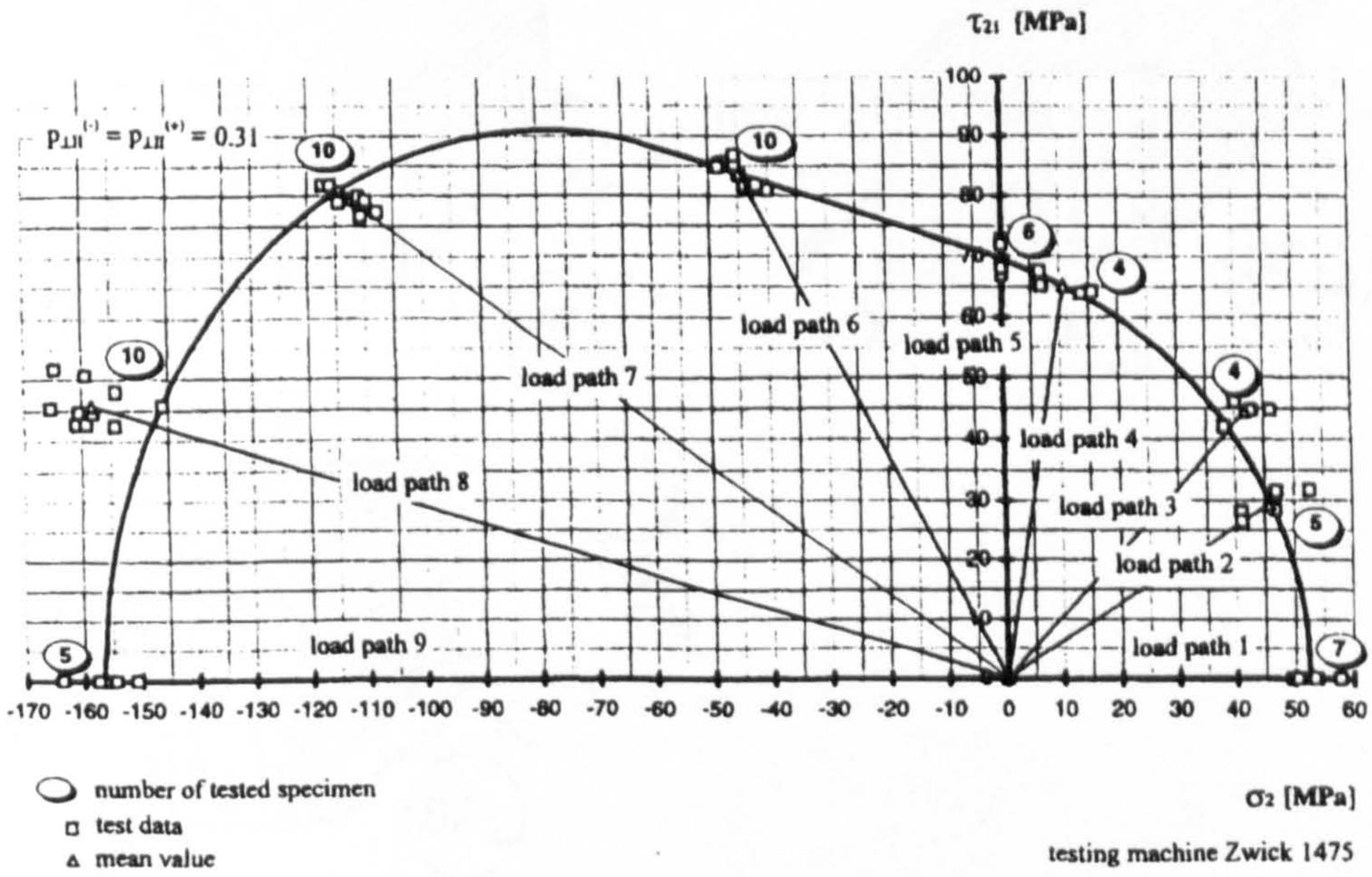

Figure 64 Comparison of tension/compression-torsion test results with theoretical predictions [135]

The work by Hashin [128] was improved by Puck in [133] who in 1969 [134] had noted two fundamental failure modes for composite materials which required two distinct failure criteria: fibre fracture (or FF, corresponding to Hashin's fibre failure modes) and inter-fibre fracture (or IFF, corresponding to Hashin's matrix failure

modes). Puck fully developed Hashin's original fundamental hypothesis and improved the results by proposing two theorems for inter-fibre fracture. The advent of better computing capabilities allowed Puck to confirm Hashin's hypothesis. The resulting failure criterion is shown in comparison with Tsai-Wu criterion in Figure 63.

The Hashin-Puck criterion was applied and experimentally verified for thick-walled laminates by Kroll and Hufenbach [135]. Results from tension/compression-torsion tests are shown in Figure 64 against the prediction from the Hashin-Puck criterion. These results confirm the maturity of this new criterion.

Cunzte proposed a new fracture-type failure criterion [136] which was based on the approach formulated by Hashin [132] and Puck [133]. The two fundamental failure modes (fibre fracture FF and inter-fibre fracture IFF) were further broken down with respect to two fracture-types: normal fracture (NF) and shear fracture (SF). These fracture-types form the physical basis of the criterion.

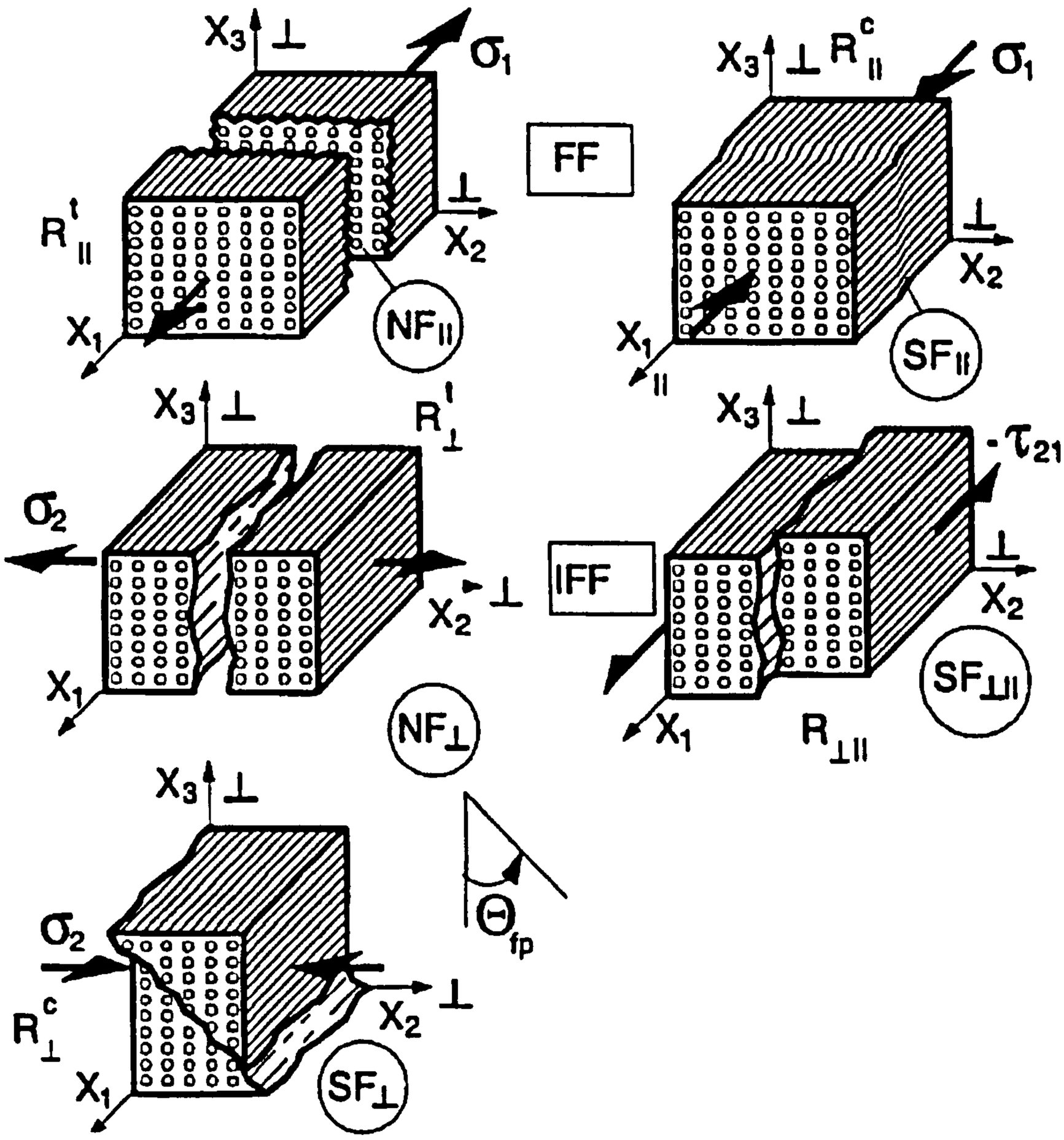

Figure 65 Fracture modes for transversely-isotropic material [131]

For a transversely isotropic material, such as a UD lamina, this gave rise to five distinct fracture modes(Figure 65).

The initial failure surface was piecewise smooth, with each branch representing a separate failure mode. Each failure mode was characterised separately and expressed in terms of the stress invariants associated with the material symmetries.

The transition between each failure mode was modelled by probabilistic means. Cuntze has shown [131] that this leads to a better fit with experimental data. Correction factors could be used if full probabilistic smoothing out of the basic failure envelope was not an option.

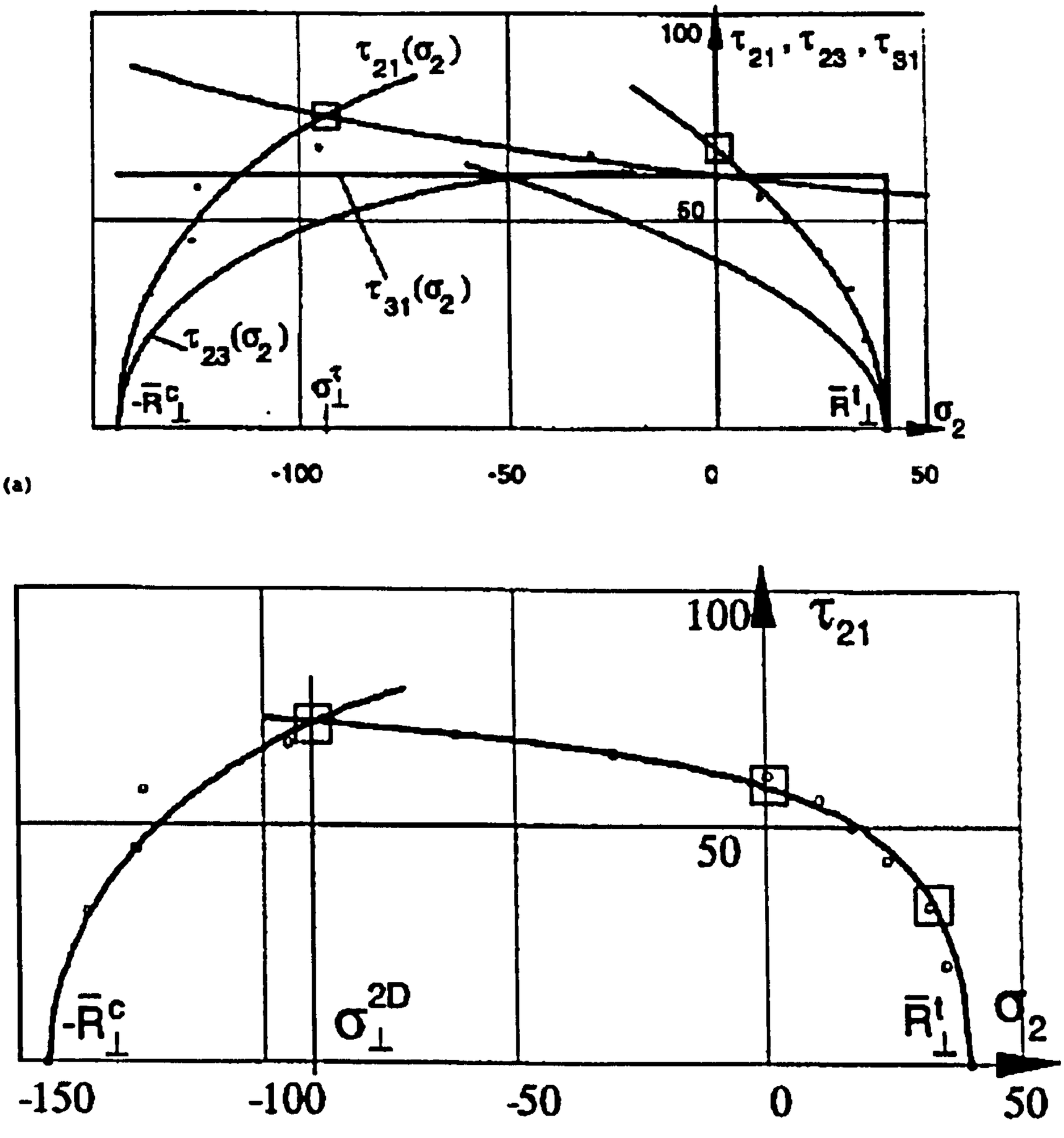

Figure 66 Comparison of Cuntze criterion with experimental results for a UD glass-epoxy lamina[131]: (a) 3D stress state (b) 2D plane stress approximation

Hart-Smith Failure Criterion

This failure criterion is based on the maximum shear stress criterion used for isotropic material such as ductile metals. It has been reformulated for transversely isotropic fibres (such as carbon fibres) in terms of strains rather than stress as done traditionally [130] with each section corresponding to a particular fibre failure mode. This constituted the basic shear envelope. Hart-Smith then proceeded to superimpose other failure modes such fibre compressive instability and brittle fracture onto the basic shear envelope.

The fibre strains were then converted into equivalent lamina strains in order to allow the characterisation of fibre failure modes on the lamina strain plane and ply by ply failure analysis. This conversion also enabled the inclusion matrix failure modes if required.

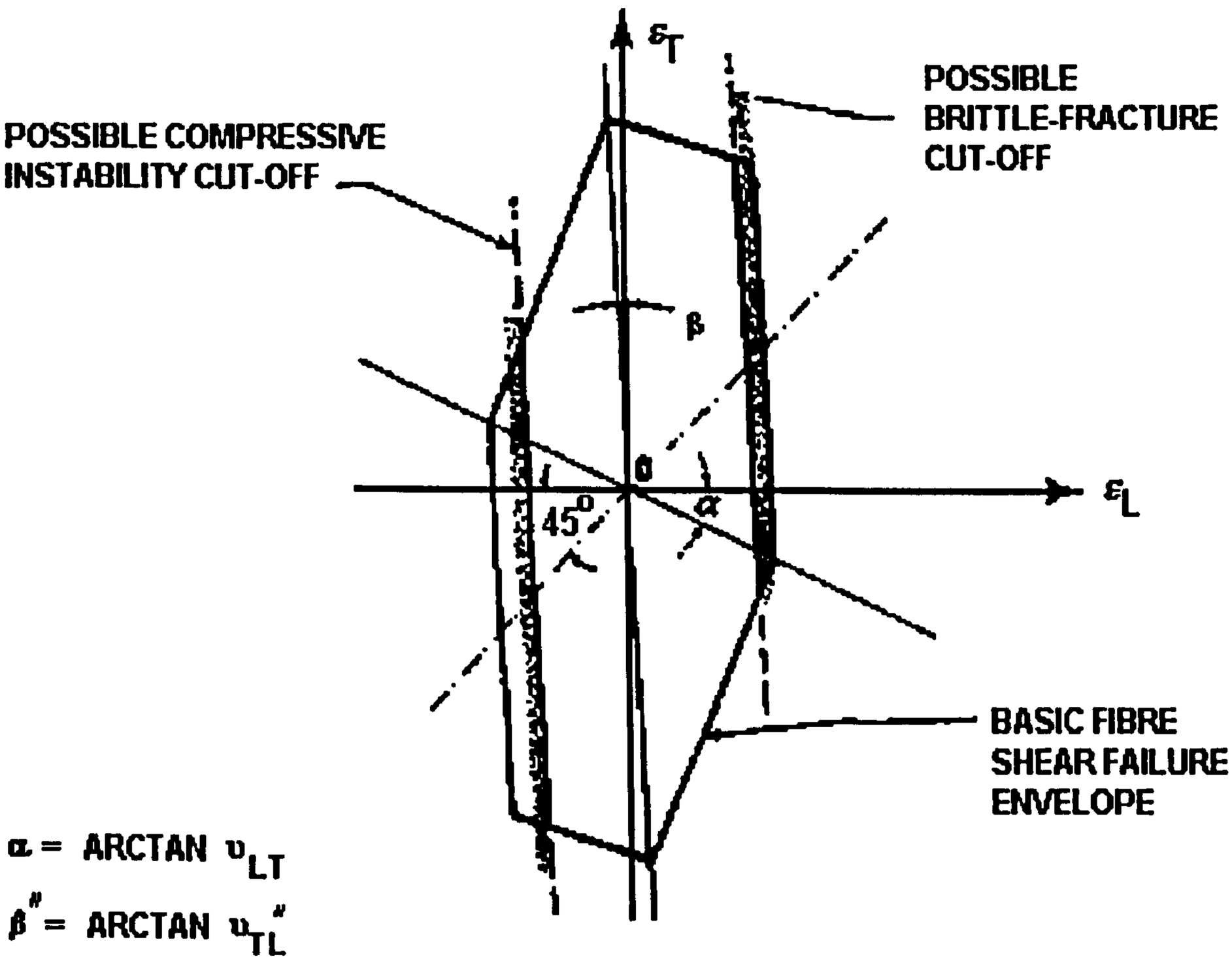

Figure 67 Fibre-failure envelope at lamina level [127]

The resulting fibre failure envelope is shown in Figure 67.

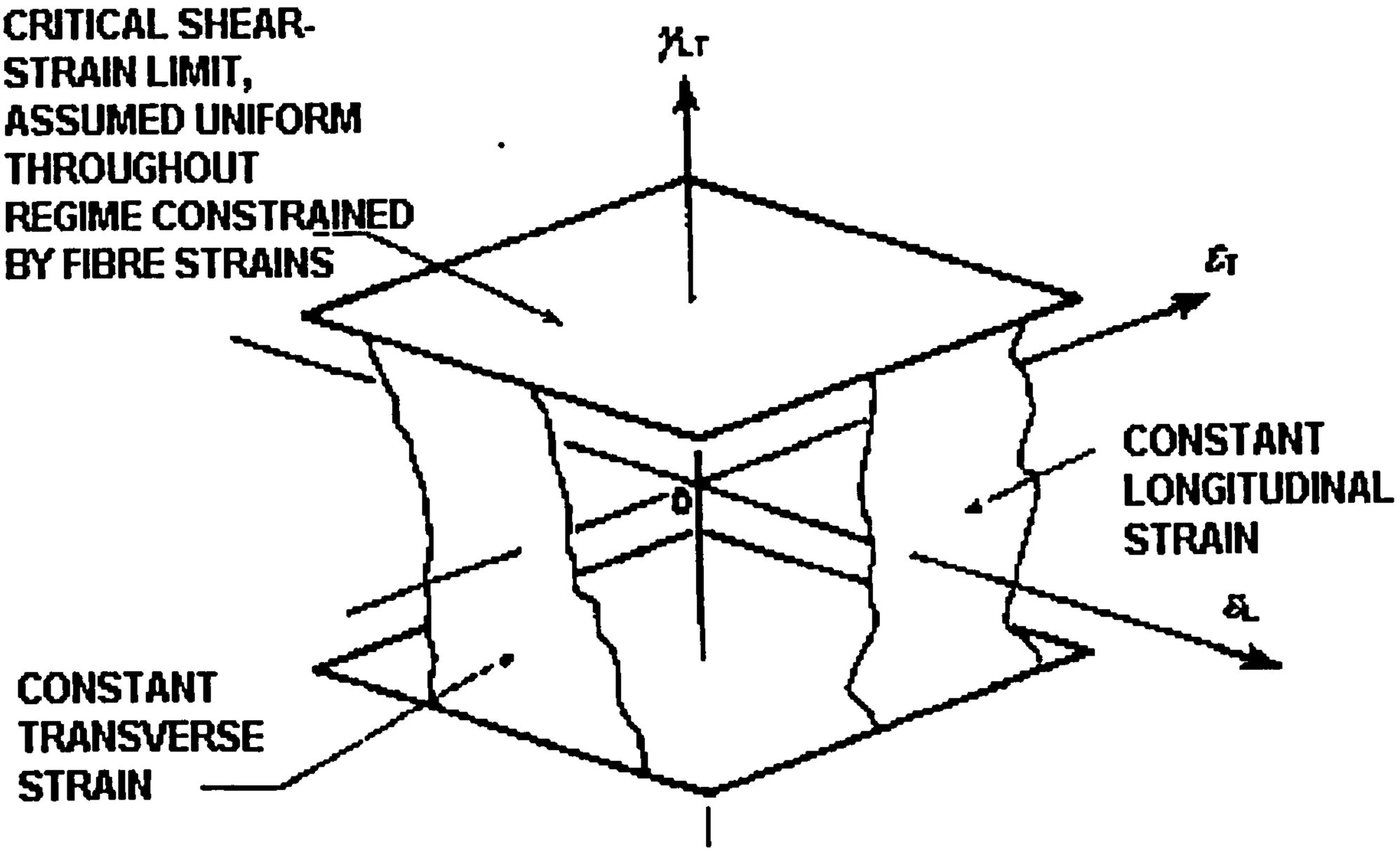

Figure 68 Matrix shear failure for polymer composites [127]

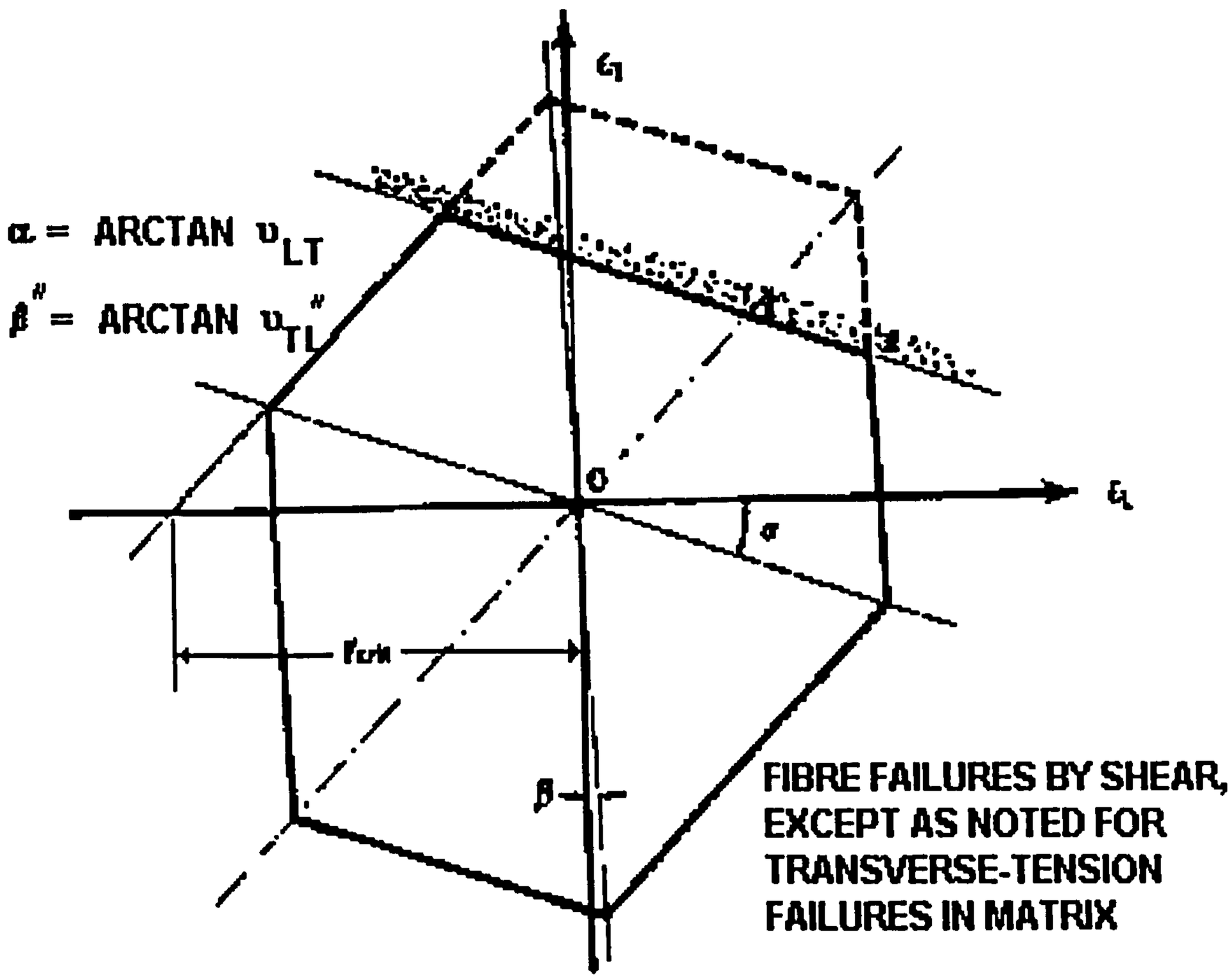

Figure 69 Matrix cracking on the lamina strain plane [127]

Although he discussed the main matrix failure modes such as in-plane shear between fibres and matrix cracking and how they can be incorporated into the strain space (Figure 68 and Figure 69 respectively), Hart-Smith argued that for most carbon-epoxy laminates used in the aerospace industry, matrix failures should be ignored [127]. This

stemmed from the fact that for these composite laminates, failure was almost always fibre dominated

Thus, the Hart-Smith criterion is best suited to composites which have fibre dominated failure modes. This category, according to Hart-Smith [127], includes all practical laminates. As such, this main limitation was not significant. However, Curtis [121] remarked that delamination which is a matrix dominated could reasonably be considered of real importance in real composite structures.

Compared to the Hashin-Puck family of failure criteria, it can be argued that Hart-Smith criterion lacks general applicability to all polymeric composites. Furthermore, with the use of fracture planes in the Hashin-Puck criteria, it can be speculated that delamination could be included as additional matrix failure mode.

4.1.1.4 - Implementation in NISA/DISPLAY FEA Package

In NISA, the composite module written in the early 1990s offers only classical failure criteria. The maximum stress criterion and both Tsai-Hill and Tsai-Wu interactive failure criteria are available. However, their availability is linked to the element types used. For the 3D composite element (NKTP-7 in NISA), the Tsai-Wu failure criterion only is available. For the 3D composite sandwich element (NKTP-33), it is the maximum stress criterion only which can be used. All three criteria are available for the 3D composite shell element (NKTP-32).

For the maximum stress criterion, each of the stress components is compared to the corresponding UD allowable strength as a ratio. For example, the ratio RXX is given by the ratio of longitudinal stress SXX over the longitudinal strengths FXT or FXC depending on the sign of SXX i.e.:

$$RXX = \frac{SXX}{FXT} \text{ for } SXX > 0$$

$$RXX = -\frac{SXX}{FXC} \text{ for } SXX < 0$$

Equation 11

The remaining ratios (RYY, RZZ, RXY, RYZ, RZX) are defined in a similar manner.

Given the available failure criteria, only first ply failure of structures can be predicted in NISA.

4.1.1.5 - Concluding Remarks on Composite Failure Criteria

It is impossible at this stage to indicate which failure theory works best. This is a task being currently carried out by a team at the *Composites Science and Technology* journal [127] in collaboration with nearly forty researchers which have proposed failure theories in the past.

While there is no doubt over the shortcomings of the interactive failure criteria, they have been used successfully in various conditions even with woven fabric composites [137, 138]. The Tsai-Wu criterion is elegant and easy to use while appearing to be mathematically complete, hence the widespread use. However, the possibility exists that the interactive failure criteria are successful for all the wrong reasons.

Physically based criteria offer a sound basis for further development in our understanding of composite materials. The fact that they can relate predicted results to experimentally observed failure modes is a great benefit. However, they remain fairly complex in nature and have not been fully tested experimentally but they do offer the best prospect of integrating full progressive damage analysis into composite failure analysis in FE packages.

4.1.2 - Adhesives in Structural Joints

The literature on the prediction of failure of adhesives used in structural joints is extensive. This review does not aim to be exhaustive but to explore critically the main aspects of the literature on adhesive failure criteria with an emphasis of their use in finite element analysis and their application to bonded composite repairs. The majority of relevant documents used in this section of the appendix have been gathered by Adam Towse and Andrew Clarke from the University of Bristol (UK) whose help is gratefully acknowledged.

4.1.2.1 - Failure Criteria

Most failure criteria for structural adhesives were devised during the study of adhesive bonded joints. They can be grouped into the following categories:

(i) maximum stress or strain criteria
(ii) critical stress or strain at a distance or over a zone
(iii) limit state criteria
(iv) fracture mechanics criteria
(v) damage mechanics criteria

The first type can be called also maximum value criteria and type (ii) finite zone criteria.

Maximum stress or strain criteria

This is by far the biggest category of failure criteria for structural adhesives. Those used in finite element analysis have evolved naturally from close form analysis criteria.

For example, in the shear lag analytical model as described by Volkersen [68] and Goland and Reissner [69], the adhesive was assumed to deform in shear only. It becomes natural to consider the maximum shear stress in the prediction of joint strength. Such an approach was used by Greenwood *et al.* [139] on single lap joints. They found that the maximum shear stress occurred in the adhesive at 45° to the loading direction. Their strength predictions overestimated the joint experimental strengths.

Using continuum mechanics, Hart-Smith showed the maximum peel stress could be used as a failure criterion for single lap joints [140]. This was also used by Crocombe and Tatarek [110]. This criterion could only be applied to a limited number of joint configurations and its effectiveness was further limited if the adherends yielded. And this yielding has been shown to occur in single lap joints by Adams and Panes [141]. Hart-Smith recommended however that peel should be minimised by design rather than be used as a design limit on the strength of bonded joints [60]. Thus the maximum peel stress should not be used as a failure criterion for most joint configurations.

Given the limitation of closed form analysis, the finite element method became the most widely used analysis method to investigate adhesive bonded joints following the pioneering work of Adams and co-workers [80, 85, 86]. Harris and Adams [142] stipulated that any realistic prediction method for single-lap joint strength should take into account at least the non-linear large displacement joint deformations and the non-linear behaviour of both adherends and adhesives on top of the variations through the glueline thickness and the geometry of the adhesive spew fillets.

The maximum principal tensile stress and maximum principal tensile strain criteria were used successfully by Harris and Adams [142] to predict the failure of single lap joints. These quantities were selected because the non-linear analysis of the critical regions revealed that their conditions were dominated by tensile principal stresses. The predicted strengths were within 10% of the experimental results. However, there was no rule as to which criterion to use with a particular adhesive but the choice seemed dependent on particular joint configuration. The maximum principal stress criterion fared well with highly ductile adhesives where the strain criterion would have intuitively been expected to be more appropriate.

Using the same set of criteria on cleavage and compressive shear test specimens, Crocombe *et al.* [143] found that the maximum principal stress criterion was more appropriate for brittle untoughened epoxy adhesives. For thoughened epoxy adhesives, this criterion was better for mode I loading and the maximum principal strain for mode II loading.

It was shown subsequently by Adams and Harris [85] that the maximum principal stress could be mesh dependent if a stress singularity was present. That would lead to erroneous predictions if the criterion was applied at the singularity. In fact in [142], the criterion was applied at the integration point (Gauss point) which was located at a small distance from the singularity. One could argue in fact that a critical stress at a distance was applied rather than a true maximum stress criterion, hence the good agreement with experimental results.

Ikegami *et al.* [94] used the maximum von Mises stress as a failure criterion for the adhesive in their investigation of bonded scarf joints between metal and composite adherends. This criterion was not very successful because of the adhesive behaviour high dependency on the joint hydrostatic stress state which could not be accounted for in the von Mises criterion. This criterion was also found ineffective on double lap joint strength predictions by Charalambides *et al.* [144].

Other possible criteria include the maximum shear strain criterion as used by Lee and Lee [145] in their study of tubular single lap joints and the effective uniaxial plastic strain by Crocombe and Adams [146] for peel test specimens where the triaxial strain was expressed as an effective uniaxial strain and compared to the bulk adhesive strain to failure.

For all the maximum stress or strain criteria described, the problem comes from the maximum value of the failure parameter considered. A bi-material wedge was shown by Bogey [147] to give rise to a singular strain distribution. As such, there will always be a singularity at the ends of idealised bonded joints. The maximum strain for such a model will coincide with the value at the singularity and thus will vary greatly with mesh refinement. If local rounding is used to remove the singularity as was done by

Harris and Adams [85], the problem is shifted toward deciding how much rounding to use in order not to affect the joint strength [148]. Knowledge of the exact end shape becomes then essential for accurate strength predictions.

Critical stress or strain at a distance or over a zone

To overcome the mesh dependency of the previous category of failure criteria, several researchers have resorted to the application of these criteria at a particular distance from the singularity or over a given zone.

Zhao [149] proposed a weighted averaged maximum stress criterion where the adhesive thickness is used as the distance over which the maximum principal stresses are averaged and compared to the adhesive yield strength. Charalambides *et al.* [92] showed that for double lap joints, the location of the maximum stress occurs further down the fillet edge, outside the averaged zone.

Clark and McGregor [87] developed a criterion similar to Zhao's [149] which stated that for failure to occur, the maximum principal stress must exceed the ultimate tensile stress of the adhesive over a finite zone (UTS over a zone), measured normal to the direction of maximum principal stress. The criterion applied to three different joints (single lap, double strap and T-peel joints) produced good agreement with experimental results. The zone size was also found to be independent of joint geometry but required some experimental calibration. Although, the UTS over a zone criterion was believed to be joint type independent, Charalambides *et al.* [144] found the predictions for double lap joints overestimated the experimental data by about 68% for long overlaps. Further problems were also found with defining what UTS value to use for the calculations.

Crocombe and Richardson [150] used critical peel stress at a distance from the singularity to predict the strength of non-cracked and cracked joints subject to mode I (opening mode) and mode II (forward shearing mode) loading. The comparison with experimental data was excellent but the criterion was found to be rather empirical. Using an effective stress at a distance, compared to the uniaxial strength of the adhesive, was less effective, especially under mixed mode loading.

Towse *et al.*[151] used a critical strain at a distance criterion on double lap joints. This criterion was used in a non-linear analysis which included also the effect of residual thermal stresses. The joint was deemed to have failed when the strain in the vicinity of the singularity reached the adhesive ultimate strain. The predictions compared well with experimental data. The same criterion was successfully used by Towse *et al.* [152] in their study of a novel comb joint. For both studies, the characteristic distance had to be determined experimentally. Although the results were very good, the required calibration of the characteristic distance put a question mark on the application of this criterion to other joints in terms of predictive capability.

One of the main difficulties in the application of this category of failure criteria is the evaluation of the characteristic distance or zone where they are applied. In the case of the UTS over a zone, there are doubts whether the zone is a truly reliable, independent feature for any joint. In most cases, the determination of the characteristic distance is not very clear (as in [150]). Using an experimental test to determine that characteristic distance appears to give very good results [151, 152] but the problem is that it becomes impossible to predict the strength of any joint which does not use the same

adherends and adhesive which was characterised. This almost defeats the purpose of being able to perform a numerical analysis.

Other Failure Criteria

Various attempts have been made to use other types of failure criterion in the search of the best criterion able to cope with any joint configuration and loading conditions. The most notable amongst those are : limit state criteria, fracture mechanics based criteria and a new concept of using damage mechanics.

Crocombe [148] proposed global yielding as a limit state failure criterion for bonded joints. The predicted results for single lap joint, double lap joint and compressive shear stress test specimens joints were in good agreement with experimental data. However, Clark and McGregor [87] pointed out that the adhesives considered were very ductile and showed little or no work hardening. These two assumptions would be invalid for rubber toughened epoxy adhesives used for bonding vehicle structures together. A point acknowledged later by Crocombe *et al.* [150].

Fracture mechanics has been a particular attraction for researchers looking for better failure criteria for adhesive bonded joints. This stems from the fact that this discipline provides the means to study structures containing flaws such as cracks and void which by their very nature are surrounded by singular stress field. The presence of a singularity at the end of idealised adhesive bonded joints suggested that fracture mechanics could be used. The evaluation of singular stress fields is done through the use of parameters such as the energy release rate G which is a measure of the energy required to advance the crack, the J-integral and stress intensity, K, which is the stress required to grow the crack length by a given length. Those parameters can be defined for each of the three opening modes: opening mode or mode I, forward shearing mode or mode II and tearing mode or mode III.

The constraints imposed by the adherends on the adhesive in a bonded joint recreates the conditions of mixed mode loading (i.e. the fracture mode is a mixture of opening and forward shear modes). Kinloch and Shaw [153] found that the energy release rate G_{IC} was controlled by the adhesive thickness using continuum fracture mechanics.

Applying the method in finite element analysis, Trantina [154] was able to investigate successfully adhesive bonded joints. Crocombe and Richardson [150] used a failure criterion based on critical opening displacement in their assessment of cracked and non-cracked adhesive joints after conventional linear fracture mechanics failed to estimate non-cracked joint strength accurately. More recently Charalambides *et al.* [144] have used a fracture mechanics based criterion to evaluate the strength of a double lap joint. The criterion used the J-integral in terms of the crack length. No other information was available on how good the predictions were.

Groth [88] pioneered the use of stress intensity at bi-material interfaces as a failure criterion. In [155] Gradin and Groth predicted failure within 10% of experimental data.

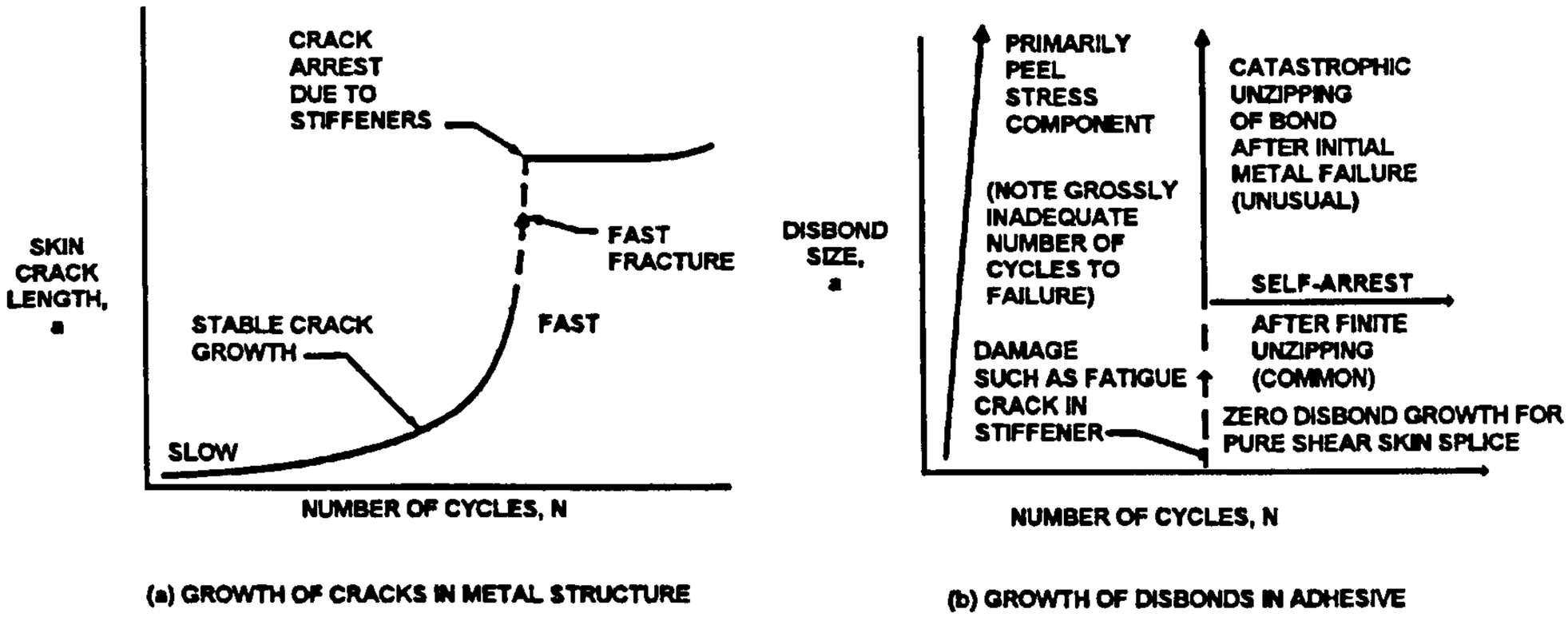

Figure 70 Crack growth in metals and adhesive bonds [156]

Although the use of fracture mechanics appears to be successful, its application to bonded joints raises some fundamental questions. Fracture mechanics was developed initially to deal with the analysis of metallic structures containing cracks. The types of cracks in metallic structures which are best handled by fracture mechanics are those which exhibit self-similar stable growth (Figure 70).

Hart-Smith [156] argued that fracture mechanics should not be used for adhesive bonded joints because the experimental observations indicated either no growth of initial flaws or catastrophic rapid growth. In addition, the actual size of the initial crack used in analysis are much bigger than anything that can be observed and thus not representative. Furthermore, Crocombe [148] noted that it was difficult to relate stress intensities to a value obtained from the bulk adhesive. Finally, fracture mechanics as such has been validate only for the most ductile adhesives and did not fare well with the most brittle ones [156].

Damage mechanics is one of the latest analysis tools being used in the assessment of adhesive bonded joints. The main idea is to use a set of laws to detect and model damage through the structures. One of the first studies have been carried out by Chow and Lu [157] who applied it to a butt joint. Although, no comparison with experimental data was made, the technique looked promising. The only drawback is that a crack was assumed present within the adhesive layer. Laschet [158] had more success using an isotropic damage model in conjunction with the material maximum principal stress/strain criterion in a finite element analysis.

4.1.2.2 - Relevance to Bonded Composite Repairs

Clearly, from the preceding paragraph, the number of possibilities in choosing a failure criterion is overwhelming. It is difficult to assess which one is the best. However, it is likely that the choice of criterion will primarily be dictated by the type of joint considered.

Table 15 Failure criteria per bonded joint types (Reference number)

Bonded Joint Types	Maximum Value Criteria	Finite Zone Criteria	Other Criteria
Single lap joint	139 140 141 142 145	87	148 158
Double lap joint	144	92 87 151	148 92
Scarf joint	94	X	X
Stepped lap joint	X	X	X
Peel Joint	146	X	X
Butt Joint	X	X	157
Others	X	87 150 152	148

Table 15 shows how the various criteria discussed above are distributed according to joint type. The single lap joint emerges as the most studied joint with the greatest number of criteria followed by the double lap joint.

The data contained in the table above have a big implication on which criterion to select for adhesively bonded repairs to composite structures. This comes from the fact that not all joint types can be used in a repair scheme. Single lap and double lap joints can be used for external repairs whilst step and scarf joints are suited for flush repairs. Thus only the failure criteria used for those joint types are relevant to bonded repairs and can be used after careful examination of the advantages and drawbacks. The rest can only be used after adaptation and if they are found relevant.

Finally, the choice of failure criterion is dependent on the repair design philosophy. If it is accepted that the repair must be designed in such a way that the adhesive is never the weak link, the selection of an adhesive failure criterion is governed essentially by the need to confirm that the adhesive will fail at a stress level well beyond that for the adherends.

4.1.2.3 - Proposed Adhesive Failure Criterion

Taking into account the main requirement of a failure criterion for bonded repairs given above, it is intended to use an average (shear) stress failure criterion (ASFC). It is an adaptation of the Brewer and Lagace criterion [159] used to determine the onset of delamination in notched composite laminates. It is a finite zone type of criterion and states that failure is deemed to have occurred when:

$$\bar{\tau}(x) = \sigma_{ys}$$

where

$$\bar{\tau}(x) = \frac{1}{d_0}\int_0^{d_0} \tau dx$$

Equation 12

σ_{ys} is the adhesive shear strength and d_0 is the characteristic distance over which the shear stress is averaged.

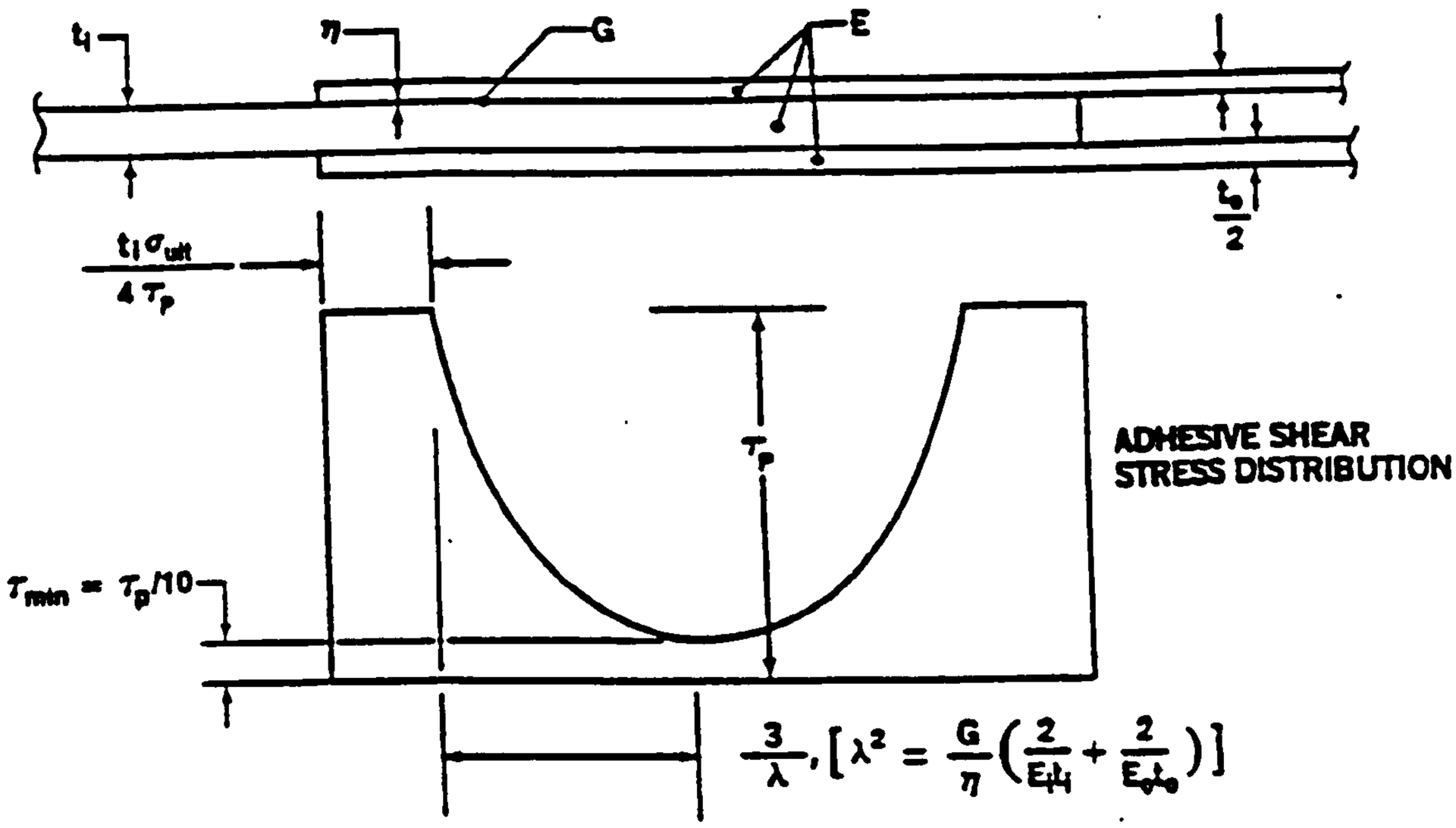

Figure 71 Double-lap joint design [156]

For an external repair, a section in the direction of loading is equivalent to a double lap joint as shown in Figure 71. The characteristic distance is set as the sum of the plastic zones which are assumed to transfer the entire strength of the adherends (following Hart-Smith design procedure for double lap joints [156]). The distance, d_0, is given by [156]:

$$d_0 = \frac{t_1 \sigma_{ult}}{2\tau_p}$$

Equation 13

where t_1 is the parent laminate thickness, σ_{ult} the parent laminate ultimate longitudinal tensile strength and τ_p, the maximum shear stress. For single material orthotropic laminates with plies laid-up in only four possible angles (0°, 90° and ±45°) and loaded uniaxially, σ_{ult} can be evaluated with Hart-Smith's refined 10% rule [160, 161, 162].

For a flush scarf repair, the characteristic distance is the joint length. This is selected because, for balanced adherends, the shear stress distribution is uniform and thus the whole joint length is considered to transfer the entire adherend strength. For unbalanced and/or thermally mismatched adherends, provided the imbalance and/or mismatch is not great, the same procedure can be followed. The predicted results are anticipated to be fairly conservative.

4.2 - Modelling Data

For this part of the work, the repaired plate only was considered. The geometric features are described along with the type of material data used in the analysis.

4.2.1 - Geometry

The geometry of the repaired panel was described extensively in Chapter 3 (p. 48). No change was made.

4.2.2 - Materials

The materials used for the models were the same as those used by Soutis and Hu. Where no information was available, an appropriate estimate of the properties was used. The parent laminate was made of HTA carbon fibres embedded in an epoxy resin (Ciba-Geigy 913). It was is symmetric and orthotropic with the following stacking sequence: $[(\pm 45/0/90)_3]_s$. The repair patches were made from the same material. Their lamination sequence was identical to the parent laminate lay-up.

Table 16 HTA/913 Material Data (Soutis and Hu [107])

PROPERTY(°)	Value	Unit
Young's modulus in x-direction (EX)	144200	MPa
Young's modulus in y-direction (EY)	9240	MPa
Young's modulus in z-direction (EZ*)	9240	MPa
In plane (XY) shear modulus (GXY)	4710	MPa
Out-of-plane (XZ) shear modulus (GXZ*)	3876	MPa
Out-of-plane (YZ) shear modulus (GYZ*)	3876	MPa
Poisson's ratio (NUXY)	0.346	
Poisson's ratio (NUXZ*)	0.192	
Poisson's ratio (NUYZ*)	0.192	
Tensile strength in x-direction (FXT)	2185	MPa
Compressive strength in x-direction (FXC)	1500	MPa
Tensile strength in y-direction (FYT)	60	MPa
Compressive strength in y-direction (FYC)	180	MPa
In-plane shear strength (FSXY)	80	MPa

* assumed

(°) nomenclature from NISA/DISPLAY

The data are given in Table 16. The strength properties were estimated from XAS/913 carbon/epoxy composite which is very similar to HTA/913.

Table 17 Araldite 2005 Material Data (Soutis and Hu [107])

PROPERTY	Value	Units
Young's modulus E	3400	MPa
Shear modulus, G	1260	MPa
Poisson's ratio	0.35	
Yield strength (estimated)	80	MPa
Shear strength	40	MPa

An epoxy adhesive (Araldite 2005) was used to repair the plate. The material data used in the analysis are given in Table 17.

4.3 - Modelling Strategy

The new Quasi-3D model described at length in Chapter 3 was used for the analysis. This model mixed composite shell elements with 3D solid elements. Composite shell elements were used for the parent laminate and the repair patches. Solid elements were used for the adhesive layers. The laminated nature of the composite adherends was maintained and the solid elements allowed a full 3D stress analysis of the adhesive layers.

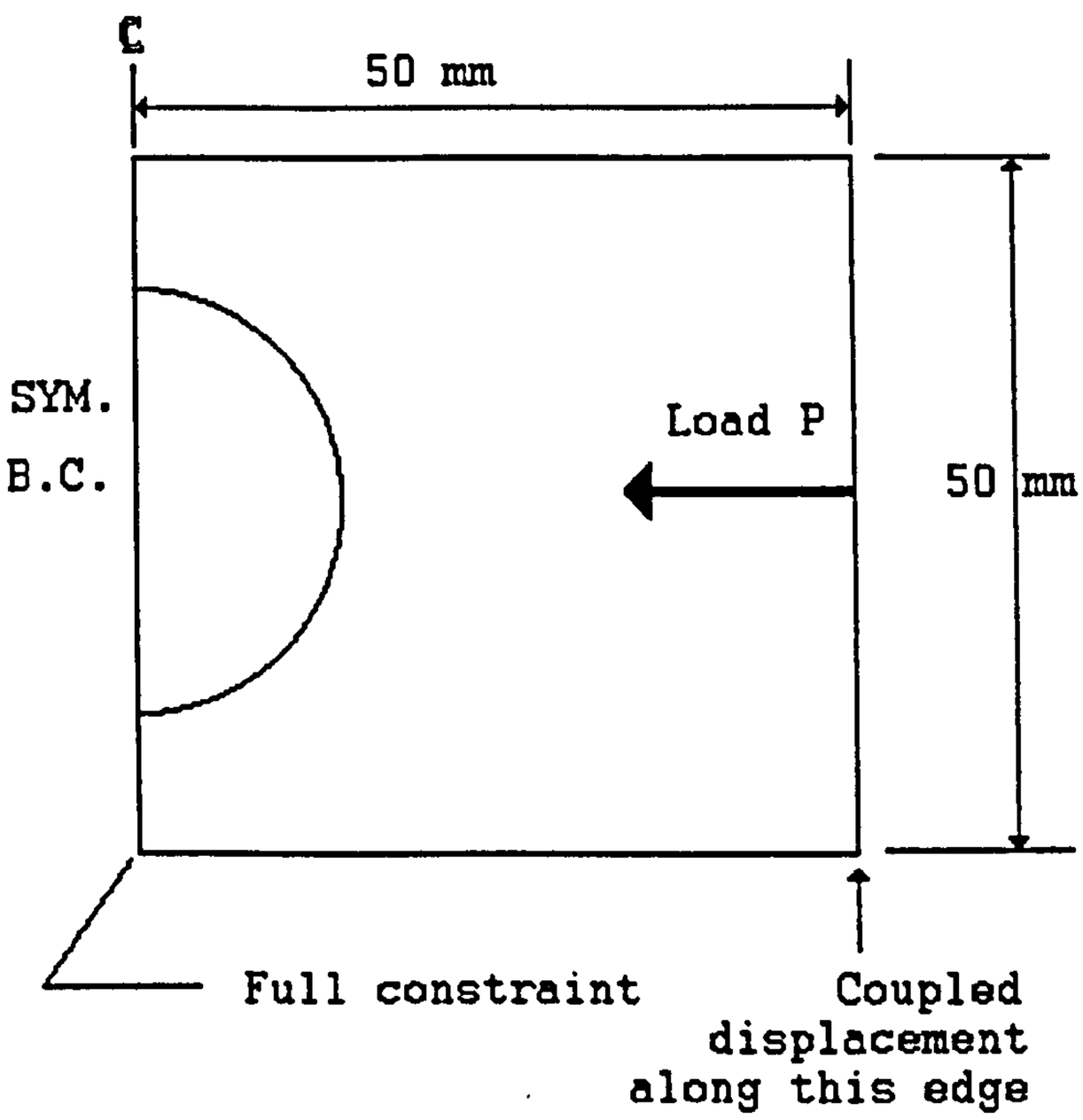

Figure 72 Boundary conditions for repaired plate

The boundary conditions used are given in Figure 72.

A linear static analysis was carried out. The analysis was carried out in two phases. The first phase investigated the plate response to an applied compressive stress of 350 MPa (52.5 kN) in order to determine stress "hot spots" and the adhesive behaviour. The second dealt exclusively with failure load predictions.

For the first phase, adhesive stresses were obtained. For the second phase, the average stress failure criterion (ASFC) was selected for the adhesive and the Tsai-Wu interactive quadratic failure criterion for the composite adherends.

4.4 - Results and Discussion

The results for both analysis phases are presented in the following sections.

4.4.1 - Repaired panel response to compressive loading

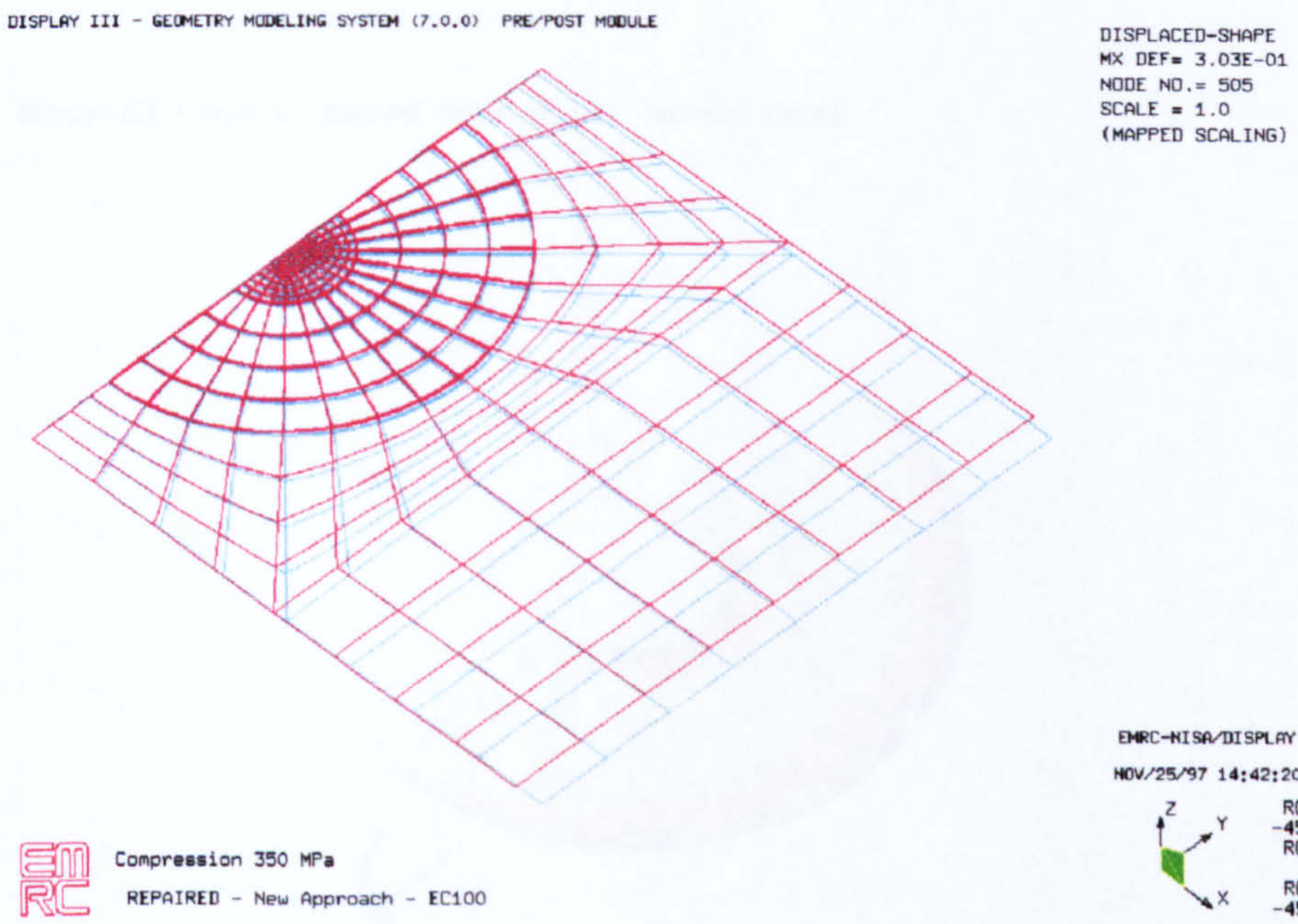

Figure 73 Deformation of the repaired plate under compression load

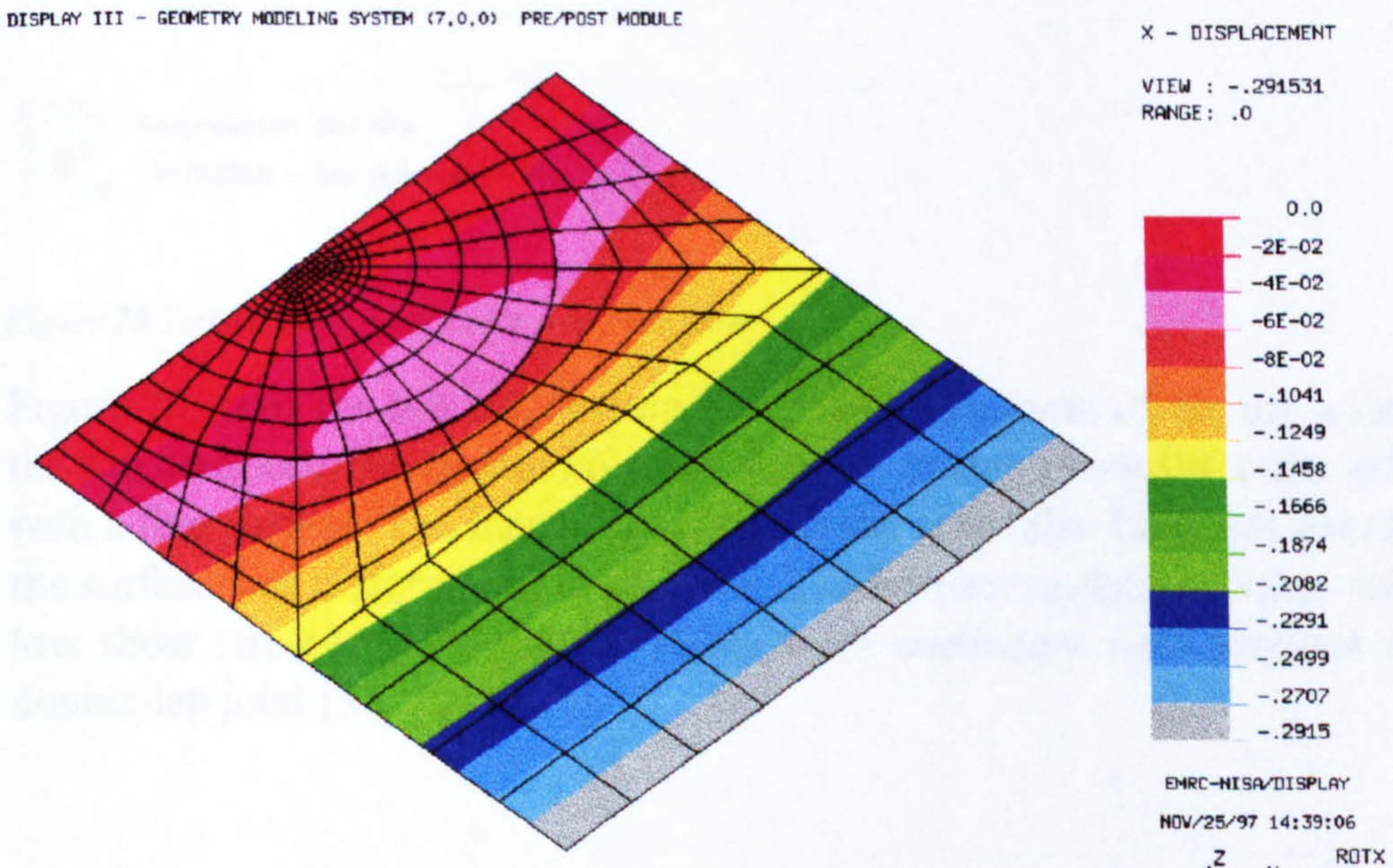

Figure 74 Longitudinal displacement for the repaired plate

The deformation of the repaired plate is shown in Figure 73. The blue lines represent the model before the load is applied and the deformed plate is shown in red. The maximum longitudinal displacement was 0.2915 mm (Figure 74).

Both the deformed shape and the maximum axial displacement were in line with what one would expect. In the case of the axial displacement, the contours show that the central area (that delimited by the patches on both sides of the parent laminate) was stiffer. Thus, the displacement bands were no longer parallel to the loading edge, as

one would have expected for an undamaged plate, but were more curved closer to the repair patch edges.

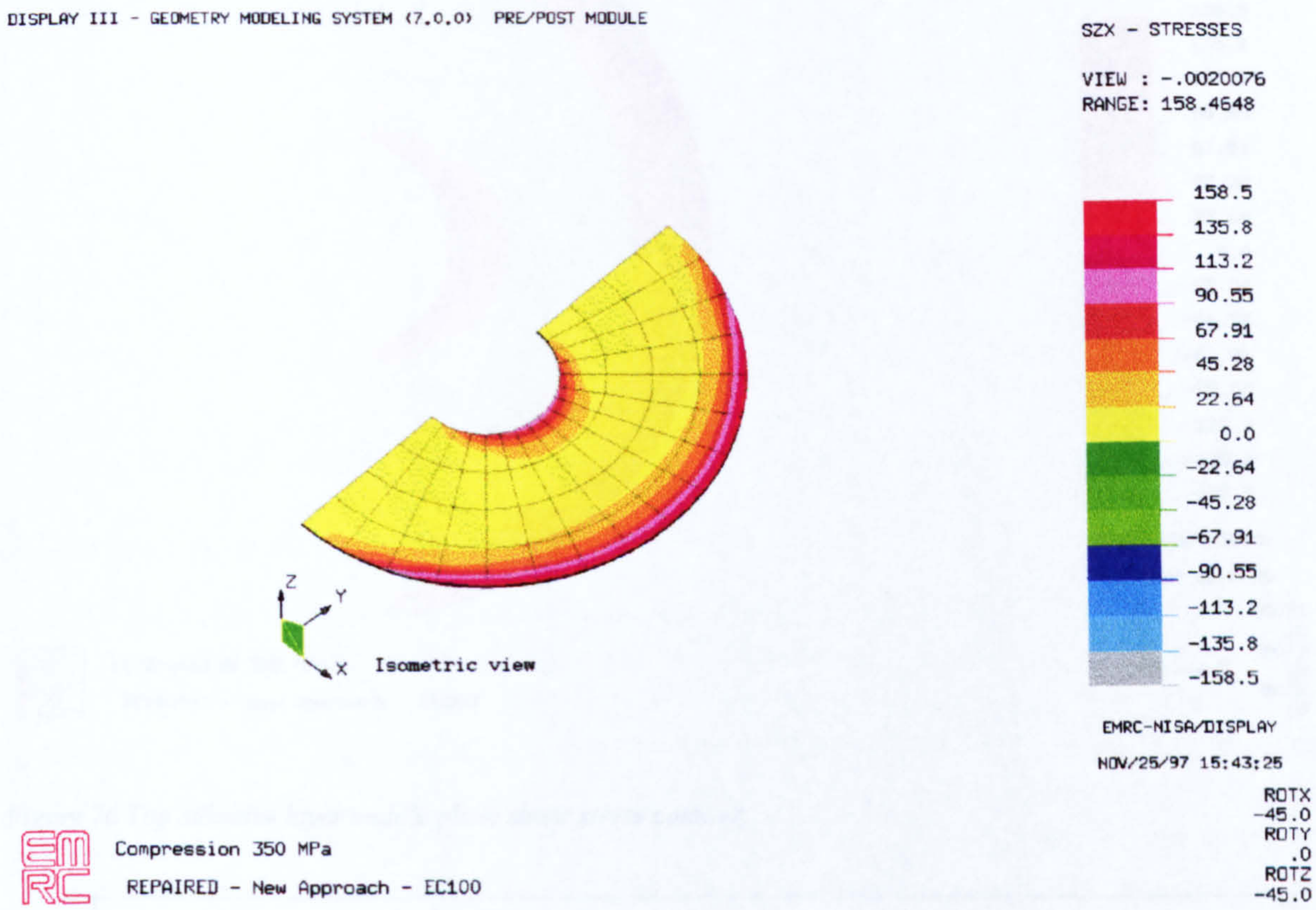

Figure 75 Top adhesive layer shear stress contour

Figure 75 show the top and bottom shear stress contours of the top adhesive layer. On the top contours, the maximum shear stresses occurs along the outer edge which ends with a free surface. The inner edge, around the hole, also had high stresses. The rest of the surface was under very low stresses. The bottom surface was also subjected to very low shear stresses. These observations were consistent with analyses carried out for double-lap joint [55, 107, 111].

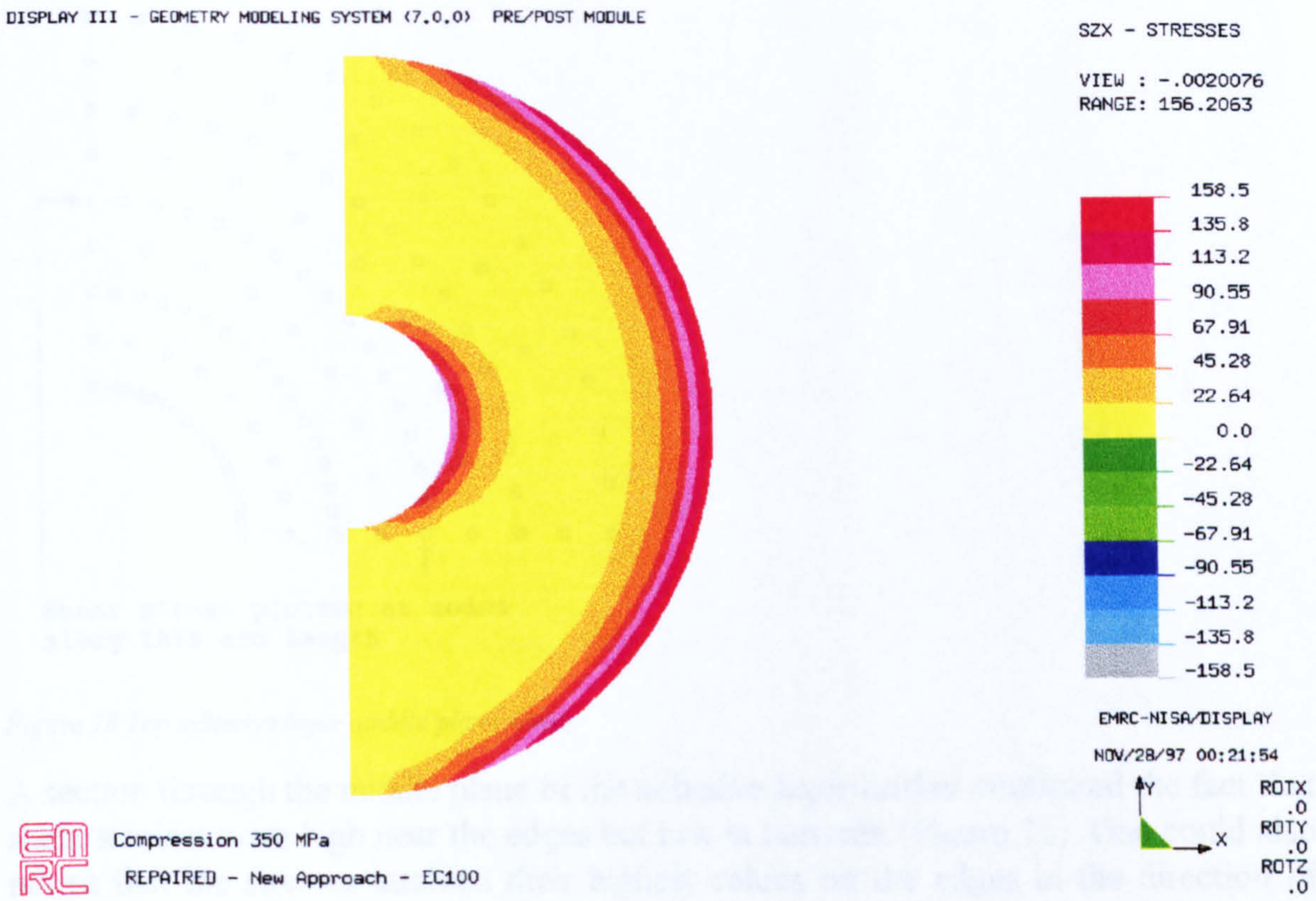

Figure 76 Top adhesive layer middle plane shear stress contour

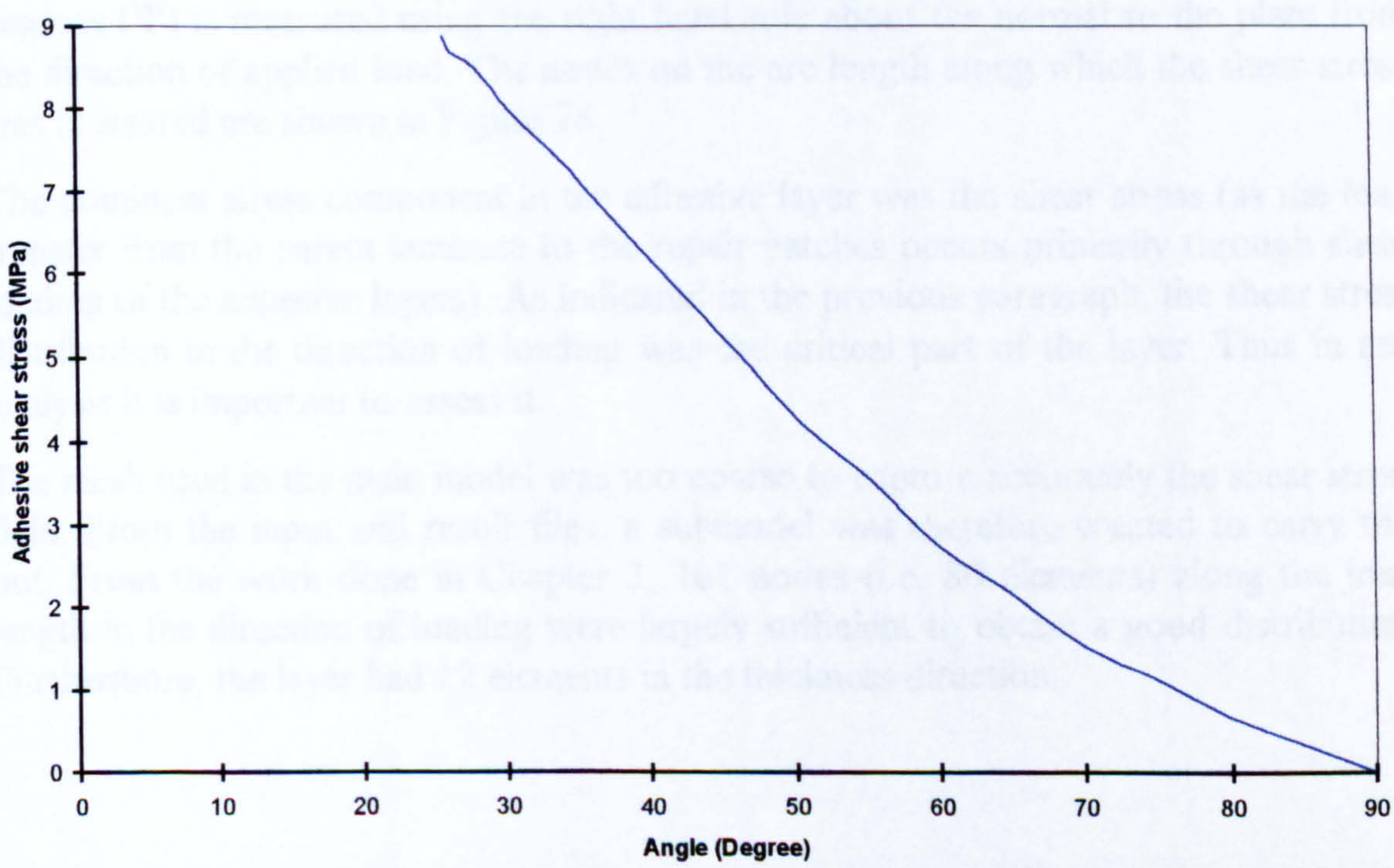

Figure 77 Shear stress distribution around the hole circumference for top adhesive layer

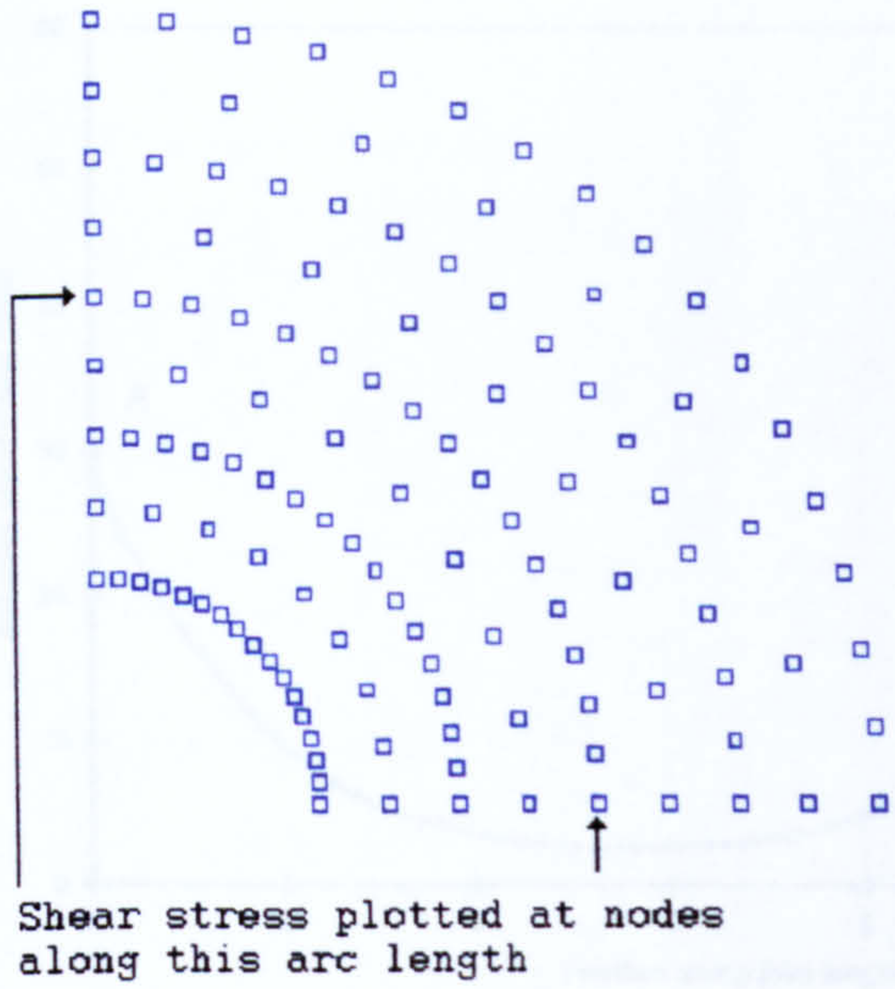

Figure 78 Top adhesive layer middle plane nodes

A section through the middle plane of the adhesive layer further confirmed the fact that shear stresses were high near the edges but low in between (Figure 76). One could also notice that the stresses attained their highest values on the edges in the direction of loading. This made the shear stress distribution in the middle plane along the loading direction the most important region of the adhesive layer (with respect to any failure predictions). This was confirmed by the graph shown in Figure 77 where the angle in degrees (Ψ) is measured using the right hand rule about the normal to the plate from the direction of applied load. The nodes on the arc length along which the shear stress was measured are shown in Figure 78.

The dominant stress component in the adhesive layer was the shear stress (as the load transfer from the parent laminate to the repair patches occurs primarily through shear loading of the adhesive layers). As indicated in the previous paragraph, the shear stress distribution in the direction of loading was the critical part of the layer. Thus in any analysis it is important to assess it.

The mesh used in the main model was too coarse to capture accurately the shear stress field. From the input and result files, a submodel was therefore created to carry this out. From the work done in Chapter 3, 161 nodes (i.e. 80 elements) along the joint length in the direction of loading were largely sufficient to obtain a good distribution. Furthermore, the layer had 12 elements in the thickness direction.

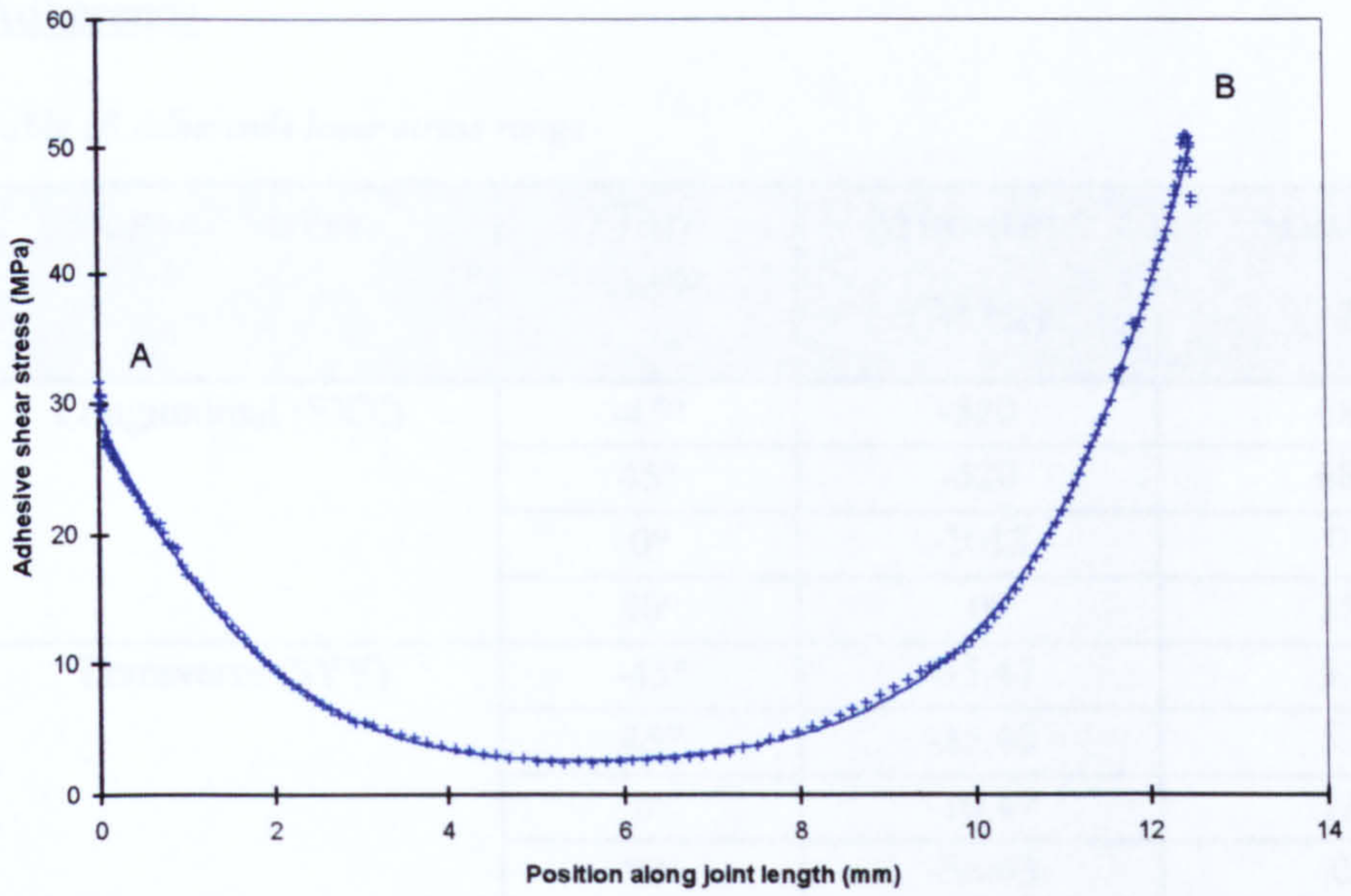

Figure 79 Top adhesive layer shear stress distribution

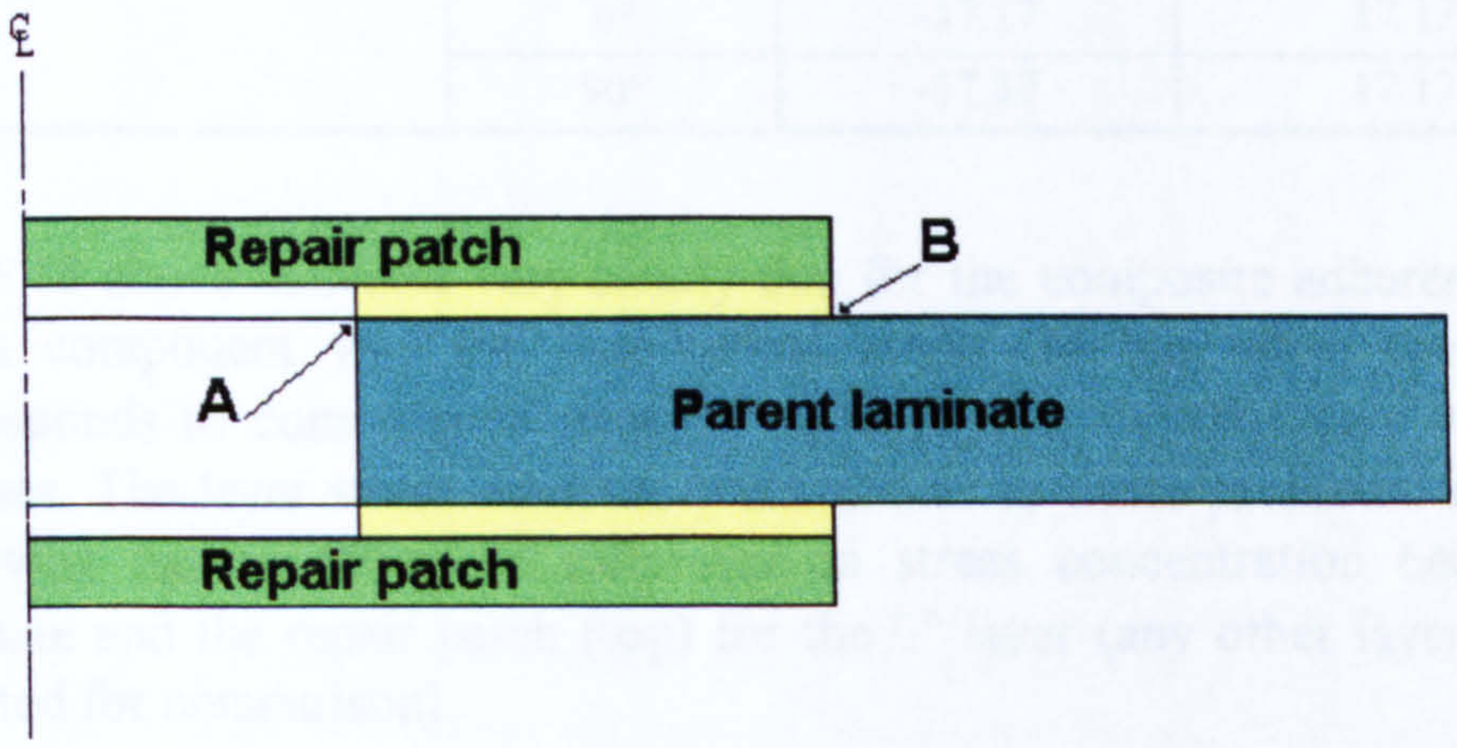

Figure 80 Section through repaired plate in the direction of loading

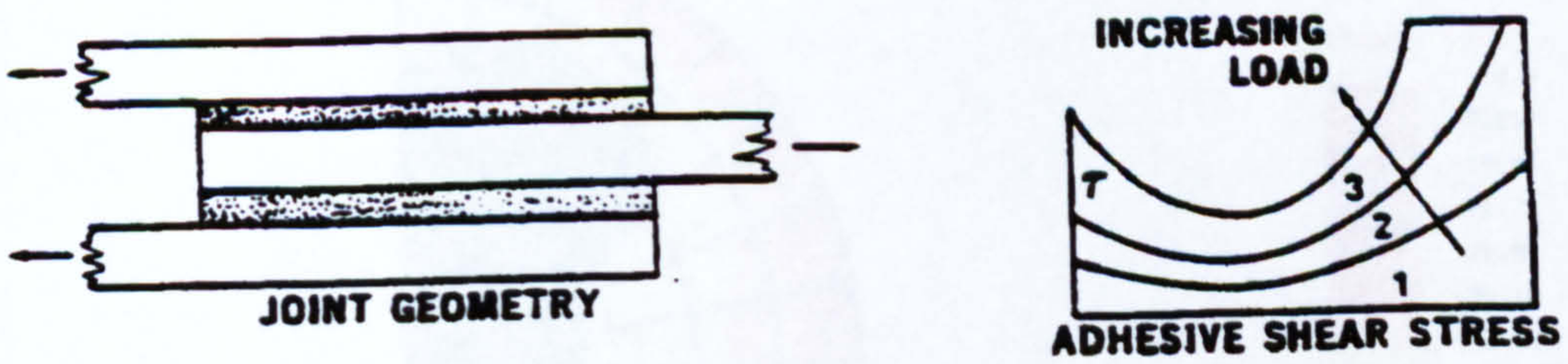

Figure 81 Effect of stiffness imbalance on double lap joint adhesive shear stress distribution [156]

The resulting curve is shown in Figure 79. The figure indicates that the curve is not symmetrical about the middle of the joint length although both adhesive ends are free surfaces. This can be explained by the stiffness imbalance between the repair patches and the parent laminate. As a result, the adhesive end near B (Figure 80) is subject to higher shear stresses compared to that near A. This is consistent with Hart-Smith parametric studies of double lap joints (Figure 81).

Adherends

Table 18 Adherends layer stress range

Layer Stress	Fibre Angle	Minimum (MPa)	Maximum (MPa)
Longitudinal (SXX)	-45°	-520	68.01
	45°	-520	68.01
	0°	-1013	0.00
	90°	0	352.7
Transverse (SYY)	-45°	-35.47	5.631
	45°	-35.46	5.631
	0°	-10.47	12.58
	90°	-58.63	0.00
Longitudinal (SXY)	-45°	0.00	44.56
	45°	-44.56	0.0
	0°	-17.17	17.17
	90°	-17.17	17.17

Table 18 above indicates very clearly that for the composite adherends, the dominant stress component was the longitudinal stress. In the table, the negative values corresponds to compressive stresses. As expected, the 0° layers were under higher stresses. The layer stress contours were similar to those presented in Chapter 3. The following figures show the difference in stress concentration between the parent laminate and the repair patch (top) for the 0° layer (any other layer could have been selected for comparison).

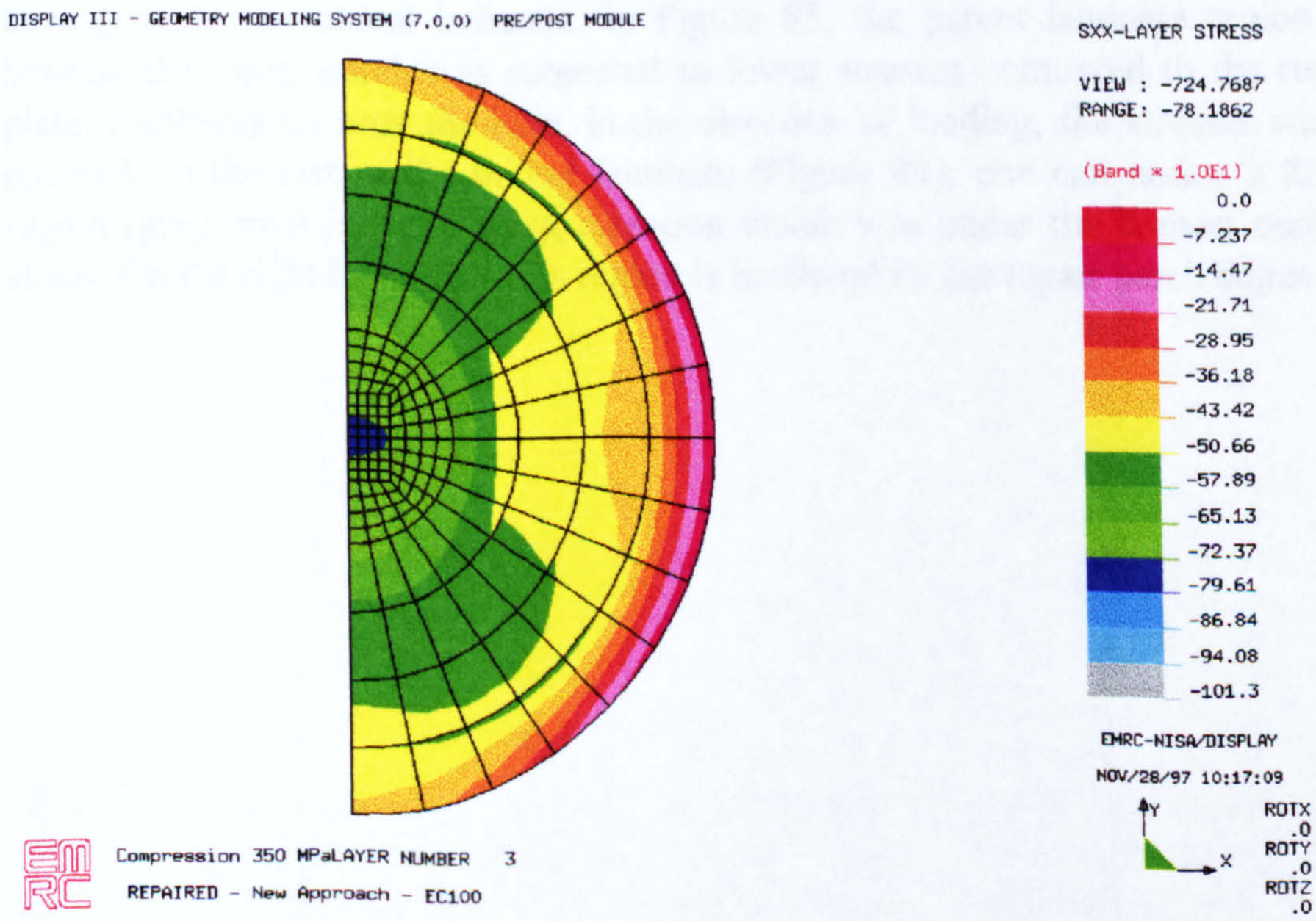

Figure 82 Top repair patch longitudinal stress contour (0° layer)

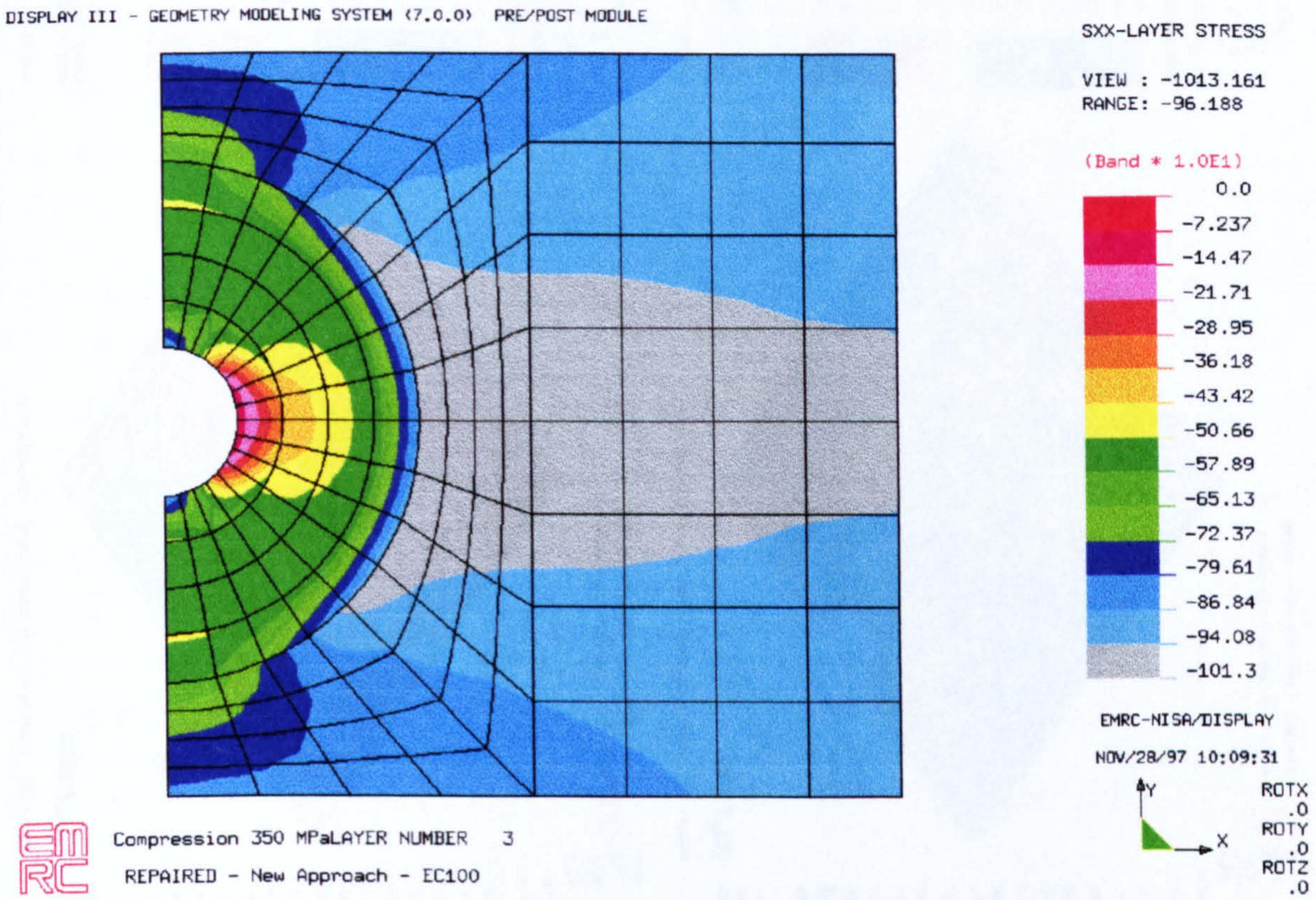

Figure 83 Parent laminate longitudinal stress contour (0° layer)

The repair patch layer shown in Figure 82 was under compressive stresses only. The maximum stress occurred at the centre of the patch (-724.77 MPa) and the minimum (-78.19 MPa) at the edge in the direction of loading . This is a clear indication that the repair patch was performing its role in "soaking up" some of the load which would have gone to the parent laminate. In Figure 83, the parent laminate region directly beneath the repair patch was subjected to lower stresses compared to the rest of the plate. Furthermore, near the hole, in the direction of loading, the stresses were much reduced. In the rest of the parent laminate (Figure 83), one can notice a funnel-like region (grey area) in the loading direction which was under the highest compressive stress. On the right hand side, this region is bordered by the repair patch edges.

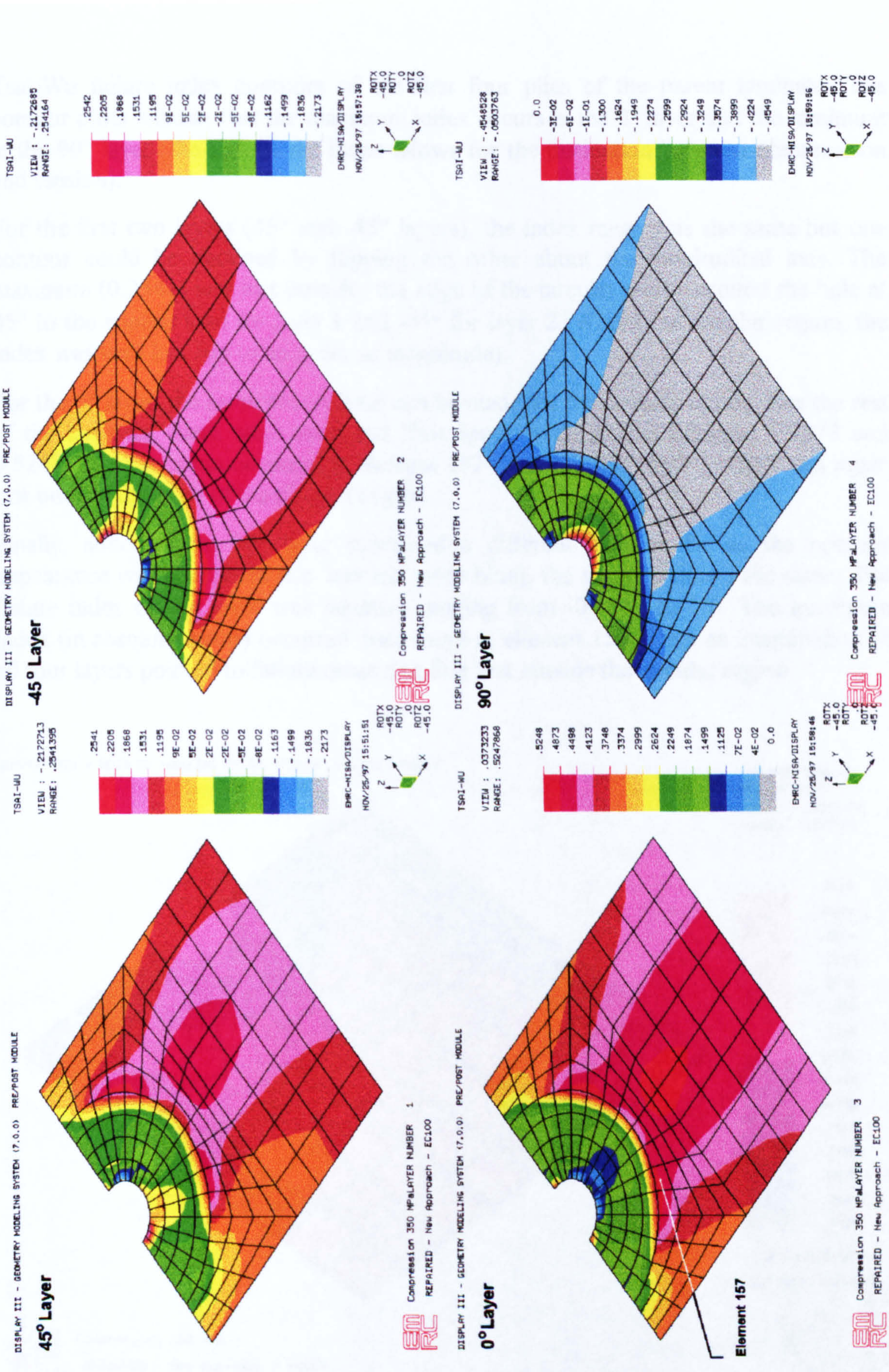

Figure 84 Parent laminate Tsai-Wu failure index contour

One of the main advantages of this modelling approach compared to traditional ones is the fact that one can investigate the structure response on a ply by ply basis. This is particularly useful for failure load prediction and locations because, with the help of composite failure criteria, one can examine the structure stress "hot spots" for each layer. This in turn gives a better idea of possible failure location. Figure 84 shows the

Tsai-Wu failure index contours of the first four plies of the parent laminate. The contour plots indicate that the maximum index occurs in the 0° layer and the minimum in the 90° layer (the sign of the index allows for the distinction between compression and tension).

For the first two layers (45° and -45° layers), the index range was the same but one contour could be obtained by flipping the other about the longitudinal axis. The maximum (0.2541) was just outside the edge of the circular region around the hole at 45° to the applied load for layer 1 and -45° for layer 2. Within the circular region, the index was very low (up to an order of magnitude).

For the 0° layer, the same observation can be made for the circular region. For the rest of the laminate, there were three red "hot spots" with indices between 0.4873 and 0.5248. The maximum occurred at element 157 (shown in Figure 84) which was again just outside the edge of the circular region.

Finally, although the 90° layer presented a different look as far as the contour appearance was concerned (i.e. less red more blue), the story remained the same. The failure index on the layer was negative ranging from -0.4549 to 0.0. The maximum index (in absolute terms) occurred once more at element 157. Thus an examination of all four layers pointed to failure occurring first just outside the circular region.

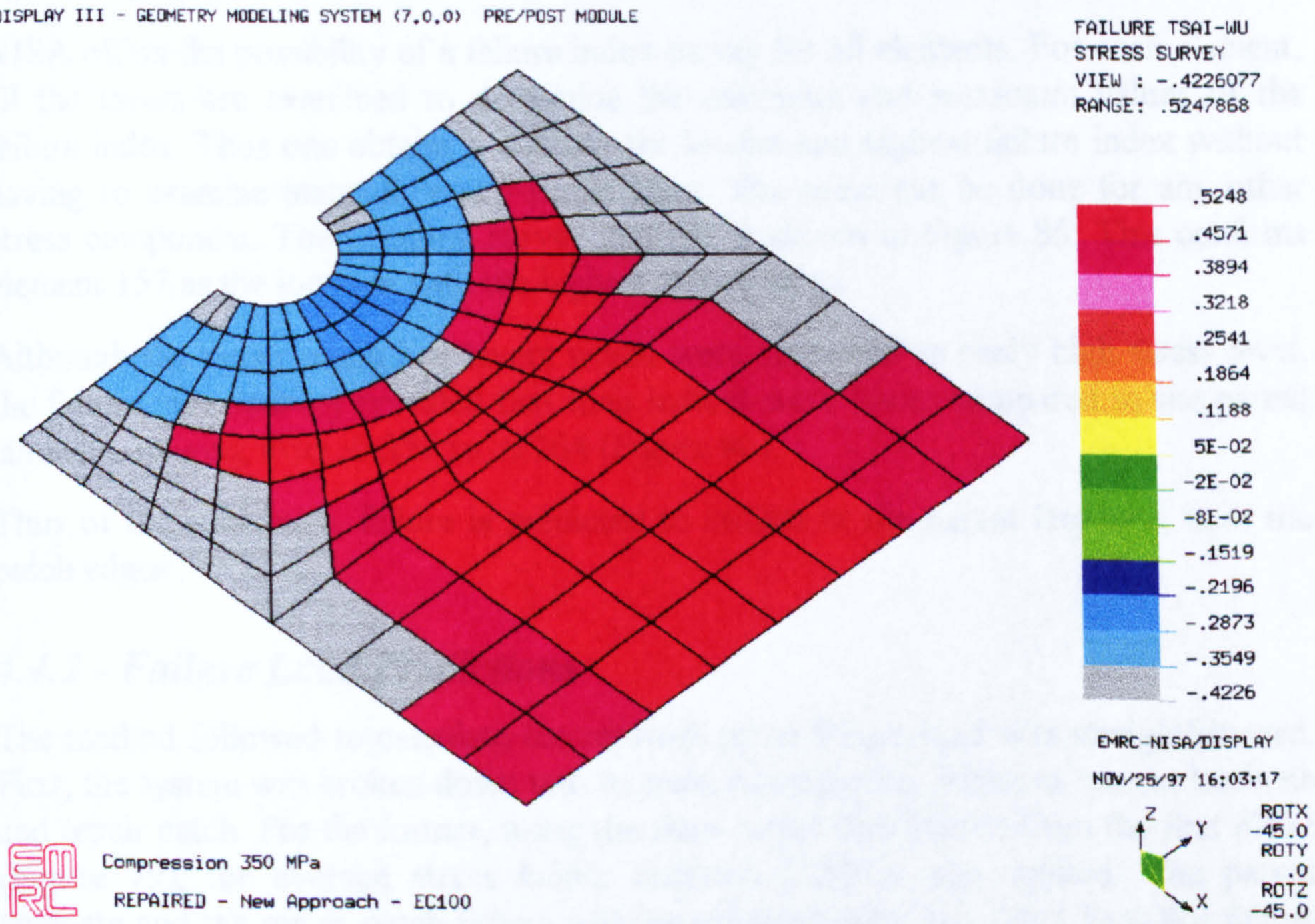

Figure 85 Parent laminate Tsai-Wu failure index survey

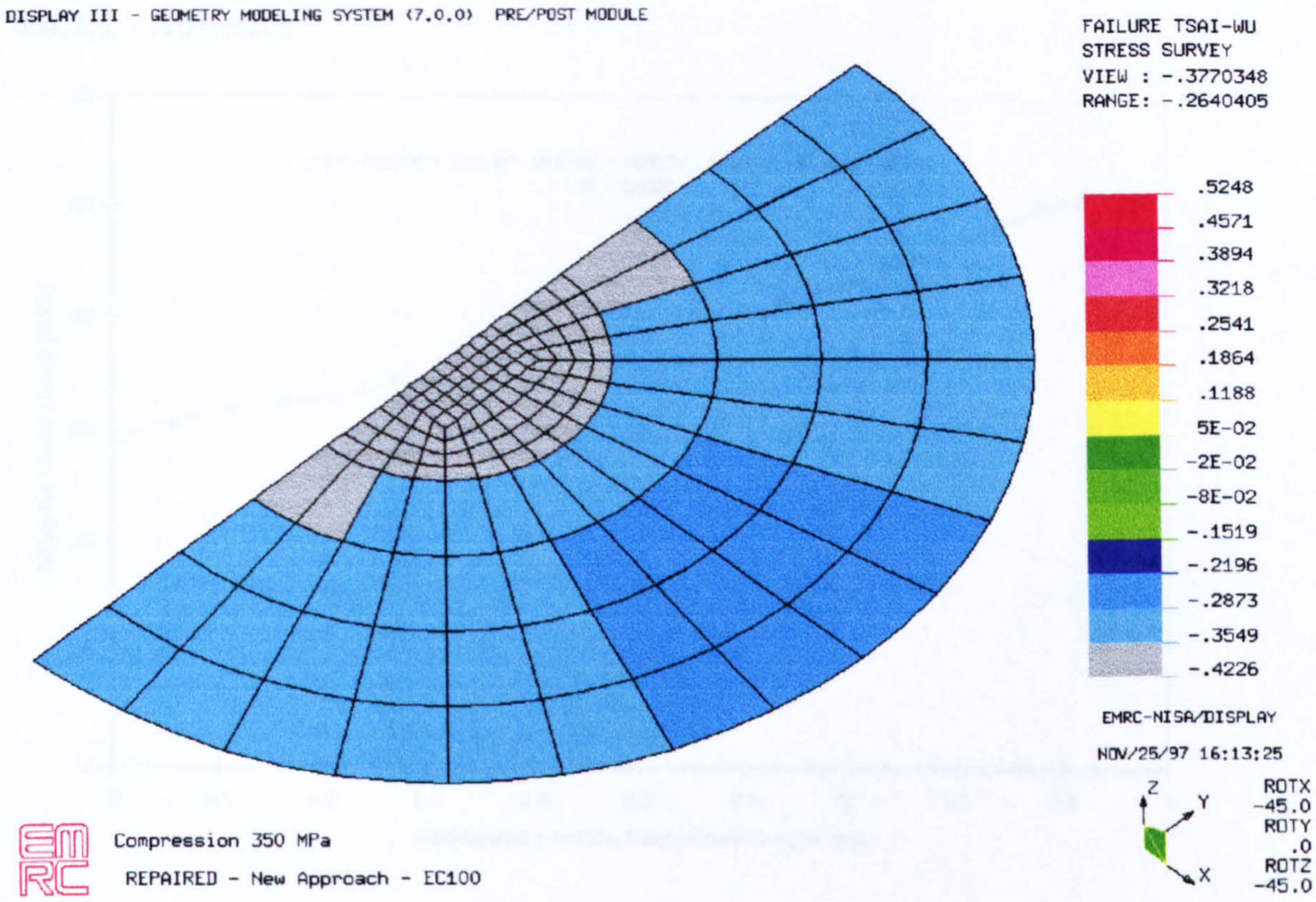

Figure 86 Top repair patch failure index survey

NISA offers the possibility of a failure index survey for all elements. For each element, all the layers are examined to determine the minimum and maximum values of the failure index. Thus one obtains a contour for lowest and highest failure index without having to examine manually every single layer. The same can be done for any other stress component. The resulting survey contour is shown in Figure 85. This confirms element 157 as the location with the highest failure index.

Although the repair patch had layers which were subjected to fairly high stress level, the failure index survey revealed that their indices were lower compared to the parent laminate, ranging from -0.377 to -0.264 (Figure 86).

Thus of the adherends, failure is predicted to initiate in the parent laminate, near the patch edges.

4.4.2 - Failure Load Predictions

The method followed to calculate the repaired panel failure load was straightforward. First, the system was broken down into its main constituents: adhesive, parent laminate and repair patch. For the former, using the shear stress distribution from the first phase (Figure 79), the average stress failure criterion (ASFC) was applied. The parent laminate and the repair patch failure was investigated using the same Tsai-Wu failure criterion. The first phase of the analysis had already shown that the parent was the critical part of the system as far as composite adherends were concerned. The predicted results are presented below with a comparison with experimental results.

4.4.2.1 - Adhesive

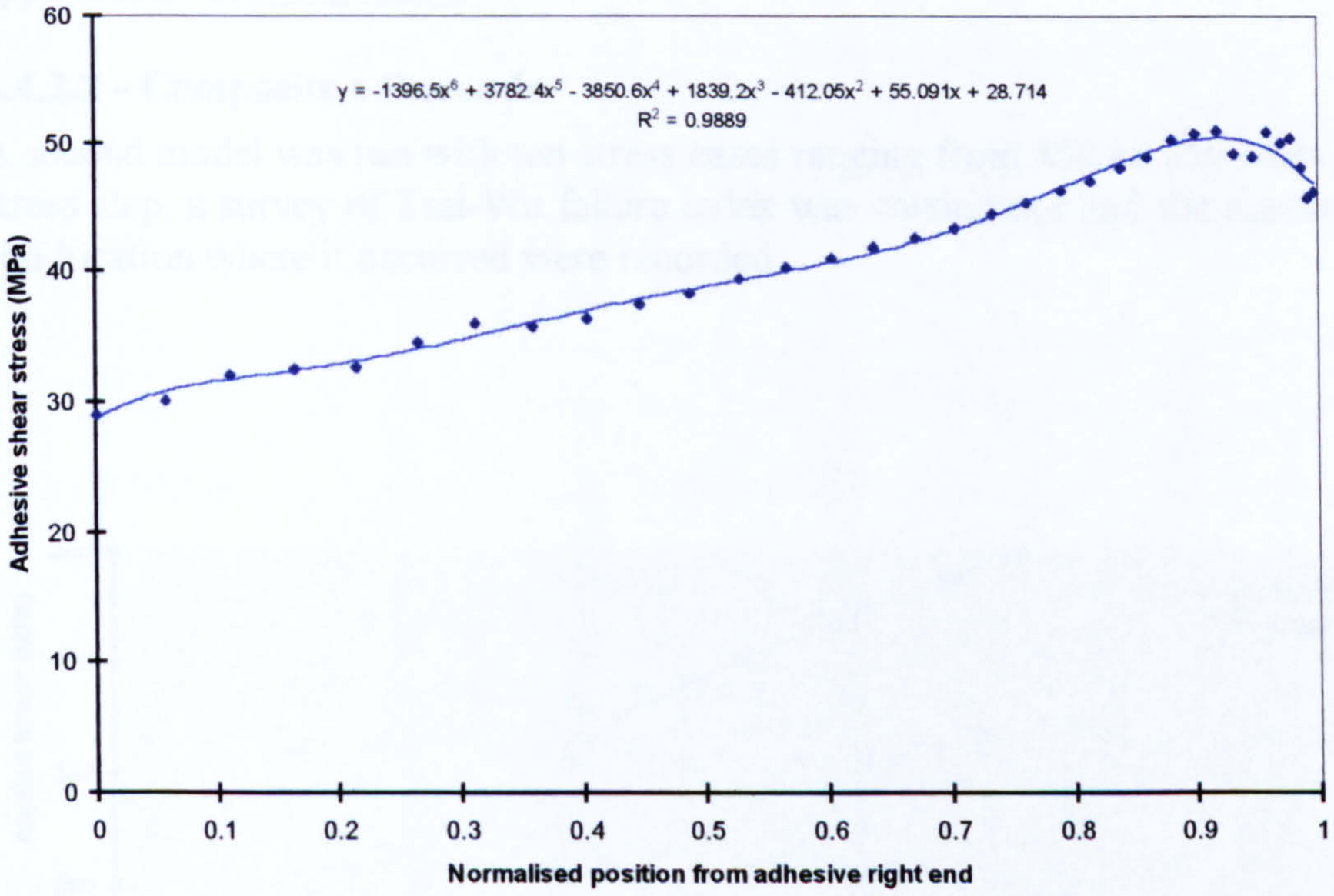

Figure 87 Shear stress curve with polynomial best fit curve

For the shear stress curve of Figure 79, only the critical end was required to calculate the adhesive failure load. The characteristic distance, d_0, was evaluated to be 0.996 mm from Soutis and Hu's parametric study[107]. The appropriate curve portion is shown in Figure 87 where it was fitted with a 6^{th} order polynomial so that the shear stress τ could be expressed as a function of position (x) along the joint length with the following expression:

$$\tau = Ax^6 + Bx^5 + Cx^4 + Dx^3 + Ex^2 + Fx + G$$

where:

$$A = -1396.5 \quad ; \quad B = 3782.4$$

$$C = -3850.6 \quad ; \quad D = 1839.2$$

$$E = -412.05 \quad ; \quad F = 55.091$$

$$G = 28.714$$

Assuming that both ends have the peak stresses, the average stress over the joint length, $\bar{\tau}$, is defined by:

$$\bar{\tau} = \frac{1}{2d_0}\int_0^{d_0} \tau dx$$

From this the averaged stress was 39.46 MPa for an applied stress of 350 MPa. This gives a ratio of averaged stress to applied stress of 0.0564 at each end. The ASFC indicates that failure is deemed to have occurred in the adhesive when the average shear stress along the joint length is equal to the adhesive shear strength. For the adhesive, the shear strength is 40 MPa. The ratio of averaged stress to applied stress

being constant for a given adhesive, the ASFC predicts failure in the adhesive at an applied load of 709.60 MPa.

4.4.2.2 - Composite adherends

A second model was run with ten stress cases ranging from 350 to 650 MPa. For each stress step, a survey of Tsai-Wu failure index was carried out and the maximum value and location where it occurred were recorded.

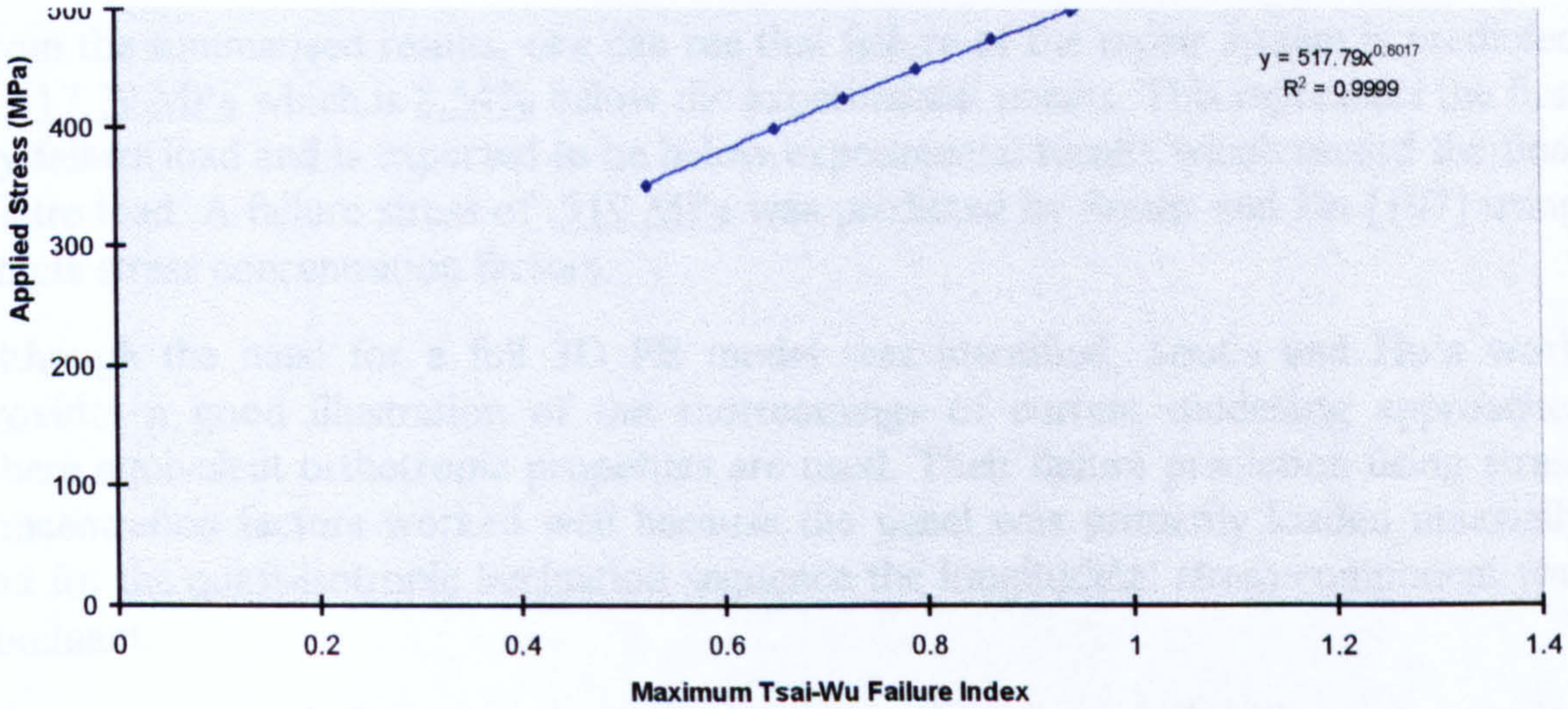

Figure 88 Composite adherend first ply failure prediction

The graph in Figure 88 shows the effect of applied load on the magnitude of the maximum Tsai-Wu failure index.

For this failure criterion, first ply failure is deemed to have occurred when the index reaches unity. The axes were chosen with the failure index along the x-axis so that the coefficient of the best fit curve (expressed by $y = ax^b$) was equal to the applied load at failure ($x=1$). From the curve above, one can determine easily that the failure index is unity when a stress of 517.79 MPa is applied. The failure location was element 157, as expected from the first phase of the analysis.

4.4.2.3 - Summary and Comparison with Experimental Data

The predicted results are summarised in the following table which includes also the recorded experimental failure load.

Table 19 Applied stress at failure

	FEA Predictions		Experimental [107]
	Tsai-Wu	ASFC	
Parent laminate	517.79	N/A	562.00
Repair patch	N/C	N/A	
Adhesive	N/A	709.60	
N/C = not calculated N/A = not applicable	all values in MPa		

From the summarised results, one can see that failure of the repair system is predicted at 517.79 MPa which is 8.54% below the experimental results. This represents the first ply failure load and is expected to be below experimental results which record the final failure load. A failure stress of 519 MPa was predicted by Soutis and Hu [107] using simple stress concentration factors.

Although the need for a full 3D FE model was identified, Soutis and Hu's work provides a good illustration of the shortcomings of current modelling approaches where equivalent orthotropic properties are used. Their failure prediction using stress concentration factors worked well because the panel was primarily loaded uniaxially and for the quasi-isotropic lamination sequence the longitudinal stress component was dominant.

The new approach for external repairs has the potential to deal with more complex loading and lay-up because it intrinsically takes into account the laminated nature of the composites. Furthermore, it offers the opportunity to assess both the composite adherends and the adhesive and the possibility to use failure criteria specific to composites.

In addition, the problem of assessing the adhesive failure is addressed by going back to the fundamentals of what a bonded repair model should be able to do within the context of an appropriate repair design philosophy. This resulted in the proposal for a criterion which is able to assess the failure load accurately enough to verify that the adhesive is never going to be the weak link in the repair.

4.5 - Conclusion

- A new adhesive failure criterion was proposed for bonded repairs to composite structures which was a simple but effective way of assessing the adhesive failure load in relation to the other repair components
- The repaired panel was predicted to fail at 517.79 MPa through the parent laminate
- The predicted results compared very well with the predictions from an older different modelling approach
- The FE predictions agreed well with experimental data

4.6 - Summary

The work carried out in this chapter has shown that the proposed new modelling approach for externally bonded patch repairs offers an improved method for the prediction of failure load and location.

The average failure criterion is useful in establishing adhesive failure load without the need to resort to expensive and potentially time consuming non-linear analysis. This is due to the fact that it inherently produces conservative results which are adequate within the context of establishing the relative position of the repair system constituents failure loads.

Despite the controversy surrounding failure criteria for composite materials, the widely used Tsai-Wu criterion provides a useful method to predict first ply failure.

The second new modelling approach is developed further through its application to real flush repairs over the next three chapters.

Chapter 5

Application to Bonded Repairs

Case Study 1: Simple Scarf Joint for Repairs

5.0 - Introduction

The preceding chapters have shown that most of the modelling approaches which have been used in the literature for the study of adhesively bonded joints are not exactly well suited to the study of bonded repairs to composite structures. A close look at what a repair model needs to be able to do has highlighted the need for a model which gives the repair designer an overall view of the situation.

The work reported in the previous two chapters has shown, that within the context of PC-based applications, such a single modelling approach cannot be used which will cater for all the various structural repair types (namely external repairs and flush repairs). At best external repairs can be modelled using a combination of 3D solid elements and 3D composite shell elements with layer stress capability. For flush repairs, it is theoretically possible to used 3D solid composite elements. In practice, this means a tedious modelling process which does not lend itself easily to quick modifications. To that effect, an alternative called the twin phase modelling concept (or 2PMC) has been devised. One model provides the displacement field which is then input into the second model which provides layer stresses and other composite relevant data.

This case study deals with the modelling of a simple scarf joint. 2D and 3D analyses are performed to assess the adhesive and adherend stresses. Failure loads are predicted in both linear and non-linear analysis using appropriate failure criteria and compared to experimental results.

The main aim of this case study was to demonstrate the importance of layers stresses in the prediction of composite adherend failure modes. The viability of the 2PM concept is also demonstrated.

5.1 - Modelling Data

The data given in this section has been kindly provided by the Structural Materials Centre (SMC - DERA Farnborough which is part of the UK Defence Evaluation and Research Agency) where the experimental work was carried out in collaboration with other partners.

5.1.1 - Geometry

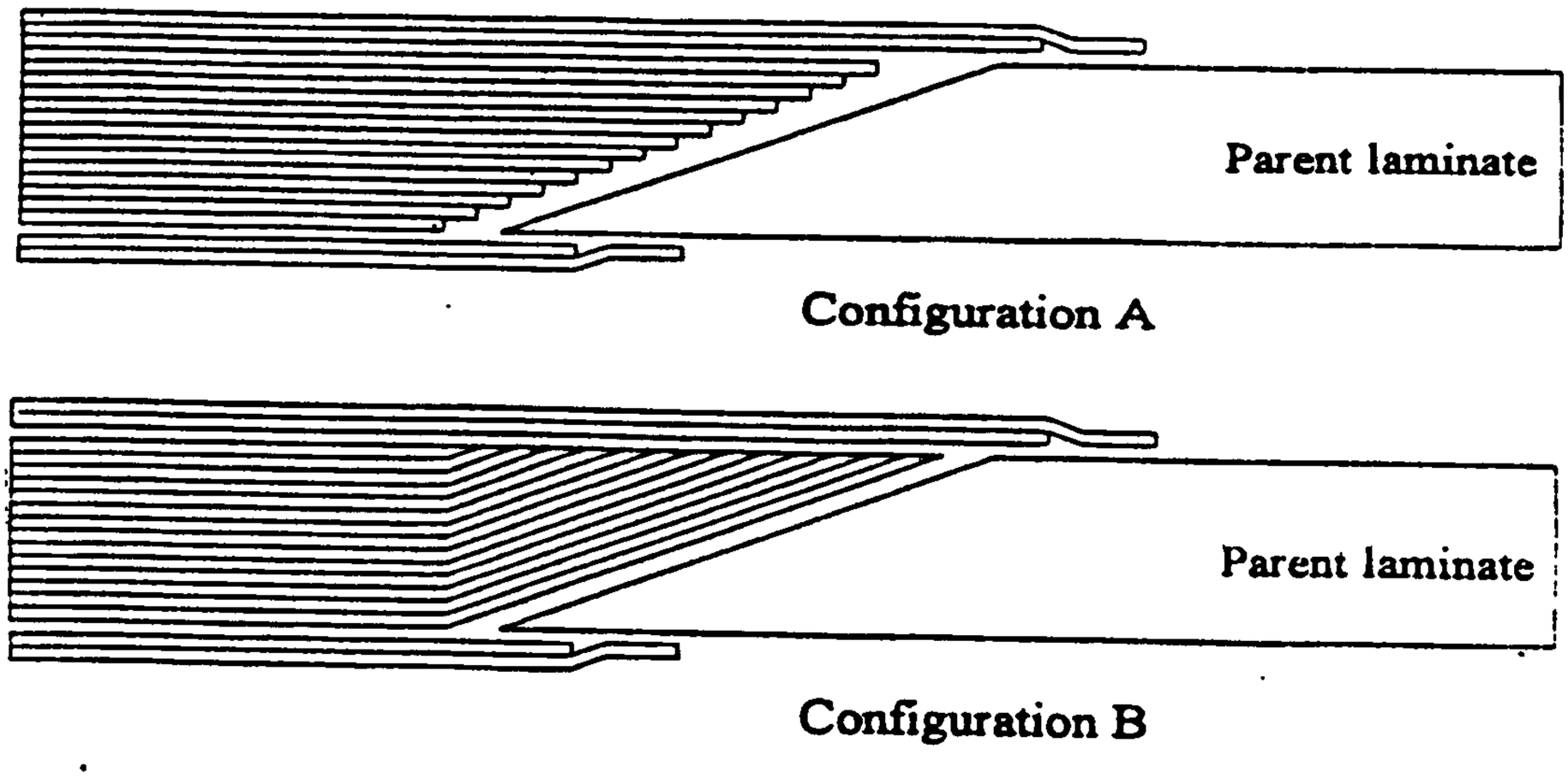

Figure 89 Alternative patch configurations for composite scarf repairs (SMC - DERA Farnborough)

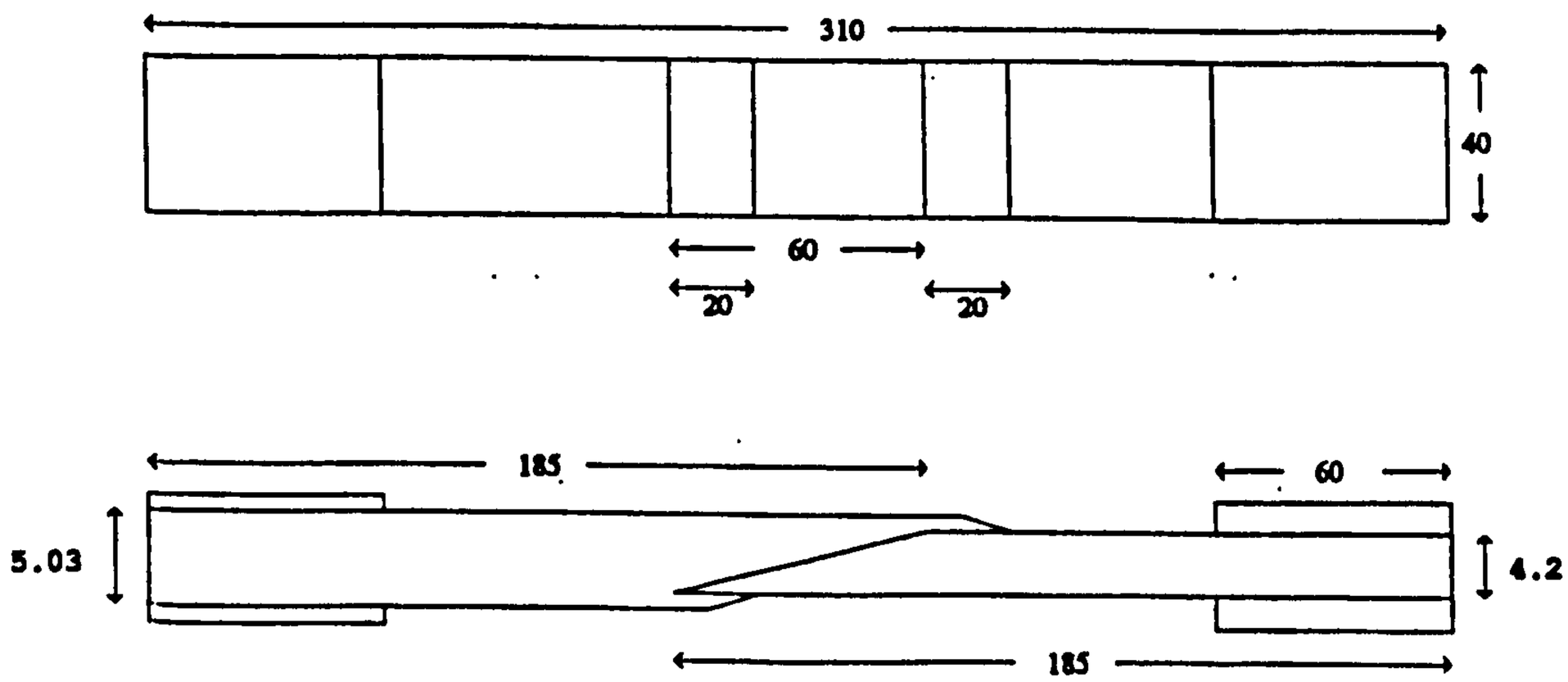

Figure 90 Test piece for adhesively-bonded scarf joints (not to scale) - (SMC - DERA Farnborough)

Two configurations A and B were considered (see Figure 89). For practical reasons, configuration B was chosen for the experimental work. The actual dimensions are given in Figure 90

The parent laminate was 4.2 mm thick with the following stacking sequence: $[\pm 45/0/90/-45/+45/0_2/\pm 45/0_2/-45/+45/90/0]_s$. Thus the parent laminate had 37% of the fibres at 0°, 50% at ±45° and 12.5% at 90°. The part modelled was that between the tabs. The repair patch was 5.03 mm thick and is made of 12 layers.

5.1.2 - Materials

Table 20 T800/924C Material Data (Source: SMC, DERA Farnborough)

PROPERTY(°)	Value	Unit
Young's modulus in x-direction (EX)	16800	MPa
Young's modulus in y-direction (EY)	9500	MPa
Young's modulus in z-direction (EZ*)	9500	MPa
In plane (XY) shear modulus (GXY)	4600	MPa
Out-of-plane (XZ) shear modulus (GXZ*)	4600	MPa
Out-of-plane (YZ) shear modulus (GYZ*)	3740	MPa
Poisson's ratio (NUXY)	0.27	
Poisson's ratio (NUXZ*)	0.27	
Poisson's ratio (NUYZ*)	0.27	
Tensile strength in x-direction (FXT)	2700	MPa
Compressive strength in x-direction (FXC)	1520	MPa
Tensile strength in y-direction (FYT)	93	MPa
Compressive strength in y-direction (FYC)	214	MPa
In-plane shear strength (FSXY)	133	MPa

* assumed (for transverse isotropy)
(°) nomenclature from NISA/DISPLAY

Table 21 T800/924C Equivalent Orthotropic Data

PROPERTY(°)	Value	Unit
Young's modulus in x-direction (EX)	80053	MPa
Young's modulus in y-direction (EY)	44534	MPa
Young's modulus in z-direction (EZ*)	44534	MPa
In plane (XY) shear modulus (GXY)	23935	MPa
Out-of-plane (XZ) shear modulus (GXZ*)	23935	MPa
Out-of-plane (YZ) shear modulus (GYZ*)	15472	MPa
Poisson's ratio (NUXY)	0.439	
Poisson's ratio (NUXZ*)	0.439	
Poisson's ratio (NUYZ*)	0.439	

* assumed
(°) nomenclature from NISA/DISPLAY

The parent laminate was made from T800 carbon fibres embedded in an epoxy matrix (Ciba-Geigy 924C). The material properties used for the linear static analysis are given in Table 20. The assumed properties were for transverse isotropy (with the exception of the YZ-plane Poisson's ratio. The data given in Table 20 was used for models which required only lamina material properties. The computer program LAP (Laminate Analysis Programme) was used with the appropriate stacking sequence and the above lamina data to generate equivalent orthotropic properties. These are given in Table 21.

Table 22 T300/LY5052 Material Data (Source: SMC, DERA Farnborough)

PROPERTY(°)	Value	Unit
Young's modulus in x-direction (EX)	58400	MPa
Young's modulus in y-direction (EY)	58400	MPa
Young's modulus in z-direction (EZ*)	58400	MPa
In plane (XY) shear modulus (GXY)	5500	MPa
Out-of-plane (XZ) shear modulus (GXZ*)	5500	MPa
Out-of-plane (YZ) shear modulus (GYZ*)	5500	MPa
Poisson's ratio (NUXY*)	0.06	
Tensile strength in x-direction (FXT)	696	MPa
Compressive strength in x-direction (FXC)	430	MPa
Tensile strength in y-direction (FYT)	696	MPa
Compressive strength in y-direction (FYC)	430	MPa
In-plane shear strength (FSXY*)	80	MPa

* assumed

(°) nomenclature from NISA/DISPLAY

Table 23 T300/LY5052 Equivalent Orthotropic Data

PROPERTY(°)	Value	Unit
Young's modulus in x-direction (EX)	51761	MPa
Young's modulus in y-direction (EY)	51761	MPa
Young's modulus in z-direction (EZ*)	51761	MPa
In plane (XY) shear modulus (GXY)	10868	MPa
Out-of-plane (XZ) shear modulus (GXZ*)	10868	MPa
Out-of-plane (YZ) shear modulus (GYZ*)	22179	MPa
Poisson's ratio (NUXY)	0.167	
Poisson's ratio (NUXZ*)	0.167	
Poisson's ratio (NUYZ*)	0.167	

* assumed

(°) nomenclature from NISA/DISPLAY

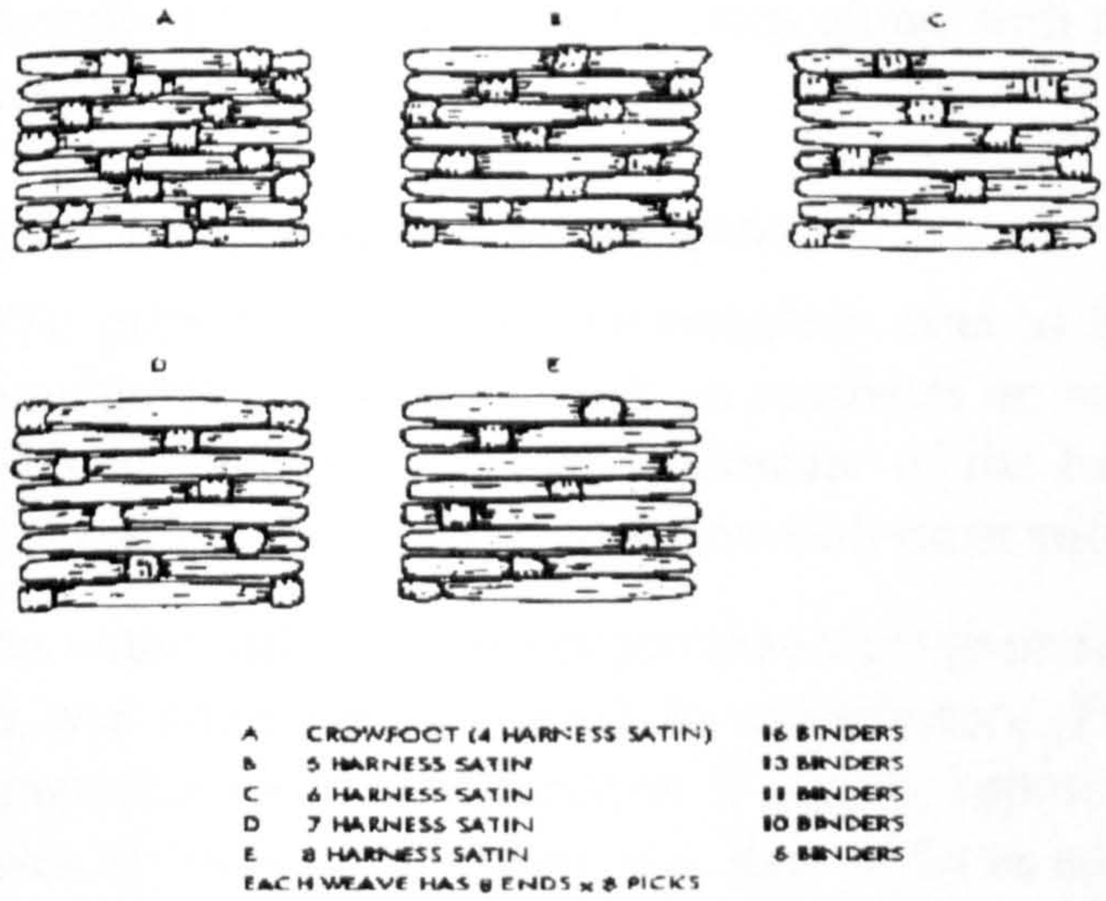

Figure 91 Five different satin weaves (Bailie [163])

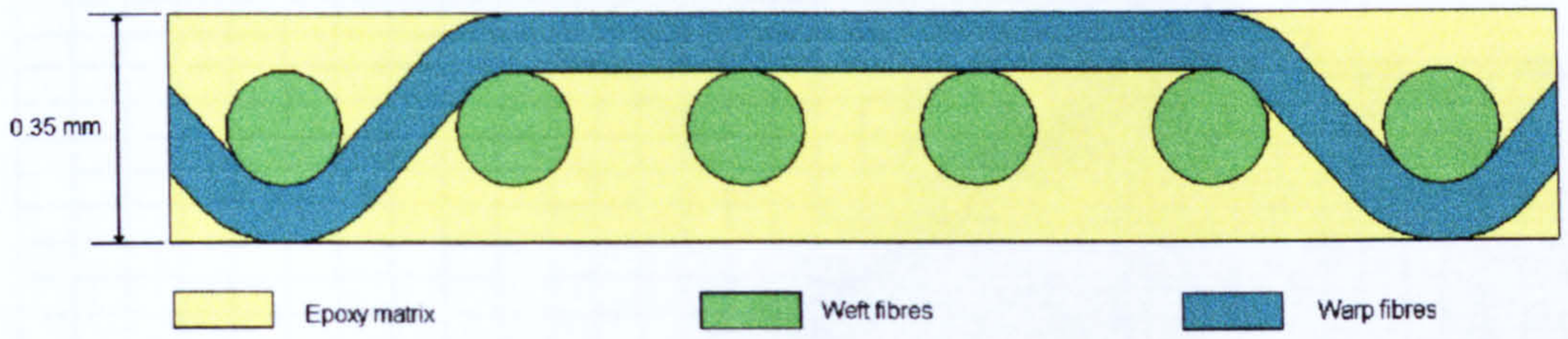

Figure 92 Section through the repair patch 5HS woven composite

The corresponding material data for the repair patch are given in Table 22 and Table 23. T300/LY5052 is a woven carbon fibre reinforced composite with 5 harness satin weave pattern (as shown in Figure 91 [163]) . The lamination sequence used was as follows: $[(\pm 45)_2/(0/90)_4/\pm 45/(0/90)_2]_s$. The repair patch was added to the parent laminate using a wet lay-up technique and then cured unto it. The patch epoxy matrix played the role of the adhesive. Along the repair joint length, pockets of epoxy existed as shown in Figure 92 which formed a bond with the parent laminate. Thus for modelling purposes, an adhesive layer was included between the parent laminate and the repair patch. This layer was 0.13 mm thick.

5.2 - Linear Static Analysis

The analysis was carried out in two main stages: one dealing essentially with linear elastic materials and the second part including the adhesive non-linear behaviour. This case study also served as a test case for the remaining cases due to the fact that the same scarf joint characteristics were used in the experimental investigation of a repaired flat panel and curved panel.

5.2.1 - Modelling Strategy

The linear static analysis was broken down into two main parts: one investigating the adhesive stress distribution for both scarf joint configurations and the second demonstrated the viability of the twin phase modelling concept. These two parts are described in the following sections along with a consideration of the method used to predict the failure loads.

5.2.1.1 - Preliminary Investigation

The primary aim of this investigation was to find out the main differences between configurations A and B with an emphasis on adhesive stresses along the joint length. This allowed an objective assessment of the two configurations without resorting to full scale analysis and comparison with experimental data.

As noted earlier, for the experimental programme, configuration B was chosen because it was comparatively easier to manufacture. From a practical point of view, repair engineers found configuration A almost impossible to realise accurately. The analysis was to check if that choice was right as far as adhesive shear stress characteristics were concerned.

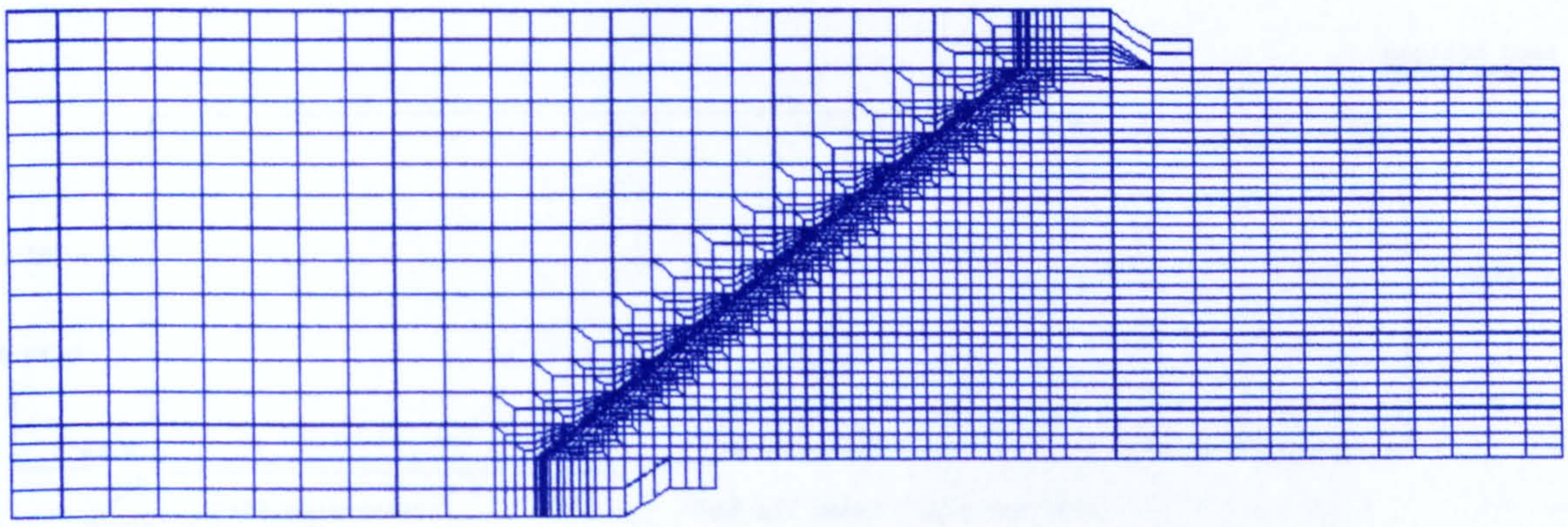

Figure 93 Configuration A - FE Mesh used

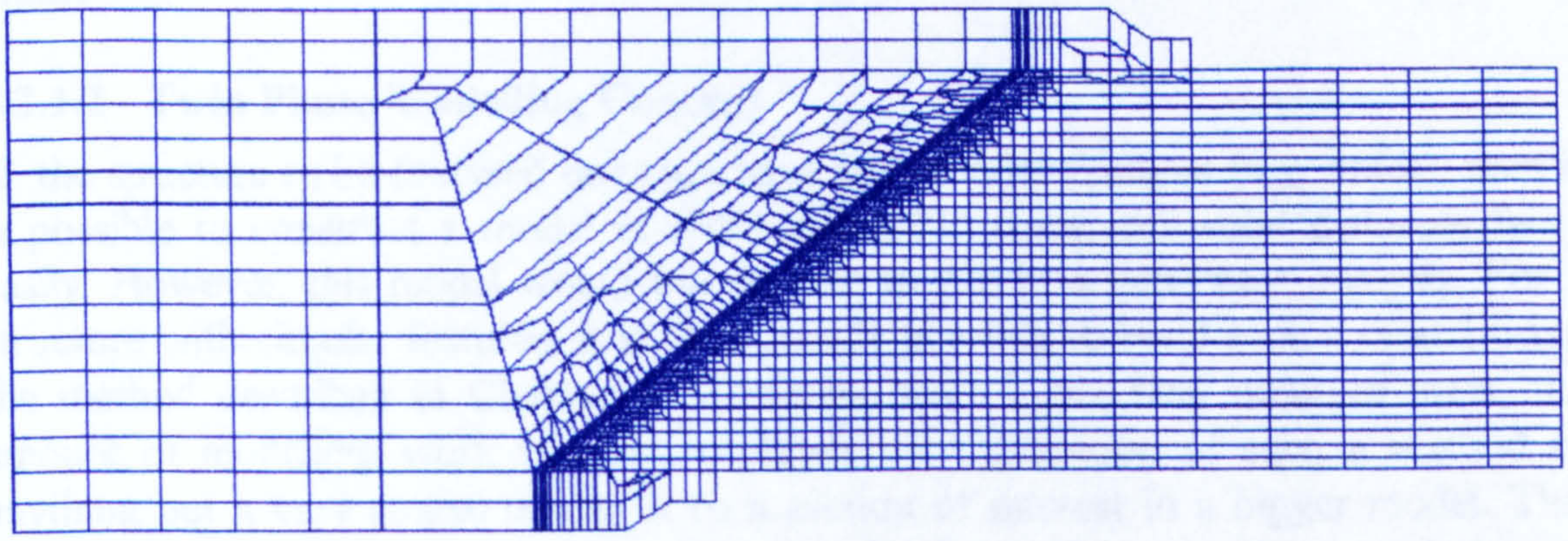

Figure 94 Configuration B - FE mesh used

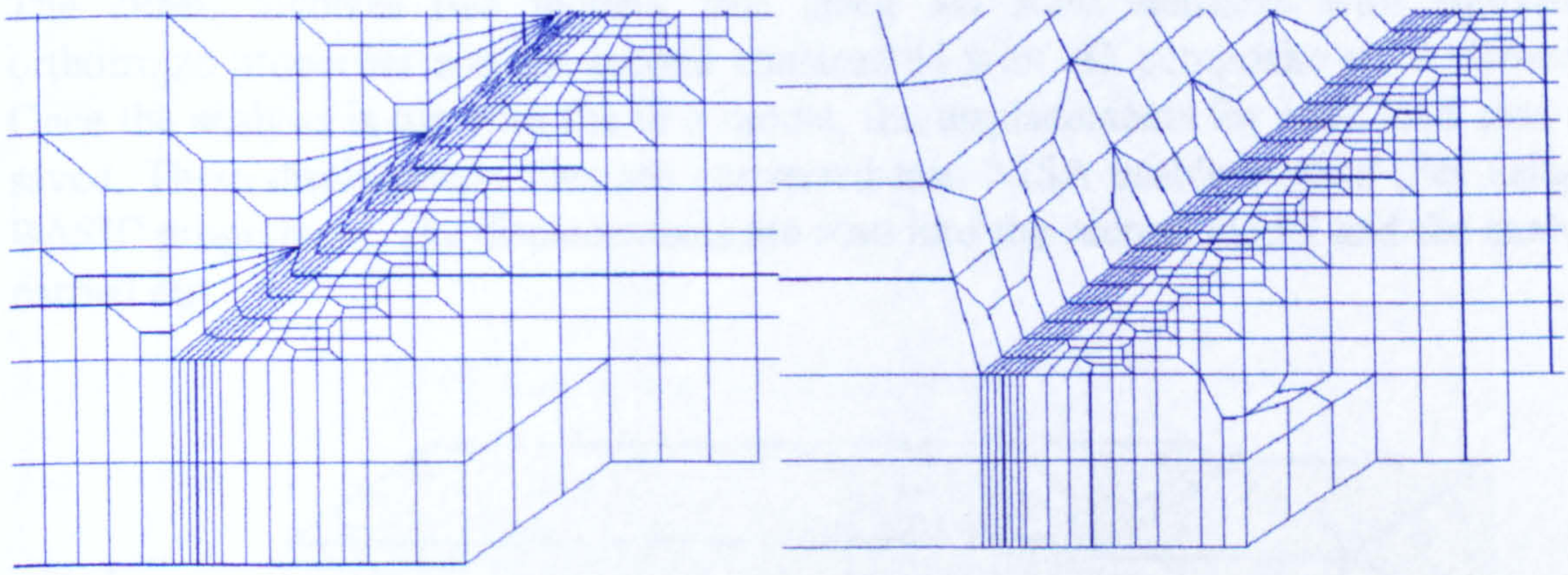

(a) *(b)*

Figure 95 Mesh close-up: (a) Configuration A (b) Configuration B

2D plane strain models of both scarf joints were built. These model used the composite equivalent properties given the preceding tables. The mesh used was quite fine, especially along the joint length to in order to capture the stress field accurately (Figure 93 and Figure 94). Following recommended practice, the adhesive layer had 6 elements along the thickness. A close-up of both meshes is shown in Figure 95.

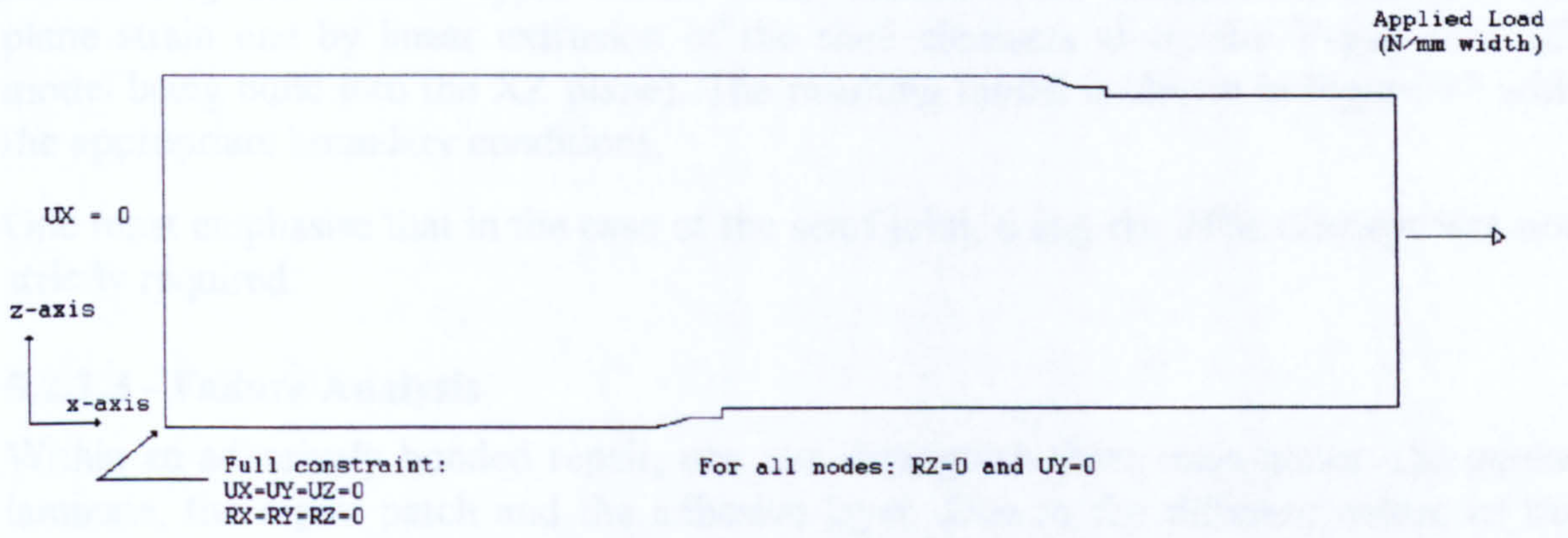

Figure 96 Boundary conditions for plane strain models

The load and displacement boundary conditions applied for both models are given in Figure 96 .

5.2.1.2 - Twin Phase Modelling Concept

If the structure to be analysed does not have any circular features (e.g. holes), then it is possible to construct a model in NISA using 3D composite solid elements fairly easily. However, this model would not be able to run in a non-linear analysis. For a structure with circular features, it is theoretically possible to build such a model using the method described in Chapter 3. However, from a practical point of view, the amount of modelling work involved prohibits the application of such a method to anything but a very coarse model or to a section of interest in a bigger model. This modelling concept has been thought of to cater for cases where non-linear analysis may be required but could not be undertaken using 3D composite solid elements

The 2PMC involves two models: one using 3D solid elements with equivalent orthotropic properties and the second constructed with 3D composite solid elements. Once the analysis is run with the first model, the displacements for each load case are saved. These displacement files are converted into NISA usable session files using a BASIC programme. The displacements are read into the second model and the analysis carried out.

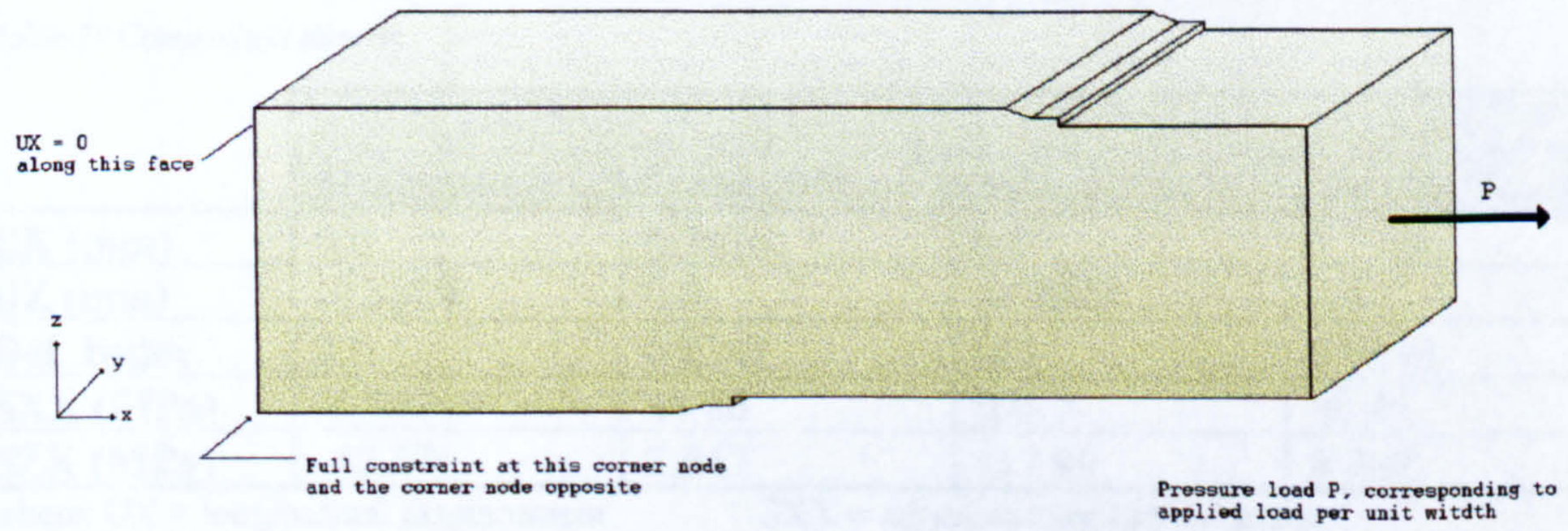

Figure 97 3D Solid model with boundary conditions

The two models are identical in every respect with the same number of elements and nodes. Only the element types differ. These models were constructed from the 2D plane strain one by linear extrusion of the shell elements along the Y-axis (the 2D model being build into the XZ plane). The resulting model is shown in Figure 97 with the appropriate boundary conditions.

One must emphasise that in the case of the scarf joint, using the 2PM concept was not strictly required.

5.2.1.3 - Failure Analysis

Within an adhesively bonded repair, one can distinguish three main zones: the parent laminate, the repair patch and the adhesive layer. Due to the different nature of the materials used in these three zone, no single failure criterion can be applied to determine the failure load.

One has to address in turn each of the three zones, applying an appropriate criterion to determine the failure load. Comparing these failure load levels enables the determination of the likely failure order and location.

For the composite adherends, three criteria have been selected: the average stress failure criterion (ASFC), the traditional Maximum Stress criterion and the Tsai-Wu interactive failure criterion. The ASFC was used by Soutis and Hu [108] to predict failure initiation in bonded scarf repairs modelled using equivalent orthotropic properties in a 3D model. This criterion was selected to check its suitability for composites structures. The other two were selected to demonstrate the necessity of using failure criteria which are specific to composites in assessing bonded repairs to composite structures.

For the adhesive, the average stress failure criterion (ASFC) has been retained as the primary failure criterion due to its inherent simplicity. Its use gives a fairly conservative estimate of the adhesive failure load, taking into account adhesive non-linearity and plastic deformation. For the adhesive, the stress is averaged over the whole joint length.

5.2.2 - Results and Discussion

5.2.2.1 - Comparison of Configuration A and B

Table 24 Comparison Results

	Configuration A		Configuration B	
	Minimum	**Maximum**	**Minimum**	**Maximum**
UX (mm)	0.0	0.7876	0.0	0.7784
UZ (mm)	-0.3329	0.0	-0.3898	0.0
Def. Index	0.0	0.8141	0.0	0.8234
SXX (MPa)	-5.947	44.80	0.0	20.43
SZX (MPa)	-42.27	7.647	-17.99	8.402

where: UX = longitudinal displacement SXX = adhesive longitudinal stress
UZ = vertical displacement SZX = adhesive out-of-plane shear stress
Def. Index = deformation index calculated from all displacements, indicates overall shape change from original shape.

Configuration A is a cross between a stepped lap joint (on the repair patch side) and a scarf joint (on the parent laminate side). This leads to a particular stress distribution as will be shown in the following figures. Configuration B has the advantage of creating a smoother scarf joint on both sides of the adherends.

The main results are summarised in Table 24. It indicates that model B extends slightly less than model A but deflects more and this results in a deformation index which is higher. The maximum longitudinal stress in A is more than twice that in B. For the shear stresses, the important set of values are the minimum one in the table (negative because of the scarf orientation and the loading in tension). Here again the value for A is twice that for B. This indicates that there are higher stress concentrations in Configuration A. Confirmation of this indication is given by the adhesive tensile and shear stress curves for both configurations.

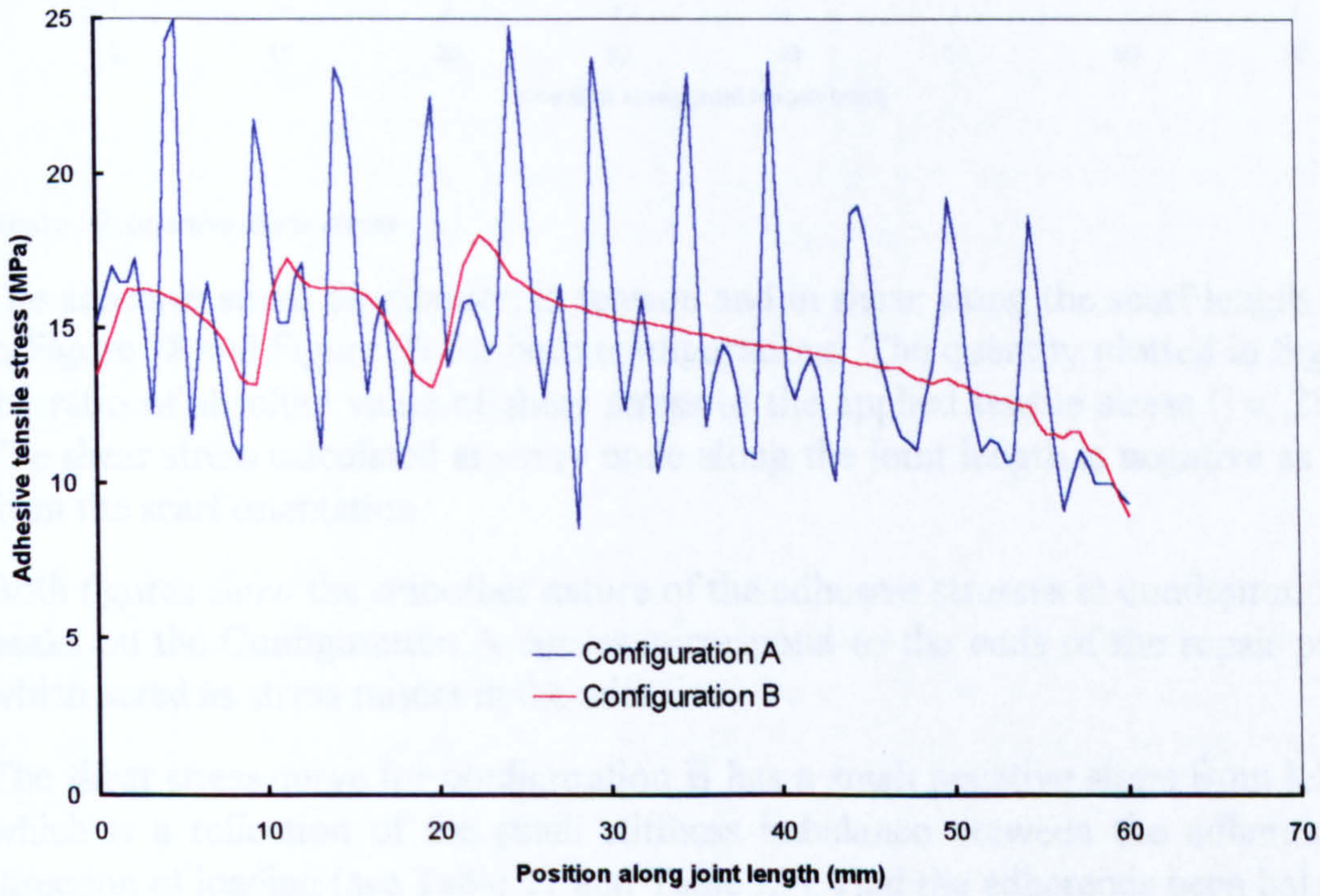

Figure 98 Adhesive tensile stress

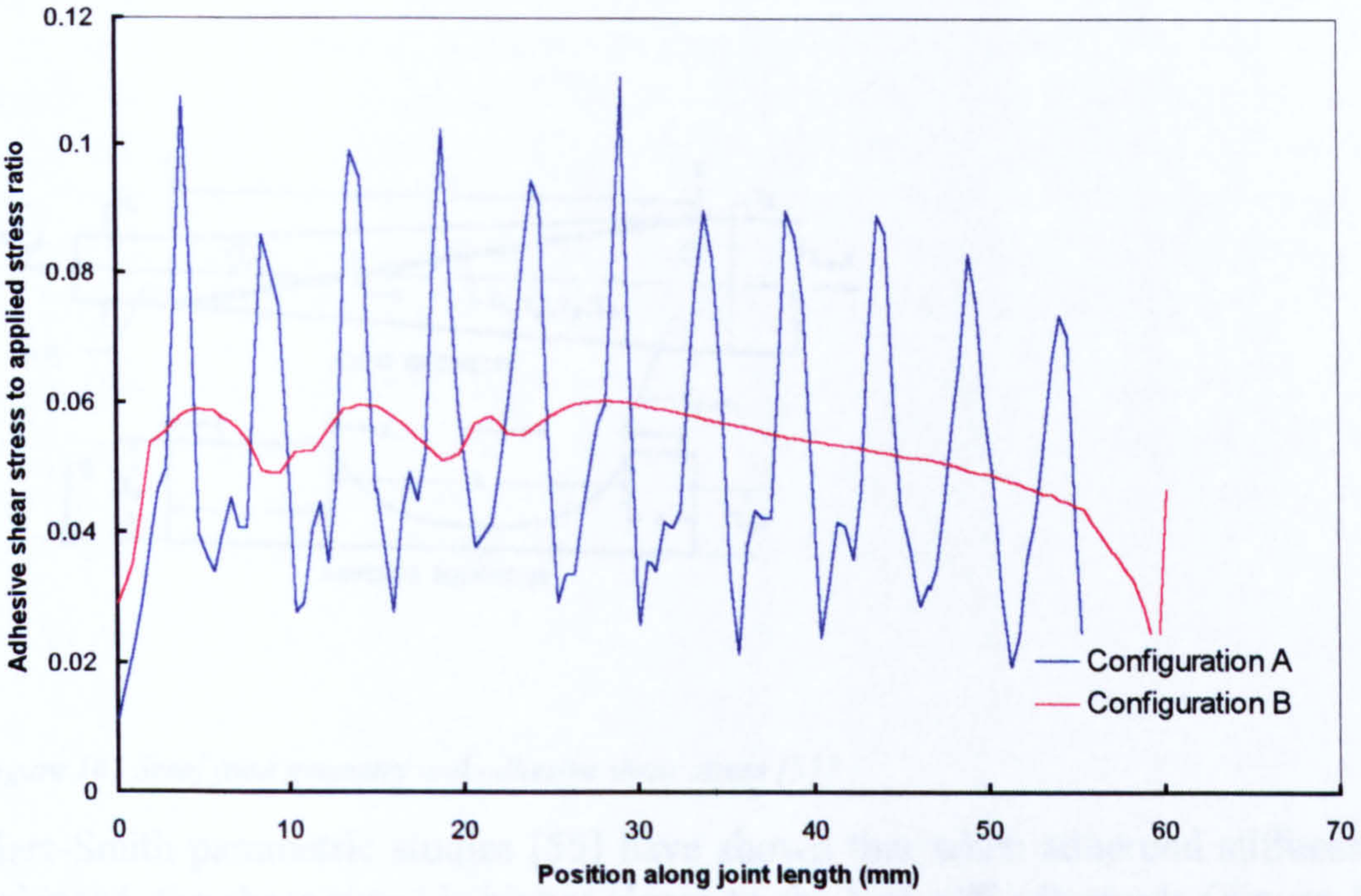

Figure 99 Adhesive shear stress

The adhesive stress distribution in tension and in shear along the scarf length is shown in Figure 98 and Figure 99 for both configurations. The quantity plotted in Figure 99 is the ratio of absolute value of shear stress to the applied tensile stress (i.e. 298 MPa). The shear stress calculated at every node along the joint length is negative as expected from the scarf orientation.

Both figures show the smoother nature of the adhesive stresses in configuration B. The peaks on the Configuration A curves correspond to the ends of the repair patch plies which acted as stress raisers in the adhesive.

The shear stress curve for configuration B has a small negative slope from left to right which is a reflection of the small stiffness imbalance between the adherends in the direction of loading (see Table 21 and Table 23). Had the adherends been balanced, the shear stress would have been uniformly flat, falling to zero at both joint ends.

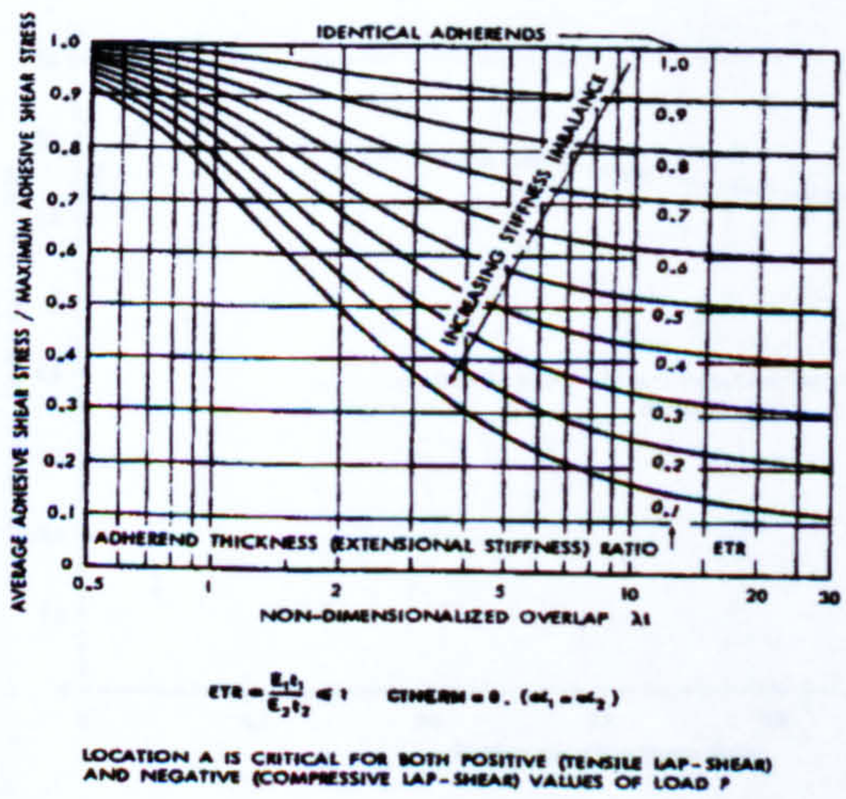

Figure 100 Effect of adherend stiffness imbalance on shear stress distribution [55]

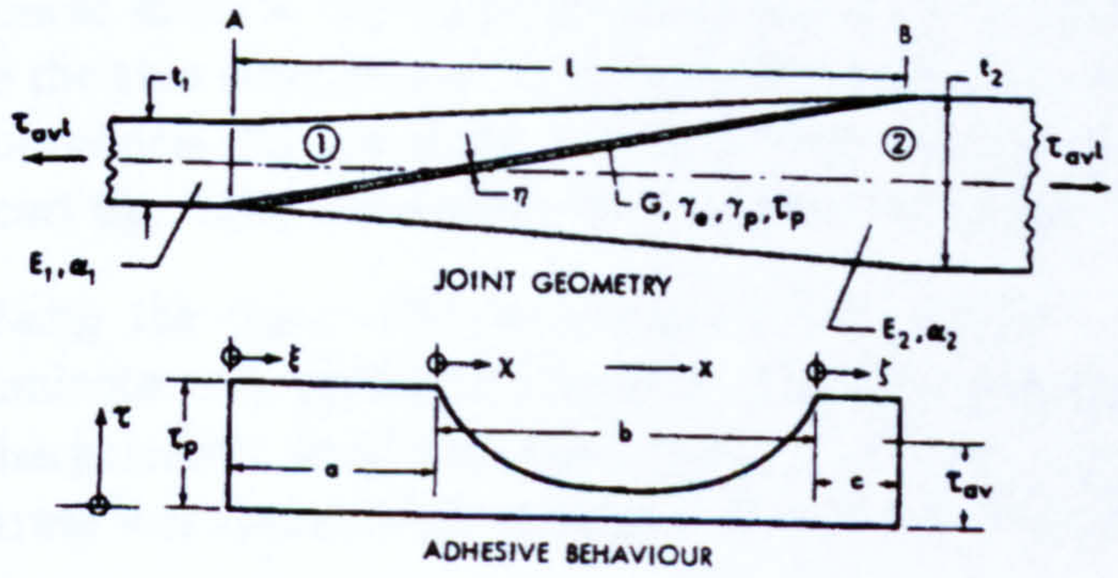

Figure 101 Scarf joint geometry and adhesive shear stress [55]

Hart-Smith parametric studies [55] have shown that when adherend stiffness are not balanced, the shear stress is higher closer to the less stiff adherends (Figure 100). The present curve shows similar trends but with some noticeable differences (namely in curve smoothness). Location A mentioned in Figure 100 is shown in Figure 101

Thus, the simple comparison of adhesive stress characteristics showed that the second configuration was overall better than the first one. For the remaining analysis, Configuration B only was considered as experimental data was available for this scarf joint.

5.2.2.2 - Failure Analysis

The 2D model allowed the preliminary investigation to be carried out efficiently. The results obtained there were used as reference to check the various 3D models analysed subsequently. Once stresses were evaluated, the appropriate failure criteria were applied to the composite adherends and then to the adhesive

Composite Adherends

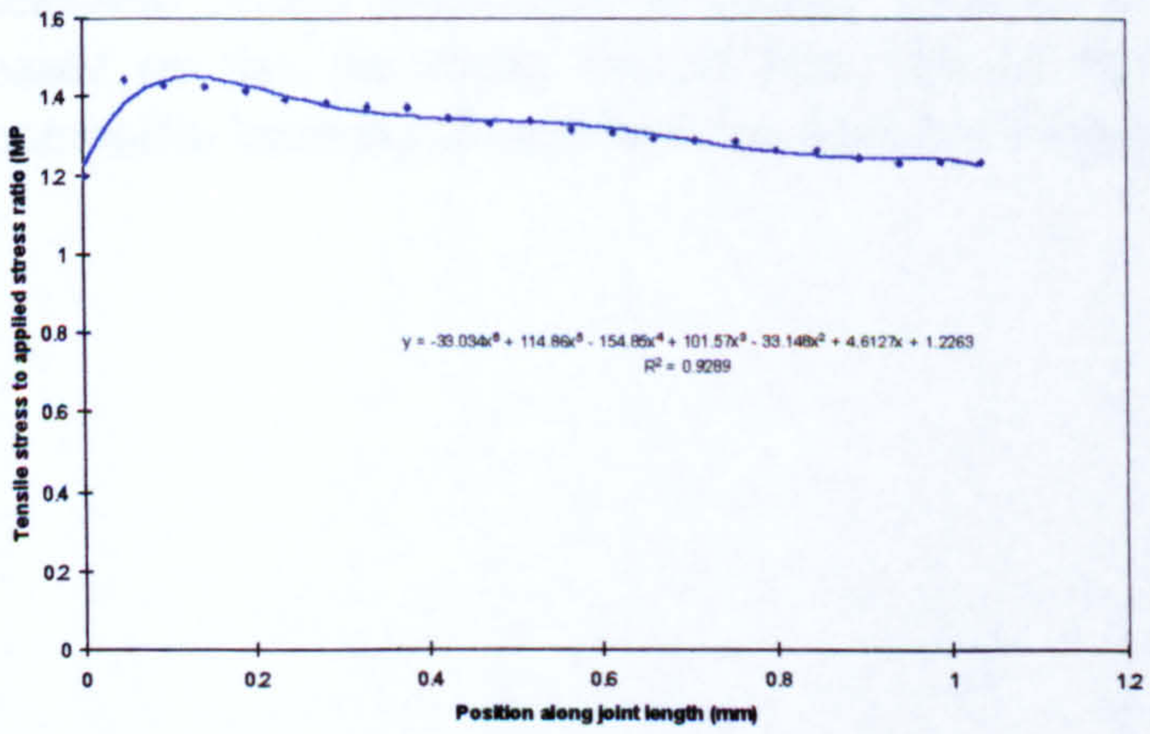

Figure 102 Parent laminate tensile stress along the joint length from scarf tip

The variation of tensile stress along the joint length in the parent laminate, obtained from the 3D solid model, is shown in Figure 102. One notices that there is no stress singularity at the tip of the scarf but a definite value. This could have been due to a coarse mesh at the tip of the scarf unable to calculate the stress field accurately or due to the two extra layers at bottom of the coupon. Successive refinements of the mesh in submodels did not show any significant change in the stress field in the vicinity of the scarf tip. Thus the absence of a stress singularity was due to these layers.

Using the curve shown in Figure 102 and the definition of the ASFC, the parent laminate was predicted to fail at 8526.3 N/mm width (2030 MPa or 341 kN). The characteristic length d_0 was chosen as 1 mm. The ratio of average stress to applied stress was found to be constant for a given characteristic length.

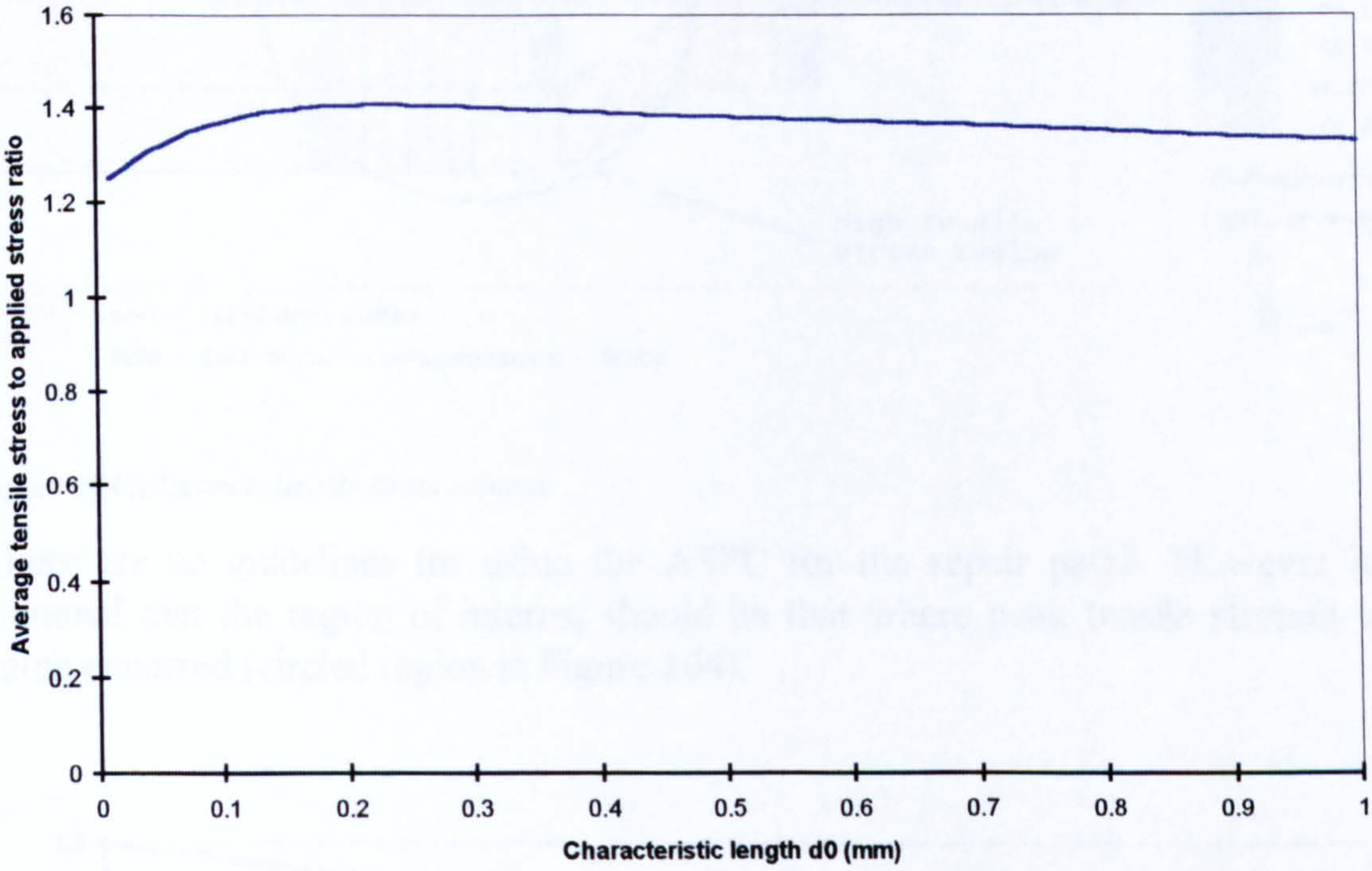

Figure 103 Effect of characteristic length on the average stress

Further investigations have shown that the characteristic length has a strong influence on the calculated average stress (Figure 103). It is not clear what should guide the selection of this adjustable parameter. Clearly, its effect is such that any prediction based on this parameter should bear that in mind. Applying such a criterion to a composite laminate should be done with due caution.

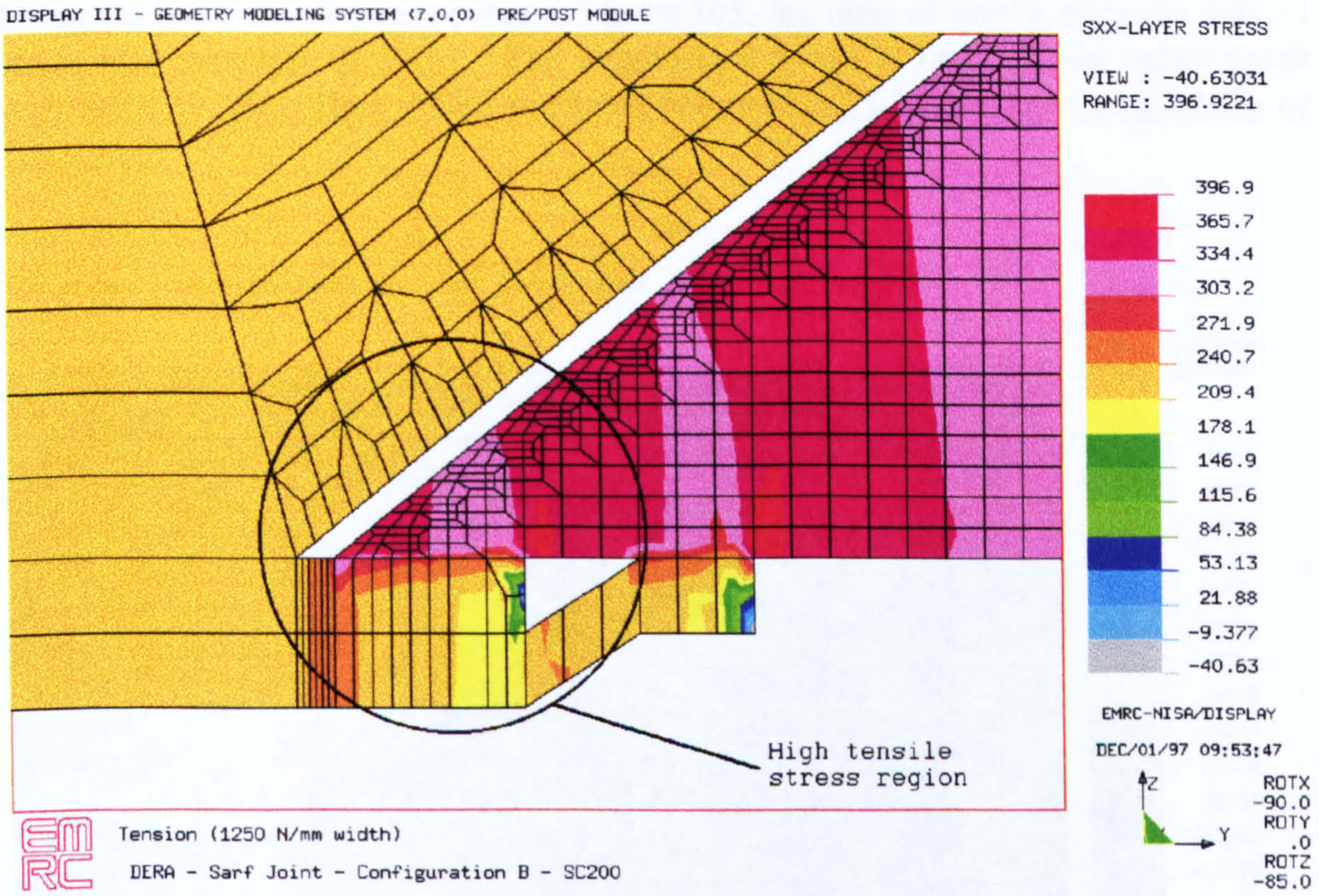

Figure 104 Adherends tensile stress contour

There are no guidelines for using the ASFC for the repair patch. However it was assumed that the region of interest should be that where peak tensile stresses in the patch occurred (circled region in Figure 104).

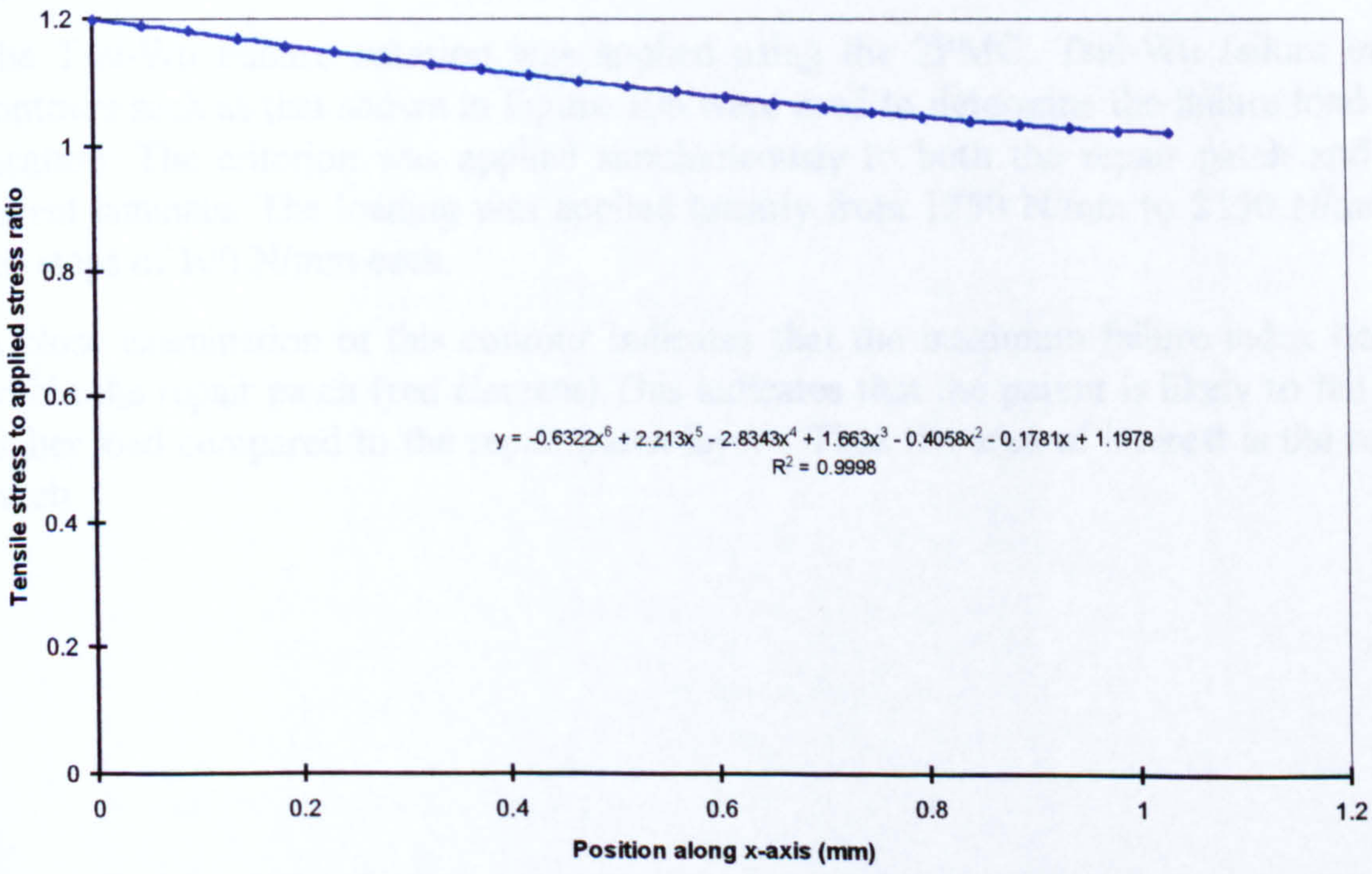

Figure 105 Repair patch tensile stress along longitudinal axis from scarf tip

Using the patch tensile stress curve in Figure 105, the ratio of tensile stress to applied stress was calculated as 1.101 . The longitudinal tensile strength of the repair patch was 696 ± 39 MPa. Thus ASFC predicted failure at 2655.3 N/mm (i.e. 632.2 MPa or 106.2 kN).

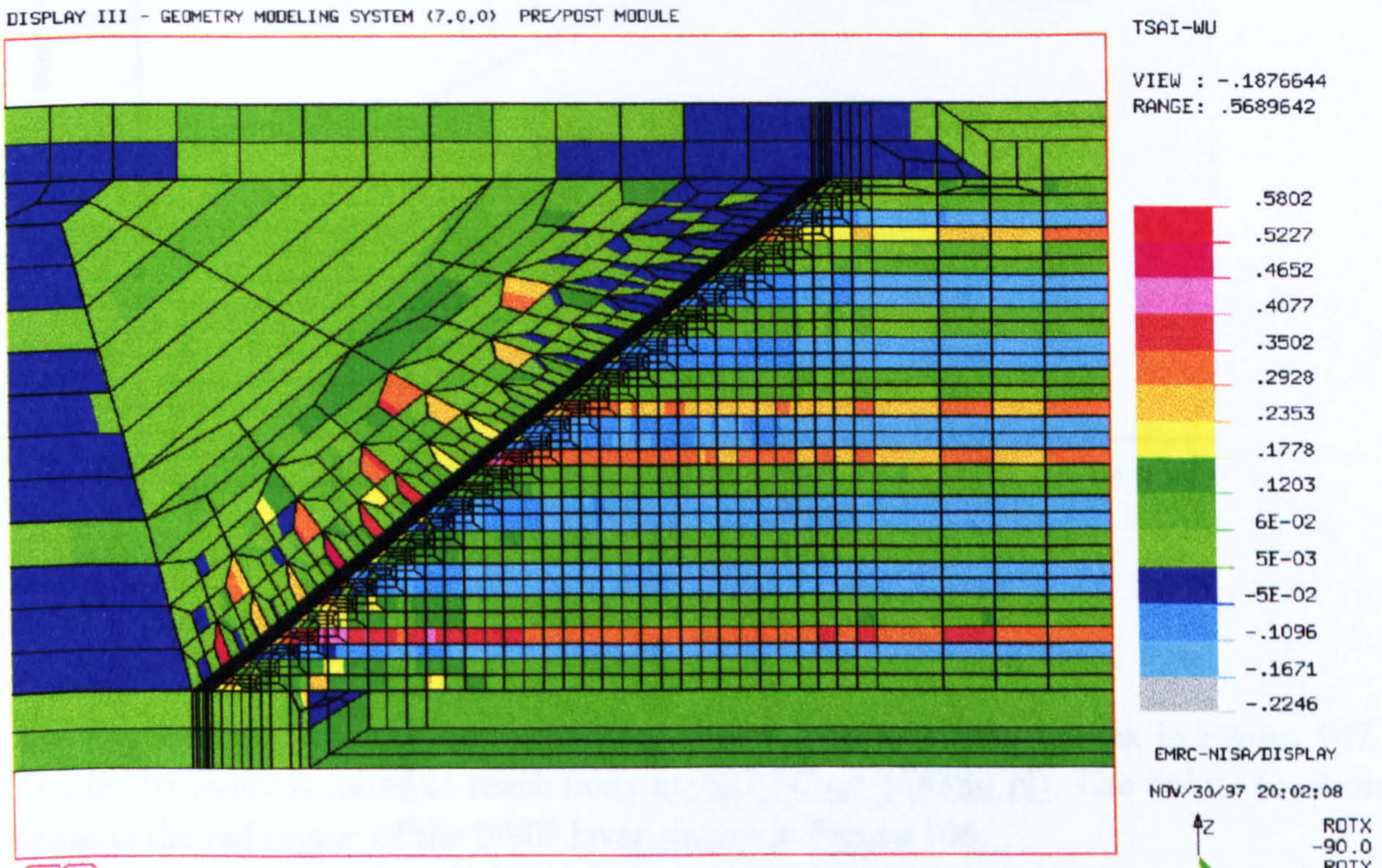

Figure 106 Tsai-Wu Failure Index Contour for applied load at 1250 N/mm (298 MPa)

The Tsai-Wu Failure criterion was applied using the 2PMC. Tsai-Wu failure index contours such as that shown in Figure 106 were used to determine the failure load and location. The criterion was applied simultaneously to both the repair patch and the parent laminate. The loading was applied linearly from 1250 N/mm to 2150 N/mm in ten steps of 100 N/mm each.

A close examination of this contour indicates that the maximum failure index occurs within the repair patch (red element).This indicates that the parent is likely to fail at a higher load compared to the repair patch layers. Thus the area of interest is the repair patch.

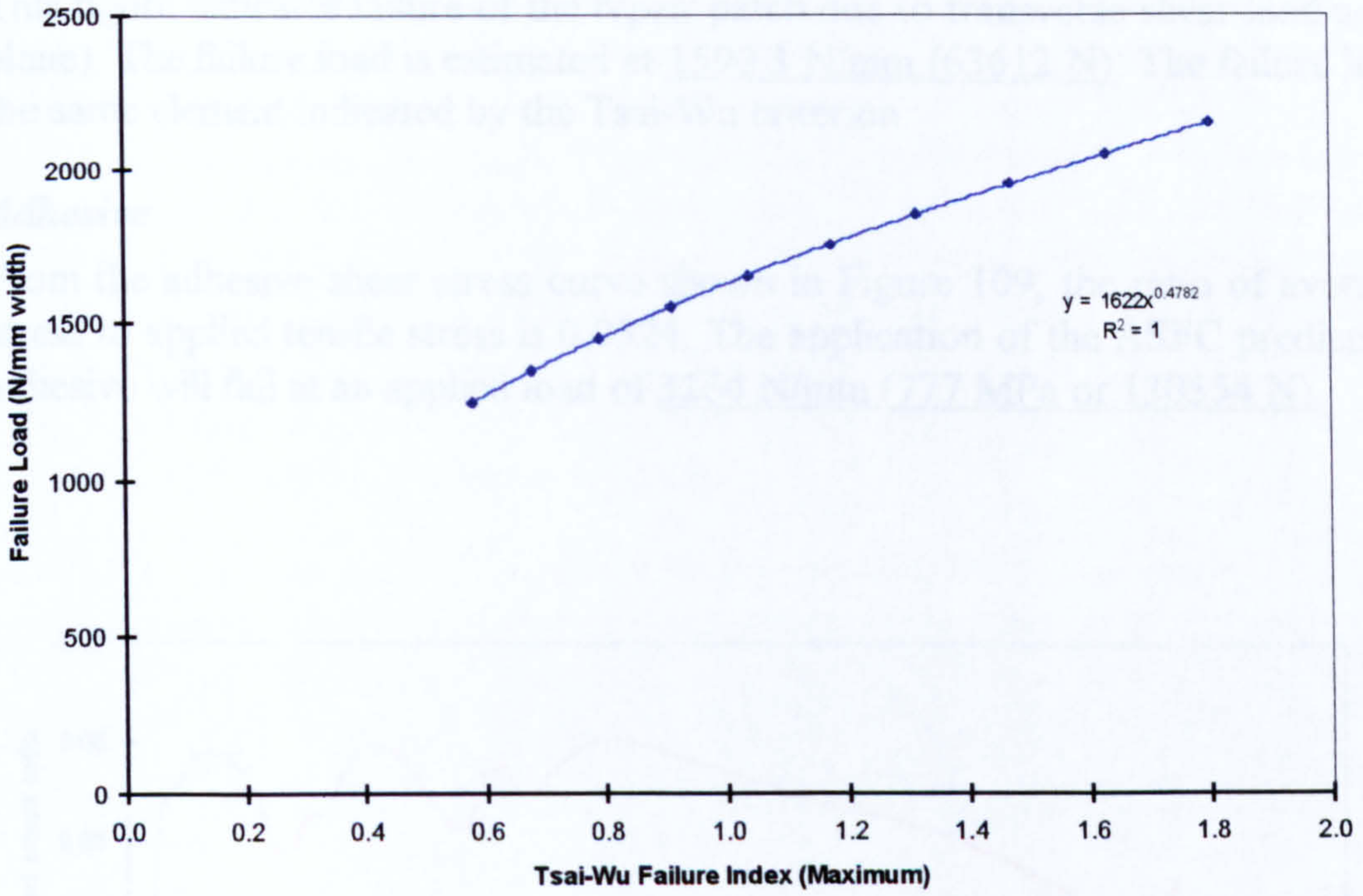

Figure 107 Maximum Tsai-Wu failure index

The applied load is plotted against the maximum Tsai-Wu failure index in Figure 107. The failure index is found to reach unity at1622 N/mm (64880 N). The failure location being in the red region of the 0/90° layer shown in Figure 106.

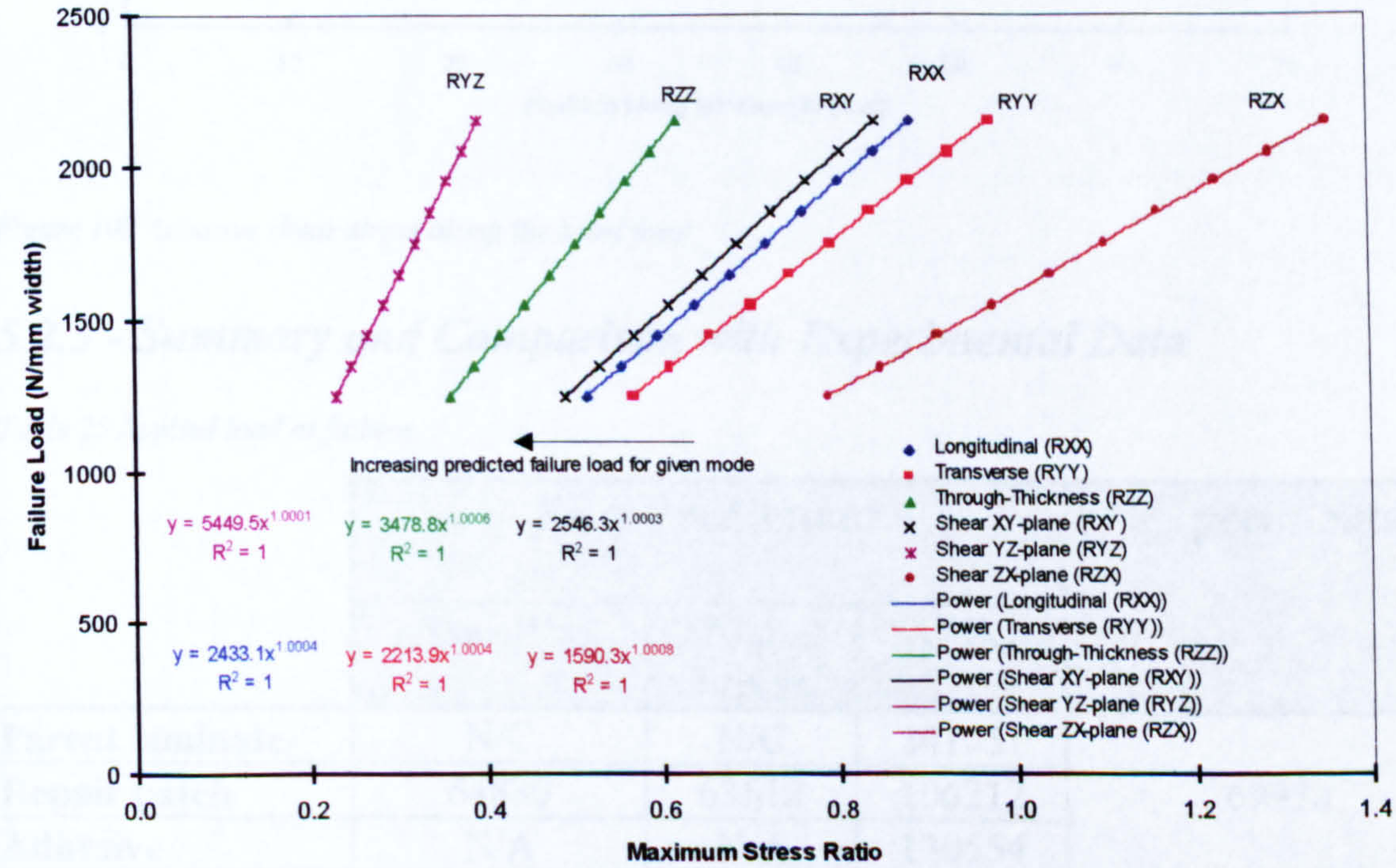

Figure 108 Maximum stress failure criterion

The maximum stress failure criterion has also been applied to the calculated layer stresses for all 10 load cases. The applied load is plotted against all six stress ratios in Figure 108.

This figure indicates failure of the repair patch due to transverse shear loading (in ZX-plane). The failure load is estimated at 1590.3 N/mm (63612 N). The failure location is the same element indicated by the Tsai-Wu criterion.

Adhesive

From the adhesive shear stress curve shown in Figure 109, the ratio of average shear stress to applied tensile stress is 0.0524. The application of the ASFC predicts that the adhesive will fail at an applied load of 3264 N/mm (777 MPa or 130554 N).

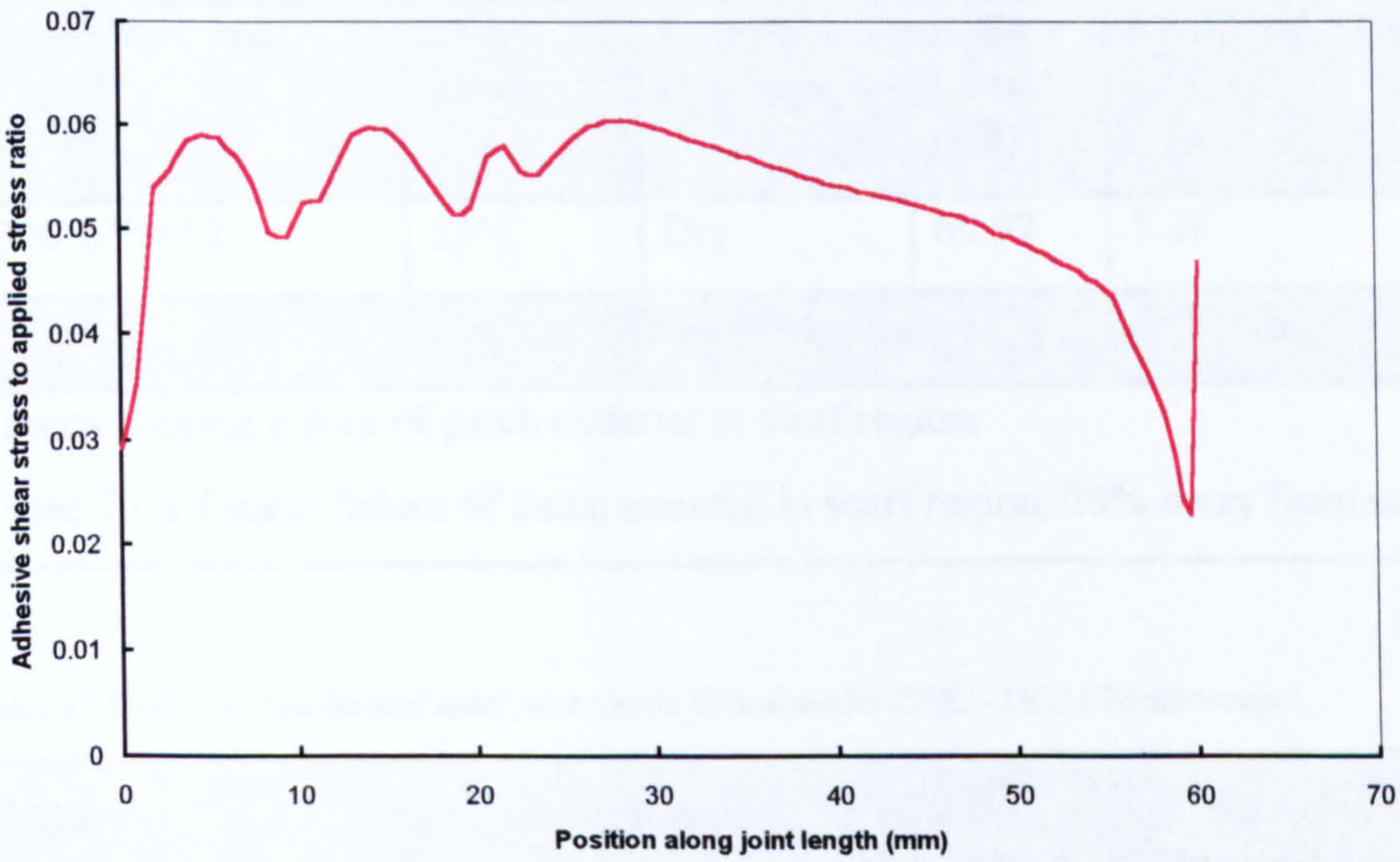

Figure 109 Adhesive shear stress along the scarf joint

5.2.3 - Summary and Comparison with Experimental Data

Table 25 Applied load at failure

	FEA Predictions			Experimental
	Tsai-Wu	**Max. Stress**	**ASFC**	
Parent laminate	N/C	N/C	341051	69970
Repair patch	64880	63612	106212	
Adhesive	N/A	N/A	130554	
% Difference with experimental results	7.84%	9.99%	51.80%	N/A
N/C = not calculated N/A = not applicable	all values in N			

From the summarised results (Table 24), the patch is predicted to be the weakest part of the joint whichever method is used. However the predicted failure load varies greatly between the ASFC (51.80%) and the two other criteria (7.84% for Tsai-Wu and 9.99% for maximum stress). The latter two predict failure loads which are closer to but lower than the experimental data. This is consistent with the fact that these predictions are for first ply failure whereas the experiment recorded final failure loads. Finally, the maximum stress criterion predicted failure through transverse shear (ZX-plane) which is consistent with the fact that composites have low transverse strengths [164]. Although woven fabric composites are an improvement on UD composites in that respect, it is still a weakness in general.

Table 26 Results of tensile test of co-bonded scarf repair joints (SMC - DERA Farnborough)

Repair Materials	**Test Temp**	**Condition Dry/Wet**	**Failure Load (kN)**	**Standard Deviation (kN)**
T300/LY5052	23°C	Dry	69.97	5.38
Failure Mode				
3 specs. Tensile failure of patch material in scarf region. 2 spec 75% Tensile failure of patch material in scarf region, 25% away from scarf				

Table 27 Summary of co-bonded scarf joint tensile failure modes (SMC - DERA Farnborough)

Failure Mode	**Description**	**No. of Specimens**	**Percentage %**
A	Tensile Failure of Patch Material in Scarf	13	10.7
B	Partial Disbond of Scarf Joint and Tensile Failure of Patch Material	40	33.1
C	100 % Disbond of Scarf Joint and Tensile Failure of Overlap Patch	52	43.0
D	Tensile Failure and Large Delamination of Patch Material	1	0.8
E	100 % Disbond of Scarf Joint and Disbond of Overlap Patch	7	5.8
F	Tensile Failure at Patch Material in Plane of the Scarf	6	5.0
G	100 % Disbond of Scarf Joint and Tensile Failure of Overlap Patch, Delamination in Parent Material	2	1.7

Total number of specimens tested = 121

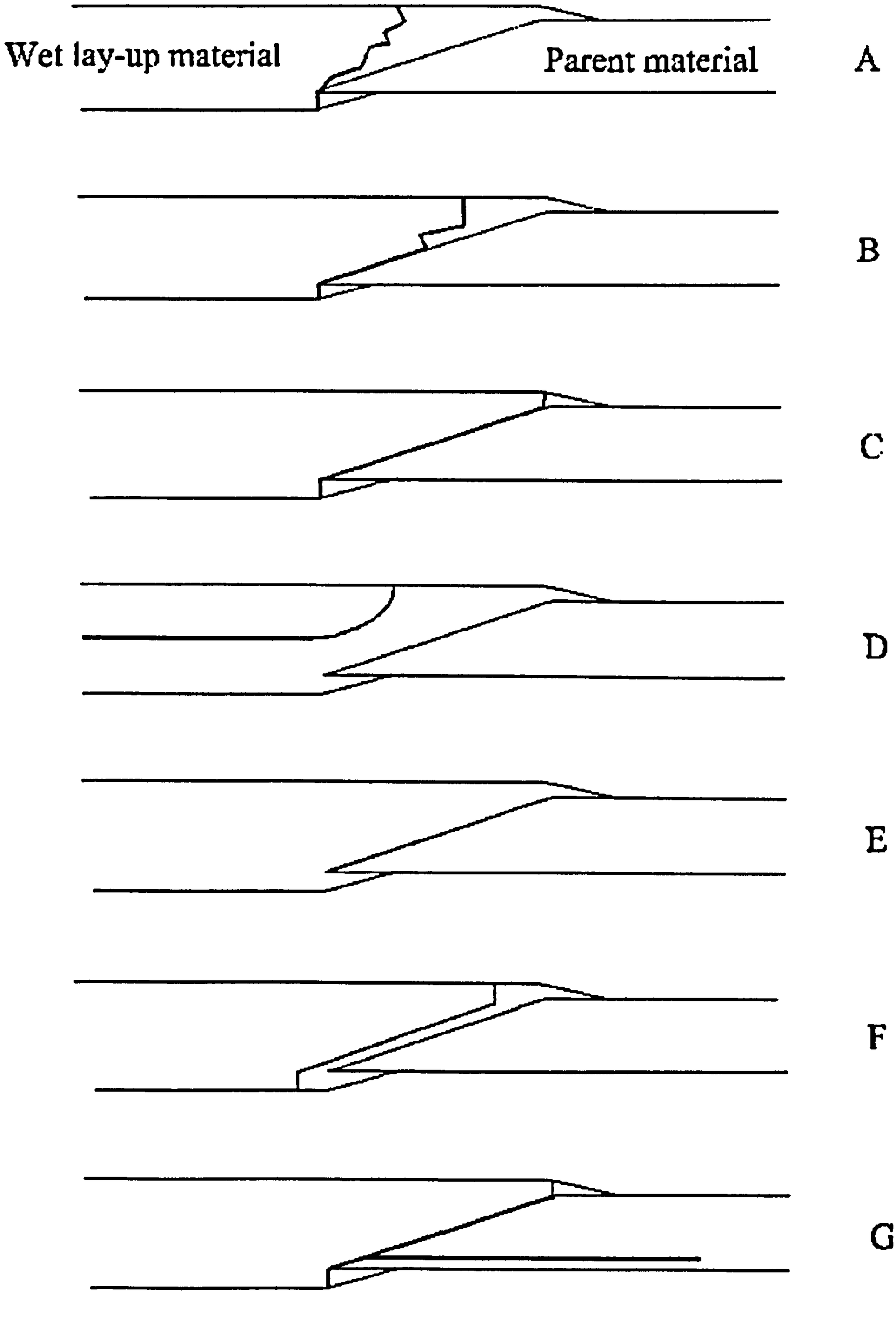

Figure 110 Schematic diagram of fracture modes observed in scarf joints (SMC - DERA Farnborough)

Table 26 shows the failure modes of the specimens tested at Farnborough. Most of these specimen failed in the scarf region. Further information about the experimental work can obtained from Table 27 which summarises the failure modes of all tested

specimens (including those from DERA partners). The failure modes are illustrated in Figure 110.

The observed fracture modes are consistent with the first ply failure location. Because the failure occurred so quickly, it was not possible to determine the sequence of events, even with the use of video equipment during the experimental phase. At the time of writing further work was being done to ascertain the correct failure sequence.

One possible explanation emerging from the FE analysis and the fracture mode schematic is that after failure was initiated in the patch, the fracture progressed to reach the interface between the woven wet lay-up material and the parent laminate which had resin rich pockets (Figure 92). This in turn lead to the degradation of bond along the scarf length.

Although in the analysis a thin uniform adhesive layer was modelled, that layer was not uniform between the patch and the parent laminate given the woven nature of the repair material. This may explain the propensity of the interface to disbond.

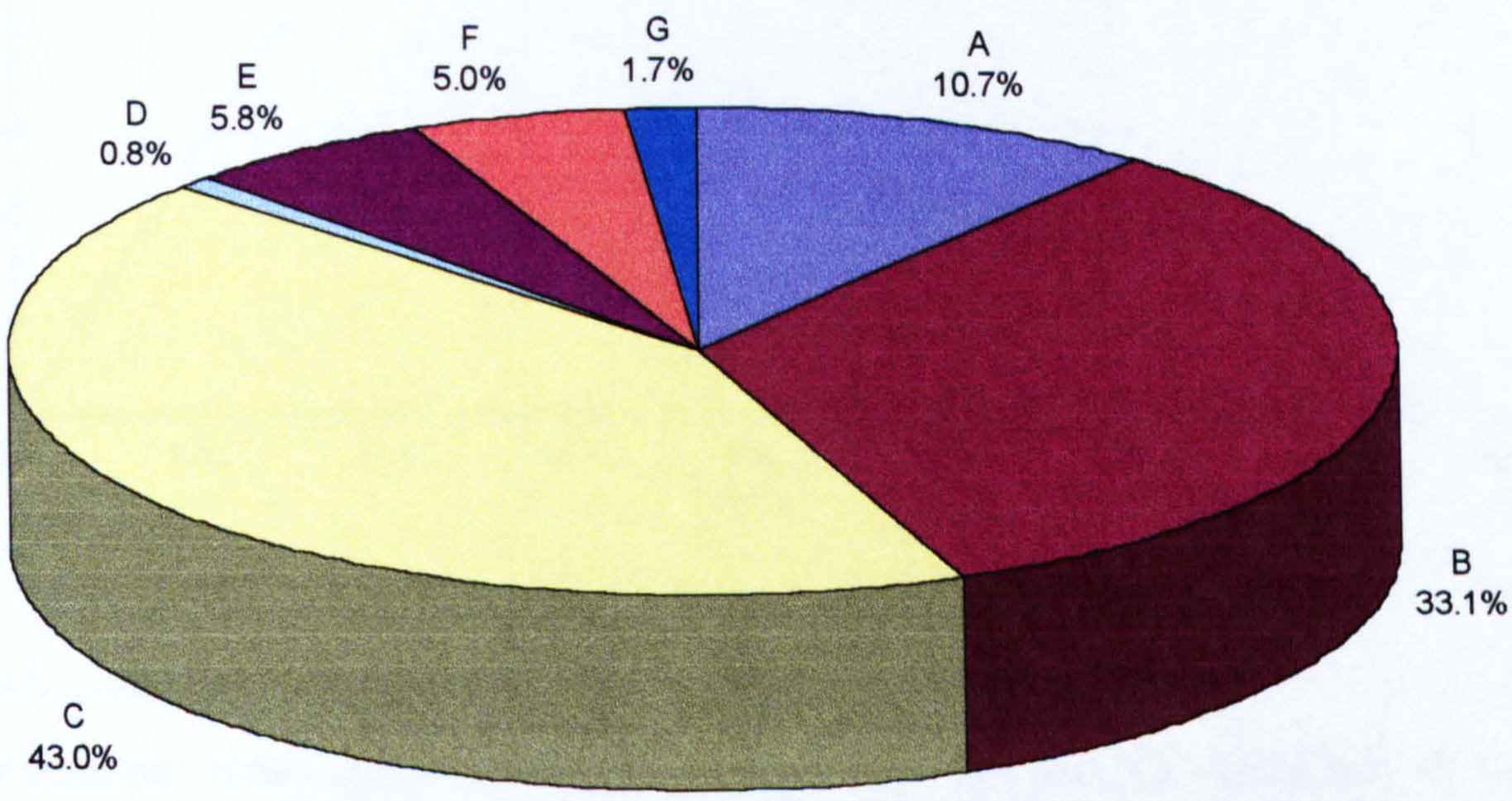

Figure 111 Scarf failure mode pie chart

The pie chart in Figure 111 indicates that most of the scarf joints failed through failure mode A, B or C. The latter being the biggest single category. These findings are further proof that the predicted FE results are in very good agreement with experimental results.

The use of the interactive failure criterion is more appropriate to predict composite failures than using a stress averaging one even if it includes the use of an adjustable parameter. The averaging of the stress hides the fact that even at low stresses, individual layers may fail leading to catastrophic failure of the whole laminate. The ASFC is more suited to predict failure in the adhesive.

5.3 - Non-linear Static Analysis

This part of the case study was carried out to ascertain the effect of the adhesive non-linear behaviour on the adhesive failure load. This was to ensure that the linear static analysis was not widely underestimating the failure load.

5.3.1 - Modelling Strategy

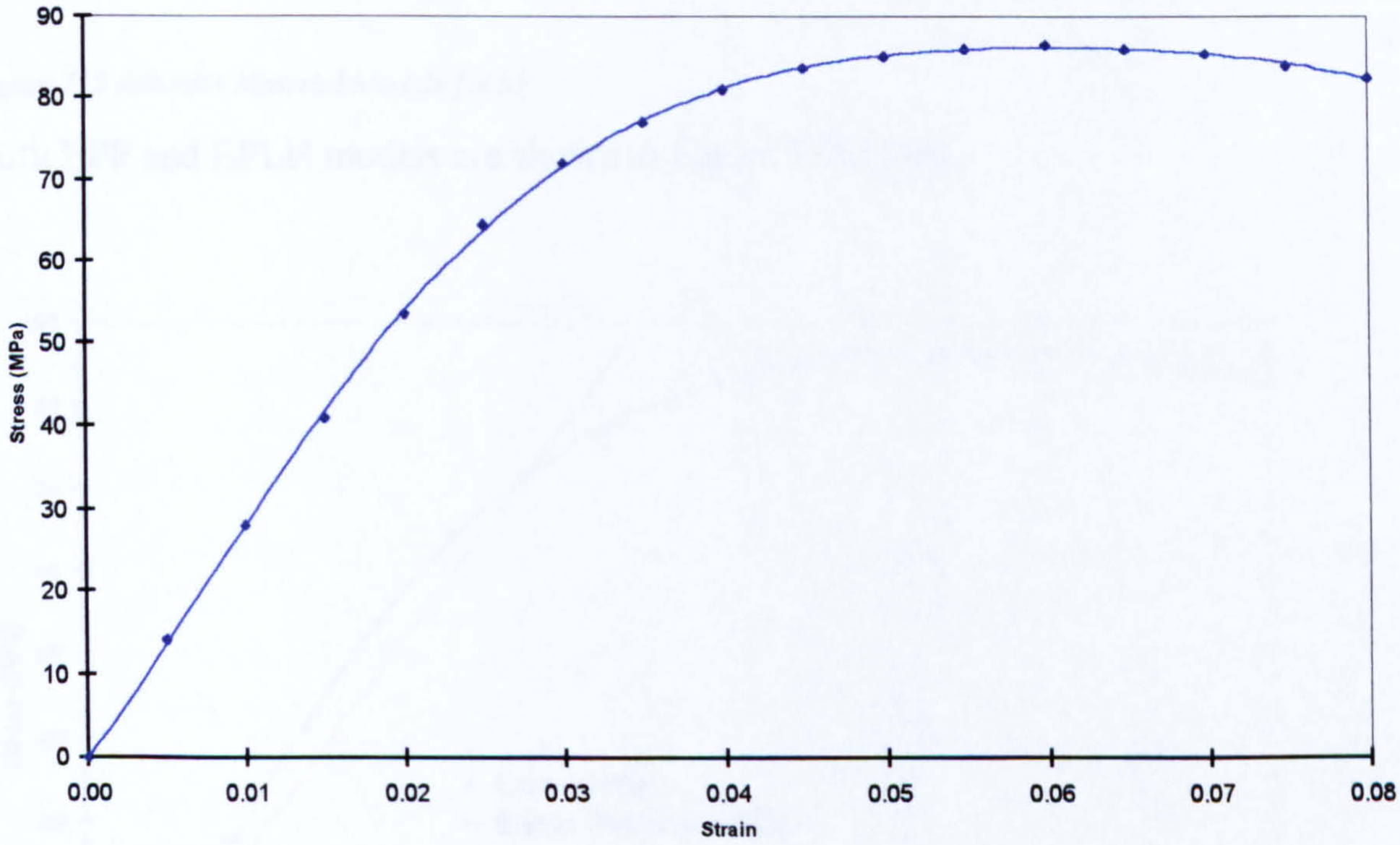

Figure 112 LY5052 Epoxy Adhesive Uniaxial Stress-Strain Curve

The non-linear static analysis deals essentially with the material behaviour of the adhesive which is represented by the uniaxial tensile stress-strain curve shown in Figure 112. The approach used here was to carry out this analysis in the first instance to find out what influence the adhesive non-linear behaviour had on the shear stress distribution and then determine the effect on the predicted failure load. To that aim, two aspects were addressed: which adhesive material model to use and which failure criterion to apply to determine the adhesive load carrying capacity.

5.3.1.1 - Adhesive Material Models

There was a choice between two material models that were selected: the traditional elastic, perfectly plastic (EPP) model favoured by most researchers and an elastic, piecewise linear hardening (EPLH) model which is closer to the true stress-strain curve of the adhesive. The EPP model was selected for its simplicity and also because it could fulfil the aim of this part of the case study. The idea was to used the EPLH model if the EPP model predicted much closer failure loads between the adhesive and the repair patch than that predicted by the linear static analysis.

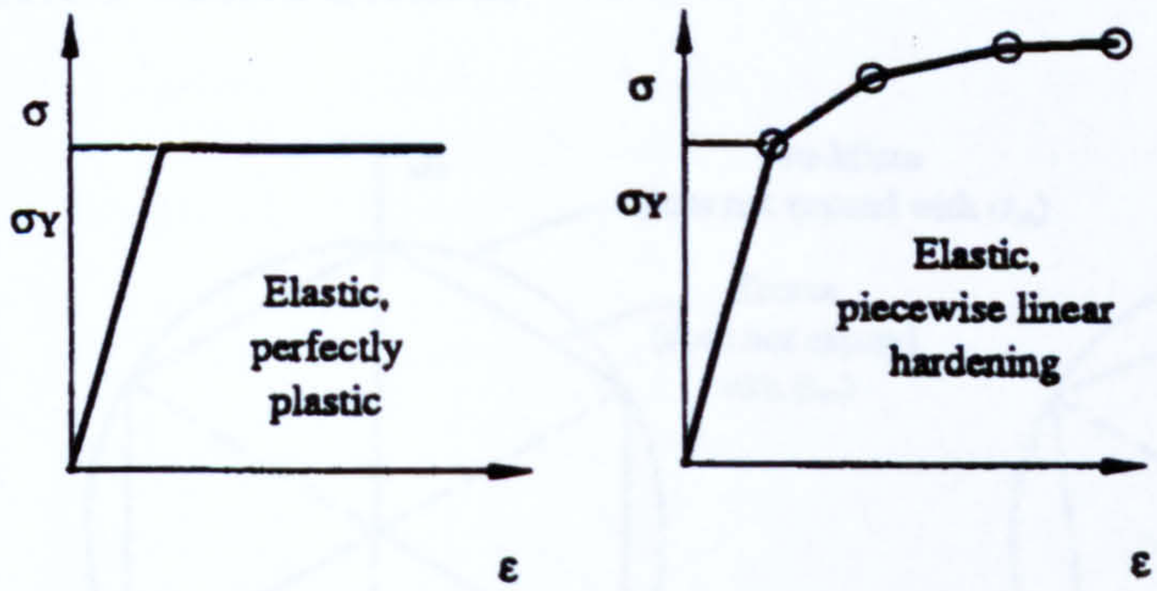

Figure 113 Adhesive Material Models [165]

Both EPP and EPLH models are shown in Figure 113 [165].

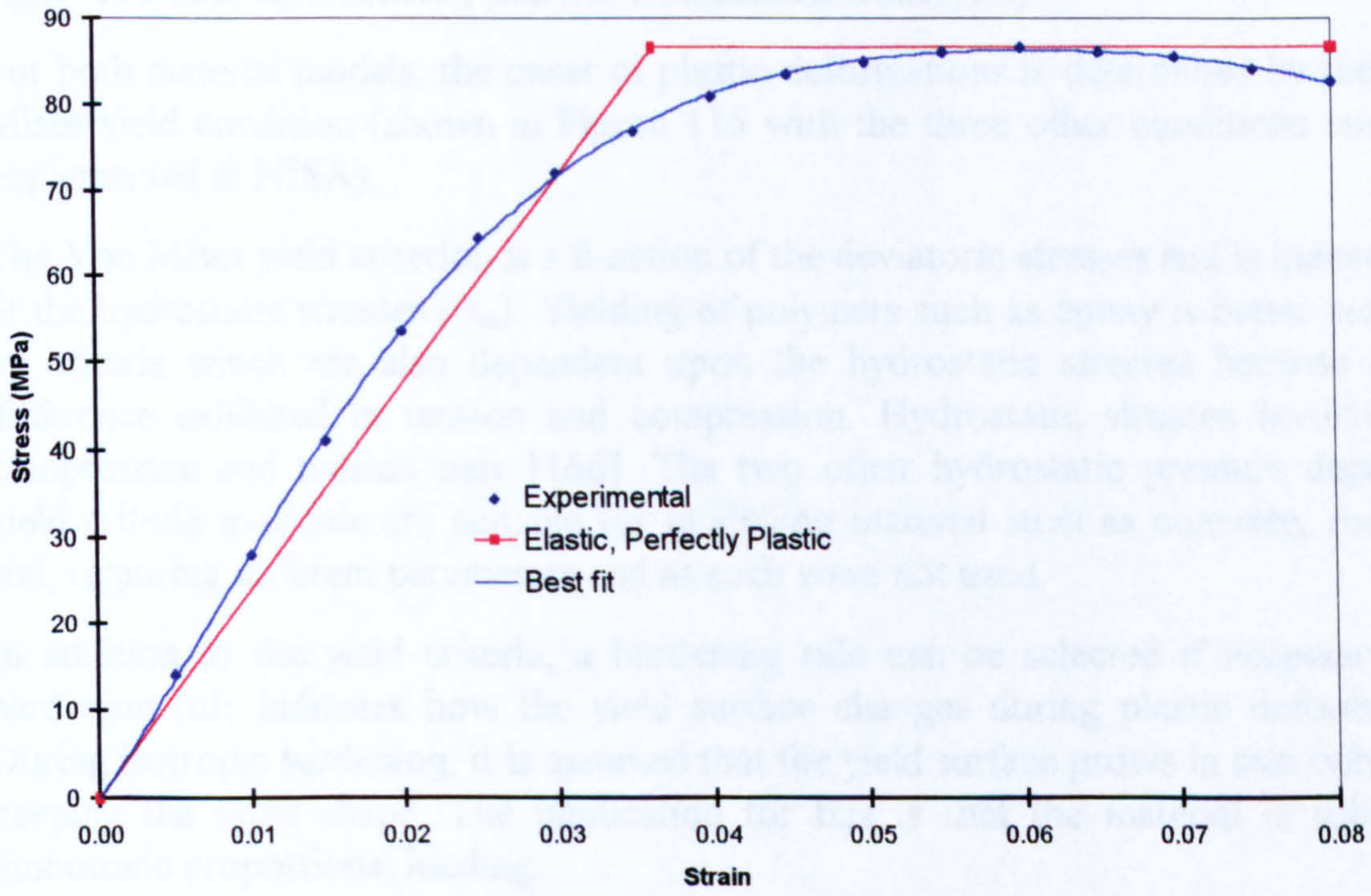

Figure 114 LY5052 Epoxy Adhesive EPP Model

The EPP curve (Figure 114) was obtained from the experimental curve using the condition that the strain energy density (represented by the area under the curve) was the same for both curves. This resulted in a lower Young's modulus for deformations up to the elastic limit (3.634%) compared to the value used in the linear static analysis. The following values were used: 2830 MPa for the Young's modulus and 0.4 for the Poisson's ratio. The initial yield stress was 86.5 MPa.

5.3.1.2 - Yield Criteria

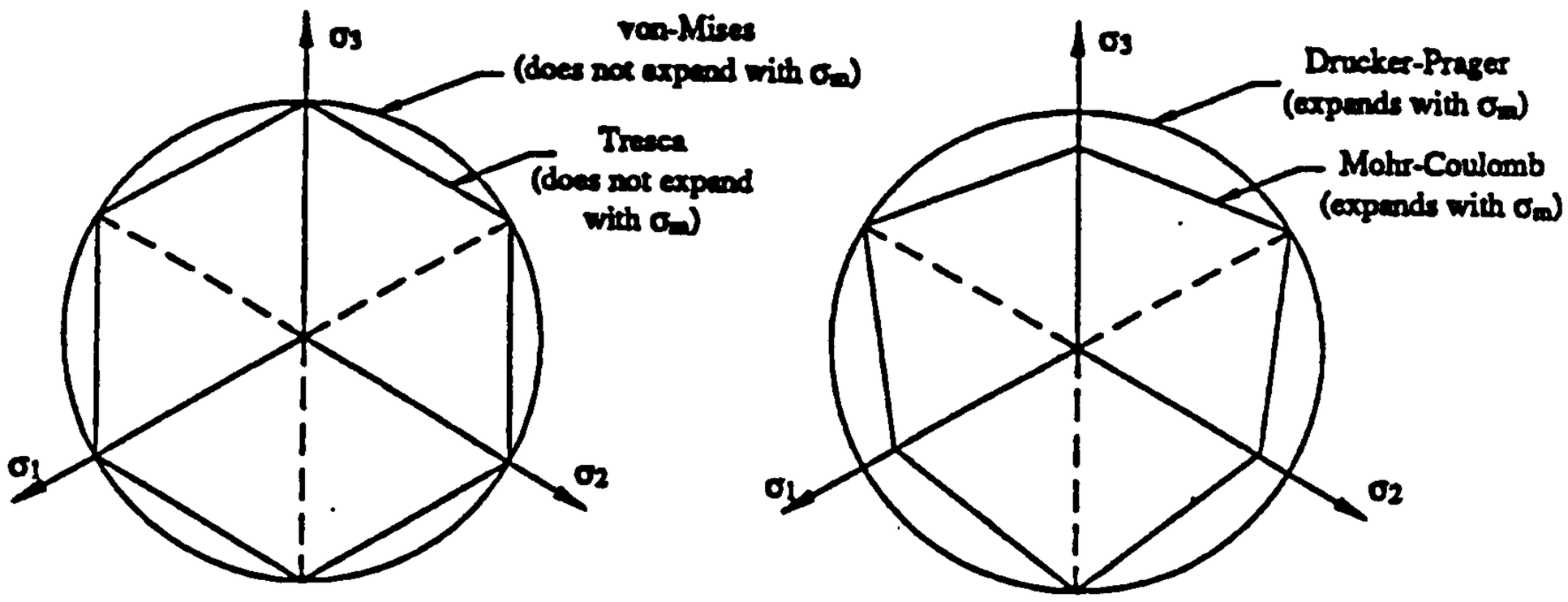

Figure 115 π-plane representation of yield criteria implemented in NISA [165]

For both material models, the onset of plastic deformations is determined by the Von-Mises yield condition (shown in Figure 115 with the three other conditions currently implemented in NISA).

The Von Mises yield criterion is a function of the deviatoric stresses and is independent of the hydrostatic stresses (σ_m). Yielding of polymers such as epoxy is better modelled by criteria which are also dependent upon the hydrostatic stresses because of the difference exhibited in tension and compression. Hydrostatic stresses involve pure compression and tension only [166]. The two other hydrostatic pressure dependent yield criteria available are suitable for modelling material such as concrete, rock and soil, requiring different parameters and as such were not used.

In addition to the yield criteria, a hardening rule can be selected if necessary. The hardening rule indicates how the yield surface changes during plastic deformations. During isotropic hardening, it is assumed that the yield surface grows in size only while keeping the same shape. The implication for this is that the material is subject to monotonic proportional loading.

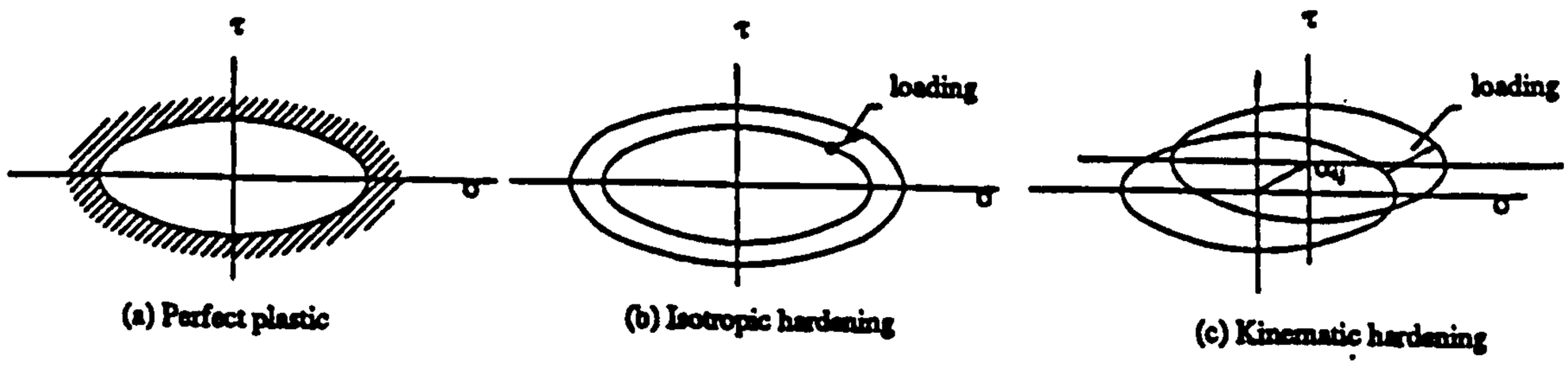

Figure 116 Hardening rule implemented in NISA [165]

3.1.2 - Failure Criteria

The non-linear analysis being concerned primarily with the adhesive behaviour, it was deemed necessary to retain the ASFC presented earlier.

5.3.2 - Results and Discussion

The non-linear analysis was carried out to ascertain the effect of the non-linear behaviour of the adhesive on the predicted failure load. Thus, the adhesive is the primary focus of the investigation.

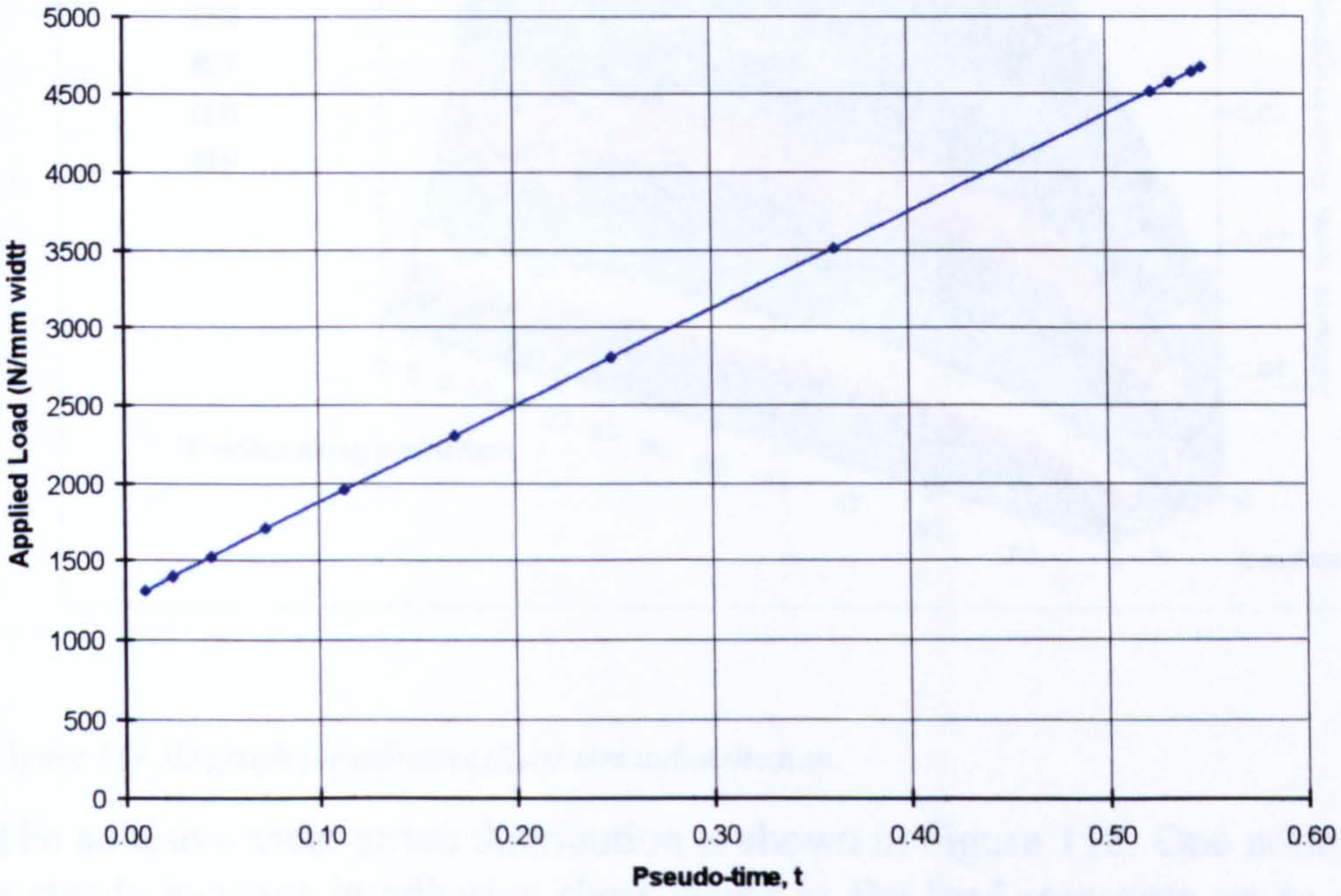

Figure 117 Loading curve

Figure 117 shows how the load was applied during the analysis. Initially, a maximum of 20 load steps was selected between 1250 N/mm and 7500 N/mm. The analysis used the auto-load stepping facility available in NISA. The analysis failed to converge after the 12th load increment at 4673.5 N/mm. The analysis ran for almost 10 hours.

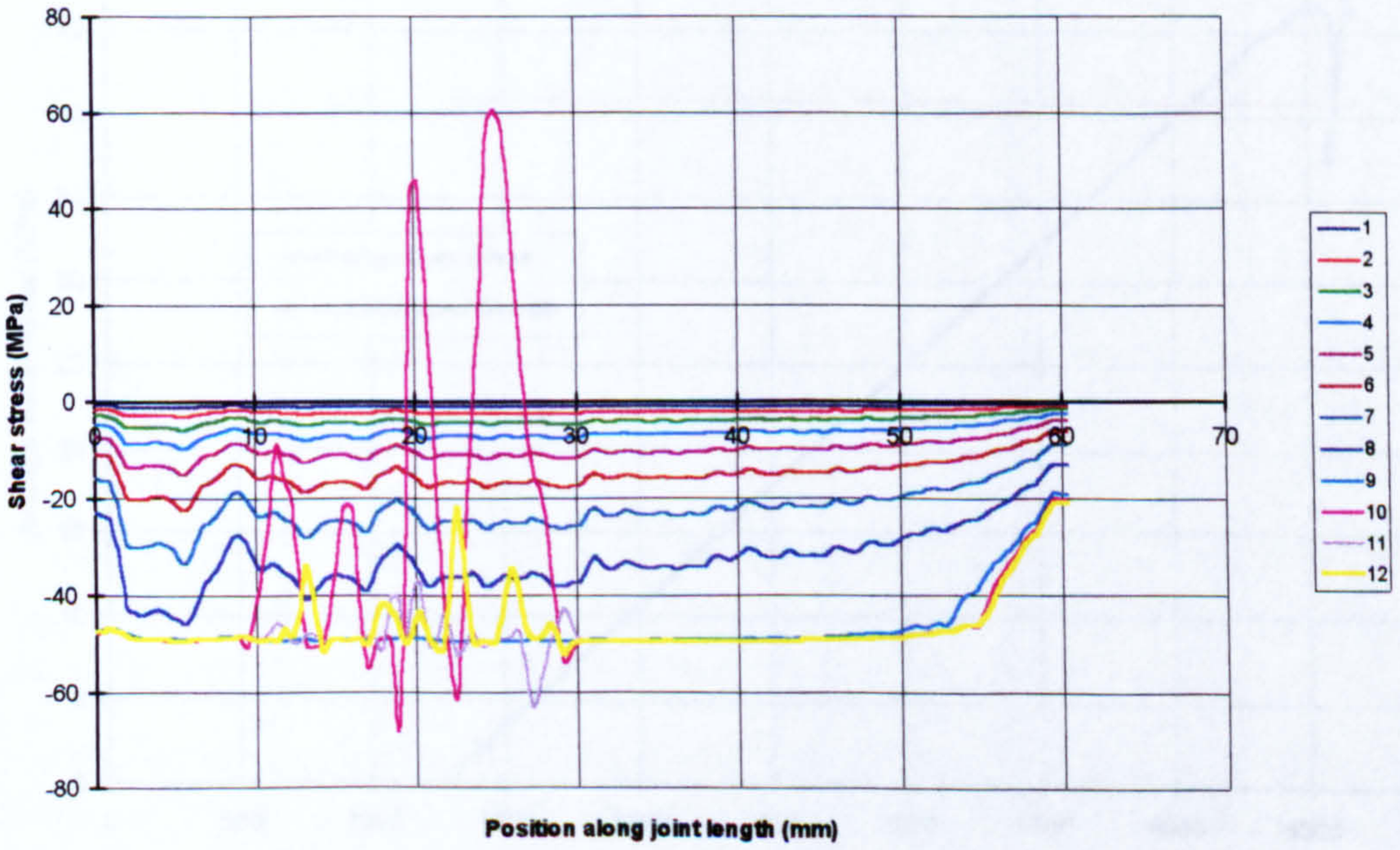

Figure 118 Adhesive shear stress distribution along scarf length

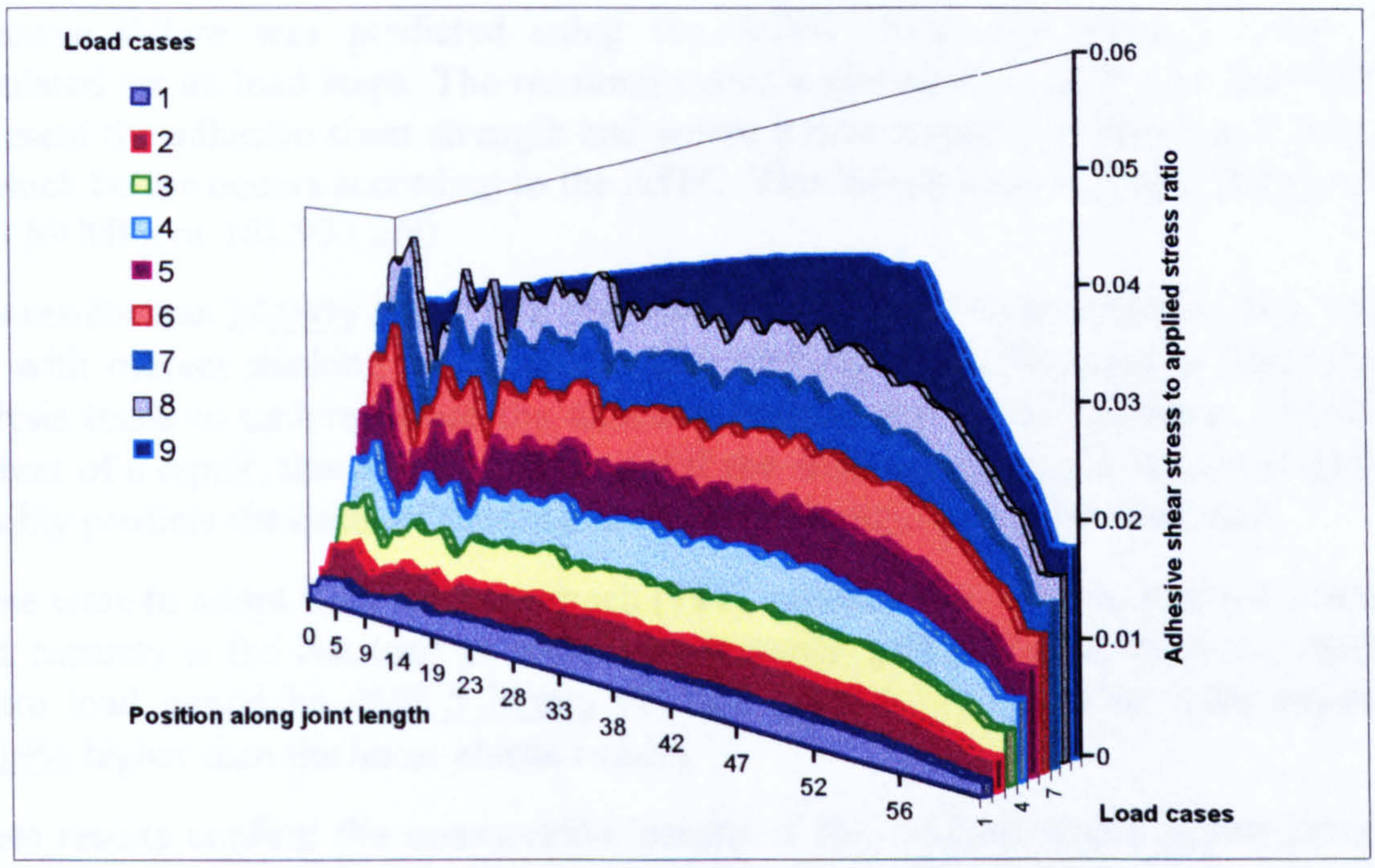

Figure 119 3D graph for adhesive shear stress distribution

The adhesive shear stress distribution is shown in Figure 118. One notices that there is a steady increase in adhesive shear stress as the load increases up to 4513.3 N/mm. Then, at the onset of yielding, the main portion of the curve becomes flatter. After the 9th load step (4513.5 N/mm), the shear stress becomes unstable. A few steps after, the solution fails to converge. Such a similar failure to converge has been reported by Callinan [111] for double lap joints. The shear stress distribution up to the 9th load step is shown in Figure 119.

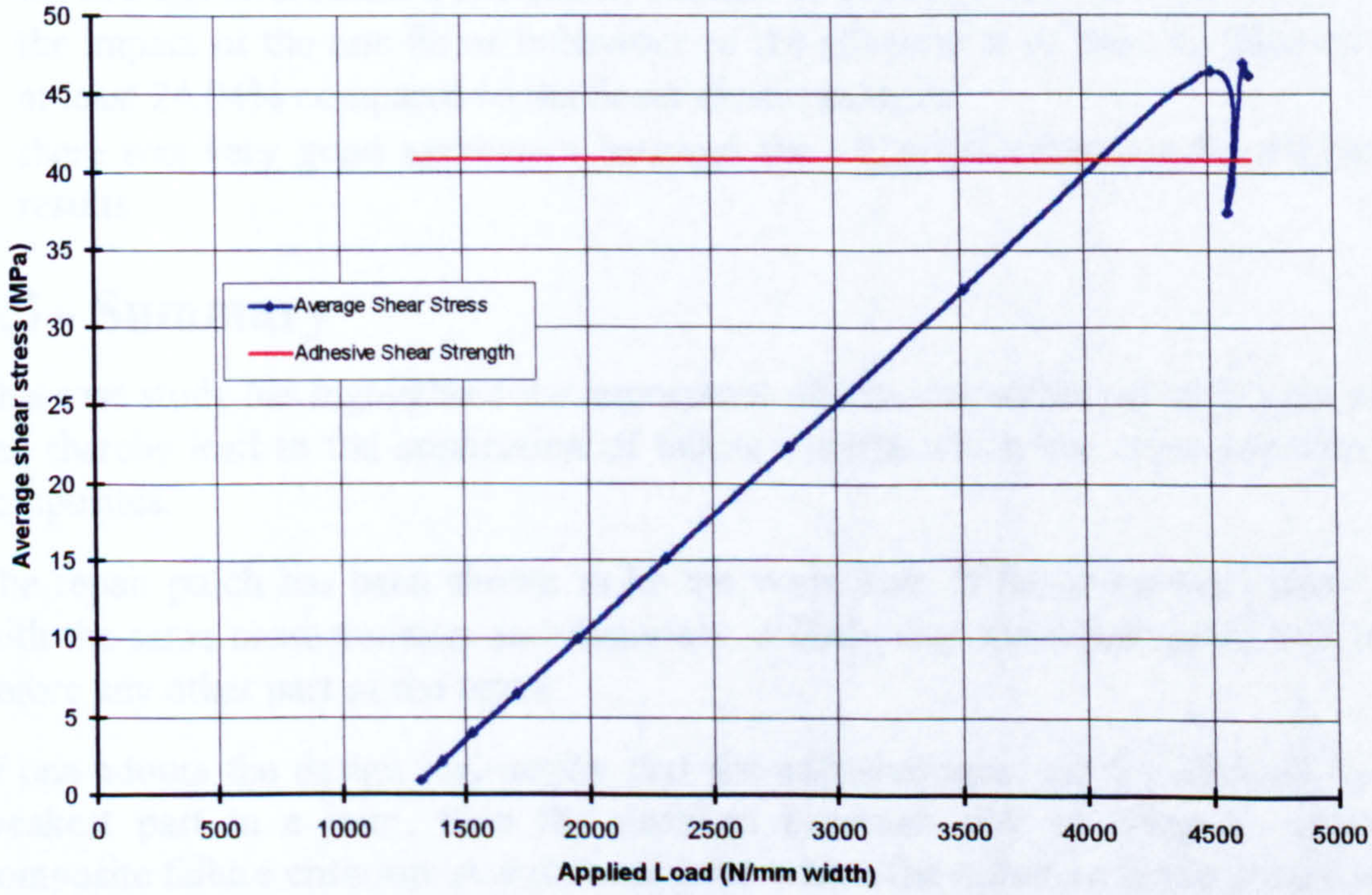

Figure 120 Average shear stress variation with applied load

Adhesive failure was predicted using the ASFC. First, the average stress was calculated for all load steps. The resulting curve is plotted in Figure 120. The red line represent the adhesive shear strength and where it first crosses the blue line is the load at which failure occurs according to the ASFC. This failure load is 4048.3 N/mm width (963.89 MPa or 161.933 kN).

This results was 24.04% above that predicted by the linear static analysis. This was in line with current thinking in the field which underlines the fact that a linear elastic analysis tends to underestimate the adhesive loading capability. However, within the context of a repair, this may not be crucial if the criterion chosen in the linear analysis sensibly predicts the order of failure and that the adhesive is not the weak link.

If one were to adopt Callinan's approach [111], which states that the ultimate adhesive load capacity is the last load at which convergence was achieved, then the adhesive failure load would be 4673.5 N/mm (1112.7 MPa or 186.94 kN). This would be 43.19% higher than the linear elastic results.

These results confirm the conservative nature of the average stress failure criterion. However this criterion is suited to the approach used in this analysis.

In the light of the results from the EPP model, it was deemed unnecessary to pursue the matter further using the EPLH material model.

5.4 - Conclusion

The results obtained have shown that:

- the repair patch will fail first at 64.88 kN in a region close to the scarf tip
- the adhesive is not the weak link
- the Tsai-Wu failure criterion predicts accurately the failure load within 7.84% of the experimental data
- the average stress failure criterion is suitable to predict adhesive failure load
- the impact of the non-linear behaviour of the adhesive is to raise its failure load by at least 24.04% compared to the linear elastic analysis
- there was very good agreement between the FE predictions and the experimental results

5.5 - Summary

This case study has highlighted the importance of a model which can give layer stresses and thereby lead to the application of failure criteria which are more appropriate for composites.

The repair patch has been shown to be the weak link. If the same scarf joint is used with the same characteristics and materials, it likely that the repair patch will fail first before any other part of the repair.

If one adopts the design philosophy that the adhesive must not be allowed to be the weakest part in a joint, then the problem becomes one of using an appropriate composite failure criterion. A structural joint where the adhesive is the critical element will require a good failure criterion, backed-up by appropriate experimental testing.

The twin phase modelling concept is a viable option for situations where it is not possible to use composite elements (e.g. non-linear analysis in NISA at present). A full non-linear analysis is not necessary for this joint system.

The very good agreement between the predicted results and the experimental data has shown that the proposed new approach for flush repairs was sound and offered improved failure prediction capabilities. In this case study, the analysis was carried out with prior knowledge of the experimental failure load. In the following chapter, the same approach is taken further by the modelling of a real scarf repair to a representative aircraft composite panel. The analysis and failure prediction are carried out without any advanced knowledge of the experimental results.

Chapter 6

Application to Bonded Repairs

Case Study 2: Flat Panel

6.0 - Introduction

The scarf patch studied in Chapter 5 has been used in the repair of a flat panel. This repair type is amongst a number of repair techniques explored experimentally by the DERA for their Aircraft Battle Damage Repair Programme.

This case study is an expansion of the application of the improved modelling approaches devised earlier to real structural repairs. It further explores the possibility of modelling much larger structures (compared to the panel repaired and modelled in Chapters 3 and 4).

Building on the experience gained in the preceding chapter, all models were constructed and analysed without prior knowledge of the experimental results. This was done in order to test the predictions for failure load and location with experimental results.

6.1 - Modelling Data

The scarf joint dimensions and characteristics were the same as that used in Chapter 5 along with all materials. However the scarfed patch was applied to a larger flat panel.

6.1.1 - Undamaged Panel

This undamaged panel was modelled for reference purposes only. The panel is 712 mm long, 508 mm wide and 4.2 mm thick. It was made of T800/924C carbon/epoxy composites. The lay-up was the same as the parent laminate of the scarf joint in Chapter 5 with 37.5% of 0° plies, 50% of ±45° plies and 12.5% of 90°. The 0° plies were in the direction of loading, along the panel length.

6.1.2 - Damaged Panel

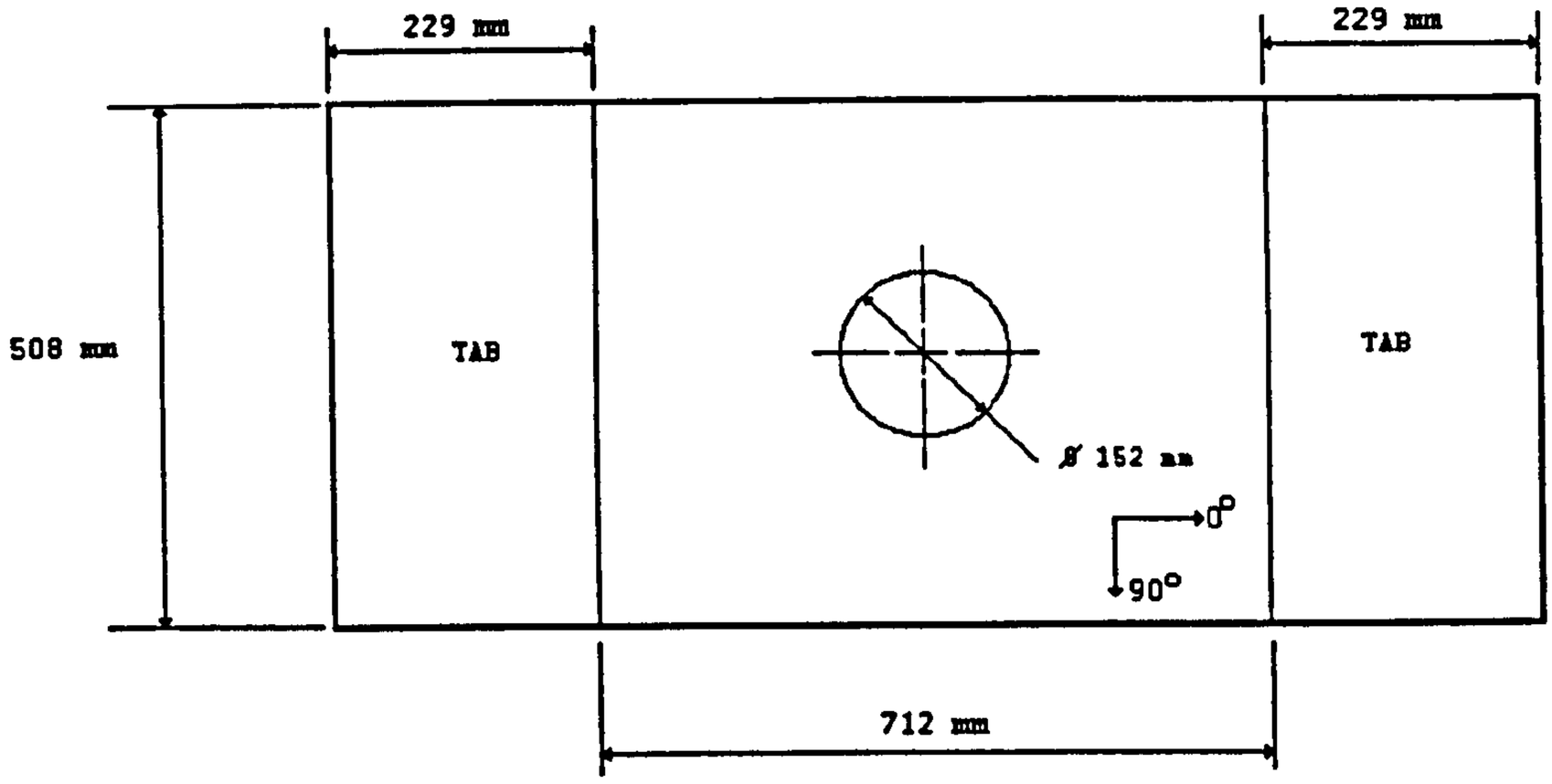

Figure 121 Damaged Panel

The damaged panel was built to the exact dimension, material and lay-up of the undamaged panel with a central hole of 152 mm in diameter which represented the amount of damaged material which was removed. The damaged panel is shown in Figure 121.

6.1.3 - Repaired Panel

The patch used for the scarf joint was used to repair the damaged panel. The scarf was circular and 5.03 mm thick with 12 plies.

6.2 - Undamaged and Damaged Panels

The modelling approach used for both damaged and undamaged panels is described next followed by the results of the analysis.

6.2.1 - Modelling Strategy

For these panels, 3D composite shell elements were used in the modelling. These elements are the main element for composite structural analysis. First, the structural response to an applied load of 1250 N/mm (298 MPa or 635 kN) was investigated for both panels to determine the appropriate load range for failure analysis. The second part of the analysis was carried out to determine failure loads and location. Ten equal load steps were applied from 1150 to 2150 N/mm.

The Tsai-Wu failure criterion was used exclusively. The results were then compared to experimental data.

6.2.2 - Results and Discussion

6.2.2.1 - Undamaged Panel

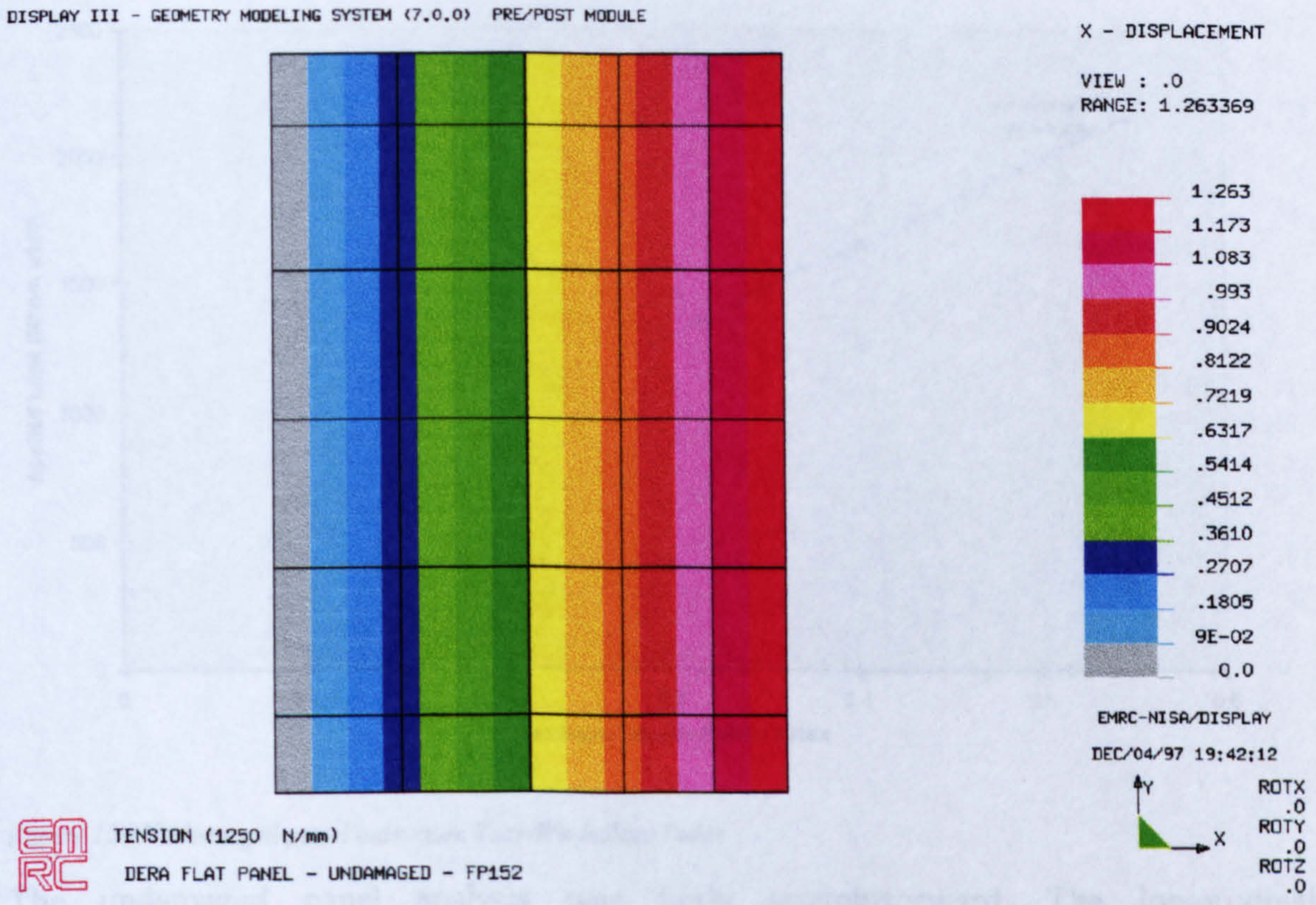

Figure 122 Undamaged panel longitudinal displacement

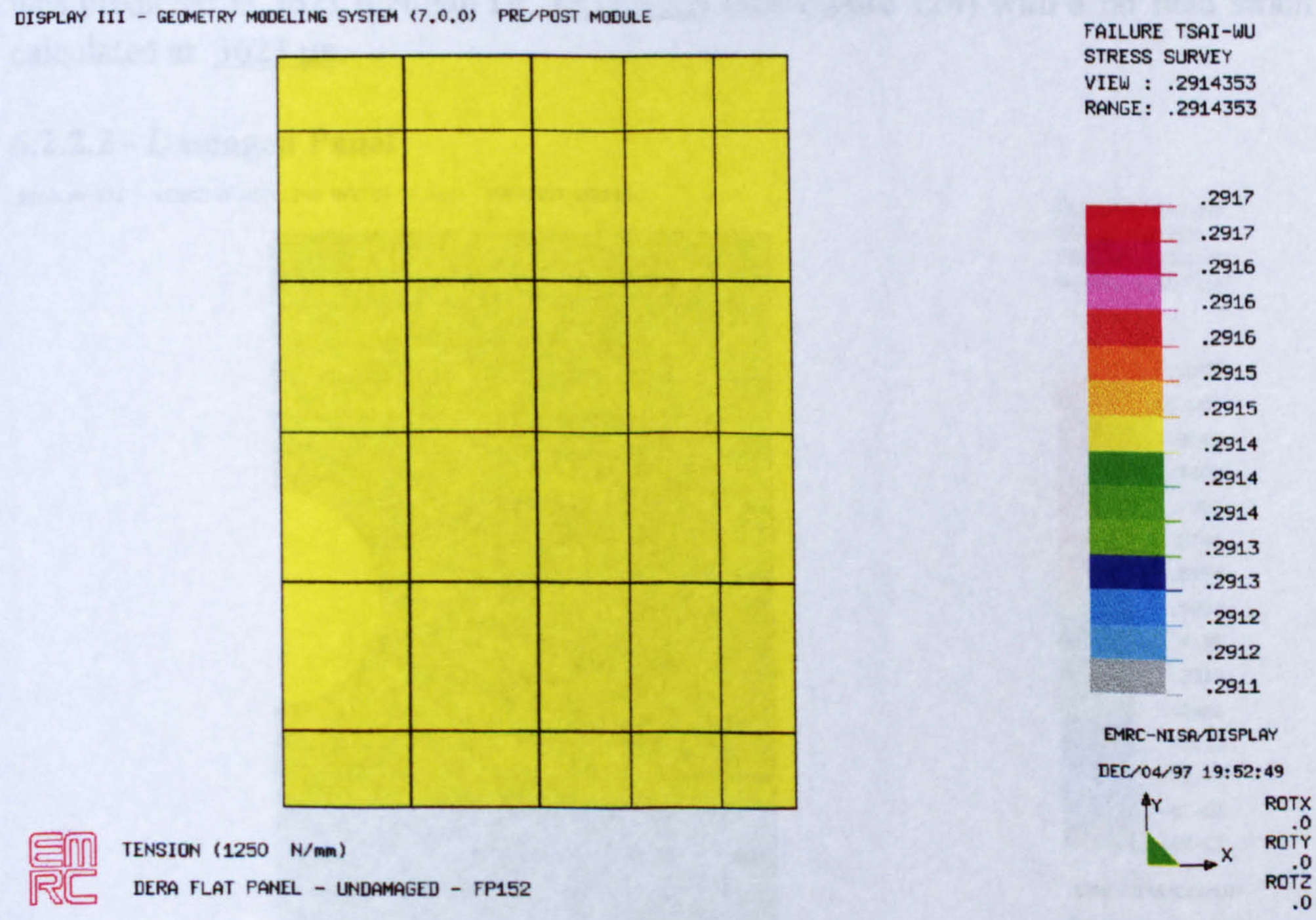

Figure 123 Tsai-Wu failure index stress survey for undamaged panel

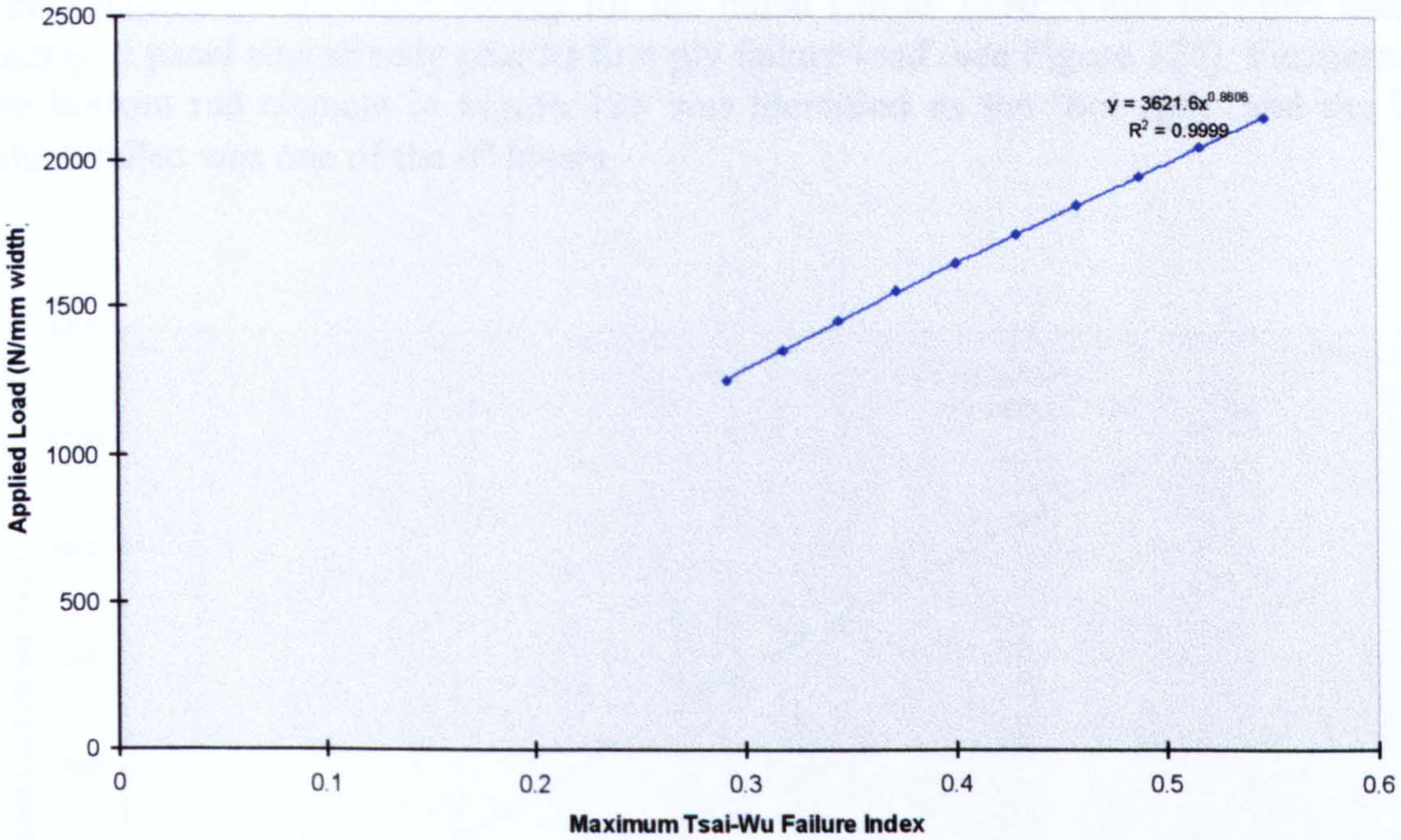

Figure 124 Undamaged panel maximum Tsai-Wu failure index

The undamaged panel analysis was fairly straightforward. The longitudinal displacement is shown in Figure 122. Figure 123 confirms a uniform failure index for the panel as one could have anticipated from classical laminate theory. First ply failure was predicted at 3621.6 N/mm i.e. 1839.8 kN (see Figure 124) with a far field strain calculated at 3623 με.

6.2.2.2 - Damaged Panel

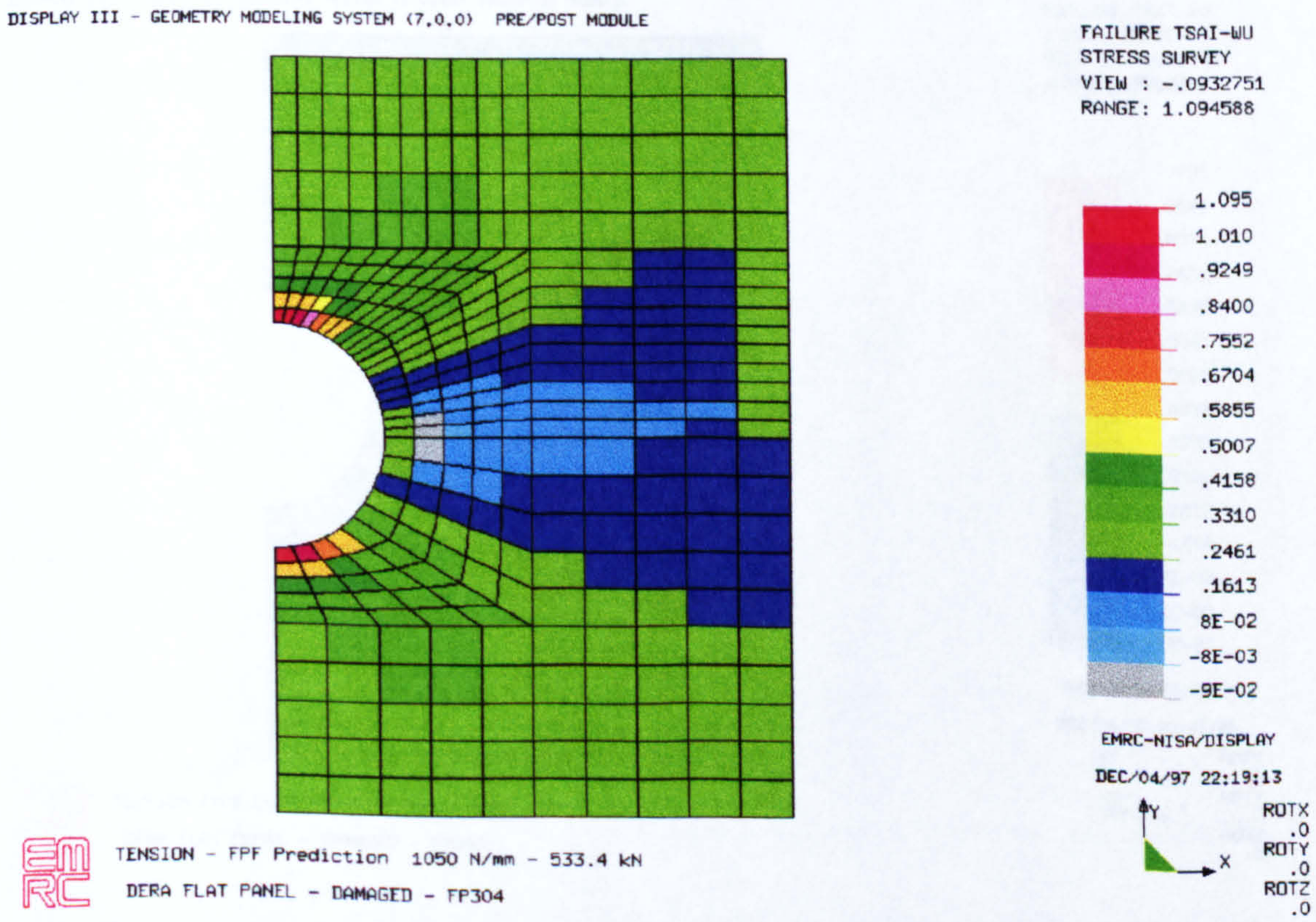

Figure 125 Tsai-Wu failure index survey for damaged panel

The Tsai-Wu failure index survey for the initial run at 1250 N/mm revealed that the damaged panel was already past its first ply failure load (see Figure 125). Furthermore, the bottom red element in Figure 125 was identified as the 'hot spot' and the layer which failed was one of the 0° layers.

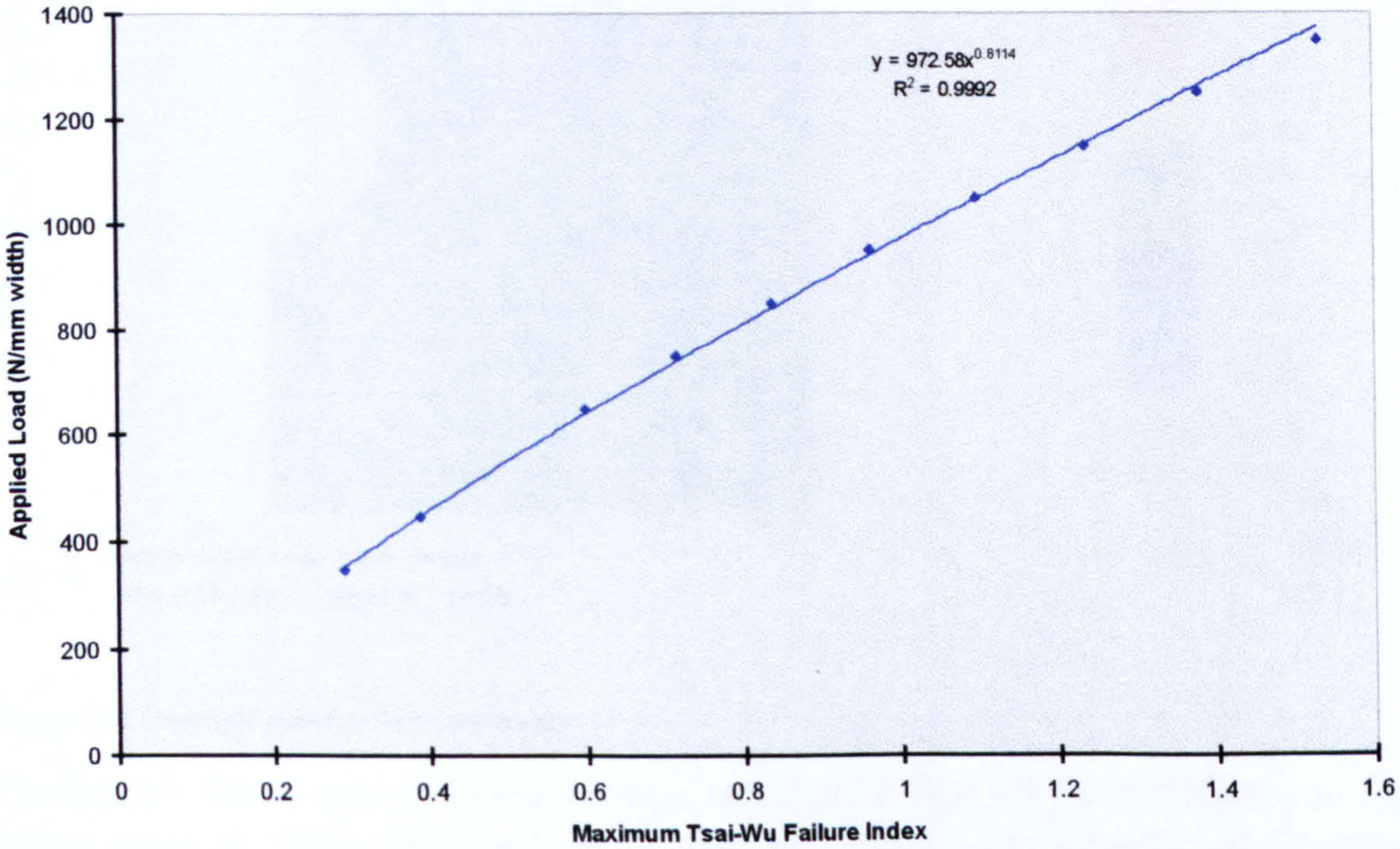

Figure 126 Damaged panel maximum Tsai-Wu failure index

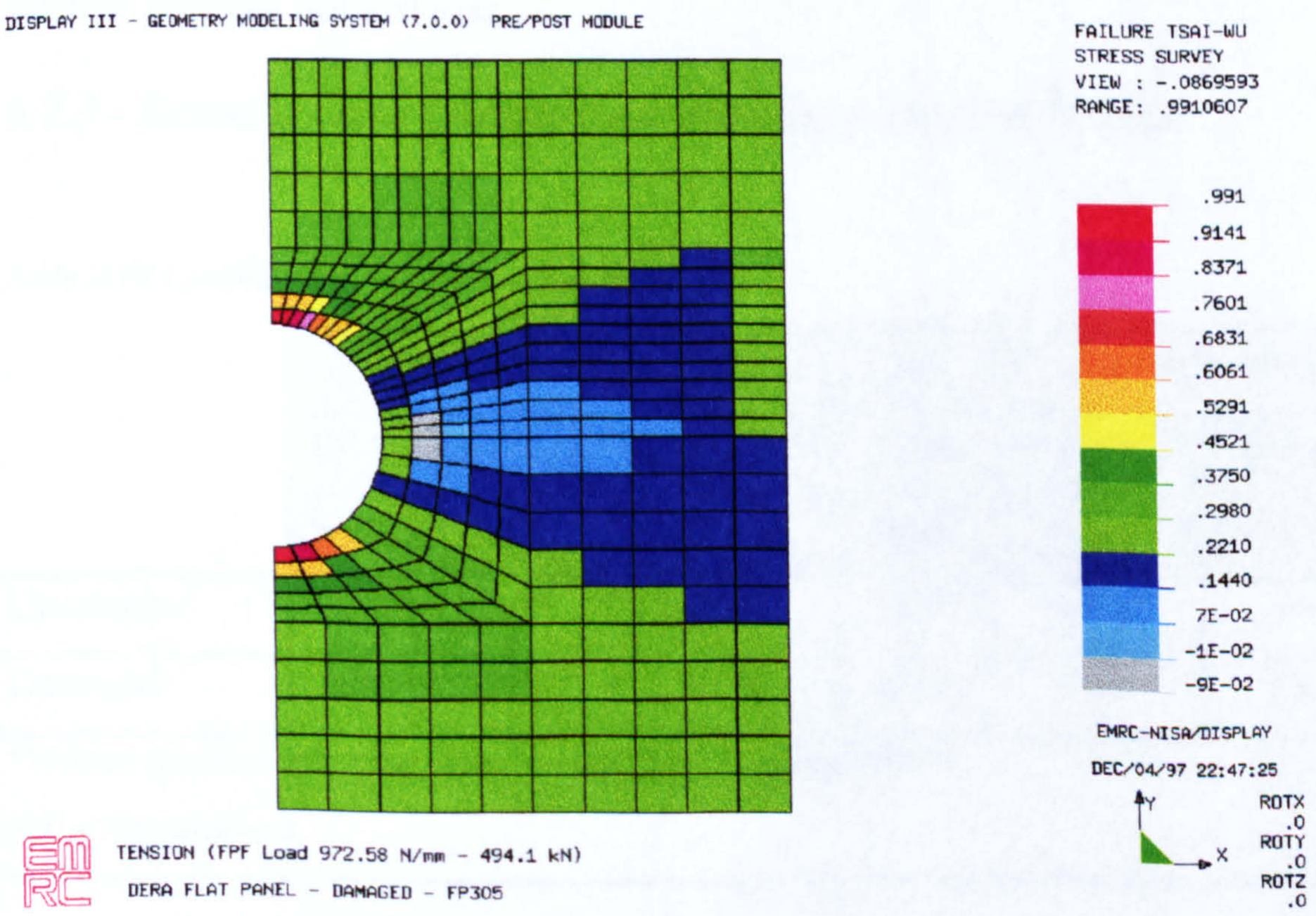

Figure 127 Damaged panel Tsai-Wu failure index survey

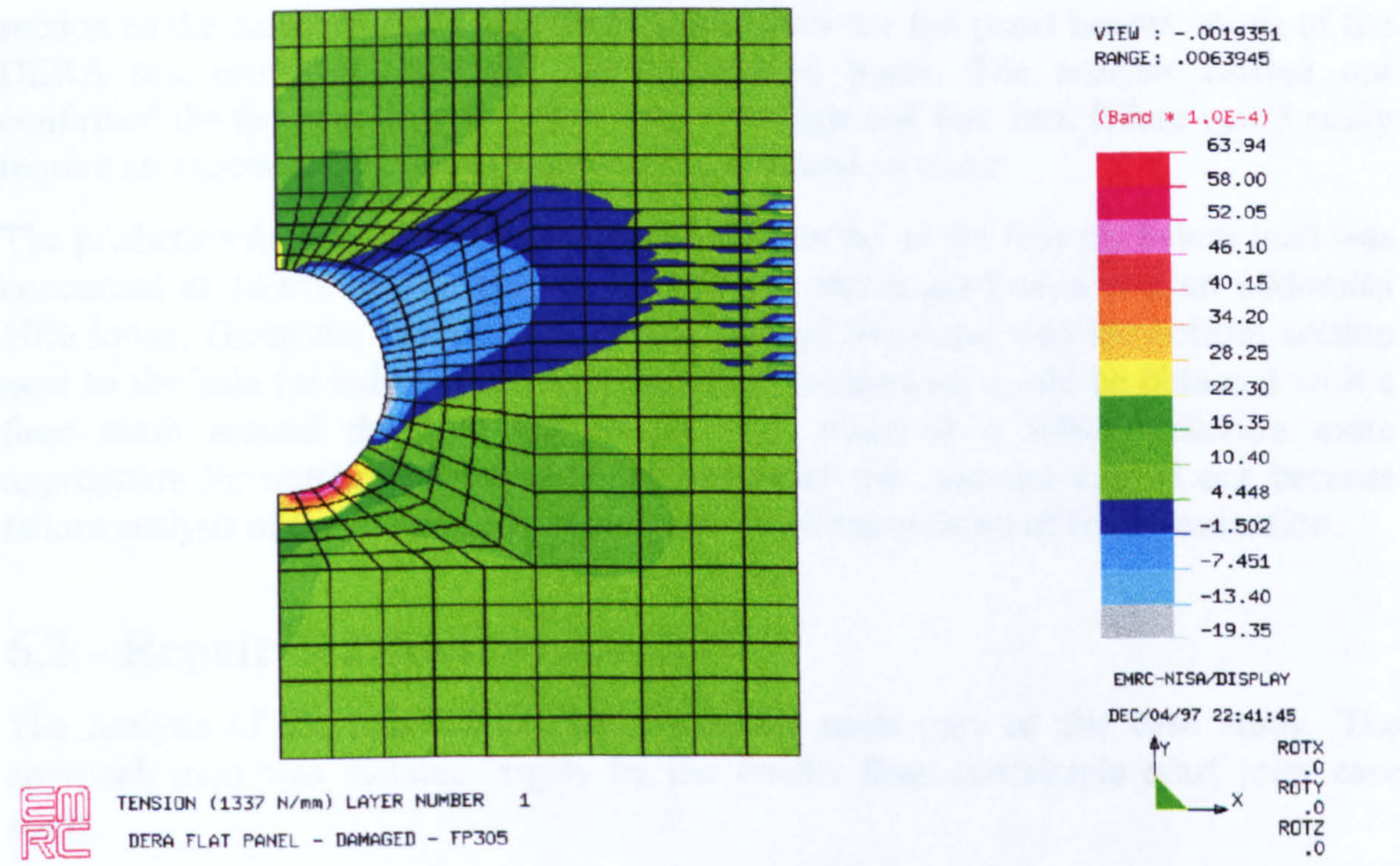

Figure 128 Damaged panel failure strain map

The first ply failure was predicted to occur at 972.58 N/mm (494.1 kN) with a far field failure strain of 3239με (Figure 126). At that load level, the longitudinal displacement reached a maximum of 1.161 mm. The failure index survey is shown in Figure 127 and the strain contour in Figure 128 . The strain shown are expressed with respect to the laminate principal material axes.

6.2.3 - Summary and Comparison with Experimental Results

Table 28 FEA predictions and experimental results summary

	Mean Failure Load			Far Field Failure Strain		
	FEA (kN)	Experim. (kN)	Difference (%)	FEA (με)	Experim. (με)	Difference (%)
Undamaged	1840	990*	N/C	3623	11990*	N/C
Damaged	494	577	16.80	3239	4090	26.27

*Waisted specimen with same central cross-section as damaged panel

N/C = Not calculated

The main results from the failure analysis are presented in Table 28 with the experimental results. The difference between FEA predictions and experimental results for the undamaged panel was not calculated because these results cannot be compared

directly. For the experimental work, a waisted specimen with the same central cross section as the damaged panel was tested rather than the full panel because none of the DERA test machines could fail the undamaged panel. The analysis carried out confirmed the fact that first ply failure load was high and that final failure could easily require an excess of 200 metric tonnes of applied load to occur.

The prediction for the damaged panel was better as far as the first ply failure load was concerned at 16.8% below. The far field failure strain prediction was an additional 10% lower. Given the fact that the critical part of the panel was the bottom section next to the hole (as indicated earlier), improved predictions could be obtained with a finer mesh around the hole but would have required a failure criterion more appropriate for notched laminates [121]. However this was not carried out because failure analysis of the damaged panel was not the primary focus of the investigation.

6.3 - Repaired Panel

The analysis of the repaired flat panel was the main part of this case study. The approach used was dictated largely by the results from the simple scarf joint case study.

6.3.1 - Modelling Strategy

The first problem faced while trying to generate the repaired panel from the 2D models used in Chapter 5, by rotation about the global z-axis, was the mesh size which was too fine. The resulting central region of the repair had in excess of 100,000 first order elements. This model could not be run on a PC with just 32 Mb of RAM.

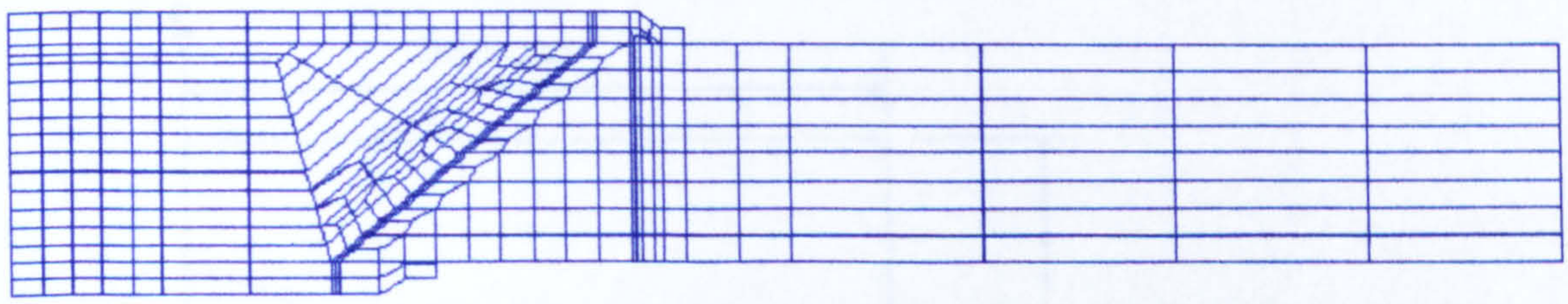

Figure 129 Repaired panel mesh (cross-section in loading plane)

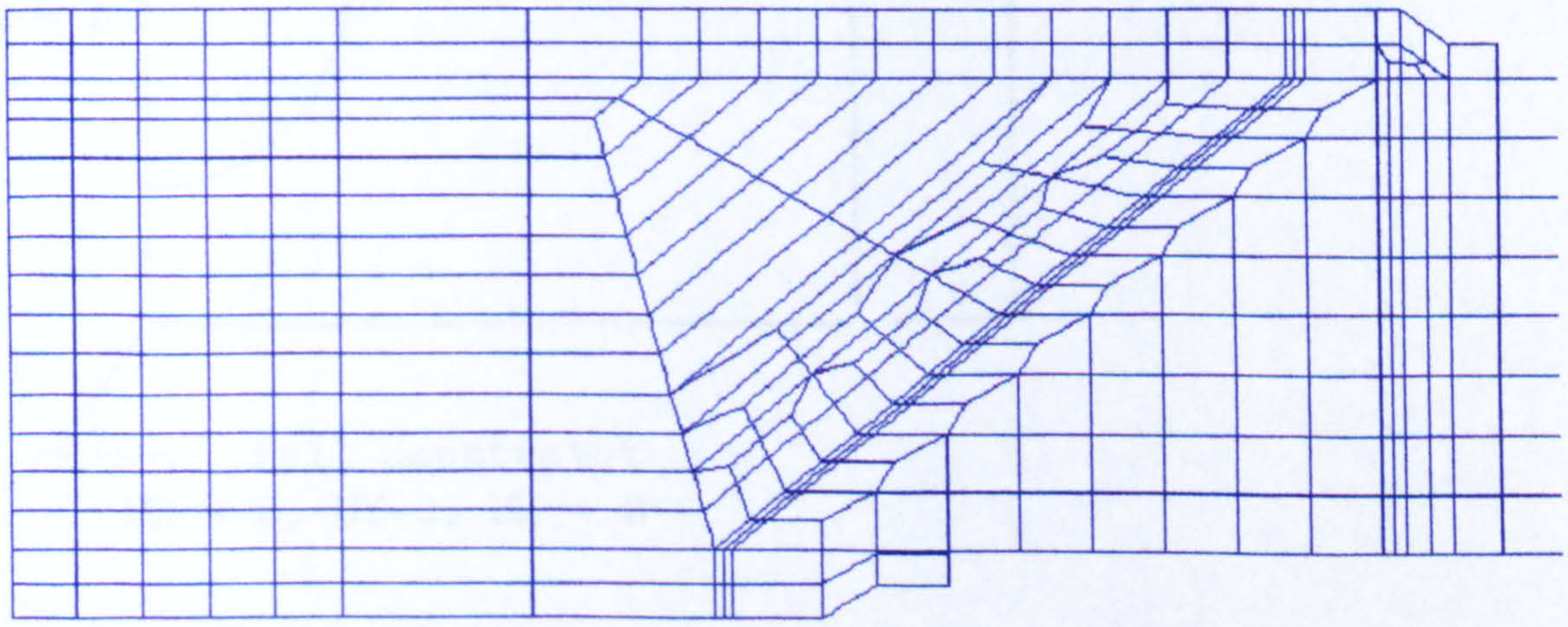

Figure 130 Repaired panel mesh (Close-up)

A coarser 2D mesh was therefore constructed and used as a starting point (Figure 129). A close-up of the mesh in shown in Figure 130.

The critical part of the repair patch was modelled using 3D composite solid elements because of the likelihood of failure occurring within the patch itself. The remaining sections were constructed from 3D orthotropic solid elements. In order to obtain a layered strain contour of the top of the panel for comparison with strain gauge measurements, the top elements were all build from 3D composite solid elements which included a thin "gauge layer". This thin gauge layer is specific to NISA and is used to obtain stresses and strain close to the region of interest because strains are calculated at element centroids. Thin gauge layers are ignored in the calculation of the stiffness matrix during problem solutions.

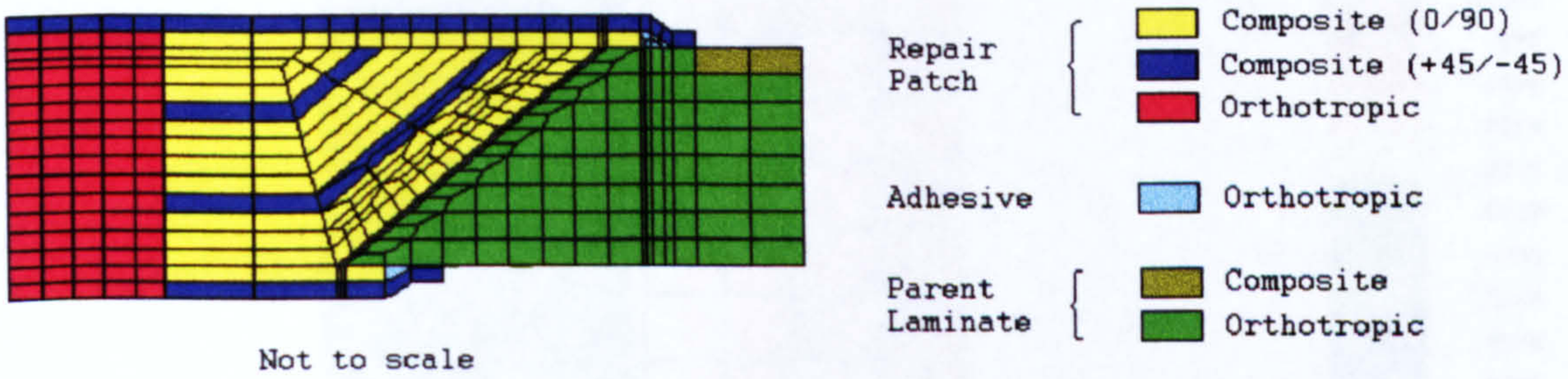

Figure 131 Repaired panel element types

Thus the resulting model had a mixture of composite and orthotropic solids. The element type distribution is shown in Figure 131.

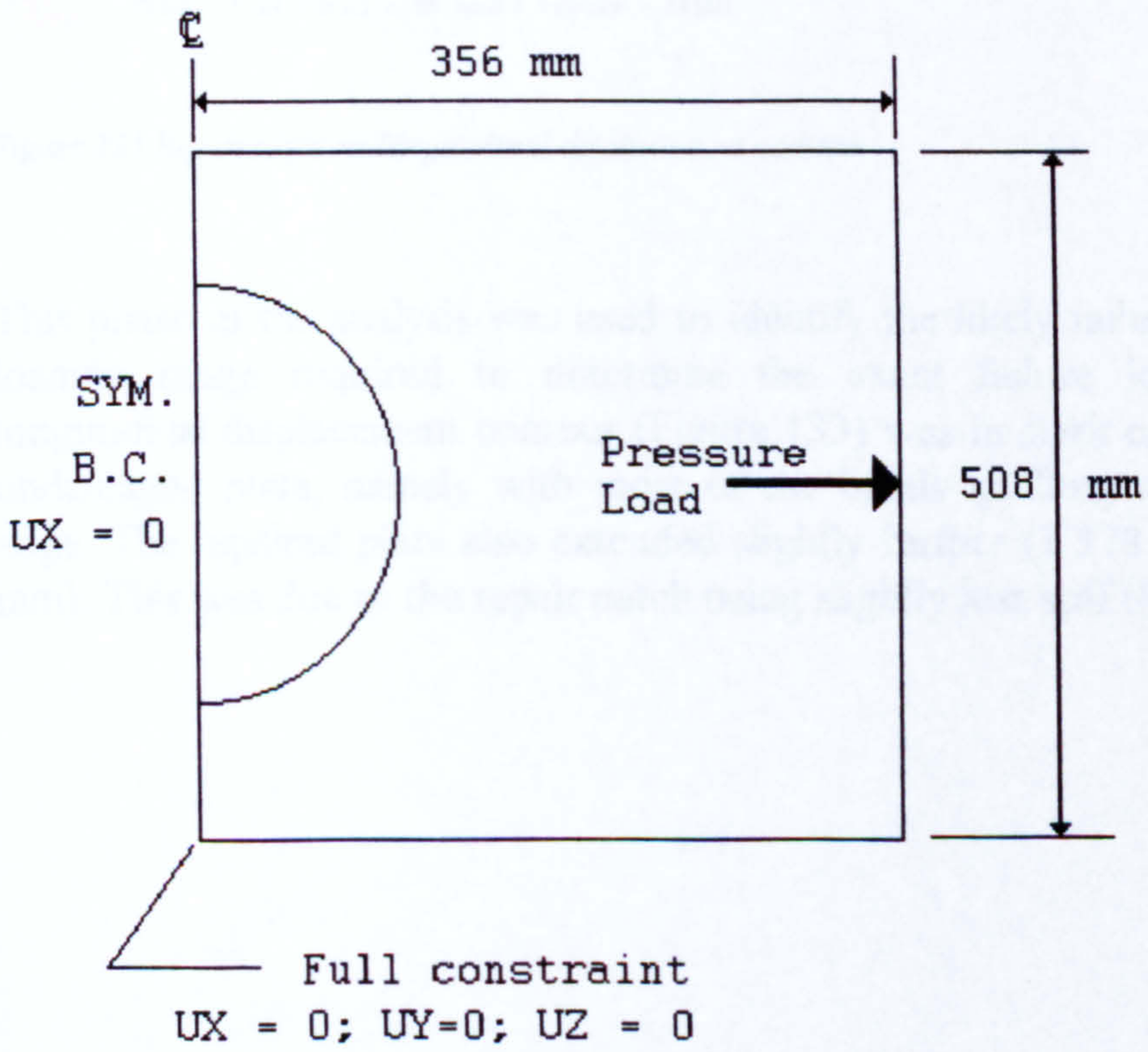

Figure 132 Repaired panel boundary conditions

The boundary conditions applied to the panel are given in Figure 132.

6.3.2 - Results and Discussion

6.3.2.1 - Structural Response to Tensile Loading

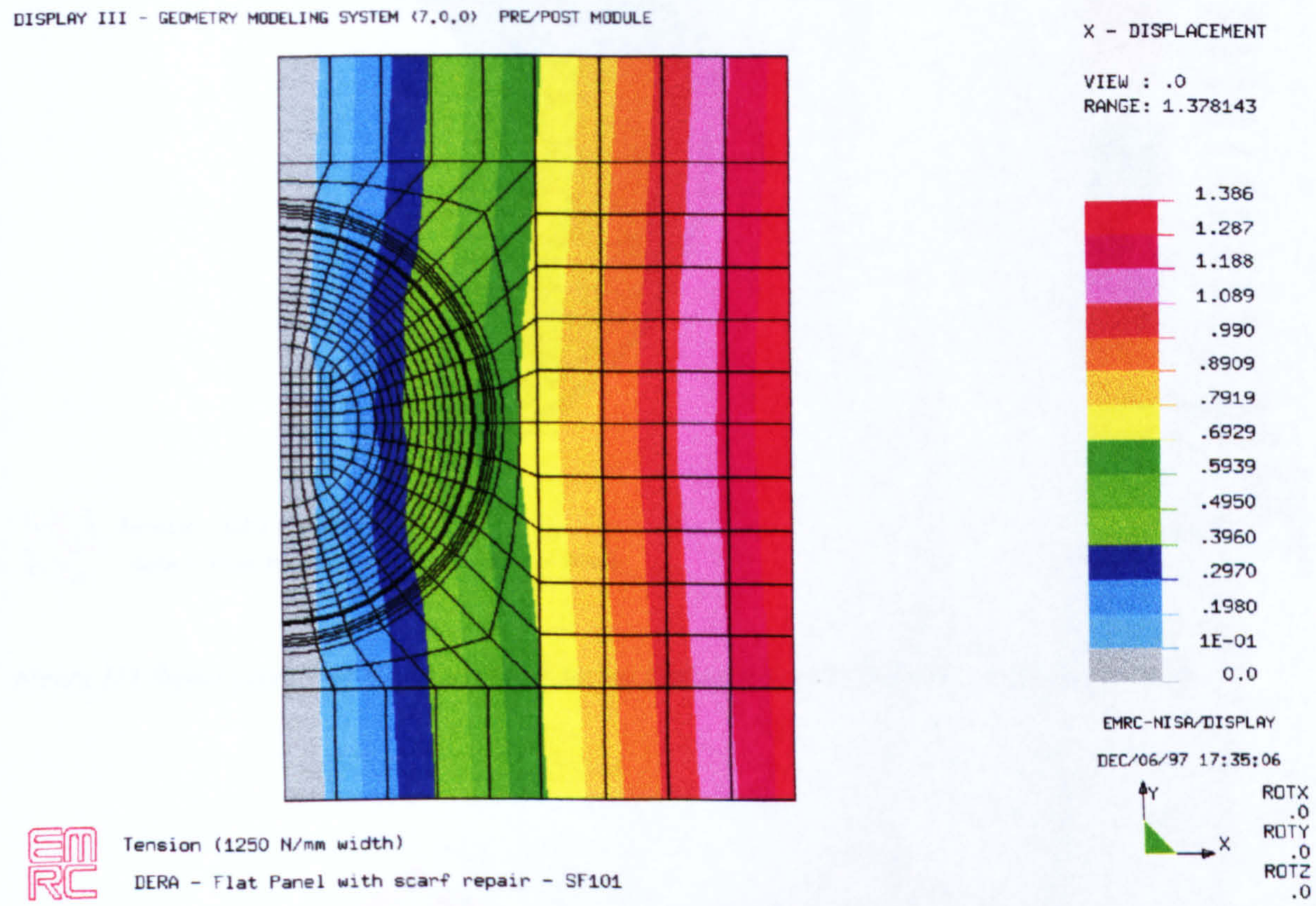

Figure 133 Repaired panel longitudinal displacement contour

This phase of the analysis was used to identify the likely failure location and also the loading range required to determine the exact failure load. As expected, the longitudinal displacement contour (Figure 133) was in stark contrast with that for the undamaged plate, namely with most of the bands no longer parallel to the loading edge. The repaired plate also extended slightly further (1.378 mm compared to 1.263 mm). This was due to the repair patch being slightly less stiff than the parent laminate.

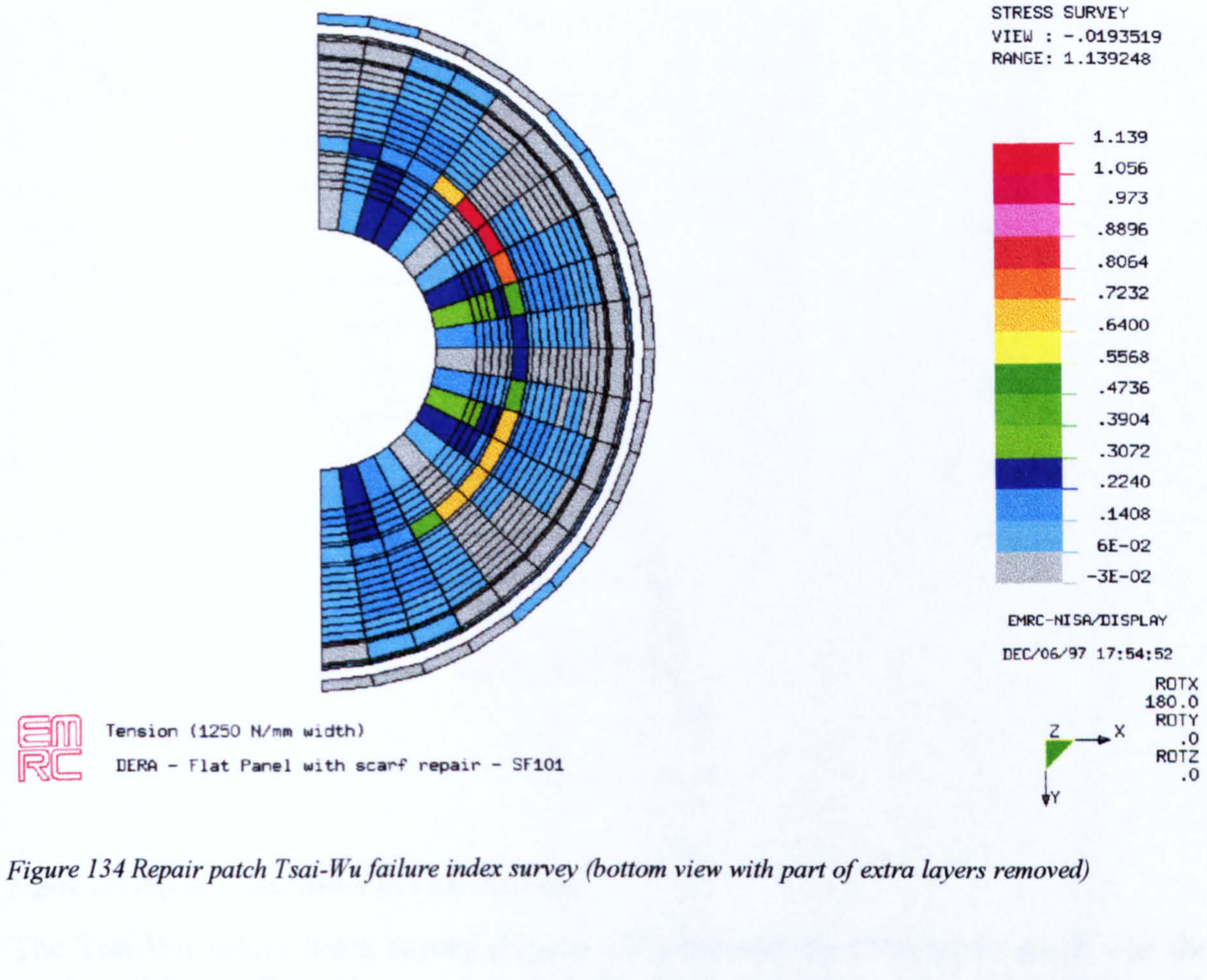

Figure 134 Repair patch Tsai-Wu failure index survey (bottom view with part of extra layers removed)

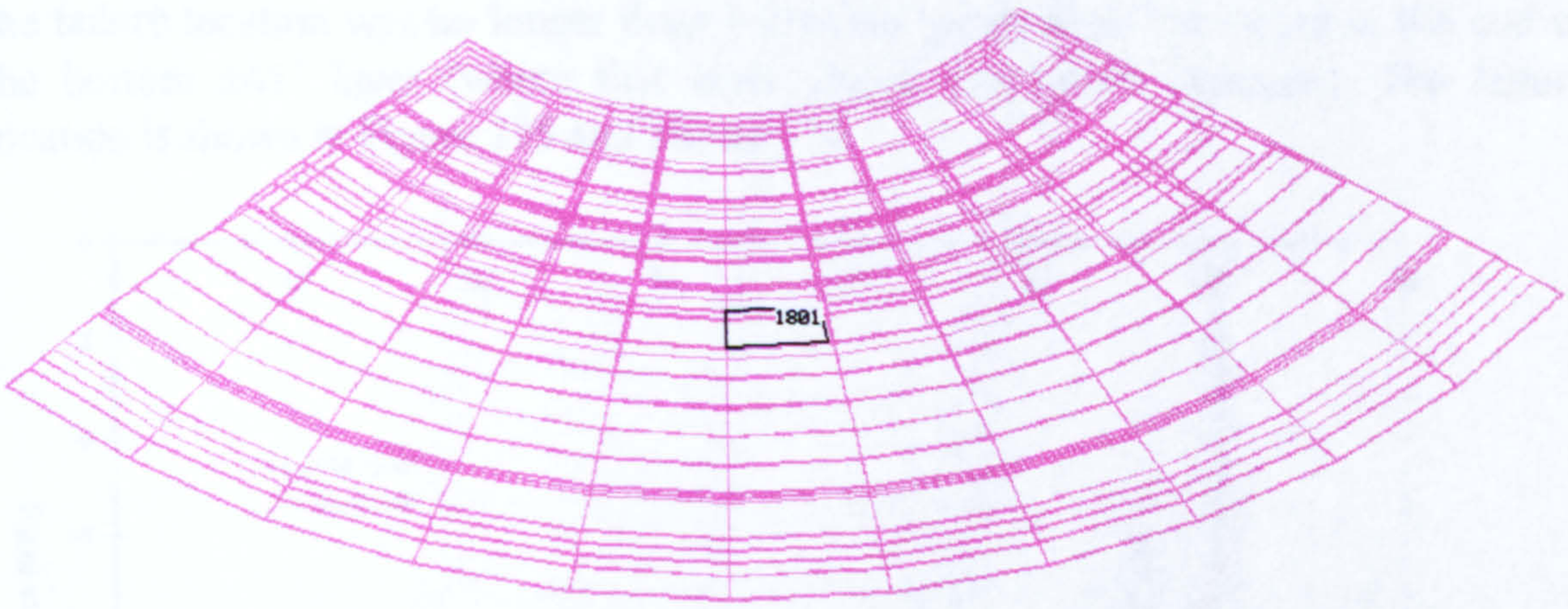

Figure 135 Repaired panel failure location

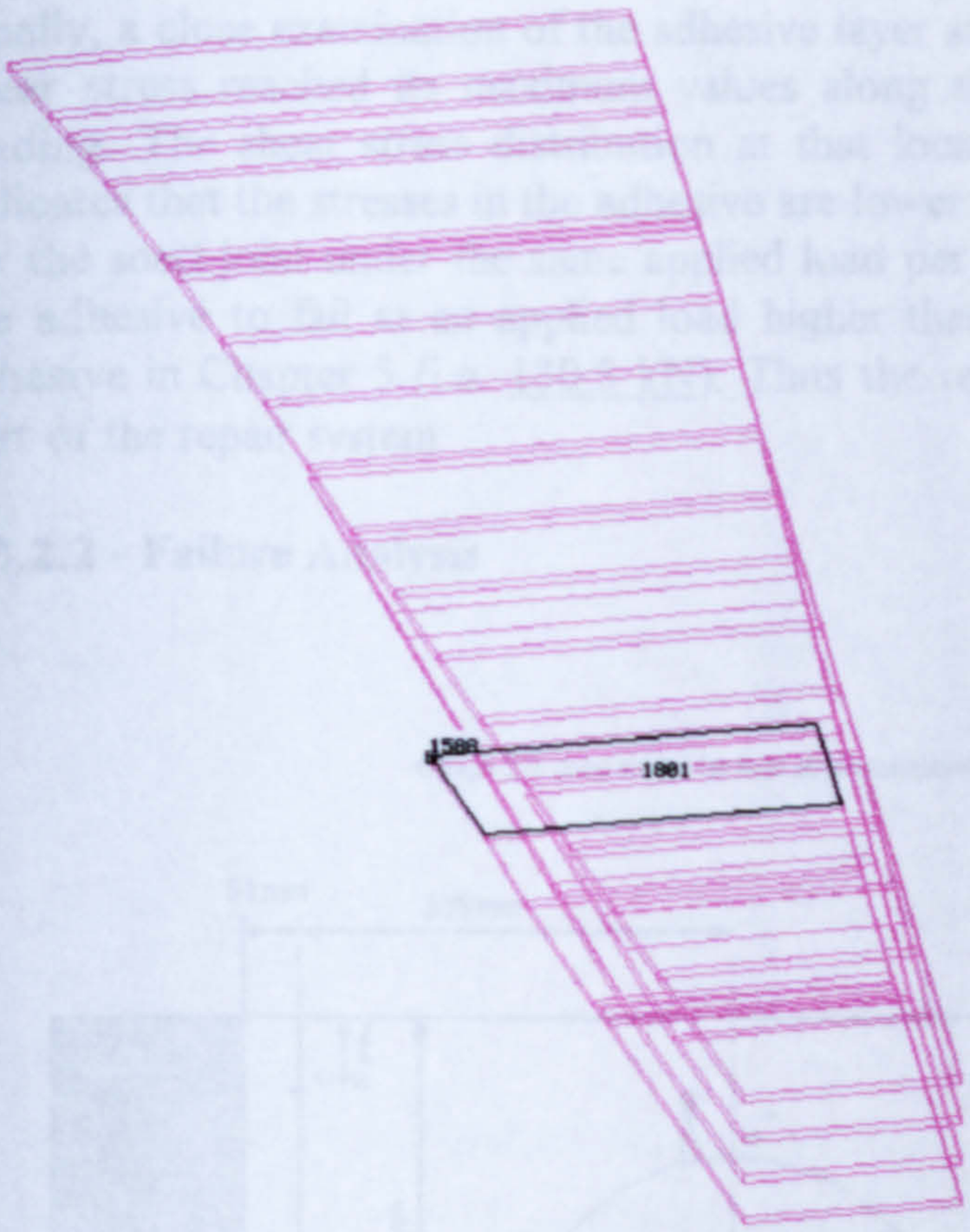

Figure 136 Repaired panel failure location (close-up)

The Tsai-Wu failure index survey (Figure 134) revealed that the repair patch was the weaker of both adherends as anticipated. However, contrary to the scarf joint model, the failure location was no longer deep within the patch itself but rather at the end of the bottom ±45° layer (where that layer joined the parent laminate). The failure location is shown in Figure 135 and Figure 136.

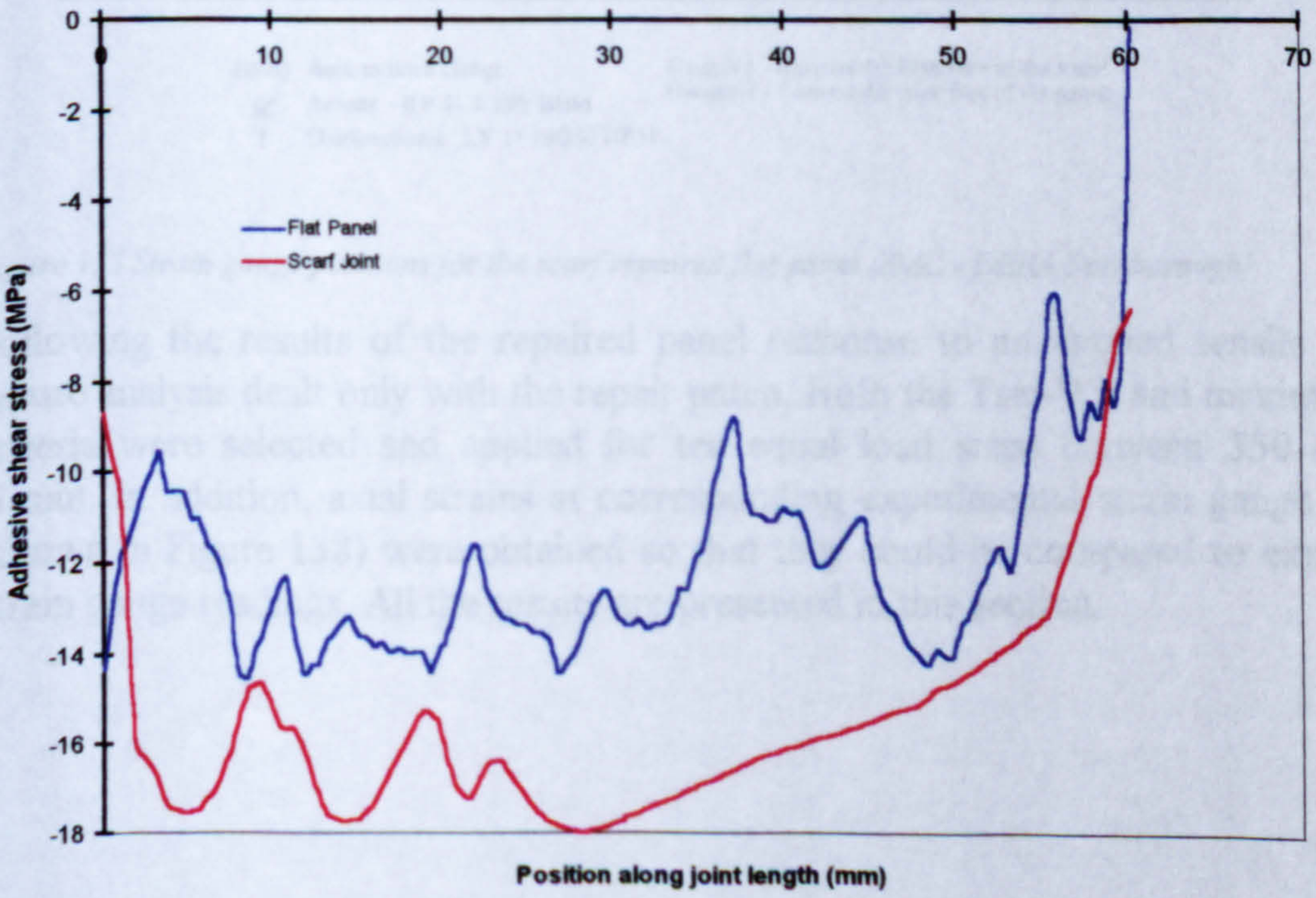

Figure 137 Flat panel adhesive shear stress distribution

Finally, a close examination of the adhesive layer stresses confirmed that the dominant shear stress reached its maximum values along the scarf length in the direction of loading. The shear stress distribution at that location is shown in Figure 137. This indicates that the stresses in the adhesive are lower for the repaired panel than they are for the scarf joint under the same applied load per unit width. Thus one could expect the adhesive to fail at an applied load higher than that predicted for the scarf joint adhesive in Chapter 5 (i.e. 130.5 kN). Thus the repair patch was indeed the weakest part of the repair system.

6.3.2.2 - Failure Analysis

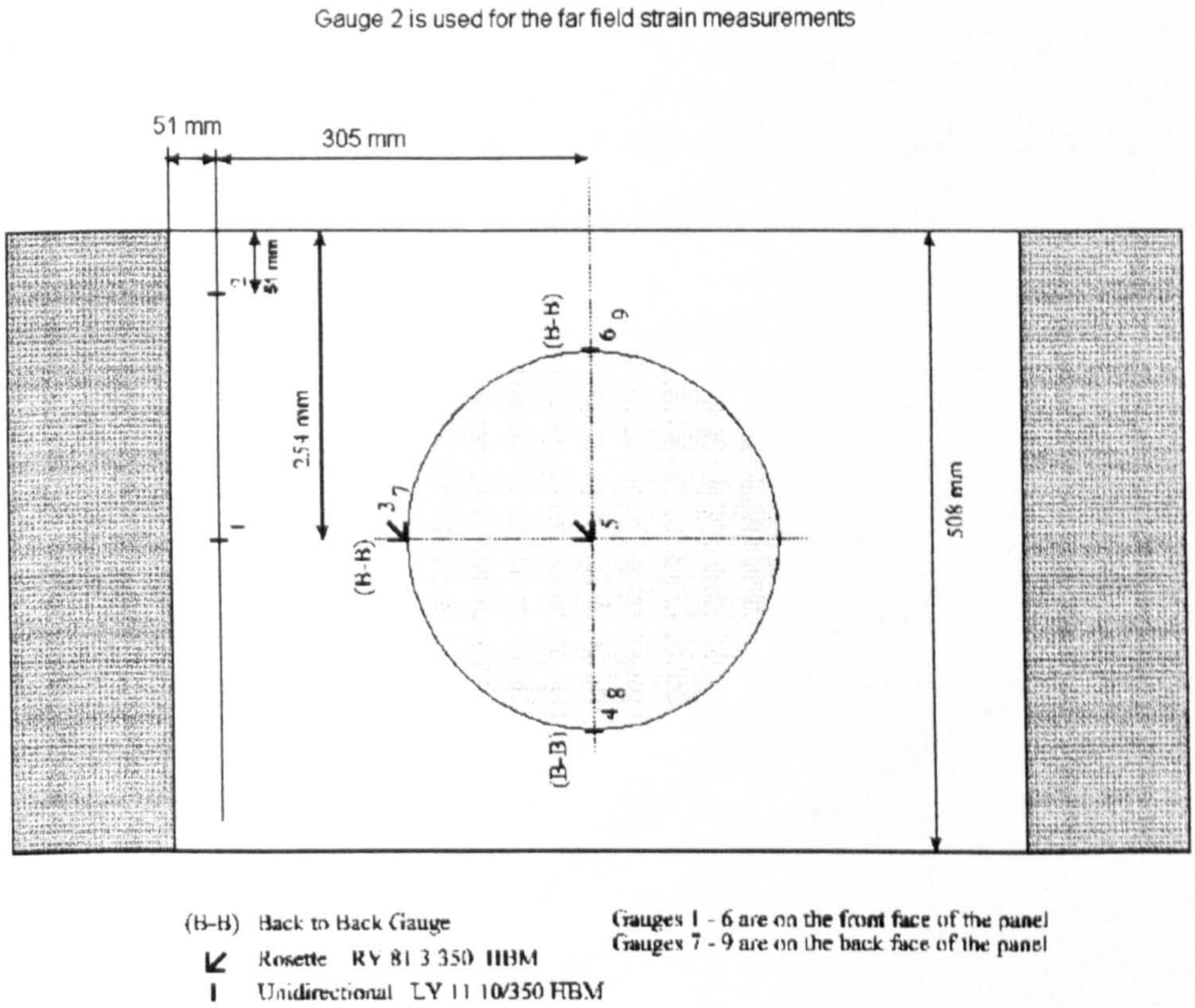

Figure 138 Strain gauge positions for the scarf repaired flat panel (SMC - DERA Farnborough)

Following the results of the repaired panel response to an applied tensile load, the failure analysis dealt only with the repair patch. Both the Tsai-Wu and maximum stress criteria were selected and applied for ten equal load steps between 350 and 1250 N/mm. In addition, axial strains at corresponding experimental strain gauge locations (shown in Figure 138) were obtained so that they could be compared to experimental strain gauge readings. All the results are presented in this section.

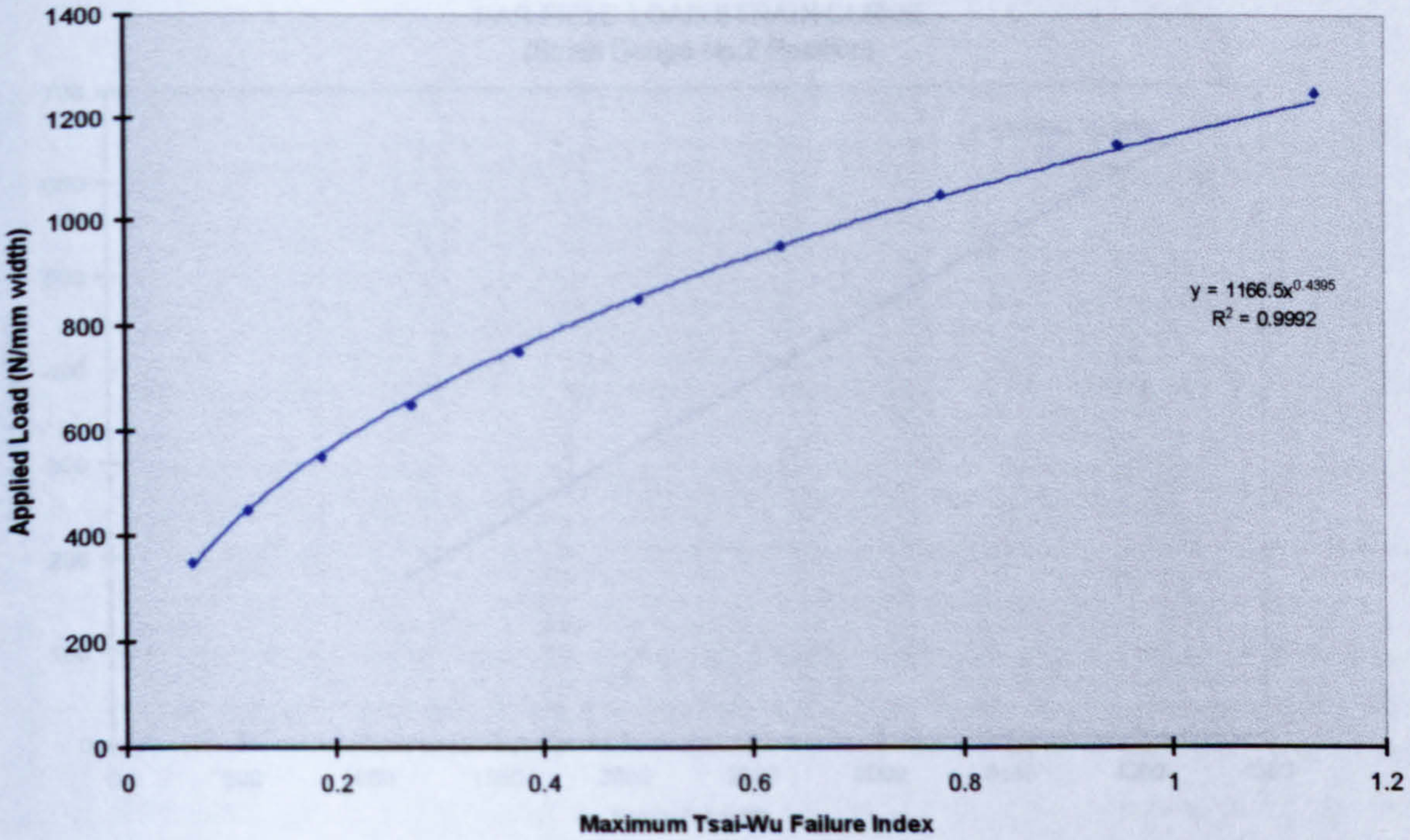

Figure 139 Repaired flat panel maximum Tsai-Wu failure index

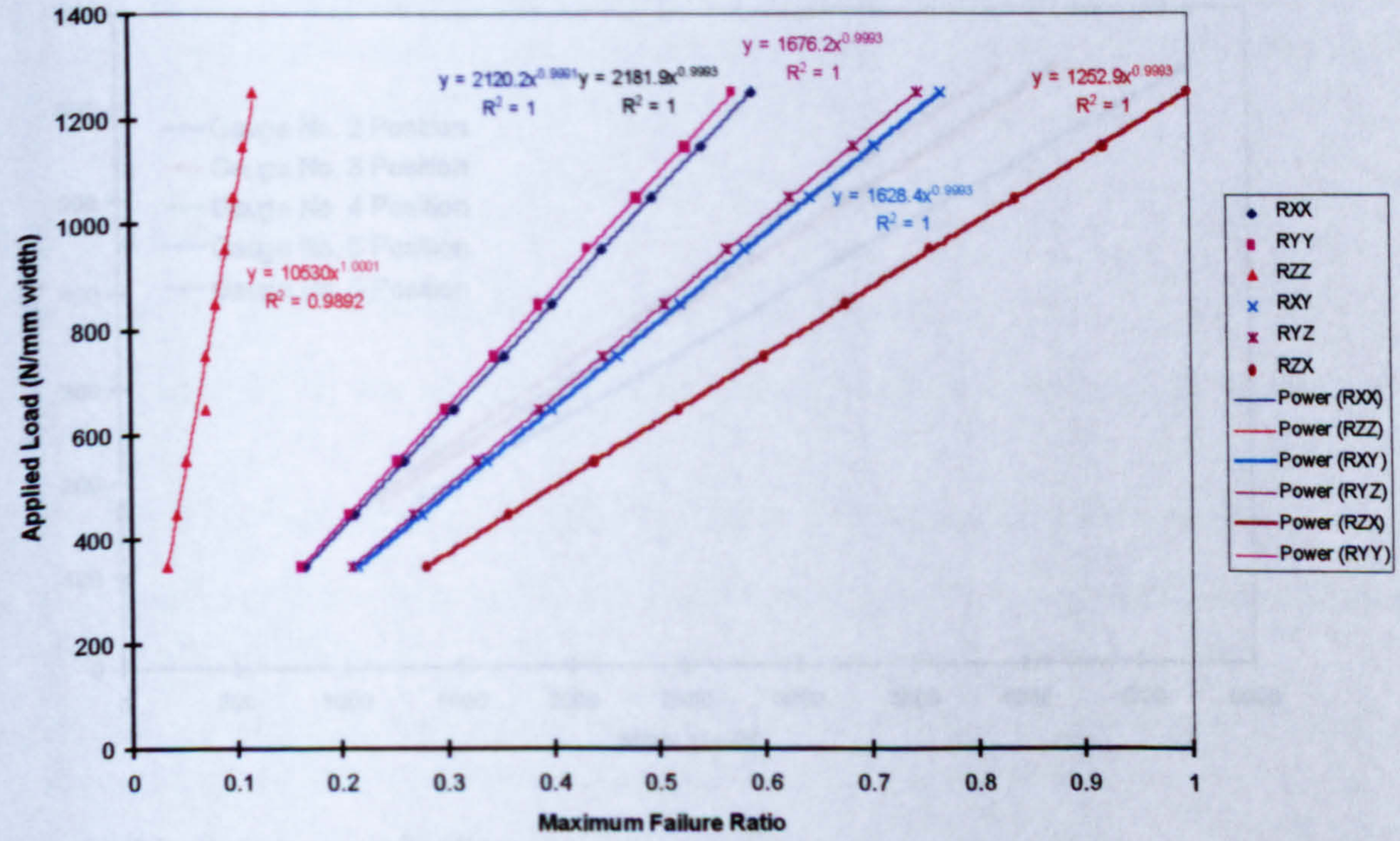

Figure 140 Repaired panel maximum stress failure ratio

From Figure 139, the Tsai-Wu failure criterion predicts that the first ply will fail in the repair patch at 1166.5 N/mm (i.e. 592.58 kN). For the maximum stress criterion (Figure 140), this is predicted at 1252.9 N/mm (i.e. 636.47 kN). Both methods agreeing on the failure location and the maximum stress indicates that this failure will occur through transverse shear stresses in the ZX-plane.

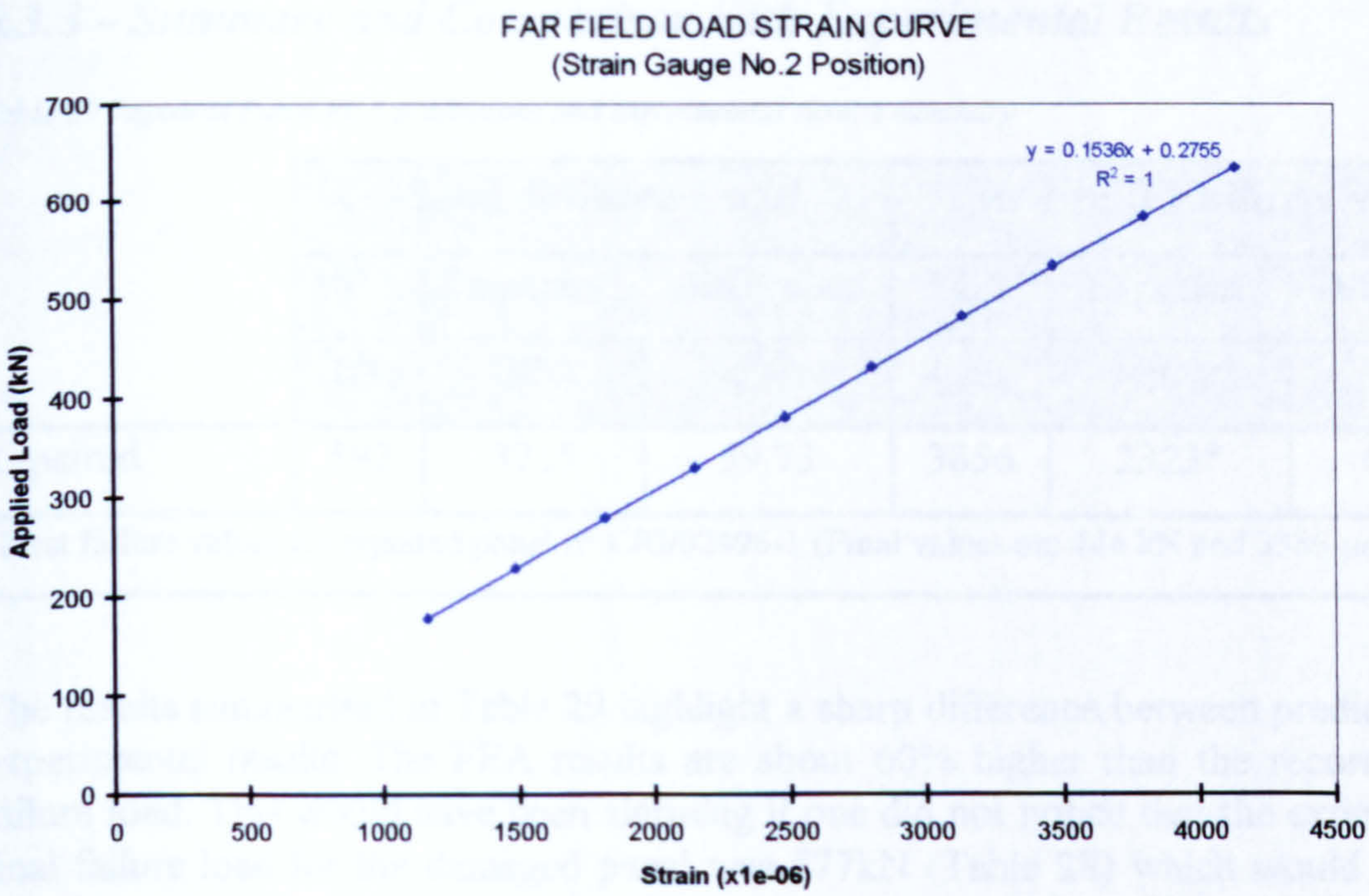

Figure 141 Far field load-strain curve

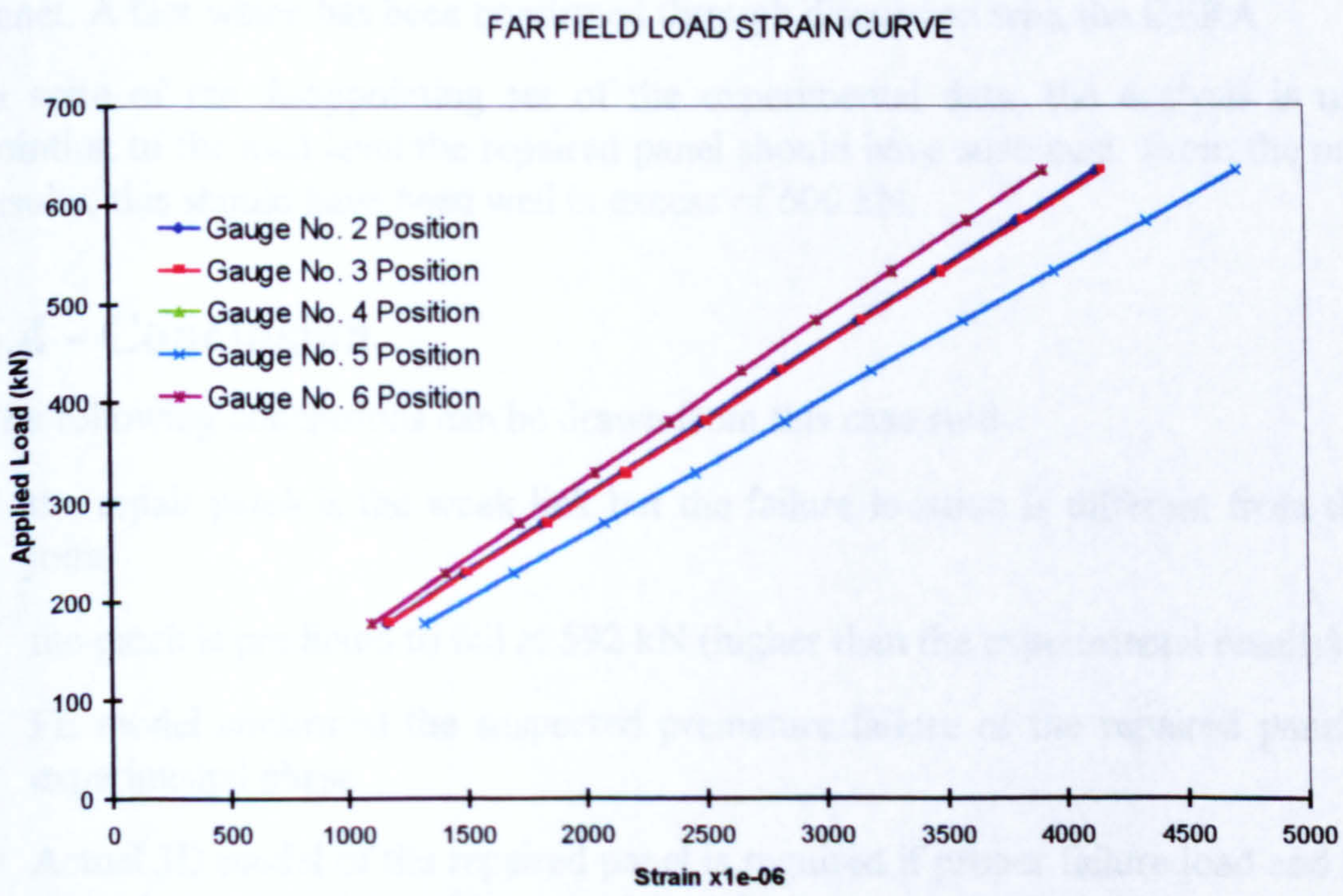

Figure 142 Load-strain curves for all top strain gauge positions

The far field strain is plotted in Figure 141 for each load step. From this curve, the far-field strain at failure is estimated at 3856 με (using Tsai-Wu failure load). The same curve is plotted for each remaining top strain gauge position and shown in Figure 142. Figure 142 shows that the strain at the edge of the patch (gauge n°3 position), in the direction of loading, is very close to the far field strain. Also, the strains at the top and bottom of the hole are very close to each other but they are lower than those in the direction of loading. Finally the remaining strains in the centre of the patch are the highest.

6.3.3 - Summary and Comparison with Experimental Results

Table 29 Repaired Panel FEA predictions and experimental results summary

	Mean Failure Load			Far Field Failure Strain		
	FEA (kN)	Experim. (kN)	Difference (%)	FEA (με)	Experim. (με)	Difference (%)
Repaired	592	371*	59.73	3856	2323*	65.99
*First failure values for repaired panel n° CRI/02496-1 (Final values are 444 kN and 3386 με)						

The results summarised in Table 29 highlight a sharp difference between predicted and experimental results. The FEA results are about 60% higher than the recorded first failure load. This would have been alarming if one did not notice that the experimental final failure load for the damaged panel was 577kN (Table 28) which would indicate that the repair was unsuccessful. This points to a premature failure of the panel, possibly due to manufacturing deficiencies or experimental errors, rather than a bad repair design. This puts a question mark over the experimental results for the repaired panel. A fact which has been confirmed through discussion with the DERA.

In spite of the disappointing set of the experimental data, the analysis is useful in pointing to the load level the repaired panel should have sustained. From the predicted results, this should have been well in excess of 600 kN.

6.4 - Conclusion

The following conclusions can be drawn from this case study:

- the repair patch is the weak link but the failure location is different from the scarf joint
- the patch is predicted to fail at 592 kN (higher than the experimental results)
- FE model confirmed the suspected premature failure of the repaired panel during experimental phase
- Actual 3D model of the repaired panel is required if proper failure load and location are to be predicted (scarf joint model useful but not representative)
- Mixed 3D composite and orthotropic elements worked well for the repaired panel model

6.5 - Summary

This case study has shown that the second new modelling approach was sound. However due to insufficient PC power, a compromise was found by using 3D composite solid elements only where required and 3D orthotropic solid elements elsewhere. The resulting model worked very well and first-ply failure was predicted correctly. The results showed that the FE method was well suited to model bonded

repairs to composite structures and the approach developed was able to cope with repairs to large panels.

This study has also revealed a difference in failure location between the repaired flat panel and the scarf joint on which the design of the repair scheme was based. This indicates that coupon testing may be of limited value for validating repair systems.

Chapter 7

Application to Bonded Repairs

Case Study 3: Curved Panel

7.0 - Introduction

The scarf patch studied in Chapter 5 was used to repair a curved panel. The analysis of this panel constitutes the third case study. The main interest is the fact that with this panel, one is getting closer to real aircraft structures and thus it becomes interesting to see how the repair fares. The fact that the panel is loaded in compression adds to the interest. This study concentrates on the repaired panel exclusively. As with the second case study in Chapter 6, this one was carried out without prior knowledge of the experimental results to further test the predictive capability of the modelling approach being proposed.

7.1 - Repaired Panel Modelling Data

The repair system used for the curved panel was very similar to that used to repair the flat panel. The main differences originated from outer dimensions and loading.

7.1.1 - Geometry

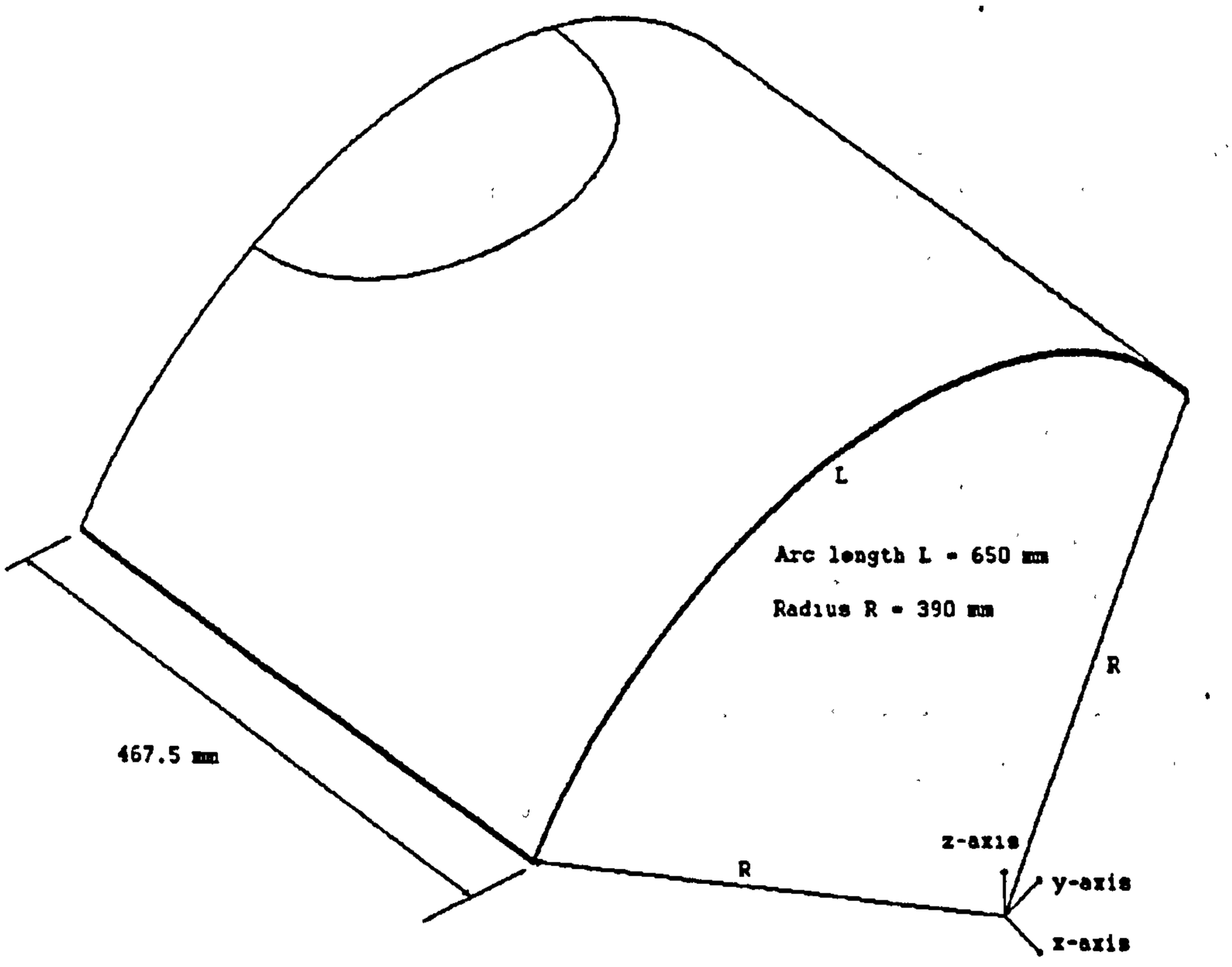

Figure 143 Curved panel geometry

The dimensions of the repaired panel are shown in Figure 143 (half the panel is represented). Before the application of the repair patch, the panel had a 156mm diameter hole in its central region. The 0° fibre direction is along the x-axis and the 90° one in the y-direction.

7.1.2 - Materials

Table 30 T800/924C Equivalent Orthotropic Data for compression loading

PROPERTY(°)	Value	Unit
Young's modulus in x-direction (EX)	77330	MPa
Young's modulus in y-direction (EY)	43894	MPa
Young's modulus in z-direction (EZ*)	43894	MPa
In plane (XY) shear modulus (GXY)	23195	MPa
Out-of-plane (XZ) shear modulus (GXZ*)	23195	MPa
Out-of-plane (YZ) shear modulus (GYZ*)	15238	MPa
Poisson's ratio (NUXY)	0.4403	
Poisson's ratio (NUXZ*)	0.4403	
Poisson's ratio (NUYZ*)	0.4403	

* assumed

(°) nomenclature from NISA/DISPLAY

The materials used in this analysis were the same as those in the preceding chapter. However, the parent material, T800/924C carbon/epoxy composite, had different Young's moduli in compression and in tension: 161 GPa for the longitudinal Young's modulus and 11.5 GPa for the transverse modulus instead of 168 GPa and 9.5 GPa respectively in tension. Thus, this had to be taken into consideration. The computer program LAP was used with the appropriate stacking sequence and the lamina data to generate equivalent orthotropic properties. These are given in Table 30.

7.2 - Modelling Strategy

The modelling strategy was based around the model used for the flat panel and as such was similar. The flat panel dimensions were extended by constructing additional elements around it. Then, each node created was translated along the z-axis. The distance,δz, by which each node was moved was calculated as follows:

$$\delta z = \sqrt{R^2 - y^2}$$

where R is curvature radius (390 mm) and y is the node co-ordinate along the y-axis. The global Cartesian co-ordinate system had its origin in the centre of the hole and the panel curvature was part of a circle of 390 mm radius centred on the co-ordinate system origin. A short program was written to assist with the task of translating all the nodes.

The first part of the analysis was concerned with the panel response to an applied compressive load of 1250 N/mm in order to determine stress "hot spots" and an appropriate load range to determine failure.

7.3 - Results and Discussion

7.3.1 - Structural Response to Compressive Loading

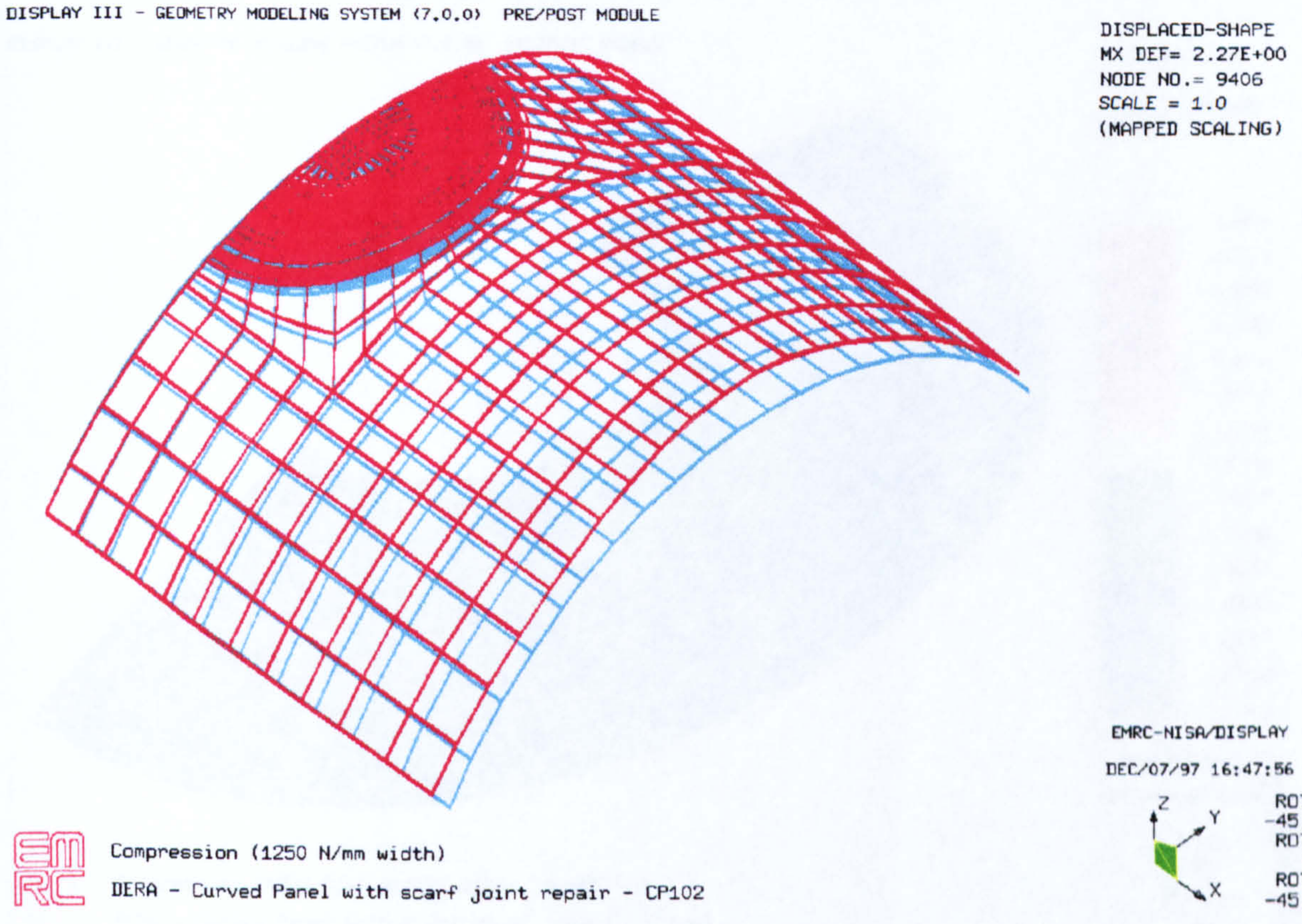

Figure 144 Repaired curved panel deflection

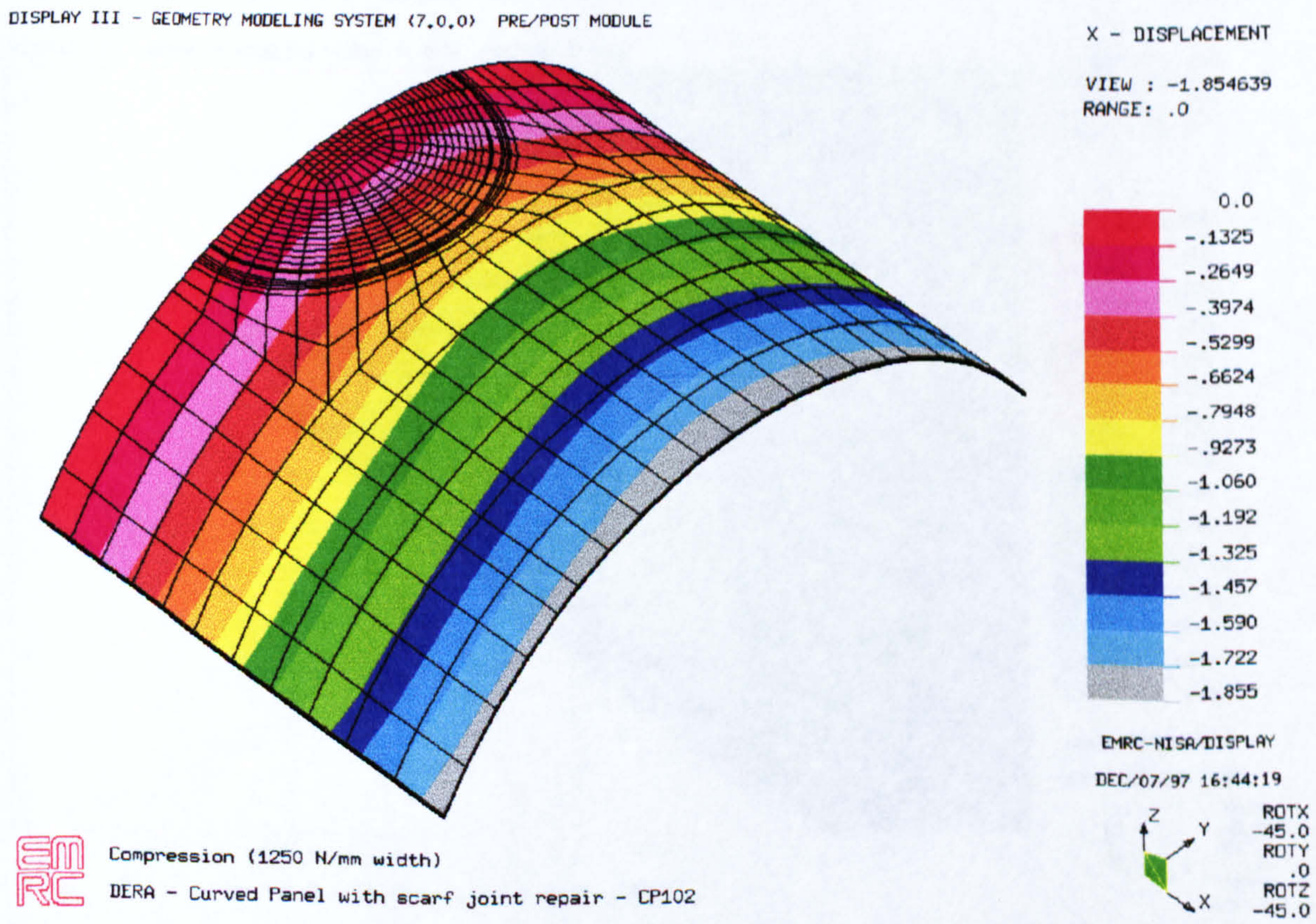

Figure 145 Longitudinal displacement

The deformation of the panel under the applied load is shown in Figure 144. The action of the repair patch is reflected in the longitudinal displacement contour (Figure 145) where the colour bands are not parallel to the loading edge as would have been expected from an undamaged panel.

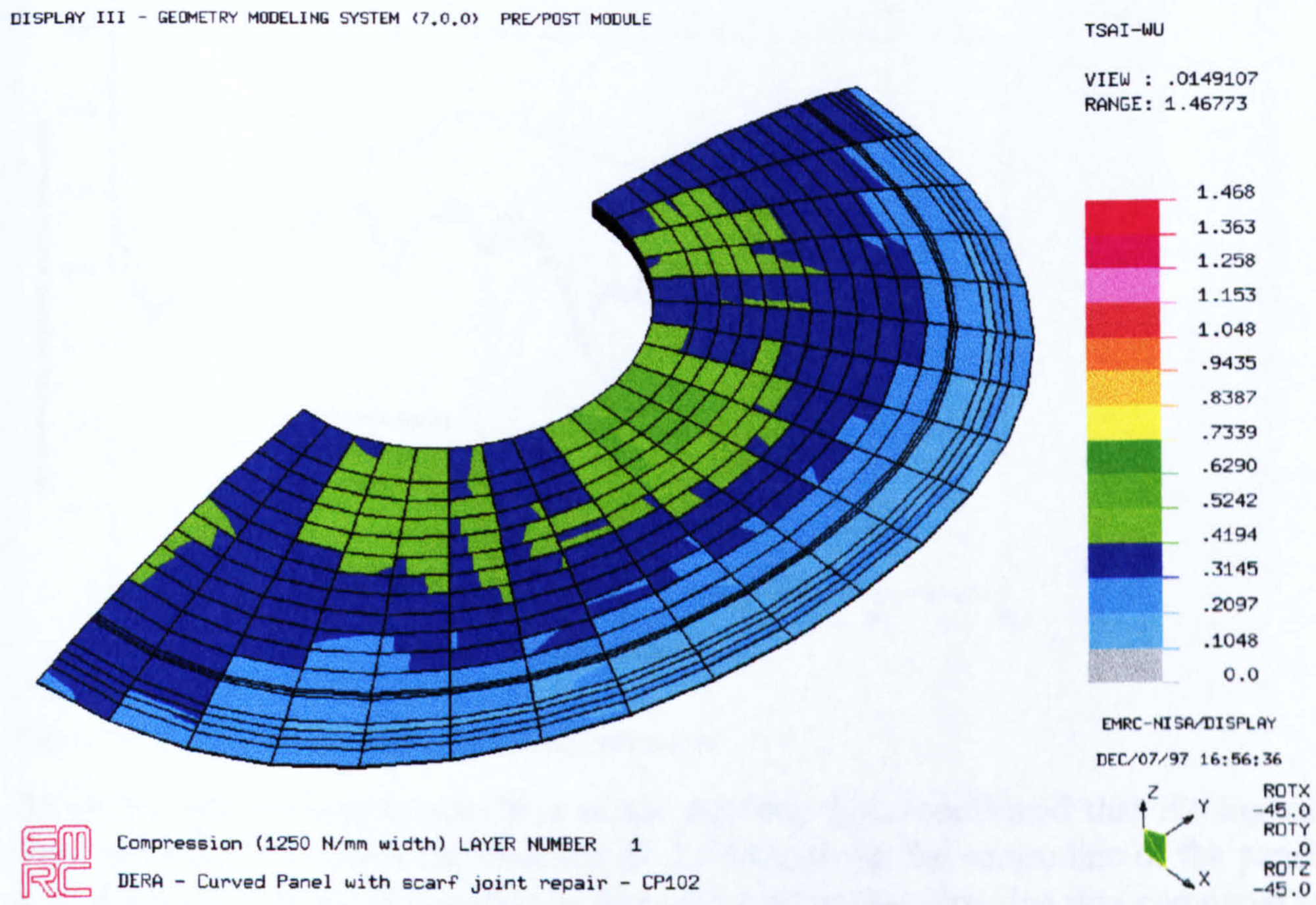

Figure 146 Repaired patch Tsai-Wu failure index contour

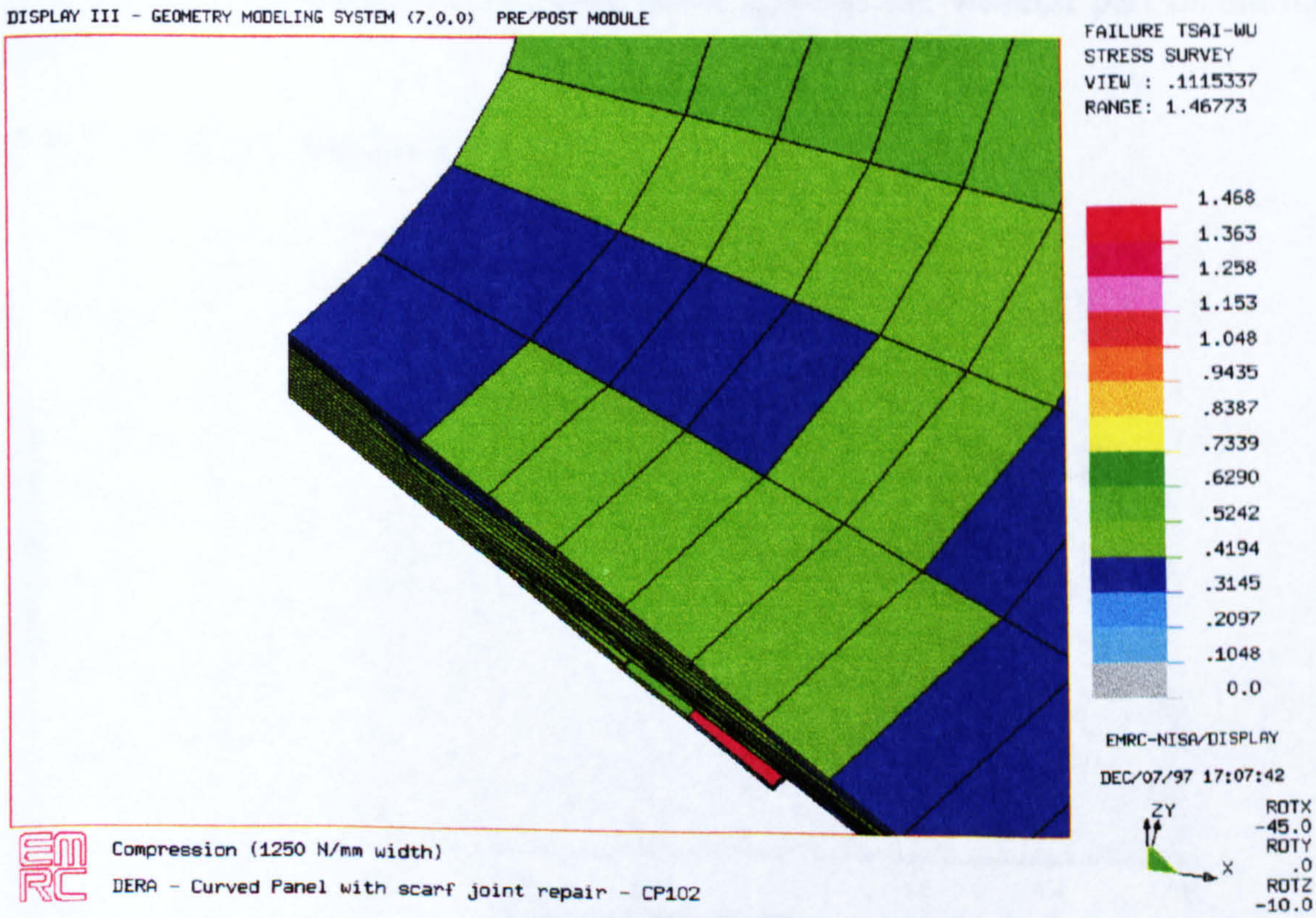

Figure 147 Failed extra layer(some patch elements removed for clarity)

The Tsai-Wu survey of the repair patch (Figure 146) shows that most of the patch has a significant amount of reserve strength (low failure index) but reveals that the extra ±45° layer is well past its first ply failure load (Figure 147). Failure is predicted to occur at the same location as the flat panel failure location (red element in Figure 147).

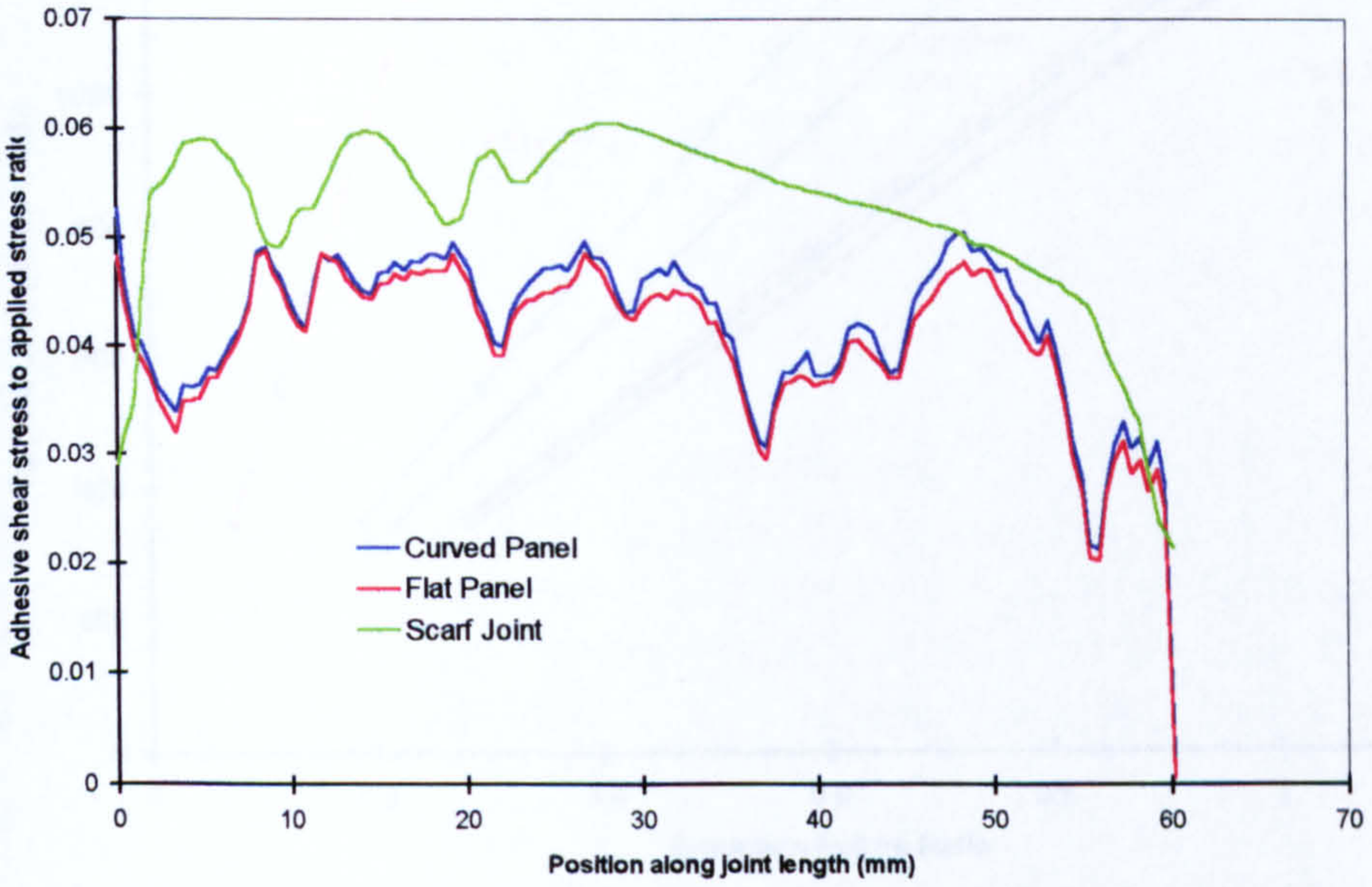

Figure 148 Repaired panel adhesive shear stress distribution

As anticipated, a close examination of the adhesive layer confirmed that the highest shear stresses occurred in the direction of loading, along the centre line of the panel. The adhesive shear stress distribution along the joint in that direction was compared to the results of the scarf joint and flat panel analysis (Figure 148). This revealed that the stresses in both panels were comparable and that they were much lower than the scarf joint results. This confirmed the repair patch again as the weakest part of the repair system.

7.3.2 - Failure Analysis

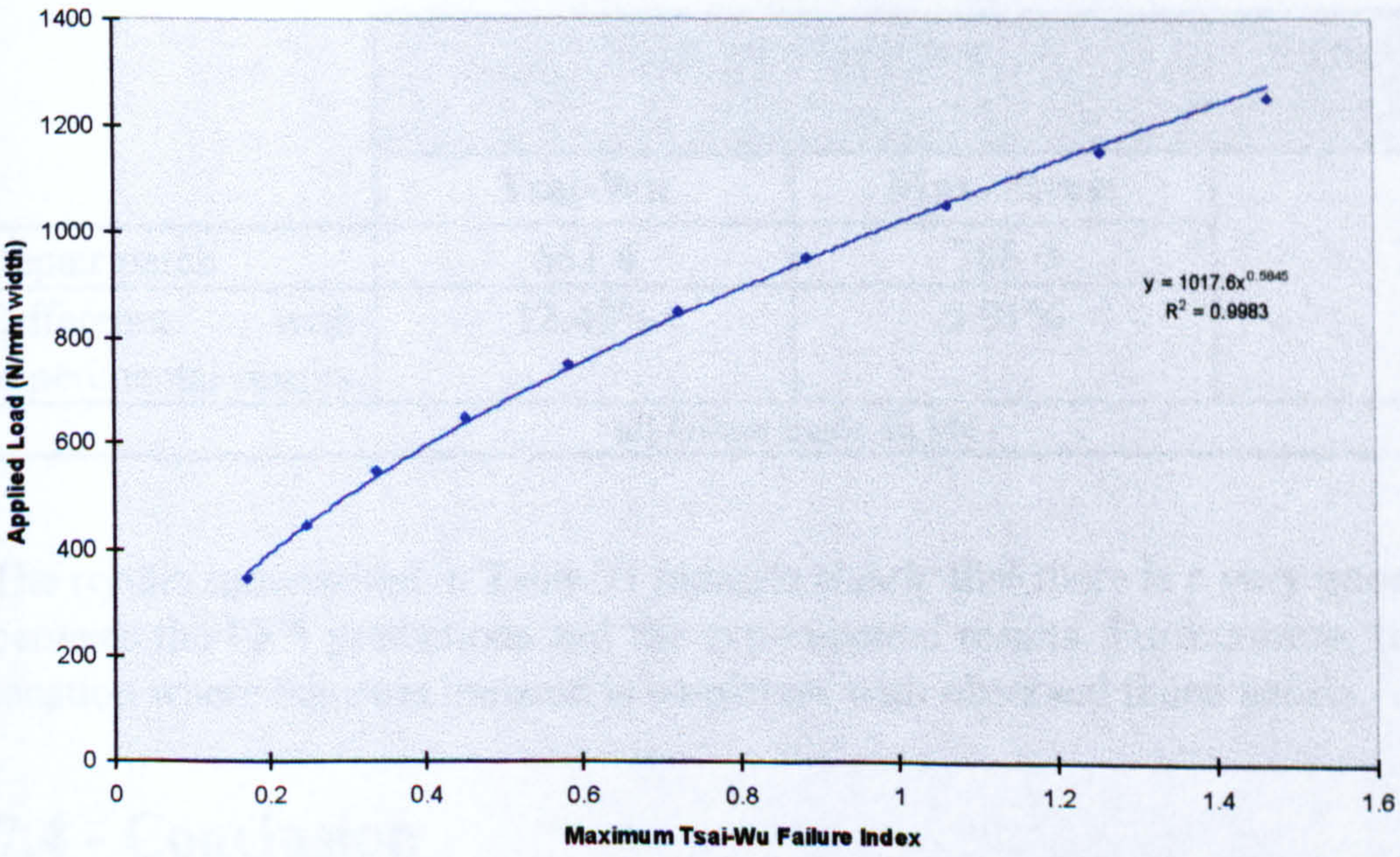

Figure 149 Maximum Tsai-Wu failure index for curved panel

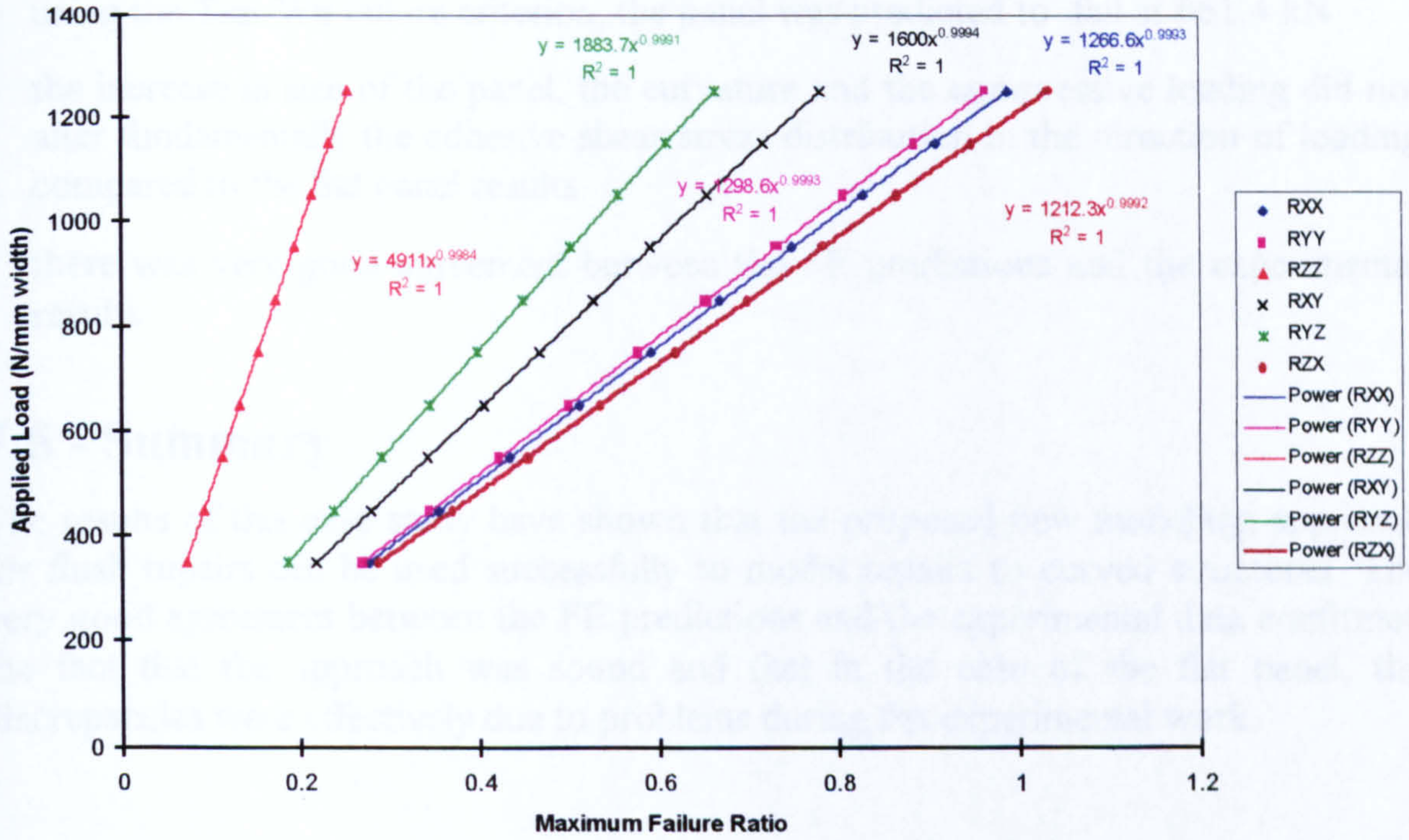

Figure 150 Maximum stress failure ratio for repaired curved panel

The failure analysis focused on the repair patch only. The Tsai-Wu and maximum stress failure criteria were used to determine the first ply failure load. The results are shown in Figure 149 and Figure 150. From the curve in Figure 149, the failure load is 1017.6 N/mm (or 661.4 kN). Using the maximum stress failure criterion (Figure 150), the failure load is 1212.3 N/mm (or 788.0 kN) due to transverse shear stresses in the ZX-plane.

7.3.3 - Summary and Comparison with Experimental Results

Table 31 Curved Panel FEA predictions and experimental results summary

	FEA Predictions		**Experimental**
	Tsai-Wu	**Max. Stress**	
Repair patch	661.4	788.0	744
Difference with experimental results	12.48%	5.91%	
all failure loads in kN			

The results summarised in Table 31 indicate clearly that there is a very good agreement between the FEA predictions and the experimental results. Furthermore, the predicted location where failure is initiated is consistent with observed failed panels.

7.4 - Conclusion

This case study has established that:

- the repair patch was the weak link
- using the Tsai-Wu failure criterion, the panel was predicted to fail at 661.4 kN
- the increase in size of the panel, the curvature and the compressive loading did not alter fundamentally the adhesive shear stress distribution in the direction of loading compared to the flat panel results
- there was very good agreement between the FE predictions and the experimental results

7.5 - Summary

The results of this case study have shown that the proposed new modelling approach for flush repairs can be used successfully to model repairs to curved structures. The very good agreement between the FE predictions and the experimental data confirmed the fact that the approach was sound and that in the case of the flat panel, the discrepancies were effectively due to problems during the experimental work.

Chapter 8

Contribution of the Current Work

General Discussion - Future Work

8.0 - Introduction

In this chapter, the work carried out and the results obtained are put within the context of the literature survey done in Chapter 1.

8.1 - Final Remarks

The project's first objective was to gain an understanding of the philosophy behind the modelling approaches that have been used in previous published works. Given the context of the work being carried out on a PC with commercial FE codes, only those modelling approaches which could be conducted within those constraints were selected. For the project, the FEM was just an analysis tool and had to be used in such a way that a practising repair engineer could use it in performing the maintenance duties assigned to him or her.

The comparative study which followed shed light on the capabilities and restrictions of the three main approaches selected. It was shown in particular that the 2D plane strain model, which evolved from earlier studies on adhesive bonded joints, was excellent for the study of the adhesive layer but had inherent short comings when it came down to adherends stresses. Although Siener [102] indicated that the model could be used for bonded repairs, this study showed that if that were the case, the information would be complete because layers stresses cannot be calculated using his model.

The innovative approach of Bair *et al.*[109] produced the reverse of Siener's model specifically in the prediction of adhesive shear stresses. In the original work, the preoccupation seemed to be the correlation of predicted strains to experimental strains which the model was able to provide. The comparative study has been able to reveal that the approach proposed by Bair and co-workers could not provide reliable shear stress data.

The 3D model with equivalent properties, as used by Soutis and Hu [107], was better than the other two models but again adherend layer stresses could not be obtained. This comparative study, believed to be the first of its kind, addresses the fundamental philosophy behind the various models providing the repair designer a common reference. It also gave a clear indication of the difference between bonded repairs and bonded joints by highlighting the inadequacy of the modelling approaches perceived by some researchers to be able to deal with repairs.

Thus the comparative study produced a complete picture of the capabilities of these approaches and also pointed to areas where improvements could be made. This resulted in two new modelling approaches for bonded repairs to composite structures

following an assessment of key areas where improvements could be effected. These key areas were: modelling components, adhesive material models and failure theories. A sound repair design philosophy was identified as necessary to underpin any improvements to those key areas.

The new approaches were thoroughly investigated in Chapter 3 and compared to more traditional models using 3D solid elements with composite equivalent properties. In particular, the new quasi-3D model for external bonded patch repairs was shown to provide better adherend layer stresses and suitable adhesive stresses (peak values being about 17% higher than traditional models). However, comparison with experimental data in Chapter 4, showed that, for properly designed bonded repairs, accurate prediction of adhesive peak stresses was not the overriding priority. The model results were in very good agreement with experimental data (8.54%). This vindicated the use of laminated elements and a composite-specific failure criterion which is an improvement compared to more traditional approaches [107]

The next stage was to test these new modelling approaches on real repairs. The literature survey had revealed that in most studies, the FE models of bonded repairs were very idealistic [107, 102] and in some cases, the dimensions of the repaired panels were so small as to be unrepresentative of actual aircraft structures [108, 144]. When they were representative, the approach used was not entirely suited for modelling repairs [46, 109]. So it was important to model representative repairs. The repairs considered for the remaining chapters were done to large components, representative of actual aircraft structures and with increasing complexity. These repairs also included features which were required from a practical point of view such as extra layers on the top and bottom of the repaired panel and cup formation for repair patch inner layers used for easy manufacture.

A detailed investigation of the scarf joint used for the repairs was carried out in Chapter 5. This showed that the repair patch was the weak link and that the adhesive failure load was well above the repair patch failure load. The non-linear analysis confirmed that the linear static analysis was underestimating the adhesive failure load by at least 24.04% thus precluding the need for such an analysis on the repaired flat and curved panels. The agreement between the FEA results and the experimental data was again very good (7.84% and 9.99%) adding further confidence in the modelling approach being used. The analysis also showed that the use of ASFC was not a good option for composite laminates in spite of its recommendation by Soutis and Hu in their analysis of scarfed repairs [108]. The results were too sensitive to the choice of characteristic distance. Also the actual failure mode could not be predicted by this method.

The analysis of the repaired flat panel helped confirm the suspected premature failure of the panels tested experimentally by predicting what the minimum experimental failure load should have been. That analysis also highlighted one of the main differences between bonded joints (such as the scarf joint in Chapter 5) and actual bonded repairs: the additional load paths around the damaged area helped reduce the shear stress loading on the adhesive and thus delayed further the adhesive failure. Furthermore, it also showed that failure was initiated at different locations: within the patch inner layers for the scarf joint but at the end of the bottom extra layer for the repaired panel. Also, there was no direct link between the failure load level per unit width of the scarf joint and that for the repaired panel. This result therefore puts a

question mark on the value of coupon testing for anything other than establishing that the adhesive layer was sufficiently stronger than the adherends. No final assessment of the repaired panel can be based on coupon testing, especially with respect to failure load and location.

Finally, the last case study confirmed the soundness of the modelling approach used for these flush scarf repairs. The predictions for the repaired curved panel were very good, between 5.91% and 12.48% below the experimental results. The failure location was the same as that for the repaired flat panel even though the loading mode was changed from tension to compression.

The different case studies have highlighted the fact that current commercial FE codes can be used in their present condition to model and analyse successfully bonded repairs to composite structures. However, these codes are not optimised to that respect but rather geared toward composite structure design and analysis.

The NISA FE package was selected for this project as it offered the best combination of elements capability for composite modelling and ease of use as well as good value for money. As such the following remarks are mostly relevant to this package. However, the main issues raised will be more or less applicable to other software packages.

In NISA, the 3D laminated shell element has been fully developed to become the main element for composite structural analysis. This element is very flexible because it can be orientated in any direction and its fibre direction can be defined easily with respect to either global co-ordinate systems or local element axes. Three different failure criteria are available and interlaminar shear stresses are offered as standard results. This element has also been modified to become a 3D laminated sandwich shell element suitable for the analysis of composite sandwich structures. As such, these composite shell elements are well suited for the design and analysis of composite structures which tend to be thin in most engineering applications.

Adhesively bonded repairs to composite structures have significant features in the through-thickness direction (such as scarf joint, spew fillets, extra-layers etc...) which need to be represented accurately. Whilst these features can be modelled to some extent for external repairs with the first new approach proposed in this thesis using 3D laminated shell elements, the same thing is impossible with flush repairs. For these, the only alternative in order to obtain layer stresses is the 3D laminated solid element.

The 3D laminated element was intended for the analysis of thick composite structures. As such, all six stress components are available but only the Tsai-Wu failure criterion can be used. Also interlaminar stresses cannot be calculated. The biggest handicap was the fibre angle definition. This can only be done using two consecutive nodes on the element bottom or top faces. This meant that preparing a model for analysis was time-consuming. Given the nature of most flush repairs, it was best to use one element per ply in order to model accurately the through-thickness features. This meant that the elements were very thin which was not exactly how they where intended to be used. The simple inclusion of the global axes as possible fibre angle reference axes would greatly increase the element flexibility and reduce the sheer amount of work required for preparing a model for analysis.

One is left with a very strong impression of using an unfinished product. However, one can understand why that was the case because such 3D elements are not really required for the design of composite structures.

The effectiveness of any finite element analysis rests ultimately upon the quality and reliability of the material data which are used. This is even more important in the case of composite structures. This project has revealed the need for an integrated approach for the design and analysis of bonded repairs to composite structures. Usually, the FE work is carried out as part of a larger research project and is often done to confirm experimental results as in [46]. The requirements of test data for the FE analysis may be different from those of the experimental phase of a project. Thus if these requirements are not considered in an integrated fashion, one can be faced, as is too often the case, with missing data which are important for the FE analysis but have not been measured because there was no need from the experimental work point of view.

8.2 - Contribution of Current Work

The work carried out in this thesis enabled the clarification of the requirements for any FE modelling of adhesively bonded repairs to composite structures. It has also provided what is believed to be the first systematic comparison of modelling approaches for analysis of bonded repairs and found them complementary but falling short of what was required.

Two new modelling approaches have been proposed for external and flush repairs which are an improvement over previous studies [46, 101, 102, 105, 106, 108, 109] because the laminated nature of the composite adherends was maintained and allowed the use of failure criteria specific to composites. Furthermore these approaches were capable of modelling repairs on structures which were truly representative of real aircraft structures. Their failure predictions were in very good agreement with experimental data.

A new adhesive failure criterion was proposed for bonded repairs to composite structures which was a simple but effective way of assessing the adhesive failure load in relation to the other repair components. The criterion, developed from Brewer and Lagace's work [159], was conservative in its failure predictions but easy to use and it precluded the need for time-consuming material non-linear analyses.

8.3 - Proposals for Future Work

The key areas which offer the biggest scope for future work are the modelling components and the failure theories. For the first one, the work should investigate the formulation of better 3D laminated elements which would have a high tolerance of poor aspect ratio while being flexible in the definition of the laminate fibre angles. The second aspect which needs to be investigated further is the development and inclusion of better physically-based failure criteria for composite materials. Such criteria have not been coded so far into FE programmes. It is the author's deeply felt opinion that these criteria offer the best hope of producing FE models able to predict final failure loads and failure progression within composite structures.

Finally, further work needs to be done on the inclusion of residual thermal stresses and the effect of hot/wet environment in the analysis which are vital for the assessment of the long-term behaviour of adhesively bonded repairs.

8.4 - Conclusions

- This thesis has provided what is believed to be the first systematic comparison of modelling approaches for PC based application which can be applied to bonded composite repairs
- Two new modelling approaches have been proposed for the analysis of external and flush bonded repairs able to investigate within a single model both adhesive and composite adherend failures.
- The project has highlighted the potential of the finite element method as an analysis tool for bonded composite repairs, especially on a PC platform and shown the need to include layer stresses and strain in order to account for composite adherend failures
- The project has shown that current commercial FE codes are not optimised for the analysis of bonded composite repairs although a significant amount of work can be undertaken successfully

APPENDIX A

Introduction to Composite Materials

Basics and Applications

A.0 - Introduction

The increasing use of composite materials in engineering structures has been spurred by the perceived advantage they have over conventional materials in terms of specific strength and modulus.

A.1 - Basic Concepts

There is no universally accepted definition of composite materials. Definitions available in the literature differ greatly because of the level considered by each author which can be elemental, microstuctural or macrostructural. For this review, the following definition will be given as to what is meant by composite materials.

Composite materials are multi-phase materials whose overall mechanical and physical properties are a result of the interaction between the phases. They usually consist of two or more separate materials combined in a structural unit at the macroscopic level. Thus if the structural unit is formed at the microscopic level such as in metallic alloys or polymer blends, it is not classified as a composite [112]. The individual constituents are generally insoluble, remain distinct within the structural unit and may be continuous or not [113].

There are several types of composite available today for structural applications. They can be classified in several ways, one of which is according to their matrix material. Thus, for this classification, the main types of composite are: ceramic matrix composites (CMC), metal matrix composites (MMC) and polymer matrix composites (PMC).

Composites can also be divided into classes according to the type of reinforcement used. Thus we have particulate-reinforced, fibre-reinforced or laminar composites. In particulate-reinforced composites, the reinforcement has roughly equal dimensions in all directions. Such reinforcement includes spheres, rods, flakes etc. Fibre-reinforced composites have reinforcements which have lengths much greater than their cross-sectional dimensions. The fibres may be short or long. In laminar composites, we have two or more layers with two of their dimensions being larger than their third.

Advanced composites usually refer to polymer matrix composites where the matrix is reinforced by carbon, boron or aramid fibres. Their main application being in the

structural components of aerial vehicles. These components are usually built up layer by layer. Each layer is called a lamina and two or more laminae form a laminate.

This review is concerned essentially with polymer matrix long fibre reinforced composites. In subsequent pages, this category of composite materials will be referred to as "composite materials" or simply "composites". Also more emphasis will be put on advanced composites.

A.2 - Matrix Materials

The choice of the material used for the matrix is strongly dependent on the particular requirements for a given application. However, whatever material is used, the matrix has to perform essentially the same role: to hold the reinforcing fibres together and distribute the applied loads to the fibres. Matrix properties will also influence such composite properties as ductility, toughness or electrical insulation.

Polymers are the most widely used matrix materials in today's composites. They are divided into two main groups: thermosets and thermoplastics. Thermosets are made up of highly cross-linked, three dimensional polymer chains which do not melt at high temperatures once cured. Thermoplastics, on the other hand, are constructed from polymer chains which do not cross-link during curing. As a result, thermoplastics can be reprocessed at high temperatures repeatedly. This cannot be done with thermosets. Until recently, thermosets dominated completely as matrix materials for composites.

A.2.1- Thermosetting Resins

Thermosets are the most widely used matrices in advanced composites for aircraft applications. Although existing thermoset matrices have shown that the full potential of the reinforcing fibres cannot not be realised because of their matrices limited ductility, they still possess a combination of characteristics which are excellent at competitive cost. The introduction of new toughened epoxies is set to continue the domination of matrix materials by thermosets despite the promises shown by thermoplastics with much better toughness properties than current thermosets. Six types of thermosets are currently in use: epoxy, polyester, vinyl ester, phenolic, polyimides and bismaleimide resins. Polyester and vinyl ester resins are the most widely used of all matrix materials by quantity. They are used mainly in commercial or industrial applications. Epoxy, polyimides and bismaleimides are used mainly in aerospace applications.

Additional information can be found in [114, 115and 167] for epoxy resins, [168] for BMI resins and [169, 170 and 171] for polyimides on various materials engineering aspects.

A.2.2 - Thermoplastic Resins

Given the limitations of thermosets, thermoplastics have been considered as potential replacement for applications requiring better toughness capabilities and better hot/wet performance. Researchers in the aerospace field even thought of thermoplastic based composites as a serious and sure candidate to create tougher and more durable composites at significantly less costs than thermosets [172]. However, the promises of the 80s fail to materialise as noted by Brandt *et al.*[173] reviewing the prospects of thermoplastic composites for future aerospace applications.

Thermoplastics are formed by long chains of repeating molecular units (monomers) with a fixed chemical structure. They are moderately elastic and chemically inert. Under the application of heating, thermoplastics will become soft and can be moulded into the appropriate shape before turning hard again on cooling. Because barely no cross linking occurs between the monomer chains in the process, thermoplastics can be reprocessed repeatedly. However there are progressive degradation and cross linking effects with repeated temperature cycling [169]. They are the only matrices available which could, in theory at least, be used with the new intermediate modulus, high strength, high strain carbon fibres to their full potential.

In their continuous fibre form, thermoplastic composites are similar to thermoset prepregs. There are two main groups: the first one which include polyamides (PA) and polypropylene (PP) are used mainly in commercial applications and the second one made of the so-called advanced engineering thermoplastics. These include polyphenylene sulphide (PPS), polyetherimide (PEI), polyethersulphone (PES) and polyetheretherketone (PEEK). PEEK is the most used thermoplastics for aerospace applications.

Despite the slow progress and the short comings, after ten years of continuous intensive research and development programmes, thermoplastics as matrix materials still look an attractive proposition in terms of low moisture absorption, better hot/wet performance and better reparability. The advent of newly developed tough thermosets no longer makes toughness the driving force for the introduction of these materials in the aerospace field [173]. Better prospects for these materials will come mainly from improvement in manufacturing processes.

A.3 - Fibre Reinforcement

The main fibre reinforcement materials used in polymer matrix composites are: glass, boron, aramid and carbon. Other fibres in development include silicon carbide (SiC) polyethylene and quartz. Extensive information about these main reinforcing materials can be found in [174,175,176,177,178,179 and 180]

A.3.1 - Glass Fibres

Glass fibres are made of silica (SiO_2) and metallic-oxide-modifying elements. The exact glass composition will provide properties suitable for particular applications. E-glass makes up the highest proportion of manufactured glass fibres along with the

modified E-glass (ECR) which has improved chemical resistance and excellent moisture resistance over a period of time. S-glass is a higher strength material with high thermal stability and is used in the aerospace industry where its higher cost is justified by improved performance.

A.3.2 - Boron Fibres

Boron filaments are different from other reinforcing fibres. Each one of them is made by chemical vapour (CVD) of boron coating on a substrate wire of tungsten (W) or carbon (C). Boron fibres are renowned among advanced fibres for their high compressive strength which come from the fibre larger diameter. They have been developed essentially by the US because of the ready availability of boron trichloride in large quantities, left over from an abandoned rocket fuel project. Their relatively high density compared to carbon fibres have made them a less attractive proposition in the aerospace industry despite their better compression properties and earlier use in large amounts during the 1970s on several American fighter aircraft. They also more expensive to produce compared to other advanced fibres

A.3.3 - Aramid Fibres

Aromatic poly**amid** (aramid) fibres are currently the main organic fibres available to reinforce polymer matrices.Their main attraction is their toughness and general damage tolerance characteristics. However, due to their toughness, aramid fibres are very difficult to cut. Special tools have been developed to cut aramid fabrics cleanly. Because the fibres are relatively flexible and non-brittle, they can be processed using most conventional textile operations which add to their diversity of applications. In the aerospace industry, aramid is often used with carbon to reinforce polymer matrices and form hybrid composites. These have a reduced weight and better toughness characteristics due to the aramid lower density and higher toughness.

A.3.4 - Carbon Fibres

Carbon fibres are the most widely used fibres in advanced composites. They combine exceptional properties with low density putting them amongst those materials with highest specific strength and modulus(i.e. strength and modulus per unit weight).

In the literature, the terms 'carbon' and 'graphite' tend to be used interchangeably, more so in American technical and scientific literature. This has led to the common belief that graphite is just an American word for carbon. However there is a difference. Graphite fibres are subjected to much higher temperature heat treatment and contain at least 99% of elemental carbon. Carbon-fibres, on the other hand, are produced at much lower temperature and have an elemental carbon content between 95 and 99%. As the reaction temperature controls the fibre ultimate properties, graphite fibres have higher

modulus than their carbon counterparts. Unfortunately, an increase in modulus usually corresponds to a decrease in ultimate strength and elongation. Thus in aircraft applications, carbon fibres are preferred because the composites parts are continually stressed and flexed and excellent strength and ductility properties are required [180].

In this review, the term 'carbon' will be used invariably to refer to carbon-based reinforcing fibres.

A.3.5 - Other Reinforcing Fibres

Silicon carbide, polyethylene and quartz fibres are under development as potential reinforcement for polymer matrices.

Silicon carbide fibres have been used predominantly to reinforce metals because they have a better resistance to oxidation. and are less prone to attack molten aluminium than boron fibres. However for polymers, the main attraction is their high temperature resistance which would be useful to reinforce polyimide resins in particular for high temperature operations. Silicon carbide fibres are manufactured by a CVD process and have mechanical properties similar to boron fibres

High strength polyethylene (PE) fibres rank amongst the best organic fibres being developed for PMC reinforcement. Although their mechanical properties are nowhere near those of advanced fibres such as carbon fibres, PE fibres have a very low density and that gives them very high specific properties. Their low melting point however is a disadvantage.

Quartz fibres are made of pure silica and have mechanical properties similar to glass fibres. They can retain them to high temperatures which make them attractive as potential reinforcing materials [167].

A.4 - Structural Applications

Although current composite technology evolved from aerospace applications, structural elements made from polymer matrix composites can be found in many engineering applications as well as in commercial and sporting goods today. In this review, more emphasis will be put on aerospace applications of composites.

A.4.1 - Non Aerospace Applications

The use of composites in non-aerospace applications has been growing steadily. It is the composites very high specific properties that have been the main attraction for designers initially. Later on, composite versatility as a material became much appreciated and this resulted in more use of composites.

In the sporting arena, less regulated and more individualistic disciplines have led the way in making the most of the advantages composites could offer: properties suited to create lighter and more efficient equipment.

Carbon fibre reinforced epoxy (C-Ep) tennis rackets are renowned for their performance compared to wooden or aluminium ones. In sport fishing, composite rods are structurally very sound and efficient. Previously constructed hollow rods used to suffer from the collapsing-straw effect which occurred when the rod was made with a material whose fibre direction did not take into account the actual stress distribution in the bending tube. Composites property tailoring capabilities have given fishing rod designers the kind of freedom that was never possible with traditional material such as metals or wood.

Golf is another sport where composites have had an important impact. The advantages of using composite to manufacture poles for pole vaulting are similar to those obtained in sports fishing rods. Glass fibre reinforced plastics (GFRP) have been used extensively. However, recent years have seen the introduction of carbon fibre reinforced plastics (CFRP) in an attempt to reduce pole weight while improving its stiffness.

In more regulated sports, composites have been mainly used for auxiliary safety equipment. These includes protective gear for baseball, hockey and cricket.

In the recreational field, GFRP, mainly glass fibre reinforced polyester composites, have been used extensively to construct pleasure boats. The main reason was to eliminate dry rot problems caused by fungus on wooden boats which had limited the service life of these boats to a few years. On top of this, the immediate benefit was the fact that with composites, boat hull could be constructed according to the stress level which varies from keel to shear. Composites have been used also as skin material for sandwich structures and also for sails.

The impact of composite materials in the sporting and recreational field has been very strong. No component has been left untouched. Thus today, these markets are almost saturated, with composites becoming the industry standard. Further improvement will come from the optimisation in using these materials [181].

Racing yachts have been the biggest users of advanced composites for marine applications. In this field like in aerospace, performance is the most important factor. However when cost is also critical but improvements in performance are still required, the use of hybrid composites made from glass fibres mixed with any advanced fibres in a matrix has been a successful compromise. Hybrid composite hovercraft blades are now common. Other applications for these materials include passenger ferries [182].

The biggest attraction for using composites on future ships and submarines is the elimination of corrosion related problems. The development of low cost materials and processes requiring no autoclaves will lead to the widespread use of composites on larger vessels such as oil tankers which would certainly benefit from a reduction in topside weight [183].

The use of composites in the automotive industry has been confined mainly to discontinuous GFR composites. This is due to the demanding requirements and extreme cost sensitivity of automotive components.

Although continuous fibres and advanced composites have made limited inroads into this industry, a lot of effort has gone into production and experimental applications which illustrate their potential for future production cars. The Ford Taurus 'tub' concept is a well known example. The whole car body is made from five composite pieces welded and bolted together producing a lighter car which is potentially less expensive to manufacture. Ford LTD sedan and Chrysler Polymeric Extra Light (PXL) cars are other American examples. In Europe, the Renault Espace also has composite parts.

Experimental PMC engines have been developed as well but their long-term service reliability remains to be demonstrated. Leaf springs for automotive vehicles have been made with significant weight savings and better fatigue resistance.

Formula 1 racing has traditionally used advanced composites because of the required improvement in performance. Automobile designers have taken full advantage of composite versatility to produce very efficient chassis. CFR toughened epoxies are now industry standards. They have demonstrated their exceptional crash worthiness qualities over the years. The use of composites in this field has paralleled their use in aerospace with aerospace engineers often drafted in Formula 1 design teams.

The use of PMC in the construction industry has concentrated mainly around E-glass fibre reinforced polyester. Applications include pedestrian bridges, building exterior panels, towers and antenna housings. Significant developments have been made which make the prospects for high volume use of composites in structural civil engineering applications brighter. The potential savings in maintenance costs if corrosion prone steel structures are replaced by GFRP structures could reach an estimated $200 Billion per year in the US alone [183].

One of the main obstacles to clear remains the lack of industry standards and long term service experience.

A.4.2 - Aerospace Applications

The main purpose in introducing composites as structural materials was the improvement of aircraft performance and fuel economy. As a result, most of the developments of these materials have occurred in the aerospace industry. The defence industry has pioneered its use for military aircraft and other related defence and space systems. The civil aviation industry has been more conservative in its approach to composites, leaving the major developments costs to the defence sector. However with defence budgets being cut regularly, this might change.

Military Aircraft

Composite technology has been pioneered by the US defence industry which foresaw the added benefits that could be gained from lighter yet stronger materials. The initial intensive development work focused on boron epoxy (B-Ep) composites. The first production part made was a B-Ep skin on the horizontal stabiliser box for the US Navy F-14 aircraft.

Since then the proportion of composites used on military aircraft has grown steadily. This is best illustrated by recent American fighter aircraft. McDonnell Douglas F-15 has B-Ep composites on its fin, rudder, stabilator and a carbon fibre reinforced epoxy (C-Ep) speed brake. Composites represented 1% of the aircraft structural weight. General Dynamics F-16 increased that figure to 2% (using mainly C-Ep composites). This included the vertical fin box, the fin leading edge, the rudder and the horizontal tail skins of the empennage. As confidence grew in composites, the next fighter, McDonnell Douglas F/A-18, made an even bigger use of this technology with 50% of the surface and about 10% of the structural weight in composites. The F/A-18 has C-Ep wing skins, horizontal and vertical tail boxes, wing and tail control surfaces, speed brake, leading edge extension and various doors. The highest point for currently operational aircraft was reached on the McDonnell Douglas/British Aerospace AV-8B/Harrier II. This vertical and short take-off and landing (VSTOL) aircraft has 26% of its structural weight made from composites. Innovations included the use of C-Ep composites for the wing substructure which was the traditional domain of aluminium.

Planned future military aircraft (F22, EF2000 and Rafale) are reported to have pushed the percentage of composites to 50%. Figures up to 80% are quoted as possible for next generation fighter aircraft with the possibility of a virtually all composite aircraft not excluded.

Rotary wing aircraft have also benefited from composite materials. The first example on helicopters was the B-Ep reinforcement of a CH-54B tail-cone stringers. Since then, a lot of progress have been made.

Composites have been used in particular for helicopter blades quite early. They give manufacturers absolute control of the final blade characteristics thanks to property tailoring. The excellent fatigue resistance of composites provides almost unlimited service life. Today composite blades are the norm for helicopters. They're usually made from GFRP but CFRP are being used more and more. Composites have spread very quickly from secondary to primary structures. Currently serving helicopters such as Sikorsky UH-60A Black Hawk utilise an extensive amount of composites for all structures. As for future trends, the US Army Advanced Composite Airframe Program (ACAP) has already demonstrated the viability of an all-composite airframe concept. Sikorsky S-75, developed under ACAP, has about 80% of its airframe weight made from composite (with 30% C-Ep, 15% Kv-Ep and 4% Gl-Ep). The next generation of helicopters to enter active service in the near future (Westland/Agusta EH101, Eurocopter Tiger) have even more composite structures. Boeing/Bell V-22 Osprey, a tilt-rotor aircraft combining some advantages of fixed wing aircraft to rotary wing aircraft, is made virtually from composites only. This concept which is far from new would not have been possible without composites.

Experimental military aircraft rely extensively on composites to achieve their desired performance goals. Grumman X-29 advanced technology demonstrator is famous for its forward swept wing made from C-Ep composites. Aeroelastic tailoring was used to make this concept viable. This was only possible because laminate geometry and properties could be selected so that the wing remained dynamically stable under twisting loads generated by aerodynamic forces. Sikorsky S-72X1 rotor system research aircraft combines rotary wing fixtures to fixed wing ones. Its vertical take-off and landing as well as hover capabilities are provided by a four bladed composite rotor/wing. Once locked into position, the rotor/wing combines with the aircraft jets to provide forward flight speed up to 0.8 Mach.

Although the number of military programmes have been reduced due to cuts in defence budgets, composites are set to be used more frequently in military aircraft as they are currently the only materials capable of providing the ever increasing performance levels required [180].

Civil Aircraft

The use of composites in civil aircraft has been slower and generally lagging behind the military. This is due mainly to the fact that in this area, cost is the most important factor. Coupled to the generally conservative attitude, it developed into a very cautious approach to composites.

Tertiary structures, i.e. any structure whose failure does not cause a direct threat to aircraft operations but can be an inconvenience to passengers and crew [11], were the first to be made from composites. These included aircraft interiors: underseats, floor panels, airstairs, flight deck panelling, bulkheads and overhead stowage bins. The process then moved to secondary structures which on failure would not cause the loss of the aircraft but would seriously compromise its capabilities and the crew's ability to control it [11]. They include control surfaces, radome, air brakes, engine cowlings and fairings. Extensive trials such as those undertaken for NASA Flight Service Evaluation and Aircraft Energy Efficiency programmes provided the required information on composite structures reliability. The success of these programmes has been a major influence in prompting aircraft manufacturers to use composites for primary structures. These being the most important structures, the loss of any of them would result in the loss of the aircraft [11]. They include the main frame, empennage and wing boxes.

Today composites can be found on all major civil transport aircraft. The Airbus A310 was the first airliner to fly with major composite components. Aerospatiale/Aeritalia ATR72 has an all-composite wing, the first for civil aviation. This trend in increased composite usage has been followed by the latest major airliner to come into service: Boeing 777.

The 777 is a 390 seat jetliner which entered service in 1995. C-Ep composites was used for floor beams and control surfaces: elevators, rudder, flaps and spoiler. The same technology which was used on earlier Boeing planes, the 757 and 767, was extended to the empennage (i.e. vertical and horizontal stabilisers). The use of composites yielded a 20-30% reduction in weight [184]. For its size (its engines alone

have the same diameter as a 737 fuselage), it is the most efficient commercial aircraft ever built.

The long term aim of composite application on large civil aircraft is the production of a virtually all-composite aircraft. This assumes the manufacture of composite fuselage. The concept has already been proven for smaller aircraft. The Lear Fan business jet and the Beech Starship turboprop executive aircraft are well known for being exclusively in composites. A study by Johnson *et al.* [185] has shown that the effectiveness of structural weight savings was a function of their position in the aircraft. This study concluded that it was more profitable to save weight in the fuselage than in the wing. Thus there are clear benefit to be gained in building lighter aircraft fuselages. However there will be a need to address complex issues such as the severe loading of fuselage shells caused by pressurisation on top of overcoming the industry notorious conservatism. This would be done in addition to the provision for adequate damage resistance and tolerance to external unexpected loads such as foreign object impacts from runways. Van Tooren *et al.* [186] have tentatively tried to address these issues and have proposed a combination of composites and sandwich structures with incorporated damage stoppers as a possible solution.

Composites have been used in other aerospace related applications. High temperature PMC have been used for aircraft engine parts: interface fairing, nose cones, external nozzle flaps, first stage vane cluster, nacelle and blades. Most of these were made from carbon fibre reinforced polyimides (notably PMR-15) [187].

Space applications include C-Ep struss structures for the Application Technology Satellite launched in 1974, space platforms, pressure vessels and tanks for liquid propulsion systems and the US space shuttle booster cases and cargo bay doors. Missile system applications include solid propellant rocket motor cases (Polaris, Trident I and Minuteman missiles) and liquid propellant rocket tanks. The latter is a growing application field. Composite manufacturing processes such as filament winding are well suited for these applications [188].

A.5 - The Potential Of Composites

The introduction of composite materials has been driven essentially by the need to produce lighter components while improving aircraft performance. Nowhere has that need been stronger than in the military aircraft area. Thus composites high specific strength and modulus have been the main attractive feature compared to other materials. And the aerospace defence industry has born most of the development costs for these new materials.

The first step in assessing the potential of composites is to compare them with the materials they were meant to replace: metals. The second step will be to look at the advances and developments in composite materials in the last decade as the first and second generations of composite structures are being replaced by newer composites. This will give an indication of the way ahead for composite usage in industry.

Although, the example of the aerospace industry will be used, what will be mentioned will be more or less true for other industries using composites.

A.5.1 - Composites vs. metals

On the basis of strength and stiffness alone, as illustrated in Table 32, polymer matrix composite do not have a significant advantage over metals. Furthermore, their elongation to fracture is much smaller. However, PMC have very low density compared to conventional engineering materials which means that their specific properties (i.e. properties per unit mass) are much higher. This feature is translated for certain components directly into weight savings. Weight is an important factor for any moving component. Lighter components can be moved with less energy which results in cost savings.

Table 32 Comparison of room temperature properties of metals and polymer matrix composites[116]

	Density (Mg/m^3)	Young's modulus (GPa)	Tensile strength (MPa)	Ductility (%)	Specific modulus [(GPa)/(Mg/m^3)]	Specific strength [(MPa)/(Mg/m^3)]
METALS						
Aluminium	2.70	69	77	47	26	29
Al Alloy (3%Zn-0.7%Zr)	2.83	72	325	18	25	115
Steel mild	7.86	210	460	35	27	59
PMC						
Nylon66 +40%carbon fib.	1.34	22	246	1.7	16	184
Epoxide + 70%glass fib.	1.90	42	750		22	395
Epoxy + 60%Aramid	1.40	77	1800		55	1286

However a single performance indicator such as specific modulus or specific strength is not sufficient to assess different materials for a whole range of service conditions. For example, to find the best material for a rod in tension, one needs to look at the quantity E/ρ whereas for a rod under compression the governing parameter is $E^{1/2}/\rho$. For a panel subjected to bending loads, the lightest panel with minimum deflection for a given load will be made from a material with the greatest value of $E^{1/3}/\rho$. Thus for a given application, a range of performance indicators needs to be investigated. This is done best by using materials property charts [189] (Figure 151). One property is plotted against another and this allows several performance indicators to be represented on the same chart. For a given indicator, the performance of materials above the line is better and that of materials below it worse. Materials on the line will perform equally well. It can be seen from Figure 151 that PMC are the best materials if all three conditions were to be met. For bending and buckling dominated applications and other ($E^{1/2}/\rho$ and $E^{1/3}/\rho$ service limited situations, composites are far better that alloys but for (E/ρ) limited applications, only some composites are better than alloys.

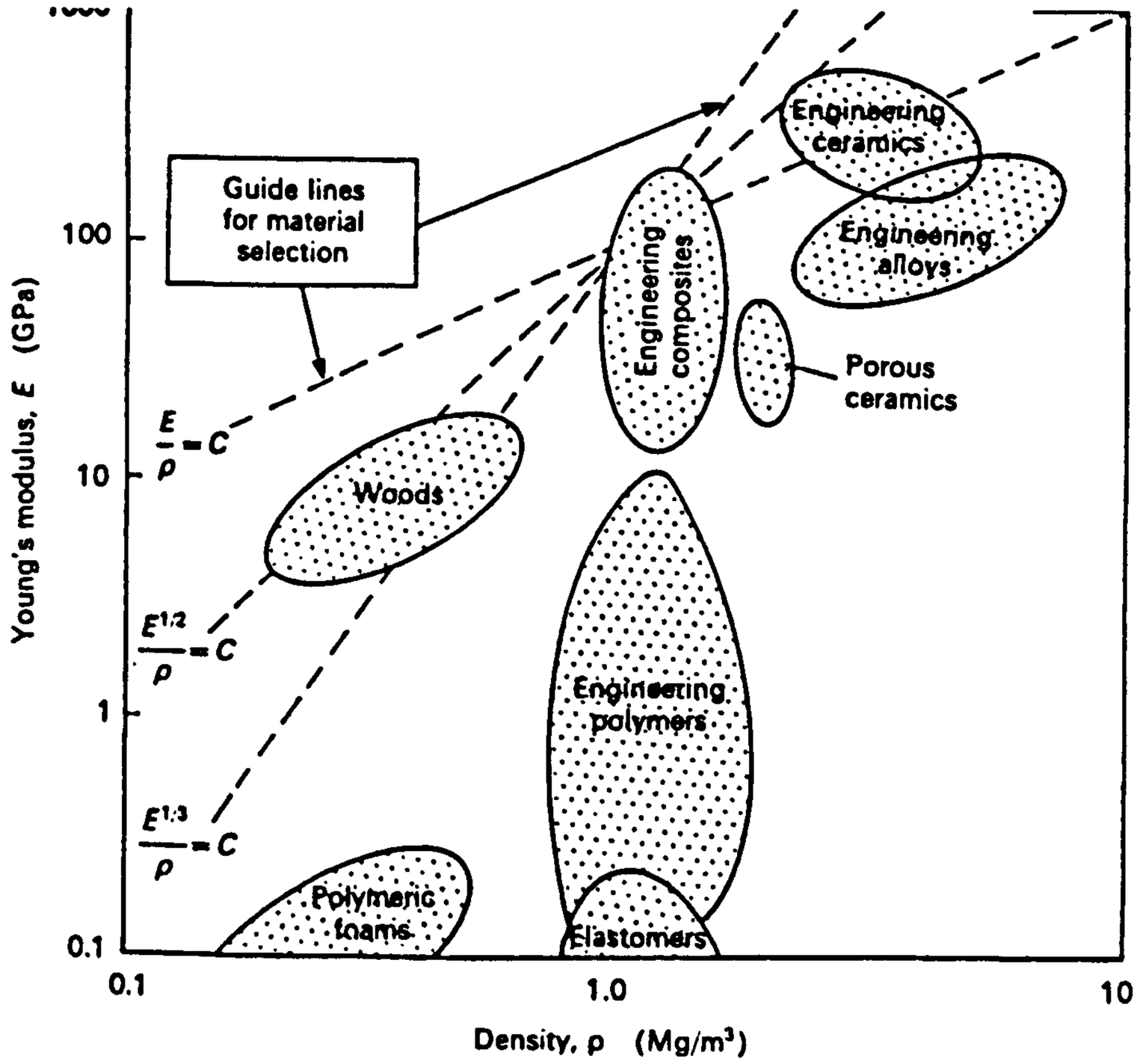

Figure 151 Materials property chart - Young's modulus against density [189]

The area of most value to the designer is the composite versatility as design material. Complex design requirement and performance targets can be met because composite properties can be tailored to suit particular needs. Their very nature lends itself to such a process. For example the stiffness of a composite can be modified by adjusting the volume fraction of fibres used as reinforcement.

Basic composite material mechanics using the rule of mixture gives the longitudinal modulus E_l of a unidirectional laminate as:

$$E_l = E_{fl}v_f + E_m v_m$$
$$= E_{fl}v_f + E_m(1 - v_f)$$

where E_{fl}= fibre longitudinal modulus

v_f = fibre volume fraction

E_m=matrix modulus

v_m = matrix volume fraction (approximated to 1- v_f if voids account for less than 1% of the laminate volume)

The variation of the longitudinal modulus with the fibre volume fraction is shown in Figure 152. This illustrates how the fibre volume fraction can be modified to change the laminate modulus. Although used for stiffness, the law can be applied to wider range of properties using the general form ($X_c = X_m v_m + X_f v_f$)

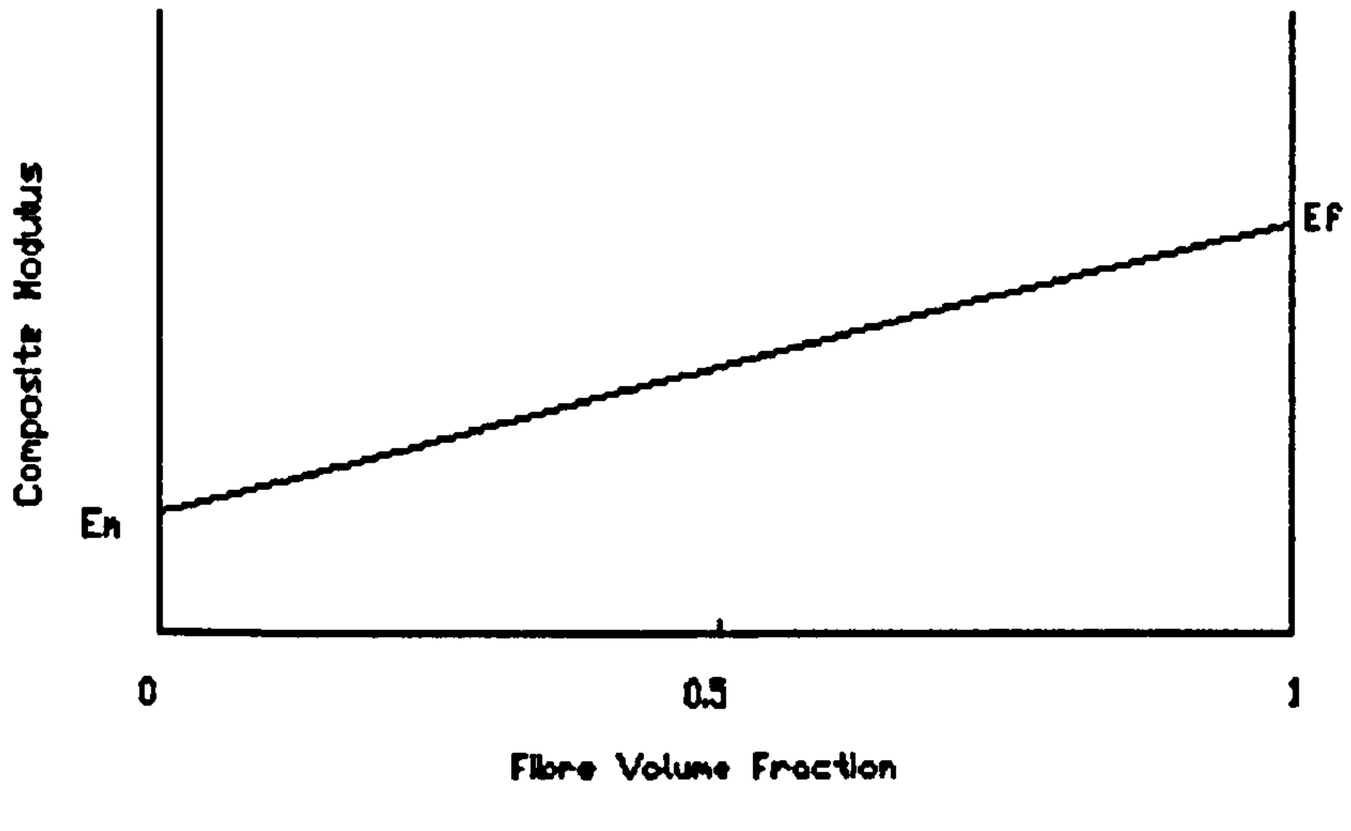

Figure 152 Variation of composite modulus with volume fraction

A.5.2 - Advances and Developments in Composites

The potential of composites can be assessed further by considering the advances that have occurred recently. At the onset of the 1980s, composites had a very promising future [1]. The advances made can be grouped in two main parts. The first one is concerned with improvements in composites intrisinc characteristics. This can be done either through the improvement of existing materials or the introduction of novel fibre or matrix materials. The second part is concerned with actual progress in composite manufacturing technology which has several processes with scope for greater automation. This has a direct impact on costs making composites more attractive to industries or areas where they are not traditionally used. This area will not be mentioned further as it falls outside the scope of this review. Emphasis will be on the advances in composite performance.

Advanced fibre manufacturers have constantly strived to improve their product characteristics to deal mainly with the aircraft industry needs. These needs were substantially for fibres with higher strain to failure because these would help increase design strength allowables and give better damage tolerance to aircraft structures.

Table 33 Carbon fibre properties

Generation	Fibre	Young's Modulus (GPa)	Tensile Strength (GPa)
1st (1970s) [1]	Toray T300	235	3.5
	Courtaulds XAS	235	3.1
2nd (1985-1988) [1]	Courtaulds Appolo HS	245	5.0
	Toray T800	294	5.6
	Hercules IM7	303	5.5
3rd (1988-) [190]	Torayca T1000	294	7.1
	Thornel P120S	827	2.2

This trend is best illustrated by development in carbon fibres as shown *in Table 33*. The improvements in tensile strength have been possible because it was shown by Johnson [191] that, for PAN-based carbon fibres, there is a direct link between fibre critical flaw size and fibre strength. These flaws are due to inclusions in the precursor or to surface contamination during manufacture. Continuing efforts have been made to decrease these flaws and stringent control of the fibre basic structure introduced. Better control of the appropriate characteristics have made possible the creation of high modulus (HM), high strength (HS) or intermediate modulus (IM) carbon fibres. The last type is an optimum combination of both strength and modulus [192].

Pitch based carbon fibres tend to give the highest modulus. Thornel P120 (Amoco Performance Products) is known to have a modulus of 827 GPa [190]. Figures up to 894 GPa have been quoted for pitch based fibres [191]. The highest reported strength are for PAN-based fibres. Torayca T1000 fibres have a tensile strength of 7 GPa (compared to a maximum of 4 GPa for pitch based fibres) [190].

Manufacturers have responded to aramid fibres moisture absorption problems with the creation of new fibres such as Kevlar 149 and Twaron HM fibres. These have lower inherent moisture absorbency properties and higher modulus. The development of new organic fibres such as the highly aligned polyethylene fibres Spectra and Dyneema has provided added incentive for existing fibres to be improved [167].

The same trend of improvement has been followed for matrix materials. The perceived competition from thermoplastics has spurred the development of toughened epoxies to deal with their well known limitation in damage tolerance. The recognition that epoxies cannot be used above a certain temperature limit without a serious degradation in their properties has prompted manufacturers to develop and improve current intermediate to high temperature thermosetting resin systems. As such, bismaleimide and polyimide resins have received very close attention to deal with their brittleness and high temperature curing requirements [168].

Overall, composites have a promising future as structural materials. As more emphasis is put on shifting away from a composite versus metal mentality, attention is drawn towards developing and improving composite intrinsic qualities to make them better materials. This would ensure that they are the best possible choice as replacement for current composite structures.

Composite materials are set to be used in an increasing number of applications because of their versatility. However the pace of progress will be governed by a better understanding of the behaviour of these materials so that they can gain more acceptance.

APPENDIX B

The Finite Element Method

Basics and Application to Composite Structures

B.0 - Introduction

The finite element method (FEM) is a general numerical method developed to solve boundary values and initial value problems including solid and structural mechanics problems with complicated geometry.

The term 'finite element' was introduced for the first time by Clough in article published in 1960 [63]. The idea of dividing a continuum into finite regions to help solve practical problems had been around in the early 1940s. The advent of digital computation in the mid-1950s allowed this technique to be implemented at a practical level, in the field of solid and structural analysis. The spectacular growth of this technique from the 1960s onwards was spurred, in parallel to the development of computers, by the realisation that the procedure could be applied to fields other than solids and structures. Another important factor in the development of the FEM was the realisation that well known weighted residual techniques such as the Galerkin method could be used as a basis for the use of the FEM in any problems which could be described mathematically by a set of partial differential equations.

Today the breadth of finite element applications is very wide indeed. Coverage of all aspects of this method is beyond the scope of this section which seeks to introduce it in relation to composite structures. Thus coverage here will , in the introductory part, be limited essentially to solid and structural analysis before shifting the emphasis on to the use of FEM to analyse composite laminates, as an illustration to its use on composite structures.

Most of the information in this section will be drawn from the excellent introduction textbook to the FEM by Astley [63] and the book by Ochoa and Reddy [64] on using the FEM to analyse composite laminates. There are several other books covering more extensively the FEM and its application to fields other than solids and structures. Among them is the definitive work by Zienkiewicz and Taylor [65, 66] in two volumes where an excellent broader treatment of the method can be found. Other books such as that by Smith and Griffiths [67] deal specifically with the computational problems in implementing the FEM.

The FEM principles will be introduced in their application to linear elastic solids and structures where they can be easily understood. The same principles form the basis of the application of the FEM in areas where their applications may be less obvious.

B.1 - Linear Elasticity Theory: Basic Principles

The main assumption behind any engineering calculations attempting to determine the stresses and deformations of a solid body is that within any volume of interest, there is a sufficiently large number of constitutive particles for the material behaviour to be independent of its fine structure. This is called the continuum assumption.

The behaviour of such a deformable body is governed by the relationship between its force and displacement states. Three conditions must be met at all points within the body:

(i) Equilibrium
(ii) Compatibility
(iii) Constitutive equations

From the first condition, a state of mechanical equilibrium must exist within the body and at its boundary. Both internal forces (i.e. forces exerted by the body particles on each other) and external forces (i.e. forces applied by an source outside the body) effects are included. The second condition implies that any deformation must be physically permissible. Thirdly, the problem is fully defined by a set of constitutive equations which relates the internal forces to the local deformation of the body. These equations usually relate stresses to strains, which in most cases are used to characterise respectively internal forces and the local deformation.

B.2 - Energy Methods

The theory of elasticity in its basic linear form is useful to solve simple continuum problems. Another approach is possible by considering energy methods. In essence, the total energy of the system under loading will be considered and a minimisation of this total energy will be an indication that stresses and displacements are correctly distributed within that system. Thus, the conditions of equilibrium, compatibility and stress-strain relations will not be through the explicit solutions of their appropriate equations.

The main advantage in re-formulating the problem at hand in a so-called **variational** (in reference to total energy variation) form is that it lends itself much more to approximation techniques because the problem becomes an optimisation one with a set of constraints. At the heart of such an approach is a set of energy principles which can be derived and stated in various ways.

The **principle of virtual work** in its general form can be stated as follows [63]:

> *A necessary and sufficient condition for static equilibrium of a system of particles is that the work done by internal forces plus the work done by the external loads during any virtual displacement is zero*

Energy is defined as the capacity of a system to work. An energy increment will occur when work is done on the system while an energy decrement will take place when work is done by the system.

The **principle of stationary total potential** can be stated as follows [63]:

> *Of all compatible displacement states of a conservative system, those that satisfy the equations of equilibrium make the total energy stationary with respect to small variations of displacement.*

A **conservative system** is one in which no energy is dissipated. For such a system, any work done on it will be totally recovered by the system doing work. The different types of energy defined above are sometimes referred to as **functionals**, i.e. they are functions of other functions. In this particular case, these other functions are provided by the displacement state of the system.

The total energy of an elastic system is then obtained by adding the strain energy expression to one or more potential energy expressions. In general, this can be expressed as:

$$\chi(\mathbf{u}) = U(\mathbf{u}) + V(\mathbf{u})$$

i.e.

$$\chi(\mathbf{u}) = \sum_{i=1}^{n} \mathbf{P}_i \cdot \mathbf{u}_i - \int_S (\mathbf{t} \cdot \mathbf{u}) dS - \int_V (\mathbf{g} \cdot \mathbf{u}) dV$$

Equation 14

where **u**(x) is the displacement field within the body.

The energy approach is a viable alternative to the linear elasticity to study the behaviour of a deformable body. This is done by casting the continuum problem in a variational form. The expressions for the total energy functional can then be used in their own right as a statement of the full continuum problem through the principle of stationary total potential.

However, the main application of this energy formulation will be as a basis for approximate, rather than exact solutions. Apart from very simple problems, it will be impractical to apply the principle of stationary total potential as suggested. This is because by considering all the possible displacement fields which give a stationary total potential, we end up with an infinite number of possibilities.

An alternative to considering all possible displacement fields, is to limit oneself to a well defined category of displacement fields which may or may not included the exact solution. However, because the choice of such a category is ultimately arbitrary, a judicious choice can be made that would provide a good approximation to the exact solution. The stationary values of the total energy functional are then determined with respect to this **trial** displacement field.

The procedure described above is called the Raleigh-Ritz method. The total energy can be written as:

$$\chi = \hat{\chi}(a_1, a_2, \ldots, a_n)$$

Equation 15

which is an approximate expression for χ. This approximate expression is a combination of kwon functions (e.g. polynomials) and unknown coefficients a_i. The stationary values are then obtained by solving the following simultaneous equations:

$$\frac{\partial \chi}{\partial a_1} = 0, \frac{\partial \chi}{\partial a_2} = 0, \ldots, \frac{\partial \chi}{\partial a_n} = 0$$

Equation 16

It can be noted that, the number of such simultaneous equations increases dramatically with the complexity of the system (systems with large number of degree of freedom). The whole procedure may then become cumbersome and difficult to follow without making serious mistakes. Also, there is a requirement to generate the trial displacement in a systematic and logical way that would enable the approximate solutions to give a good result.

The finite element method is introduced in the next section as an application of the Raleigh-Ritz procedure.

B.3 - Displacement Finite Element Method

The finite element method is now introduced as an application of the principle of stationary total energy through a systematic approach of the Raleigh-Ritz method, It is one of the many ways in which this topic has been presented. As the method grew from trying to solve structural problems in civil engineering (2-D, 3-D frame problems), the direct stiffness approached has often been used because it is the most straightforward. However, this may obscure the fact that the method is a general one which can be applied to systems which do not readily exhibit stiffness attributes. An other approach, which has been favoured by mathematicians, is the Galerkin or **weighted residual method**. This method has a broader application and deals comfortably with application fields not traditionally associated with finite elements. However, this method relates directly to the physical problem.

The approach used here has been chosen because it was felt to be easier to introduce many of the concepts behind the finite element method as an essentially approximate method to solve continuum problems. The aim being pursued is simply to present the method, its advantages and limitations as an engineering tool. Readers interested in other approaches will find in Chap. 9 of Zienkiewicz and Taylor [65] a superb presentation of both variational and weighted residual method formulations with a proof establishing the equivalence of the two methods. The question as to which methods is best is clearly beyond the scope of such an introduction to finite elements.

The main feature of the finite element method as application of the Raleigh-Ritz method is that the trial functions required are generated automatically when the continuum is replaced by a system of discrete elements. Within each element, interpolations functions are given which characterise it. These same interpolation

functions are then used as basis functions of the Raleigh-Ritz expansion (Equation 15). and the unknown coefficients, a_i, are replaced by the **nodes** (points where elements connect with each other) displacements, δ_i.

The finite element procedure follows a well defined number of steps, no matter how complex the problem is. These are: element definition (nodes), element interpolation (which will be such as to fulfil the displacement conditions at known element points - e.g. nodes), calculation of element energy (strain and potential) , assembly and energy minimisation (which give a set of simultaneous equations).When these sets of simultaneous linear equations are solved, the finite element solution is complete.

Solving the simultaneous equations is the most time consuming part of the finite element process. A variety of techniques exist which allow this task to be done efficiently using computers extensively. Discussions about the practical aspect of solving these equations can be found in Chapter 5 of Astley [94] where techniques such as the Gaussian elimination and Choleski factorisation and their implementation are presented. Also included in this chapter, is general consideration of the difficulties in storing the vast amount of data that can be generated from different matrices. This includes a short introduction to the effects of nodes and element numbering on the efficiency of a finite element code and present the principles behind the so-called **frontal solvers** used in many modern codes.

A variety of elements, notably 2D and 3D elements, are offered in commercial codes. The main difference between them lies in the order and constitution of the shape matrix $\mathbf{N}^e$ and the strain-displacement matrix $\mathbf{B}^e$ (both governed by the element shape functions). Furthermore, any type of engineering materials can be considered provided the strain-stress matrix $\mathbf{D}^e$ can be evaluated. Such a matrix constitution will be governed by the stress-strain relationship for the material considered. Information about different element types can be found in Chapters 6,8, 9 and 10 of Astley [63] which presents them in an accessible way for novices to the finite element field. More advanced knowledge can be gained from Chapter 7 of [65] and Chapters 1 and 2 of [66].

To be able to apply the finite element method to composites, it necessary to be able to define the strain-displacement and stress-strain matrices for any composite element. This in turn suggests that one is able to describe quantitatively these various characteristics for composites. This will be possible through a knowledge of composite materials mechanics. The topic is introduced in the next section.

B.4 - Composite Laminate Mechanics

To fully understand the mechanics of composites materials, it necessary to be familiar with anisotropic elasticity theory on which the behaviour of these materials is based. It will be evident later that isotropic elasticity theory is a particular case of anisotropic elasticity which is much broader in its application.

B.4.1 - Anisotropic elasticity theory

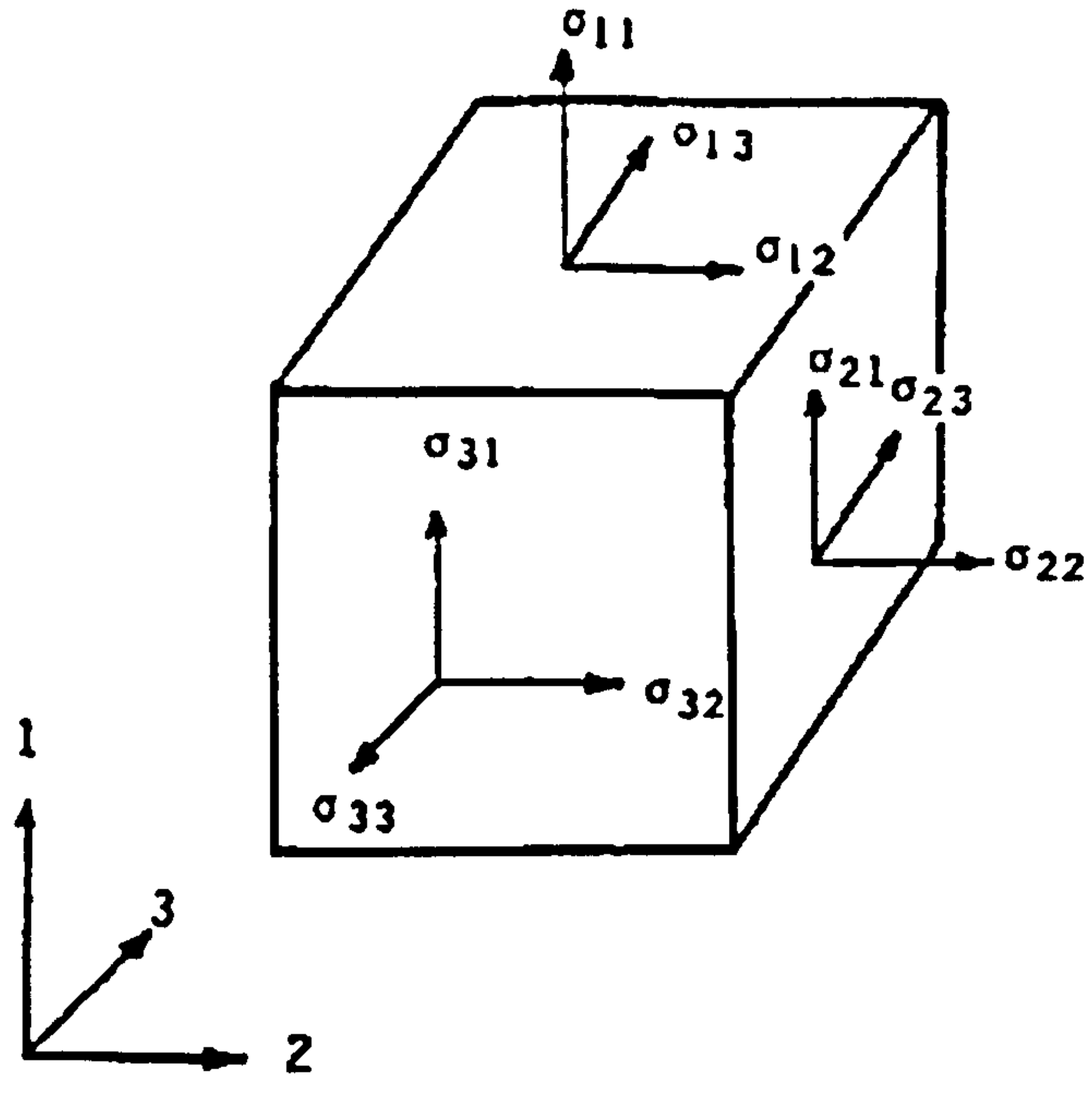

Figure 153 Cartesian co-ordinate system [64]

Consider the three-dimensional Cartesian co-ordinate system shown in Figure 153. For the remaining part of this section and for subsequent sections, it may be more convenient to adopt a single subscript notation based on the following convention:

$$\sigma_1 = \sigma_{11} \qquad \varepsilon_1 = e_1$$
$$\sigma_2 = \sigma_{22} \qquad \varepsilon_2 = e_2$$
$$\sigma_3 = \sigma_{33} \qquad \varepsilon_3 = e_3$$
$$\sigma_4 = \tau_{23} \qquad \varepsilon_4 = 2\gamma_{23}$$
$$\sigma_5 = \tau_{13} \qquad \varepsilon_5 = 2\gamma_{13}$$
$$\sigma_6 = \tau_{12} \qquad \varepsilon_6 = 2\gamma_{12}$$

Equation 17

The constitutive relation established for isotropic materials, which links stress to strain, can be shown to exist for any material and is expressed more generally as:

$$\sigma_k = C_{kj}\varepsilon_j \qquad (k = 1,2,\ldots,6)$$

Equation 18

C_{kj} are entries in the *k*-th row and *j*-th column of a 6 x 6 square matrix called the **elastic coefficients matrix**. The equation given above is an abbreviated form of the generalised Hooke's law.

The elastic coefficient matrix is symmetrical. Only 21 constants are required to characterise completely an anisotropic material. Thus we have:

$$\begin{Bmatrix}\sigma_1\\ \sigma_2\\ \sigma_3\\ \sigma_4\\ \sigma_5\\ \sigma_6\end{Bmatrix} = \begin{bmatrix} C_{11} & C_{12} & C_{13} & C_{14} & C_{15} & C_{16} \\ & C_{22} & C_{23} & C_{24} & C_{25} & C_{26} \\ & & C_{33} & C_{34} & C_{35} & C_{36} \\ & & & C_{44} & C_{45} & C_{46} \\ & & & & C_{55} & C_{56} \\ & sym. & & & & C_{66} \end{bmatrix} \begin{Bmatrix}\varepsilon_1\\ \varepsilon_2\\ \varepsilon_3\\ \varepsilon_4\\ \varepsilon_5\\ \varepsilon_6\end{Bmatrix}$$

Equation 19

In general, the value of the coefficients given above is dependent upon the Cartesian co-ordinate system used. However for an isotropic material, their value will be the same independently of the co-ordinate system.

Different materials will have a different elastic matrix. However a given class of material will display similar features which will be reflected in their elastic matrix structures. When anisotropic materials possess some material symmetry, their constitutive behaviour will be described by fewer than 21 independent constants.

Orthotropic materials have three planes of symmetry which are mutually perpendicular. They require only nine independent elastic coefficients. For such materials, we have the following relation:

$$\begin{Bmatrix}\sigma_1\\ \sigma_2\\ \sigma_3\\ \sigma_4\\ \sigma_5\\ \sigma_6\end{Bmatrix} = \begin{bmatrix} C_{11} & C_{12} & C_{13} & 0 & 0 & 0 \\ & C_{22} & C_{23} & 0 & 0 & 0 \\ & & C_{33} & 0 & 0 & 0 \\ & & & C_{44} & C_{45} & 0 \\ & & & & C_{55} & 0 \\ & sym. & & & & C_{66} \end{bmatrix} \begin{Bmatrix}\varepsilon_1\\ \varepsilon_2\\ \varepsilon_3\\ \varepsilon_4\\ \varepsilon_5\\ \varepsilon_6\end{Bmatrix}$$

Equation 20

Along the material co-ordinates, during loading, there is no coupling between elongation and shear deformations. The elastic coefficients, sometimes called **stiffness** coefficients, are related to the material engineering constants. **Isotropic** materials have no preferred direction, thus they posses an infinite number of planes of symmetry. They are completely defined by two elastic coefficients

Composite materials are anisotropic because their properties are different depending on the direction considered. However a good approximation is obtained if all the fibres are considered parallel to each other within a lamina. This assumption allows these materials to be considered as orthotropic and homogeneous and forms the basis of the constitutive equations for a lamina. These are given next.

B.4.2 - Lamina Constitutive Equations

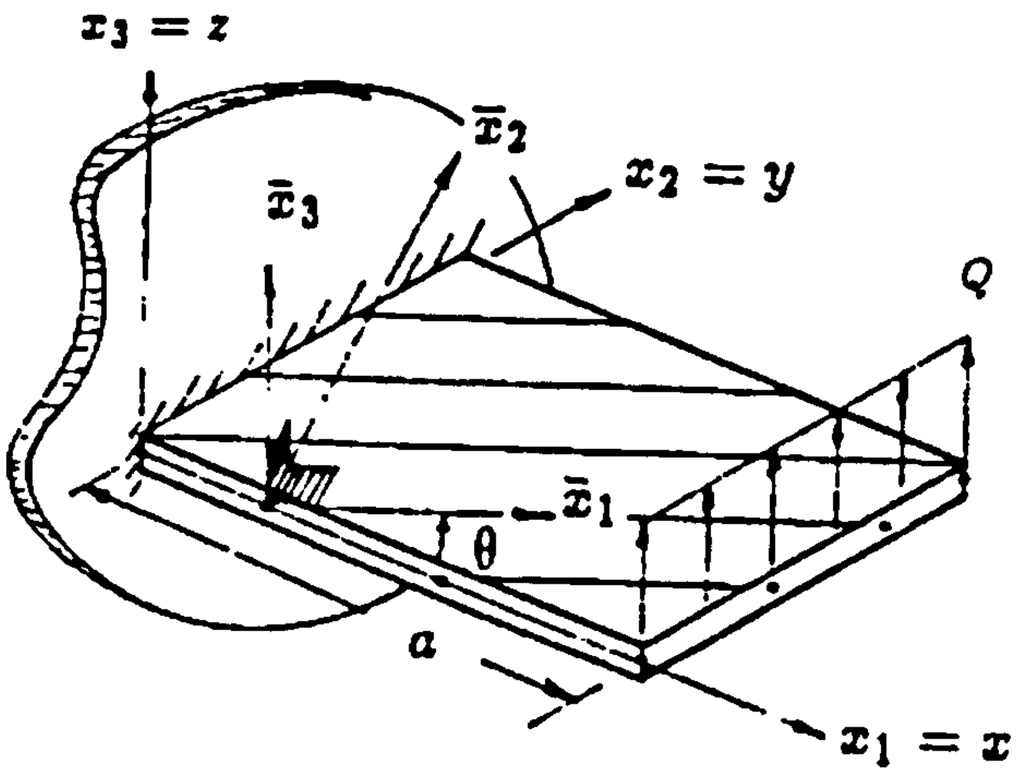

Figure 154 Composite orthotropic laminate [64]

Consider the lamina shown in Figure 154. For such a laminate, the in-plane stresses are related to the strains by the following relation:

$$\begin{Bmatrix} \bar{\sigma}_1 \\ \bar{\sigma}_2 \\ \bar{\sigma}_3 \end{Bmatrix} = \begin{bmatrix} \bar{Q}_{11} & \bar{Q}_{12} & 0 \\ \bar{Q}_{12} & \bar{Q}_{22} & 0 \\ 0 & 0 & \bar{Q}_{66} \end{bmatrix} \begin{Bmatrix} \bar{\varepsilon}_1 \\ \bar{\varepsilon}_2 \\ \bar{\varepsilon}_3 \end{Bmatrix}$$

Equation 21

These are given in relation to the material co-ordinate system $(\bar{x}_1, \bar{x}_2, \bar{x}_3)$ shown in Figure 154 and which is different from the structure co-ordinate system (x_1, x_2, x_3).

A transformation matrix is used to obtain the stresses in the global co-ordinate system when the material directions are not aligned with the global co-ordinate system. The angle θ is called the **lamination angle** and is measured anti-clockwise between the material first direction and the global x-axis.

Although its constitutive equations are useful in gaining an insight into composites behaviour, a lamina is not very useful on its own for any structural purpose. Composites structures are often made from a series of laminae bonded together, forming a laminate. The laminates that are used often have their thickness which is much smaller than the other two dimensions. Thus two-dimensional theories can be used successfully to describe their behaviour. The classical laminated plate theory (CLPT) is such a theory and is presented in the next section.

B.4.3 - Classical Laminated Plate Theory

The classical laminated plate theory is an extension of the classical plate theory to encompass the laminated nature of composite structures. As such, both theories share the same assumptions. Namely that straight lines perpendicular to the mid-plane before deformation remain, after it:
(1) straight

(2) inextensible
(3) normal to the mid-surface.
Thus this theory does not account for transverse deformation and stress state. In effect, the plates are considered to be infinitely rigid in the transverse direction which is not true in reality because composite plates tend to be weaker in this direction. However, these assumptions yield satisfactory results for thin plates (plates which have their thickness smaller than the other dimensions by two orders of magnitude).

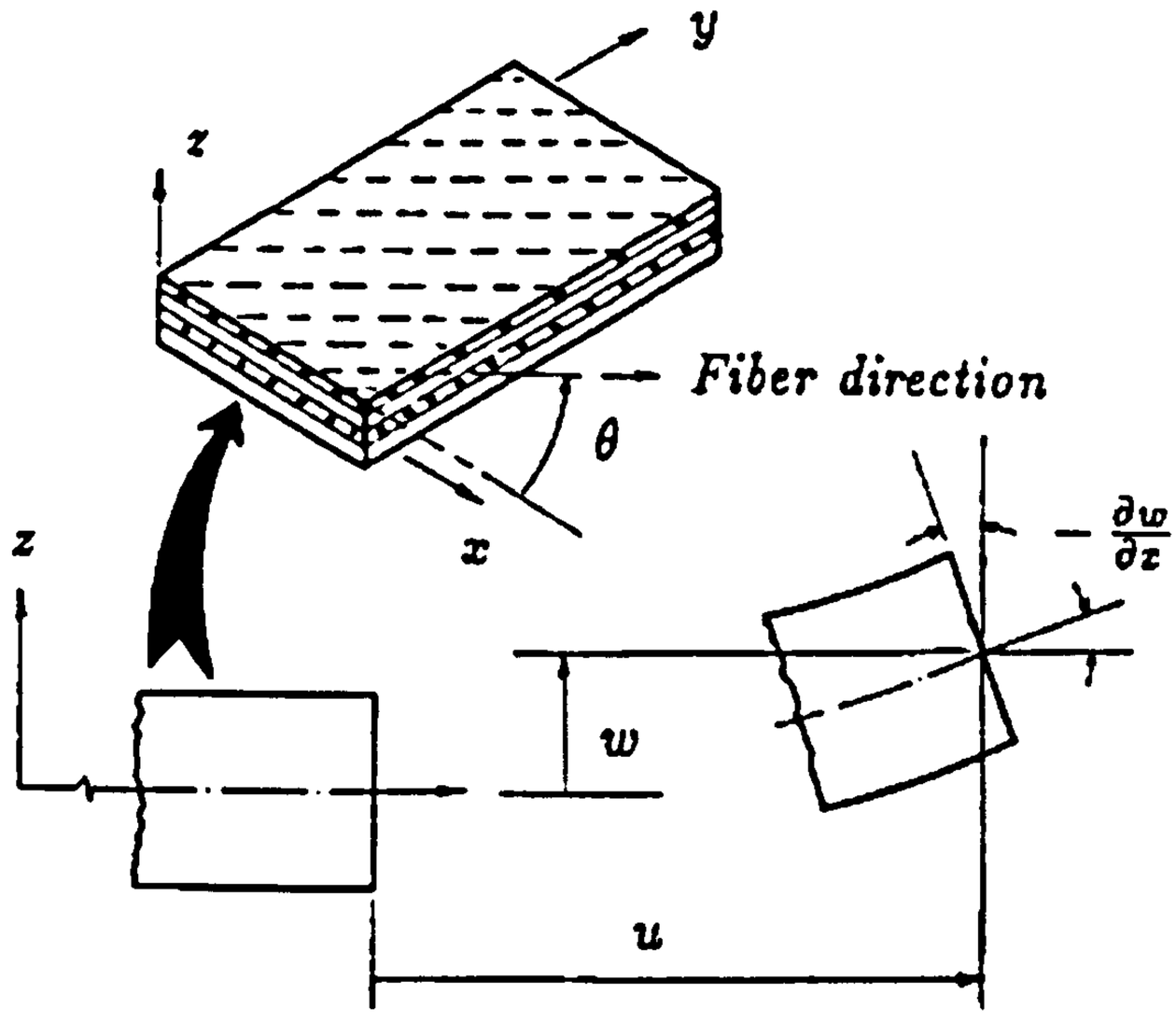

Figure 155 Thin composite laminate in bending [64]

The laminate shown in Figure 155 has *N* orthotropic layers and is of total thickness, *h*. Each layer fibres lay at angle θ_1 to the laminate co-ordinate, *x*. The layers are perfectly bonded together. The material in each one is considered linearly elastic as well as orthotropic. Each layer is of uniform thickness. The strains are assumed small and implicitly that they are continuous through the thickness of the plate.

Now the displacement field, (u_1, u_2, u_3) at any point is such that:

$$u_1(x,y,z,t) = u(x,y,t) + z\phi_1(x,y,t)$$
$$u_2(x,y,z,t) = v(x,y,t) + z\phi_1(x,y,t)$$
$$u_3(x,y,z,t) = w(x,y,t)$$

Equation 22

where (u, v, w) are the displacements of a point on the mid-plane of the laminate and ϕ_1 and ϕ_2, transverse normal rotations about the *y*-axis and *x*-axis respectively. The transverse normal rotations are given by:

$$\phi_1 = -\frac{\partial w}{\partial x}, \phi_2 = -\frac{\partial w}{\partial y}$$

Equation 23

The strain-displacement relations are:

$$\varepsilon_{ij} = \frac{1}{2}\left(\frac{\partial u_i}{\partial x_j} + \frac{\partial u_j}{\partial x_i} + \frac{\partial u_m}{\partial x_j}\frac{\partial u_m}{\partial x_i}\right) \qquad (i,j = 1,2,3)$$

Equation 24

where $(x_1, x_2, x_3) = (x, y, z)$ and a summation is implied for the repeated subscript *m*. Thus, strains are non-linear functions of the displacement gradients. If small strains are considered and only moderate rotations (up to 15°) are considered, the strains can be written simply as:

$$\varepsilon_{xx} = \frac{\partial u_1}{\partial x} + \frac{1}{2}\left(\frac{\partial u_3}{\partial x}\right)^2$$

$$\varepsilon_{yy} = \frac{\partial u_2}{\partial y} + \frac{1}{2}\left(\frac{\partial u_3}{\partial y}\right)^2$$

$$\varepsilon_{zz} = \frac{\partial u_3}{\partial z}$$

$$\varepsilon_{xy} = \frac{1}{2}\left(\frac{\partial u_1}{\partial y} + \frac{\partial u_2}{\partial x} + \frac{\partial u_3}{\partial x}\frac{\partial u_3}{\partial y}\right)$$

$$\varepsilon_{xz} = \frac{1}{2}\left(\frac{\partial u_1}{\partial z} + \frac{\partial u_3}{\partial x} + \frac{\partial u_3}{\partial z}\frac{\partial u_3}{\partial x}\right)$$

$$\varepsilon_{yz} = \frac{1}{2}\left(\frac{\partial u_2}{\partial z} + \frac{\partial u_3}{\partial y} + \frac{\partial u_3}{\partial z}\frac{\partial u_3}{\partial y}\right)$$

Equation 25

The so-called **von Karman strains**.

Using the strain-displacement relations, the strains in the laminate are given by:

$$\varepsilon_1 = \frac{\partial u}{\partial x} + \frac{1}{2}\left(\frac{\partial w}{\partial x}\right)^2 - z\frac{\partial^2 w}{\partial x^2}$$

$$\varepsilon_2 = \frac{\partial v}{\partial y} + \frac{1}{2}\left(\frac{\partial w}{\partial y}\right)^2 - z\frac{\partial^2 w}{\partial y^2}$$

$$\varepsilon_6 = \frac{\partial u}{\partial x} + \frac{\partial v}{\partial y} + \frac{\partial w}{\partial x}\frac{\partial w}{\partial y} - 2z\frac{\partial^2 w}{\partial x \partial y}$$

Equation 26

The last term on the right hand side of the above equation represents the bending contributions to strain, also called **curvatures** denoted by $\varepsilon_i^{(0)}$, whereas the others represent the in-plane shearing and stretching of the mid-plane (the so-called **membrane stains,** $\varepsilon_i^{(1)}$). Thus the strains are of the general form:

$$\varepsilon_i = \varepsilon_i^{(0)} + z\varepsilon_i^{(1)} \qquad (i = 1,2,6)$$

where:

$$\varepsilon_1^{(0)} = \frac{\partial u}{\partial x} + \underline{\frac{1}{2}\left(\frac{\partial v}{\partial x}\right)^2}, \varepsilon_1^{(1)} = -\frac{\partial^2 w}{\partial x^2}$$

$$\varepsilon_2^{(0)} = \frac{\partial v}{\partial y} + \underline{\frac{1}{2}\left(\frac{\partial w}{\partial y}\right)^2}, \varepsilon_2^{(1)} = -\frac{\partial^2 w}{\partial y^2}$$

$$\varepsilon_6^{(0)} = \frac{\partial u}{\partial x} + \frac{\partial v}{\partial y} + \underline{\frac{\partial w}{\partial x}\frac{\partial w}{\partial y}}, \varepsilon_6^{(1)} = -2\frac{\partial^2 w}{\partial x \partial y}$$

Equation 27

The underlined terms are called the **von Karman non-linear strains**.

Now using the principle of virtual displacements, the following equations of motions are obtained:

$$\frac{\partial N_1}{\partial x} + \frac{\partial N_6}{\partial y} = I_0 \ddot{u} - I_1 \frac{\partial \ddot{w}}{\partial x}$$

$$\frac{\partial N_6}{\partial x} + \frac{\partial N_2}{\partial y} = I_0 \ddot{v} - I_1 \frac{\partial \ddot{w}}{\partial y}$$

$$\frac{\partial^2 M_1}{\partial x^2} + 2\frac{\partial^2 M_6}{\partial y \partial x} + \frac{\partial^2 M_2}{\partial y^2} + N(w) + q = I_0 \ddot{w} + I_2\left(\frac{\partial^2 \ddot{w}}{\partial x^2} + \frac{\partial^2 \ddot{w}}{\partial y^2}\right) + I_1\left(\frac{\partial \ddot{u}}{\partial x} + \frac{\partial \ddot{v}}{\partial y}\right)$$

Equation 28

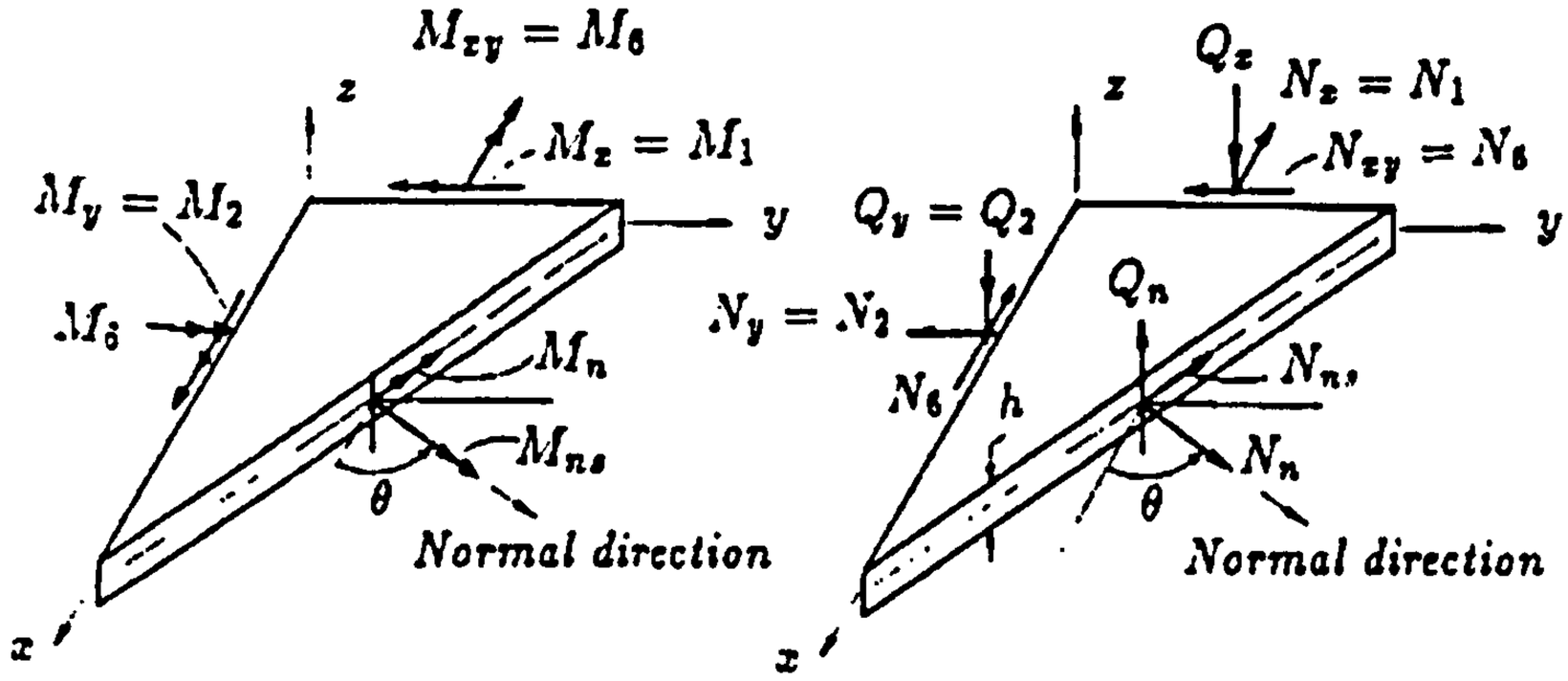

Figure 156 Laminate stress resultants [64]

where from Figure 156, q is the distributed transverse load, (N_i, M_i) are the force and moment resultants.

We also have:

$$N(w) = \frac{\partial}{\partial x}\left(N_1\frac{\partial w}{\partial x} + N_6\frac{\partial w}{\partial y}\right) + \frac{\partial}{\partial y}\left(N_6\frac{\partial w}{\partial x} + N_2\frac{\partial w}{\partial y}\right)$$

Equation 29

which is non-linear and:

$$\begin{Bmatrix} N_1 \\ N_2 \\ N_6 \end{Bmatrix} = \int_{-h/2}^{h/2} \begin{Bmatrix} \sigma_1 \\ \sigma_2 \\ \sigma_6 \end{Bmatrix} dz, \qquad \begin{Bmatrix} M_1 \\ M_2 \\ M_6 \end{Bmatrix} = \int_{-h/2}^{h/2} \begin{Bmatrix} \sigma_1 \\ \sigma_2 \\ \sigma_6 \end{Bmatrix} dz$$

Equation 30

$$\begin{Bmatrix} I_0 \\ I_1 \\ I_2 \end{Bmatrix} = \int_{-h/2}^{h/2} \begin{Bmatrix} 1 \\ z \\ z^2 \end{Bmatrix} \rho dz$$

Equation 31

For the arbitrary edge of laminate shown in the same Figure 156, the above equations are subject to geometric and force boundary conditions which are the boundary conditions of the theory:

$u_n, u_{ns}, w, \frac{\partial w}{\partial n}$ (geometric boundary conditions)

N_n, N_{ns}, Q_n, M_n (force boundary conditions)

Equation 32

The generalised Hooke 's law applied to orthotropic materials is used to express the stresses in terms of strains. These stresses are then substituted into the force and moment equations which, after integration, gives the following laminate constitutive equations:

$$\begin{Bmatrix} N_1 \\ N_2 \\ N_3 \end{Bmatrix} = \begin{bmatrix} A_{11} & A_{12} & A_{16} \\ A_{12} & A_{22} & A_{26} \\ A_{16} & A_{26} & A_{66} \end{bmatrix} \begin{Bmatrix} \varepsilon_1^{(0)} \\ \varepsilon_2^{(0)} \\ \varepsilon_6^{(0)} \end{Bmatrix} + \begin{bmatrix} B_{11} & B_{12} & B_{16} \\ B_{12} & B_{22} & B_{26} \\ B_{16} & B_{26} & B_{66} \end{bmatrix} \begin{Bmatrix} \varepsilon_1^{(1)} \\ \varepsilon_2^{(1)} \\ \varepsilon_6^{(1)} \end{Bmatrix}$$

Equation 33

$$\begin{Bmatrix} M_1 \\ M_2 \\ M_3 \end{Bmatrix} = \begin{bmatrix} B_{11} & B_{12} & B_{16} \\ B_{12} & B_{22} & B_{26} \\ B_{16} & B_{26} & B_{66} \end{bmatrix} \begin{Bmatrix} \varepsilon_1^{(0)} \\ \varepsilon_2^{(0)} \\ \varepsilon_6^{(0)} \end{Bmatrix} + \begin{bmatrix} D_{11} & D_{12} & D_{16} \\ D_{12} & D_{22} & D_{26} \\ D_{16} & D_{26} & D_{66} \end{bmatrix} \begin{Bmatrix} \varepsilon_1^{(1)} \\ \varepsilon_2^{(1)} \\ \varepsilon_6^{(1)} \end{Bmatrix}$$

Equation 34

A_{ij}, D_{ij} and B_{ij} are called the laminate **extensional** stiffnesses, **bending** stiffnesses and **bending-extensional coupling** stiffnesses respectively. They are given by:

$$\left(A_{ij}, B_{ij}, D_{ij}\right) = \sum_{k=1}^{N} \int_{z_k}^{z_{k+1}} Q_{ij}^{(k)} \left(1, z, z^2\right) dz$$

Equation 35

where $Q_{ij}^{(k)}$ represent the k-th lamina material stiffnesses referred to the laminate co-ordinates and are constant within each layer. The k-th lamina material stiffnesses referred to the laminate co-ordinates are obtained from those referred to the material co-ordinates using the appropriate transformation equations.

The next step is to substitute the strain-displacement equations into the laminate constitutive equations. The relation which results from this operation is then used to substitute for the laminate forces and moments into the equations of motion. We obtain then a system of three partial differential equations (PDE) in three displacements (u, v, w). These PDE, being lengthy, are not included here but they can be derived easily. For orthotropic laminates, as there is no bending-extension coupling, $B_{ij} = 0$ and also $A_{16} = A_{26} = D_{16} = D_{26} = 0$. The PDE are then reduced accordingly. Further simplification occurs if the material is isotropic.

Given, the limitations of this theory, notably in accounting for shear deformations effects, several attempts have been made to improve it.

The first-order shear deformation theory (FSDT) has been developed to obtain a strain distribution through the plate thickness which was closer to the true strain state. It is commonly known as the **Mindlin plate theory**. It is based on the same displacement field as that of the classical laminated plate theory, i.e.:

$$u_1(x,y,z,t) = u(x,y,t) + z\phi_1(x,y,t)$$
$$u_2(x,y,z,t) = v(x,y,t) + z\phi_1(x,y,t)$$
$$u_3(x,y,z,t) = w(x,y,t)$$

The main difference is that one of the three assumptions of the CLPT has been removed. In the FSDT, a straight line normal to the laminate mid-plane remains straight and inextensible after deformation but not necessarily perpendicular to it. In, essence, the rotations ϕ_1 and ϕ_2 of a transverse normal are now considered independent of $\frac{\partial w}{\partial x}$ and $\frac{\partial w}{\partial y}$.

This leads to the transverse shear forces Q_i being defined as:

$$\begin{Bmatrix} Q_1 \\ Q_2 \end{Bmatrix} = \int_{-h/2}^{h/2} \begin{Bmatrix} \sigma_4 \\ \sigma_5 \end{Bmatrix} dz = \begin{bmatrix} A_{55} & A_{45} \\ A_{45} & A_{44} \end{bmatrix} \begin{Bmatrix} \varepsilon_5 \\ \varepsilon_4 \end{Bmatrix}$$

where:

$$A_{ij} = K_{ij} \int_{-h/2}^{h/2} Q_{ij}^{(k)} dz \qquad (i,j = 4,5)$$
$$= K_{ij} \sum_{k=1}^{N} Q_{ij}^{(k)} (z_{k+1} - z_k)$$

Equation 36

K_{ij} are called the shear correction coefficients. Now the equations of motion can be expressed in terms of the displacements (u, v, w, ϕ_1, ϕ_2) following a procedure similar to that outlined for the CLPT.

The FSDT is one of several theories developed in an attempt to improve on the CLPT. A review of these theories can be found in [64]. The FSDT is by far the most efficient because the increase accuracy is gained without increasing the computational costs. Higher order refined theories do give better accuracy but at the cost of substantially increasing computation efforts. However, above the third-order, they become cumbersome due to the increased number of unknowns.

Now that we are able to describe the behaviour of composite laminates mathematically, we can turn our attention to the use of the finite element method to solve the differential equations derived earlier. This is considered in the next section.

B.5 - Finite Element Analysis of Composite Laminates

In this section, a finite element model for the classical laminated plate theory is described. This will be a displacement model similar to those introduced for the classical plate theory. Displacement finite elements are based on the principle of virtual displacements: i.e. all governing equations are expressed in terms of the displacements. They are different from equilibrium models which are based on the principle of virtual forces. In mixed and hybrid models, both displacements and stresses are independently approximated. Of the three types of models, the displacement type is the most widely used in commercial codes.

The main feature in displacement FE models is the approximation of the displacement fields using appropriate interpolation functions. Thus we have for a given element:

$$u(x) \approx U_e(x) = \sum_{j=1}^{n} U_j^e \psi_j^e(x)$$

Equation 37

where the displacement u is expressed in terms of the nodal displacement U_e (which takes the value U_j^e at the j-th node) and the interpolation function $\psi(x)$. If matrix notation is used, we have:

$$\mathbf{u} = \mathbf{Y}^e \mathbf{d}^e$$

Equation 38

where $\mathbf{Y}^e$ is the element shape matrix and $\mathbf{d}^e$ the nodal displacement vector. From this point, a procedure similar to the one adopted in Section 3.2 can be followed to obtain a finite element model. This is using the principle of stationary total energy through a systematic approach of the Raleigh-Ritz method. This was used because it introduced the finite element concepts in a natural way appropriate to the introductory nature of Section 3.2 In the following parts, the model will be obtained directly from the governing equations of motion derived earlier for the CLPT.

The first step is to re-cast the governing differential equations in a **weighted-integral** form. This form allows the derivation of a set of linearly independent equations between the nodal displacements and forces. Although the weighted-integral statement is obtained directly from the equations of motions, it is possible to derive it using the principle of virtual displacements. The second step is to use an appropriate approximation of the nodal displacement, such as the one described by Equation 37, and substitute it into the integral statement obtained in the first step, the so-called **weak form** of the equations of motion. Both steps are carried out for the CLPT.

We recall the governing equations for this theory. For the static case, they are:

$$-\left(\frac{\partial N_1}{\partial x}+\frac{\partial N_6}{\partial y}\right)=0$$

$$-\left(\frac{\partial N_6}{\partial x}+\frac{\partial N_2}{\partial y}\right)=0$$

$$-\left(\frac{\partial^2 M_1}{\partial x^2}+2\frac{\partial^2 M_6}{\partial x\partial y}+\frac{\partial^2 M_2}{\partial y^2}+N(w)+q\right)=0$$

Equation 39

The weak form of the above equations of motion can be obtained by multiplying them by appropriate weight functions and integrating them over a typical element, Ω^e, whose boundary is Γ^e. As the weight functions are chosen arbitrarily, they are chosen so that they correspond to virtual variations in the displacement field (u, v, w). Thus the following weight functions are chosen: δ_u, δ_v, δ_w. Now using the first equation of motion from the above equation, multiplying it with δ_u and integrating over the element domain Ω^e gives:

$$\int_{\Omega^e}\delta u\left[-\frac{\partial N_1}{\partial x}-\frac{\partial N_6}{\partial y}\right]dxdy=0$$

Equation 40

Now using integration-by-parts we have:

$$\int_{\Omega^e}\left(\frac{\partial \delta u}{\partial x}N_1+\frac{\partial \delta u}{\partial y}N_6\right)dxdy-\int_{\Gamma^e}N_n\delta u ds=0$$

Equation 41

This is called the weak form of the first equation of motion. N_1 and N_6 are functions of the derivatives of the displacements u,v and w. To evaluate the first equation of motion as described before, for any element, N_1 and N_6 need to be differentiable twice. If the weak form is used instead then N_1 and N_6 need only be differentiable once. Thus a weaker continuity of the dependent variables, i.e. the displacements u,v, and w, is required. Hence the name **weak form** given to Equation 41. Following the same procedure, the weak form of the remaining equations can be found.

For the second part of the procedure, the displacements (u, v, w) are approximated over the element using interpolations of the form:

$$u=\sum_{j=1}^{n}u_j\psi_j(x,y)$$

$$v=\sum_{j=1}^{n}v_j\psi_j(x,y)$$

$$w=\sum_{j=1}^{m}u_j\phi_j(x,y)$$

Equation 42

where (u_j, v_j) are the nodal values of (u, v) and Δ_j those of w and its derivatives.

The interpolated displacement field is then substituted into the weak form of the equations of motions and using $\delta u = \psi_i, \delta v = \psi_i, \delta w = \phi_i$ we obtain the following finite element model:

$$\int_{\Omega^e}\left(\frac{\partial \psi_i}{\partial x}N_1 + \frac{\partial \psi_i}{\partial y}N_6\right)dxdy - \int_{\Gamma^e} N_n \partial\psi_i ds = 0$$

$$\int_{\Omega^e}\left(\frac{\partial \psi_i}{\partial x}N_6 + \frac{\partial \psi_i}{\partial y}N_2\right)dxdy - \int_{\Gamma^e} N_{ns} \partial\psi_i ds = 0$$

$$-\int_{\Omega^e}\left(\frac{\partial^2 \phi_i}{\partial x^2}M_1 + 2\frac{\partial^2 \phi_i}{\partial x \partial y}M_6 + \frac{\partial^2 \phi_i}{\partial y^2}M_2 + \phi_i q\right)dxdy - \int_{\Gamma^e}\left(\phi_i V_n + \frac{\partial \phi_i}{\partial t}M_n\right)ds$$

Equation 43

which can be expressed in matrix form as :

$$[K^e]\{\Delta^e\} - \{F^e\} = 0$$

Equation 44

This equation is then assembled for each element using the fact that the nodal displacements are continuous at the element interfaces and that nodal forces are in balance. Once this assembly process is carried out for the whole laminated structure, it is possible to write for the whole structure domain :

$$[K]\{\Delta\} - \{F\} = 0$$

Equation 45

We have a set of simultaneous equations to be solved for nodal displacements of the total mesh subject to displacement and force boundary conditions.

Once the nodal displacements are calculated at any arbitrary mid-plane we obtain the total displacement at any point (x, y, z). From the displacement field, strains are calculated and from strains, stresses are found.

The procedure described above can easily be applied for first order shear theory to obtain a corresponding finite element model for that laminated plate theory

B.6 - Conclusions

While there is only one finite element method, for a given problem there can be several finite element models all differing because of the assumptions implied from the choice of elements and the accuracy of results required. The actual computational aspects of implementing such models has not been covered as it is outside the scope of this review. Only a feel for the potential of the finite element method in dealing with complex materials and complex structures has been given. More information on can be found in chapter 3 of Ochoa and Reddy [64] on various aspects of computer implementations of these models alongside other more refined ones.

APPENDIX C

FE Software Selection

C.0 - Introduction

This appendix details the selection of a finite element analysis package to model the repair of aircraft composite structures. This selection process deals with four packages: ANSYS, COMPOSIC, LUSAS and NISA. The search for a suitable package was narrowed to these four packages after a software demonstration session at Imperial College on 22 June 1995. The only criterion used at this session was simply based on the first impressions.

It must be emphasised that ultimately the choice of a finite element package is closely link to the type of analysis and the type of work envisaged. At this stage of the work, the final research topic has not been completely defined. However there is a need to select a package in order to proceed with the necessary familiarisation with the new tool before the actual analysis work begins.

The software demonstration session was part of a wider course looking at the computer aided analysis and modelling of composites. As such, a greater understanding of the rationale behind the finite element method was gained, giving much more confidence to proceed with the selection of a package even though the research topic was not completely defined.

Bearing these limitations in mind, the selection proceeded in two phases. The first one relied on the impressions from the software session, combined with the result of a brief information gathering exercise about each of the packages, through preliminary contacts with the marketing companies. At the end of this phase, a decision was made to select only two packages for further investigation in phase two.

C.1 - Phase One

From the software demonstration session, COMPOSIC emerged as the most impressive package. It is a unique programme which was designed by FRAMASOFT+CSI to model exclusively composite structures. As such, the whole architecture of the programme has been set up with the composite designer in mind. ANSYS looked an attractive option as its latest version runs under Windows NT. NISA seemed also promising with its strong emphasis on its composite element library and other features. FEA Ltd demonstration of LUSAS was excellent.

A first look at COMPOSIC showed the programme to be a good option. The cost for running a licence was quoted at £3250 per annum. The programme has only a UNIX version. It has a wide variety of composite elements (beams, shells, 3D). Micromechanical characteristics of each ply are used to set up material databases integrated into the package. To take into account of particularities associated with local effects (free edges, loaded edges, inserts, bonding etc.), it includes a dedicated module CLEOPS (separately priced at £1250). Optimisation facilities are included in the package.

LUSAS literature revealed that the programme had only one composite element in its library. A new element capable of looking at edge effects and delamination would be available with the latest version of the programme.

ANSYS and NISA both had a decent number of composite elements. The cost of running ANSYS in its educational version would be around £450. An educational version of NISA (limited to 5000 elements) was quoted at £750.

At the end of this phase, it was decided to have a closer look at ANSYS and NISA which were the most promising packages over all. LUSAS was not selected because of its narrow composite element range. COMPOSIC was not selected mainly on cost grounds.

C.2 - Phase Two

The comparison of the two packages was done under five main headings: composite features, linear static analysis, non-linear static analysis, pre-processing and post-processing. The results of the comparison are given below. The left bullet lists give information for NISA and those on the right information for ANSYS.

C.2.1 - Composite Features

C.2.1.1 - Composite Element Library

NISA	ANSYS
• 3D Layered Composite Shell NKTP32	• 16 Layer Structural Shell SHELL91
• 3D Layered Sandwich Shell NKTP33	• 100 Layer Structural Shell SHELL99
• 3D Composite Solid NKTP7	• 3D Layered Solid SOLID46
	• User-Defined Element

3D Layered Composite Shell (NKTP=32)	16 Layer Structural Shell (SHELL91)
This a 3-D shell element which includes deformation due to membrane, bending, membrane-bending coupling and transverse shear effects. It is used for moderately thick to thin laminates with degrees of freedom per nodes. It can be shaped as a 4 to 12 node quadrilateral or as a 3 or 6 node triangle	This element may be used for layered application of a structural shell model. Up to 16 different layers are permitted. It has six degree of freedom per node, with eight or six nodes per element. It has non-linear capabilities.

3D Layered Sandwich Shell (NKTP=33)
This element includes similar effects to NKTP=32 but is used to model sandwich structures with two or more thin and stiff face sheets and one or more relatively thick and flexible cores.

100-Layer Structural Shell (SHELL99)
This element may be used for layered application of a structural shell model. Up to 100 different layers are permitted. If more than 100 are required, a user-input constitutive matrix option is available. has six degree of freedom per node, with eight or six nodes per element.

3D Composite Solid (NKTP = 7)
This element is based on a general 3D state of stress and is suited for modelling thick laminated composite structures. It is an 8 or 20 node solid hexahedron element.

3D Layered Solid (SOLID46)
Up to 100 uniform or 50 tapered layers of composite laminae. It is an 8 node solid hexahedron element. No non-linear capabilities

C.2.1.2 - Analysis Features

NISA	ANSYS
• No restriction on the number of layers	• Choice of up to 16 or 100 layers
• Variable thickness and rotation angles for each layer	• Variable thickness and rotation angles for each layer
• Edge effects and delamination	• Nodal temperatures and temperature gradients
• Nodal temperatures and temperature gradients	• Temperature dependent material properties
• Temperature dependent material properties	• Interlaminar shear stresses
• Interlaminar stresses consistent with 3D equilibrium equations	

C.2.1.3 - Modelling Features

NISA	ANSYS
• Graphical representation of lamina thickness and angles	• Display of composite material layers and orientations for layered elements

C.2.1.4 - Failure Theories

NISA	ANSYS
• Maximum stress	• Maximum stress
• Modified Hill-Mises	• Maximum strain
• Tsai-Wu	• Tsai-Wu
• Delamination	• 6 User-defined failure criteria

C.2.1.5 - Output

NISA	ANSYS
• Plots of original and/or deformed geometry • Contour plots of displacement, stress components and stress resultants in any layer • Filtered stress output • Stress survey plots • Largest magnitudes of the displacement vector • Highest stress resultants in descending order of magnitudes	• Original and/or deformed geometry plot • Contour plots (displacement, stress components, stress resultants)

From the information given above, it can be seen that ANSYS and NISA offer similar composite features in general terms. However, there are significant differences which need to be emphasised.

NISA composite element library is more extensive than ANSYS. Whereas ANSYS only offers second order elements, there is a choice of first to third order elements in NISA (The higher the element order, the higher the accuracy of computed results but also the higher the computing time required - but this option can be useful in certain cases . It is widely accepted now that second order element offer the best compromise). NISA also has a dedicated sandwich element which is very useful for modelling a variety of sandwich structures. ANSYS provides the capability for user-defined element through the use of FORTRAN subroutines linked to the ANSYS object code. This provides significant flexibility and potential power to users with special requirements.

An additional capability of NISA not provided in ANSYS is the possibility of including edge effects and delamination as well as the use of the Autolayup facility for fabric-type composites. It has been widely recognised now that edge effects and delamination are very important aspects of composite analysis and probably more so where composite repair are concerned (e.g. peel stresses at the edges of the patch can cause delamination or debonding of the patch from the parent laminate)

NISA provides a modified Hill-Mises and a delamination criterion in addition to Tsai-Wu and Maximum Stress criteria as failure theories. ANSYS on the other hand has a Maximum Strain criterion in addition and allows up to six user defined failure criteria, again through FORTRAN subroutines.

C.2.2 - Linear Static Analysis

C.2.2.1 - Features

NISA	ANSYS

- Multiple load cases
- Automatic wave front optimisation
- Interlaminar shear and edge effects for composite elements
- Automatic submodeling in user-defined regions for more accurate stress calculations
- Restarts

- Multiple load cases
- Automatic wavefront optimisation
- Interlaminar shear stresses for composites
- Automatic sub-modelling capability in user-defined regions
- Reactivate and deactivate element option

C.2.2.2 - Material Properties

NISA

- Isotropic, orthotropic, temperature dependent
- Directional tensile, compressive, and shear failure stresses for composites
- Tsai-Wu coupling coefficients for composites

ANSYS

- Isotropic, orthotropic, temperature dependent
- Directional tensile, compressive, and shear failure stresses for composites
- Tsai-Wu coupling coefficients
- Matrix input form for composite elements

C.2.2.3 - Loading

NISA

- Point force, moment on nodes or range of nodes in local or global co-ordinate system
- Distributed force, pressure load
- Linear, angular acceleration
- Thermal loading
- Specified displacement

ANSYS

- Point force, moment on nodes or range of nodes in local or global co-ordinate system
- Distributed force, pressure load
- Linear, angular acceleration
- Thermal loading
- Specified displacement

C.2.2.4 - Printed and Graphical Output

NISA

- Displacements, stresses, and strains at elements and nodes
- Principal stresses and their directions
- von Mises, maximum shear, and octahedral shear stresses
- Averaged and unaveraged nodal stresses, element stresses at Gauss points and centroid
- Error plots

ANSYS

- Element and node displacements, stresses and strains
- Principal stresses
- von Mises, maximum shear
- Interlaminar shear stresses at centroid
- Evaluation on error due to mesh discretization

C.2.2.5 - Boundary Conditions

NISA	ANSYS
• Specified nodal displacements	• Specified nodal displacements
• Coupled displacements	• Coupled displacements
• Multipoint constraints	• Multipoint constraints

The linear static analysis capability of both programmes are very similar. Attractive features on both side include sub-modelling in user-defined regions as this allows a region of interest to be modelled accurately without the need for extensive remodelling work. Again, NISA differs from ANSYS in including edge effects and the possibility of printing out averaged and unaveraged nodal stresses, element stresses at Gauss points and centroids. This last capability can be very useful for in-depth look at the programme results and for assessing the likelihood of accurate representation of the model behaviour. ANSYS on the other hand offers a useful tool in providing the user with a matrix form to input element material properties as an alternative to the layer form (the matrices must be computed outside the ANSYS programme) if a greater number of layers than the maximum of 100 is required.

C.2.3 - Non-linear Static Analysis

C.2.3.1 - Material Non-linearity

NISA	ANSYS
• Material models included: von Mises, Tresca, Mohr-Coulomb, and Drucker-Prager yield criterion.	• Models: Bi- or Multilinear Kinematic hardening, Bi- or Multilinear Isotropic Hardening, Drucker-Prager
• Elastic perfectly plastic, elastoplastic with isotropic, kinematic or mixed work hardening	• Multilinear elasticity
• Uniaxial stress-strain curve description include elastic perfectly plastic, elastic linear hardening, elastic piece-wise linear hardening and Ramberg-Osgood curve.	• Anand model
• Hyperelasticity and rubber-like material behaviour (generalised Mooney-Rivlin, Blatz-Ko, Alexander models etc.)	• Anisotropic behaviour
• Creep laws (Norton, McVetty, Soderberg, Dorn, ORNL, etc. as function of tie, stress, and temperature)	• Hyperelasticity (Mooney-Rivlin)
• Anisotropic elastoplastic material model with linear or piece wise linear hardening for composite shell element.	• Blatz-Ko function
• Temperature dependent inelastic properties.	• Viscoplasticity
	• Creep
	• Swelling (user FORTRAN routine)
	• Viscoelasticity
	• User-defined material models using FORTRAN routines

C.2.3.2 - Geometric Non-linearity

NISA	ANSYS
• Large displacements, large rotations, finite strains • Total and updated Lagrangian formulation • Stress stiffening • Post buckling analysis	• Large strain • Large deflection • Stress stiffening • Spin softening • Non-linear buckling

C.2.3.3 - Loading

NISA	ANSYS
• Fixed direction force, moment and pressure • Non-conservative loading (deformation dependent follower concentrated force and follower pressure) • Body forces (weight and inertia) • Thermal loading	• Point loads • Surface loads • Body loads • Inertia

C.2.3.4 - Output

NISA	ANSYS
• Output at each load step or at every 'N' load step • Stress output in second Piola-Kirchhoff or Cauchy stress for geometric non-linearity • Nodal, Gauss point, and centroidal stresses and strains • Multiple displacement history and stress contours	• Output at each load step or at every user defined step • Nodal and Gauss point stresses and strains • Centroidal interlaminar shear stresses • Multiple displacement history and stress contours

C.2.3.5 - Solution Procedure

NISA	ANSYS
• Incremental-iterative solution procedure • Full or modified Newton-Raphson techniques • Special formulation for pure incremental analysis with no iterations • Equal, user-defined or automatic load steps	• Load is ramped from initial value up to final value • Automatic load stepping • Automatic time stepping • ARC-length method used in the solution for snap-through problems and non-linear buckling cases • Convergence enhancement features

- Line search for faster convergence
- Convergence checks with displacements, rotation, force, moment, and energy criterion
- ARC-length method to improve convergence characteristics specially for post-buckling and snap through problems
- Time integration schemes for dynamics, creep and viscous effects including Newmark, Wilson-Theta Central difference and Houbolt methods
- Restart from the last converge load step

including prediction, bisection, line search and adaptive ascent methods for faster convergence
- Incremental-iterative solution procedure
- Use of Newton-Raphson method

The two programmes provide most of the basic features required for non-linear analysis of engineering structures. They also provide facility to take into account non-linearity existing in composites, namely anisotropy for material non-linearity. The solution procedures are also similar and most of the basic convergence techniques are used. One of the main difference again is that ANSYS offers the possibility of user-defined non-linear features through FORTRAN routines. On the other hand, NISA has a wider range of non-linear features for the user to choose from.

C.2.4 - Pre Processing

NISA	ANSYS
• Automatic and mapped mesh generation for 2D and 3D geometry using shells and solids	• Automatic 2D and 3D mesh generation including free meshing, mapped meshing and adaptive meshing
• Excellent CAD interface, direct or through IGES	• Extensive CAD interface capability direct or through IGES, VDAFS or PDES/STEP
• Capabilities to model complex 3D geometry using lines, arcs, surfaces, solids, and NURBS curves and surfaces	• Bi-directional translator with MSC/NASTRAN
• Comprehensive drawing tool set	• Extensive model generation features with solid modelling or direct generation capability
• On-Line Help	• Solid modelling using top-down or bottom-up method
• Solid Modelling capabilities	• Capabilities to model 3D geometries using NURBS curves and surfaces
• Extensive macros for parametric modelling and database queries	• Co-ordinate systems include Cartesian, cylindrical, spherical, elliptical and toroidal systems
• Unique fill-in form interface and completely mouse driven	• Cross reference checking available
• Bending moment and shear force diagrams for beams	• Close link to ANSYS Parametric Design Language
• Extensive model checking capabilities, distortion index, boundary check, normal check, duplicate element check	
• Special pre-processing for composites	

• Large database of AISC, CISC and European beam sections
• On-Line Help

Both programmes make extensive use of powerful interactive graphics in the pre-processors. The features offered are comparable.

C.2.5 - Post Processing

NISA	ANSYS
• Forms based post-processing eliminates the need for guess work by displaying all logical choices • Graphic display of analysis results includes contours, deformations, animation, history data and graphs • All plots can be fully customised using controls provided • Extensive features for composite elements • Interactive query of results • Preparation of tables for reports	• Graphic displays and/or tabular report form for displacements, stresses and strains • All requested data save in a file for later use • Entire model results can be interpreted in the general post-processor (POST 1) • Selected portions can be displayed in the time-history results post-processor (POST 26) • Contours, Vector display, deformations • Element tables • Error estimation techniques

Again post-processing features of ANSYS and NISA are generally comparable. However NISA has a single pre- and post-processor, DISPLAY III whereas ANSYS has one pre-processor and two post-processors.

C.3 - Conclusions

Although the two programmes satisfy most of the basic requirements for the analysis of composite structures, the implementation of the different features is done differently on each one. From this comparison, it emerges that ANSYS has an open architecture, allowing the user to add additional features to suit his/her needs while NISA relies heavily on its greater variety of analysis tools available to satisfy each user's particular requirements. This is by far the biggest difference between the two programmes.

An other difference is that NISA FE code is independent of the platform it is used on whereas ANSYS capabilities are strongly tied to the platform, mainly as far as most of the user programmable features are concerned. This aspect has important implications.

The NISA composite elements have more capabilities than those offered by ANSYS specially with respect to interlaminar stresses, edge effects and delamination. But this is balanced by ANSYS providing the user with the possibility of defining his/her own element. This feature is available on all platforms.

NISA offers only a limited number of failure criteria, including delamination but has no room for any user-defined criteria which ANSYS does provide. This may represent an advantage for ANSYS.

Considering all the points mentioned above, it emerges that NISA might be better suited for the modelling of composite structures on a PC as most of the user-programmable features which make ANSYS an attractive proposition in a research environment are not available. If another platform is considered such as a workstation then it might be worth looking again at the problem taking into account other important aspects such as cost.

BIBLIOGRAPHY

1. ANSYS Revision 5.1 Technical Description of Capabilities Manual

2. ANSYS Revision 5.0 Elements Manual

3. NISA/DISPLAY Brochure

4. NISA/DISPLAY Element Library Manual

5. The Composite Modelling Features of NISA II / DISPLAY III, Training Course Notes

6. FRAMASOFT+CSI COMPOSIC Brochures

7. FEA LUSAS Leaflets

8. FEA LUSAS Element Library Manual

PUBLICATIONS

1. ODI, R A; FRIEND, C M; "Finite element analysis of bonded repairs in composite structures", Proceedings 4th International Conference on Deformation and Fracture of Composites, Manchester, UK, 24-27 March 1997

2. ODI, R A; FRIEND, C M; "Bonded repairs in composite structures: a finite element approach", Proceedings 11th International Conference on Composite Materials (ICCM-11), Gold Coast, Australia, 14-18 July 1997

3. ODI, R A; FRIEND, C M; "An improved 2D model for bonded composite joints", Proceedings 5th International Conference on Structural Adhesives in Engineering, Bristol, UK, 1-3 April 1998 - *in print*

4. ODI, R A; FRIEND, C M; "Bonded external patch repairs to composite structures: an improved FE approach for PC-based applications", Proceedings 8th European Conference on Composite Materials, Naples, Italy, 3-6 June 1998 - *in print*

REFERENCES

1 BASHFORD, P D; "The potential of composite materials", Composite Materials in Aircraft Structures, ed D H Middleton, Longman Group UK Ltd, 1990, pp. 9-16.

2 BAKER, A A; JONES, R; CALLINAN, R J; "Damage Tolerance of graphite/epoxy composites", Composite Structures, Vol. 4, 1985, pp. 15-44.

3 ADAMS, R D; CAWLEY, P; "A review of defect types and non-destructive testing techniques for composites and bonded joints", Seminar "Bonding and Repair of Composites", Birmingham, UK, 1989, pp. 1-15.

4 HESLEHURST, R B; "Analysis and modelling of damage and repair of composite materials in aerospace", Numerical Analysis and Modelling of Composite Materials, ed. J W Bull, Chapman and Hall, 1996, pp. 28-59.

5 DAVIES, P; "Delamination", Advanced Composites, ed. I K Partridge, Elsevier Applied Science, 1989, pp. 303-329.

6 SMITH, B A; "Airframers stress durability in composites", Aviation Week & Space Technology, 6 Feb 1995, pp. 60-61.

7 DASTIN, S; "Repairing advanced composite materials", Machine Design, February 1986, pp. 86-90.

8 DEXTER, H B; "Long term environmental effects and flight service evaluation", Applications and Experience, Composites, Engineered Materials Handbook, Volume 1, ASM International, 1987, pp. 823-831.

9 TEAGLE, P R; "Non destructive evaluation of composite aerospace components", Composite Materials in Aircraft Structures, ed. D H Middleton, Longman Group UK Limited, 1990, pp. 190-206.

10 WEGMAN, R F; TULLOS, T R; "Handbook of adhesive bonded structural repair", Noyes Publications, USA, 1992, pp. 199-215.

11 ROBSON, J E; "The repair of composite materials", PhD Thesis, 1993, Imperial College

12 MYHRE, S H; LABOR, J D; "Repair of advanced composite structures", Journal of Aircraft, Vol. 18, No. 7, 1981, pp. 546-552.

13 HESLEHURST, R B; "Field level damage analysis of composite structures by a handheld calculator", Proceedings 3rd Annual SAMPE Symposium, Australian Chapter, North Ryde, NSW, Australia, 1990.

14 HESLEHURST, R B; "Evaluation of techniques for the damage analysis of composite aircraft structures", Master's Thesis, Royal Melbourne Institute of Technology, Melbourne, 1990.

15 PIPES, R B; PAGANO, N J; "Interlaminar stresses in composite laminates under uniform extension", Journal of Composite Materials, Vol. 4, 1970, pp. 538-548.

16 O'BRIEN, T K; "Characterization of delamination onset and growth in composite laminates", ASTM STP 775, ASTM Philadelphia, PA, USA, 1982, pp. 140-167.

17 WHITNEY, J M; "Structural analysis of laminated anisotropic plate", Technomic, Lancaster, PA, 1987.

18 COOK, T N; RENIERI, M; BREAULT, G B; COX, R; "Advanced composite structures R&M design and repair guide", USAACOM Report No. TR-85-D-12, USA, 1986, pp. 5.1-5.5.

19 ANONYMOUS, "Advanced Composite Repair Guide", NOR 82-60, Northrop Corporation, Hawthorne, NV, 1982.

20 HESLEHURST, R B; "Which is best, a bolted or a bonded patch ?", Composite Structural Repairs, SAE TOPTEC Conferences Series, Seattle, WA, USA, 1-2 Nov 1993.

21 BAKER, A A; "Repair techniques for composite structures", Composite Materials in Aircraft Structures, ed. D H Middleton, Longman Group UK Ltd, 1990, pp. 207-227.

22 DONNELLAN, T M; ROSENWEIG, E L; TRABOCCO, R E; WILLIAMS, J G; "Repair of composites", Composite Structure Repair, AGARD-R-716-Addendum, AGARD, NATO, Neuilly-sur-seine FRANCE, 1984, pp. 1.1-1.10.

23 MYHRE, S H; BECK, C E; "Repair concepts for advanced composite structures", Journal of Aircraft, Vol. 16, No. 10, 1979, pp. 720-728.

REFERENCES

24 ROBSON, J E; MATTHEWS, F L; KINLOCH, A J; "The strength of composite repair patches: a laminate analysis approach", Journal of Reinforced Plastics and Composites, Vol. 11, July 1992, pp. 729-742.

25 MATTHEWS, F L; "Load-carrying joints", Composite Materials in Aircraft Structures, ed. D H Middleton, Longman Group UK Ltd, 1990, pp. 142-155.

26 HART-SMITH, L J; "The design of repairable advanced composite structures", SAE Paper 851830, Aerospace Technology Conference and Exposition, Long Beach, California, USA, 14-17 Oct 1985, 15 pp.

27 BORDER, J; "The heat's on for quick composite repair", Machine Design, 7 Mar 1991, pp. 71-74.

28 VARADAN, V K; VARADAN, V V; "Microwave joining and repair of composite materials", Polymer Engineering and Science, Vol. 31, Apr 1991, pp 470-486

29 MYHRE, S H et al.; "Advanced composite repair guide", AFWAL-TR-83-3092, Air Force Wright Aeronautical Lab, USA, 1982.

30 MYHRE, S H; " Advanced composite repair – recent developments and some problems", Composite Repair SAMPE Monograph I, ed. H. Brown, SAMPE, Covina, CA, USA, pp. 14-25.

31 KNAUSS, J F; STONE, R H; "Demonstration of repairability and repair quality on graphite/epoxy structural subelements", Composite Repair SAMPE Monograph I, ed. H. Brown, SAMPE, Covina, CA, USA, pp. 40-51.

32 STONE, R H; "Development of repair procedures for graphite/epoxy structures on commercial transports", Composite Repair SAMPE Monograph I, ed. H. Brown, SAMPE, Covina , CA, USA, pp. 26-39.

33 BROWN, H; "Composite Repair SAMPE Monograph I", SAMPE, Covina, CA, USA, 1985.

34 ANONYMOUS, "The repair of aircraft structures involving composite materials", AGARD-CP-402, AGARD, Neuilly-Sur-Seine, France, 1986.

35 THIELE, TH; "Repair procedures for composite parts on the Alpha Jet", AGARD-CP-402, AGARD, Neuilly-sur-Seine, France, 1986, pp. 2.1-2.7.

36 HELLARD, G; "La conception et le controle des réparations des volets hypersustentateurs de l'ATR-42 en carbone", AGARD-CP-402, AGARD, Neuilly-sur-Seine, France, 1986, pp. 5.1-5.18.

37 TORRES, M; PLISSONNEAU, B; "Repair of helicopter composite structure: techniques and substantiations", AGARD-CP-402, AGARD, Neuilly-sur-Seine, France, 1986, pp. 6.1-6.21.

38 CHAUMMETTE, D; HENRIOT, F; "Réparation de dommages en service des structures composites - Applications au Mirage 2000", AGARD-CP-402, AGARD, Neuilly-sur-Seine, France, 1986, pp. 12.1-12.10.

39 ARMSTRONG, K B; "British Airways experience with composite repairs", AGARD-CP-402, AGARD, Neuilly-sur-Seine, France, 1986, pp. 21.1-21.12.

40 GUNTHER, G; LEMMER, L; "Composite repair of cocured J-stiffened panels - design and test verification", AGARD-CP-402, AGARD, Neuilly-sur-Seine, France, 1986, pp. 8.1-8.19.

41 LEDWA, K; "Composite repair techniques for J-stiffened composite fuselage structures", AGARD-CP-402, AGARD, Neuilly-sur-Seine, France, 1986, pp. 14.1-14.11.

42 ANONYMOUS, "Composite repair of military aircraft structures", AGARD-CP-550, AGARD, Neuilly-Sur-Seine, France, 1995.

43 FRAILEY, J A; CARTER, D W; "Rapid repair of large area damage to contoured aircraft structures", AGARD-CP-550, AGARD, NATO, 1995, pp. 12.1-12.9.

44 BAUER, J; MAIER, A; " "on aircraft" repair verification of a fighter a/c integrally stiffened fuselage skin", AGARD-CP-550, AGARD, NATO, 1995, pp. 11.1-11.14.

45 MAIER. A E; "Composite repair of a CF18 - Vertical stabilizer leading edge", AGARD-CP-550, AGARD, NATO, 1995, pp. 13.1-13.16.

46 BAKER, A A; CHESTER, R J; HUGO, G R; RADTKE, T C; "Scarf repairs to graphite/epoxy components", AGARD-CP-550, AGARD, NATO, 1995, pp. 19.1-19.12.

REFERENCES

47 ELALDI, F; LEE, S; SCOTT, R F; "Scarf joint technique with cocured and precured patches for composite repair", AGARD-CP-550, AGARD, NATO, 1995, pp. 20.1-20.12.

48 WOLF, K; SCHINDLER, R; "External patch repair of CFRP/Honeycomb sandwich", AGARD-CP-550, AGARD, NATO, 1995, pp. 18.1-18.11.

49 COCHRAN, R; TRABOCCO, R; MEHRKAM, P; DIBERARDINO, M; "Field repair materials for naval aircraft", AGARD-CP-550, AGARD, NATO, 1995, pp. 10.1-10.7.

50 HEIMERDINGER, M W et al.; "Repair technology for thermoplastic aircraft structures", AGARD-CP-550, AGARD, NATO, 1995, pp. 15.1-15.12.

51 JONES, J S; GRAVES, S R; "Repair techniques for Celion/LARC-160 Graphite / polyimide composite structures", NASA Report No. CR-3794, 1984, 209 pp.

52 KLEIN, A J; "Repair of composites", Advanced Composites, July/Aug 1987, pp. 50-62.

53 McCONNELL, V P; "In need of repair", Advanced Composites, May/June 1989, pp. 60-70.

54 HALL, S R; RAIZENNE, M D; SIMPSON, D L; "A proposed composite repair methodology for primary structures", Composites, Vol. 20, No. 5, Sept 1989, pp. 479-483.

55 HART-SMITH, L J; "Analysis and design of advanced composite bonded joints", NASA contractor Report CR-2218, 1974.

56 HART-SMITH, L J; "Adhesive bonded joints for fibrous composite structures", Douglas Paper - presented at International Symposium, " Joining and repair of fibre reinforced plastics", Imperial College, 1986.

57 HART-SMITH, L J; "Adhesive bonded scarf and stepped lap joints", NASA Contractor Report CR 112237, 1973.

58 HART-SMITH, L J; "Further developments in the design and analysis of adhesive-bonded structural joints", Joining of Composite Materials, ASTM STP 749, K T Kedward, Ed., American Society for Testing and Materials, 1981, pp. 3-31.

59 SANDOW, F; "A computer aided aircraft structural composite repair system", Proceedings 32nd International SAMPE Symposium, 1987, pp. 551-557.

60 HART-SMITH, L J; "Designing to minimize peel stresses in adhesive joints", ASTM STP 876, 1985, pp. 238-266.

61 PARTRIDGE, P W; BREBBIA, C A; WROBEL, L C; "The dual reciprocity boundary element method", Computational Mechanics Publications, Elsevier Science Publishing Co., 1992, 279 pp.

62 SMITH, G D; "Numerical solution of partial differential equations: the finite difference methods", Oxford Applied Mathematics and Computing Science Series, Oxford University Press, Second Edition, 1978, 299 pp.

63 ASTLEY, R J; "Finite elements in solids and structures - An introduction", 1st edition, 1992, Chapman & Hall, London, UK, 345 pp.

64 OCHOA, O O; REDDY, J N; "Finite element analysis of composite laminates", Solid Mechanics and its applications Series, Kluwer Academic Publishers, Dordrecht, The Netherlands, 1992, 197pp.

65 ZIENKIEWICZ, O C; TAYLOR, R L; "The finite element method", 4th Edition, Volume 1, McGraw-Hill, 1989, 648 pp.

66 ZIENKIEWICZ, O C; TAYLOR, R L; "The finite element method", 4th Edition, Volume 2, McGraw-Hill, 1991, 807 pp.

67 SMITH, I M; GRIFFITHS, D V; "Programming the finite element method", 2nd Edition, John Wiley and Sons Ltd, 1988, 469 pp.

68 VOLKERSEN, O; " Die Niet Kraft vertelung in Zug bean Spruchten Niet verb bind ungen mit Konstanten Lasch enguerschnitten", Luftfahrt, No. 15, 1938, pp.41-47

69 GOLAND, M; REISSNER, E; "Stresses in cemented joints", ASME Journal of Applied Mechanics, Vol. 11, 1947, pp. A.17-A-27.

REFERENCES

70 SZEPE, F; "Strength of adhesive bonded joints with respect to temperature and fatigue", Experimental Mechanics, Vol. 6., 1966, pp. 280-286.

71 DE BRUYNE, N A; "The strength of glued joints", Aircraft Engineering, Vol. 16, 1944, pp. 115-118.

72 KUTSCHA, D; HOFER, K E; "Feasibility of joining advanced composite flight vehicles", AFML-TR-68-391, January 1969.

73 VINSON, J R; SIERAKOWSKI, R L; "Joints", Chapter 8, The behavior of structures composed of composite materials, Mechanics of Structural Systems Series, ed. Przemieniecki J S and Oravas, G AE, Martinus Nijhoff Publishers, Dordrecht, The Netherlands, 1985, pp. 239-283.

74 MATTHEWS, F L; KILTY, P F; GODWIN, E W; "A review of the strength of joints in fibre reinforced plastics part 2: Adhesively bonded joints", Composites, Vol. 13, 1982, pp. 29-37.

75 ADAMS, R D; "Theoretical stress analysis of adhesively bonded joints", Chapter 5, Joining of Fibre-reinforced Plastics, ed. F L Matthews, Elsevier, 1987, pp. 185-226.

76 RENTON, W J; VINSON, J R; "The efficient design of adhesive bonded joints", Journal of Adhesion, Vol. 7, 1975, 175-193.

77 RENTON, W J; VINSON, J R; "The efficient design of adhesive bonded joints", Journal of Adhesion, Vol. 7, 1975, p.175.

78 RENTON, W J; VINSON, J R; "On the behaviour of bonded joints in composite materials", Engineering Fracture Mechanics, Vol. 7, 1975, p.41

79 ALLMAN, D J; "A theory for elastic stresses adhesive bonded lap joints", Quarterly Journal of Mechanics and Applied Mathematics, Vol. XXX, 1977, p. 4.

80 ADAMS, R D; PEPPIAT, N A; Journal of Strain Analysis, Vol. 9, 1974, p. 185.

81 HART-SMITH, L J; "Joints", Composite Structures Analysis and Design, Composites, Engineered Materials Handbook, Volume 1, ASM International, 1987, pp. 479-495.

82 HART-SMITH, L J; "Developments in Adhesives - 2", Ed. A J Kinloch, Applied Science Publishers, London, UK, 1981, p. 1.

83 ADAMS, R D; WAKE, W C; "The nature and magnitude of stresses in adhesive joints", Structural Adhesive Joints in Engineering , Chapter 2, Elsevier Applied Science Publishers, 1984, pp. 14-114

84 WOOLEY, G R; CARVER, D R; Journal of Aircraft, Vol. 8, 1971, p.817

85 ADAMS, R D; HARRIS, J A; "Influence of local geometry on the strength of adhesive joints", International Journal of Adhesion and Adhesives, Vol. 7, No. 2, 1987, pp. 68-80.

86 ADAMS, R D; ATKINS, R W; HARRIS, J A; KINLOCH, A J; "Stress analysis and failure properties of carbon-fibre reinforced plastic/steel double lap-joint", Journal of Adhesion, Vol. 20, 1986, pp. 29-33.

87 CLARKE J.D. AND MCGREGOR I.J., 'Ultimate tensile stress over a zone: A new failure criterion for adhesive joints', Journal of Adhesion, Vol. 42, 1993

88 GROTH, H L; "Stress singularities and fracture at interface corners in bonded joints", International Journal of Adhesion and Adhesives, Vol. 8, No. 2, 1988, pp. 107-113.

89 KINLOCH, A J; SHAW, S J; Journal of Adhesion, Vol. 12, 1981, pp.59-77.

90 REMY, J; LASCHET, G; JEUSETTE, J P; "Non-linear finite element analysis of joints adhesively bonding composite materials", Mechanics and Mechanisms of Damage in Composites and Multi-Materials, ESIS11 (Edited by D. Baptiste), 1991, Mechanical Engineering Publications, London, pp. 301-318.

91 JOHN, S J; KINLOCH, A J; MATTHEWS, F L; "Measuring and predicting the durability of bonded fibre/epoxy composite joints", Composites, Vol. 22, 1991, pp. 121-127.

92 CHARALAMBIDES, M N; MATTHEWS, F L; KINLOCH, A J; "Failure criterion for a double lap joint", Case Study Notes, Computer-Aided Analysis of Composite Materials Short Course, Imperial College, London UK, 23 June 1995

REFERENCES

93 LEE, R J; McCARTHY, J C; "Design of bonded structures", Advanced Composites, Chapter 8, ed. I K Partridge, Elsevier Applied Science, 1989, pp. 269-301.

94 IKEGAMI M., KISHIMOTO W., OKITA K, NAKAYAMA H. AND SHIRATO M., 'Strength of adhesively bonded scarf joints between glass fibre reinforced plastics and metals', Proceedings of Structural Adhesives in Engineering II, 1989

95 GALI, S; ISHAI, O; "Interlaminar stress distribution within an adhesive layer in the non-linear range", International Journal of Adhesion, Vol. 19, 1978, pp. 253-256.

96 PICKETT, A K; HOLLOWAY,L; "The analysis of elastic-plastic adhesive stress in bonded lap joints in FRP structures", Composite Structures, Vol. 4, 1985, pp. 135-160.

97 GROSSFIELD, H; ISHAI, O; "The effect of cyclic loading on residual stresses and strains in a bonded joint", International Journal of Adhesion, 1982, pp. 155-160.

98 WRIGHT, M D; "Stress distribution of a butt strap joint in CFRP", Composites, Vol. 9, No. 4, Oct 1978, p.259.

99 WRIGHT, MD; "Stress distribution in carbon fibre-reinforced plastic joints", Composites, Vol. 11, No. 1, Jan 1980, p. 46.

100 RHAGAVA, R; CADDELL, R M; YEH, G S; "The macroscopic yield behaviour of polymers", Journal of Material Science, Vol. 8, 1973, pp. 225-232.

101 LOSS, K R; KEDWARD, K T; "Modelling and analysis of peel and shear stresses in adhesively bonded joints", Paper 84-0913, AIAA, 1984.

102 SIENER, M P; "Stress field sensitivity of a composite patch repair as a result of varying patch repair thickness", ASTM STP 1120, "Composite Materials: Testing and Design, Volume 10, 1992, pp. 444-464.

103 CHICKEN, S H; "Repair of military aircraft composites", Proceedings of the RAeS Damage, Assessment and Repair Conference, London, UK, 1996, pp. 3.1-3.11.

104 DAVIS, M J; "The development of an engineering standard for composite repair", AGARD-CP-550, AGARD, NATO, 1995, pp. 24.1-24.11.

105 HUNTER, M W; "Modeling and analysis of orthotropic plate with circular cut-out and adhesive bonded patch", Master Thesis, Air Force Institute of Technology, USA, 1990

106 JONES, R; CALLINAN, R J; AGGARWAL, K C; "Analysis of bonded repairs to damaged fibre composite structures", Engineering Fracture Mechanics, Vol. 17, No. 1, 1983, pp. 37-46.

107 SOUTIS, C; HU, F Z; "Design and performance of bonded patch repairs of composite structures", presented at the IMechE Conference on Airworthiness Aspects of New Technologies, 10 November 1996, Bristol, UK, 17 pp.

108 SOUTIS, C; HU, F Z; "Repair design of composites and efficiency of scarf patch repairs", Proceedings 11th International Conference on Composite Materials, Vol. VI, July 1997, Woodhead Publishers, pp. 395-404

109 BAIR, D L; HUDSON, P O; GHANIMATI, G R; "Analysis and repair of damaged composite laminates", Proceedings 36th International SAMPE symposium, SAMPE, Covina, CA USA, Vol. 36, Book2, 1991,pp. 2264-2278.

110 CROCOMBE A.D. AND TATAREK A., 'A unified approach to adhesive joint analysis', *Proceedings of Adhesives, Sealants and Encapsulants 85*, Plastics and Rubber Institute, 1985

111 CALLINAN, R J; "FE analytical requirements for bonded joints analysis - Statement of minimum model requirements", ICCM-11 Workshop on Practical Adhesive Bonding for Performance and Durability: Standards and Standardisation, Brisbane, 11 July 1997, 25 pp.

112 GIBSON, R F; "Principles of composite material mechanics", Engineering Mechanics Series, Mc Graw-Hill International Editions, 1994, 425 pp.

113 VINSON, J R; SIERAKOWSKI, R L; "The behavior of structures composed of composite materials", Mechanics of Structural Systems Series, ed. Przemieniecki J S and Oravas, G AE, Martinus Nijhoff Publishers, Dordrecht, The Netherlands, 1985, 323 pp

114 MIDDLETON, D H, "Composite Materials in Aircraft Structures", Longman Group UK Ltd, 1990, 393 pp.

REFERENCES

115 POWELL, P C; "Engineering with fibre-polymer laminates", 1st Edition, Chapman & Hall, London, 1994, 441 pp.

116 MATTHEWS, FL; RAWLINGS, R D; "Composite Materials: Engineering and Science", Chapman and Hall, 1994 , 470 pp.

117 DATOO, M H; "Mechanics of fibrous composites", Elsevier Applied Science, Elsevier Science Publishers Ltd, Barking, UK, 1991, 636 pp.

118 DANIEL, I M; ISHAI, O; "Engineering Mechanics of Composite Materials", Oxford University Press, Oxford, UK, 1994, 395 pp.

119 HOSKIN, B C; BAKER, A A (Editors); "Composite Materials for Aircraft Structures", AIAA Education Series, AIAA, New York, 1986, 237 pp.

120 SANDHU, R S; " A survey of failure theories of isotropic and anisotropic materials", Air Force Flight Dynamics Laboratory, Technical Report AFFDL-TR-72-71, Wright Aeronautical Labs , Dayton OH, USA, 1972

121 CURTIS, P T; "Theoretical prediction of strength and failure mechanisms in polymeric composite materials", Technical Report TR-92057, Defence Research and Evaluation Agency, Farnborough, UK, 1992.

122 TSAI, S W; WU, E M; "A general theory of strength for anisotropic materials", Journal of Composite Materials, Vol. 5, 1971, pp. 58-80.

123 TENNYSON, R C; NANYARO, A P; WHARRAM, G E; "Application of the cubic polynomial strength criterion to the failure analysis of composite materials", Journal of Composite Materials Supplement, Vol. 14, 1980, pp. 28-41.

124 TENNYSON, R C; ELLIOT, W G; "Failure analysis of composite laminates including biaxial compression", NASA Contractor Report, CR 172192, 1983.

125 TENNYSON, R C; MacDONALD, D; NANYARO, A P; "Evaluation of the tensor polynomial failure criterion for composite materials", Journal of Composite Materials, Vol. 12, 1978, pp. 63-75.

126 JIANG, Z; TENNYSON, R C; "Closure of the cubic tensor polynomial failure surface", Journal of Composite Materials, Vol. 23, 1989, pp. 208-231.

127 HART-SMITH, L J; "The first fair dinkum macro-level fibrous composite failure criteria", Proceedings 11th International Conference on Composite Materials, Vol. I, 1997, pp. 52-87.

128 HASHIN, Z; "Failure criteria for unidirectional fiber composites", Journal of Applied Mechanics, Vol. 47, June 1980, pp. 329-333.

129 PIPES, R B; COLE, B W; "On the off-axis strength test for anisotropic materials", Journal of Composite Materials, Vol. 7, 1973, p.246.

130 HART-SMITH, L J; "A strain-based maximum shear stress failure criterion for fibrous composites", Proceedings 31st AIAA/ASME Structures, Structural Dynamics and Materials Conference, California, USA, April 1990.

131 CUNTZE, R G; "Evaluation of multiaxial test data of UD laminae by so called Fracture-Type Strength Criteria and by supporting probabilistic means", Proceedings 11th International Conference on Composite Materials, Gold Coast, Australia, July 1997, Vol. II, pp. 273-289.

132 HASHIN, Z; ROTEM, A; " A fatigue failure criterion for fibre-reinforced materials", Journal of Composite Materials, Vol. 7, 1973, pp. 448

133 PUCK, A; "Festigkeitsanalyse von Faser-Matrix-Laminaten - Modelle fur die Praxis", Munchen, Carl Hanser Verlag, 1995.

134 PUCK, A; "Calculating the strength of glass fibre plastics laminates under combined load", German Plastics [English issue of Kunststoffe], Vol. 59, pp. 18-19.

135 KROLL, L; HUFENBACH, W; "Physically based failure criterion for dimensioning of thick-walled laminates", Applied Composite Materials, Vol. 4, No. 5, 1997, pp. 321-332.

REFERENCES

136 CUNTZE, R G; "Fracture-type strength criteria formulated by invariants which consider the material symmetries of the isotropic/anisotropic materials used", Proceedings ESA-CNES-DARA Conference on Spacecraft Structures, Materials and Mechanical Testing, Noordwijk, March 1996.

137 TENNYSON, R C; WHARRAM, G E; "Development of failure criterion for Kevlar/Epoxy fabric laminates", NASA CR 172465, July 1984.

138 TENNYSON, R C; WHARRAM, G E; "Evaluation of failure criterion for graphite/epoxy fabric laminates", NASA CR 172547, February 1985.

139 GREENWOOD L., BOAG T.G. AND MCLAREN A.S., 'Stress distributions in lap joints, Adhesion: Fundamentals and practice, McLaren, 1969

140 HART SMITH L.J., 'Adhesive bonded single lap joints', *Technical Report CR-112236*, NASA, Langley Research Centre, 1973

141 ADAMS R.D., AND PANES G.A., 'The effect of three dimensional stresses on the failure of single lap joints', Proceedings of Euradh 94, Institute of Materials, 1994

142 HARRIS J.A., AND ADAMS R.D., 'Strength prediction of bonded single lap joints by non-linear finite element methods', International Journal of Adhesion and Adhesives, Vol. 4, No.2, 1984

143 CROCOMBE A.D., BIGWOOD D.A. AND RICHARDSON G., 'Analysing structural adhesive joints for failure', International Journal of Adhesion and Adhesives, Vol. 10, No. 3. 1990

144 CHARALAMBIDES, M N; KINLOCH, A J; MATTHEWS, F L; "Strength prediction of bonded joints", AGARD Conference on Bolted/Bonded Joints in Polymeric Composites, AGARD Conference Proceedings CP-590, 1997, pp. 10.1-10.10

145 LEE S.J AND LEE G.L., 'Development of a failure model for the adhesively bonded tubular single lap joint', Journal of Adhesion, Vol. 40, 1992

146 CROCOMBE A.D. AND ADAMS R.D., 'An elastoplastic investigation of the peel test', Journal of Adhesion, Vol. 13, 1982

147 BOGEY, D B; "Edge bonded dissimilar orthogonal elastic wedges under normal and shear loading", Transactions ASME Journal of Applied Mechanics, Vol. 35, 1968.

148 CROCOMBE A.D., 'Global yielding as a failure criteria for bonded joints', International Journal of Adhesion and Adhesives, Vol. 9, No. 3, 1989

149 ZHAO X, PhD. Thesis, Bristol, 1991

150 CROCOMBE A D, RICHARDSON G., AND SMITH P.A., 'A unified approach for predicting the strength of cracked and non-cracked adhesive joints', *Journal of Adhesion*, 1994

151 TOWSE, A; DAVIES, R G H; CLARKE, A; WISNOM, M R; ADAMS, R D; POTTER, KD; "The design and analysis of high load intensity adhesively bonded double lap joints", Proceedings 4th International Conference on Deformation and Fracture of Composites, Manchester, UK, 1997, pp. 479-488.

152 TOWSE, A; POTTER, K D; WISNOM, M R; ADAMS, R D; "A novel comb joint concept for high strength unidirectional carbon fibre bonded joints", Proceedings 11th International Conference on Composite Materials, Gold Coast, Australia, 1997, Vol. VI, pp. 95-101.

153 KINLOCH A.J. AND SHAW S.J., 'The fracture resistance of a toughened epoxy adhesive', Journal of Adhesion, Vol. 12, 1981

154 TRANTINA G.C., 'Fracture mechanics approach to adhesive joints', Journal of Composite Materials, Vol. 6, 1972

155 GRADIN P.A. AND GROTH H.L., 'A fracture criterion for adhesive joints in terms of material induced singularities', Report No. 83-12, The Royal Institute of Technology Stockholm Sweden, 1984

156 HART-SMITH, L J; "Simple practical joint design methodology" ICCM-11 Workshop on Practical Adhesive Bonding for Performance and Durability: Standards and Standardisation, Brisbane, 11 July 1997, 38 pp.

157 CHOW C.L. AND LU T.J., 'Analysis of failure properties and strength of structural adhesive joints with damage mechanics', International Journal of Damage Mechanics, Vol. 1, 1992

REFERENCES

158 LASCHET,G; "Numerical strength predictions of adhesively bonded multimaterial joints", AGARD Conference on Bolted/Bonded Joints in Polymeric Composites, AGARD-CP-590, 1997, pp. 11.1-11.8

159 BREWER, J C; LAGACE, P A; "Quadratic stress criterion for initiation of delamination", Journal of Composite Materials, Vol. 22, 1988, pp. 1141-1151

160 HART-SMITH, L J; "Simplified estimation of stiffness and biaxial strengths for design of laminated carbon-epoxy composite structures", Douglas Paper 7548, McDonnell Douglas Aerospace, Long Beach, CA, 1985

161 HART-SMITH, L J; "The ten-percent rule for preliminary sizing of fibrous composite structures", Aerospace Materials, Vol. 5, No. 2, August-October 1993, pp. 10-16.

162 HART-SMITH, L J; "Expanding the capabilities of the ten-percent rule for predicting the strength of fibre-polymer composites", McDonnell Douglas Paper MDC 97K0012, 1997 appear in Composite Science and Technology

163 BAILIE, J A; "Woven fabric aerospace structures", Handbook of Composites, Vol.2 - Structure and Design, Chapter 7, Ed. C T Herakovitch and Y M Tarnopol'skii, Elsevier Science Publishers, 1989, p.359

164 ADAMS, R D; WAKE, W C; "The nature and magnitude of stresses in adhesive joints", Chapter 2, Structural Adhesive Joints in Engineering, Elsevier Applied Science Publishers, 1984, pp. 15-114.

165 ANON., NISA II User manual, EMRC, Troy Michigan, USA, 1995 p. 3.9-2

166 DIETER, G E; Mechanical Metallurgy, McGraw-Hill, 2nd Ed., 1976, 774 pp.

167 LOVELL, D R; "Types of materials", Composite Materials in Aircraft Structures, ed. D H Middleton, Longman Group UK Ltd, 1990, pp 17-38.

168 SEN, Z Q; "Modification of BMI and QY8911 BMI resin systems", Proceedings 38th International SAMPE Symposium, Vol. 38, Book 1 , 1993, pp. 909-923.

169 REINHART, T J; " Introduction to composites", Composites, Engineered Materials Handbook, Volume 1, ASM International, 1987, pp. 1-42.

170 SCOLA, D A; "Polymide resins", Properties of Constituent Materials, Composites, Engineered Materials Handbook, Volume 1, ASM International, 1987, pp. 78-89.

171 GREEN, G E; "Matrices for advanced structural composites", Composite Materials in Aircraft Structures, ed. D H Middleton, Longman Group UK Ltd, 1990, pp 39-49.

172 BROWN, A S; "Thermoplastic composites: material of the '90s?", Aerospace America, Vol. 28, Jan 90, pp. 28-31.

173 BRANDT, J; DRECHSLER, K; RICHTER, H; "The use of high-performance thermoplastic composites for structural aerospace applications - status and outlook", ICCM/9, Composites: Properties and Applications, Volume VI, Woodhead Publishing Ltd, 1993, pp. 143-150.

174 WATSON, J C; RAGHUPATHI, N R; "Glass Fibers", Constituent Material Form, Composites, Engineered Materials Handbook, Volume 1, ASM International, 1987, pp. 107-111.

175 MILLER, D M; "Glass Fibers", Properties of Constituent Materials, Composites, Engineered Materials Handbook, Volume 1, ASM International, 1987, pp. 45-48.

176 SCHOENBERG, T; "Boron and silicon carbide fibres", Properties of Constituent Materials, Composites, Engineered Materials Handbook, Volume 1, ASM International, 1987, pp. 58-59.

177 BASCOM, D W; "Other continuous fibers", Constituent Material Forms, Composites, Engineered Materials Handbook, Volume 1, ASM International, 1987, pp 117-118.

178 PIGLIACAMPI, J J; "Aramid fibers", Constituent Material Forms, Composites, Engineered Materials Handbook, Volume 1, ASM International, 1987, pp. 114-116.

179 PIGLIACAMPI, J J; "Organic fibres", Properties of Constituent Materials, Composites, Engineered Materials Handbook, Volume 1, ASM International, 1987, pp. 54-57.

180 SCHWARTZ, M M; "Composite materials handbook", 2nd Edition, McGraw-Hill, 1992.

REFERENCES

181 SPRY, W J; "Sports and recreational equipment", Applications and Experience, Composites, Engineered Materials Handbook, Volume 1, ASM International, 1987, pp. 845-847

182 SUMMERSCALES, J; "Marine applications", Applications and Experience, Composites, Engineered Materials Handbook, Volume 1, ASM International, 1987, pp. 837-844.

183 KELLY, J; SPERO, A; DORR, J; CORONA, K; "Development of organic matrix composites for transport aircraft, marine and civil structures", ICCM/9, Composites: Properties and Applications, Volume VI, Woodhead Publishing Ltd, 1993, pp. 283-290.

184 FENBERT, H R; "Composites in commercial aircraft - a production cost perspective ICCM/9, Composites: Properties and Applications, Volume VI, Woodhead Publishing Ltd, 1993, pp. 159-165.

185 THORBECK, J; "Economical view on composite structures maintenance", Advanced Materials: Cost Effectiveness, Quality Control, Health and Environment, ed. Kwakernaak, A and van Arkel, L, SAMPE, Elsevier Science Publishers B.V., 1991, pp. 323-335.

186 VAN TOOREN, M J L; VAN BEIJNEN, M N; VAN STIJN, I P M; "Towards an all composite aircraft fuselage", ICCM/9, Composites: Properties and Applications, Volume VI, Woodhead Publishing Ltd, 1993, pp. 166-173.

187 ANGLIN, J M; "Aircraft applications", Applications and Experience, Composites, Engineered Materials Handbook, Volume 1, ASM International, 1987, pp. 801-809.

188 POLICELLI, F J; VICARIO, A A; "Space and missile systems", Applications and Experience, Composites, Engineered Materials Handbook, Volume 1, ASM International, 1987, pp. 816-822.

189 ASHBY, M F; "On the engineering properties of materials", Acta Metallugica., Vol. 37, 1989, p. 1273

190 JONES, F R; "Carbon fibres from PAN - preparation and properties", Fibrous Reinforcements for Composite Materials, Handbook of Polymer-Fibre Composites, ed. F R Jones, Polymer Science and Technology Series, Longman, UK, 1994, pp. 19-24.

191 JOHNSON, D J; "Chemistry and physics of carbon", Ed., P A Thrower, Marcel Dekker, New York, 1987.

192 JOHNSON, D J; "Carbon fibres from PAN - structure", Fibrous Reinforcements for Composite Materials, Handbook of Polymer-Fibre Composites, ed. F R Jones, Polymer Science and Technology Series, Longman, UK, 1994, pp. 24-29.